ANNUAL REPORT 2004

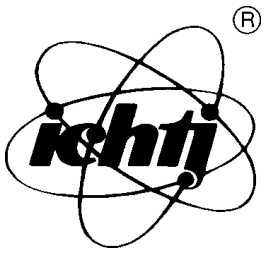

INSTITUTE
OF NUCLEAR CHEMISTRY
AND TECHNOLOGY

EDITORS

Prof. Jacek Michalik, Ph.D., D.Sc.
Wiktor Smułek, Ph.D.
Ewa Godlewska-Para, M.Sc.

PRINTING

Sylwester Wojtas

CONTENTS

GENERAL INFORMATION

The Institute of Nuclear Chemistry and Technology (INCT) is one of the successors of the Institute of Nuclear Research (INR) which was established in 1955. The latter Institute, once the biggest Institute in Poland, has exerted a great influence on the scientific and intelectual life in this country. The INCT came into being as one of the independent units established after the dissolution of the INR in 1983.

At present, the Institute research activity is focused on:

- radiation chemistry and technology,
- radiochemistry and coordination chemistry,
- radiobiology,
- application of nuclear methods in material and process engineering,
- design of instruments based on nuclear techniques,
- trace analysis and radioanalytical techniques,
- environmental research.

In the above fields we offer research programmes for Ph.D. students.

At this moment, with its nine electron accelerators in operation and with the staff experienced in the field of electron beam (EB) applications, the Institute is one of the most advanced centres of radiation research and EB processing. The accelerators are installed in the following Institute units:

- pilot plant for radiation sterilization of medical devices and transplants,
- pilot plant for radiation modification of polymers,
- experimental pilot plant for food irradiation,
- pilot plant for removal of SO_2 and NO_x from flue gases,
- pulse radiolysis laboratory, in which the nanosecond set-up was put into operation in 2001. A new 10 MeV accelerator was constructed in the INCT for this purpose.

Based on the technology elaborated in our Institute an industrial installation for electron beam flue gas treatment has been implemented at the EPS "Pomorzany" (Dolna Odra PS Group). This is the second full scale industrial EB installation for SO_2 and NO_x removal all over the world.

***

In 2004 the INCT scientists published 74 papers in scientific journals registered in the Philadelphia list, among them 31 papers in journals with an impact factor (IF) higher than 1.0. The INCT research workers are also the authors of 19 chapters in scientific books published in 2004.

The Ministry of Science and Information Society Technologies (MSIST) approved the INCT application to set up the Centre of Excellence "EKO-NUKLEON – Centre of Proecologic Nuclear Technologies" and the Centre was established in the INCT in November 2004.

In 2004 the Ministry of Science and Information Society Technologies granted 7 research projects and one implementation project to the INCT research teams. The INCT started participating in 3 integrated research projects ordered and supported financially by MSIST.

The European Commission (EC) in 2004 approved three new research projects:

- *Advanced methods for environment research and control*
  principal investigator: Dr. **Grażyna Zakrzewska-Trznadel**

- *Chemical studies for design and production of new radiopharmaceuticals*
  principal investigator: Prof. **Jerzy Ostyk-Narbutt**
- *European research program for the partitioning of actinides from high active wastes issuing the reprocessing of spent nuclear fuels*
  principal investigator: Prof. **Jerzy Ostyk-Narbutt**

Altogether the INCT is carrying out 6 research projects supported financially by EC.

Annual rewards of the INCT Director-General for the best publications in 2004 were granted to the following research teams:

- First award to Dr. **Dariusz Pogocki** for presenting an innovatory approach in a series of papers to the formation of sulphuranyl oxides, using modern techniques of molecular modelling.
- Second award to Dr. **Leon Fuks**, Assoc. Prof. **Marcin Kruszewski**, **Elżbieta Boużyk**, **Hanna Lewandowska-Siwkiewicz** for a series of papers concerning interdisciplinary studies on synthesis of platinum and palladium complex compounds and their biological activity of antitumor characteristics.
- Third award to Dr. **Andrzej Deptuła**, **Wiesława Łada**, **Tadeusz Olczak** for a series of papers on the formation of new materials using sol-gel technique enabling practical application of the obtained results.

The INCT activity in organizing the scientific meetings should be especially stressed. In total, in 2004, seven international meetings have been organized:

- 2nd Research Coordination Meeting of the International Atomic Energy Agency "*Remediation of Polluted Waters and Wastewaters by Radiation Processing*";
- IAEA Consultants Meeting "*Preparation of a Technical Document on Radiotracers and Labelling Compounds for Applications in Industry and Environment*";
- International Symposium on *Advanced Oxidation Technologies for Wastewater Treatment*;
- Conference on *Tracer and Tracing Methods*;
- 2nd Congress "*Food, Nutrition and Health in Poland Integrated with European Union*";
- II Conference on *Problems of Waste Disposal*;
- Kick-off Workshop on the Project "*Chemical Studies for Design and Production of New Radiopharmaceuticals (POL-RAD-PHARM)*".

The international journal for nuclear research – NUKLEONIKA, published by the INCT, was mentioned in the SCI Journal Citation List.

MANAGEMENT OF THE INSTITUTE

MANAGING STAFF OF THE INSTITUTE

Director
Assoc. Prof. **Lech Waliś**, Ph.D.

Deputy Director for Research and Development
Prof. **Jacek Michalik**, Ph.D., D.Sc.

Deputy Director for Maintenance and Marketing
Roman Janusz, M.Sc.

Accountant General
Barbara Kaźmirska/Małgorzata Otmianowska-Filus

HEADS OF THE INCT DEPARTMENTS

- Department of Nuclear Methods of Material Engineering
  Wojciech Starosta, M.Sc.
- Department of Radioisotope Instruments and Methods
  Prof. **Piotr Urbański**, Ph.D., D.Sc.
- Department of Radiochemistry
  Prof. **Jerzy Ostyk-Narbutt**, Ph.D., D.Sc.
- Department of Nuclear Methods of Process Engineering
  Prof. **Andrzej G. Chmielewski**, Ph.D., D.Sc.
- Department of Radiation Chemistry and Technology
  Zbigniew Zimek, Ph.D.
- Department of Analytical Chemistry
  Prof. **Rajmund Dybczyński**, Ph.D., D.Sc.
- Department of Radiobiology and Health Protection
  Prof. **Irena Szumiel**, Ph.D., D.Sc.
- Experimental Plant for Food Irradiation
  Assoc. Prof. **Wojciech Migdał**, Ph.D., D.Sc.
- Laboratory for Detection of Irradiated Foods
  Wacław Stachowicz, Ph.D.
- Laboratory for Measurements of Technological Doses
  Zofia Stuglik, Ph.D.

SCIENTIFIC COUNCIL (2003-2007)

1. Prof. **Grzegorz Bartosz**, Ph.D., D.Sc.
   University of Łódź
   • biochemistry
2. Assoc. Prof. **Aleksander Bilewicz**, Ph.D., D.Sc.
   Institute of Nuclear Chemistry and Technology
   • radiochemistry, inorganic chemistry
3. Prof. **Krzysztof Bobrowski**, Ph.D., D.Sc. (Chairman)
   Institute of Nuclear Chemistry and Technology
   • radiation chemistry, photochemistry, biophysics
4. **Sylwester Bułka**, M.Sc.
   Institute of Nuclear Chemistry and Technology
   • electronics
5. Prof. **Witold Charewicz**, Ph.D., D.Sc.
   Wrocław University of Technology
   • inorganic chemistry, hydrometallurgy

6. Prof. **Stanisław Chibowski**, Ph.D., D.Sc.
   Maria Curie-Skłodowska University
   • radiochemistry, physical chemistry
7. Prof. **Andrzej G. Chmielewsk**i, Ph.D., D.Sc.
   Institute of Nuclear Chemistry and Technology
   • chemical and process engineering, nuclear chemical engineering, isotope chemistry
8. Prof. **Jadwiga Chwastowska**, Ph.D., D.Sc.
   Institute of Nuclear Chemistry and Technology
   • analytical chemistry
9. Prof. **Rajmund Dybczyński**, Ph.D., D.Sc.
   Institute of Nuclear Chemistry and Technology
   • analytical chemistry
10. Prof. **Zbigniew Florjańczyk**, Ph.D., D.Sc.
    (Vice-chairman)
    Warsaw University of Technology
    • chemical technology
11. Prof. **Leon Gradoń**, Ph.D., D.Sc.
    Warsaw University of Technology
    • chemical and process engineering
12. Assoc. Prof. **Edward Iller**, Ph.D., D.Sc.
    Radioisotope Centre POLATOM
    • chemical and process engineering, physical chemistry
13. Assoc. Prof. **Marek Janiak**, Ph.D., D.Sc.
    Military Institute of Hygiene and Epidemiology
    • radiobiology
14. **Iwona Kałuska**, M.Sc.
    Institute of Nuclear Chemistry and Technology
    • radiation chemistry
15. Assoc. Prof. **Marcin Kruszewski**, Ph.D., D.Sc.
    Institute of Nuclear Chemistry and Technology
    • radiobiology
16. Prof. **Marek Lankosz**, Ph.D., D.Sc.
    AGH University of Science and Technology
    • physics, radioanalytical methods
17. Prof. **Janusz Lipkowski**, Ph.D., D.Sc.
    Institute of Physical Chemistry, Polish Academy of Sciences
    • physicochemical methods of analysis
18. **Zygmunt Łuczyński**, Ph.D.
    Institute of Electronic Materials Technology
    • chemistry
19. Prof. **Andrzej Łukasiewicz**, Ph.D., D.Sc.
    Institute of Nuclear Chemistry and Technology
    • material science
20. Prof. **Bronisław Marciniak**, Ph.D., D.Sc.
    Adam Mickiewicz University
    • physical chemistry
21. Prof. **Józef Mayer**, Ph.D., D.Sc.
    Technical University of Łódź
    • physical and radiation chemistry
22. Prof. **Jacek Michalik**, Ph.D., D.Sc.
    Institute of Nuclear Chemistry and Technology
    • radiation chemistry, surface chemistry, radical chemistry
23. Prof. **Jerzy Ostyk-Narbutt**, Ph.D., D.Sc.
    Institute of Nuclear Chemistry and Technology
    • radiochemistry, coordination chemistry
24. **Jan Paweł Pieńkos**, Eng.
    Institute of Nuclear Chemistry and Technology
    • electronics
25. Prof. **Leon Pszonicki**, Ph.D., D.Sc.
    Institute of Nuclear Chemistry and Technology
    • analytical chemistry
26. Prof. **Sławomir Siekierski**, Ph.D.
    Institute of Nuclear Chemistry and Technology
    • physical chemistry, inorganic chemistry
27. Prof. **Sławomir Sterliński**, Ph.D., D.Sc.
    Central Laboratory for Radiological Protection
    • physics, nuclear technical physics
28. Prof. **Irena Szumiel**, Ph.D., D.Sc.
    Institute of Nuclear Chemistry and Technology
    • cellular radiobiology
29. Prof. **Jerzy Szydłowski**, Ph.D., D.Sc.
    Warsaw University
    • physical chemistry, radiochemistry
30. Prof. **Jan Tacikowski**, Ph.D.
    Institute of Precision Mechanics
    • physical metallurgy and heat treatment of metals
31. Prof. **Marek Trojanowicz**, Ph.D., D.Sc.
    Institute of Nuclear Chemistry and Technology
    • analytical chemistry
32. Prof. **Piotr Urbański**, Ph.D., D.Sc.
    (Vice-chairman)
    Institute of Nuclear Chemistry and Technology
    • radiometric methods, industrial measurement equipment, metrology
33. Assoc. Prof. **Lech Waliś**, Ph.D.
    Institute of Nuclear Chemistry and Technology
    • material science, material engineering
34. Assoc. Prof. **Andrzej Wójcik**, Ph.D., D.Sc.
    (Vice-chairman)
    Institute of Nuclear Chemistry and Technology
    • cytogentics
35. Prof. **Zbigniew Zagórski**, Ph.D., D.Sc.
    Institute of Nuclear Chemistry and Technology

- physical chemistry, radiation chemistry, electrochemistry
- electronics, accelerator techniques, radiation processing

36. **Zbigniew Zimek**, Ph.D.
Institute of Nuclear Chemistry and Technology

HONORARY MEMBERS OF THE INCT SCIENTIFIC COUNCIL (2003-2007)

1. Prof. **Antoni Dancewicz**, Ph.D., D.Sc.
   - biochemistry, radiobiology

SCIENTIFIC STAFF

PROFESSORS

1. **Bobrowski Krzysztof**
   radiation chemistry, photochemistry, biophysics
2. **Chmielewski Andrzej G.**
   chemical and process engineering, nuclear chemical engineering, isotope chemistry
3. **Chwastowska Jadwiga**
   analytical chemistry
4. **Dybczyński Rajmund**
   analytical chemistry
5. **Leciejewicz Janusz**
   crystallography, solid state physics, material science
6. **Łukasiewicz Andrzej**
   material science
7. **Michalik Jacek**
   radiation chemistry, surface chemistry, radical chemistry
8. **Ostyk-Narbutt Jerzy**
   radiochemistry, coordination chemistry
9. **Piekoszewski Jerzy**
   solid state physics
10. **Pszonicki Leon**
    analytical chemistry
11. **Siekierski Sławomir**
    physical chemistry, inorganic chemistry
12. **Szumiel Irena**
    cellular radiobiology
13. **Trojanowicz Marek**
    analytical chemistry
14. **Urbański Piotr**
    radiometric methods, industrial measurement equipment, metrology
15. **Zagórski Zbigniew**
    physical chemistry, radiation chemistry, electrochemistry

ASSOCIATE PROFESSORS

1. **Bilewicz Aleksander**
   radiochemistry, inorganic chemistry
2. **Grigoriew Helena**
   solid state physics, diffraction research of non-crystalline matter
3. **Grodkowski Jan**
   radiation chemistry
4. **Kruszewski Marcin**
   radiobiology
5. **Legocka Izabella**
   polymer technology
6. **Migdał Wojciech**
   chemistry, science of commodies
7. **Pogocki Dariusz**
   radiation chemistry, pulse radiolysis
8. **Waliś Lech**
   material science, material engineering
9. **Wójcik Andrzej**
   cytogenetics
10. **Żółtowski Tadeusz**
    nuclear physics

SENIOR SCIENTISTS (Ph.D.)

1. **Bartłomiejczyk Teresa**
   biology
2. **Borkowski Marian**
   chemistry
3. **Buczkowski Marek**
   physics
4. **Cieśla Krystyna**
   physical chemistry

5. **Danilczuk Marek**
chemistry
6. **Danko Bożena**
analytical chemistry
7. **Dembiński Wojciech**
chemistry
8. **Deptuła Andrzej**
chemistry
9. **Dobrowolski Andrzej**
chemistry
10. **Dudek Jakub**
chemistry
11. **Dźwigalski Zygmunt**
high voltage electronics, electron injectors, gas lasers
12. **Frąckiewicz Kinga**
chemistry
13. **Fuks Leon**
chemistry
14. **Gniazdowska Ewa**
chemistry
15. **Grądzka Iwona**
biology
16. **Harasimowicz Marian**
technical nuclear physics, theory of elementary particles
17. **Kierzek Joachim**
physics
18. **Krejzler Jadwiga**
chemistry
19. **Kunicki-Goldfinger Jerzy**
conservator/restorer of art
20. **Machaj Bronisław**
radiometry
21. **Mikołajczuk Agnieszka**
chemistry
22. **Mirkowski Jacek**
nuclear and medical electronics
23. **Nowicki Andrzej**
organic chemistry and technology, high-temperature technology
24. **Owczarczyk Andrzej**
chemistry
25. **Owczarczyk Hanna B.**
biology
26. **Palige Jacek**
metallurgy
27. **Panta Przemysław**
nuclear chemistry
28. **Pawelec Andrzej**
chemical engineering
29. **Pawlukojć Andrzej**
physics
30. **Polkowska-Motrenko Halina**
analytical chemistry
31. **Przybytniak Grażyna**
radiation chemistry
32. **Ptasiewicz-Bąk Halina**
physics
33. **Rafalski Andrzej**
radiation chemistry
34. **Sadło Jarosław**
chemistry
35. **Samczyński Zbigniew**
analytical chemistry
36. **Skwara Witold**
analytical chemistry
37. **Sochanowicz Barbara**
biology
38. **Stachowicz Wacław**
radiation chemistry, EPR spectroscopy
39. **Strzelczak Grażyna**
radiation chemistry
40. **Stuglik Zofia**
radiation chemistry
41. **Szpilowski Stanisław**
chemistry
42. **Tymiński Bogdan**
chemistry
43. **Warchoł Stanisław**
solid state physics
44. **Wąsowicz Tomasz**
radiation chemistry, surface chemistry, radical chemistry
45. **Wierzchnicki Ryszard**
chemical engineering
46. **Wiśniowski Paweł**
radiation chemistry, photochemistry, biophysics
47. **Wojewódzka Maria**
radiobiology
48. **Zakrzewska-Trznadel Grażyna**
process and chemical engineering

49. Zielińska Barbara
chemistry

50. Zimek Zbigniew
electronics, accelerator techniques, radiation processing

RADIATION CHEMISTRY
AND PHYSICS,
RADIATION TECHNOLOGIES

SPECTRAL AND CONDUCTOMETRIC PULSE RADIOLYSIS STUDIES OF RADICAL CATIONS DERIVED FROM *N*-ACETYLATED OLIGOPEPTIDES CONTAINING METHIONINE AND GLYCINE RESIDUES

Krzysztof Bobrowski, Dariusz Pogocki, Gordon L. Hug[1/], Christian Schöneich[2/]

[1/] Radiation Laboratory, University of Notre Dame, USA

[2/] Department of Pharmaceutical Chemistry, University of Kansas, Lawrence, USA

In our previous reports we have shown that the sulfide radical cation of *N*-acetylmethionine amide (*N*-Ac-Met-NH_2) might associate with the deprotonated amide nitrogen localized either N- or C-terminally to methionine [1-2]. In *N*-acetylmethionine methyl ester (*N*-Ac-Met-OMe), a derivative lacking the C-terminal amide, such association is limited to the N-terminally localized nitrogen atom [3]. Mechanistically, the association with the N-terminal amide nitrogen has to be preceded by the formation of the sulfur-oxygen bond (in a seven-membered ring) followed by the -C(=O)NH- deprotonation and O-to-N migration of the sulfide radical cation resulting in the sulfur-nitrogen bond formation (in a favorable five-membered ring). Analogous processes involving sulfide radical cation should be observed in oligopeptides containing internal methionine residues. In order to check whether such mechanisms are possible, we have selected two *N*-acetylated oligopeptides containing internal methionine residues: *N*-Ac-Gly-Met-Gly and *N*-Ac-Gly-Gly-Gly-Met-Gly-Gly-Gly.

Time-resolved conductivity experiments with *N*-Ac-Gly-Met-Gly have shown low amplitude of negative conductivity at pH 5.45, recorded 20 μs after pulse irradiation (Fig.1A). The maximum loss of equivalent conductivity indicates very low yields of radical cations (**1**) and/or (**2a**,**b**) (Chart 1). This was confirmed by time-resolved optical spectroscopy (*vide infra*).

The •OH-induced reaction pathways in *N*-Ac-Gly-Met-Gly have been characterized by the complementary pulse radiolysis measurements coupled to time-resolved UV-VIS spectroscopy. The optical spectrum recorded 20 μs after pulse irradiation is well deconvoluted into contributions from: the two-α-(alkylthio)alkyl radicals (**3a**,**b**), the intermolecularly sulfur-sulfur three-electron bonded dimeric radical cation (**1**), the intramolecular sulfur-oxygen bonded radical cations (**2a**,**b**), the C_α-centered radical (**4**), and the glycyl radical (**5**) (Chart 1,

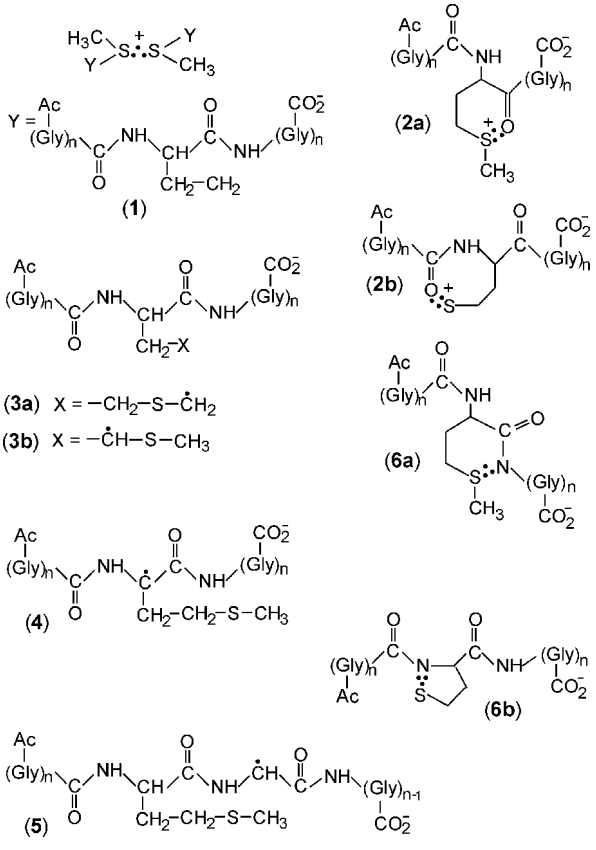

Chart 1.

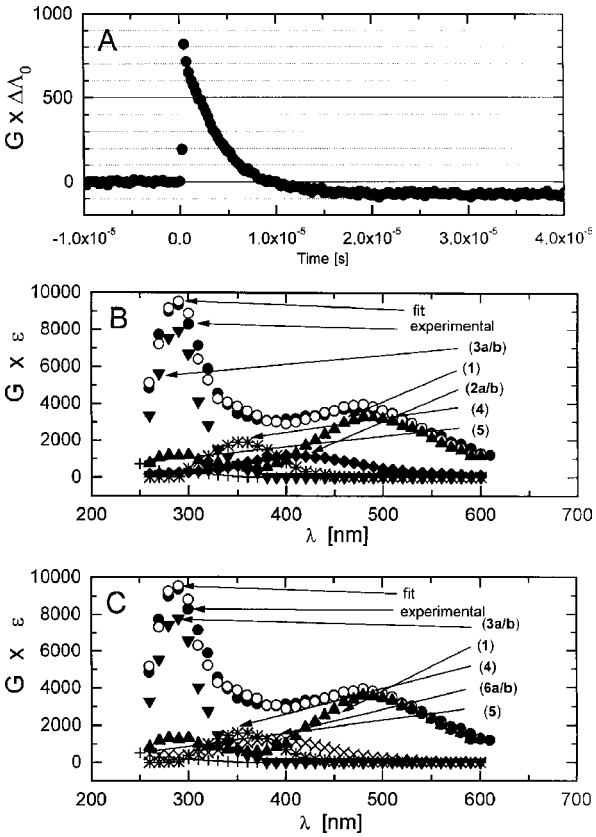

Fig.1. A – Equivalent conductivity changes represented as ($G \times \Delta\Lambda_0$) *vs*. time profile following the •OH-induced oxidation of *N*-Ac-Gly-Met-Gly (0.2 mM) in N_2O-saturated aqueous solutions at pH 5.45; B and C – resolution of the spectral components in the transient absorption spectra following the •OH-induced oxidation of *N*-Ac-Gly-Met-Gly (0.2 mM) in N_2O-saturated aqueous solutions at pH 5.45 taken 20 μs after the pulse.

Fig.1B). While the deconvolution results in the total yield of radical cations, $G_{1+2a,b}=1.2$, the discrepancy between G(ions)=0.7 and $G_{1+2a,b}=1.2$ is unacceptable. Best results are obtained when the deconvolution takes into account the formation of (**1**) and intramolecular sulfur-oxygen bonded radical cations (**2a**,**b**) are replaced by intramolecular sulfur-nitrogen bonded radical cations (**6a**,**b**), yielding a good match between G(ions)=0.7 and $G_{1+2a,b}=0.6$. Without any doubt, the existence of the **6a**,**b** transients is confirmed at longer times by applying complementary time-resolved conductivity and spectrophotometric measurements.

Similar spectral and conductance features have been observed in *N*-Ac-Gly-Gly-Gly-Met-Gly-Gly-Gly. Together with the spectral deconvolution of the optical spectrum recorded after 20 μs after pulse irradiation into contributions from species (**1**), (**3a**,**b**), (**4**), (**5**), and (**6a**,**b**) and based on G(ions)=0.5, we conclude that the only species absorbing around 390 nm is (**6a**,**b**).

The following differences between two peptides in the transient yields are: a preference for the intramolecular sulfur-nitrogen bonded radical cations (**6a**,**b**) over the intermolecularly sulfur-sulfur three-electron bonded dimeric radical cations (**1**) and substantially higher yields of C_α-centered radicals (**4**) and glycyl radicals (**5**), as the size of the model peptide increases.

In this report, by applying complementary time-resolved conductivity and UV-VIS spectrophotometric measurements in *N*-acetylated oligopeptides containing internal methionine residue, we provide further experimental proof for the formation of the sulfur-nitrogen bonded intermediate (**6a**,**b**) (Chart 1).

This report is a part of the original paper [4] and was presented during the 9th International Symposium on Organic Free Radicals (Porto Vecchio, France).

References

[1]. Schöneich C., Pogocki D., Wiśniowski P., Hug G.L., Bobrowski K.: J. Am. Chem. Soc., 122, 10224-10225 (2000).

[2]. Bobrowski K., Pogocki D., Hug G.L., Schöneich C.: Spectral and conductometric pulse radiolysis studies of radical cations derived from *N*-acetyl-methionine amide. In: INCT Annual Report 2002. Institute of Nuclear Chemistry and Technology, Warszawa 2003, pp.23-25.

[3]. Bobrowski K., Pogocki D., Hug G.L., Schöneich C.: Spectral and conductometric pulse radiolysis studies of radical cations derived from *N*-acetyl-methionine methyl ester. In: INCT Annual Report 2003. Institute of Nuclear Chemistry and Technology, Warszawa 2004, pp.20-22.

[4]. Schöneich C., Pogocki D., Hug G.L., Bobrowski K.: J. Am. Chem. Soc., 125, 13700-13713 (2003).

BIMOLECULAR HOMOLYTIC SUBSTITUTION (S_H2) REACTION WITH HYDROGEN ATOMS. TIME-RESOLVED ELECTRON SPIN RESONANCE DETECTION IN THE PULSE RADIOLYSIS OF α-(METHYLTHIO)ACETAMIDE

Paweł Wiśniowski[1,2/], Krzysztof Bobrowski[2/], Ian Carmichael[1/], Gordon L. Hug[1/]

[1/] Radiation Laboratory, University of Notre Dame, USA

[2/] Institute of Nuclear Chemistry and Technology, Warszawa, Poland

One of the classic reaction pathways available to free radicals ($R_1^\bullet$) is bimolecular homolytic substitution (S_H2) [1]:

$$R_1^\bullet + R_2\text{-}A \rightarrow R_2^\bullet + R_1\text{-}A$$

The most common reactions of this type are the simple radical abstractions occurring at monovalent centers. However more complex S_H2 mechanisms are also seen at multivalent atoms, usually at reactions sites with the capacity of behaving hypervalently. Work on such reactions was a very active area of research [2] among a small number of investigators in the 1960's and 1970's. In addition to the main body of this work that involved organic radicals, the early studies of S_H2 reactions included chemical systems where the reacting partners were multivalent metallic centers having low-lying unfilled orbitals [3].

S_H2 reactions involving organic molecules with hypervalent atoms have also been studied extensively in the gas phase. There are examples of detailed experimental and theoretical studies [4,5] of S_H2 radical processes at multivalent sites in the gas phase. These gas-phase investigations have been prevalent in the field of mass spectroscopy [6]. On the other hand, in solution, recent work on S_H2 reactions is more limited. In particular, bimolecular homolytic substitution reactions with the simplest free radical containing a nucleus, the hydrogen atom, are almost nonexistent. For instance, in the 1988 comprehensive listing [7] of H-atom rate constants with 574 compounds, there are only five S_H2 reactions [8-10] listed that are not simple abstractions (hydrogen or halogen atoms).

Since hydrogen is the simplest radical with a nucleus, it is a useful probe for elucidating the mechanisms of solution-phase studies of S_H2 reactions at multivalent reaction centers. One convenient way to study the kinetics of hydrogen atom reactions in solution is to generate them by pulse radiolysis of aqueous solutions.

The primary radicals were produced with 0.5 μs pulses of 2.8 MeV electrons from a Van de Graaff accelerator and were detected with time-resolved electron spin resonance (TRESR) [11-13].

The TRESR spectrum following pulse radiolysis of an N_2O-aqueous solution of α-(methylthio)ace-

tamide at pH 1 is shown in Fig. The time window for the spectrum is 8.5 to 11.5 μs after the 0.5 μs electron pulse. The spectrum is strongly polarized with the low-field lines in emission and the high--field lines in enhanced absorption. The radical can be assigned by analyzing the splitting patterns. The three large groups of lines are separated by a hyperfine coupling constant of a_H=21.1 G. An analysis of the low-field lines is illustrated in Fig. with stick diagrams indicating additional hyperfine coupling constants of a_H=2.81 G, a_H=2.35 G, and a_N=1.9 G.

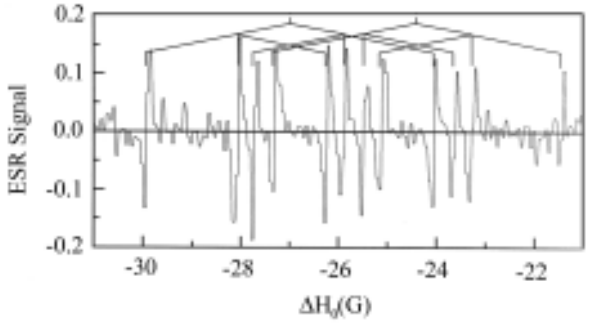

Fig. TRESR spectrum showing acetamide radicals from pulse radiolysis of 2 mM aqueous solutions of α-(methylthio)acetamide, N_2O-saturated, at pH 1.2. Time window 8.5 to 11.5 μs; dose such that primary radicals concentration ≈32 μM; origin of the abscissa corresponds to the static magnetic field, H_0, at which g=2.00043, the hydrated electron's g-factor.

A similar analysis applies to the central group of lines if the lines are considered as being doublets. The doubling of lines in the central band group, and lack of doubling of the low- and high-field groups is characteristic of second-order splitting [14] associated with 1:2:1 patterns due to two magnetically equivalent protons with a large hyperfine coupling, *i.e.* a_H=21.1 G. The center of the spectrum is at a magnetic field offset, ΔH_0, that computes into g=2.0030 [15]. (The origin of the ΔH_0 scale corresponds to g=2.00043, the center of the hydrated electron line.) The observed g-factor for the unknown transient and the hyperfine splittings have been previously reported and assigned to the acetamide radical, $^{\bullet}CH_2C(O)NH_2$ [16]. From the computation methodology described above, calculations gave g=2.00336, $a_H(CH_2)$=-21.2 G, a_N=0.9 G, and, for the two inequivalent -NH_2 protons, a_H(NH)=-1.9 G and a_H(NH)=-2.5 G. For additional confirmation of our assignment of the transient, the spectrum in Fig. was also obtained following irradiation of an N_2O-saturated aqueous solution of acetamide at pH 7 (phosphate buffer). A similar TRESR spectrum was observed following pulse radiolysis of an N_2O-saturated aqueous solution of 5 mM α-(methylthio)acetamide at pH 7 (phosphate buffer).

Acetamide radicals were identified in the pulse radiolysis of aqueous solutions of α-(methylthio)acetamide. The source of these radicals appears to be a bimolecular homolytic substitution (S_H2) of the acetamide radical fragment in α-(methylthio)acetamide by hydrogen atoms. The yields of the acetamide radical tracked the H atoms yields. Furthermore, controlled scavenging reactions, with t-BuOH and oxygen, point to H atoms as being the precursors of the acetamide radical. These same experiments eliminate $^{\bullet}$OH as being the precursor of the acetamide radical. A separate control experiment whereby sulfur-centered radical cations were formed directly, but with no observed acetamide radicals, further eliminates the possibility that the acetamide radicals are formed from sulfur-centered radical cations, whether or not the sulfur-centered radical cations come *via* $^{\bullet}$OH radicals or by other pathways.

This report is a part of original paper [17] and a part of the material presented during Trombay Symposium on Radiation and Photochemistry – TSRP-2004 (Mumbai, India, January 8-12, 2004).

References

[1]. Fossey J., Lefort D., Sorba J.: Free Radicals in Organic Chemistry. John Wiley&Sons, Chichester, New York 1995.
[2]. Ingold K.U., Roberts B.P.: Free-Radical Substitution Reactions. Wiley-Interscience, New York 1971.
[3]. Davies A.G., Roberts B.P.: Bimolecular homolytic substitution at metal centers. In: Free Radicals. Ed. J.K. Kochi. Wiley-Interscience, New York 1973, pp.547-589.
[4]. Resende S.M., De Almeida W.B.: J. Phys. Chem. A, 101, 9738-9744 (1997).
[5]. Syrstad E.A., Stephens D.D., Turecek F.: J. Phys. Chem. A, 107, 115-126 (2003).
[6]. Turecek F.: Transient intermediates of chemical reactions by neutralization-reionizatin mass spectrometry. In: Topics in Current Chemistry. Ed. C.A. Schalley. Springer, Berlin 2003.
[7]. Buxton G.V., Greenstock C.L., Helman W.P., Ross A.B.: J. Phys. Chem. Ref. Data, 17, 513-886 (1988).
[8]. Navon G., Stein G.: Isr. J. Chem., 2, 151-154 (1964).
[9]. Jayson G.G., Stirling D.A., Swallow A.J.: Int. J. Radiat. Biol. Relat. Stud. Phys. Chem. Med., 19, 143-156 (1971).
[10]. Grachev S.A., Kropachev E.V., Litvyakova G.I., Orlov S.P.: J. Gen. Chem. USSR, 46, 1813-1817 (1976).
[11]. Verma N., Fessenden R.W.: J. Chem. Phys., 65, 2139-2155 (1976).
[12]. Fessenden R.W., Hornak J.P., Venkataraman B.: J. Chem. Phys., 74, 3694-3704 (1981).
[13]. Madden K.P., McManus H.J.D., Fessenden R.W.: Rev. Sci. Instrum., 65, 49-57 (1994).
[14]. Fessenden R.W.: J. Chem. Phys., 37, 747-750 (1962).
[15]. Jeevarajan A., Fessenden R.W.: J. Phys. Chem., 93, 3511-3514 (1989).
[16]. Livingston R., Zeldes H.: J. Chem. Phys., 47, 4173-4180 (1967).
[17]. Wisniowski P., Bobrowski K., Carmichael I., Hug G.L.: J. Am. Chem. Soc., 126, 14468-14474 (2004).

PHOTOCHEMISTRY OF 4-(METHYLTHIO)PHENYLACETIC ACID. STEADY-STATE AND LASER FLASH PHOTOLYSIS STUDIES

Piotr Filipiak[1/], Gordon L. Hug[2/], Krzysztof Bobrowski, Bronisław Marciniak[1/]

[1/] Faculty of Chemistry, Adam Mickiewicz University, Poznań, Poland

[2/] Radiation Laboratory, University of Notre Dame, USA

In recent years there has been interest in the nature of photolytic C-S bond cleavage, specifically whether it leads to radical-like or ionic products [1-2]. Furthermore, the relatively low ionization potential of sulfur centers in molecules make photoionization also a potential source of sulfur-centered radicals following photoexcitation. The source of photochemically generated sulfur radicals is the subject of the current work. The molecule chosen for investigation, 4-(methylthio)phenylacetic acid (4-MTPA, H_3C-S-C_6H_4-CH_2-COOH), has a C-C bond that is photolabile and provides a standard against which to measure C-S bond cleavage. Sensitized photooxidation of variuos aromatic sulfur--containing carboxylic acids has been recently described [3].

In the present work, the mechanisms of direct photolysis of the aromatic sulfur-containing carboxylic acid, 4-MTPA, are elucidated using steady--state and laser flash photolysis. A variety of primary stable photoproducts was found under steady--state, 254 nm irradiation of acetonitrile solutions including carbon dioxide (photodecarboxylation), phenylacetic acid, dimethyl disulfide, methyl *p*-tolyl sulfide, 4-(methylthio)benzaldehyde, 4-(methylthio)benzyl alcohol, benzaldehyde, 1,2-diphenylethane. These stable photoproducts were identified and characterized using HPLC, GC, GC-MS, and UV-VIS techniques.

Following laser flash photolysis (266-nm Nd:YAG laser) a variety of transients (*e.g.*, the 4-MTPA triplet state and the sulfur-centered radical cation, H_3C-$S^{+\bullet}$-C_6H_4-CH_2-COOH) was found (Fig.). Inset (a) in Fig. shows a 390 nm kinetic trace on an expanded time scale. This kinetic trace can be fitted to an exponential decay with a rate constant of 8.6×10^5 s^{-1} or a lifetime of 1.1 μs. In the presence of oxygen, the 390 nm transient decays with a rate constant of 6.2×10^7 s^{-1} or a lifetime of 16 ns. This enhanced decay in the presence of oxygen can be explained as being due to the rapid quenching of the triplet state of 4-MTPA by oxygen. On the same time scale, the kinetic trace at 560 nm (Fig., inset (b)) shows a decay with a rate constant equal to 2.6×10^5 s^{-1} or a lifetime of 3.8 μs which is different from that recorded at 390 nm. We did not observe any faster decay at 560 nm absorption band when oxygen was present. This is consistent with the assignment of the 560 nm band being due to the sulfur-centered radical cation because such radicals normally have small rate constants for their reactions with oxygen.

A detailed mechanism of the primary and secondary processes is proposed and discussed. The photoinduced C-C bond cleavages are shown to result from an excited singlet reaction pathway, and the C-S bond cleavages follow a triplet pathway. The validity of this proposed mechanism was supported by an analysis of the quantum yields of stable products and their transient precursors. The results from excited-state quenching by oxygen are also consistent with the proposed mechanism.

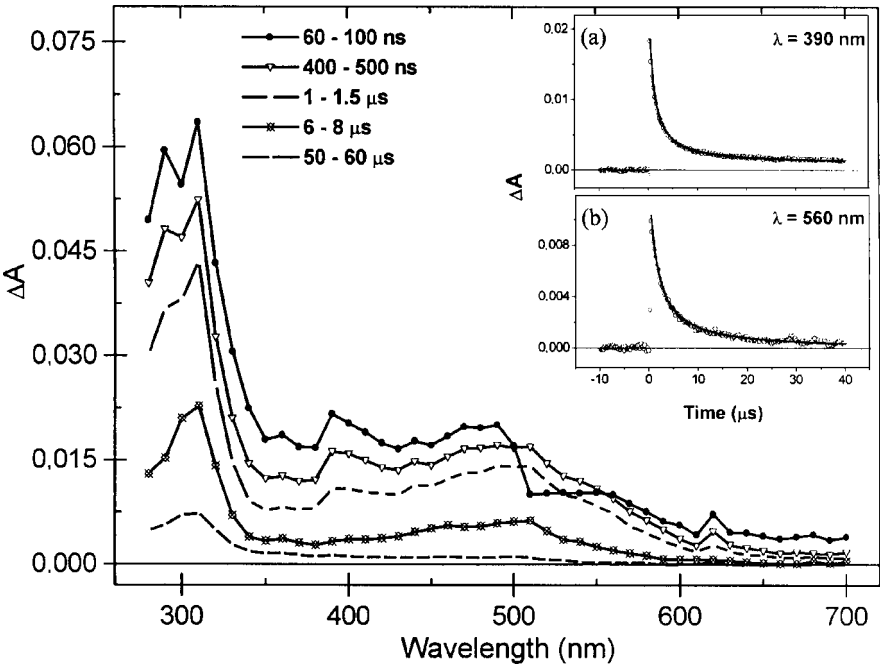

Fig. Transient absorption spectra following 266 nm laser flash photolysis of 4-MTPA in Ar-saturated acetonitrile, recorded at 5 different delays times, relative actinometry – [T]=23.4 μM. Insets show experimental trace for decays taken at 390 nm ((a) – triplet state of 4-MTPA) and 560 nm ((b) – sulfur-centered radical cation).

This report is a part of the original paper [4] and was presented during the 9th International Symposium on Organic Free Radicals (Porto Vecchio, France).

References

[1]. Vialaton D., Richard J.: J. Photochem. Photobiol. A, 136, 169-177 (2000).
[2]. Baciocchi E., Del Giacco P., Elisei F., Gerini M.F., Lapi A., Liberali P., Uzzoli B.: J. Org. Chem., 69, 8323-8330 (2004).
[3]. Filipiak P., Hug G.L., Carmichael I., Korzeniowska-Sobczuk A., Bobrowski K., Marciniak B.: J. Phys. Chem. A, 108, 6503-6512 (2004).
[4]. Filipiak P., Hug G.L., Bobrowski K., Marciniak B.: J. Photochem. Photobiol. A (2005), in print.

RADIATION-INDUCED MODIFICATION OF SHORT PEPTIDES MODELLING ENKEPHALIN FRAGMENTS

Gabriel Kciuk, Gordon L. Hug[1/], Krzysztof Bobrowski

[1/] Radiation Laboratory, University of Notre Dame, USA

Enkephalins are pentapeptides containing a tyrosine residue, two glycine residues, a phenylalanine residue, and a methionine or a leucine residue, depending on the enkephalin [1]. They are in the class of opioid peptides and play roles as neurotransmitters or neuromodulators. Moreover, they have shown immunoregulatory activity [2]. The three amino acid residues tyrosine, phenylalanine, and methionine are especially susceptible to oxidation in these peptides. Such reaction pathways are relevant to biological systems exposed to conditions of oxidative stress [3,4].

The pulse radiolysis results of enkephalins presented in our previous report are complex [5]. In order to determine the exact nature of the transient species involved in the processes following the pulse radiolysis of these pentapeptides, we oxidized model compounds having fragments that mimic different structural features of the enkephalins. Our recent studies have also focused on the interaction of the generated transients with protons.

Hydroxyl radicals (•OH), produced in the radiolysis of water, were used as one electron oxidants. The resulting transient species were examined by pulse radiolysis with optical detection. In the case of tyrosine, the hydroxyl radical reacts mainly by addition to the aromatic ring, creating the dihydroxycyclohexadienyl radical. This radical can undergo dehydration and form a tyrosyl radical, but other reaction pathways (*i.e.* disproportionation) are also possible. However, of these reactions, only dehydration can be catalyzed by protons. In our research we have concentrated on the yield and the rate of build-up of tyrosyl radicals as a function of:

- adjacent amino acid residues and/or functional groups (*i.e.* carboxyl or amino group),
- concentration of protons,
- position of selected residue in the peptide chain (*e.g.* tyrosine in N-terminal position, in C-terminal position, or in the middle of chain).

In the case of peptides containing tyrosine and methionine, the tyrosyl radical is generated in two steps, and protons accelerate only one of these steps. The first step (the faster one) is the result of an electron transfer between the radical centered on the methionine residue and tyrosine residue itself. The second step (the slower one, which is accelerated by protons) shows a pH dependence. In the peptides Tyr-Met and Met-Tyr, the specific sequence of these two residues has a distinct influence on the oxidative pathway of the dipeptides. This sequence dependence can be clearly seen in the transient spectra following pulse irradiation of these two dipeptides (Fig.1). Probably in the Met-Tyr case, radicals centered on the methionine are stabilized by three electron bonds S∴N. However, this issue needs further examination due to the overlapping of the absorption of the tyrosyl radicals with the absorption of the three electron bonded

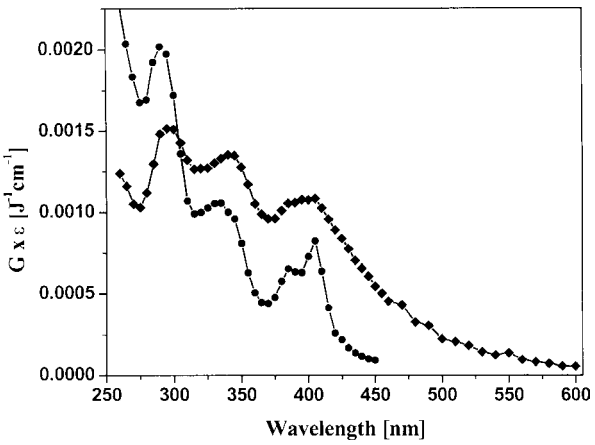

Fig.1. Transient spectra recorded 3 μs after pulse irradiation of an N_2O saturated aqueous solution containing: (◆) 0.2 mM Met-Tyr, pH 6.6; (●) 0.2 mM Tyr-Met, pH 6.1.

S∴N species. In the other peptides examined (tyrosine with others amino acid residues), no electron transfer was observed.

The rate of the dehydration reaction of the dihydroxycyclohexadienyl radical (catalyzed by protons) depends on the position of the tyrosine residue in the peptide chain. Generally, when the tyrosine residue is C-terminal, the rate of dehydration is faster than for tyrosine alone. When tyrosine is the N-terminal residue, the opposite effect can be observed. These observations can be clearly seen in the peptides Tyr-Gly and Gly-Tyr (Fig.2). The rate of tyrosyl radical formation are $k=1.8\times10^7$ dm^3 mol^{-1} s^{-1} and $k=9.4\times10^7$ dm^3 mol^{-1} s^{-1}, respectively and for tyrosine alone $k=2.9\times10^7$ dm^3 mol^{-1} s^{-1}. The hypothesis that the transient products in the reaction

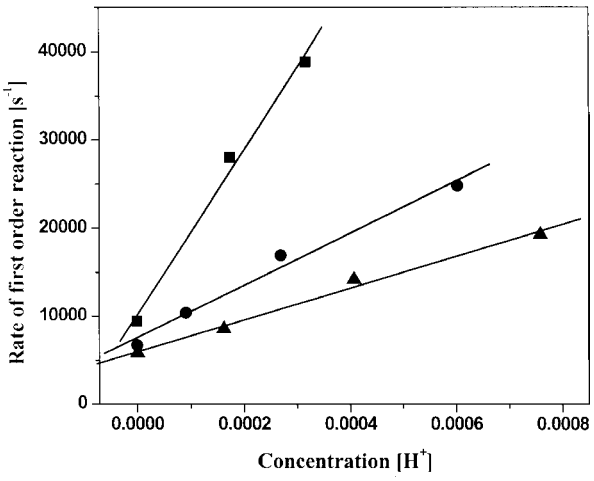

Fig.2. First order rate of tyrosyl radical formation *vs*. proton concentration for the following compounds: (■) Gly-Tyr peptide, (●) Tyr, (▲) Tyr-Gly peptide.

pathway between the dihydroxycyclohexadienyl radical and tyrosyl radical, called radical cation, is stabilized by the peptide bond or negative charge on the carboxyl group, is not confirmed by our pulse radiolysis studies with optical detection. The situation is complicated since the shape of absorption of the radical cation might be identical with the shape of tyrosyl radical [6]. This hypothesis can be confirmed most easily by the computational chemistry. Tentative computational surveys confirm this hypothesis.

In contrast, radicals centered on the aromatic ring of the phenylalanine residues are pH independent.

The following conclusions can be drawn:

- We cannot easily extrapolate the chemistry of isolated amino acids to the reactivity of their residues, even for short peptides containing highly-reactive and slowly-reactive amino acid residues like tyrosine and glycine, respectively.
- Peptide bonds and neighboring amino acid residues have some effect on the aromatic ring in the tyrosine residue.
- When the tyrosine is a C-terminal residue, the rate of reaction of dehydration is faster than when the tyrosine is N-terminal.

This work was partly supported by the International Atomic Energy Agency (IAEA Fellowship POL/00107 for Gabriel Kciuk) and by Research Training Network SULFRAD (HPRN-CT-2002184).

References

[1]. Goldstein A.: Science, 193, 1081-1086 (1976).
[2]. Smith E.M., Harbour-McMenamin D., Blalock J.E.: J. Immunol., 135, 779s-782s (1985).
[3]. Davies M.J., Dean R.T.: Radical-mediated protein oxidation. From Chemistry to Medicine. Oxford University Press, Oxford 1997.
[4]. Stadtman E.: Free Radicals, Oxidative Stress, and Antioxidants. Ed. T. Özben. Plenum Press, New York 1998, pp.131-143.
[5]. Kciuk G., Mirkowski J., Bobrowski K.: Short-lived oxidation products derived from enkephalins. In: INCT Annual Report 2001. Institute of Nuclear Chemistry and Technology, Warszawa 2002, pp.23-24.
[6]. Tripathi G.N.R., Yali Su: J. Phys. Chem. A, 108, 3478-3484 (2004).

ELECTRON PARAMAGNETIC RESONANCE STUDY OF RADIATION-INDUCED RADICALS IN 1,3,5-TRITHIANE AND ITS DERIVATIVES

Grażyna Strzelczak, Aneta Janeba[1/], Bronisław Marciniak[1/]

[1/] Faculty of Chemistry, Adam Mickiewicz University, Poznań, Poland

It is known that trithiane compounds (containing sulfur atoms) are involved in radiation-induced polymerization in the solid state. Sulfide groups increase the refractive index of the polymer due to the high polarizability of the sulfur atom, and in the polymerization product can improve its hydrophobic properties. Sulfides can also act as oxidizable compounds for the reduction of oxygen inhibition [1].

Radicals formed in gamma-irradiated 1,3,5-trithiane (TT) and its derivatives at room temperature have been studied by electron paramagnetic resonance (EPR) spectroscopy by Andrzejewska *et al*. [2].

In this paper we report results of EPR studies of radicals formed at low temperatures (77 to 293 K) in various trithiane compounds.

1,3,5-Trithiane, α-2,4,6-trimethyl-1,3,5-trithiane (α-TMT), β-2,4,6-trimethyl-1,3,5-trithiane (β-TMT), and 2,4,6-trimethyl-2,4,6-triphenyl-1,3,5-trithiane (MTFT) were prepared according to the methods described in the literature [3].

The samples were irradiated with a dose of about 4 kGy in a ^{60}Co source (Mineyola; at the Institute of Nuclear Chemistry and Technology) in liquid nitrogen. The EPR measurements were performed using a Bruker-EPS 300 spectrometer operating in the X-band (9.5 GHz) equipped with a cryostat and a variable temperature unit over the temperature range of 77-293 K.

Measurement parameters were following: microwave frequency – 100 kHz, microwave power – 1 mW, modulation amplitude – 0.2 mT.

The main component of the EPR spectrum recorded at 77 K for TT, α-TMT, β-TMT, and TMTFT was an anisotropic singlet with $g_{||}=2.011$, $g_{\perp}=2.005$ attributed to the monomeric sulfur radical cation $>S^{+\bullet}<$ (Fig.1). Similar spectral features were observed previously [4]. Warming the samples of α-TMT to 150 K resulted in the appearance of a four-line component with g=2.004 and a=1.7 mT attributed to the carbon-centered radical ($-C^{\bullet}-CH_3$) that might result from deprotonation of the mo-

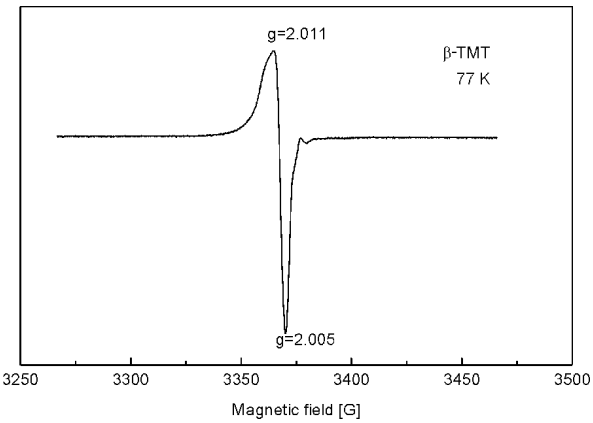

Fig.1. EPR spectrum of gamma-irradiated at 77 K β-TMT recorded at 77 K, assigned to the monomeric sulfur radical cation (-$S^{+\bullet}$-).

nomeric sulfur radical cation (Chart 1). At the same temperature, the EPR spectrum indicated in β-TMT the presence of a four-line component with g=2.004 and a=1.7 mT assigned to the carbon-centered radical (-C$^{\bullet}$-CH_3), and in the samples of TT, EPR spec-

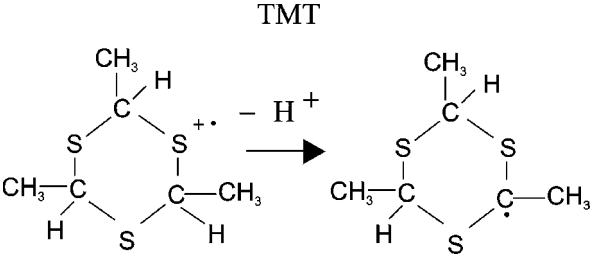

Chart 1.

trum indicated a dublet component with g=2.004 and a=1.7 mT assigned to the carbon-centered radical (-$^{\bullet}$CH). These radicals might result from deprotonation of the respective monomeric sulfur radical cations. The spectra are very unstable compared to the EPR spectrum obtained for the sample of α-TMT (Fig.2).

At room temperature, EPR spectra indicated a new broad anisotropic singlet with $g_{||}$=2.052 and $g_{\perp}$=2.000 for the samples of TT, α-TMT and β-TMT. The anisotropic singlet can be attributed to the sulfur-centered radical type RS$^{\bullet}$ resulted from the fragmentation of the respective molecules. Similar spectral features were observed previously for the aliphatic sulfur-centered radicals [5]. For the samples of α-TMT, a four-line component is stable at room temperature. For the TT and β-TMT samples, carbon-centered radicals disappeared, and EPR spectra consisted only of an anisotropic singlet which can be assigned to the sulfur-centered radicals obtained after the fragmentation of the molecules.

In the samples of TMTFT, EPR spectrum recorded at 77 K consists of an asymmetric singlet assigned to the monomeric sulfur radical cation >$S^{+\bullet}$< which is very long lived up to 180 K. Warming the sample to 250 K resulted in the appearance of a triplet with g=2.0045 and a=1.85 mT (due to interaction with two protons). The triplet can be assigned to the carbon-centered radicals obtained after H abstraction from the methyl group. This radical disappears at room tempera-

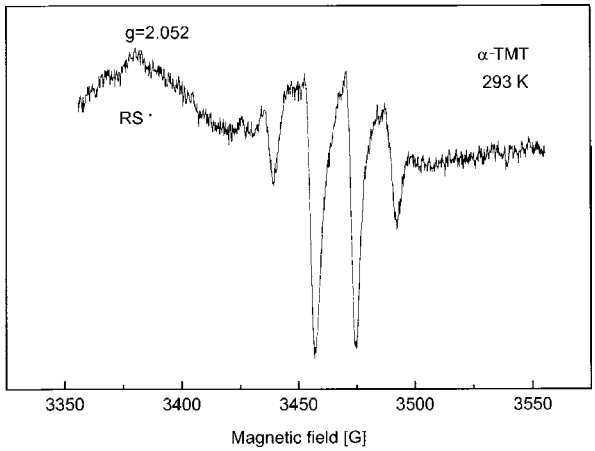

Fig.2. EPR spectra of gamma-irradiated at 77 K α-TMT recorded at 293 K, consist of: anisotropic singlet of RS$^{\bullet}$ type radicals and four-line component of (-$^{\bullet}$C-CH_3) radicals.

ture and a new EPR signal is seen (a broad singlet with g=2.0085 and ΔH=1.5 mT). This spectrum can be assigned to the radical with a spin localization on the sulfur atom in the ring. In the case of TMTFT samples (which contain the phenyl group) we have not observed RS$^{\bullet}$ type radicals. This might suggest that the phenyl group in the molecule is a protective agent.

In the present work, radical cations and radicals formed in trithiane compounds (containing sulfur atoms) were produced by gamma irradiation at 77 K. The sulfur monomeric radical cations (>$S^{+\bullet}$<) were formed as a result of direct ionization of the sulfur atom in the parent molecule. The sulfur monomeric radical cations decay by two competitive pathways:

- deprotonation from the Cα adjacent to the sulfur (producing carbon-centered radicals),
- fragmentation *via* the cleavage of the C-S bond, producing RS$^{\bullet}$ type radicals.

Radical formation and stabilization depends on the isomeric form of investigated TMT compounds (α or β).

The presence of the phenyl group in the molecule has a protective effect on the stabilization of trithiane compounds.

References

[1]. Andrzejewska E.: Polymer, 34, 3899 (1993).
[2]. Andrzejewska E., Żuk A., Krzyminiewski R., Pietrzak J.: J. Polym. Sci., A 25, 3363 (1987).
[3]. El-Hewehi Z., Hempel D.: J. Prakt. Chem., 21 (1963).
[4]. Strzelczak G., Bobrowski K., Kozubek H., Michalik J.: Nukleonika, 45, 93 (2000).
[5]. Chatgilialoglu C., Bertrand M.P., Ferreri C.: Sulfur-centered radicals in organic synthesis. In: S-centered radicals. Ed. Z.B. Alfassi. John Wiley & Sons Ltd., Chichester 1999, p.311.

PULSE RADIOLYSIS STUDY OF THE RADICAL REACTIONS IN IONIC LIQUIDS. INTERMEDIATE SPECTRA IN THE SYSTEM $Br_2^{\bullet-}/Br^-/SCN^-$ IN THE IONIC LIQUID METHYLTRIBUTYLAMMONIUM BIS[(TRIFLUOROMETHYL)SULFONYL]IMIDE

Jan Grodkowski, Małgorzata Nyga, Jacek Mirkowski

Room temperature ionic liquids [1-3] are non-volatile and non-flammable and serve as good solvents for various reactions and have been proposed as solvents for green processing [3]. To understand the effect of these solvent on the chemical reactions, the rate constants of several elementary reactions in ionic liquids have been studied by the pulse radiolysis technique [4-8].

Fast kinetic measurements were carried out by pulse radiolysis using 10 ns, 10 MeV electron pulses from a LAE 10 linear electron accelerator [9] delivering the dose up to 20 Gy per pulse. The details of a computer controlled measuring system were described before [10]. 8 MB maximum memory for data recording covers a time range from single nanoseconds to milliseconds, depending on the oscilloscope settings, after every single electron pulse. Useful spectral range for the experiments with methyltributylammonium bis[(trifluoromethyl)sulfonyl]imide (R_4NNTf_2) was from ~350 to ~800 nm.

In this study of the reactions of $Br_2^{\bullet-}$, anion radicals with thiocyanate anions in the ionic liquid R_4NNTf_2 have been examined. $Br_2^{\bullet-}$ in the R_4NNTf_2 ionic liquid has been produced as before [9] *via* the reaction of solvated electrons with 1,2-dibromoethane (DBE):

$$e^-_{sol} + BrCH_2CH_2Br \rightarrow Br^- + {}^{\bullet}CH_2CH_2Br \quad (1)$$

$$^{\bullet}CH_2CH_2Br \rightarrow CH_2{=}CH_2 + Br^{\bullet} \quad (2)$$

$$Br^{\bullet} + Br^- \leftrightarrows Br_2^{\bullet-} \quad (3)$$

The spectra following pulse irradiation of solution 0.013 mol L^{-1} DBE in R_4NNTf_2 recorded at 80, 300 and 4000 ns after the pulse are presented in Fig.1. The data at 80 ns after the pulse correspond to the solvated electron. The spectrum – 4000 ns after the pulse is ascribed to $Br_2^{\bullet-}$ anion radical. Its yield is equal to the reported value of the yield of the solvated electrons in R_4NNTf_2 $G=0.7$ mol J^{-1} [7]. However, for higher concentrations of DBE, the yield of $Br_2^{\bullet-}$ is increased due to scavenging of dry electrons. The second order decay rate constant of the reaction (1) was calculated to be $k_1=(1\text{-}2)\times10^8$ L mol^{-1} s^{-1}.

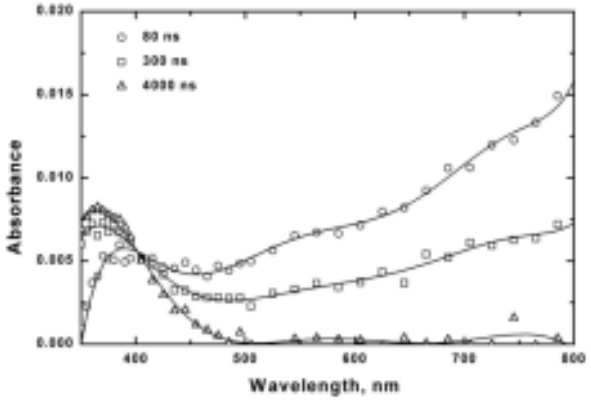

Fig.1. Transient optical spectra monitored by pulse radiolysis of deoxygenated R_4NNTf_2 containing 0.013 mol L^{-1} DBE. The spectra were taken 80 ns (○), 300 ns (□), and 4000 ns (△) after the pulse. Dose was 11 Gy.

After addition of SCN^- ions in the pulse irradiated solution, several reactions initiated by $Br_2^{\bullet-}$ anion radicals have been considered:

$$Br_2^{\bullet-} + SCN^- \rightarrow 2Br^- + SCN^{\bullet} \quad (4)$$

$$Br_2^{\bullet-} + SCN^- \rightarrow BrSCN^{\bullet-} + Br^- \quad (5)$$

$$SCN^{\bullet} + Br^- \leftrightarrows BrSCN^{\bullet-} \quad (6)$$

$$Br^{\bullet} + SCN^- \leftrightarrows BrSCN^{\bullet-} \quad (7)$$

$$SCN^{\bullet} + SCN^- \leftrightarrows (SCN)_2^{\bullet-} \quad (8)$$

$$BrSCN^{\bullet-} + SCN^- \leftrightarrows (SCN)_2^{\bullet-} + Br^- \quad (9)$$

From the intermediates listed above, $Br_2^{\bullet-}$, $BrSCN^{\bullet-}$ and $(SCN)_2^{\bullet-}$ are observed in R_4NNTf_2. Their contribution to the overall kinetics and the resulting spectra depends on the relative concentrations of Br^- and SCN^- ions. Their contribution to the overall kinetics and the resulting spectra is dependent on the relative concentrations of Br^- and SCN^- ions (Figs.2 and 3).

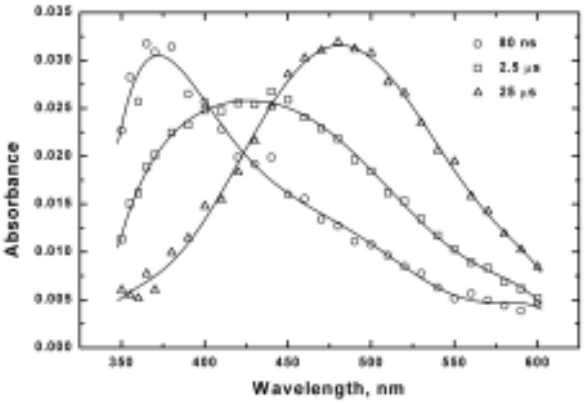

Fig.2. Transient optical spectra monitored by pulse radiolysis of deoxygenated R_4NNTf_2 containing 0.19 mol L^{-1} DBE and 0.04 mol L^{-1} SCN^-. The spectra were taken 80 ns (○), 2.5 µs (□), and 25 µs (△) after the pulse. Dose was 18.5 Gy.

In the case when there is no Br^- added (Fig.2), spectra recorded at 80 ns, 2.5 µs and 25 µs after the pulse, only the last one corresponds to a single intermediate, namely $(SCN)_2^{\bullet-}$. The others are a mixture of all the three components: $Br_2^{\bullet-}$, $BrSCN^{\bullet-}$ and $(SCN)_2^{\bullet-}$ with their relative proportions changing with progressing $Br_2^{\bullet-}$ transformation into $(SCN)_2^{\bullet-}$.

Pulse radiolysis of the solution containing 0.18 mol L^{-1} DBE, 0.006 mol L^{-1} SCN^- and additional 0.09 mol L^{-1} Br^- in R_4NNTf_2 produces significantly different spectra. In the case presented in Fig.3 the participation of $(SCN)_2^{\bullet-}$ in the resulted spectra is negligible. This is probably the first direct observation of the spectrum of $BrSCN^{\bullet-}$ anion radical; previous spectra were extracted from the composite results [11].

The rates of the $Br_2^{\bullet-}$ anion radicals with thiocyanate are of the same order of magnitude as observed before for the reaction with chlorpromazine

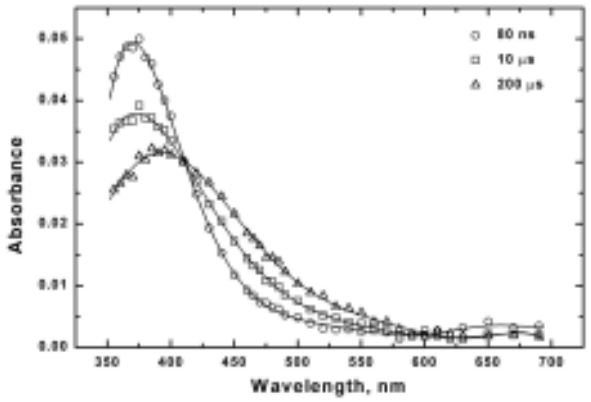

Fig.3. Transient optical spectra monitored by pulse radiolysis of deoxygenated R_4NNTf_2 containing 0.19 mol L^{-1} DBE, 0.006 mol L^{-1} SCN^- and 0.09 mol L^{-1} Br^-. The spectra were taken 80 ns (○), 10 μs (□), and 200 μs (△) after the pulse. Dose was 16.5 Gy.

in R_4NNTf_2 [6]. It was suggested that the energy of solvations is the main factor which affects the driving force of $Br_2^{\bullet-}$ reactions. In the present report, only the intermediates involved are discussed. The more complete description including evaluation of the particular reactions rates and equilibria, will be done after completion of the experiments with a wider range of concentration of concerned species.

References

[1]. Welton T.: Chem. Rev., 99, 8, 2071-2083 (1999).
[2]. Wasserscheid P., Keim W.: Angew. Chem. Int. Ed., 39, 21, 3772-3789 (2000).
[3]. Ionic liquids: Industrial application to green chemistry. Eds. R.D. Rogers, K.R. Seddon. 2002, ACS Symp. Ser. No. 818.
[4]. Grodkowski J., Neta P.: J. Phys. Chem. A, 106, 22, 5468-5473 (2002).
[5]. Grodkowski J., Neta P.: J. Phys. Chem. A, 106, 39, 9030-9035 (2002).
[6]. Grodkowski J., Neta P.: J. Phys. Chem. A, 106, 46, 11130-11134 (2002).
[7]. Wishart J.F., Neta P.: J. Phys. Chem. B, 107, 30, 7261-7267 (2003).
[8]. Grodkowski J., Neta P., Wishart J.F.: J. Phys. Chem. A, 107, 46, 9794-9799 (2003).
[9]. Zimek Z., Dźwigalski Z.: Postępy Techniki Jądrowej, 42, 9-17 (1999), in Polish.
[10]. Grodkowski J., Mirkowski J., Płusa M., Getoff N., Popov P.: Rad. Phys. Chem., 69, 379-386 (2004).
[11]. Schöneshöfer M., Henglein A.: Ber. Bunsen-Ges. Phys. Chem., 73, 3, 289-293 (1969).

SINGLET OXYGEN-INDUCED DECARBOXYLATION OF CARBOXYL SUBSTITUTED THIOETHERS

Monika Celuch, Dariusz Pogocki

Singlet oxygen ($^1O_2$) could be generated in biological systems by a range of endogenous and exogenous processes (*e.g.* enzymatic and chemical reactions, UV or visible light in the presence of a sensitizer) [1]. Numerous data show that proteins are major targets for $^1O_2$, with damage occurring preferentially at aromatic and sulfur-containing amino acid residues (Trp, His, Tyr and Cys and Met) [1]. Reaction with each of these residues gives rise to further reactive species.

For example, reaction of $^1O_2$ with thioether sulfur of methionine (Met) leads to the formation of peroxysulfoxide – reaction (1) [2,3]:

$$^1O_2 + >S \rightarrow >S^{(+)}O\text{-}O^{(-)} \qquad (1)$$

which is in equilibrium with superoxide radical-anion ($O_2^{\bullet-}$) and respective sulfur-centered radical-cation – reaction (2):

$$>S^{(+)}O\text{-}O^{(-)} = >S^{\bullet+} + O_2^{\bullet-} \qquad (2)$$

Peroxysulfoxide may react with the second molecule of thioether leading to the formation of two molecules of respective sulfoxide – reaction (3) [2,3]:

$$>S^{(+)}O\text{-}O^{(-)} + >S \rightarrow 2\ >S{=}O \qquad (3)$$

Reaction (3), then occurring intramolecularly in the peptides containing two or more Met residues, has the potential to be a convenient way to evaluate the flexibility of the polypeptide backbone. Since, double methionine sulfoxide (2MetS=O) arises in the process that requires direct contact of two backbone-separated side chains of Met [4,5]. Therefore, chromatographic quantification of 2MetS=O produced in the $^1O_2$-induced oxidation "coupled" with molecular modeling techniques may help to understand the structure dependent mechanism of free radicals related cytotoxicity of some proteins [6]. Among them are such "prominent" proteins as the human prion protein that contains nine Met residues [7].

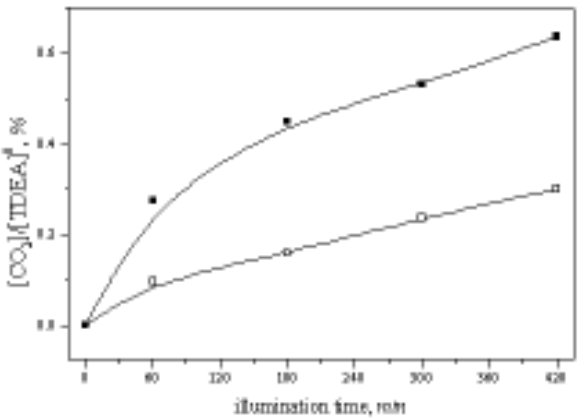

Fig.1. Efficiency of $^1O_2$-induced CO_2 formation normalized to the initial concentration of thioether *vs*. time of illumination in solutions containing 50 mM TDEA, 22 μM RB, (■) 1.045 or (□) 0.219 mM O_2 at pH 6.

However, for quantitative use of reaction (3) in the field of peptide dynamics study, the deeper knowledge on the competitive processes is required. Therefore, we are involved in the research

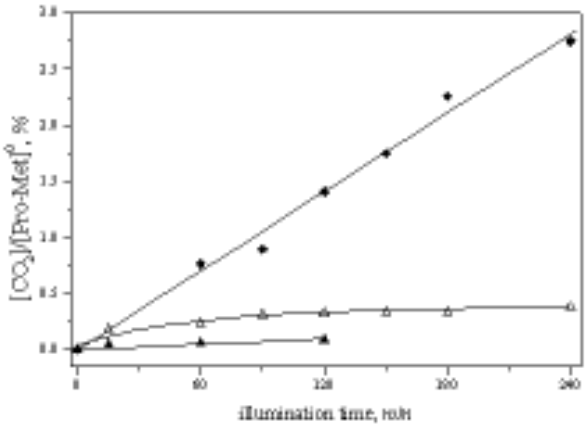

Fig.2. Efficiency of $^1O_2$-induced CO_2 formation normalized to the initial concentration of thioether *vs*. time of illumination in air saturated solutions (0.219 mM O_2) containing 22 μM RB and (◆) 1, (△) 3 or (▲) 10 mM of Pro-Met at pH 6.

aimed at characterization of some irreversible processes, which may accompany the $^1O_2$-induced oxidation of thioether group in peptides, such as dethioethers, illuminated by visible light in the presence of rose bengal (RB) as a photosensibilizer [8]. Formation of CO_2 has been monitored by means of head-space gas chromatography.

For both investigated compounds, the $^1O_2$-induced oxidation leads to the release of CO_2. Observed decarboxylation occurs most probably due to the intramolecular electron transfer from deprotonated carboxylic functionality to sulfur-centered radical-cation [9]. The yield of decarboxylation obviously depends on the concentration of oxygen in solution – crucial for the initial yield of $^1O_2$ (see an example in Fig.1). Since the dissociation of peroxysulfoxide to superoxide radical-anion and sulfur-centered radical-cation (being the precursor of decarboxylation [9]), reaction (2), compete with intermolecular reaction (3), therefore increase of the thioethers concentration leads to decrease of decarboxylation yield (see an example in Fig.2). The idea that sulfur-centered radical-cation is indeed the precursor of decarboxylation has an additional support in the pH dependence of the efficiency of CO_2 release (Fig.3). It suggests that the formation

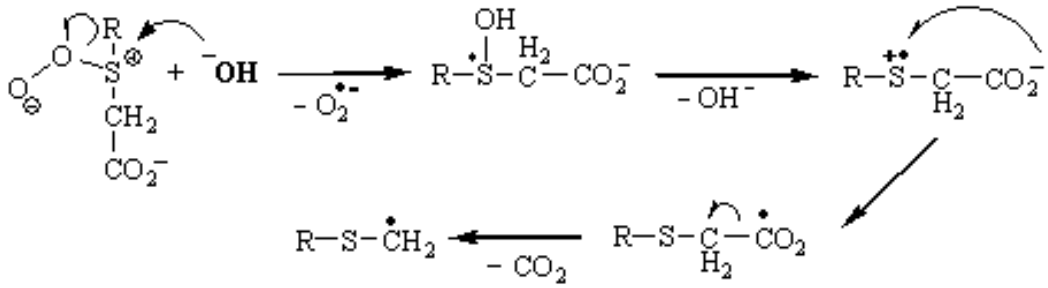

Scheme 1.

protonation and decarboxylation of sulfur-centered radical-cation of C-terminal Met residues.

Two model thioethers have been chosen for our investigation: thiodiethanoic acid (easy available carboxylic derivative of dimethylsulfide) and Pro-Met (dipeptide being a simple model of C-terminal part of Met-$(Pro)_n$-Met oligopeptide investigated in [4]). Singlet oxygen has been produced in aqueous, oxygen (or air) saturated solutions of

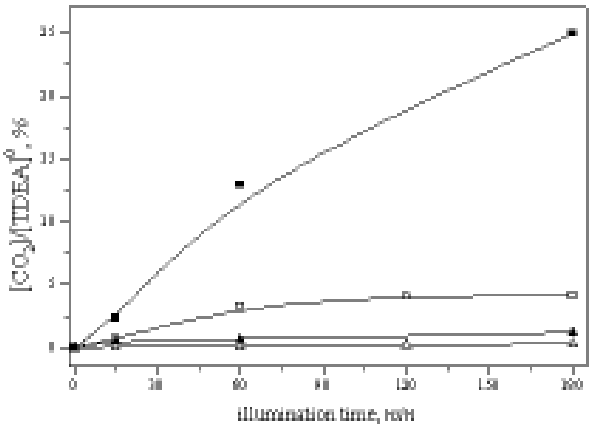

Fig.3. Efficiency of $^1O_2$-induced CO_2 formation normalized to the initial concentration of thioether *vs*. time of illumination in air saturated solutions (0.219 mM O_2) of TDEA containing 22 μM RB and: 30 mM TDEA pH 9 (■) and 30 mM TDEA pH 6 (□); 3 mM TDEA pH 9 (▲) and 3 mM TDEA pH 6 (△).

of CO_2 may by catalyzed by the presence of Levis bases. At first sight, it seems that this reaction (drafted for 2,2'-thiodiacetic acid – TDEA in Scheme 1) can be described by nuclephilic substitution at the thioether sulfur, in which week nuclephile $O_2^{\bullet-}$ ($pK_A(HO_2^{\bullet}/O_2^{\bullet-})\approx4.8$ [10]) by much stronger nuclephile OH^-. The reaction may occur in the

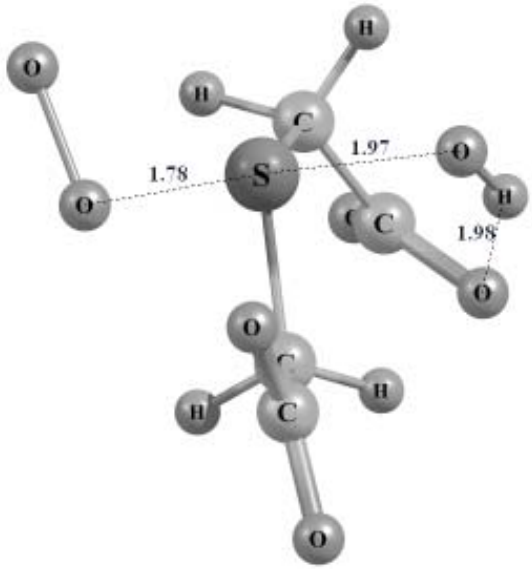

Fig.4. The B3LYP/6-31G(d)/IEFPCM calculated geometry of the nuclephilic substitution transient product for TDEA (distances are shown in [Å]).

way analogous to S_N2 mechanism usually occurring at sp^3 hybridized carbon [11]. However, our recent DFT (density functional theory) calculations [12] failed in prediction of a transient state, instead they predict formation of the tetravalent transient product (Fig.4) that seems stable in vacuum an solvent cage as well. This makes the case slightly more complicated, therefore further clarification of the mechanism requires additional experimental and computational effort.

The work was sponsored by the State Committee for Scientific Research (KBN) – grant No. 3 T09A 066 26.

References

[1]. Davies M.J.: Photochem. Photobiol. Sci., 3, 17-26 (2003).
[2]. Clennan E.L.: Acc. Chem. Res., 34, 875-884 (2001).
[3]. Jensen F., Greer A., Clennan E.L.: J. Am. Chem. Soc., 120, 4439-4449 (1998).
[4]. Pogocki D., Ghezzo-Schöneich E., Celuch M., Schöneich C.: Singlet oxygen induced oxidation as a benchmark of the conformational flexibility of Met-$(X)_n$-Met peptides. In: Europhysics conference abstracts. Vol. 28A. European Physical Society, 2004, p.77.
[5]. Pogocki D.: Wewnątrzcząsteczkowe przemiany rodnikowe z udziałem utlenionego centrum siarkowego w modelowych związkach tioeterowych o znaczeniu biologicznym. Instytut Chemii i Techniki Jądrowej, Warszawa 2004, 87p. Raporty IChTJ. Seria A No. 2/2004, in Polish.
[6]. Pogocki D.: Acta Neurobiol. Exp., 63, 131-145 (2003).
[7]. Zahn R. *et al.*: Proc. Natl. Acad. Sci. USA, 97, 145-150 (2000).
[8]. Nowakowska N., Kępczyński M., Dąbrowska M.: Macromol. Chem. Phys., 201, 1679-1688 (2001).
[9]. Bobrowski K., Pogocki D., Schöneich C.: J. Phys. Chem., 97, 13677-13684 (1993).
[10]. Bartosz G.: Druga twarz tlenu. Wolne rodniki w przyrodzie. Wydawnictwo Naukowe PWN, Warszawa 2003, pp.1-447, in Polish.
[11]. Smith M.B., March J.: March's advanced organic chemistry reactions, mechanisms, and structure. John Wiley, New York 2001.
[12]. Frisch M.J. *et al.*: Gaussian 03. (Rev. B.03). Gaussian Inc., Pittsburgh, PA 2003.

ELECTRON PARAMAGNETIC RESONANCE STUDY OF ETHYL RADICALS TRAPPED IN SYNTHETIC H-rho ZEOLITE

Marek Danilczuk, Hirohisa Yamada[1/], Jacek Michalik

[1/] National Institute of Material Science, Tsukuba, Japan

Depending on the adsorption pressure, two types of ethyl radicals were observed in γ-irradiated H-rho zeolite exposed to C_2H_4. The first type of ethyl radical has shown hyperfine couplings with α and β protons very similar to those observed for ethyl radicals in liquid hydrocarbons at low temperature. The hyperfine coupling with α-protons (A_α=1.47 mT, A_β=2.7 mT, g_{iso}=2.0029) of second ethyl radical is significantly reduced suggesting a strong interaction of ethyl radical with zeolite through the methylene group.

The primary radiolytic processes of small organic molecules have been one of the most fundamental subjects in radiation chemistry. A number of EPR (electron paramagnetic resonance) and optical absorption studies have been reported for organic radicals stabilized in different halocarbon matrices at low temperature. Also inert gas matrices have been utilized for that purpose very successfully. Synthetic zeolites because of the crystalline lattice structure, variable pore size and ion exchange properties, are unique to study the chemistry of reactive intermediates in heterogeneous systems. The EPR technique and related methods like ENDOR (electron nuclear double resonance) as well as NMR (nuclear magnetic resonance) spectroscopy are among the most appropriate methods for the investigation of molecules or radicals trapped in different zeolites [1,2].

The EPR spectra of ethyl radicals generated in liquid or solid phase or trapped on solid surfaces at low temperature are well known. In liquids, ethyl radicals have been characterized by isotropic hyperfine parameters. In contrast, radicals adsorbed on a surface have an asymmetric line profiles typical for axially symmetric spin Hamiltonian parameters [3,4].

The NaCs-rho zeolite synthesized by the modified Robson's method in cationic form was exchanged three times with 20% solution of NH_4NO_3 followed by calcination at 573 K in air for 20 h to prepare the protonic form of zeolite [5].

The samples of H-rho zeolite were placed into Suprasil EPR tubes and dehydrated *in vacuo*, whilst gradually raising temperature to 473 K. Then oxidation with static O_2 at 573 K was carried out for 2 h. The oxygen was pumped off at the same temperature for the next 2 h. The adsorption of ethylene was carried out at room temperature at a pressure of 0.4 and 8 kPa for 24 h and then the zeolite samples were irradiated in a ^{60}Co source at the liquid nitrogen temperature (77 K) with a dose of 5 kGy. The EPR measurements were carried out with an X-band Bruker ESP-300E spectrometer equipped with a Bruker ER 4111 VT variable temperature unit operating in the temperature range 110-370 K. The g-value was determined using a DPPH specimen for field calibration.

The EPR spectrum of γ-irradiated H-rho/C_2H_4 zeolite exposed to 0.4 kPa of ethylene at room temperature and recorded at 110 K consists of two sets of lines: **A** – relatively intensive multiplet (A_α=2.7 mT, A_β=2.15 mT, g_{iso}=2.0028) of ethyl radicals and triplet **B** – representing $^{\bullet}CH_2$ radicals (A_{iso}=2.0 mT, g_{iso}=2.0027) (Fig.1). The hyperfine coupling constants are independent of temperature and are very similar to hyperfine constants of ethyl radicals in other matrices – in frozen hydrocarbons or at the

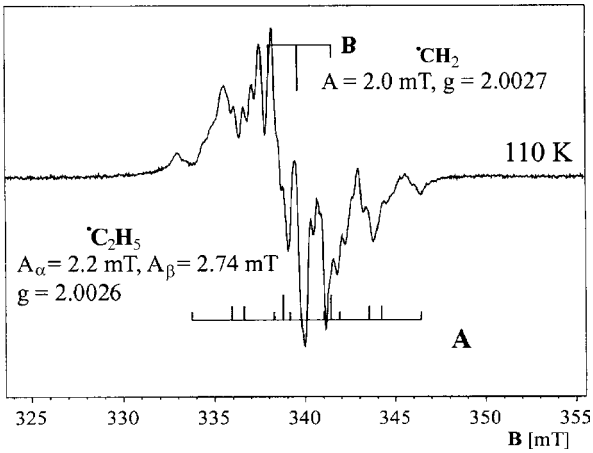

Fig.1. The EPR spectrum of γ-irradiated H-rho zeolite exposed to 0.4 kPa of C_2H_4 recorded at 110 K.

surface of silica gel at low temperature. The EPR spectrum of the ethyl radicals was observed in the temperature range 110 to 250 K. Isotropic hyperfine parameters and high thermal stability suggest that ethyl radicals are trapped in the middle of α-cages and do not interact with surface of zeolite. The observed line broadening of $^{\bullet}C_2H_5$ lines can originate from hindered rotation of the CH_3 group at lower temperatures. It is worthy of mention that we did not observed the EPR spectrum of vinyl radicals although the radiolysis of liquid ethylene leads to the formation of that radical product.

The EPR spectrum of H-rho zeolite with ethylene adsorbed under a pressure of 8 kPa and recorded at 230 K is shown in Fig.2a. Spectrum of

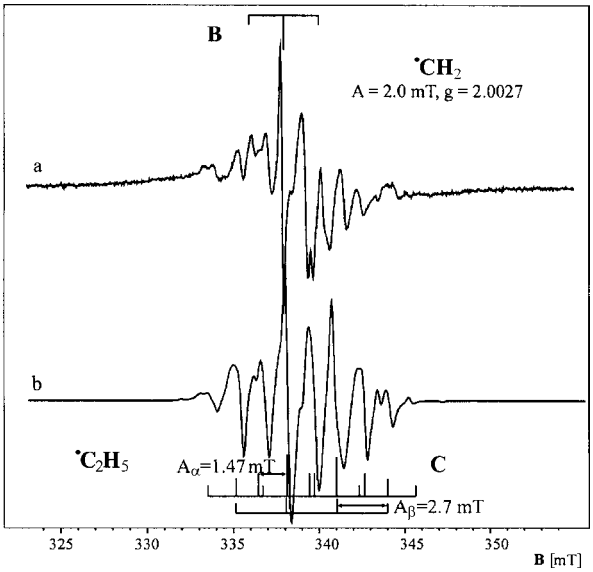

Fig.2. The experimental (a) and simulated (b) EPR spectra of γ-irradiated H-rho zeolite with ethylene adsorbed under a pressure of 8 kPa.

this radical is observed in the temperature range 150-310 K and is completely different from the spectrum of ethyl radicals presented in Fig.1. It consists of two overlapping EPR spectra of two different radicals: **B** – triplet of $^{\bullet}CH_2$ radical with EPR parameters (A_{iso}=2.0 mT, g_{iso}=2.0027) similar to those in rho zeolite exposed to 0.4 kPa of C_2H_4 and **C** – multiplet with anisotropic spin Hamiltonian parameters (A_{α}=1.47 mT, A_{β}=2.7 mT, $g_{\perp}$=2.0026, $g_{||}$=2.0029) similar to the spectrum of ethyl radicals adsorbed on VYCOR glass surface [6]. That spectrum was assigned to the ethyl radical strongly interacting with the surface of zeolite. The spectrum in Fig.2b presenting the sum of two EPR spectra simulated with the following parameters: **A** – A_{iso}=2.0 mT, g=2.0027 and ΔH_{pp}=0.15 mT; **B** – A_{α}=1.47 mT, A_{β}=2.7 mT, $g_{\perp}$=2.0026, $g_{||}$=2.0029 and ΔH_{pp}=0.75 mT is in good agreement with experimental spectrum.

It is interesting that α hyperfine constant of $^{\bullet}C_2H_5$ (**C**) is distinctly different from α hfc of typical ethyl radical (**A**), while β hfc constants in both types of ethyl radicals are nearly the same. It might be due to the strong interaction of ethyl radical with trapping sites (Brönsted acid sites and/or exchangeable cation sites) through the methylene group. Another possible origin of the large difference in α hyperfine constant of both types of $^{\bullet}C_2H_5$ radicals might be related to the pressure of adsorbed gas. It is postulated that at higher pressure C_2H_4 molecules migrate to the less accessible sites in zeolite framework. Then methylene groups could be trapped in octagonal windows or prisms while CH_3 groups would stay outside and not participate in the strong interaction with zeolite.

It has been proved that H-rho zeolite shows unique properties for stabilization of small alkyl radicals. Those radicals, usually very reactive, in H-rho lattice are stable even at 310 K. Depending on the adsorption conditions, two different types of ethyl radical were observed. The first type is characterized by isotropic spin Hamiltonian parameters and corresponds to freely tumbling radical stabilized in electrostatic field of zeolite. The second type strongly interacts or even is chemically bonded to the aluminasilica framework. In γ-irradiated zeolite rho containing ethylene, the EPR spectra of ion-radicals were not observed. Thus, it seems reasonable to assume that $^{\bullet}CH_2$ radicals are formed as a result of fragmentation of ethylene molecules.

References

[1]. Toriyama K., Nunome K., Iwasaki M.: J. Chem. Phys., 77, 5894 (1999).
[2]. Iwasaki M., Toriyama K., Muto H., Nunome K., Fukaya M.: J. Phys. Chem., 85, 1326 (1981).
[3]. Fessenden R.W., Schuler R.H.: J. Chem. Phys., 39, 2447 (1963).
[4]. Shiga T., Lund A.: J. Phys. Chem., 77, 453 (1973).
[5]. Robson H.E., Shoemaker D.P., Ogilvie R.E., Manor P.C.: Adv. Chem. Ser., 121, 106 (1973).
[6]. Katsu T., Yanagita M., Fujita Y.: J. Phys. Chem., 75, 4064 (1971).

ESR AND ESEEM STUDY OF SILVER CLUSTERS IN SAPO-17 AND SAPO-35 MOLECULAR SIEVES

Jarosław Sadło, Jacek Michalik, Adekkanatu Prakash[1/], Larry Kevan[2/]

[1/] Department of Chemical Engineering, Auburn University, USA

[2/] Department of Chemistry, University of Houston, USA

The aim of this work is to study silver agglomeration processes and the interaction of silver species with molecular adsorbates in AgH-SAPO-17 and AgH-SAPO-35 molecular sieves. SAPO-17 and SAPO-35 are small pore molecular sieves with eight-membered ring pore openings. The structure of calcined SAPO-17 is analogous to the natural zeolite erionite with hexagonal symmetry and lattice parameters a=1.33 nm and c=1.53 nm. The secondary structure consists of double hexagonal cages, cancrinite cages and distinctly larger erionite cages. SAPO-35 has a structure similar to zeolite levyne. The polyhedral cages in calcined SAPO-35 are hexagonal prisms and levyne cages. The levyne cages are connected by six-ring and double six-ring windows and are accesible through eight-membered windows of dimension 0.36x0.48 nm.

Up to now, only limited number of both electron spin resonance (ESR) and electron spin echo envelope modulation (ESEEM) studies were undertaken to investigate the radiation induced silver agglomeration and the interaction of silver clusters with molecular adsorbates in SAPO molecular sieves. The use of continuous wave ESR method allows usually to deduce the nature of paramagnetic species, but the determination of interaction of these species with adsorbates in the host lattice is not so evident because of the limited resolution of ESR spectra for the weak dipolar interactions. In contrast to conventional ESR technique, the resolution of ESEEM spectroscopy is usually high enough to resolve these interactions and determine the surrounding of paramagnetic center. For example, ESEEM technique allowed to explain the differences in silver agglomeration in isostructural zeolite A and SAPO-42 molecular sieve [1]. In AgH-SAPO-5 and AgH-SAPO-11 the ESEEM results indicate that organosilver radicals are located in twelve-ring (SAPO-5) and ten-ring (SAPO-11) channels and are coordinated by two nonequivalent methanol molecules. In contrast, the Ag_2^+ cluster is located in a six-ring channel in both frameworks and is stabilized by the interaction with three methanol molecules [2].

SAPO-17 and SAPO-35 molecular sieves were synthesized by hydrothermal crystallization under autogenous pressure without agitation using cyclohexylamine and hexamethylamine as organic template, respectively [3]. Silver forms of SAPOs were obtained by ion exchange with 1 M $AgNO_3$ solution at room temperature overnight in darkness. For ESR and ESEEM measurements, the samples

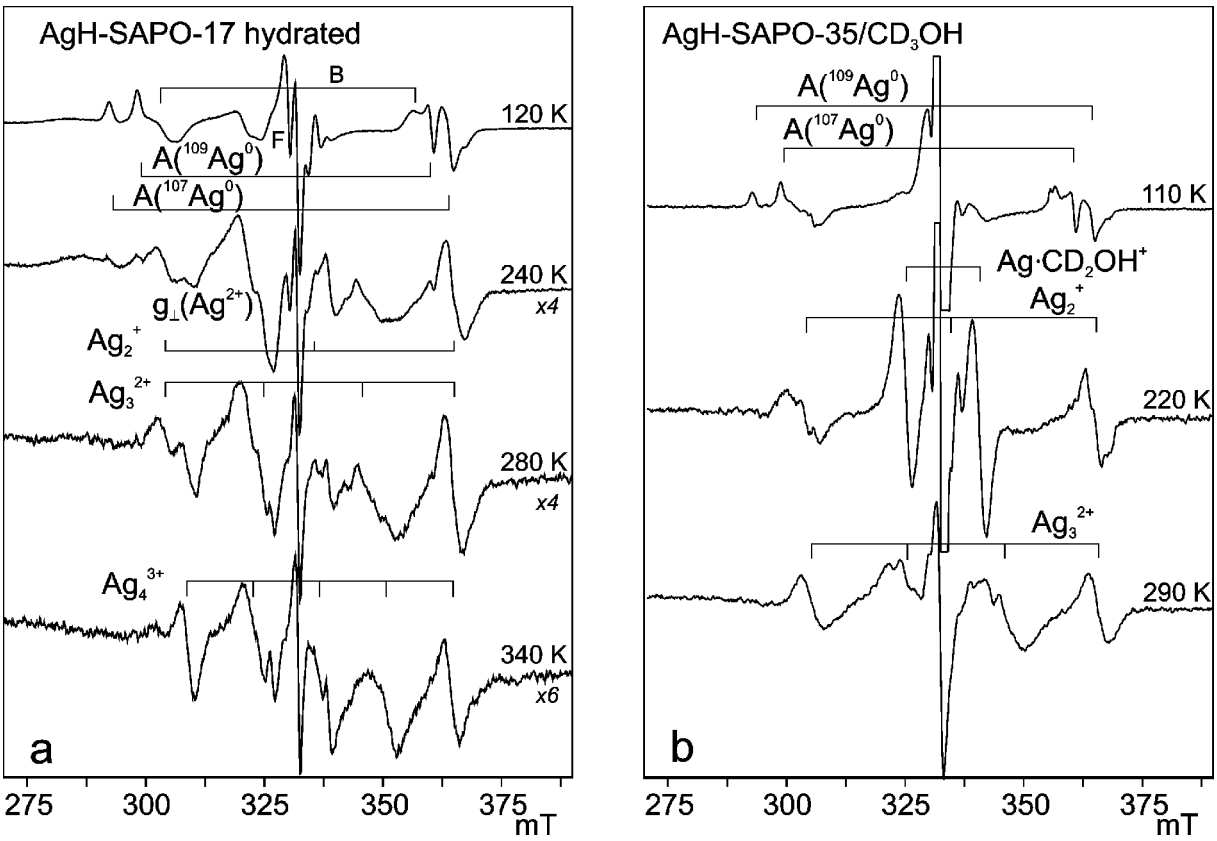

Fig.1. ESR spectra of (a) hydrated AgH-SAPO-17 and (b) AgH-SAPO-35/CD_3OH molecular sieves irradiated at 77 K and recorded at temperature indicated on the spectrum.

were placed into Suprasil quartz tubes and evacuated to a final pressure of 10^{-2} Pa. All samples were γ-irradiated at 77 K in a ^{60}Co source with a dose of 4 kGy. ESR spectra were recorded on a Bruker ESP-300E X-band spectrometer at various temperatures in the range 110-300 K by using a variable-temperature Bruker unit. ESEEM signals were measured on a Bruker ESP-380 FT pulse spectrometer in the temperature range 4.5-5 K using a helium flow cryostat. For three-pulse experiments, a pulse sequence of 90°-τ-90°-T-90° was employed and T was swept. Simulations of the experimental data were performed by using the analytical expressions derived by Dikanov *et al*. [4].

In hydrated AgH-SAPO-17 at 110 K (Fig.1a), three ESR signals representing silver species are observed: isotropic doublets A with narrow lines (H_{pp}=1.3 mT) of $^{107}Ag^0$ atoms (A_{iso}=61.3 mT, g_{iso}=2.0023) and $^{109}Ag^0$ (A_{iso}=70.7 mT, g_{iso}=2.0025), doublet B with distinctly broader lines (H_{pp}=5.2 mT) and lower hyperfine splitting A_{iso}=55.4 mT of silver atoms in different site and anisotropic doublet of Ag^{2+} cations ($g_{\perp}$=2.750, $g_{||}$=2.345). A singlet F at g=2.009 was assigned to the radiation-induced paramagnetic centers in silicaaluminaphosphate framework. After annealing at 240 K, the doublets of Ag^0 atoms decay and the observed spectrum is composed of a triplet C (A_{iso}=30.5 mT, g_{iso}=1.985) of Ag_2^+ clusters and quartet D (A_{iso}=20.5 mT, g_{iso}=1.975) of Ag_3^{2+} trimers. Above 280 K a new signal appears – a pentet E with A_{iso}=13.9 mT and g_{iso}=1.975, which we assigned to Ag_4^{3+} cluster, identical as stabilized in AgCs-rho zeolite [5]. Tetrameric silver clusters are also stabilized in AgH-SAPO-17 samples exposed to methanol and annealed to room temperature after irradiation at 77 K. In hydrated AgH-SAPO-35 at 110 K, there is only one doublet with broad lines: A_{iso}=59.7 mT, g_{iso}=1.978, H_{pp}=5.2 mT representing silver atoms. On thermal annealing at 200 K the Ag^0 doublet transforms into a triplet (A_{iso}=30.6 mT, g_{iso}= 1.990) of Ag_2^+ dimer. The Ag_2^+ spectrum is also observed at room temperature with slowly decreasing intensity.

When AgH-SAPO-35 is exposed to D_2O, the ESR spectra recorded at 110 and 290 K are similar to the spectra observed for the hydrated sample. Only silver dimers are stabilized at room temperature in the presence of water molecules, whereas in the presence of methanol the Ag_3^{2+} clusters are produced. The ESR spectra of AgH-SAPO-35/CD_3OH recorded during the thermal annealing are shown in Fig.1b. At 110 K the narrow lines of two doublets A of $^{107}Ag^0$ (A_{iso}=61.3 mT, g_{iso}=2.0023) and $^{109}Ag^0$ (A_{iso}=71.3 mT, g_{iso}= 2.0023) overlap with a third doublet B with larger linewidth and hyperfine splitting about 50 mT. The doublets of silver atoms disappear above 200 K and then a new doublet with distinctly smaller hyperfine splitting A_{iso}=15.3 mT and g_{iso}= 2.0023, assigned to hydroxymethyl radical ion $Ag{\cdot}CD_2OH^+$, appears. The outer lines of ESR spectrum recorded at 225 K belong to Ag_2^+ cluster (A_{iso}=30.0 mT, g_{iso}=1.980). The central line of Ag_2^+ triplet is overlapped by a strong singlet of framework paramagnetic centers. On annealing at 290 K, the only spectrum of silver species is quartet of Ag_3^{2+} cluster (A_{iso}=20.1 mT, g_{iso}=1.980). Silver trimers in SAPO-35 can be observed for a few hours at room temperature.

Dehydrated samples of AgH-SAPO-17 after irradiation at 77 K show only sharp lines of $^{107}Ag^0$ (A_{iso}=7.3 mT, g_{iso}=2.0023) and $^{109}Ag^0$ (A_{iso}=66.5 mT, g_{iso}=2.0023) which decay above 180 K. No ESR multiplets of cationic silver clusters were observed during their decay. Also in dehydrated AgH-SAPO-35 decay of Ag^0 atoms is not associated with cluster formation.

Pulse ESR experiments were carried out only for Ag_2^+ cluster in AgH-SAPO-35/D_2O and Ag_3^{2+} in AgH-SAPO-35 exposed to CD_3OH and CH_3OD. Magnetic field was set at the low and high field lines of Ag_2^+ triplet. The best simulation parameters are collected in Table. For both settings, the best simulations were obtained by assuming the interaction with four deuterium nuclei at a distance of 0.35 nm. These values are consistent with two D_2O molecules coordinated with Ag_2^+ cluster. Based on these

Table. Parameters used for the simulations of ESEEM results of AgH-SAPO-35 molecular sieve.

Shell	N	R [nm]	A [MHz]
Ag_2^+ in AgH-SAPO-35/D_2O			
1	4	0.351	0.1
Ag_3^{2+} in AgH-SAPO-35/CD_3OH			
1	12	0.411	0.12
Ag_3^{2+} in AgH-SAPO-35/CH_3OD			
1	4	0.444	0.06

results, we postulate that Ag_2^+ dimer is located in hexagonal prism and is coordinated by two water molecules occupying positions in two levyne cages connected by the hexagonal prism.

For ESEEM experiment for Ag_3^{2+} in AgH-SAPO-35 exposed to CD_3OH and CH_3OD the field was set at the first and third line of Ag_3^{2+} quartet. The simulation of the ESEEM spectra for both settings gave the best results for twelve deuterium nuclei at the distance of 0.44 nm for CD_3OH and

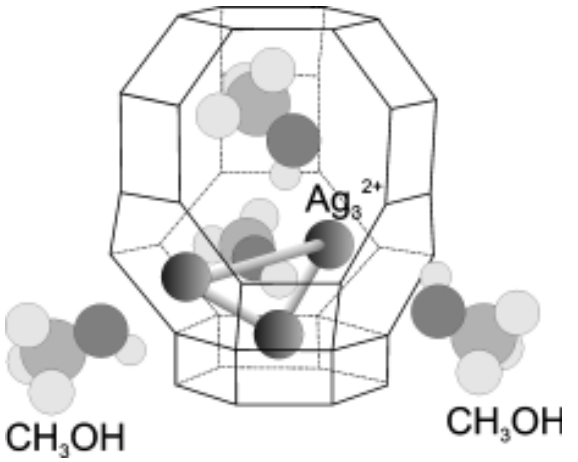

Fig.2. The geometrical arrangement of Ag_3^{2+} and methanol molecules in relation to levyne cage in AgH-SAPO-35 molecular sieve.

for four D nuclei at the distance of 0.41 nm for CH_3OD. These results indicate that four methanol molecules are coordinated by Ag_3^{2+} trimer in SAPO-35 with their molecular dipoles directed into the cluster. We proposed that Ag_3^{2+} is located in levyne cage close to hexagonal prism. In that region cationic sites are situated close each to the others, thus Ag_3^{2+} could be formed by short-distance migration of Ag^0 and Ag^+ species. The proposed coordination geometry is the following: one CH_3OH molecule is located in the same cage when Ag_3^{2+} is stabilized and three other molecules there are in the adjacent levyne cages. Their molecular dipoles are directed through hexagonal windows towards Ag_3^{2+} cluster (Fig.2).

A comparison of silver agglomeration processes in SAPO-17 and SAPO-35 univocally proves that small structural cages are indispensable for stabilization of cationic silver clusters in molecular sieves.

However, for molecular sieves with low cation capacity this condition is not sufficient. The important role plays also the molecular adsorbates. They can affect agglomeration process not only by blocking migration path of silver species, but also reacting chemically with active radiolytical products.

References

[1]. Michalik J., Zamadics M., Sadlo J., Kevan L.: J. Phys. Chem., 97, 10440-10444 (1993).
[2]. Michalik J., Azuma N., Sadlo J., Kevan L.: J. Phys. Chem., 99, 4679-4686 (1995).
[3]. Prakash A.M., Kevan L.: Langmuir, 13, 5341-5348 (1997).
[4]. Dikanov S.A., Shubin A.A., Parmon V.N.: J. Magn. Reson., 42, 474 (1981).
[5]. Michalik J., Sadlo J., Yu J-S., Kevan L.: Colloids Surf. A: Physicochem. Eng. Aspects, 115, 239-247 (1996).

SILVER AGGLOMERATION IN ANALCIME

Janusz Turek, Jacek Michalik

Molecular sieves have unique abilities to stabilize small cationic silver clusters generated radiolytically or by hydrogen reduction. The most stable cationic silver clusters are silver hexamers – Ag_6^{5+} found in A-type zeolite and silver tetramers – Ag_4^{3+} in Cs-rho zeolite. However, these clusters are stable only in vacuum and decay quickly in the present of air.

Recently, we carried out experiments with a new zeolite type – analcime (ANA) containing silver. Analcime is a channel type zeolite with a small diameter of channels. ANA contains sixteen monovalent cations per unit cell to compensate the negative charge of zeolite network. It turned out that silver clusters produced in this system did not decay when the zeolite had been exposed to air or pure oxygen at room temperature.

We studied Ag-ANA samples with different silver content: Na_{16}-ANA (without silver), $Ag_{0.3}Na_{15.7}$-ANA, Ag_1Na_{15}-ANA, Ag_4Na_{12}-ANA, $Ag_{10}Na_6$-ANA and Ag_{16}-ANA (fully loaded with silver). All samples were dehydrated at 480°C in vacuum for 2 h. Next, the samples were oxidized for 2 h and degassed for 1 h. After that, the samples were irradiated in a γ-source over night in liquid nitrogen (77 K).

EPR (electron paramagnetic resonance) measurements were made using a Bruker ESP-300 spectrometer equipped with a nitrogen cryostat. The EPR spectra were measured in temperature range 100-350 K.

The EPR spectra of dehydrated Ag_{10}-ANA zeolite are presented in Fig.1. Spectrum recorded at 100 K shows the following signals:

- a strong anisotropic doublet of divalent silver, Ag^{2+} charcterized by $g_{||}=2.305$ and $g_{\perp}=2.043$;
- a doublet of silver atoms with $A_{iso}=63.2$ mT showing an additional structure due to overlapping signals of silver dimers and trimers.

At 200 K, the intensity of Ag^0 lines decreases and the quartet of Ag_3^{2+} cluster becomes visible. At

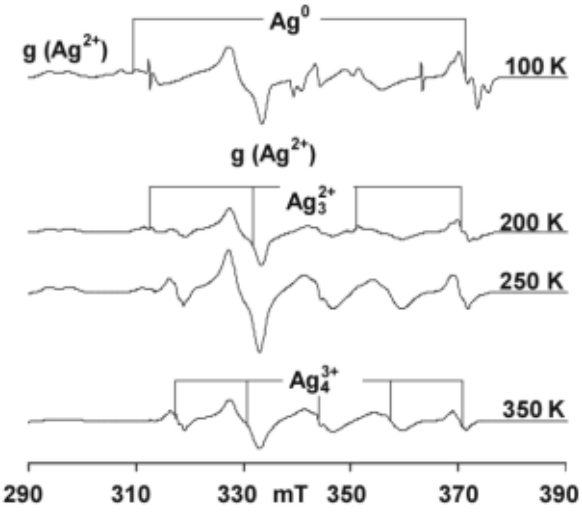

Fig.1. The EPR spectra of dehydrated Ag_{10}-ANA samples at different temperatures.

250 K, the Ag_3^{2+} quartet overlaps with Ag_4^{3+} quintet. At higher temperatures, Ag_3^{2+} decays completely and at 350 K only the Ag_4^{3+} quintet is recorded.

The transformation of EPR spectra on thermal annealing clearly indicates that the silver agglomeration process, initiated by radiation-induced reduction of Ag^+ cations – reaction (1), requires the mobility of silver species and proceeds by gradual addition of Ag^+ cation to silver clusters – reaction (2).

$$Ag^+ + e^- \rightarrow Ag^0 \qquad (1)$$

$$Ag^0 + Ag^+ \rightarrow Ag_2^+ \xrightarrow{Ag^+} Ag_3^{2+} \xrightarrow{Ag^+} Ag_4^{3+} \qquad (2)$$

It is worthy of mention that silver tetramers are formed in the analcime lattice even when Ag^+ loading is very low. The transformation of EPR spectra on thermal annealing in $Ag_{0.3}Na_{15.7}$-ANA is similar to zeolite with higher Ag^+ content, however the process is slower and the intensity of cluster spectra is lower. At 280 K, the intense quartet

of Ag_3^{2+} is still overlapping the quintet of Ag_4^{3+} cluster (Fig.2). This means that Ag^+ cations are able

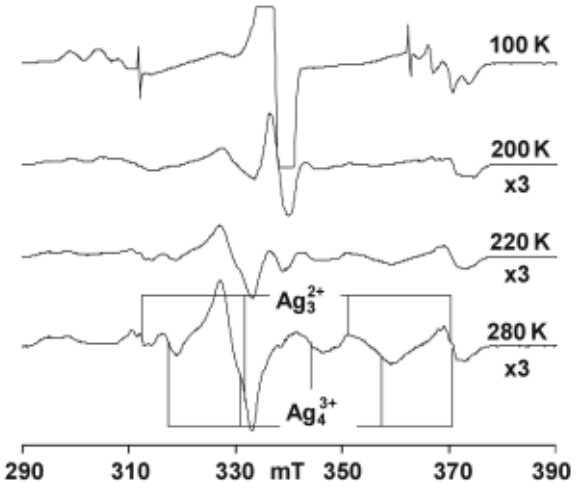

Fig.2. The EPR spectra of dehydrated $Ag_{0,3}$-ANA samples at different temperatures.

to move through many cages until they find the silver atom or cluster to react with.

The most interesting feature of silver tetramers in analcime structure is their stability. The ESR signal of Ag_4^{3+} is still recorded in the degassed samples heated at 100°C. It also does not decay in the samples exposed to air at room temperature. After adsorption of pure oxygen under the pressure of 300 Torrs, the signal intensity remains unchanged for several days. This is probably due to the small dimensions of lattice windows connecting analcime cages which makes difficult the penetration of O_2 molecules through analcime channels.

Silver tetramers in analcime framework show unique stability at room temperature in the presence of air. It opens completely new experimental possibilities leading to better characterization of Ag_4^{3+} in solid state. In the nearest future we plan to perform XRD (X-ray diffraction) and electron microscopy experiments with unirradiated and irradiated Ag-ANA samples. We also will be applying for Hasylab grant to use a synchrotron beam in order to study Ag_4^{3+} structure and location in the lattice. The efficiency of Ag_4^{3+} formation in hydrogen reduced Ag-ANA will be also checked in 2005.

INFLUENCE OF IONISING RADIATION ON POLY(SILOXANEURETHANES)

Ewa Kornacka, Izabella Legocka, Krzysztof Mirkowski, Jarosław Sadło, Grażyna Przybytniak

According to the general guidelines for selection of radiation-stable materials (ISO 11137-1995, Annex A) both polyurethanes and silicones are qualified as the materials possessing excellent or good radiation stability (aliphatic and aromatic). Therefore, medical devices fabricated from these polymers are recommended for radiation sterilisation. To combine good mechanical properties of polyurethanes with biostability and biocompatibility of silicones, a new class of materials was prepared – poly(siloxaneurethanes). In order to determine the chemical effect of ionising radiation on the new copolymers designed as potential materials for medical applications we studied mechanisms of radiolytically initiated processes using two methods, EPR (electron paramagnetic resonance) and GC (gas chromatography). Investigated block copolymers consist of rigid segments (isophorone diisocyanate – IPDI fragments common for all samples) and flexible ones (oligosiloxanediols).

Samples of segmented poly(siloxaneurethanes) and their monomers (Table) were irradiated in presence of oxygen with an electron beam (accelerator LAE 13/9) to the indicated doses at ambient temperature and in a gamma source ^{60}Co (Mineyola) in liquid nitrogen with a dose of 4 kGy. For EPR experiments, the monomers and polymers were frozen in liquid nitrogen and irradiated at 77 K. After irradiation, EPR signals were measured with a Bruker X-band ESR 300 spectrometer using a microwave power of 1 mW. EPR spectra were recorded at 77 K and on annealing to the required

Table. Chemical composition of poly(siloxaneurethanes).

Number of sample	Chemical structure of samples			
	NCO/OH ratio	Oligosiloxanediol		
1	2:1	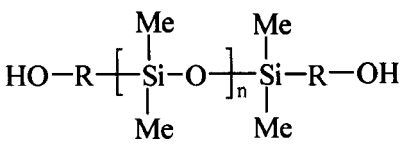	n=30	R= -$(CH_2)_6$-
2	3.5:1		n=30	R= -$(CH_2)_6$-
3	2:1		n=40	R= -$(CH_2)_3$-O-$(CH_2)_2$-
4	3.5:1		n=40	R= -$(CH_2)_3$-O-$(CH_2)_2$-
5	2:1		n=10	R= -$(CH_2)_6$-
6	3.5:1		n=10	R= -$(CH_2)_6$-
7	3.5:1		n=20	R= -$(CH_2)_3$-O-$(CH_2)_2$-

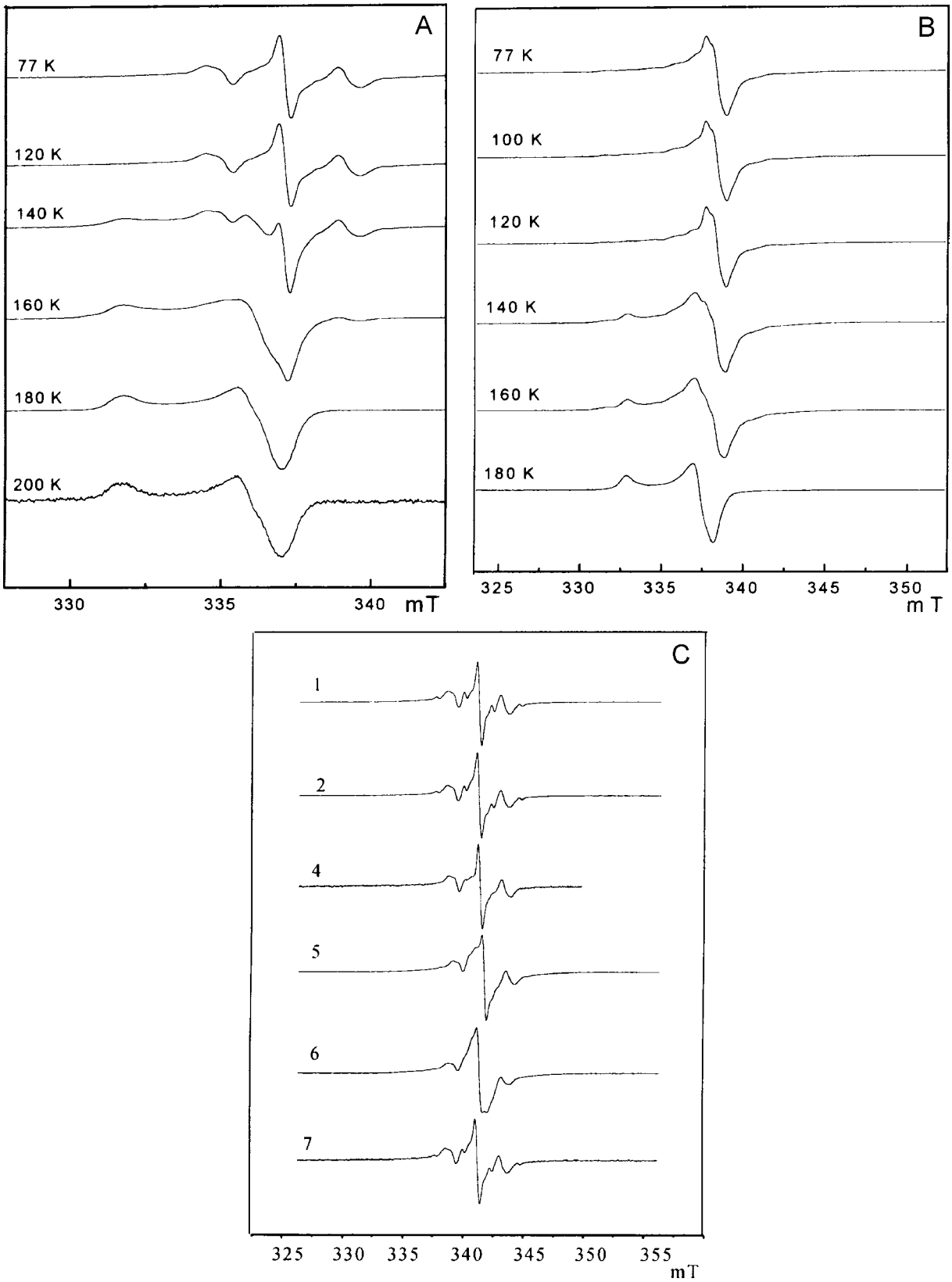

Fig.1. EPR spectra of monomers: diisocyanate (A) and oligosiloxanediol (B), upon irradiation at 77 K and on annealing to indicated temperatures. C – series of EPR spectra of poly(siloxaneurethanes) presented in Table, measured upon irradiation at 77 K.

temperature controlled by a cryostat. The yield of hydrogen in the gas phase evolved from irradiated polymers were determined with gas chromatograph Shimadzu-14B.

On the basis of EPR spectra (Fig.1) we found that the irradiation of dimethylsiloxanes causes both Si-CH_3 and $SiCH_2$-H scissions involving abstraction of hydrogen and methyl groups. At last stage of processes, radicals produced by irradiation are rapidly scavenged by oxygen to form corresponding peroxyl radicals. According to Miller [1], the $SiCH_2OO^{\bullet}$ is ultimately oxidised to carbonyl group

SiCOOH, while the $SiOO^{\bullet}$ is a radical forming the residual links. The character of spectra obtained for irradiated poly(siloxaneurethanes) is similar to that recorded for dimethylsiloxane oligomers. Although

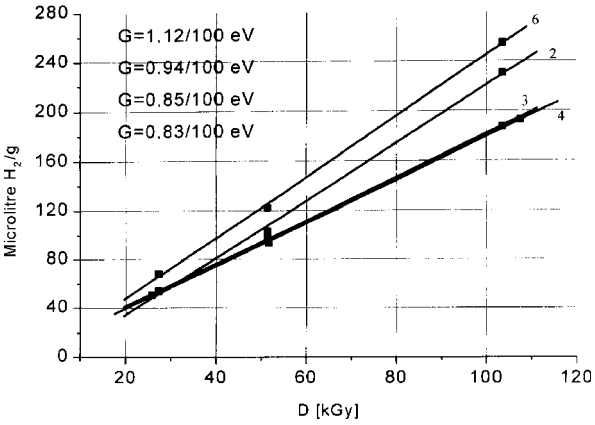

Fig.2. Yield of hydrogen released from selected poly(siloxaneurethanes) in function of ionising radiation dose.

energy is deposited in all fragments of copolymer, the radicals are produced predominantly in the siloxane segments. Methyl radical decays already at 77 K [2], therefore only in some irradiated samples the intermediate was identified. Recombination of the two types of polymer radicals, $Si^{\bullet}$ and $SiCH_2^{\bullet}$, can lead to three types of crosslinks. Consequently, a correspondence between gas and crosslinking yields should be expected. However, the effect is partly suppressed by molecular oxygen. The relationship presented in Fig.2 shows that the production of hydrogen depends on the siloxane segments – the longer is the unit, the smaller is the release of H_2. The ratio NCO:OH does not change the yield of hydrogen release.

Upon radiolysis unstable radicals are generated mainly at the siloxane segments. Such selective processes must lead to the crosslinking predominantly at these parts of copolymers. The yield of abstracted hydrogen is inversely proportional to the length of siloxane units. Therefore the presence of numerous $(CH_3)Si(CH_3)$ groups involves competing reactions which results in the breakage of Si-C bonds rather than C-H bonds.

References

[1]. Miller A.A.: J. Phys. Chem., 82, 3519-3527 (1960).
[2]. Menhofer H., Heusinger H.: Radiat. Phys. Chem., 29, 243-251 (1987).

RADIATION-INDUCED MODIFICATION OF FILLERS USED IN NANOCOMPOSITES

Zbigniew Zimek, Izabella Legocka, Krzysztof Mirkowski, Grażyna Przybytniak, Andrzej Nowicki

Nanofillers are a new class of particles that are applied to composite polymers and other materials with new properties. As nanofillers the following are used: oxides, carbides, simple and composite salts and other compounds.

The main problem in the mixing process of polymers and fillers is the incompatibility of these materials. Inorganic compounds are hydrophilic, while main types of polymers are hydrophobic. For good mixing, the fillers should be modified to obtain hydrophobic layer at the surface. The modification is possible in many ways; the most popular is the impregnation of fillers with bi-functional molecules, containing in one molecule hydrophobic (*e.g.* long alkyl) and hydrophilic (*e.g.* ionic or polar) groups. A typical example is the impregnation with ammonium salts having a long alkyl chain [1-7].

In previous work conducted at the Institute of Nuclear Chemistry and Technology (INCT) another way of the modification of mineral fillers was tested. The grafting process of vinyl monomers on inorganic surface was followed by radiation-induced radicals of fillers [8,9].

The preliminary studies on modification of nanofillers with unsaturated monomers using ionizing radiation were conducted for popular and low-cost compounds: zinc oxide and magnesium oxide. Some vinyl monomers were used as modifying agents: maleic anhydride, methacrylic acid and methyl methacrylate. Main conclusion from works on the model compounds was that it is possible to graft vinyl monomers on inorganic surface using ionizing radiation. In addition, the optimal range of ionizing radiation doses in a laboratory process was found to be compatible with filler production.

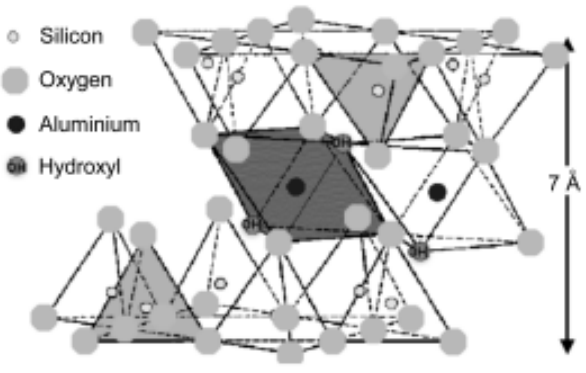

Fig.1. Structure of montmorillonite.

In the present studies, the following commercial materials of nanostructure were used [7] (Fig.1):

- unmodified bentonite Tixogel VP produced by Riedel-deHaen containing >90% montmorillonite as sodium salt (catalogue No. 18609) – "RdH",
- two kinds of unmodified Polish bentonites (Mine Works "Zebiec", Starachowice): "Special" containing more than 70% of pure montmorillonite

and type "SW" containing *ca*. 50% of pure montmorillonite.

For modification of fillers, maleic anhydride was selected as unsaturated, unable to homopolymerize monomer. The polar carboxylic groups of maleic anhydride interacting with polar centers of montmorillonite facilitate dispensability of nanoparticles in the polymer and prompt bond formation between nanofillers and the polymer.

Maleic anhydride was absorbed on bentonites from 2.5% w/w. solution in acetone. The samples with absorbed monomer were irradiated by 10 MeV electron beam. The overall dose was 26 kGy. After irradiation, the samples were immediately investigated by the electron spin resonance (ESR) method. Beside hyperfine splitting of ^{27}Al (S=5/2) (6 lines at a distance of 10 mT) the signal from maleic anhydride radicals was confirmed.

Mixtures of modified nanoparticles with commercial polypropylene (type J601, from the Polish concern "Orlen") were made. For comparison, unmodified bentonite and non-irradiated samples of modified bentonite were prepared. The products were washed with an excess of acetone (to remove maleic anhydride) and dried for 6 h at 250°C.

The mixtures of polypropylene and bentonites were prepared in a Brabender mixer in the temperature range from 185 to 210°C. The mechanical properties: tensile stress, stress at yield and tensile strain were tested using the universal testing machine Instron 5565, while the thermal properties were tested using the differential scanning calorimeter MDSC2920CE in standard mode.

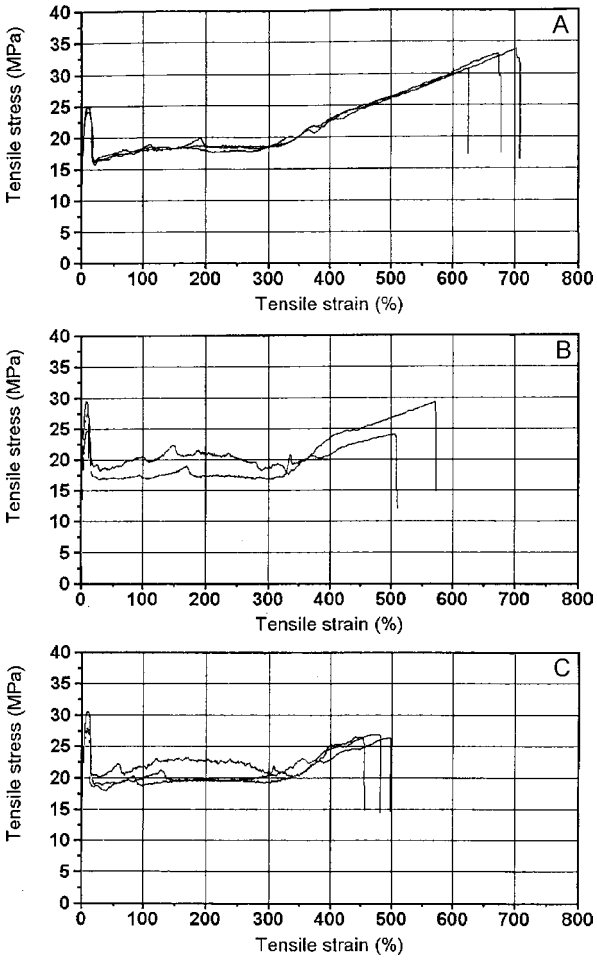

Fig.2. Mechanical properties of polypropylene mixed with modified montmorillonites: A – "Special" (3 samples), B – "RdH" (2 samples), C – "SW" (3 samples).

All samples of polypropylene mixed with unmodified bentonite showed insufficient mechanical properties: they were very fragile and cracked at low elongation, *ca*. 10-15%. Addition of more than 5% w/w. of the filler into polypropylene causes a significant growth of hot mixture viscosity. Therefore, the next experiments were performed at concentration of modified fillers equal to 2.9% w/w.

The best mechanical properties were obtained for polypropylene filled with modified bentonite "Special" (Fig.2A). The results obtained for other fillers show that the optimization of the amount of added maleic anhydride is necessary. The quality of modified bentonite "RdH" and "SW" is low probably due to impurities present in the fillers (Fig.2).

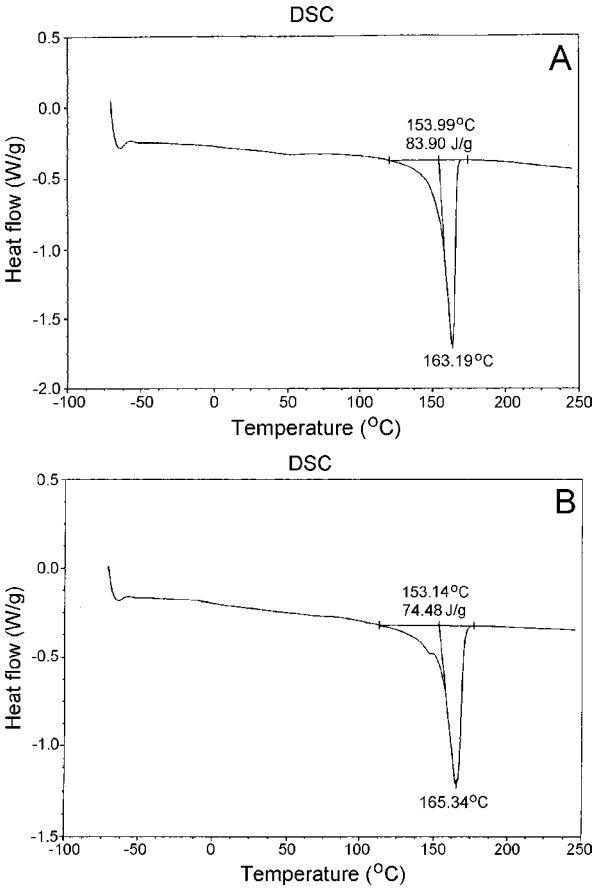

Fig.3. DSC (exothermic – up) study of polypropylene mixed with modified montmorillonites: A – "RdH" (second heating cycle), B – "Special" (first heating cycle).

Thermal testing provides additional information about the properties of obtained mixtures. In DSC (differential scanning calorimetry) experiments, the second heating cycle of the mixture with modified bentonite "RdH" is regular (Fig.3A), contrary to the first one. However, endothermic peak at about 55°C indicates that a low amount of free maleic anhydride is included in the material. The results confirm a suggestion from mechanical testing that careful selection of the contribution of modifying agent is essential together with optimization of mixing process.

Thermal properties of polypropylene mixed with modified "Special" bentonite also offer interesting information. No free maleic anhydride was detected and the melting peak is split because of the presence of two polymer phases characterized by different melting temperatures (Fig.3B). The temperature of transition is about 2°C higher than that for the mixture containing "RdH" bentonite.

Conclusion: Modification of the different types of bentonite by ionizing radiation and maleic anhydride as a modifying agent shows that the particles obtained in this process are good fillers for production of nanocomposites on the basis of polypropylene. The properties of some final materials were better than those of initial polypropylene.

References

[1]. Fujiki K. *et al*.: Polym. J., 22(8), 661 (1990).
[2]. Golubiv V.N. *et al*.: Dokl. Akad. Nauk SSSR, 198, 1085 (1977), in Russian.
[3]. Guanglin H.: Radiat. Phys. Chem., 42, 61 (1993).
[4]. Korsak V.V. *et al*.: Vysokmol. Soedin., A20(5), 1010 (1978), in Russian.
[5]. Tsubokawa N. *et al*.: Polym. J., 22(9), 827 (1990).
[6]. Yuding F. *et al*.: Radiat. Phys. Chem., 42, 77 (1993).
[7]. Viville P. *et al*.: J. Am. Chem. Soc., 126, 9007 (2004).
[8]. Zimek Z. *et al*.: Radiat. Phys. Chem., 57, 411 (2000).
[9]. Legocka I. *et al*.: Preliminary study on application of the PE filler modified by radiation. E-MRS Fall Meeting, Warsaw, Poland, 6-10 September 2004, Conference Materials, p.215.

RADIATION CHEMISTRY OF RADIOACTIVE TRANSURANIUM (TRU) WASTE, TO BE STORED IN THE WASTE ISOLATION PILOT PLANT (WIPP) REPOSITORY: FINAL CONCLUSIONS

Zbigniew Paweł Zagórski

The engagement of the Institute of Nuclear Chemistry and Technology (INCT) in the introduction of radiation chemistry to the management of radioactive waste was duly documented in the INCT Annual Reports and here is the next installment. Our paper in the "INCT Annual Report 2002" [1] has described starting information about the role of radiation chemistry in the project. Radiation chemistry is fundamentally involved in management of radioactive waste on every time scale, from the zero point of waste generation through its preliminary storage and processing, transportation and final rest in geological repositories. All experimental approaches are possible only with the assistance of tools of radiation chemistry, which are not in disposition of Los Alamos National Laboratory (USA). Equipment for radiation chemistry, in particular intensive sources of radiation are not very common and study of chemical effects with radiochemical apparatus is difficult, sometimes impossible and time consuming.

The key hardware in the realization of the project are electron accelerators in the Department of Radiation Chemistry and Technology (INCT) able to simulate any dose, dose rate and linear energy transfer (LET) value of ionizing radiation. The last mentioned property of electrically generated ionizing radiation is especially important in the project, as the main radioactive contaminant in waste under consideration is plutonium, which emits high LET alphas. The simulation of higher LETs is achieved by increasing the dose rate from straight beam of electrons, concentrated in small volume of the condensed phase material. At such conditions, spurs overlap creating conditions in which single ionization spurs behave like multi-ionization spurs.

Usual analytical methods applied in radiation chemistry for so called product analysis are not applicable in the discussed problems. All analytical methods applied in the project have a specific mode of application being realized on line with the electron beam. An example is a gas chromatography method combined with electron beam irradiation. That combination of irradiation and hydrogen determination helped to determine most dangerous product of waste radiolysis, *i.e*. molecular hydrogen from contaminated polymers. The other examples are spectral investigations and pH-metry.

Intensive research, in which several members of the Department staff were involved, has helped to solve problems successfully and results have been published in part, after presentation and discussion on the International Conference "Plutonium Futures" [2,3]. The paper describes preliminary results of radiolytic effects of plutonium decay, on materials contaminated during plutonium production, applications and reprocessing of nuclear weapons, during production of MOX fuel *etc*. The most important conclusions were the yields of molecular hydrogen, much lower than assumed, generated by most hydrogen bearing polymers. No chemical chain reaction was found, which could increase hydrogen yield above $G_{H2}=5$ per 100 eV of absorbed energy. On the contrary, the hydrogen yields were lower than expected from the crosslinking results, as found later in 2004, because some reactions of increasing the molecular weight run as entanglements, described as supramolecular chemistry.

Figure shows typical production of hydrogen in the function of absorbed dose, from polyethylene without additives (curve a) and from an elastomer (curve b). The latter shows initially lower yield of hydrogen, due to additives and two times lower general yield of hydrogen, due to the use of half of the absorbed energy for formation of entanglements of the polymer. After examination of all polymers which can occur in the plutonium contaminated waste, it became evident that only polyethylene without additives can be taken as stan-

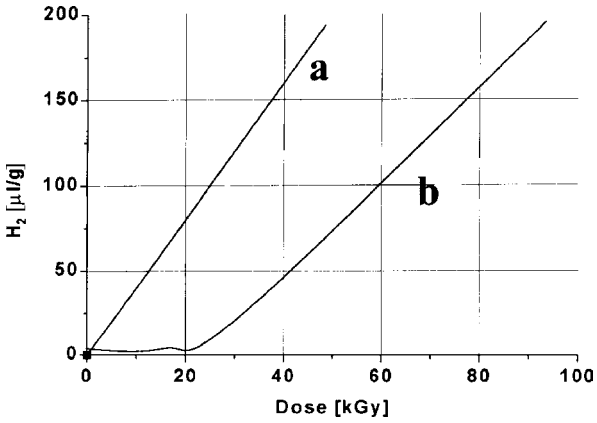

Fig. Production of radiolytic hydrogen from typical polymers in the waste in the function of absorbed dose of ionizing radiation. (Explanations in text.)

dard for the worst case anticipation of hydrogen production.

By occasion of the execution of investigations, time and again the observations were made that radiochemists do not accept fully the facts of chemical reactions generated by ionizing radiation. Therefore, the purpose of full report of investigations (*vide infra*) will mean a proposal to consider by radiochemists, especially those dealing with radioactive waste management. Relations between radiochemistry and radiation chemistry are still insufficiently close and unsatisfactory. Radiochemists do not have the access to the tools and methods of modern radiation chemistry, *i.e.* powerful sources, especially to accelerators of electrons. Hopefully, the problem of radiation-induced chemical effects connected with handling of radioactive materials, especially in the case of long time waste storage, can be solved with the help of radiation chemistry. The Department of Radiation Chemistry and Technology is ready to consult problems connected with chemical aspects of waste management, in particular of long time storage. The Department is ready to supply a full range of help, from consultation to experimental projects and computer assisted simulation of expected chemical effects.

Specific problem connected with radioactive waste management is connected with far shot analysis what can happen with salt deposits after thousands of years. The mentioned techniques are adapted to simulate what will happen if radioactive, long-lived material included in salt deposits, will be attacked by sipping water, turning the deposit into saturated NaCl brine, radiolyzed in completely different manner, in comparison to previous, initial solid state radiolysis. The system is in fact the radiation chemistry of saturated salt solutions, bringing complications connected with direct action of radiation on the solute. Our experimental approach is prepared to overcome that complication. As a comparison and control of experiment, the simulation is done also by computer assisted simulation. In 2004, it has been done with the help of Chemsimul programme, developed in the Risø National Laboratory (Denmark) and installed in the Department. The author of the report is licensed to use the programme freely and to obtain help from the authors of the programme, if needed. The case of salty brine has been originally developed for the case of chemical changes caused by potassium-40, the β emitter in prebiotic conditions on Earth, in particular in early oceans, seas and lakes.

Precision and accuracy of measurements were under control. All reported investigations have been performed under rigorous conditions of Quality Assurance (QA), as demanded by proper basic research and/or commercial radiation processing, controlled by the ASTM/ISO standards and traced to NIST samples. Reliable results have economic importance. Proper use of the experimental approach to the questions of dangers, connected with radiolytic products of waste management and storage, can mean substantial savings. For instance, the drum containing waste can be considered of too high activity of plutonium and before storage has to be repacked at the expense of tens of thousand of USD. Our investigations have shown upper limits of permissible activity, producing hydrogen from most dangerous plastics. These data show, that the activity inside drums can be left much higher than the earlier accepted value, thus avoiding repackage and cutting high additional costs.

During the year 2004, the work was continued, tending to formulate final conclusions to be found in a high volume INCT report.

References

[1]. Dziewinski J., Zagórski Z.P.: Role of radiation chemistry in waste management. In: INCT Annual Report 2002. Institute of Nuclear Chemistry and Technology, Warszawa 2003, p.44.

[2]. Zagórski Z.P., Dziewinski J., Conca J.: Radiolytic effects of plutonium. In: Plutonium Futures – the Science. Third Topical Conference on Plutonium and Actinides. Ed. G.D. Jarvinen. American Institute of Physics, Melville, New York 2003, p.336. AIP Conference Proceedings, Vol.673.

[3]. Zagórski Z.P.: Postępy Techniki Jądrowej, 46, 3, 34 (2003), in Polish.

ALIPHATIC-AROMATIC POLYMER BLENDS AS A PROPOSAL FOR RADIATION RESISTANCE

Wojciech Głuszewski, Zbigniew Paweł Zagórski

Several applications of polymers demand resistance towards ionizing radiation, *e.g.* for single use medical devices radiation sterilized, for nuclear medicine devices, for outer space research, *etc*. Ionizing radiation can cause different effects, from positive, like crosslinking, to negative as degradation and

formation of low molecular debris of the chain. Traditional preventive approach consists in additives, mainly typical, used widely, securing resistance of the material to sunlight and increased temperature [1]. These additives can have adverse effect in applications, *e.g.* for medical purposes, therefore other proposals are looked for. Most additives of stabilizing action are aromatic compounds and their activity towards photochemical action consists in direct absorption of UV-VIS quanta and change of ionizing energy into harmless heat or to longer wavelength light not able to cause photochemical changes. However, the direct action in radiation chemistry is proportional to the participation of additives in the pool of electrons, that means it is low. However, the observed protection effect is higher than that resulting from additives percentage, what means that there must be energy transfer from the ionized main constituent of the material to the protecting additive. The best explanation is the concept of the positive hole (h^+) transfer over the chain to the energetically attractive site, like the neighborhood of aromatic additive. That effect occurs in the case of 80% of deposited energy in single ionization spurs. The remaining 20% are deposited in the multi-ionization spurs, causing serious radiation damage, chain scission and formation of low molecular weight debris [2-8].

The idea of the present investigation is the application of aromatic polymers instead of traditional low molecular weight additives. Aromatic polymers can be used in higher concentrations than additives, thus improving mechanical properties of the material and securing radiation resistance. Stabilizers and other additives will no longer introduce complications and adverse effects of mostly strange chemistry of additives. Even if the applied results will not successfully compete with conventional solutions, the basic research results will justify the research. The knowledge of energy transfer in polymers is far from perfect and the research will contribute to better basic understanding of radiation chemistry of polymers.

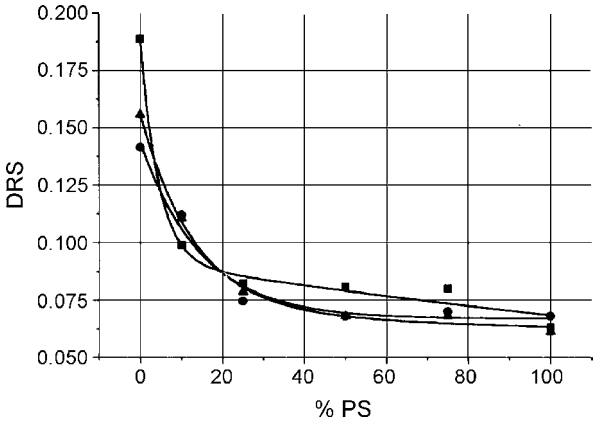

Fig. Dependence of peak intensity at $\lambda = 290$ nm in the DRS spectrum from the PS content in the blend, for three media of irradiation: pure oxygen (squares), air (triangles), argon (circles).

The main constituent of polymer blends, the polypropylene (PP) has been chosen, as the most popular polymer for the application in construction of medical devices, due to the hardness and temperature resistance. Unfortunately, the virgin PP is of low resistance towards ionizing radiation, already to sterilization doses [9] and cannot be applied without additives. Following the idea expressed above, as a simple aromatic polymer, polystyrene (PS) was applied and both polymers were used as blends in different proportion and prepared in a variety of ways. Mechanical properties of blends were investigated in collaboration with the Wrocław Technical University [10,11].

Main recognition of the protection effect has been done by the diffused reflection spectroscopy (DRS), developed in the Department of Radiation Chemistry and Technology (Institute of Nuclear Chemistry and Technology) for the application to irradiated polymers [12]. The dependence of intensity of bands in the DRS spectrum, attributed to ketone groups, which are final products of oxidation, shows clearly the protection effect of PP, executed by PS (Fig.). One can assume that the contact between PP and PS chains is not intimate enough to accept all positive holes and electrons released in the primary process. Therefore, hydrogen is detached from PP, forming alkyl radicals on the chain. The PS competes successfully with oxygen for these centers, preventing the oxidation of polymers. The aromatics free PP is oxidized easily, whereas the presence of PS prevents this reaction.

It is obvious that the study of hydrogen detachment can clear these assumptions, as it has been indicated in first experiments [13]. The detachment of hydrogen is unknown in the classical chemistry of polymers. Molecular hydrogen is not released in conventional methods of crosslinking; it appears as a variety of compounds depending on the kind of crosslinking agent. Our investigations, limited by temporary access to a gas chromatograph, have shown the radiation yield connected with the participation of PP in the blend.

Results of our investigations have been compared with the measurements of mechanical properties, performed at the Wrocław Technical University, *i.e.* mass flow rate, elongation, coefficient of direct elasticity, viscosity. Results obtained, after comparison with commercial data of traditional PP compositions, indicate a possible application of our approach.

All reported investigations have been performed under rigorous conditions of Quality Assurance (QA), as demanded by proper basic research and/or commercial radiation processing, controlled by the ASTM/ISO standards and traced to NIST samples. These conditions have to be fulfilled, if the medical devices shall be permitted for application [14]. Applied radiation techniques [15-18] secure proper dosimetry, maximum to minimum dose ratio, *etc.*

References

[1]. Żuchowska D.: Polimery konstrukcyjne. Wyd. II. WNT, Warszawa 2000, in Polish.
[2]. Zagórski Z.P.: Polimery, 42, 141 (1997), in Polish.
[3]. Zagórski Z.P.: Radiat. Phys. Chem., 56, 559 (1999).

[4]. Zagórski Z.P.: Postępy Techniki Jądrowej, 43, 4, 2 (2000), in Polish.
[5]. Zagórski Z.P.: Radiat. Phys. Chem., 63, 9 (2002).
[6]. Zagórski Z.P.: Role of spurs in radiation chemistry of polymers. In: Advances in radiation chemistry of polymers. IAEA, Vienna 2004, IAEA-TECDOC, in print.
[7]. Zagórski Z.P.: Radiat. Phys. Chem., 71, 263-267 (2004).
[8]. Zagórski Z.P.: Postępy Techniki Jądrowej, 46, 4, 10 (2003), in Polish.
[9]. Rafalski A.: Unstable products of polypropylene radiolysis. Ph.D. Thesis. Warszawa 1998, in Polish.
[10]. Żuchowska D., Zagórski Z.P.: Polimery, 44, 514 (1999), in Polish.
[11]. Żuchowska D., Zagórski Z.P., Przybytniak G.K., Rafalski A.: Int. J. Polymer. Mater., 52, 335 (2003).
[12]. Zagórski Z.P.: Int. J. Polymer. Mater., 52, 323 (2003).
[13]. Zagórski Z.P., Głuszewski W.: Irreversible radiolytic dehydrogenation of polymers – the key to recognition of mechanisms. In: INCT Annual Report 2003. Institute of Nuclear Chemistry and Technology, Warszawa 2004, p.40.
[14]. Zagórski Z.P.: Sterylizacja Radiacyjna. PZWL, Warszawa 1981, 188 p., in Polish.
[15]. Zagórski Z.P.: Thermal and electrostatic aspects of radiation processing of polymers. In: Radiation Processing of Polymers. Eds. A. Singh, J. Silverman. Hanser Publishers, Monachium, Vienna, New York 1992, pp.271-287.
[16]. Zagórski Z.P.: Pulse radiolysis of solid and rigid systems. In: Properties and Reactions of Radiation Induced Transients. Ed. J. Mayer. PWN, Warszawa 1999, pp.219-233.
[17]. Zagórski Z.P.: Radiat. Phys. Chem., 22, 409 (1983).
[18]. Zagórski Z.P., Głuszewski W., Rzymski W.M.: Plast. Rev., 7(20), 23 (2002).

CHEMICAL CONSEQUENCES OF NUCLEAR STABILITY

Przemysław P. Panta

The matter around us contains chemical elements in the elemental state and in a variety of combinations. Some materials consist of two or more elements joined in chemical compounds, or are mixtures of elements or compounds or both.

Very early, in the opinion of XVIII century chemists all chemical elements should be treated as "eternal". However, after Becquerel's discovery of radioactivity of certain atomic nuclei such invariability became problematic and depended only on longevity of a given time scale. A chemical element can consist of different isotopes (stable or radioactive) as was firmly established by J.J. Thompson. In chemistry, atomic binding energies (*i.e.* energies of chemical bonds) are of the order of eV, whereas the level of many MeV is useful in nuclear physics. Electron structure of atom determines its chemical behaviour, and the nucleus binding energy decides about its stability. About 273 different nuclei are stable because they lack enough mass to break up into separate nucleons. The energy equivalent of the missing mass of a nucleus is called the binding energy of the nucleus. The greater its binding energy, the more energy must be supplied to break up the nucleus. For given nucleus, the binding energy per nucleon is found by dividing the total binding energy of the nucleus by the number of nucleons, A, it contains.

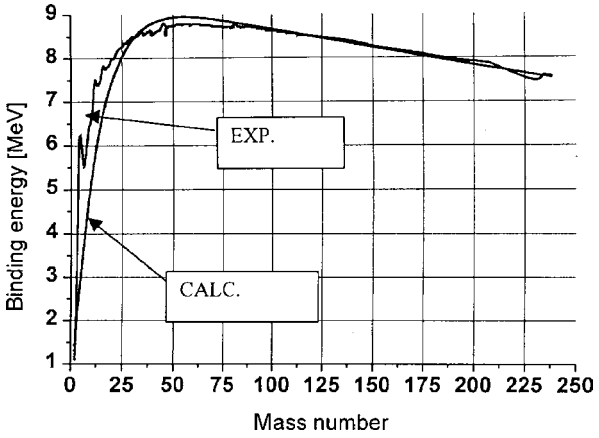

Fig. Binding energy per nucleon plotted against mass number A (experimental and calculated values, respectively).

The greater the binding energy per nucleon the more stable the nucleus. The graph (Fig.) illustrating the relationship between binding energy and mass number has its maximum at 8.8 MeV/nucleon when the number of nucleons is 56. The nucleus that has 56 protons and 56 neutrons is ^{56}Fe, the iron main isotope. This is the most stable nucleus, since the highest energy is needed to pull a nucleon away from the iron nucleus. All the larger nuclei are unstable and decay radioactively.

It is an empirical fact that the binding energy per nucleon is roughly the same for all stable nuclei, *i.e. ca.* 8 MeV. As the mass number increases, the binding energy per nucleon gradually decreases. This systematic trend is a consequence of the electrostatic energy repulsion of the protons within the nucleus. The binding energy curve is the key to energy production in the universe, mainly nuclear fusion leading to nucleosynthesis of heavy elements. The graph has a good claim of being the most significant in the whole science. The fact that the binding energy exists in general means that the nuclei more complex than the single proton of hydrogen (A=1) can be stable. This stability, in turn, accounts for the existence of the various chemical elements and, consequently, for the existence of the truly enormous amount of chemical compounds and their mixtures we see around us. For example, there are several millions of known and described chemical compounds, and even theoretically about 10^{48} of different proteins.

The semi-empirical mass formula (SEMF) was originally devised by C.F. Weizsacker [1] to represent the known nuclear masses in term of a few (five) adjustable parameters and enable useful estimates to be made of the masses of unknown nuclei. In the SEMF, the total binding energies expressed as a sum of five terms:

$$\frac{BE}{A} = A_v \cdot A - A_s \cdot A^{2/3} - A_c \cdot Z^2/A^{1/3} - A_a \cdot (N - Z)^2/A \pm \Delta$$

where: A – mass number, A_v – volume binding term, A_s – surface term, A_c – Coulomb term, A_a – asymmetry term, BE – binding energy, Δ – pairing term, Z – atomic number, N – neutron number.

These five adjustable parameters were obtained by fitting the formula to the experimentally determined values. There are significant differences between the values of the above five adjustable parameters reported by various authors [2-7], for example, 31% for the surface term and 28% for the asymmetry term.

Instead, in this paper is propose another approximation of binding energy per nucleon, BE, in the form of the difference of two simple exponential functions of mass number, A-1 (because BE of the nucleus of the lightest hydrogen isotope is equal to zero, then the ordinate should be shifted by one unit on the mass number scale, A).

$$\frac{BE}{A} = E_{extr} \cdot (e^{-\lambda \cdot (A-1)} - e^{-((\lambda \cdot C)/\alpha) \cdot (A-1)})$$

where: C – the Euler-Mascheroni constant, α – the Sommerfeld's fine structure constant, E_{extr} – extrapolation constant, e – a base of natural logarithm, λ – exponent of exponential function.

The three applied constants terms (*i.e.* two exponents: λ and $C/\alpha \cdot \lambda$ and proportionality coefficient, A_{extr}) are a simple combination of some mathematical and physical constants, and not need any fitting for observation.

This formula predicts the binding energy per nucleon for the mass number greater than 25 (Fig. – calculated values). For singular isobars the precision is sufficient, and only in the case of an isobaric triad the maximal error is equal to 2.4%.

References

[1]. Weizsacker C.F.: Z. Phys., 96, 431-458 (1935), in German.
[2]. Pitzer K.: Quantum Chemistry. J. Wiley, New York 1954, pp.409-411.
[3]. Friedlender G., Kennedy J.W.: Nuclear and Radiochemistry. J. Wiley, New York 1955, p.41.
[4]. Evans R.D.: The Atomic Nucleus. Mc Graw Hill, New York 1955; Reprint 1975, p.368.
[5]. Haissinsky M.: La chimie nucleaire et ses applications. Masson et Cie, Paris 1957, p.61, in French.
[6]. Williams W.S.C.: Nuclear and Particle Physics. Clarendon Press, Oxford 1992, p.60.
[7]. Lilley J.: Nuclear Physics. J. Wiley, Chichester-New York 2001, p.41.

RADIOLYTIC DEGRADATION OF HERBICIDE 4-CHLORO-2-METHYLPHENOXYACETIC ACID (MCPA) BY γ-RADIATION FOR ENVIRONMENTAL PROTECTION

Anna Bojanowska-Czajka, Przemysław Drzewicz, Grzegorz Nałęcz-Jawecki[1/], Józef Sawicki[1/], Czesław Kozyra[2/], Marek Trojanowicz

[1/] Department of Environmental Health Sciences, Warsaw University of Medicine, Warszawa, Poland
[2/] Organika Sarzyna SA, Nowa Sarzyna, Poland

Worldwide application of intensive methods in modern agriculture in the last few decades results in the presence of variety of agrochemicals in the environment. Many pesticides that are commonly used are resistant to natural degradation in the environment, hence, there is a great concern about possible adverse effects for human health and for equilibrium in ecosystems [1-3]. Chlorophenoxy herbicides, which have potential toxicity towards humans and animals [4], and are suspected mutagenes and carcinogens, are used worldwide on a large scale as plant growth regulator for agricultural and non-agricultural purposes. Among them, 4-chloro-2-methylphenoxyacetic acid (MCPA) is used in amounts exceeding 2000 tons per year in West European countries [5]. In commercial preparations it is used as dimethylammonium, potassium or sodium-potassium salts, very often in mixtures together with other chlorophenoxy pesticides (2,4-dichlorophenoxyacetic acid – 2,4-D, 3,6-dichlorophenoxyacetic acid – dicamba, 4-(4-chloro-2-methylphenoxy)butyric acid – MCPB), but also with other groups of pesticide compounds. In aqueous solutions, it occurs mainly in anionic form (pK_a=3.1), and its reported field half-life time ranges from 6 to 60 days, which is longer than, for instance, reported for 2,4-D or dicamba [6].

In the literature on degradation or removal of MCPA for environmental purposes, mostly photodegradation methods have been reported [7-10]. In electrochemical degradation, oxidation was carried out with hydroxyl radicals produced from Fenton's reaction between Fe(II) and hydrogen peroxide generated in anodic reaction that can be additionally accelerated using a photoperoxi-coagulation treatment under UV irradiation of solutions, providing more hydroxyl radicals [11]. Other methods reported in the literature include ultrasonic decomposition in an argon atmosphere [12], biodegradation using a microcosmic technique [13], and removal of MCPA from aqueous solutions by acid-activated spent bleaching earth, which is a solid waste from edible oil processing industry [14].

The aim of this work was to study chromatographically the effectiveness of degradation and to identify products of degradation of MCPA in synthetic aqueous solutions and industrial wastes from the production of this herbicide. The chromatographic determinations of MCPA and products of its radiolytic decomposition were determined in a reversed-phase high pressure liquid chromatography (RP-HPLC) system using a Shimadzu chromatograph with a diode array UV-VIS detector, using a column C18 Luna ODS2 (5 μm, 250×4.6 mm) and

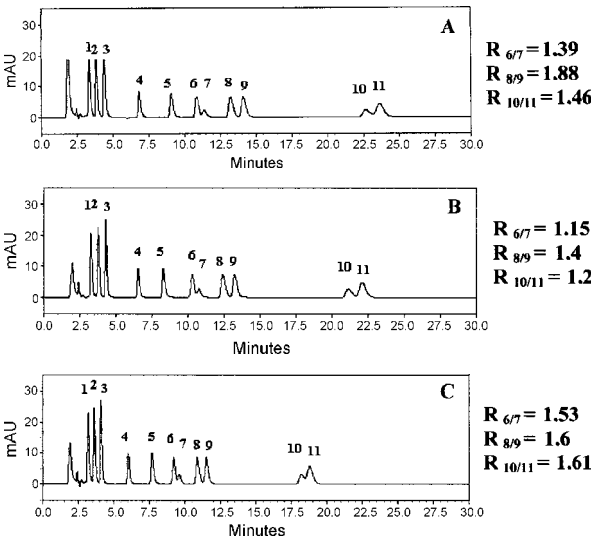

Fig.1. Effect of temperature on the separation of a mixture of standards containing 10 mg/l of each solute with UV detection at 280 nm. Eluent: 2 g/l citric acid with ACN-gradient program. Column: Phenomenex C18 Luna ODS2 (5 μM, 250×4.6 mm), flow rate – 1 ml/min. Peaks: (1) hydroquinone, (2) methylhydroquinone, (3) catechol, (4) phenol, (5) salicylic acid, (6) o-cresol, (7) MPA, (8) 4-chlorophenol, (9) 3-chlorophenol, (10) MCPA, (11) 4-chloro-2-methylphenol in different temperature: A – 25°C, B – 40°C, C – 65°C. R is resolution for indicated peaks.

a guard column from Phenomenex. The sample injection volume was 20 μL. Simultaneously, changes of toxicity of irradiated solutions were monitored using a commercial bioluminescence bacterial test Microtox.

The application of the developed earlier RP-HPLC isocratic method for simultaneous determination of 2,4-D and its main degradation products – chlorophenols [15], was not satisfactory for separation of MCPA and the main product of its degradation in mild conditions 4-chloro-2-methylphenol. In order to improve separation of these two analytes, the effect of temperature in isocratic conditions was examined. It was found that the separation does not depend practically on temperature (Fig.1). The next step in optimisation of separation was to examine two different gradient procedures. The separation was optimised for a mixture of MCPA

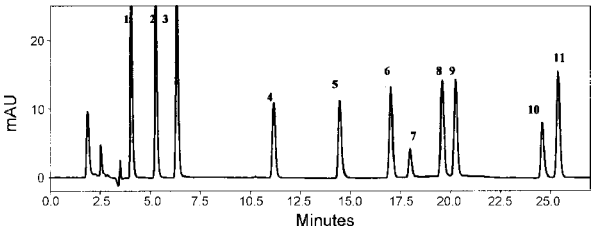

Fig.2. Chromatogram obtained for a mixture of standards containing 10 mg/l of each solute in optimized conditions with UV detection at 280 nm. Eluent: 2 g/l citric acid with ACN-gradient program. Column: Phenomenex C18 Luna ODS2 (5 μM, 250×4.6 mm), flow rate – 1 ml/min. Peaks: (1) hydroquinone, (2) methylhydroquinone, (3) catechol, (4) phenol, (5) salicylic acid, (6) o-cresol, (7) MPA, (8) 4-chlorophenol, (9) 3-chlorophenol, (10) MCPA, (11) 4-chloro-2-methylphenol.

with several chlorophenols, dihydroxybenzenes and 4-chloro-2-methylphenol. The optimum separation, illustrated by chromatogram shown in Fig.2 for the synthetic mixture, was obtained for the system with solution A containing 5% acetonitrile (ACN) in aqueous solution of citric acid g/l and B which was pure ACN. The linear change of solution A in the eluent was applied from 79 to 42% in 45 min. For all examined solutes a base-line resolution was obtained.

As MCPA is a weak acid (pK_a=3.1), the effect of pH value of irradiated MCPA solutions on effectiveness of radiolytic decomposition was examined. The experiments were carried out at pH values 1.5 (where MCPA is almost completely protonated), 7.0 and 11.5, where MCPA is present in anionic form. Initial solutions containing 100 ppm MCPA were irradiated with doses up to 4 kGy. It was found that the main product of radiolytic degradation of MCPA was identified as 4-chloro-2-methylphenol in these experimental conditions. Besides, 4-chloro-2-methylphenol as other products of radiolytic degradation of MCPA also catechol, phenol, o-cresol and 3-chlorophenol were identified, and their decomposition is also more effective in acidic than in neutral or alkaline solutions (Fig.3). As industrial wastes are strongly acidic, in practical applications no additional neutralisation would be required.

In order to examine the possibility of chemical enhancement of radiolytic degradation, the radiolytic decomposition of MCPA was carried out also

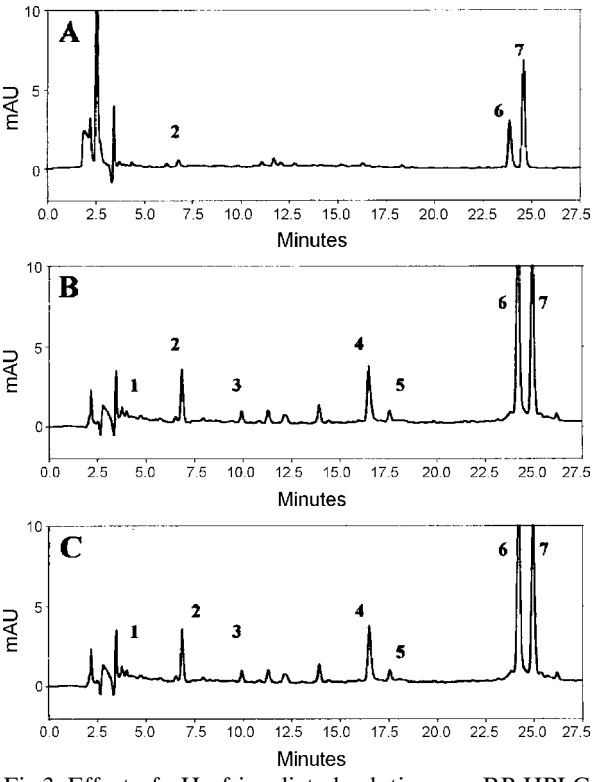

Fig.3. Effect of pH of irradiated solutions on RP-HPLC chromatograms for 100 ppm solution of MCPA obtained after γ-irradiation with 3 kGy dose: A – pH 1.5, B – pH 7.0, C – pH 11.5. Peak assignements: (1) hydroquinone, (2) catechol, (3) phenol, (4) o-cresol, (5) 4-chlorophenol, (6) MCPA, (7) 4-chloro-2-methylphenol.

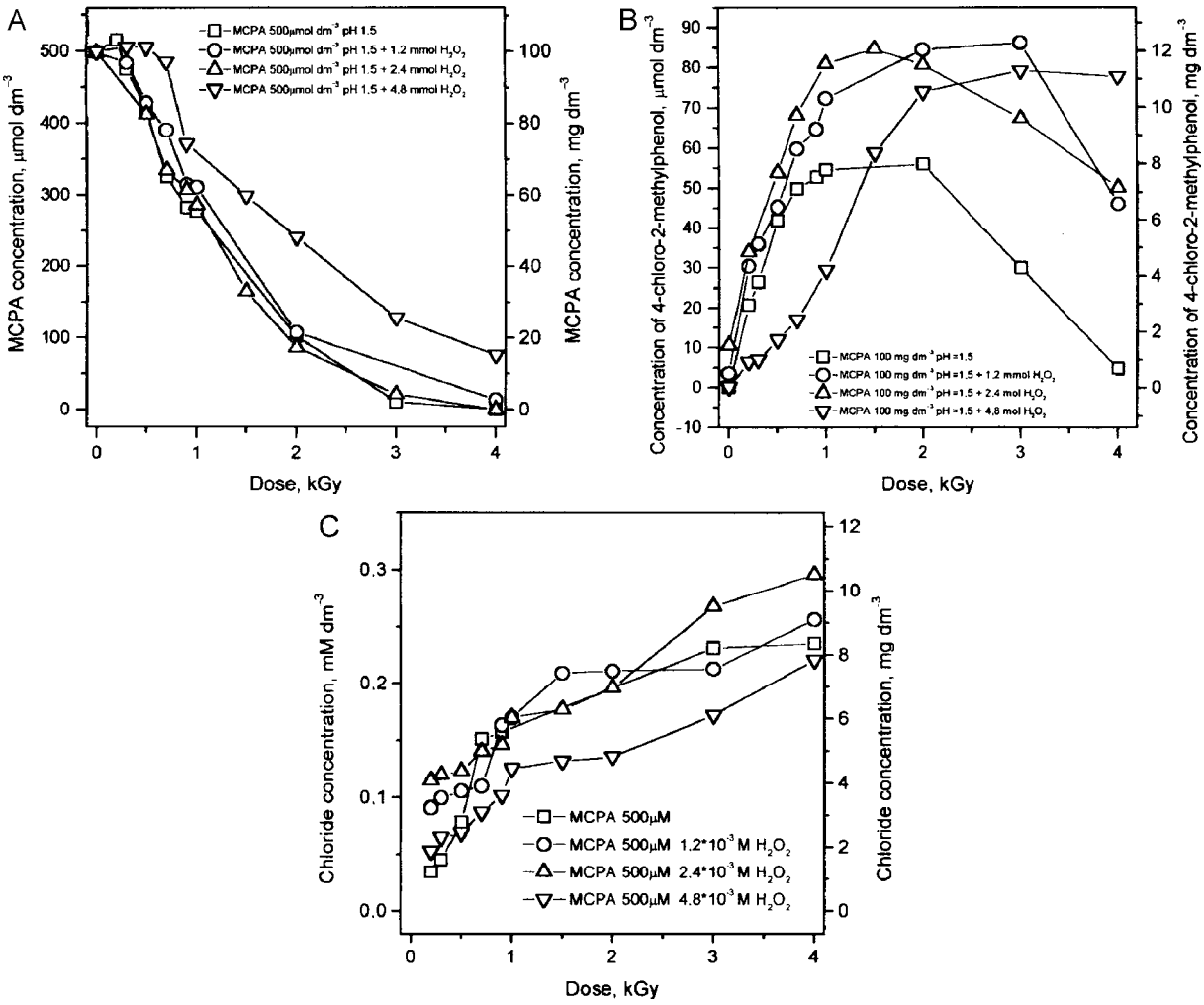

Fig.4. Yield of decomposition of MCPA (A) and formation of 4-chloro-2-methylphenol (B) and chloride (C) at different doses during γ-irradiation of 100 ppm solution of MCPA without hydrogen peroxide (□), in the presence of 1.2 mM hydrogen peroxide (○), 2.4 mM hydrogen peroxide (△) and 4.8 mM hydrogen peroxide (▽).

in the presence of 4.8 mM hydrogen peroxide, which is a stoichiometric amount needed for oxidation of 100 ppm MCPA and also smaller amounts 2.4 and 1.2 mM. As can be seen from Fig.4, at doses below 4 kGy the added hydrogen peroxide acts evidently as scavenger of hydroxyl radicals, giving less efficient decomposition of MCPA, and less effective formation of 4-chloro-2-methylphenol. The larger concentration of hydrogen peroxide, the larger scavenging effect was observed.

The effect of the presence of hydrogen peroxide in irradiated samples was also examined for samples of industrial waste from the production of MCPA. The consecutive steps of industrial synthesis of MCPA include condensation of sodium o-cresolate with chloroacetic acid in alkaline medium, which is followed by separation of 2-methylphenoxyacetic acid (MPA) by precipitation and acidification with hydrochloric acid, and by chlorination of MPA that leads to obtaining MCPA. The product is filtered and dried. The wastes disposed after filtration of MCPA were taken for treatment with γ-radiation. The effect of irradiation dose up to 10 kGy on decomposition of MCPA, and the product of its radiolytic degradation in irradiated waste is shown in Fig.5. Contrary to irradiation of pure MCPA solutions, almost in each examined case the addition of hydrogen peroxide, in this measurements used at 39 mM (1.32 g/l) level, affected positively the yield of processes. Complete decomposition of MCPA without hydrogen peroxide was observed at 10 kGy, while in the presence of hydrogen peroxide already half of this dose was sufficient for complete decomposition of MCPA. A substantial positive effect of addition of hydrogen peroxide was observed in case of decomposition of 3-chlorophenol and especially 4-chloro-2-methylphenol.

For examination of the effect of matrix components in wastes on yield of irradiation process, also irradiation of pure MCPA solutions were carried out at the same level as it was found in industrial waste from synthesis of MCPA. Irradiation of this solution was carried out at three different levels of added hydrogen peroxide 19, 39 and 58 mM. As it is illustrated by data plotted in Fig.6, the yield of degradation of MCPA was evidently better at the same doses in waste matrix than in pure water. For synthetic aqueous solutions of MCPA, addition of hydrogen peroxide at three different levels practically does not affect the yield of decomposition. One may conclude that hydrogen peroxide added in case of wastes may significantly accelerate decomposition of 4-chloro-2-me-

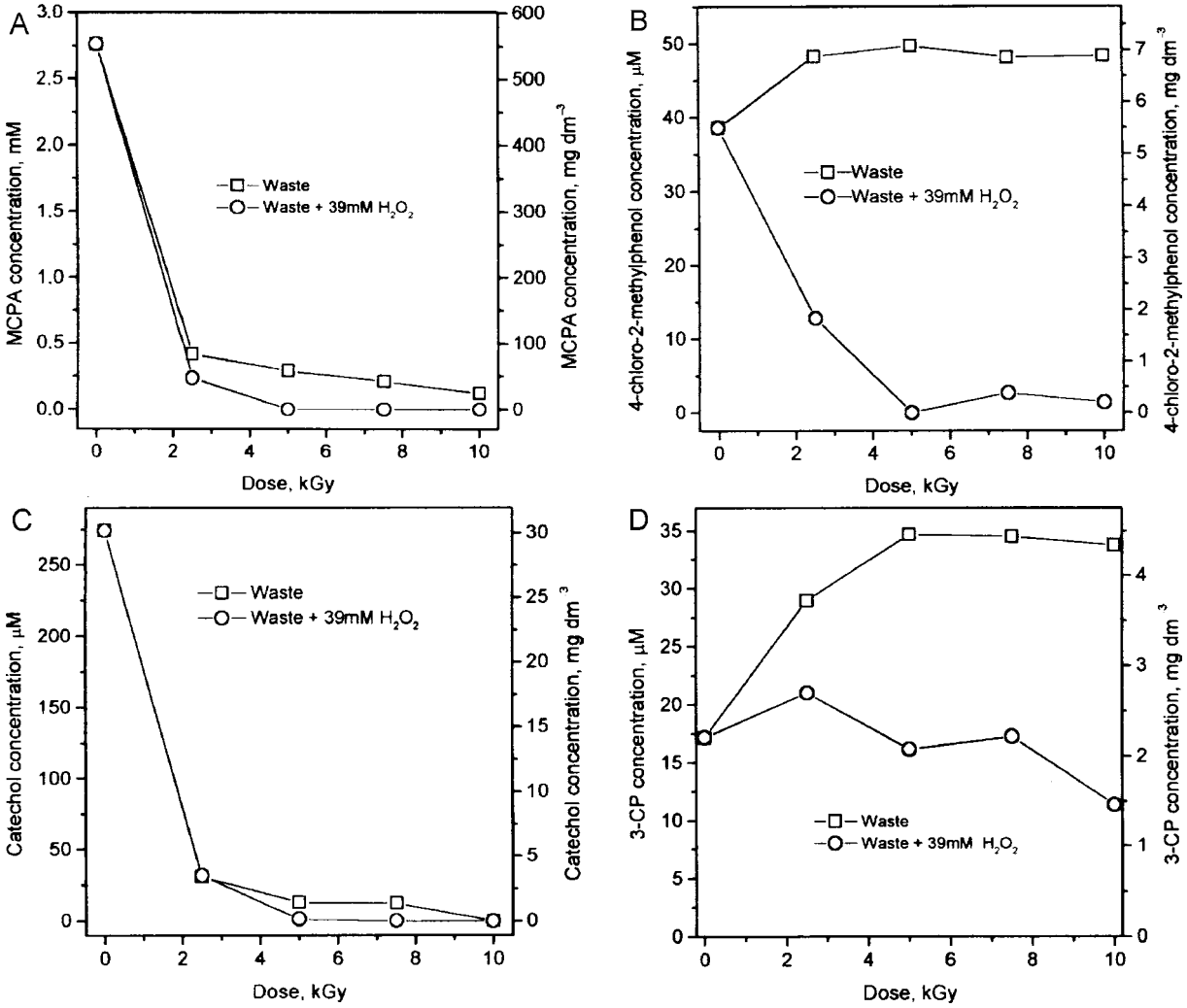

Fig.5. Decomposition of MCPA (A) and formation of 4-chloro-2-methylphenol (B), catechol (C) and 3-chlorophenols (D) at different doses during γ-irradiation of waste from production of MCPA without hydrogen peroxide (□), and with 39 mM hydrogen peroxide (○).

thylphenol or 4-chloro-2-methylphenol is not formed, because decomposition of MCPA occurs in the presence of waste constituents in different mechanisms with participation of other radical species formed during irradiation. One of the possible hypothesis is participation in these processes of chloride, present in high concentration in wastes 81 g/dm^3. For the reaction: $Cl^- + OH^\bullet \leftrightarrow ClOH^-$ there are

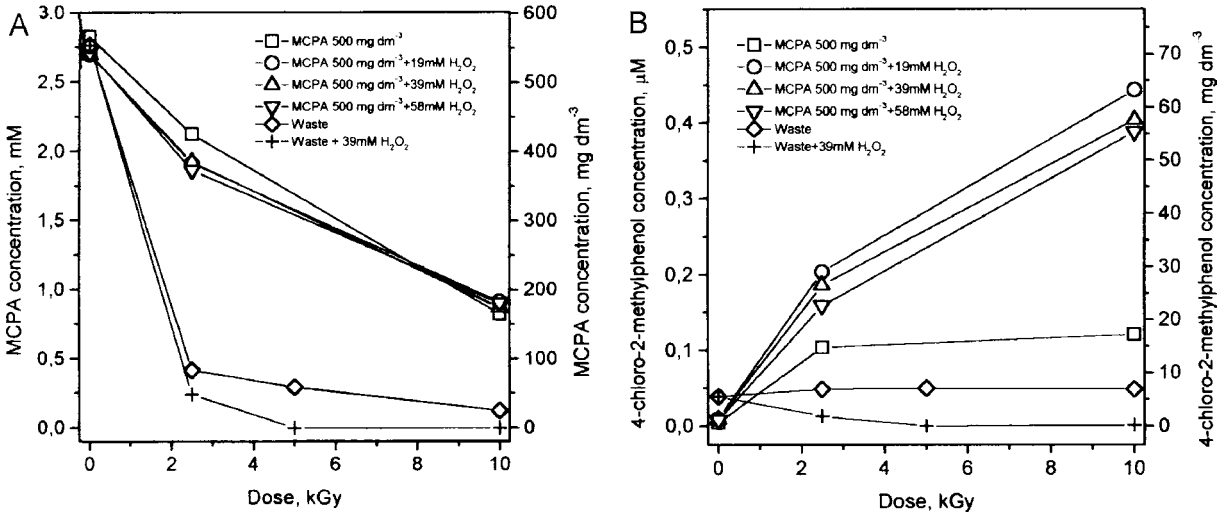

Fig.6. Decomposition of MCPA (A) and formation of 4-chloro-2-methylphenol (B) during irradiation of solution 500 mg dm^{-3} MCPA (□), 500 mg dm^{-3} MCPA with 19 mM hydrogen peroxide (○), 500 mg dm^{-3} MCPA with 39 mM hydrogen peroxide (△), 500 mg dm^{-3} MCPA with 58 mM hydrogen peroxide (▽), waste (◇), waste with 39 mM hydrogen peroxide (+).

known rate constants $K_+ = 4.3 \times 10^{10}$ $M^{-1}s^{-1}$ and in reverse direction $K_- = 6 \times 10^9$ $M^{-1}s^{-1}$ [16]. Formation of strong oxidants $HClO_2$ and $HClO_4$ [17] may accelerate oxidation of MCPA in waste compared to pure aqueous solutions.

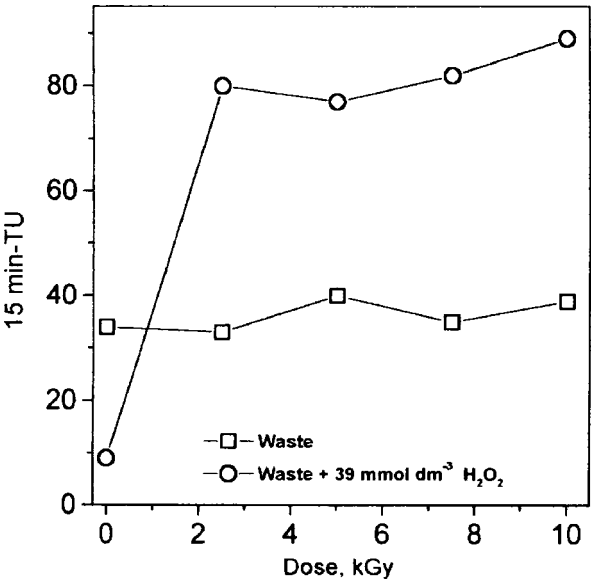

Fig.7. Changes of toxicity of irradiated waste from production of MCPA without hydrogen peroxide (□) and with hydrogen peroxide in irradiated solution (○).

In the irradiated sample of industrial waste without addition of hydrogen peroxide the toxicity level was practically not changed in the dose range up to 10 kGy (Fig.7). After addition of hydrogen peroxide to raw waste prior to irradiation, the toxicity of waste solution has decreased by about 70%. Irradiation of this sample containing hydrogen peroxide resulted, however, in about ten fold increase of toxicity at doses above 2 kGy. The exact reason of this significant change is not known, as yet. It can be caused not only by products of radiolytic degradation of MCPA, but also by products of other reactions taking place in irradiated waste. Formation of other toxic compounds such as chlorinated alkanocarboxylic acids may be responsible for this effect and requires further investigation.

References

[1]. Environmental Chemistry of Herbicides. Eds. R. Grover, A.J. Cessna. CRC Press, Boca Raton 1991.
[2]. Hodgson E., Levi P.E.: Environ. Health Perspect., 104, 97 (1996).
[3]. Blair A., Malker H., Cantor K., Burmeister L., Wiklund K.: J. Work Environ. Health, 11, 397 (1985).
[4]. Hoar S.K., Blair A., Holmes F.F., Boysen C.B., Robel J.R., Hoover R., Fraumeni H.: J. Am. Med. Assoc., 256, 1141 (1986).
[5]. Fielding M., Barcelo D., Helweg A., Torstennson L., van Zoonen P., Angeletti G.: Pesticides in Ground and Drinking Water (Water Pollution Research Report, 27). Commission of the European Communities, Brussels 1992, pp.1-136.
[6]. Hornsby A.G., Wouchope R.D., Herner A.E.: Pesticide Properties in the Environment. Springer Verlag, New York 1996.
[7]. Soley J., Vicente M., Clapés P., Esplugas S.: Ind. Eng. Chem. Prod. Res. Dev., 25, 645 (1986).
[8]. Clapés P., Soley J., Vicente M., Rivera J., Caixach J., Ventura F.: Chemosphere, 15, 395 (1986).
[9]. Topalov A., Abramovic B., Molnar-Gabor D., Csanadi J., Arcson A.: J. Photochem. Photobiol., 140, 249 (2001).
[10]. Brillas E., Boye B., Dieng M.M.: J. Electrochem. Soc., 150, 583-589 (2003).
[11]. Boye B., Brillas E., Dieng M.M.: J. Electroanal. Chem., 540, 25 (2003).
[12]. Fujita T., Ona E.P., Kojima Y., Matsuda H., Koda H., Tanahashi N., Asakura Y.: J. Chem. Eng. Jpn., 36, 806 (2003).
[13]. Harrison L., Leader R.U., Higgo J.J.W., Williams G.M.: Chemosphere, 36, 1211 (1998).
[14]. Mahramanlioglu M., Kizilcikli I., Bicer I.O., Tuncay M.: J. Environ. Sci. Health, Part B, B38, 813 (2003).
[15]. Drzewicz P., Trojanowicz M., Zona R., Solar S., Gehringer P.: Radiat. Phys. Chem., 69, 281 (2004).
[16]. von Gunten U.: Wat. Res., 37, 1469 (2003).
[17]. Getoff N.: Peroxyl Radicals in the Treatment of Waste Solutions. In: Peroxyl Radicals. Ed. Z. Alfassy. Wiley, Chichester 1997, pp.483–506.

PROGRESS IN THE DETECTION OF IRRADIATED FOODSTUFFS IN THE INCT

Wacław Stachowicz, Kazimiera Malec-Czechowska, Katarzyna Lehner

In recent period, the Laboratory for Detection of Irradiated Foods (Institute of Nuclear Chemistry and Technology – INCT) notes a significant increase of the number of foodstuffs delivered by various firms and institutions from the country and from abroad to be examined whether were or were not treated with ionising radiation. In 2003, the total number of samples analysed in the Laboratory was 122, while this year the number approaches 540 (Fig.1). The majority of samples comes from Germany, but we receive a lot of foodstuffs for analysis from Italy, the United Kingdom, Thailand. The number of samples delivered in 2004 from the country amounts to about 140 and reflects the growing tendency, too. It has to be noted that the majority of the samples is examined by the thermoluminescence method (European Standard PN-EN 1788 [1]). It is mainly so because of the assortment of samples

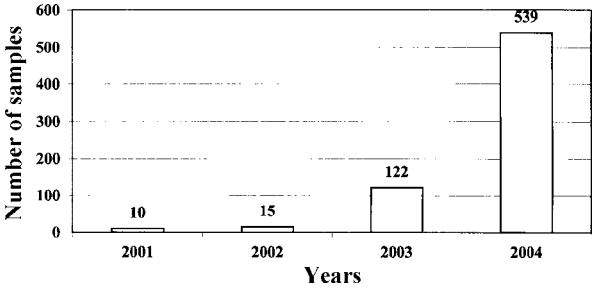

Fig.1. The number of food samples analysed in the Laboratory from 2001 to 2004.

delivered. However, this year about 5% of samples was analysed by the electron paramagnetic resonance (EPR) method, too (European Standards PN-EN 1786 [2] and PN-EN 1787 [3]). A significant increase of the number of orders for the detection of irradiation in various foodstuffs has probably its source in the execution of the European Union (EU) Commission requirements, Directives 1999/2/EC [4] and 1999/3/EC [5]. The Directives regulate the condition of radiation treatment and distribution of irradiated foods within the EU countries. Actually, it is allowed to distribute within the European food market only three groups of foodstuffs treated with ionising radiation. These are herbs, spices and seasonings. All other products cannot be legally distributed in Europe. The Directive 1999/2/EC states in addition that all irradiated food products should be labelled including those containing the irradiated stuff as small admixture to the other non-irradiated ingredients that appear in abundance. It is why more and more blends and composed food products containing spices and herbs is delivered to the Laboratory for the analysis in this year. Under this new situation, the Laboratory is faced today how to analyse complex samples to obtain reliable results and how to treat those samples which cannot deliver reliable results and hence, will not undergo classification whether irradiated or non-irradiated. The problem finds very often its solution in the modification of the preparation technique leading to more effective isolation of mineral fraction and/or in the increase of the mass of a single sample to be examined. Sometimes, however, the separation of silicate minerals remains still unsuccessful. Under such condition, the examination of a sample is not satisfactory and thus the test report cannot include the statement whether sample was or was not irradiated. According to the Laboratory instruction clients include to the order or attach an additional sheet with information on the composition of the sample and its state (for example fine powder). As a rule, if such information is not included, the Laboratory ask the client to deliver it by fax or e-mail. Having a practice, concerning the treatment of typical complex and powdered samples, the Laboratory can expect in advance that serious analytical problems may appear with some samples. Thus, we inform the client in advance that such situation may appear and the receiving of reliable result of the analysis may be rather problematic. Nevertheless, until now in all these cases the clients decided to continue the examination on their own risk. Among *ca*. 50 samples of this kind analysed this year in the Laboratory, 18 remained unclassified.

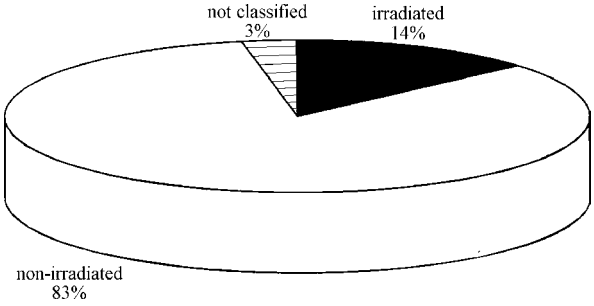

Fig.2. Classification of food samples delivered to the Laboratory in 2004.

It seems necessary today to proceed the work on the modification or development of detection methods that meet the requirement of complex foodstuffs.

Among 539 food samples analysed this year 83% were found not to be irradiated, 14% irradiated, while 3% samples remained not classified (Fig.2).

The assortment of foodstuffs that were examined in 2004 (Fig.3) compiles:

- spices and herbs and blends that contain small admixture of irradiated spices added to non-irradiated stuff (39%);
- seasonings, vegetables and sauces containing spices (29%);
- fresh shrimps (13%);
- powdered herbal pharmaceutics (13%);
- some other products like herbal extracts, bone containing foods (poultry and fish) and nuts in shell (6%).

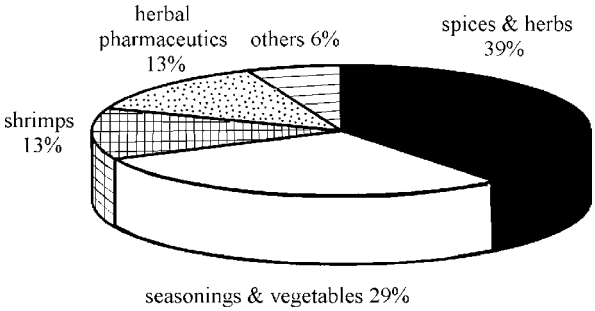

Fig.3. The assortment of food products analysed in the Laboratory in 2004.

In accordance with EU regulation, the Chief Sanitary Inspector of Poland obliged this year the heads of the Sanitary-Epidemiological Stations of all 16 Poland's provinces (voivodeship) to provide the control of the irradiation of imported food products in their regions. The INCT Laboratory is the only one in the country that is responsible for the examination of these products and authorised to issue the test reports with the classification of a products whether irradiated or not.

References

[1]. PN-EN 1788:2002. Foodstuffs – Thermoluminescence detection of irradiated food from which silicate minerals can be isolated.

[2]. PN-EN 1786:2000. Foodstuffs – Detection of irradiated food containing bone. Method by ESR spectroscopy.

[3]. PN-EN 1787:2001. Foodstuffs – Detection of irradiated foods containing cellulose. Method by ESR spectroscopy.

[4]. Directive 1999/2/EC, 22 February 1999 on the approximation of the Member States concerning food and food ingredients treated with ionising radiation. Off. J. European Communities L 66/16-23 (13.3.1999).

[5]. Directive 1999/3/EC, 22 February 1999 on the establishment of Community list of food and food ingredients treated with ionising radiation. Off. J. European Communities L 66/24-25 (13.3.1999).

DETECTION OF IRRADIATED SPICES ADDED TO MEAT PRODUCTS

Kazimiera Malec-Czechowska, Wacław Stachowicz

Detection of admixtures in irradiated spices and herbs to reprocessed meat products is today a crucial analytical problem in view of European Union (EU) regulations defined in Directive 1999/2/EC [1] and in the decree issued by the Polish Ministry of Health on 15th January 2003 [2], respectively. Both documents refer to food and food ingredients treated with ionising radiation which must be labelled, while only herbs, spices and seasonings are allowed to be present in EU food market. Our proposal is to apply a method based on the thermoluminescence (TL) measurements of silicate minerals separated from foodstuff. The method is standardised to food products which contain silicate minerals but refers rather to food articles irradiated in the bulk (PN-EN 1788) [3]. Model samples of meat products with a known content of irradiated spices have been prepared in the Laboratory for Detection of Irradiated Foods (Institute of Nuclear Chemistry and Technology – INCT). Hundred grams of ground mixed (pork and beef) meat was taken to form forcemeat balls with an admixture of spices. The irradiated spices were: powdered sharp paprika exposed to 7 kGy of gamma rays in a ^{60}Co source "Issledovatel" of the Department of Radiation Chemistry and Technology (INCT) and powdered black pepper exposed to 6 kGy of 7 MeV electron beam generated in the linear electron accelerator "Elektronika 10-10" installed in the Experimental Plant for Food Irradiation (INCT).

The concentration of irradiated components in the samples of meat was 0.1, 0.3, 0.5 and 1.0%, respectively. In parallel, the samples which contained 0.1% of non-irradiated spices were also prepared.

In order to isolate silicate minerals from the samples, the hydrolysis with 6 mol/l of aqueous HCl solution was applied. The sample (forcemeat ball) was placed in a round button beaker, treated with HCl solution and heated at 50°C ±5°C in a water bath during 3 hours. Then the pulp was diluted with re-distilled water and filtered through nylon sieves 125 mesh. From the filtrate, the mineral fraction was separated by sedimentation technique. In order to separate the silicate minerals, the procedure given in the PN-EN 1788 standard and in our earlier publications was applied [4,5].

The TL of silicate minerals was measured with the use of a TL reader (model TL/OSL; Risø National Laboratory, Denmark). The measuring conditions were similar to those routinely used in the Laboratory [4,5]. After Glow 1 curve has been recorded, the minerals were irradiated with a normalised dose of 1 kGy in the gamma source. Subsequently, Glow 2 curve was registered.

For the evaluation of samples whether irradiated or not, a criterion given in PN-EN 1788 standard was adapted. The shapes of both Glow 1 and Glow 2 TL curves were analysed, while the integrated glow ratio was calculated within the temperature range 214-284°C. The TL maximum be-

Table 1. TL intensities (Glow 1 and Glow 2) integrated over the temperature range 214-284°C and TL glow ratio of silicate minerals isolated from control samples of minced meat enriched with 0.1% of non-irradiated pepper, and at different concentrations of pepper irradiated with 6 kGy by electron beam.

Percentage of pepper	TL intensity Glow 1 (214-284°C)	TL intensity Glow 2 (214-284°C)	TL glow ratio Glow 1/Glow 2 (214-284°C)
0.1 non-irradiated	12164	2436800	0.005
	9726	1200208	0.008
	8456	944000	0.009
0.1 irradiated	2036547	817409	2.49
	9130432	4929884	1.84
	7323815	3421138	2.14
0.3 irradiated	25390016	14747925	1.72
	24579191	8747223	2.81
	20873128	9324815	2.23
0.5 irradiated	20849992	6841794	3.05
	11778646	4110629	2.86
	15469327	5708239	2.71
1.0 irradiated	2949100	951925	3.10
	64210162	17189166	3.73
	117434465	4270358	2.75

Table 2. TL intensities (Glow 1 and Glow 2) integrated over the temperature range 214-284°C and TL glow ratio of silicate minerals isolated from control samples of minced meat enriched with 0.1% of non-irradiated paprika and at different concentrations of paprika irradiated with 7 kGy of gamma rays.

Percentage of paprika	TL intensity Glow 1 (214-284°C)	TL intensity Glow 2 (214-284°C)	TL glow ratio Glow1/Glow2 (214-284°C)
0.1 non-irradiated	10469	4068323	0.002
	7232	2169605	0.003
	14853	2970615	0.005
0.1 irradiated	3690910	2553301	1.44
	8183133	5355352	1.53
	5162432	4266473	1.21
0.3 irradiated	13224788	13036892	1.01
	15978387	17316917	0.92
	14539337	13701104	1.06
0.5 irradiated	27581269	24000815	1.15
	3897257	2938503	1.33
	12212577	11806334	1.03
1.0 irradiated	2550077	2773775	0.92
	12261268	14803812	0.83
	8347283	7258507	1.15

tween 150 and 250°C is a proof of irradiation. The TL maximum recorded over 300°C originates from natural luminescence. Glow 1/Glow 2 ratio higher than 0.1 proves a typical radiation treatment of a sample. In the case when glow ratio is lower than 0.1 while the shape of Glow 1 curve is typical of an irradiated sample (maximum between 150 and 250°C) the decisive is the shape proving that the sample was irradiated.

In Tables 1, 2 and in Fig.1, the results of the TL analysis of minerals separated from model samples were comprehended. It has been proven that the concentration of irradiated paprika and pepper powders in meat at a level of 0.1% and higher are detectable by the TL method. The shapes of the Glow 1 curves have the maxima between 150 and 250°C, while the respective glow ratios were always higher than 0.1 despite the dose applied and the irradiation source used. The results document and show conclusively that the TL method could be successfully used for the detection of irradiated admixtures (spices and herbs) to meat products.

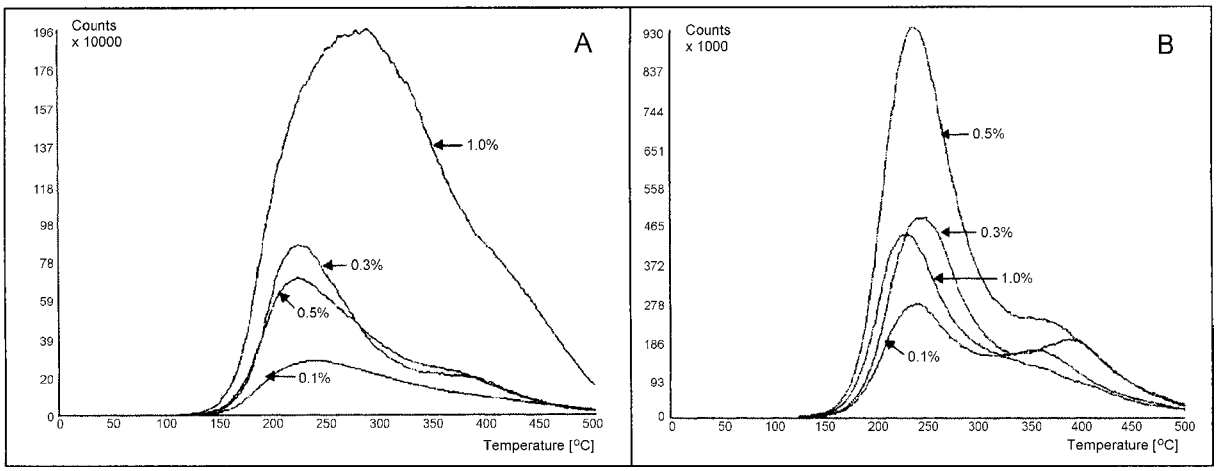

Fig.1. TL Glow 1 curves of silicate minerals isolated from the samples of minced meat containing: (A) different concentrations of pepper irradiated with a dose of 6 kGy of electron beam radiation and (B) different concentrations of paprika irradiated with a dose of 7 kGy of gamma radiation.

References

[1]. Directive 1999/2/EC, 22 February 1999 on the approximation of the Member States concerning foods and food ingredients treated with ionising radiation. Off. J. European Communities L 66/16-23 (13.3.1999).

[2]. Rozporządzenie Ministra Zdrowia z dnia 15 stycznia 2003 r. w sprawie warunków napromieniowania środ-

ków spożywczych, dozwolonych substancji dodatkowych lub innych składników żywności, które mogą być poddane działaniu promieniowania jonizującego, ich wykazów, maksymalnych dawek napromieniowania oraz wymagań w zakresie znakowania i wprowadzania do obrotu. Dz. U. z 2003 r. Nr 37, poz. 327.
[3]. Standard PN-EN 1788:2002. Foodstuffs – Thermoluminescence detection of irradiated food from which silicate minerals can be isolated.
[4]. Malec-Czechowska K., Strzelczak G., Dancewicz A.M., Stachowicz W., Delincée H.: Eur. Food Res. Technol., 216, 157-165 (2003).
[5]. Malec-Czechowska K., Stachowicz W.: Nukleonika, 48, 3, 127-132 (2003).

PROPERTIES OF THE FILMS BASED ON MILK PROTEINS RELATED TO THE INTERACTION IN THE NON-IRRADIATED AND GAMMA-IRRADIATED PROTEIN-POLYSACCHARIDE SYSTEM

Krystyna Cieśla, Stephane Salmieri[1/], Monique Lacroix[1/]

[1/] Canadian Irradiation Center, Research Laboratories in Sciences Applied to Food, INRS-Institute Armand Frappier, University of Quebec, Laval, Canada

Our work concerns the current problem of the edible packaging materials and methods for improvement of their functional properties using modified composition and gamma irradiation [1-4]. Our previous results dealing with the films prepared using non-irradiated and irradiated solutions of calcium caseinate-whey protein isolate (WPI)-glycerol (1:1:1) have shown that improvement of the films properties after irradiation corresponds to the changes in protein conformation. Reorganisation of aperiodic helical phase and β-sheets, in particular the increase in β-strands content [3] was discovered after irradiation. It was also found that addition of polysaccharides (at the level of 10% of total protein mass) led to an essential modification of films properties [4].

The present studies were directed to the interaction between calcium caseinate and WPI taking place in a mixed calcium caseinate-WPI-glycerol system. For this purpose, the properties of gels formed in the presence of calcium salt using a mixed composition were examined and related to the properties of gels prepared using separately calcium caseinate and WPI. Modification resulting in this composition after irradiation were related to the structural changes occurring in calcium caseinate-glycerol and in WPI-glycerol compositions. Moreover, the studies were carried out concerning the influence of polysachaccharide addition on the properties of gels formed using non-irradiated and irradiated proteins. The following polysaccharides were selected for this purpose: potato starch, soluble potato starch and sodium alginate. Structural properties of proteins and interactions with polysaccharides in gels were related to the functional properties and microstructure of the films resulting as the final product.

Calcium caseinate (New Zealand Milk Product Inc.) and WPI (BiPro Davisco) and chemical grade glycerol were used. Potato starch, soluble potato starch and sodium alginate were all Sigma products. Irradiation of solutions was carried out with gamma rays from Co-60 applying a dose of 32 kGy at a dose rate of 7 Gys^{-1}. The control non-irradiated solutions, were also prepared. Gel formation in calcium salt solutions and gel fracture strength measurements were realised according to the procedure described in [2,4]. The films were prepared and examined according to the procedures described in [1] and [4]. In particular, water vapour permeability (WVP) and puncture strength were determined.

FTIR (Fourier transform infrared spectroscopy) measurements were done using a Perkin-Elmer spectrophotometer in conditions described in [3]. TEM (transmission electron microscopy) studies were carried out using a Hitachi 7100 transmission electron microscope. A Stevens LFRA Texture Analyser Model TA/100 was applied for mechanical measurements of gels and films. The SAS statistical package was applied to analyse statistically the results dealing with gel fracture strength and functional properties of the films [1,4]. Differences between means were considered significant when $p \leq 0.05$.

The irradiation increased capability to connect calcium ions by mixed calcium caseinate-WPI system results due to the increase in β-structure content and to its further ordering [3], accompanied by a decrease in the content of aperiodic phase and turns rather than α-helices. It is connected to the fact that calcium binding leading to gel formation is more possible in the cases when the more strongly crosslinked β-sheets and β-strand are present.

Table 1. Strength of gels formed after addition of calcium salt to the non-irradiated and irradiated proteins compositions. Means followed by different letters are significantly different.

Dose [kGy]	CC[1)]	WPI	CC[1)]-WPI
0	16.7 ± 2.0^{a}	189.7 ± 10.4^{d}	48.0 ± 4.7^{b}
32	120.9 ± 7.0^{c}	293.3 ± 2.0^{e}	413.6 ± 30.5^{f}

[1)] calcium caseinate.

Gels formed after addition of calcium salt to the non-irradiated calcium caseinate are soft (Table 1) in regard to the small content of β-structure in these proteins resulting after heating. On the contrary, large strength of gels formed using the non-irra-

diated WPI shows a high efficiency in the formation of crosslinked β-structure during heating. The strength of gels, prepared using calcium caseinate--WPI composition, considerably smaller than the average value obtained separately in the case of calcium caseinate and WPI gels can be attributed to the smaller content of β-structure in the mixed system than can be expected considering contribution of the two components.

Addition of any polysaccharide does not induce the essential change in strength of gels prepared using the non-irradiated proteins solution, although the differences were found between the properties of the films formed using these solutions (Table 2). Addition of potato starch and sodium alginate to the irradiated solution induces a decrease in gel strength (Figs.1 and 2). On the contrary, addition of soluble potato starch led to the formation of stronger gels (Figs.1 and 2). Comparison of the action of particular polysaccharides shows that the gels containing polysaccharides are softer in these cases when the corresponding films were stronger and had better barrier properties (shown by the higher tensile strength and lower WVP value, respectively). Moreover, a linear dependence was found between the average values of gels strength prepared after addition of polysaccharide and the average values of puncture strength (Fig.1) and WVP (Fig.2). This result was related to the compatibility between proteins and polysaccharides in solution increasing in the following sequence: sodium alginate<potato starch<soluble potato starch.

Table 2. Strength of gels and properties of films (tensile strength and WVP) produced using the non-irradiated calcium caseinate-WPI solutions. Means followed by different letters in each column are significantly different.

Composition	Gel strength [N]	Tensile strength of films [Nmm]	WVP of films [g·mm/m^2·d·mm Hg]
CC-WPI[1)]	48.0 ± 4.7^b	53.9 ± 2.6^b	168.6 ± 10.1^c
CC-WPI-PS[2)]	42.7 ± 5.0^a	52.3 ± 2.6^b	133.1 ± 9.7^b
CC-WPI-SPS[3)]	46.2 ± 2.6^b	41.0 ± 3.4^a	171.9 ± 12.0^c
CC-WPI-Al[4)]	48.2 ± 3.0^b	60.1 ± 4.1^c	113.8 ± 7.2^a

[1)] calcium caseinate-WPI.
[2)] calcium caseinate-WPI-potato starch.
[3)] calcium caseinate-WPI-soluble potato starch.
[4)] calcium caseinate-WPI-sodium alginate.

Irradiation induces a 7.2-fold increase in strength of calcium caseinate gels and a 1.6-fold increase in strength of WPI gels. The difference between the irradiation effect confrms the much higher efficiency of irradiation in the formation of crosslinks between caseinate than between WPI chains. The increase in gel strength, after irradiation of calcium caseinate-WPI composition, larger (8.6-fold) than separately for calcium caseinate and WPI demonstrates a higher efficiency of crosslinking taking place in the mixed proteins composition than separately in calcium caseinate and in WPI. This conclusion is confirmed by the higher strength of gels obtained in the case of calcium caseinate-WPI than the value obtained by summarising the contribution from both proteins (207.2 N).

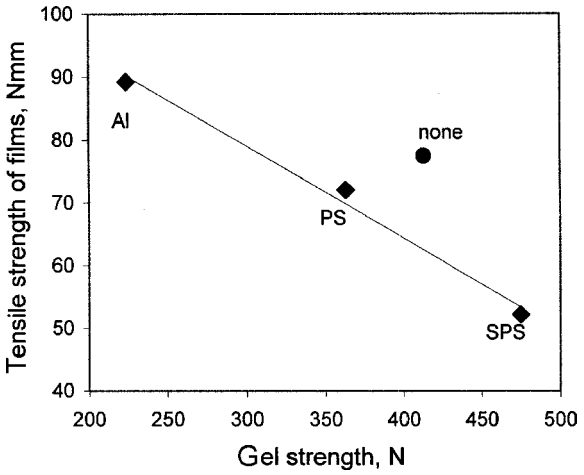

Fig.1. Dependence of the mean values of WVP obtained for the calcium caseinate-WPI films containing polysaccharides on the mean strength of gels formed after addition of $CaCl_2$: Al – alginate, PS – potato starch, SPS – soluble potato starch. Additionally, the point shown is representing pure calcium caseinate-WPI composition.

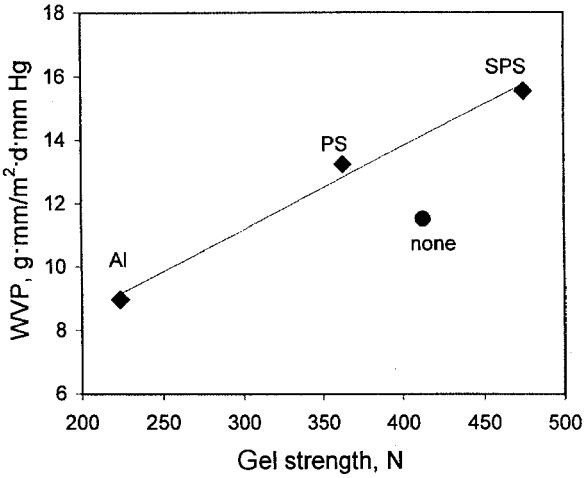

Fig.2. Dependence of the mean values of puncture strength obtained for the calcium caseinate-WPI films containing polysaccharides on the mean strength of gels formed after addition of $CaCl_2$: Al – alginate, PS – potato starch, SPS – soluble potato starch. Additionally, the point shown is representing pure calcium caseinate-WPI composition.

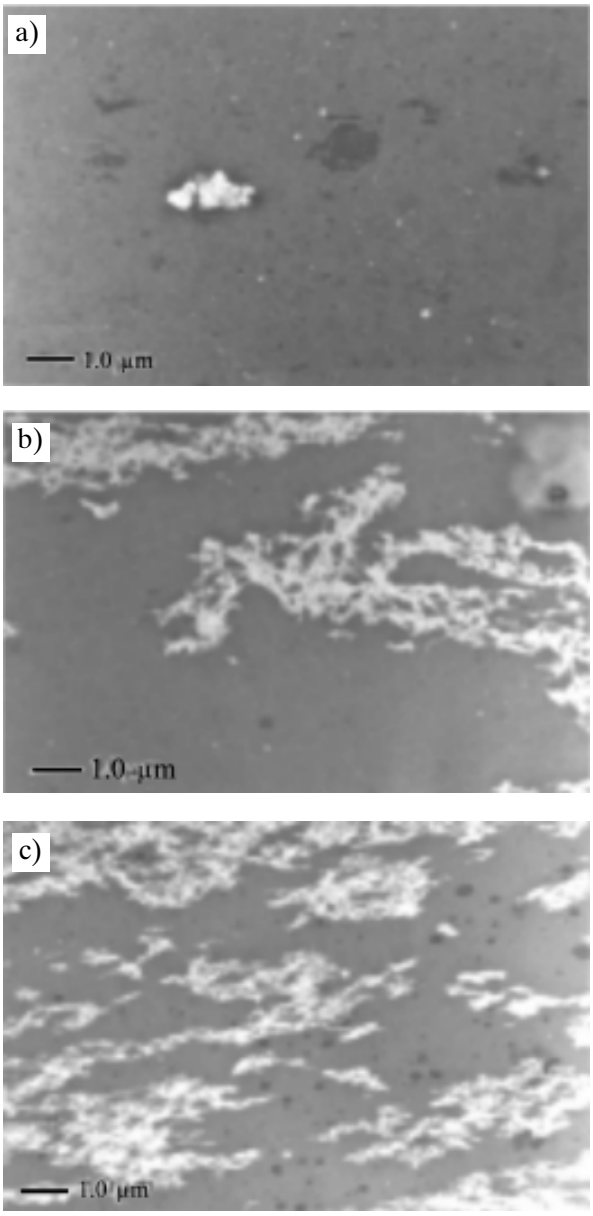

Fig.3. TEM photos of the selected films: a) control calcium caseinate-WPI, b) control calcium caseinate-WPI-alginate, c) calcium caseinate-WPI-alginate irradiated with a 32 kGy dose.

Examination of the film microstructure by TEM has indicated on the granular structure of the calcium caseinate-WPI films, with the presence of small holes and some spots (Fig.3). No particular differences were noticed between the irradiated and non-irradiated films, except that none spots and slightly more holes, but with smaller dimensions, were present in the irradiated film as compared to those present in the non-irradiated ones.

The films prepared using the non-irradiated solution with an additive of sodium alginate have revealed the appearance of some incorporated material with bonded chain structure (Fig.3). Distribution of these chains was more homogeneous in all the bulk material in the films obtained after addition of sodium alginate to the irradiated solution. Orientation of the chains in direction parallel to the film surface is also improved after irradiation.

Our results have shown that the interaction with caseinate has negative effect on binding of calcium ions to the control WPI and that radiation-induced formation of the strongly bonded β-strands occurs more effectively in the mixed calcium caseinate-WPI composition than separately in calcium caseinate or in WPI composition. Using of the irradiated mixed composition is expected thus to lead to films with better properties than using these proteins irradiated separately. It was also found that better films were obtained after addition of polysaccharide (potato starch, soluble potato starch or sodium alginate) in the case of the higher incompatibility of the protein-polysaccharide pair in solution. The improvement of the irradiated films properties after addition of alginate results moreover due to the stiffening of the proteins chain in the incorporated alginate network. More homogeneous distribution of the alginate network within the irradiated proteins network results in the improvement of the functional properties of the final films.

The financial support of the International Atomic Energy Agency (fellowship of Krystyna Cieśla, C6/POL/01003P) enabling to perform experiments with films is kindly acknowledged.

References

[1]. Brault D., D'Aprano G.D., Lacroix M.: J. Agric. Food Chem., 45, 2964-2969 (1997).
[2]. Ressouany M., Vahon C., Lacroix M.: J. Agric. Food Chem., 46, 1618-1623 (1998).
[3]. Cieśla K., Salmieri S., Lacroix M., Le Tien C.: Radiat. Phys. Chem., 71, 95-99 (2004).
[4]. Cieśla K., Salmieri S., Lacroix M.: Modification of the milk proteins films properties by gamma irradiation and starch polysaccharides addition. J. Sci. Food Agric., submitted.

POLYESTER FILMS MODIFIED BY CHEMICAL COMPOSITION AND PHYSICAL TREATMENT STUDIED BY X-RAY DIFFRACTION METHODS

Krystyna Cieśla, Ryszard Diduszko[1/]

[1/] Industrial Institute of Electronics, Warszawa, Poland

Thermal treatment is a well known method applied for modification of polymer structure. Application of ionising radiation for these purposes also increases in last years. The use of heavy ion irradiation is connected to the specific physicochemical changes on the way of ion path in materials [1].

Our previous work has concerned heavy ion irradiation effects on the films made from poly(ethyl-

eneterephthalate) (PET) and poly(butyleneterephthalate) (PBT) and several copolymers of PET and PBT, containing various amounts of crystalline material as well as those biaxially oriented. Crystallinity of the films was adapted by modification of the preparation conditions. Destruction of the crystalline ordering was discovered by means of WAXS (wide angle X-ray scattering), DSC (differential scanning calorimetry) and volume crystallinity data [2-6]. Scission of polymer chains accompanied by the simultaneous crosslinking was discovered after heavy ion irradiation [2].

At present, the studies are carried out dealing with the influence of thermal treatment and heavy ion irradiation on the amorphous phase ordering in a series of polyester films with a modified chemical composition and crystallinity. Commercial granulates of PET and PBT as well as PET copolymer with lactic acid – PET-LA (kindly supplied by Dr. K. Grzebieniak from the Institute of Chemical Fibers, Łódź, Poland) were used for film preparation. The films were obtained by hot pressing under modified conditions and submitted afterwards to thermal treatment followed by irradiation with heavy ions.

The films were characterized using standard WAXS diffraction, density measurements and molecular mass analysis. Two PET films, two PBT films and one PET-LA film differing in molecular mass as well as in volume and WAXS crystallinities were then selected for further studies by means of the radial distribution function (RDF). All the films have contained a large amount of amorphous phase, while one PET film has appeared to be totally amorphous.

PET and PBT films were irradiated with ^{40}Ar (5.5 MeV/amu) or ^{84}Kr (6.5 MeV/amu) applying ion fluencies in the range from $5x10^{-10}$ to $5x10^{11}$ ions x cm^{-2}. PET-LA film was irradiated with ^{209}Bi ions (11.4 MeV/amu, 10^{-10} ions x cm^{-2}). Heavy ion irradiation was carried out at the Centre de Recherche du Cyclotron (Whatman Company), Louvain-la-Neuve, Belgium (Ar), Joint Institute for Nuclear Research, Dubna, Russia (Kr) and Gesellschaft für Schwerionenforschung mBh, Darmstadt, Germany (Bi).

Standard WAXS measurements were done using an HZG4C diffactometer with a generator IRIS-3M and a proportional counter. $Cu_{K\alpha}$ radiation was applied with a tube voltage of 35 kV and a tube current of 25 mA. WAXS crystallinity was determined using the integral method [7] on the basis of diffraction patterns recorded in a 2θ range 8-70 with a step of 0.05 and counting time of 28 s. Volume crystallinities were determined on the basis of density data using values for the crystalline and amorphous standards given in [2] and [4].

WAXS diffraction patterns appropriate for RDF analysis were obtained using a Siemens D500 diffractometer equipped with a K800 generator and a semiconductor detector Si[Li]. Measurements were done in a 2θ range 6-145 with a step of 0.1 and a constant number of counts at the point equal to 4000 applying $Cu_{K\alpha}$ radiation with a tube voltage of 40 kV and a tube current of 40 mA. RDF analysis was carried out after subtracting the "crystalline" reflections using the programme XVIEW elaborated by R. Diduszko and H. Marciniak [8].

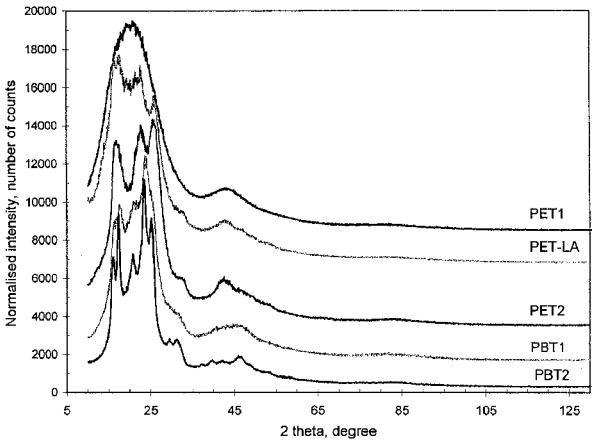

Fig.1. X-ray diffraction pattern of the selected polyester films used for RDF analysis.

WAXS diffraction patterns of the selected non-irradiated films are shown in Fig.1. On the basis of different solutions of G(r) and P(r) functions obtained for the particular films, it can be stated that atomic ordering in the amorphous PBT phase was better developed as compared to that in the amorphous phases in PET and PET-LA films. It can be related to the stiffening of the longer aliphatic chains in PBT, as compared to PET and a stronger tendency of PBT for formation of the crystalline phase during preparation of films. No small-distance ordering (apart from that connected to the benzene rings) can be deduced in the case of the totally amorphous PET film (distance *ca*. 1.4 and 2.5 Å) (Fig.2). In the case of all the semi-crystalline PET and PBT films, some ordering in amorphous phase can be stated on the basis of the maxima in G(r) function corresponding to the distance of *ca*. 6.0, 8.5 and 11.5 Å (Fig.3). Such ordering was not discovered, however, in the case of partially crystalline PET-LA film.

Heating of PET and PBT films led to development of the atomic ordering in amorphous phase accompanied by an increase in the content of the crystalline phase. These physical changes correspond to an increase in Mn.

No differences were discovered between atomic ordering in the initial and in the irradiated PET

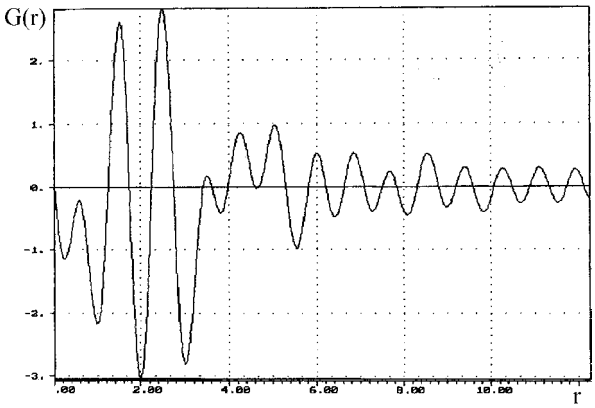

Fig.2. G(r) transform of the final reduced intensity F(k) determined for the totally amorphous PET1 film.

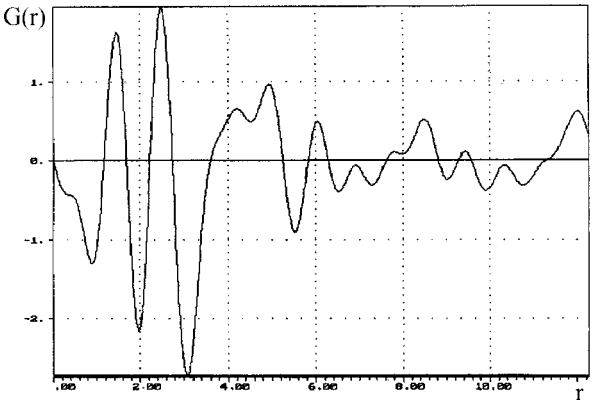

Fig.3. G(r) transform of the final reduced intensity F(k) determined for the annealed PBT film (volume crystallinity equal to 0.191, WAXS crystallinity equal to 0.304).

and PBT films, though chemical changes and/or decrease in crystallinity were found for these films. On the contrary, the appearance of short range ordering can be deduced after irradiation of PET-LA film, accompanying by a decrease in Mn. Lack of the modification of RDF reflections corresponding to the benzene rings after heavy ion radiation shows that irradiation does not influence the benzene rings in the polymer, although some essential chemical changes occur, in particular degradation and crosslinking.

The authors would like to acknowledge the heavy ion iradiation performed by: Dr. Etienne Ferain from Centre de Recherche du Cyclotron (Whatman Company), Dr. Aleksandr Didyk from Joint Institute for Nuclear Research and Dr. Johann Vetter from Gesellschaft für Schwerionenforschung mBh.

References

[1]. Fleisher R.L., Price P.B., Walker R.M.: Nuclear tracks in solids; principles and applications. University of California Press, Berkeley 1975.
[2]. Cieśla K., Starosta W.: Nucl. Instrum. Meth. Phys. Res. B, 105, 115-119 (1995).
[3]. Cieśla K.: Polimery, 44, 120-126 (1999), in Polish.
[4]. Cieśla K.: Proceedings of SPIE, 4240, 27-32 (2000).
[5]. Cieśla K., Trautmann Ch., Vansant E.F.: Nukleonika, 40, 3, 141-152 (1995).
[6]. Cieśla K.: J. Thermal. Anal. Calorim., 56, 1141-1146 (1999).
[7]. Cieśla K., Gwardys E., Żółtowski T.: Starch/Stärke, 43, 251-253 (1991).
[8]. Diduszko R.: Application of the non-conventional X-ray diffraction methods in the studies of carbon materials. Ph.D. Thesis. Institute of Physics, Polish Academy of Sciences, Warszawa 1995, in Polish.

"SELF-CALIBRATED" EPR DOSIMETERS WITH ALANINE AND SUGAR AS RADIATION SENSITIVE MATERIALS

Zofia Peimel-Stuglik, Sławomir Fabisiak

The alanine-EPR (electron paramagnetic resonance) dosimetry method is widely used in the high--dose reference laboratories owing to its accuracy and excellent metrological properties. The way of the same method towards industrial applications is much more difficult. Until now, alanine-EPR dosimetry is very occasionally used in irradiation plants and the resistance of the old-school industrial dosimetrists accustomed to optical methods is only one part of the problem. The more important reason seems to be non-conformity of the method to the industrial requirements: to be cheap, simple, fast and easy to handle.

The first barrier is a low choice and high cost of compact and easy-to-use EPR spectrometers. For instance, "e-scan Alanine Dosimeter Reader" from Bruker is very suitable to dosimetry, but its price (~100 000 USD) is too high for the most routine dosimetry laboratories working for the middle size irradiation plants. Some companies produce cheaper (20 000-40 000 USD) EPR spectrometers to different applications. Such devices are usually suitable for dosimetry, but because of rather difficult measurement procedures they had to be operated by highly educated and EPR experienced staff. It also creates costs.

The difficulty of quantitative EPR measurements arises from the fact that the intensity of EPR signal depends not only on the number of paramagnetic centre, but also on the instrumental and environmental parameters (gain, microwave power, modulation, time constant, sample position, dielectric constants of tube and dosimeter material, humidity, *etc*.). Because of that the intensity of dosimetric signal had to be normalised to the intensity of EPR standard (ruby, Mn^{2+}, others).

Generally, EPR standard is placed outside the dosimeter and measured before, after or simultaneously with it. A good idea leading to considerable simplification of quantitative EPR measurements was put forward by Prof. N.D. Yordanov from the Bulgarian Academy of Sciences. He invented and promoted the so-called "self-calibrated" EPR dosimeters containing three constituents: radiation sensitive material (RSM), radiation insensitive, but EPR active substance (Mn^{2+}/MgO) and a binder. Fine-grained Mn^{2+}/MgO, evenly distributed inside the dosimeter offers a better solution of the normalization problem than standards placed outside. It reflects not only changes in instrumental parameters and atmospheric conditions, but also in actual field conditions (RSM and the standard are situated exactly at the same place). Because of that, it should be possible to get accurate dosimetry results even with less sophisticated EPR spectrometers operated by the technical staff.

Each batch of "self-calibrated" dosimeters is characterised by the dose respond coefficient K_{dr} given as:

$$K_{dr} = (I_{RSM}/I_{Mn})/D \qquad (1)$$

where: I_{RSM} – intensity [a.u.] of the central line of the RSM, measured in "self-calibrated" dosimeter

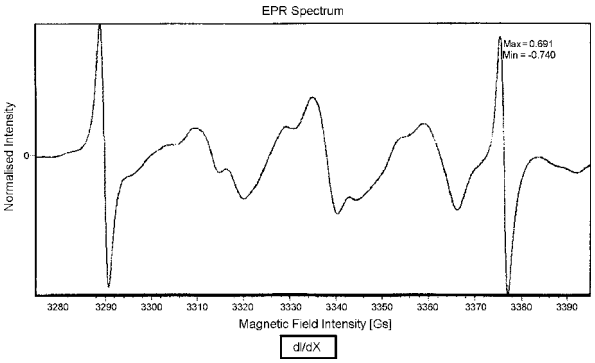

Fig.1. EPR spectrum of "self-calibrated" alanine dosimeter.

irradiated to the known dose; I_{Mn} – intensity [a.u.] of the one or two Mn^{2+} lines simultaneously recorded in the same dosimeter; D – absorbed dose [kGy].

Once determined K_{dr} is used for the evaluation of unknown dose D_x according to the relation:

$$D_x = (I^X_{RSM}/I^X_{Mn})/K_{dr} \quad (2)$$

So, in this idea only one calibration irradiation is necessary to read unknown dose. Of course, the dosimeters used to K_{dr} and D_x evaluation had to belong to the same batch.

In this report there are presented some results of experiments directed to study dosimetric properties of "self-calibrated" dosimeters.

We had to our disposal "self-calibrated" EPR dosimeters with alanine and sugar as the radiation sensitive materials. The concentration of the Mn^{2+}/MgO in both kind dosimeters was 5% and the concentration of paraffin – 35%. Both, alanine and sugar were ground to fine powder and sieved. The diameters of RSM particles was lower than 100 μm. The dosimeters has the shape of rods with a diameter of ~4 mm and the lengths from 10 to 11 mm. They were irradiated in the Institute of Nuclear Chemistry and Technology in a ^{60}Co calibration gamma source "Issledovatel" with a dose rate traceable to the National Physical Laboratory (Teddington, the United Kingdom) primary standard. Uncertainty of the dose measurements has been estimated as 2.4% at a 95% confidence level.

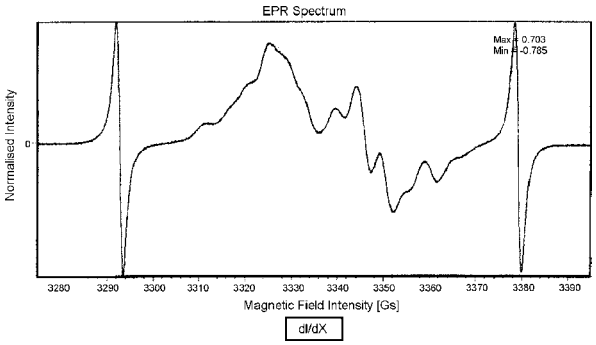

Fig.2. EPR spectrum of "self-calibrated" sugar dosimeter.

The dosimeters were irradiated at a temperature of 14-22°C and in approximate electronic equilibrium conditions. Before and after irradiation they were stored in dark envelopes in room conditions.

The EPR measurements were done on an EPR-10 MINI spectrometer manufactured by the

Table 1. Determination of K_{dr} for an alanine "self-calibrated" dosimeter.

D* [kGy]	Irradiation temperature [°C]	$I_{Mn(III)}$	$I_{Mn(IV)}$	$I_{Mn(III)}/I_{Mn(IV)}$	I_{RSM}	$I_{Mn}=(I_{Mn(III)}+I_{Mn(IV)})/2$	$K_{dr}=(I_{RSM}/I_{Mn})/D^*$
1.17	14.7	7.196	6.912	1.041	1.280	7.054	0.155
2.34	17.9	6.812	6.572	1.037	2.576	6.692	0.165
5.34	21.5	6.764	6.304	1.073	5.536	6.534	0.159
8.34	17.9	6.325	5.765	1.097	8.235	6.045	0.163
						Average	0.160
						Standard deviation	0.0043
						Relative standard deviation	2.7%

* D – dose.

Table 2. Determination of K_{dr} for a sugar "self-calibrated" dosimeter.

D* [kGy]	Irradiation temperature [°C]	$I_{Mn(III)}$	$I_{Mn(IV)}$	$I_{Mn(III)}/I_{Mn(IV)}$	I_{RSM}	$K_{dr\ Mn(III)}=(I_{RSM}/I_{Mn(III)})/D^*$	$K_{dr\ Mn(IV)}=(I_{RSM}/I_{Mn(IV)})/D^*$
1.17	14.7	7.854	7.708	1.019	0.850	0.092	0.094
2.34	17.9	7.683	7.571	1.015	1.633	0.091	0.092
5.34	21.5	7.046	7.238	0.974	3.317	0.088	0.086
8.34	17.9	7.420	7.255	1.023	4.955	0.080	0.082
					Average	0.088	0.089
					Standard deviation	0.0055	0.0057
					Relative standard deviation	6.3%	6.4%

* D – dose.

Table 3. Short-time stability of the intensity and related parameters in an alanine "self-calibrated" dosimeter.

D* [kGy]	Time after irradiation [h]	$I_{Mn(III)}$	$I_{Mn(IV)}$	$I_{Mn(III)}/I_{Mn(IV)}$	I_{RSM}	$I_{Mn}=(I_{Mn(III)}+I_{Mn(IV)})/2$	$K_{dr}=I_{RSM}/I_{Mn}$
2.34	2	6.812	6.572	1.037	2.576	6.692	0.385
2.34	72	6.844	6.716	1.019	2.636	6.780	0.389
V_{72} - V_2** [%]		0.5	2.2	-1.7	2.3	1.3	1.0

* D – dose.
** V_n – the value of the measurand read-out "n" hours after irradiation.

Sankt-Petersburg Instruments Ltd. Except for the experiments whose results are presented in Tables 3 and 4, the EPR measurements were performed 70 to 76 hours after the irradiation. The settings were as follow: microwave power – 1 mW, time constant – 0.01 s, modulation amplitude – 0.48 G, gain – 50-250, scans – 10, sweep width – 120 G (from 3275 to 3395 G). The difference between the highest and the lowest point of EPR spectrum of RSM was chosen as a dosimetric signal.

The EPR signals of alanine dosimeter is shown in Fig.1 and of sugar dosimeter in Fig.2.

In the case of sugar dosimeters, Mn^{2+} lines are better separated from the dosimetric signal than in the case of alanine. So, according to Prof. N.D. Yordanov suggestion we calculated K_{dr} for sugar using 3rd or 4th Mn^{2+} line and for alanine using the average intensity of both the lines.

In Tables 1 and 2, there are shown the results of consecutive irradiation of one piece of dosimeter. Regardless of Mn^{2+} line chosen to calculation, K_{dr} value was ~13% higher for the first irradiation than for the last one. At the moment we cannot say if it arises from the spontaneous or from radiation induced decay of paramagnetic centre or both. Irrespective of the reason, K_{dr} value calculated for the first measurement is probably more proper than the other ones.

Table 4. Short-time stability of the intensity and related parameters in sugar "self-calibrated" dosimeter.

D* [kGy]	Time after irradiation [h]	$I_{Mn(III)}$	$I_{Mn(IV)}$	$I_{Mn(III)}/I_{Mn(IV)}$	I_{RSM}	$K_{dr\ Mn(III)}$	$K_{dr\ Mn(IV)}$
2.34	2	7.683	7.571	1.015	1.633	0.213	0.216
2.34	72	7.746	7.592	1.020	1.692	0.218	0.223
V_{72} - V_2** [%]		0.8	0.3	0.5	3.5	2.3	3.2

* D – dose.
** V_n – the value of the measurand read-out "n" hours after irradiation.

In the case of sugar dosimeters, Mn^{2+} lines are better separated from the dosimetric signal than in the case of alanine. So, according to Prof. N.D. Yordanov suggestion we calculated K_{dr} for sugar using 3rd or 4th Mn^{2+} line and for alanine using the average intensity of both the lines.

In Tables 1 and 2, there are shown the results of consecutive irradiation of one piece of dosimeter. The short-time signal stability (2-72 h) of the alanine dosimeter was presented in Table 3 and sugar dosimeter in Table 4.

In the case of alanine dosimeter, the spread of each kind of measured value was at a level of 2% and can be recognised as accidental. In the case of sugar dosimeter, increase of Mn^{2+} signals was small and recognised as incidental, whereas increase of intensity for sugar dosimetric signal was probably significant. The experiment should be repeated.

In Tables 5 and 6 there are presented some results illustrating the benefits of using "self-calibrated" dosimeters on the decrease of experimental errors connected with positioning of dosimeters inside the cavity.

Table 5. The influence of the sample position in the cavity on measured amplitudes of Mn^{2+} signals and alanine dosimetric signals and also on the K_{dr} value.

D* [kGy]	Position**	$I_{Mn(III)}$	$I_{Mn(IV)}$	$I_{Mn(III)}/I_{Mn(IV)}$	I_{RSM}	$I_{Mn}=(I_{Mn(III)}+I_{Mn(IV)})/2$	$K_{dr}=I_{RSM}/I_{Mn}$	Deviation of K_{dr} from the average value [%]
2.34	A	5.516	5.268	1.047	1.992	5.392	0.369	-2.2
	B	6.832	6.568	1.040	2.528	6.700	0.377	-0.1
	C	6.844	6.716	1.019	2.636	6.780	0.389	2.9
	D	6.888	6.628	1.039	2.584	6.758	0.382	1.2
	E	5.652	5.444	1.038	2.06	5.548	0.371	-1.7
max - min [%]		21.6	23.6	2.7	27.3	22.3	5.3	

* D – dose.
** A – upper surface of dosimeter at the level of cavity centre, B – between A and C, C – standard position – centre of the sample at the centre of cavity, D – between C and E, E – bottom surface of the sample at the level of cavity centre.

In the case of alanine, a stochastic spread of K_{dr} value was observed and RSD value was less than 3%. In the case of sugar, the situation was differ-

Table 6. The influence of sample position in the cavity on measured amplitudes of Mn^{2+} signals and sugar dosimetric signals and also on the K_{dr} value.

D* [kGy]	Position**	$I_{Mn(III)}$	$I_{Mn(IV)}$	$I_{Mn(III)}/I_{Mn(IV)}$	I_{RSM}	$K_{dr\ Mn(III)}$	Deviation of $K_{drMn(III)}$ from the average value [%]	$K_{dr\ Mn(IV)}$	Deviation of $K_{drMn(IV)}$ from the average value [%]
2.34	A	5.517	5.333	1.034	1.208	0.219	-0.7	0.227	0.2
	B	6.854	6.704	1.022	1.496	0.218	-1.0	0.223	-1.3
	C	7.746	7.592	1.020	1.692	0.218	-0.9	0.223	-1.5
	D	7.550	7.392	1.021	1.663	0.220	-0.1	0.225	-0.5
	E	6.017	5.850	1.028	1.363	0.226	2.6	0.233	2.9
max - min [%]		37.0	38.6	1.4	35.5	0.9		1.7	

* D – dose.

** A – upper surface of dosimeter at the level of cavity centre, B – between A and C, C – standard position – centre of the sample at the centre of cavity, D – between C and E, E – bottom surface of the sample at the level of cavity centre.

The results from both the tables clearly show that the use of "self-calibrated" EPR dosimeters decrease drastically the uncertainty of EPR measurements connected with positioning of dosimeters inside the cavity.

On the basis of the results have obtained hitherto we can conclude that "self-calibrated" EPR dosimeters:

- allow to do quantitative EPR measurements without any external EPR intensity standard;
- shorten the measurement time using for positioning and weighting;
- spare the time for performing a calibration curve; unknown dose can be calculated just after one experiment needed to K_{dr} determination;
- decrease drastically the uncertainty of EPR measurements connected with positioning of dosimeters inside the cavity;
- allow to use not very sophisticated and thereby cheaper EPR spectrometers.

However,

- dosimeters used for dose measurement should be from the same batch as used for K_{dr} determination,
- all dosimeters from the one batch must have the same concentration of constituents,
- radiation sensitive material must have linear signal-to-dose characteristics.

Authors thank very much Prof. N.D. Yordanov (Bulgarian Academy of Sciences) to make available "self-calibrated" dosimeters to study.

RADIOCHEMISTRY
STABLE ISOTOPES
NUCLEAR ANALYTICAL METHODS
GENERAL CHEMISTRY

A NEW STRONTIUM-82/RUBIDIUM-82 GENERATOR

Aleksander Bilewicz, Barbara Bartoś, Ryszard Misiak[1/], Barbara Petelenz[1/]

[1/] The Henryk Niewodniczański Institute of Nuclear Physics, Polish Academy of Sciences, Kraków, Poland

Due to similarity of rubidium and potassium cations, the radionuclide ^{82}Rb, a positron emitter, has been used in nuclear medicine to characterize myocardial perfusion with high sensitivity and specificity [1-3]. The advantage of ^{82}Rb positron emission tomography (PET) *vs.* classical SPECT with ^{201}Tl is the short half-life of ^{82}Rb ($T_{1/2}$=75 s) which allows one to scanning of the patients every 10 minutes and to reduce the exposure of patient to radiation. Additionally, ^{82}Rb is a generator produced from the longer lived parent radionuclide ^{82}Sr ($T_{1/2}$=25.55 days), which permits clinical PET studies also in hospitals which do not have expensive on-site cyclotrons. Numerous methods for manufacturing the ^{82}Sr/^{82}Rb generator have been already described [4,5]. All these procedures, however, suffer from various limitations, *e.g.* a complicated multi-step separation of ^{82}Sr from a rubidium target, insignificant radiation resistance of the organic extractans and ion exchange resins, *etc*. To avoid these disadvantages, we used for the separation an inorganic ion exchanger – cryptomelane MnO_2. Cryptomelane MnO_2 has a tunnel-framed structure with exchangeable alkali or alkali earth cations. The average tunnel diameter is 280 pm, therefore the sorbent is selective for the cations with crystal ionic radii of 130-150 pm, *e.g.* K^+, Rb^+, Ba^{2+} and Ra^{2+}. To find optimum conditions for Rb^+-Sr^{2+} separations, the distribution coefficients (K_d) of Rb^+ and Sr^{2+} on cryptomelane MnO_2 were determined as a function of HNO_3 concentration. The influence of the HNO_3 concentration on the K_d for Sr^{2+} and Rb^+ on cryptomelane MnO_2 is shown in Fig.1. It can be seen that K_d for Rb^+ is very high even at 1 M HNO_3. This confirms high affinity of

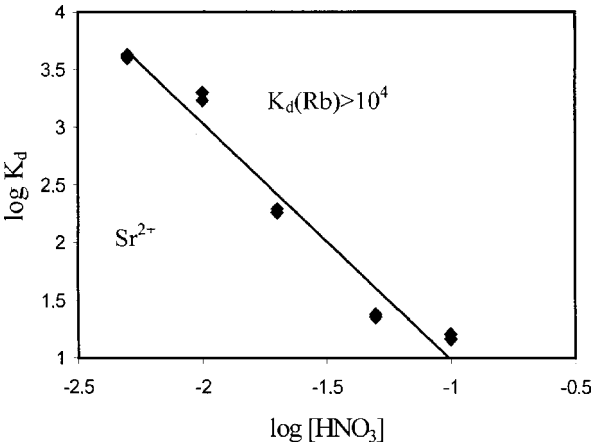

Fig.1. Dependence of Sr^{2+} and Rb^+ distribution coefficients on HNO_3 concentration.

cryptomelane MnO_2 for cations with ionic radii close to 150 pm. For Sr^{2+}, whose ionic radius is lower (118 pm), K_d decreases with increasing concentration of H^+ ions. For the efficient separation of the Rb^+-Sr^{2+} pair, 0.5 mol dm^{-3} HNO_3 was chosen as optimal solution. In this system, the K_d for Rb^+ on cryptomelane MnO_2 is greater than 10^4,

Table. Radionuclides detected in the ^{nat}RbCl target after irradiation with 48 MeV proton beam.

Radionuclide	$T_{1/2}$ [days]	Activity [MBq]	Nuclear reaction
^{82}Sr	25.5	6.49	^{85}Rb(p,4n)^{82}Sr
^{83}Sr	1.35	4.45	^{85}Rb(p,3n)^{83}Sr
^{85}Sr	64.8	8.55	^{85}Rb(p,n)^{85}Sr ^{87}Rb(p,3n)^{85}Sr
^{83}Rb	86.2	18.60	^{83}Sr(EC,β^+)$\rightarrow$^{83}Rb
^{84}Rb	32.9	14.29	^{85}Rb(p,pn)^{84}Rb
^{86}Rb	18.7	18.66	^{85}Rb(n,γ)^{86}Rb

while for Sr^{2+} it is close to 1. This allows one to perform a simple and quantitative separation of ^{82}Sr from the irradiated rubidium target.

The isotope ^{82}Sr was produced on an AIC-144 cyclotron located at the Institute of Nuclear Physics (Kraków, Poland). In the pilot experiment, a target of 0.133 g RbCl of natural isotopic abundance (72.17% ^{85}Rb, 27.83% ^{87}Rb) was irradiated with an internal proton beam of 48 MeV, 0.5 μA, during 4 hours. At this energy, proton activation of the natural rubidium target leads to direct or indirect formation of ^{82,83,85}Sr and ^{82,83,84,86}Rb isotopes. These radionuclides detected by gamma spectrometry in the irradiated target are presented in Table.

After 8 days of waiting period, which is enough for the decay of ^{83}Sr, the RbCl target was dissolved in 0.5 M HNO_3 solution. The solution was then passed through a cryptomelane MnO_2 column (d=3 mm, h=30 mm). The inactive rubidium (target material) and ^{83,84,86}Rb were quantitatively adsorbed on cryptomelane MnO_2. The effluent from the column was alkalized by 1 M NaOH to pH=6-8. Afterward, the strontium radionuclides from the neutralized solution were loaded on the top of a SnO_2

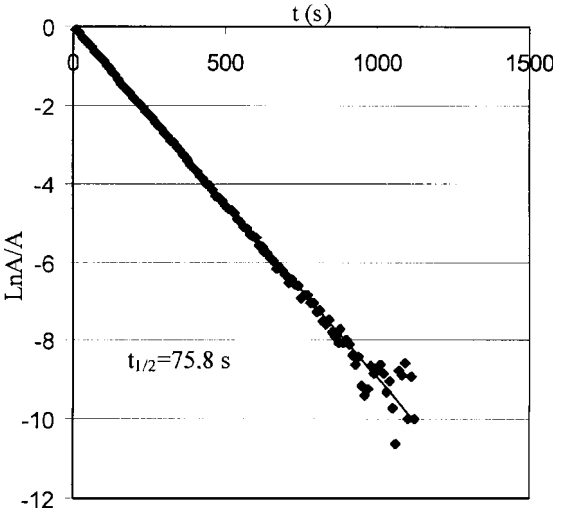

Fig.2. Decay curve of ^{82}Rb fraction.

aq. column. The inorganic ion exchanger – tin oxide was prepared by acidification of sodium stannate solution according to the procedure described in [6]. The ^{82}Rb formed from the decay of ^{82}Sr was eluted from the column by 0.9% NaCl (physiological saline). The elution was repeated every 10 minutes. The radionuclide purity of the effluent was measured by gamma spectrometry after the decay of ^{82}Rb. Additionally, we measured also the decay curves of the effluent fractions (Fig.2). The ^{82}Sr and ^{85}Sr breakthroughs measured by gamma spectrometry were lower than the established limits. After passing 1 liter of 0.9% NaCl through the column, no significant breakthrough was observed either by gamma spectrometry or by analyzing the decay curves. The half-life of the eluted ^{82}Rb, determined from the decay curve measured for more than 6 expected half-lives, is identical with the literature value.

References

[1]. Anderson C.J., Welch M.J.: Chem. Rev., 99, 2219 (1999).
[2]. Parkash R., DeKemp R.A., Ruddy T.D.: J. Nucl. Cardiol., 11, 440 (2004).
[3]. Epstein N.J. *et al.*: Appl. Radiat. Isot., 60, 921 (2004).
[4]. Brihaye C., Guillaume M., Cogneau M.: J. Biophys. Med. Nucl., 6, 151 (1982).
[5]. Vallabhajosula S. *et al.*: J. Nucl. Med., 22, 76 (1981).
[6]. Clearfield A.: Inorganic Ion Exchange Materials. CRC Press, Inc., Boca Raton, Florida 1982, p.144.

APPROACHES TO ESTIMATE THE IONIC RADIUS OF Po^{2+}

Krzysztof Łyczko, Aleksander Bilewicz, Willy Brüchle[1/], Brigitta Schausten[1/], Mathias Schädel[1/]

[1/] Gesellschaft für Schwerionenforschung (GSI), Darmstadt, Germany

Due to the relativistic stabilisation of $6p_{1/2}$ electrons, polonium – usually present in the 4+ oxidation state – can be reduced to the 2+ oxidation state. This cation has outside its filled $[Xe]4f^{14}5d^{10}$ electron shells – two electron pairs: $6s^2$ and $6p^2_{1/2}$. No information is available about the ionic radius of Po^{2+} and about the coordination number of Po^{2+} in aqueous solutions. The measurement of the ionic radius could be the first step towards a better understanding of the contribution of Po^{2+} electron orbitals to the chemical bonding.

The goal of our studies was to estimate the ionic radius of hydrated Po^{2+} from a comparison of the distribution coefficients (K_d) for Po^{2+} with K_d values of divalent metal cations of the second group of the Periodic Table (Ca^{2+}, Sr^{2+} and Ba^{2+}). This is based upon a well established linear correlation between ionic radii (known for Ca^{2+}, Sr^{2+} and Ba^{2+}) and the K_d values. This correlation is valid for ions with similar coordination numbers. K_d values can be obtained from the maxima of elution peaks in liquid chromatography experiments. Earlier a cation exchange study of Po^{4+} in acid solutions ($HClO_4$, H_2SO_4, H_3PO_4, CH_3COOH and oxalic acid) was reported [1].

We eluted polonium from the cation exchange resin Dowex 50W-X8, 200-400 mesh, with 3 M $HClO_4$ and 3.3 M CF_3SO_3H (triflic acid), both in SO_2 water solution. Perchloric and triflic acids were used because of their non-complexing properties for metal cations [2]. In order to reduce Po(IV) to Po(II), sulfur dioxide was applied. It is commonly known that sulfur dioxide and hydrazine reduce polonium to oxidation state +2 in acidic solution [3]. As we were using low-level radioactive tracer solutions of ^{210}Po, the measurement of α-activity from this samples was mandatory. Therefore, we were only able to use sulfur dioxide as the reducing agent. The use of hydrazine was impossible due to white salt residues which appeared during the evaporation step for α-sample preparation.

The used radiotracers ^{47}Ca (40 Bq/mg) and ^{85}Sr (3.3 kBq/mg) were produced at the Mainz TRIGA reactor. While the calcium tracer had a very low specific activity, the commercially available ^{133}Ba was carrier free. The tracer solutions were prepared by dissolving the irradiated oxides in perchloric acid or trifluoromethanesulphonic acid and aliquots were loaded onto the column: 46 mm length and 3.2 mm inner diameter. Elutions were performed at a rate of about 3.3 ml min^{-1}.

From the maxima of the elution position in 3 M $HClO_4$, we determined K_d values equal to 2, 7 and 24 for $^{47}Ca^{2+}$, $^{85}Sr^{2+}$, and $^{133}Ba^{2+}$, respectively. The corresponding literature [4] values are 10.4, 13.4 and 25.1. Presumably, the lower K_d values for calcium and strontium in comparison with the literature values from [4] result from the use of relatively large amounts of carrier material in our experiment. It should also be noted here that our calcium and strontium elution curves were rather wide and exhibited considerable tailings. For the elution with 3.3 M CF_3SO_3H, the K_d values were 11 for strontium and 37 for barium.

Then we studied the behaviour of polonium during the elution using 3 M $HClO_4$ both with and without SO_2. The elution curves for both solutions were similar. Peaks were very broad with maxima appearing only after 65-75 ml giving incomprehensibly large K_d values (~450-550). As an additional surprise, we measured a large elution maximum at about 25 ml, corresponding to a K_d of ~150, with 3.3 M CF_3SO_3H in SO_2 water. One would not expect such a large, if any, difference in the elution of Po^{2+} with 3.3 M CF_3SO_3H and 3 M $HClO_4$.

Therefore, we interpret the large K_d values for polonium observed in both systems in terms of incomplete reduction of polonium to the +2 oxidation state by sulfur dioxide. The observation of the different elution position in the two acids can possibly be explained by the oxidizing properties of $HClO_4$. In the perchloric acid solution we most likely could not reduce Po(IV) to the lower oxidation state at all.

The next step in these experiments will be the application of hydrazine as a reductant when using

γ-emitting ^{206}Po, or liquid scintillation counting to measure the α-active ^{210}Po in solution.

References

[1]. Ampelegova N.I.: Soviet Radiochem., 17, 52 (1974),
[2]. Cotton F.A. *et al.*: Advanced Inorganic Chemistry. 6th edition. Chapter 2. J. Wiley & Sons, 1999.
[3]. Gmelin Handbook: Polonium. Suppl. Vol. 1, part 11.
[4]. Marhol M.: Ion Exchangers in Analytical Chemistry. Czechoslovak Academy of Sciences, Prague 1981, p.493.

CHARACTERIZATION STUDIES AND CYTOTOXICITY ASSAYS OF Pt(II) CHLORIDE COMPLEXED BY N-(2-METHYLTETRAHYDROFURYL)THIOUREA

Leon Fuks, Marcin Kruszewski, Nina Sadlej-Sosnowska[1/], Krystyna Samochocka[2/]

[1/] National Institute of Public Health, Warszawa, Poland

[2/] Maria Skłodowska-Curie Memorial Cancer Center and Institute of Oncology, Warszawa, Poland

The ultimate target for platinum-based therapeutic complexes is generally accepted to be DNA, although the exact way whereby *cis*platin induces the toxic event for cell death is still in dispute. Inhibition of DNA synthesis has been often cited as the way of *cis*platin action [1,2] but in the early eighties evidence had been presented for an *in vivo* activity of this drug at the transcriptional level [1]. The cytotoxic effects of *cis*platin should perhaps be better considered as the combined effects of various DNA lesions [3].

The usefulness of *cis*platin in clinical use is limited by the enhancement of the resistance after continued treatment; at least, three resistance mechanisms have been recognized: reduced transport across the cell membrane [4], strong binding to inactivating thiolate ligands inside the cell [5] and repair of platinated lesions on DNA by enzymes [6]. In particular, bindings to methionine, S-thiolate (*e.g.* glutathione) and the cysteine-rich proteins (metallothioneins) are normally considered for *cis*platin as inactivation steps. So, the use of thiol-based or sulfur-containing ligands had been tested in order to reduce *cis*platin acquired resistance [7].

In the last two decades, the interest toward Pt(II) complexes containing nitrogen- and sulfur-donor ligands has increased, directed on obtaining metal-based drugs of the high anticancer activity and/or reduced toxicity in relation to known complexes exhibiting therapeutic properties [8]. Numerous modern chemotherapeutic procedures try to apply different Pt(II) compounds with ligands containing S-donor groups against platinum-based side effects as so called chemoprotectants. In particular, thiocarbonyl and thiol group donors have shown promising properties in chemical modulating *cis*platin nephrotoxicity [7,9]. As a result of these studies, a number of Pt(II) complexes sufficiently interesting for clinical trials have been produced but none of these has overcome the parent drug in efficacy [10].

The knowledge of the relationship between the ligand structure and the cytotoxicity of the platinum-based complexes is still limited [6] even if several rules may be apparent [11]. A general assumption is that, in order to be cytotoxic, the compound should present two *cis*-coordinated amino ligands as non-leaving groups, each carrying at least one N-H bond. Anyway, Farrell and others [12-14] reported on examples which do not follow this structure-activity relationship.

The substitution of ammonia by chelate ligands [15-17] yields bicyclic chelate Pt(II) complexes with different biological activities including cases of reduced cross-resistance. Some recent examples are *cis*-aminodichloropicolineplatinum(II) [18,19] and the *trans*platinum complexes with isoquinoline [20,21] or 1-(2-aminophenyl)isoquinoline ligands [22].

The main objective of our studies was to synthesize N-(2-methyltetrahydrofuryl)thiourea (**1**), in the following assigned as MTHFTU, a derivative of simple thiourea containing the moiety able by itself to link to DNA and test the neutral Pt(II) complex as a potential antitumor drug. So, the question arises if the $\mathbf{M}(R_1R_2tu)_x^{2+}$, where (R_1R_2tu) denotes the differently substituted (tu) molecule, might exhibit the desired biological activity. The antitumor activity of the complex was tested against standard the L1210 murine leukemia cell line. Because of serious difficulties in obtaining crystals suitable for X-ray diffraction (XRD) investigations, infrared (IR) spectra in connection with the quantum chemical calculations appeared to be the main source of the structural information. It has been already

Table 1. Selected IR frequencies [cm^{-1}].

	ν_{as}(NH)	ν_s(NH)	ν_s(CH_2)	ν_{as}(CH_2)	δ_s(HNH)	δ_{as}(HNH)	ν_{as}(CN)+ δ_s(HNH)	ν(CHOCH)	ρ(HNH)	ν_{as}(COC)	ν_s(COC)		δ_s(NCN)+ ν(CS)	ω(HNH)
MTHFTU (**1**)	3292	3183	2976	2876	1631	1546	1509	1183	1063	1021	954	924	754	591
Pt(MTHFTU)Cl_2 (**2**)	3274	3185	2973	2878	1649	1603	1521	1187	1071	1020	953	923	699	627

shown that the calculations reflect the main structural features of the Pt(II) complexes in the proper way [23]. Assignment of the main vibrational bands (both experimentally registered and theoretically

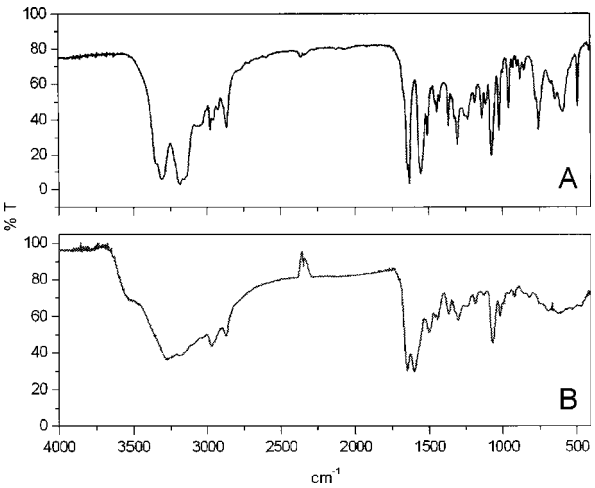

Fig.1. IR spectra of MTHFTU (**1**) and Pt(MTHFTU)Cl_2 (**2**).

calculated) for the MTHFTU ligand, **1**, and title complex **2** is presented in Table 1. Figure 1, in turn, shows a comparison of the spectra registered for the above species.

and scissoring δ(NCN) vibrations (754 cm^{-1}) shifts by about 50 cm^{-1}, but in the opposite direction. Lowering of the latter frequencies found in the spectra may be attributed to the reduction of the CS bond force constant and bond order in the complex, relatively to the free ligand molecule. Slight movement of the band corresponding to the $\nu_{as}(CN)+\delta_s(HNH)^{ic}$ vibrations (1509 cm^{-1}) towards greater wavenumbers may be associated with the increase in the C-N bond energy (and order). It can be assumed that formation of the S→M bonds stabilizes the polar structure analogical to that mentioned in the literature for the (tu) molecule and its derivatives. The observed shift of both δ(HNH) peaks associated with their approachingmay serves, in turn, as a proof that the NH_2 groups participate in the hydrogen bond network existing in the crystalline form.

As the starting point for the studies, we checked three hypothetical structures of the complex (Fig.2): one linear with a single coordination bond between the cation and the ligand (**I**) and two cyclic structures (**II** and **III**). Structure **II** contains a seven-membered ring, whereas **III** – a four-membered one. All the structures fulfill the analytically found requirements for the Pt:Cl mol ratio equal to 2.

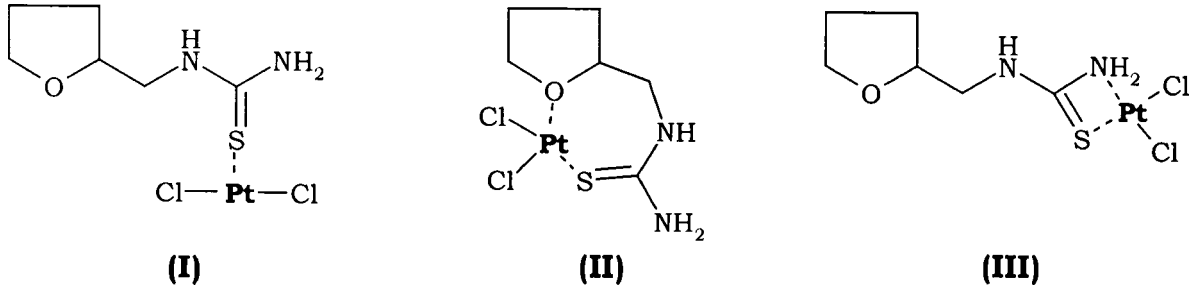

Fig.2. Hypothetical structures of the complex studied.

It can be concluded from these data that the positions of peaks representing the same modes of vibrations occurring within the (MTHFTU) ligand for a free and complexed molecule significantly differ. In particular, the band corresponding to the wagging ω(HNH) vibration at 591 cm^{-1} (free molecule) shifts by about 40 cm^{-1} towards greater wavenumbers upon complexation. On the contrary, the peak assigned to the combination of stretching ν(CS)

As the first step, several conformers of each structure were found on the molecular mechanics (MMFF force field) and semiempirical PM3 levels. At the latter, energy difference between the lowest energy conformers of **I** and **II** is 96 kcal/mol; none of the conformers of **III** could be optimized at this level.

As the second step, several lowest energy conformers of each structure were optimized at the

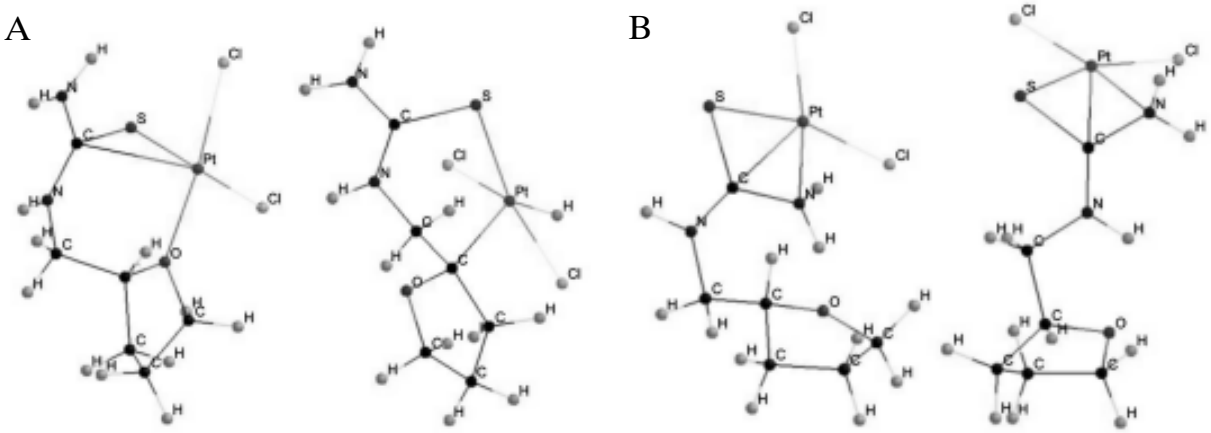

Fig.3. Hypothetical structures with seven-membered ring (**IIa** and **IIb** – A) and four-membered ring (**IIIa** and **IIIb** – B) formed by a ligand and the Pt(II) cation.

MPW1PW/LanL2DZ level. At this point, the issue becomes entangled. Namely, none conformer of **I** could be optimized. That is why only a single point

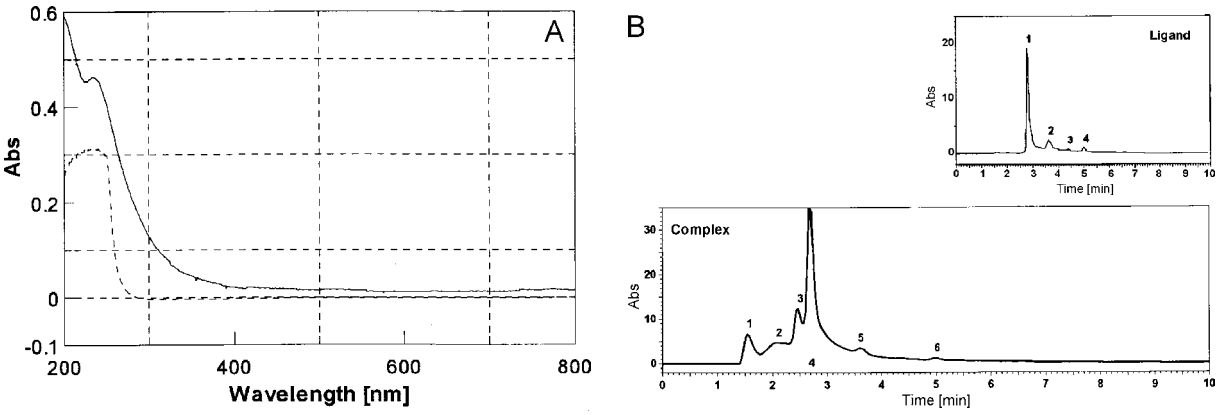

Fig.4. UV-VIS spectrum (A) and the HPLC (B) of the title complex **2** registered as the aqueous solutions. (Dotted line in the UV-VIS spectrum represents the ligand and solid complex (both at the same concentrations). Small diagram in the part B of the Fig. represents chromatograms of the ligand.)

energy was calculated for a few conformers of **I**. On the other hand, upon the optimization the initial structures of **II** and **III** were subjected to certain modifications which resulted in the structures shown below. For **II**, two different structures were obtained, marked as **IIa** and **IIb**. It can be seen that in structure **IIb** the second coordination bond Pt····O is broken and a new Pt-C bond created. Its length (Pt-C2) is equal to 2.108 Å. As a result, one can observe the formation of a six-membered ring. Both isomers are shown in Fig.3A. Structure **IIa**, of lower (by 4.37 kcal/mol) energy preserves the seven-membered ring. The additional Pt-C1 bond can be assumed to be an artifact, because the Pt-C1 distance is equal to 2.660 Å. In the case of four-membered structure **III**, all attempts of the optimization resulted in preservation of the four-membered ring. However, an additional bond between Pt and C (2.252 Å) was found. Two lowest energy conformers of **III** are shown in Fig.3B. The most stable structure, **IIIa**, is stabilized by two short hydrogen bonds: H3····O (1.593 Å) and H12-Cl1 (2.926 Å). Other conformers of **III** are similar to **IIIa**, the differences concern mainly the relative positions of the tetrahydrofuran and the four-membered rings. In one of the higher energy conformers, **IIIb**, the shortest distance between Cl and H

Table 2. Survival fraction and estimated ID_{50} of L1210 cells treated with a Pt(II) complex or ligand, respectively.

Dose [mM]	MTHFTU (**1**)		$Pt(MTHFTU)Cl_2$ (**2**)	
	Surviving fraction [%]	SD	Surviving fraction [%]	SD
1500	4.015	3.291	6.970	2.587
750	25.17	3.579	3.675	1.381
375	55.32	11.340	13.33	0.324
187.5	83.38	2.226	46.36	10.34
93.75	90.45	5.879	58.33	16.24
46.87	94.86	6.878	88.26	10.93
23.44	90.67	4.757	95.48	4.17
11.72	98.05	0.867	97.66	3.906
5.86	104.2	4.117	98.82	8.046

ID [μM][a]		
	MTHFTU (**1**)	$Pt(MTHFTU)Cl_2$ (**2**)
50% inhibition dose (ID_{50})	449.2	123.3
90% inhibition dose (ID_{90})	1202	396.3

Therapeutic Index (TI)[b]		
MTHFTU (**1**)	$Pt(MTHFTU)Cl_2$ (**2**)	*cis*platin
2.68	3.21	8.1 [26]

[a] calculated using the "best fitting curve".
[b] $TI = ID_{90}/ID_{50}$.

is 3.86 Å, and between H and O – 2.010 Å. Hydrogen bonds, if exist, are weaker than the hydrogen bonds in **IIIa**. Regarding the linear structure of **I**, the MPW1PW/LanL2DZ optimization resulted in its transformation into **IIa**. Thus it can be assumed that only the theoretical structures containing an internal ring have to be considered as representing the actual one.

The energy difference between the most stable ring conformers **IIIa** and **IIa** is 3.51 kcal/mol, so the seven-memebered structure appears to be more stable than the four-membered one, at least in the hypothetical gas phase.

The stability of **2** in the aqueous solution (0.9% of NaCl; commercial peritoneal injection solution produced by Baxter Terpol, Ltd., Sieradz, Poland, contains 154 mmol dm^{-3} of natrium and 154 mmol dm^{-3} of chloride ions, pH=6.7) was studied by registering its UV-VIS and IR spectra *vs*. time (Fig.4). Within one week no changes in the spectra have been detected. Also the HPLC results obtained for the saline solution of **2** (isocratic elution using the CH_3CN-H_2O mixture, vol:vol=20:80; 230) do not exhibit distinct changes during one week.

Cytotoxicity of the investigated species was estimated *in vitro* by means of a relative growth test with 1 h exposure to the drug, as described earlier [24]. Studies were performed with mouse lymphoma cell line L1210. The detailed results are presented in Table 2 and Fig.5. L1210 cells were treated with the investigated Pt(II) complex, **2**, or with the free MTHFTU, **1**, respectively. The reference values for the *cis*platin were already obtained by the authors under the same experimental conditions [25,26]. If the toxicity of the reference *cis*platin was found to be ID_{50}=5 μM [23], the ID_{50} of species investigated in the presented paper appeared to be about 450 or 100 μM and the ID_{90} about 1440 or 260 μM for **1** or **2**, respectively (Fig.5). Therapeutic index for both ligand and the Pt(II) complex appear to be 2.7 and 3.2, respectively (*i.e*. 3 and 2.5 times smaller than that for the *cis*platin).

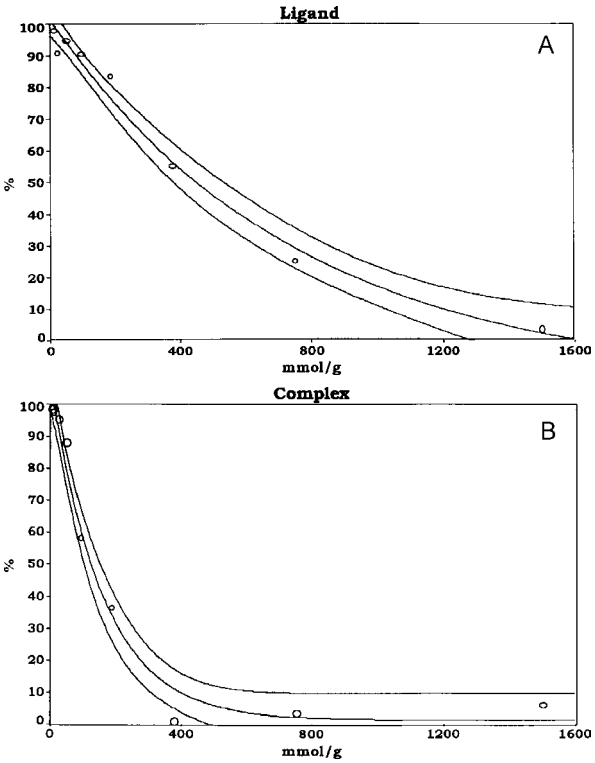

Fig.5. Toxicity against the L1210 cell cultures caused by **1** (A) or **2** (B) at a 95% confidence level.

No significant cytotoxicity of the already studied complex $Pt(tu)_4Cl_2$ – the 50% inhibition dose (ID_{50}) values being greater than 1500 μM [23] in relation with the obtained here data – remains in accordance with the earlier [23] hypothesis that substituted (tu) molecules as ligands for the Pt(II) cations might create complexes exhibiting the desired biological activity.

The work has beem undertaken as the statutory research of the National Institute of Public Health and the Institute of Nuclear Chemistry and Technology. We thank Prof. Adam Krówczyński (Department of Chemistry, Warsaw University) for synthesis of the ligand.

References

[1]. Meijer C., Mulder N.H., Hospers G.A.P., Uges D.R.A., deVries E.G.E.: Br. J. Cancer, 62, 72-76 (1990).
[2]. Eastman A., Schulte N.: Biochemistry, 27, 4730-4734 (1988).
[3]. Dorr R.T.: Platinum and Other Metal Coordination Compounds in Cancer Chemotherapy. Vol.2. Plenum Press, New York 1996, pp.131-154.
[4]. Farrell N.: Catalysis by Metal Complexes, Transition Metal Complexes as Drugs and Chemotherapeutic Agents. Vol.11. Kluwer Academic, Dordrecht 1989, pp.44-46.
[5]. Alberts D.S., Canetta R., Mason-Liddil N.: Semin. Oncol., 17, 1, Suppl. 2, 54-60 (1990).
[6]. Sherman S.E., Lippard S.J.: Chem. Rev., 87, 1153-1181 (1987).
[7]. Eastman A.: Pharmacol. Ther., 34, 155-166 (1987).
[8]. Molecular Aspects of Anticancer Drug Action. Eds. S. Neidle, M.J. Waring. MacMillan, London 1983, pp.183-231.
[9]. Farrel N.: Cancer Invest., 11, 578-589 (1993).
[10]. Woud W.R.: Cancer Res., 47, 6549-6555 (1987).
[11]. Hambley T.W.: Coord. Chem. Rev., 166, 181-223 (1997).
[12]. Farrell N., Kelland L.R., Roberts J.D., Van Beusichem M.L.: Cancer Res., 52, 5065-5072 (1992).
[13]. Deacon G.B.: Platinum and Other Metal Coordination Compounds in Cancer Chemotherapy. Plenum Press, New York 1991, pp.139-150.
[14]. Bierbach U., Hambley T., Farrell W.N.: Inorg. Chem., 37, 708-716 (1998).
[15]. Kidani Y., Inagaki K., Iigo M., Hoshi A., Kuretani K.: J. Med. Chem., 21, 1315-1319 (1978).
[16]. Noji M., Okamoto K., Kidani Y., Tashiro T.: J. Med. Chem., 24, 508-515 (1981).
[17]. Rezler E.M., Fenton R.R., Esdale W.J., McKeage M.J., Russel P.J., Hambley T.W.: J. Med. Chem., 40, 3508-3515 (1997).
[18]. Holford J., Raynaud F., Murrer B.A., Grimaldi K., Hartley J.A., Abrams M., Kelland J.R.: Anticancer Drug Des., 13, 1-18 (1998).
[19]. Chen Y., Guo Z., Parsons S., Sadler P.J.: Chem. Eur. J., 4, 672-678 (1998).
[20]. Bierbach U., Farrel N.: Inorg. Chem., 36, 3657-3665 (1997).
[21]. Farrel N.: Met. Ions Biol. Syst., 32, 603-639 (1996).
[22]. von Nussbaum F., Miller B., Wild S., Hilder C.S., Schumann S., Zorbas H., Beck W., Steglich W.: J. Med. Chem., 42, 3478-3485 (1999).

[23]. Fuks L., Sadlej-Sosnowska N., Samochocka K., Starosta W.: Characterization studies and cytotoxicity assays of Pt(II) chloride complexed by N-(2-methyltetrahydrofuryl)thiourea. J. Mol. Struct., in print.
[24]. Samochocka K., Kruszewski M., Szumiel I.: Chem.-Biol. Interact., 105, 145-155 (1997).
[25]. Fuks L., Samochocka K., Anulewicz-Ostrowska R., Kruszewski M., Priebe W., Lewandowski W.: Eur. J. Med. Chem., 38, 775-780 (2003).
[26]. Bertini I., Gray H., Lippert S.J., Valentine J.S.: Bioinorganic Chemistry. University Science Books, Mill Valley 1994, p.526.

TRANSITION METAL COMPLEXES WITH URONIC ACIDS

Dorota Filipiuk[1/], Leon Fuks, Marek Majdan[2/]

[1/] Białystok Technical University, Poland
[2/] Maria Curie-Skłodowska University, Lublin, Poland

Heavy metals are known to be essential for almost all kinds of living organisms. However, when their concentrations exceed certain limits, these metals can become toxic and harmful to the living beings. For this reason, authorities responsible for control of the environmental pollution have imposed operations on the discharge of industrial wastewater containing heavy metals entering natural watercourses. As a result, many companies have already developed more or less cheap, but efficient methods to reduce the metal content of the commercial effluences.

Biosorption of heavy and/or radioactive metals can be considered as an alternative technology competitive with respect to conventional technologies [1,2] applied in the wastewater treatment. To sequester the aforementioned metals from aqueous solutions cheap adsorption materials are used mainly of natural origin. These materials can accumulate metal to levels that can be much higher than those in the liquid phase. Thus, biosorption can serve to reduce the waste volume. Instead of dealing with large volumes of liquid waste, only a small volume of solid waste could be treated, *e.g.* by combustion or deposition in landfills [3,4].

Process of heavy metals biosorption can be explained by considering different kinds of chemical and physical interactions between the heavy metals in solution and the functional groups present in the cell wall components: carboxylic, phosphate, sulfate, ammino, amidic, and hydroxylic groups are the most commonly found [5-7]. Vibrational spectroscopy can reveal detailed information concerning the properties and structure of materials at the molecular level. Infrared (IR) spectroscopy until recently was the most widely used technique for studying natural products. This spectroscopic method presents three main advantages: it is fast, non-destructive, and it demands small sample quantities [8]. The aim of the present work was to initialize more complex studies on species formed by alginic acid with different metal cations.

Alginic acid is a naturally occurring hydrophilic, colloidal polysaccharide obtained from various kinds of brown seaweeds (*i.e.* algae, *Phaeophyceae*). This common name is given to the family of linear polysaccharide-like polymers containing three different functional groups: -COO^- (carboxylate), -C-O-C- (ether) and -OH (alcohol). The acid consists of 1,4-linked β-D-mannuronic (**M**) and α-L-guluronic (**G**) acid residues arranged in non-regular blocks forming long chains. The most pronounced sequences are -$\mathbf{M}(\ldots)_{n1}\mathbf{M}$-, -$\mathbf{G}(\ldots)_{n2}\mathbf{G}$- or -$\mathbf{MG}(\ldots)_{n3}\mathbf{GM}$- (Scheme 1) [9].

In modeling studies on metal biosorption it is commonly assumed that there is only one general type of functional group (represented as $\mathbf{R}^{2-}$) in the metal ion binding process. It has been already found that at pH 4-6 a certain number of protons from the carboxylic groups may be displaced by metal cations sorbed. However, in an aqueous solution of metal salts this exchange takes place together with other kinds of bonding formation. The cumulative reaction may be presented as:

$$\mathbf{M}^{2+} + [\mathbf{H}_2\mathbf{R}] \Leftrightarrow 2\,\mathbf{H}^{+} + [\mathbf{M}\mathbf{R}]$$

The most important vibrational modes of alginic acid together with the transition metal complexes are presented in Table 1, while the selected FT-IR (Fourier-transform infrared) spectra are drawn in Fig.1. In the above, alginic acid is treated not only as a reference which permits a comparison with the complexes studied, but it also permits a comparison with the existing literature data for sodium alginate (discussed later).

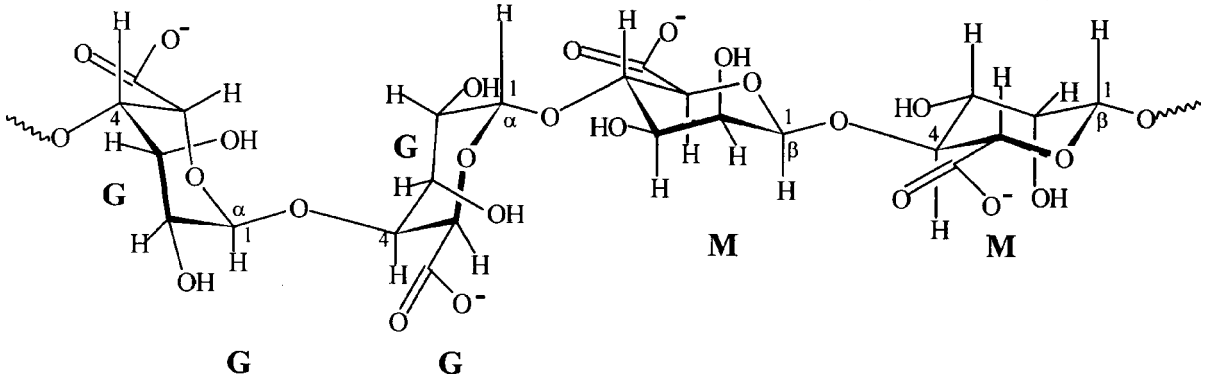

Scheme 1. Chain sequence of alginic acid.

Table 1. Assignment of the main vibrational modes for the investigated species made with help of [10,11] and papers cited there.

Assignment	Alginic acid	Na(I) alginate*	Mn(II) alginate	Co(II) alginate	Ni(II) alginate	Cu(II) alginate	Zn(II) alginate	Cd(II) alginate
	[cm^{-1}]							
ν(OH)	3482	3429	3381	3376	3385	3415	3483	3376
ν(CH) – α-anomer	2926.1	2921	2928.1	2927.2	2936.4	2927.9	2924.0	2928.1
$\nu(COO^-)_{sym}$	1737.9	1743	1752.2	1754.3	1759.0	1750.5	1760.3	1746.6
$\nu(COO)_{sym}$	1653.1	1620	1629.3	1616.0	1629.8	1629.1	1622.9	1622.9
$\nu(COO)_{as}$	1461.4	1419	1425.6	1424.9	1425.7	1416.8	1424.4	1430.6
δ(CCH) + δ(COH)	1248.1	1320.7	1313.8	1309.8	1306.1	1310.7	1307.3	1297.9
ν(CO) + ν(CCC)	1091.4	1102	1076.4	1079.1	1094.0	1087.1	1081.8	1102.8
ν(CO) + δ(CCO) + δ(CC)	1033.7	1026.9	1032.2	1033.5	1021.5	1028.3	1033.3	1026.3
δ(CH) β-anomer	875.5	889.7	870.9	878.58	876.2	881.6	882.0	878.9
δ(CH) α-anomer	812.8	821.5	810.4	807.7	821.3	819.2	825.1	815.3
$\delta_r(H_2O)$	671.7	654.1	650.7	652.6	643.6	637.4	636.3	658.2
$\delta_w(H_2O)$	611.1	608.8	605.0		620.0	613.1	614.9	606.2

* literature data [12].

Broad absorption peaks in the region of 3250-3400 cm^{-1} indicate the existence of hydroxyl groups involved in the H-bond network [10,11]. The peak observed at 2926 cm^{-1} (alginic acid) can be assigned as due to vibration of the CH group [12]. The spectrum displays also the absorption peak at 1738 cm^{-1} corresponding to the stretching band of the free carboxyl anions, COO^- [13]. The complexed carboxylate group exhibits two bands: a strong asymmetrical stretching band (for alginic acid at 1618 cm^{-1}) and a weaker symmetrical stretching band (at 1420 cm^{-1}). The peak around 1740 cm^{-1} (C=O stretching) almost completely disappears for the metal-laden biomass, while the peak around 1620 cm^{-1} (C=O chelate stretching) becames higher. The broad band at 1091 cm^{-1} is due to the

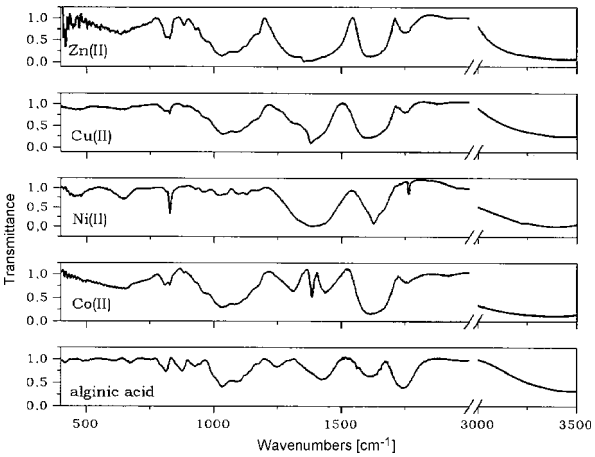

Fig.1. IR spectra of alginic acid and the selected transition metal complexes.

C-O stretching of both hydroxylic and ether groups. Peaks at 672 and 611 cm^{-1} (alginic acid) may be assigned to bending vibrations of the coordinated water molecules [14].

The most important differences in the vibrational spectra of the particular metal complexes seem to occur for the symmetric, $\nu_{sym}(COO^-)$, and asymmetric, $\nu_{asym}(COO^-)$, stretching vibrations of the carboxylic group. It has been already found, that carboxylic group can coordinate cations in different ways, *e.g.* monodentate, bidentate or bridging (Fig.2) [15,13]. Qualitatively, they can be determined after numerous rules presented in the existing literature.

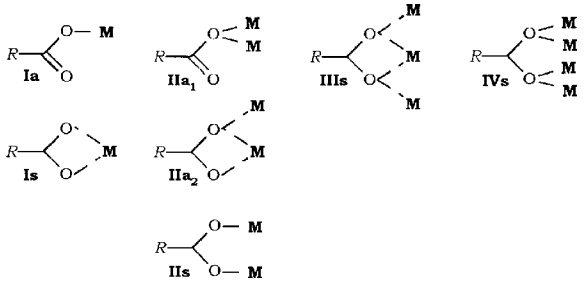

Fig.2. Different types of the carboxylate complexes proposed by Nakamoto [14].

The $\Delta\nu(COO^-)$ values of the studied complexes ($\Delta\nu \cong 190$ cm^{-1}) appear to be smaller than that for sodium alginate ($\Delta\nu \cong 201$ cm^{-1}) and shifted in agreement with the relation describing the bidentate chelating coordination mode. Slight increase in the $\Delta\nu$ values with increasing reciprocal of the cationic radii ($1/r_{ion}$) may be connected with an increase in the symmetry and equalization of the bond lengths in the carboxylate group of the investigated species [16].

Beacuse the carboxylate groups in the alginate resin play an important role in binding metal ions, the percentage of ionic bonding (PIB) can be defined as [17]:

$$\bullet\bullet\bullet\bullet \frac{\nu.... - \nu....}{\nu.... - \nu.....}$$

Table 2. PIB estimated for the transition metal alginates.

Cation	Mn(II)	Co(II)	Ni(II)	Cu(II)	Zn(II)	Cd(II)
$R_{ion}/(R_{ion}^{-1})$ [pm]	$80/1.235\cdot10^{-2}$	$72/1.389\cdot10^{-2}$	$69/1.449\cdot10^{-2}$	$72/1.408\cdot10^{-2}$	$74/1.351\cdot10^{-2}$	$97/1.087\cdot10^{-2}$
PIB [%]	84.3	80.2	79.5	86.8	85.7	88.8

where ν is the frequency of the asymmetric vibration of the carboxylate group. In the above formula the denominator is the IR frequency shift of the asymmetric C-O vibration from the typical covalent bonding (carboxylic acid) to the typical ionic bonding (sodium carboxylate), whereas the numerator term is the frequency shift of the same vibration when a particular metal ion is bound. On the basis of the FT-IR frequencies presented in Table 1, the PIB values were calculated and presented in Table 2 and in Fig.3. It is interesting to find that the PIB values are independent of the metal ions.

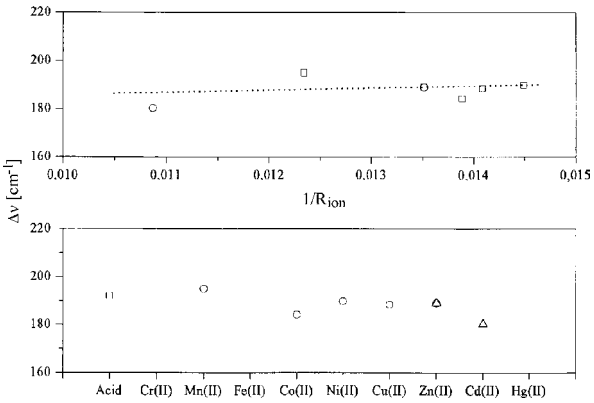

Fig.3. $\Delta\nu(COO^-)$ for the investigated complexes.

Absorption bands of bonded water molecules in the hydrated salts, generally appearing at about 3400 cm^{-1}, interfere with the strong H-bonding system of alginic acid in these salts. It can be seen that in the course of complexation, the peak at 672 cm^{-1} shifts towards 650 cm^{-1} which may be attributed to stronger interactions of water molecules with the cation, weakening the H-O bond strength in the water molecules.

The work has been undertaken as the statutory research of the Institute of Nuclear Chemistry and Technology and the Białystok Technical University.

References

[1]. Volesky B.: Hydrometallurgy, 59, 203 (2001).
[2]. Kratochvil D., Volesky B.: Trends Biotechnol., 16, 291 (1998).
[3]. Encyclopedia of Bioprocess Engineering. Eds. M.C. Flickinger, S.W. Drew. Wiley, New York 1999.
[4]. Schiewer S., Volesky B.: Biosorption by marine algae in Remediation. Ed. J.J. Valdes. Kluwer, Dodrecht, the Netherlands 2000, pp.139-169.
[5]. Veglio F., Beolchini F.: Hydrometallurgy, 44, 301 (1997).
[6]. Plette C.C.A., Benedetti M.F., van Riemsdijl W.H.: Environ. Sci. Technol., 30, 1902 (1996).
[7]. Pagnanelli F., Petrangeli Papini M., Trifoni M., Toro L., Veglio F.: Environ. Sci. Technol., 34, 2773 (2000).
[8]. Mouradi-Givernaud A.: Recherches Biologiques et Biochimiques pour la Production d'Agarose chez Gelidium latifolium. Ph.D. Thesis. Université de Caen, 1992, pp.231-251, in French.
[9]. Haug A., Larsen B., Smisroed O.: Acta Chem. Scand., 20, 183 (1966).
[10]. Vien-Lin D., Colthup N.B., Fateley W.G., Grasselli J.C.: The Handbook of Infrared and Raman Characteristic Frequencies of Organic Molecules. Academic Press, San Diego 1991.
[11]. Kapoor A., Viraraghavan T.: Bioresour. Technol., 61, 221 (1997).
[12]. Fourest E., Volesky B.: Environ. Sci. Technol., 30, 277 (1996).
[13]. Mizuguchi M., Nara M., Kawano K., Nitta K.: FEBS Lett., 417, 153 (1997).
[14]. Nakamoto K.: Infrared Spectra of Inorganic and Coordination Compounds. J. Willey, New York 1997.
[15]. Ishioka T., Shibata Y., Takahashi M., Kanesaka I.: Spectrochim. Acta A, 54, 1811 (1998).
[16]. Kalinowska M., Swislocka R., Fuks L., Koczon P., Lewandowski W.: Spectroscopic Studies on Metal Complexes with Benzoic Acid and its Derivatives. Spectrochim. Acta A, submitted for publication.
[17]. Chen J.P., Hong L., Wu Sh., Wang L.: Langmuir, 18, 9413 (2002).

TRICARBONYL(N2-METHYL-2-PYRIDINECARBOAMIDE)CHLORORHENIUM(I) AS A PRECURSOR OF RADIOPHARMACEUTICALS

Leon Fuks, Ewa Gniazdowska, Jerzy Narbutt, Wojciech Starosta

Progress in the medicinal chemistry, and especially in the nuclear medicine, requires new tissue-specific radiopharmaceuticals for both diagnosis and therapy of diseases. So, in the last two decades, the coordination chemistry of technetium and rhenium has been directed towards finding novel radiopharmaceuticals [1,2].

A great number of currently applied radiopharmaceuticals containing the ^{99m}Tc or ^{188}Re radioisotopes use precursors or complexes in their higher oxidation states [3,4]. However, more kinetically inert compounds of the monovalent cations have recently received more attention [4-9]. These soft metal cations show an increased inertness and low affinity for hard nitrogen or oxygen donor atoms, readily present in the blood serum. This characteristic feature protects the complexes *in vivo* against ligand dissociation and ligand exchange.

The aim of our studies was to synthesize and characterize physicochemically a rhenium(I) tri-

carbonyl complex with N2-methyl-2-pyridinecarboamide, $C_7H_8N_2S$ (**1**) – a compound similar to its thio-analogue recently studied [10].

The title complex $Re(CO)_3LCl$ (**3**), where L denotes (**1**), was obtained from the precursor (**2**) following the synthetic procedure worked out at the Paul Scherrer Institute, Switzerland [11].

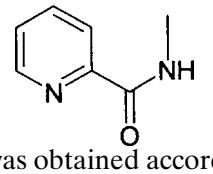

Ligand (**1**) was obtained according to the general procedure described in [12]. (Calcd: %C=64.86, %H=5.40, %N=20.05; found: %C=64.75, %H=5.50, %N=19.89.)

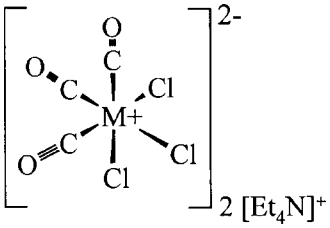

The Re(I) precursor (**2**) was obtained according to the general procedure described in [13].

Molecular structure of the $Re(CO)_3LCl$ complex (**3**) is presented in Fig.1. As it was expected, the ligand coordinates the cation bidentately: *via* the pyridine nitrogen and the oxygen atoms and forms a five-membered ring with the metal center. Main crystallographic data are presented in Table 1.

Unfortunately, we failed in the obtaining ligand (**1**) crystals suitable for X-ray diffraction studies.

Infrared (IR) spectra of the investigated species are shown in Fig.2. The detailed assignment of the peaks was made according to [10] and the references cited therein. The main FT-IR (Fourier-transform infrared spectroscopy) bands of ligand (**1**) and the title complex (**3**), ν [cm^{-1}] are listed in Table 2 together with proposition of their assignment. As one can see, all the main bands of the pyridinecarbomides can be found in both spectra. Two characteristic peaks of the Re-(CO) vibrations clearly appear in the spectrum of the complex and confirm the existence of the typical rhenium – tricarbonyl core.

One of the most important features in medicine is the biodistribution of drugs. The biodistribution to a great extent depends on the lipophilicity of the species. The drug injected into the human body

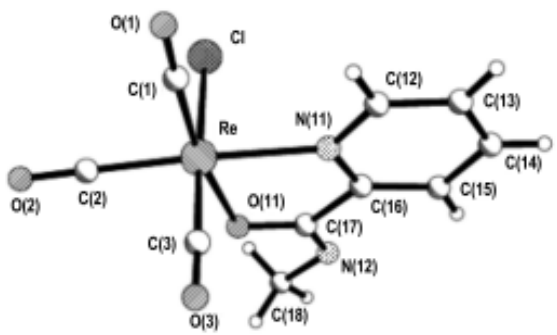

Fig.1. Molecular structure of the title complex (**3**).

Table 1. Selected bond lengths [pm] and angles [°] in the $Re(CO)_3LCl$ complex (**3**).

Bond lengths	
C16-N11	1.3343 (0.0077)
C16-C17	1.4771 (0.0089)
O11-C17	1.2515 (0.0075)
C17-N12	1.3041 (0.0082)
N12-C18	1.4461 (0.0107)
Re-C1	1.8806 (0.0068)
Re-C2	1.9122 (0.0069)
Re-C3	1.8862 (0.0067)
Re-N11	2.1764 (0.0051)
Re-O11	2.1635 (0.0045)
Re-Cl	2.4571 (0.0020)
Angles	
N11-Re-O11	73.99
N11-C16-C17	113.22 (0.52)
C17-O11-Re	117.02 (0.42)
C16-C17-O11	118.82 (0.55)
C16-N11-Re	116.61 (0.42)
N12-C17-C16	119.67 (0.60)
N12-C17-O11	118.82 (0.55)

is transported with blood to the targeted tissue or organ and passes the cell barrier by active or passive diffusion. We have determined the lipophilicity of **3** by liquid-liquid partition experiments in the *iso*octanol – 0.9% NaCl aqueous solution system. The aqueous phase composition is closely related to the human extracellular liquid (c_{Na}=140 mmol dm^{-3}, c_{Cl}=120 mmol dm^{-3}). The obtained value of partition constant of **3**, log P_3=0.85 ±0.09, is greater than the corresponding value for its thio-analogue, logP=0.57 ±0.15 [10].

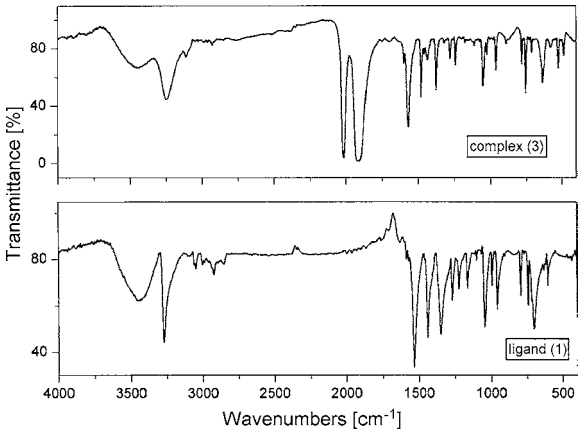

Fig.2. FT-IR spectra of ligand (**1**) and complex (**3**).

Table 2. Main IR bands [cm^{-1}] and their vibrational assignments (KBr pellets).

Assignment*	Ligand (1)	Complex (3)	Assignment*	Ligand (1)	Complex (3)
$\nu_{NH_3,as}$	3590		$\delta_{C\text{-}H,asym}$	1398	
$\nu_{NH_3,sym}$	3294	3320	$\nu_{C\text{-}N}$	1287	1257
$\nu_{C\text{-}H}$ (aromatic ring)	3057	3094		1158	1185
$\nu_{CH_3,as}$	2943	2949	A1 cumulative vibration of the pyridine ring	1088	
Re-(CO)	-	2085		997	1008
Re-(CO)	-	1998	B1 cumulative vibration of the pyridine ring	957	
$\nu_{C\text{-}O}$, amide vibration I	1591	1639	$\delta_{C\text{-}H}$ (2H vibration of the 2-substituted pyridine ring)	822	759
$\delta_{N\text{-}H}$, amide vibration II	1569	1608	Group vibrations of the aromatic ring	695	
$\nu_{C\text{-}N}$, amide vibration III	1539	1555		621	
$\delta_{C\text{-}H,sym}$	1435	1477	$\delta_{N\text{-}C=O}$, called as the amide vibration IV	605	592

* ν – stretching, δ – bending vibrations.

Stability of **3** towards oxidation was studied in aerated aqueous solution by registering its UV-VIS spectrum as a function of time. Within one week (*ca*. ten half-life periods of ^{188}Re) no distinct change in the spectrum was detected (Fig.3).

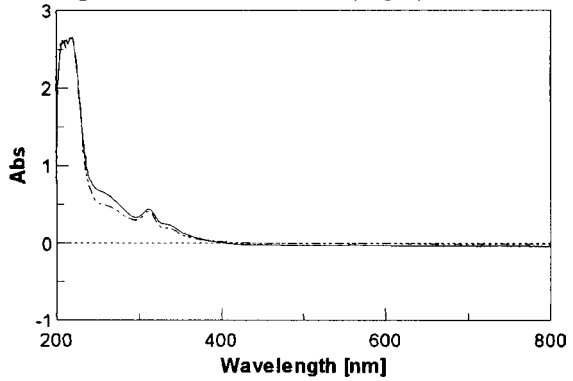

Fig.3. UV-VIS spectra of the title complex (**3**) registered at the beginning of the experiment (solid line) and after a week (dotted line).

Further studies on the title complex are in progress.

The work was supported by the State Committee for Scientific Research (KBN) – grant No. 4 TO9A 110 23.

References

[1]. Volkert W.A., Hoffman T.J.: Chem. Rev., 99, 2269-2292 (1999).
[2]. Liu S., Edwards E.S.: Bioconjugate Chem., 12, 7-34 (2001).
[3]. Ferro-Flores G., Pimentel Gonzalez G., Gonzales-Zavala M.A., Artega de Murphy C., Melendez Alafort L., Tendilla J.I., Croft B.Y.: Nucl. Med. Biol., 26, 57-62 (1999).
[4]. Karacay H., McBride W.J., Griffiths G.L., Sharkley R.M., Barbet J., Hansen H.J., Goldenberg D.M.: Bioconjugate Chem., 11, 842-854 (2000).
[5]. Wenzel M., Saidi M.: J. Labelled Compd. Rad., 33, 77-80 (1993).
[6]. Minutolo F., Katzenellenbogen J.A.: J. Am. Chem. Soc., 120, 4514-4515 (1998).
[7]. Prakash S., Went M.J., Blower P.J.: Nucl. Med. Biol., 23, 543-549 (1996).
[8]. Top S., Morel P., Pankowski M., Jaouen G.: J. Chem. Soc., Dalton Trans., 3611-3612 (1996).
[9]. Mullen G.E.D., Blower P.J., Price D.J., Powell A.K., Howard M.J., Went M.J.: Inorg. Chem., 39, 4093-4098 (2000).
[10]. Fuks L., Gniazdowska E., Mieczkowski J., Narbutt J., Starosta W., Zasępa M.: J. Organomet. Chem., 89, 4751 (2004).
[11]. Fuks L., Gniazdowska E.: Unpublished results obtained at the Institute of Chemistry, University of Zurich, and at the Paul Scherrer Institute, Villigen, Switzerland, 2002.
[12]. Neuere Methoden der Präparativen Organischen Chemie. Band III. Verlag Chemie, 1961, p.30, in German.
[13]. Schibli R.: Normaldrucksynthese von $(TcCl_3(CO)_3)^{2-}$ und $(ReCl_3(CO)_3)^{2-}$ und ihr Substitutionsverhalten im Hinblick auf Anwendungen in der Nuklermedizin. Ph.D. Thesis. Paul Scherrer Institute, Villigen, Switzerland, 1996, in German.

DENSITY FUNCTIONAL CALCULATIONS ON TRICARBONYLTECHNETIUM(I) COMPLEXES WITH AMIDES OF PICOLINIC AND THIOPICOLINIC ACIDS AND RELATED LIGANDS

Marian Czerwiński[1/], Jerzy Narbutt

[1/] Chemistry Institute, Jan Długosz University, Częstochowa, Poland

Tricarbonyl complexes of technetium(I), the derivatives of *fac*-$[^{99m}Tc(CO)_3(H_2O)_3]^+$ (**1**), containing a chelating ligand in the molecule [1], meet a great interest in radiopharmaceutical chemistry. The or-

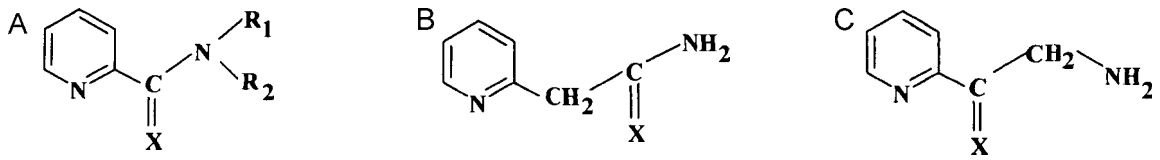

Scheme.

ganometallic precursor **1** has three coordination sites occupied by labile H_2O molecules – only these sites are available for substitution by other ligands. The other three sites are blocked by tightly bound CO ligands which withdraw electron density from the metal by π-backbonding. That is why **1** in aqueous solution behaves as an aqua-ion of unusually low coordination number, CN=3. This makes it easily coordinated by numerous bi- and tridentate ligands. Thermodynamically stable chelates with ligands of soft donor atoms (N_{aromat}, S, P) seem particularly promising in this respect [2]. Another feature of such chelates is their high kinetic inertness – an important quality of radiopharmaceuticals.

The aim of this work was to study theoretically a series of neutral $[Tc(CO)_3LX]$ complexes with various L, where X is the monovalent anion and L is the neutral chelating ligand of soft donor atoms N_{aromat} and S, in order to select, from the group of N-substituted amides of thiopicolinic acid, these ligands which form the most stable chelates. The effect of the substituents on the chelate stability was investigated. For comparison, we also studied the oxygen-containing analogues of these N,S-ligands, the picolinamides, and also some homologous ligands with an additional CH_2 group located in two different places of the molecule. This made us possible to compare the stability of chelates formed by analogous amide N,O- and N,S-ligands, by homologous amide ligands forming five- and six-membered chelate rings, and – finally – by ligands with the donor O (or S) atoms belonging to either (thio)amide or (thio)carbonyl groups.

Quantum-mechanics calculations were already carried out by other authors both on the tricarbonyltechnetium(I) precursor (**1**) [3] and on some picolinamide ligands [4]. Following a similar way we optimized the gas-phase structures and calculated the total energies of **1**, its neutral chloride form, $[Tc(CO)_3(H_2O)_2Cl]$ (**2**), twelve free ligands studied, and their twelve tricarbonylchlorotechnetium(I) complexes. The energies of complex formation were then calculated as the differences between the total energies of the products and substrates of the gas-phase reaction.

Density functional calculations were used, based on the density functional theory (DFT), as described in an earlier paper [5]. Three-parameter Becke functionals of B3LYP type were used with the Lanl2dz basis set, which made it possible to consider relativistic and polarization effects for Tc. Berny geometry-optimization algorithm was applied to calculate the geometry of the species studied. All the numerical calculations were carried out using Cray J90 and Cray Y-MP supercomputers, based on the implementation of the GAUSSIAN-98 program [6].

The calculations were carried out for ligands of three different classes shown on Scheme.

The numbering of important atoms in the class **A** ligands begins from the pyridine N and C atoms: N1-C6-C7(X8)-N9, *etc*.

Table 1 presents some selected bond lengths and ligand bites in optimized L^2 and L^6, the representative of class **A** molecules. Our recent experimental (single crystal X-ray) data for L^6 [7] are shown for comparison. Table 1 also shows some data for the optimized *fac*-$[Tc(CO)_3LCl]$ chelates with these ligands together with the experimental data [7,8] for their rhenium analogues. The other

Table 1. Selected bond lengths and ligand bites [pm] in the molecules of the free L^2, L^6 ligands and their $[M(CO)_3LCl]$ chelates, calculated (DFT) for M=Tc and experimental (X-ray) for M=Re. For the ligand specification, see Table 2.

	Ligand L^2 (X=O)				Ligand L^6 (X=S)			
	DFT, M=Tc		X-ray, M=Re [8]		DFT, M=Tc		X-ray, M=Re [7]	
	ligand	chelate	ligand	chelate	ligand	chelate	ligand	chelate
C7-X8	126.4	127.7	no data	125.2	172.3	174.4	167.3	166.9
N1-C6	136.1	137.0	"	133.4	136.5	137.1	132.4	136.1
C6-C7	151.2	150.1	"	147.7	150.5	149.2	150.7	147.1
C7-N9	136.4	135.4	"	130.4	135.2	134. 5	129.0	132.7
M-N1	-	219.5	-	217.6	-	219.1	-	219.2
M-X8	-	220.3	-	216.4	-	262.2	-	244.4
M-Cl	-	253.7	-	245.7	-	255.5	-	247.6
M-C[a)]	-	191.7	-	189.3	-	191.9	-	190.7
N1...X8	361	266	no data	261	404	307	~396	296

[a)] The mean length of three bonds.

geometrical data calculated for these systems and all the data calculated for the other ligands studied and their technetium chelates are collected in supporting information available from the authors. All the ligands studied have been specified in Table 2.

Table 2. Specification of the ligands studied, L^i (i=1-12), Mulliken charges on some atoms in the $[Tc(CO)_3L^iCl]$ chelates, the change in the total charge on the neutral L^i ligands upon chelating, and the energy of the chelate formation in the gas state [kJ/mol].

Ligands			q_{Tc}		q_X		Δq[a)]		ΔE	
abbreviation[b)]	class	NR_1R_2	X=O	X=S	X=O	X=S	X=O	X=S	X=O	X=S
$2H_2O$[c)]	-	-	0.33	-	-	-	-0.30	-	-259	-
L^1, L^5	**A**	NH_2	0.30	0.13	-0.31	0.14	-0.36	-0.50	-197	-183
L^2, L^6	**A**	$NHCH_3$	0.31	0.14	-0.33	0.12	-0.37	-0.51	-201	-186
L^3, L^7	**A**	NHC_6H_5	0.32	0.14	-0.34	0.18	-0.35	-0.51	-190	-178
L^4, L^8	**A**	$N(CH_3)_2$	0.31	0.16	-0.35	0.09	-0.38	-0.50	-222	-217
L^9, L^{10}	**B**	NH_2	0.28	0.10	-0.36	0.18	-0.41	-0.55	-207	-190
L^{11}, L^{12}	**C**	NH_2	0.29	0.08	-0.27	0.25	-0.35	-0.52	-213	-209

[a)] Transfer of electron density (charge) in a chelate molecule from L to $Tc(CO)_3Cl$.
[b)] The lower number in each pair of ligands corresponds to X=O, the higher – X=S.
[c)] Two water ligands in **2.**

A significant shortening of the C7-N9 bond is observed in amide and thioamide ligands, both free and bound, to *ca*. 135 pm in comparison to the C-N bond length in aliphatic compounds, of *ca*. 148 pm. This effect is due to the conjugation of the lone electron pair on the N9 atom with π-electrons of the C7-X8 bond, which makes the C7-N9 bond of some double-bond character. The $C\text{-}N_{amine}$ bonds of *ca*. 147 pm in the L^{11} and L^{12} ligands already have a "normal" aliphatic character. The N1-C6 and C7-O8 distances in the L^1 and L^4 ligands are by *ca*. 1-2 pm shorter and by *ca*. 3-4 pm longer, respectively, than those calculated (DFT, HF and MP2) by Wipff *et al*. [4].

The optimization of the free ligand molecules in the gas phase led to their configurations differing in the torsion angles (θ) between the planes of pyridine and of the X8-C7-N9 atoms, rotating around the C6-C7 bond. Assuming for the *cis* configuration of the donor N1 and X8 atoms in the planar molecules (as in the chelates) θ=0°, the minimum energies corresponded to θ≅180°, *i.e*. to the planar *trans* configurations, except for L^4 (θ≅155°) and L^8 (θ≅139°). For comparison, the gas-phase configuration of L^1 calculated by Wipff gave θ≅141° [4] and the experimental solid state structures gave θ≅162° for L^1 [9] and θ≅173° for L^6 [7].

The N1…X8 distances (ligand bites) in the class **A** planar N,O- and N,S-ligands and in their chelates are very close to those calculated for the respective L^2 and L^6 species (Table 1). In the twisted free L^4 and L^8 ligands, the bites are shorter (357 and 389 pm) than in the planar ones. The bites in non-amide, class **C** ligands (360 and 402 pm) and in their chelates (264 and 302 pm) are nearly the same as in the class **A** species. On the contrary, the bites in the respective class **B** ligands (432 and 475 pm) and in their six-membered ring chelates (293 and 329 pm) are significantly longer.

Mulliken charges on the donor atoms in all the ligand studied, except for L^{11} and L^{12}, are equal to *ca*.: $q_{N1}=-0.1\pm0.05$ e, $q_O\cong-0.3$ e and $q_S\cong-0.1$ e. The charge on the amide (amine) nitrogen strongly depends on the substituents; it is markedly negative (-0.3 to -0.6 e) except for L^4 (-0.12) and L^8 (-0.03). The charges on the donor atoms of the L^1 and L^4 ligands are less negative than those calculated by Wipff *et al*. [4], but their mutual relations are almost the same.

The bond lengths calculated for **1** and **2** are: Tc-C=191.7 and 191.0 pm; Tc-O=223.6 and 222.7 pm, respectively, and Tc-Cl=255.5 pm. The charges on Tc in **1** and **2** are 0.49 and 0.33 e, respectively, and the charge on the Cl atom in **2** is -0.36 e. The data for **1** are very close to the corresponding values calculated (DFT) in [3]. The calculations show that all the ligands substitute two water molecules in **2** and bond to Tc by means of the N1 and X8 atoms forming this way either five- or six-membered chelate rings (Fig.).

The chelate formation is accompanied by small changes in the geometrical parameters of both L and **2**, and in the charge distribution on their atoms. A comparison of both calculated and experimental bond lengths in the molecules of free and chelated ligands shows that complex formation results in a significant elongation of bonds involving the donor atoms (C7-X8 and N1-C6) and shortening the neighbour bonds in the ligand. The cal-

culated (gas phase, 0 K) bond lengths are, as a rule, somewhat (1-6 pm) longer than the respective experimental values (crystal, 298 K). Similar small differences between the calculated and experimental distances observed for other metal complexes were explained as the effect of libration of atoms in the real molecules, which made the experimental bond lengths shorter than those in the virtual

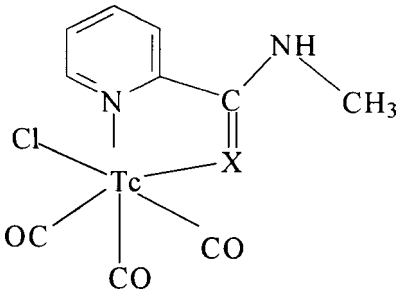

Fig. Stick formula of the *fac*-[$Tc(CO)_3LCl$] chelates with the L^2 and L^6 ligands.

"frozen" molecule [10]. On the other hand, a much greater difference (*ca*. 18 pm) found in the M-S distances, was accompanied by non-planarity of the chelate ring, observed in the optimized structures of the technetium chelates with the N,S-ligands. The S atoms in the Tc-N-C-C-S and Tc-N-C-C-C-S rings are shifted by *ca*. 80 pm over the plane of the remaining atoms. On the contrary, the Re-N-C-C-S ring in the crystalline *fac*-[$Re(CO)_3L^6Cl$] chelate is planar [7]. This difference seems not to be the result of insufficient quality of the calculations. To check this, we additionally optimized the structures of the L^2, L^6 ligands by means of more accurate *ab initio* (unrestricted HF) method with the 6-311G** basis. The new structures appeared very similar to those obtained by DFT with B3LYP potential. Therefore, we may expect that the non-planar structures of the chelate rings are not artifacts, and the planarity of the sulphur-containing chelate ring in the crystal results from interactions between the chelate molecules in the solid state. Supplementary calculations on this hypothetical "packing" effect, carried out for systems consisting of two, three and four [$Tc(CO)_3L^6Cl$] molecules, indicate that with increasing number of closely packed chelate molecules both the deformation of the chelate ring and the length of the Tc-S bond decrease.

Table 2 presents Mulliken charge distribution on the metal and the O and S donor ligand atoms in the [$Tc(CO)_3LCl$] chelates studied. Charge transfer from the ligands to the central metal ion upon chelate formation, decreases the positive charge on Tc and increases the negative charge on both donor atoms in the coordinated N,O-ligands, just as reported in [4]. The charges on the N1 donor atoms in the chelates with the five-membered rings are nearly constant, q_{N1}=-0.22 to -0.24 e, as well as the charges on the Cl atoms in the chelates, q_{Cl}=-0.32 to -0.34 e, except -0.41 e for L^7.

In the case of the N,S-ligand chelates a moderate increase in the negative charge on the N1 atoms is also observed, however, the decrease in the positive charge on the metal is large, at the expense of large changes in q_S. The significant positive charges on the S atoms in the chelates, compared to $q_S \cong$-0.1 e in the free ligands, give evidence of a greater charge transfer than that from the N,O-ligand chelates, consistent with the greater total charge transfer from L to $Tc(CO)_3Cl$, Δq. These high (0.3-0.5 e) Δq values give evidence of the significant covalencies of both Tc-O and Tc-S bonds and the greater values for the chelates with N,S-ligands (Table 2) support our expectation that these chelates would be more stable than their N,O-analogues.

However, the above conclusion seems inconsistent with the calculated energy changes of chelate formation, ΔE, calculated as the differences of the total energies of the chelates and those of $Tc(CO)_3Cl$ and L. The ΔE values include the energies necessary for attaining *cis* configurations by the free L^i ligands, the values of *ca*. 63 kJ/mol as calculated [4] for L^1. That is why the energy of attaching two water ligands to $Tc(CO)_3Cl$ is more negative than those for all the L^i ligands. Rather unexpectedly, the ΔE values appeared more negative for the N,O- than N,S-ligand chelates, and moreover, the correlation between the Δq and ΔE values was poor (Table 2).

The less negative ΔE values for the N,S-ligand chelates, in spite of the greater charge transfer than in their N,O-analogues, can result from the deformation of the Tc-N-C_n-S (n=2 or 3) rings (see above). The stabilizing π-π interactions in the analogous nearly planar Tc-N-C_n-O rings make the ΔE values of the chelates with N,O-ligands more negative. Moreover, when comparing theoretical and experimental interaction energies one must not neglect solvent effects. The expected stronger hydration energy of the N,O-ligands would affect the energies of formation of their chelates in aqueous solution more strongly than those of chelates with the analogous N,S-ligands. This would make the energies of chelate formation by analogous N,O- and N,S-ligands in solution more-or-less equal to each other. This is in agreement with our experimental data. Some of the ligands studied: L^2, L^6, L^7 and L^8 were synthesized [7,11] and their chelates – [$^{99m}Tc(CO)_3LOH$] – obtained at the non-carrier-added level following Alberto's procedure [1]. The equilibrium yields of two analogous chelates with L^2 and L^6 ligands are very close to each other [11] which may be considered as a proof of their similar stability. Also the yields of the chelates with L^7 and L^6 are close to each other [11].

Poor correlation between the Δq and ΔE values is mainly due to the much more negative ΔE values for $Tc(CO)_3L^4Cl$ and $Tc(CO)_3L^8Cl$, also inconsistent with the experiment which gives a low yield of [$^{99m}Tc(CO)_3L^8OH$] [11]. On the other hand, the calculated ΔE sequence for the pair of $Tc(CO)_3L^1Cl$ and $Tc(CO)_3L^4Cl$ chelates is in agreement with that calculated (HF) for the EuL^1Cl_3 and EuL^4Cl_3 pair (-272 *vs*. -314 kJ/mol) [4]; the greater negative values for the latter pair being probably due to the greater formal charge on Eu^{III} than on Tc^I. A reason for these strongly negative ΔE values seems to be the non-planar configuration of the substrates – the free L^4 and L^8 ligands. The *cis* configuration of L ($\theta \cong 0^o$), necessary to form

the chelate, is expected to be by a few tens of kJ/mol closer for L^4 ($\theta \cong 155^o$) and L^8 ($\theta \cong 139^o$) than for the other ligands of *trans* configuration ($\theta \cong 180^o$) in the gas state. However, this can be not the same in an aqueous solution because the free ligand configurations in solution need not be the same as in the gas state. Recent DFT (ADF) calculations on other bidentate ligands, using the COSMO methodology [12], resulted in a strong dependence of ligand configuration and energy on the dielectric constant of the electrostatic field in which the ligand molecule was embedded in order to model solvent effects [13]. Further calculations of the solvent effects would modify the formation energies of tricarbonyl complexes of technetium(I) with the ligands studied, making it better comparable with the experiment.

Nevertheless, both Δq and ΔE values significantly greater for $Tc(CO)_3L^9Cl$ and $Tc(CO)_3L^{11}Cl$ than for $Tc(CO)_3L^1Cl$ chelates, and also greater for $Tc(CO)_3L^{10}Cl$ and $Tc(CO)_3L^{12}Cl$ than for the $Tc(CO)_3L^5Cl$ ones, allow us to conclude on the chelate stabilizing effects both of six-membered over five-membered ring, and of the (thio)carbonyl – amine over the (thio)amide group in the chelating ligands. These conclusions indicate directions for further synthesis of ligands able to form stable tricarbonyltechnetium(I) chelates – potential radiopharmaceuticals.

The work was supported by the State Committee for Scientific Research (KBN) – grant No. 4 TO9A 110 23.

References

[1]. Alberto R., Schibli R., Waibel R., Abram U., Schubiger A.P.: Coord. Chem. Rev., 190-192, 901 (1999).
[2]. Technetium, Rhenium and Other Metals in Chemistry and Nuclear Medicine. 6. Eds. M. Nicolini and U. Mazzi. SGEditoriali, Padova 2002, pp.739.
[3]. Xiangyun W., Yi W., Xinqi L., Taiwei C., Shaowen H., Xionghui W., Boli L.: Phys. Chem. Chem. Phys., 5, 456-460 (2003).
[4]. Baaden M., Berny F., Madic C., Schurhammer R., Wipff G.: Solvent Extr. Ion Exch., 21, 199-220 (2003).
[5]. Narbutt J., Czerwiński M., Krejzler J.: Eur. J. Inorg. Chem., 3187 (2001).
[6]. Frish M.J. *et al.*: GAUSSIAN 98. Revision A.5. Gaussian, Inc., Pittsburgh PA 1998.
[7]. Fuks L., Gniazdowska E., Mieczkowski J., Narbutt J., Starosta W., Zasępa M.: J. Organomet. Chem., 689, 4751-4756 (2004).
[8]. Fuks L., Gniazdowska E., Narbutt J., Starosta W.: Tricarbonyl(N2-methyl-2-pyridinecarboamide)chlororhenium(I) as a precursor of radiopharmaceuticals. In: INCT Annual Report 2004. Institute of Nuclear Chemistry and Technology, Warszawa 2005, pp.69-71.
[9]. Takano S., Sasada Y., Kakudo M.: Acta Crystallogr., 21, 514 (1966).
[10]. Frąckiewicz K., Czerwiński M., Siekierski S.: Secondary Periodicity in the Tetrahalogeno Complexes of the Group 13 Elements. Eur. J. Inorg. Chem., submitted.
[11]. Zasępa M., Mieczkowski J., Narbutt J.: ^{99m}Tc(I) Tricarbonyl Complexes with N-Methylamides of Picolinic and Thiopicolinic Acids. to be published.
[12]. Klamt A., Jones V.: J. Chem. Phys., 105, 9972 (1996).
[13]. Drew M.G.B.: Personal communication, 2005.

GALLIUM ISOTOPES EFFECTS IN THE DOWEX 50-X8/1.5÷3.0 M HCl SYSTEMS

Wojciech Dembiński, Irena Herdzik, Witold Skwara, Ewa Bulska[1/], Irena A. Wysocka[1/]

[1/] Faculty of Chemistry, Warsaw University, Poland

The occurrence of gallium isotope effect ($^{69/71}$Ga) in the strong cation exchanger/HCl system, first announced in [1], has been confirmed in a series of separation experiments. The concentration of acid in the system was in the range 1.5÷3.0 M HCl. The range was chosen because it covers the left branch of U-shape relation between K_d and the acid concentration (Fig.1). It was of interest to recognize if the value of K_d influences unit separation factors of the gallium isotopes.

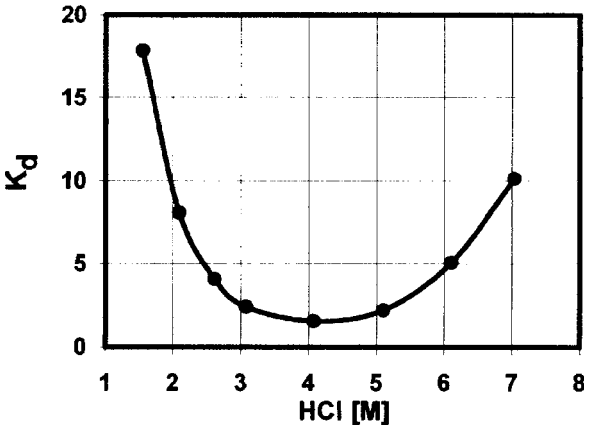

Fig.1. K_d *vs*. concentration of HCl.

The resin was a strong acidic cation exchanger, Dowex 50-X8, 200-400 mesh. The column was 100 cm high and 0.5 cm in inner diameter.

The slurred resin was packed into the column and the hydrochloric acid of proper concentration was flowed for at least 24 h with a flow rate of 0.3 ml/min. Then, the band of gallium chloride was created at the top of the column by injecting a sample solution containing 2.7 mg Ga in 2 M HCl. The band was eluted by hydrochloric acid with a flow rate of 0.11 ml/min. The band was repeatedly cycled over the column in order to increase the number of theoretical plates. After a certain number of cycles, the band was eluted to fraction collector in 1÷2 ml portions.

The gallium content in consecutive fractions was followed qualitatively by spot tests with Rhodamine B [2] and then determined quantitatively by atomic absorption analysis with flame atomisation.

The isotope ratio $^{69/71}$Ga (R) in selected fractions was determined by an inductively-coupled-plasma mass spectrometer, ICP-MS Elan 9000, Perkin

Elmer Sciex. Prior to the analysis the chlorides were removed from the samples containing more than 5 μg Ga by evaporation with 4 M HNO_3 to dryness and dissolving the residue in 0.1 M HNO_3. The relative standard deviation of a measurement was usually 0.05%.

The local separation factor defined as $q_i = R_i/R_{feed\,I}$ or the local separation gain defined as $\varepsilon = \ln(q_i)$ were calculated from the data.

The change of the local separation gain observed as a function of the eluted fraction of gallium (Δn/n) is shown in Fig.2. The S-shape relation was typical

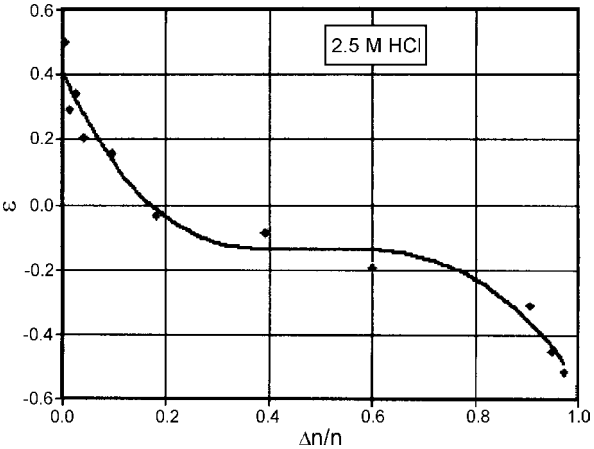

Fig.2. Isotope separation gain (ε) *vs*. eluted fraction of gallium (Δn/n).

of all the experiments. It revealed that the front part of the band is enriched in the lighter isotope, ^{69}Ga, whereas the rear part of the band in heavier isotope, ^{71}Ga. In other words, it may be stated that the lighter isotope is fractionated into the solution, whereas the heavy isotope into in the resin phase.

The results of the experiments are shown in Table.

Table. Results of separation experiments.

HCl [M]	K_d	N	Q_{max}	ε x 10^{-5}
1.5	19	4000	1.002	~1
2.0	9.1	2650	1.007	2.4
2.25	6.5	3150	1.008	2.8
2.5	4.1	3700	1.010	3.3
3.0	2.6	4100	1.011	2.7

N is the number of theoretical plates calculated as $N=8*(V_{el}/\beta)$, where β is the band width at the concentration C_{max}/e.
Q_{max} is the process separation factor equal to the ratio $R_{(front\ end)}/R_{(rear\ end)}$, where both R values observed are extreme.
$\varepsilon=\ln(q_i)$ is the unit separation gain equal to $S/N^{0.5}$, where S is the slope of linear function n of ε against the Δn/n value at another X-axis scaled in standardize differences (Z) of normal distribution (Fig.3). The same result could be obtained by plotting ε against Δn/n on a probability graph paper.

The value of the separation factor was found to be within the range expected for such systems, which is $10^{-4} \div 10^{-6}$, as follows from the review of

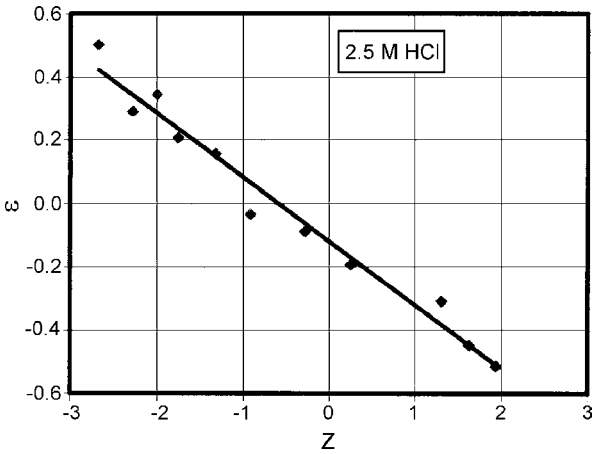

Fig.3. Isotope separation gain (ε) *vs*. eluted fraction (Δn/n) in Z units.

separation data obtained for other elements. Higher values were usually observed in electron exchange systems, or when more sophisticated exchangers, like crown ethers or cryptants, were used.

The classic theory of isotope effects [3] yields the following expression of ε in terms of the reduced partition function ratio (RPFR) and molar fractions of gallium species involved in the system, $x_i y_i$:

$$\varepsilon = \ln(x_1 f_{Ga+3} + x_2 f_{GaCl+2} + \cdots)_{resin} - \ln(y_1 f_{Ga+3} + y_2 f_{GaCl+2} + \cdots)_{sol}$$

where *f* is RPFR. Difference in respect to the hydration spheres around metal ions is omitted for simplicity.

As ε is not equal to zero, the summing up in brackets (if possible) should result in higher value of the sum for the resin than for the solution. This means, according to classic theory (based on the analysis of vibration energy), that the resin phase creates the stronger bonds to the element involved in the isotope exchange reaction than the liquid phase does. This statement should be a subject of further consideration.

The work is in progress.

This work was supported by the State Committee for Scientific Research (KBN) – grant No. 4 T09A 057 25.

References

[1]. Dembiński W., Herdzik I., Skwara W., Bulska E., Wysocka A.: Preliminary results of fractionation of gallium isotopes in the DOWEX 50-X8/HCl system. In: INCT Annual Report 2003. Institute of Nuclear Chemistry and Technology, Warszawa 2004, pp.69-70.
[2]. Feigl F., Anger V.: Spot tests in inorganic analysis. Elsevier, 1972, p.233.
[3]. Bigeleisen J., Mayer M.G.: J. Chem. Phys., 15, 261 (1947).

EFFECT OF TEMPERATURE AND THE MECHANISM OF BAND SPREADING IN CATION EXCHANGE SEPARATION OF RARE EARTH ELEMENTS BY ION CHROMATOGRAPHY

Krzysztof Kulisa, Rajmund Dybczyński

The temperature effect on the ion exchange separations and the mechanism of zone spreading has been investigated in previous years on an example of anions [1,2] as well as alkali metals, alkaline earth cations and amines [3]. An ion chromatograph Dionex 2000i/SP equipped with Dionex Ion Pac type analytical columns was used in this work.

Rare earth elements (REE) are considered as important elements from a geochemical, industrial and agricultural point of view. According to IUPAC recommendation the term of "rare earth elements" refer to the lanthanides as well as Sc, Y and La [4]. The chemical separation and determination of REE as simple trivalent cations are generally difficult and complex because of the similarity of their chemical properties and small differences in ionic radii.

Ion chromatography (IC) as a fast and practical method for separation and determination of REE became very popular in recent years employing both anion and cation exchange mechanisms of ion exchange reactions. When attempting to reproduce a procedure for the determination of REE by IC on a column with strongly acidic functional groups and gradient elution with α-hydroxyisobutyric acid (α-HIBA) [5] it was found that the quality of separation of some adjacent lanthanides was much poorer than described in the literature. Moreover, in these conditions, the peaks of Dy^{3+} and Y^{3+} (which accompany heavier lanthanides) remained unresolved. To optimize the method, several isocratic separations of REE were performed including also temperature as an additional factor influencing the separation.

In order to carry out isocratic elutions, REE cations have been divided into two groups composed of cations showing a lower and higher affinity to the ion exchanger, respectively. One isocratic elution run appeared to be impossible because of extremely high retention times and very low separation efficiency of strongly retained cations. Ion Pac CS3 column with Ion Pac CG3 guard containing $-SO_3^-$ functional groups were used in this study. The first group of cations included: Sc^{3+}, Lu^{3+}, Yb^{3+}, Tm^{3+}, Er^{3+}, Ho^{3+}, Y^{3+}, Dy^{3+} and Tb^{3+}. These cations were eluted from the Ion Pac CS3 column with the use of 80 mmol·L^{-1} α-HIBA. The second group consisted of Eu^{3+}, Sm^{3+}, Nd^{3+}, Pr^{3+}, Ce^{3+} and La^{3+}, the cations being eluted using 220 mmol·L^{-1} α-HIBA. Gd^{3+} cation was not taken into account in the study because of its interference with Eu^{3+} in these conditions. Concentration of both eluents used were established experimentally in order to achieve possibly efficient separation of all REE cations studied in a reasonable low time of elution. Flow rate of the eluents was 1 mL·min^{-1}. All the injections were performed manually with a 100 μL Tefzel sample loop (Dionex).

The REE compounds in the eluate have been converted into colour complexes with the use of a post-column complexing reagent PAR (4-(2-pyridylazo)resorcinol) in the Dionex Ion Pac Membrane Reactor. Post-column reagent flow rate was 0.7 mL·min^{-1}. Coloured REE complexes were detected by photometric detection at 520 nm using the Dionex UV/VIS Variable Wavelength Detector VDM II.

The chromatograms were obtained in all experiments as a function of column temperature. Changes of chromatographic parameters of 14 lanthanide cations, Sc^{3+} and Y^{3+} were established in the range of column temperature 10-65°C when separating the cations studied using both gradient and isocratic elution modes. The chromatograms were recorded at 10, 25, 35, 45 and 65°C.

Elution curves of Sc^{3+}, Lu^{3+}, Yb^{3+}, Tm^{3+}, Er^{3+}, Ho^{3+}, Y^{3+}, Dy^{3+} and Tb^{3+} cations obtained during isocratic elution at 25 and 65°C on an Ion Pac CS3 column are presented in Fig.1a and b, respectively. The increase of the temperature from 10 up to 65°C caused an increase in retention factors of all REE's studied. This means that the overall ion exchange-complexation reaction revealed endothermic character for all REE studied. The Sc^{3+} cation showed very low affinity to the ion exchange resin in these conditions. Y^{3+} and Dy^{3+} coeluted at lower tem-

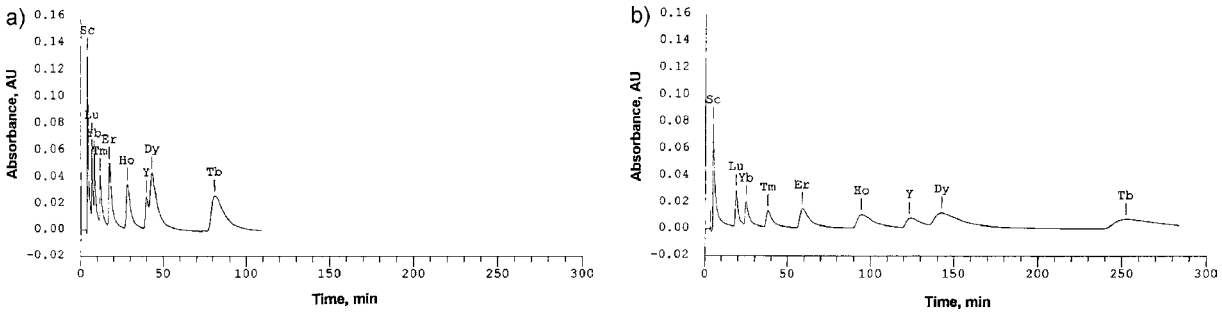

Fig.1. Elution curves of Sc^{3+}, Lu^{3+}, Yb^{3+}, Tm^{3+}, Er^{3+}, Ho^{3+}, Y^{3+}, Dy^{3+} and Tb^{3+} obtained during isocratic elution at 25°C (a) and 65°C (b). Column – Ion Pac CS3 and CG3, eluent – 80 mmol·L^{-1} α-HIBA, flow rate – 1 mL·min^{-1}. Sample: Sc^{3+} – 5 mg·L^{-1}; Lu^{3+}, Yb^{3+}, Tm^{3+} and Y^{3+} – 10 mg·L^{-1}; Er^{3+} and Ho^{3+} – 20 mg·L^{-1}; Dy^{3+} – 30 mg·L^{-1}; Tb^{3+} – 40 mg·L^{-1}.

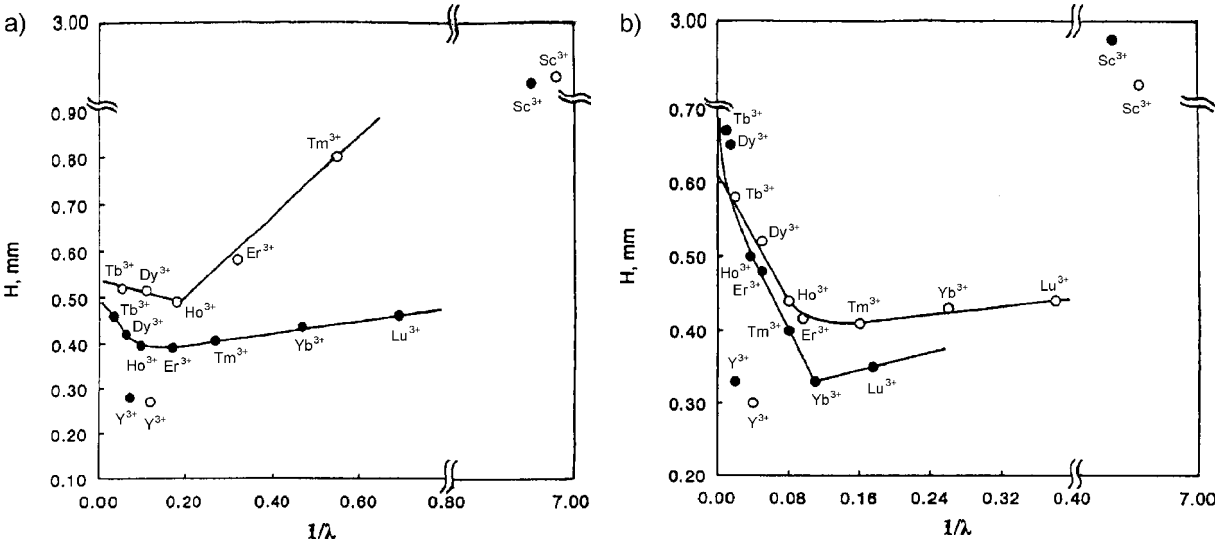

Fig.2. Plate heights calculated from elution curves of Sc^{3+}, Lu^{3+}, Yb^{3+}, Tm^{3+}, Er^{3+}, Ho^{3+}, Y^{3+}, Dy^{3+} and Tb^{3+} obtained on Ion Pac CS3 + CG3 column and 80 mmol·L^{-1} α-HIBA eluent at: a) 10°C – open circles and 25°C – full circles; b) 45°C – open circles and 65°C – full circles. Flow rate: 1 mL·min^{-1}; sample: Sc^{3+} – 5 mg·L^{-1}; Lu^{3+}, Yb^{3+}, Tm^{3+} and Y^{3+} – 10 mg·L^{-1}; Er^{3+} and Ho^{3+} – 20 mg·L^{-1}; Dy^{3+} – 30 mg·L^{-1}; Tb^{3+} – 40 mg·L^{-1} as a function of reciprocal of the distribution coefficient.

peratures. The best separation of these cations was achieved at 65°C.

The plate heights, H, calculated from elution curves of REE cations taken at 10, 25, 45 and 65°C are shown in Fig.2. Values of H calculated for Sc^{3+}, Lu^{3+}, Yb^{3+}, Tm^{3+}, Er^{3+}, Ho^{3+}, Y^{3+}, Dy^{3+} and Tb^{3+} are plotted *vs.* reciprocal of the weight distribution coefficient, 1/λ in Fig.2. At low temperature (10°C), column efficiency of lanthanide cations (Dy^{3+}, Tb^{3+}) showing a high affinity to the ion exchanger (λ>9) was poorer than that of Ho^{3+} (λ=5.5). The H *vs.* 1/λ plot after initial decrease, reached a minimum and then increased. This tendency became more intense at higher temperature (25°C), and the column efficiency of Ho^{3+} (λ=10.5) was slightly poorer than that observed for Er^{3+} (λ=6.1). Further temperature increase caused substantial intensification of the phenomenon. At 45°C, a slight decrease of column efficiency was observed for Er^{3+} (λ=10.5) compared with Tm^{3+} (λ=6.4), while at 65°C column performance for Tm^{3+}, showing only a moderate affinity to the ion exchanger, was distinctly poorer than that calculated for Yb^{3+} and Lu^{3+} (Fig.2b).

Changes of column efficiency observed for Sc^{3+} and Y^{3+} differed considerably from other REE cations. Values of the plate height of Y^{3+} were as a rule distinctly lower than those for other REE cations studied of similar ionic radius values at each column temperature, while the plate heights calculated for Sc^{3+} were considerably higher. The points referring to the values of the plate height of Y^{3+} and Sc^{3+} as a function of 1/λ are marked in Fig.2 to illustrate this phenomenon. The differences in chromatographic behaviour between Sc^{3+} and Y^{3+} and the lanthanides would indicate that the 4*f* electrons may contribute to the complex formation reaction. The results from isocratic elution experiments made it possible to derive an improved procedure for the separation of all REE by gradient elution with α-HIBA (Fig.3).

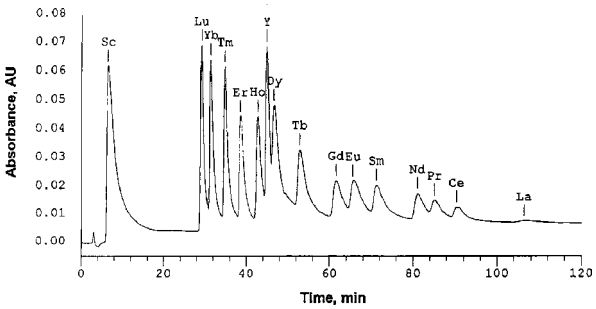

Fig.3. Elution curve of 14 lanthanides, Sc^{3+} and Y^{3+} obtained during gradient elution. Column: Ion Pac CS3 and CG3; eluent: time 0 min – 56 mmol·L^{-1} α-HIBA, time 85 min – 280 mmol·L^{-1} α-HIBA; temperature: 65°C; flow rate: 1 mL·min^{-1}; sample: each cation – 10 mg·L^{-1}.

Table. Details of gradient pump program.

Time [min]	Eluent 1 Millipore superpure water (18 MΩ·cm) [%]	Eluent 2 0.4 mol·L^{-1} α-HIBA [%]	Temperature [°C]
0.0	86	14 (56 mmol·L^{-1} α-HIBA)	65
13.0	86	14 (56 mmol·L^{-1} α-HIBA)	65
60.0	60	40 (160 mmol·L^{-1} α-HIBA)	65
85.0	30	70 (280 mmol·L^{-1} α-HIBA)	65

To achieve a good separation of REE cations (14 lanthanides, Y^{3+} and Sc^{3+}), a combined linear gradient and isocratic elution mode was applied employing gradient pump (Dionex, AGP). Details of gradient pump program have been established experimentally and are given in Table.

The studies confirmed that similarly to anions as well as alkali metal, alkaline earth cations and amines also in the case of REEs the longitudinal diffusion in the resin phase may contribute to the total column plate height for some cations showing high distribution coefficients. The column temperature may serve as an important parameter influencing the column performance during REE cation exchange separations. The increased temperature usually improved column efficiency by decreasing the plate height of REE cations showing a low or moderate affinity to the resin phase, although for cations strongly retained by the ion exchanger the reverse tendency was observed with the rise in temperature.

References

[1]. Kulisa K., Dybczyński R.: The study on the influence of temperature on ion exchange separations of anions and the stability of anion exchange columns in isocratic ion chromatography. In: INCT Annual Report 2003. Institute of Nuclear Chemistry and Technology, Warszawa 2004, pp.74-76.
[2]. Dybczyński R., Kulisa K.: Chromatographia, 57, 475-484 (2003).
[3]. Kulisa K.: Chem. Anal. (Warsaw), 49, 665-689 (2004).
[4]. Henderson P.: Rare Earth Element Geochemistry. Elsevier, Amsterdam 1984.
[5]. Heberling S.S., Riviello J.M., Shifen M., Ip A.W.: Res. Dev., 74 (September 1987).

ACTIVATION ANALYSIS OF SOME ESSENTIAL AND TRACE ELEMENTS IN BLACK AND GREEN TEA

Ewelina Chajduk-Maleszewska, Rajmund Dybczyński, Andrea Salvini[1/]

[1/] Laboratorio Energia Nucleare Applicata, University of Pavia, Italy

Trace elements play an important role in human health, both as essential elements, which have to be maintained at an optimum level, and as toxic elements, which have harmful effects even at low levels. There are at least 40 elements that are vital for well being of humans. Metals and other elements are present in food either naturally, or as a result of human activities (*e.g.* industrial and agricultural practices) or from contamination during processing and storage or added deliberately (supplementation).

Tea is probably most widespread type of beverage among all nations. Tea leaves are used in many diverse ways, not only as extracts, but also as a constituent of medicines and cosmetics. Thus, the chemical components in this type of materials have received great interest because they are related to health and disease. The chemical constituents present in the plants are responsible for their medicinal as well as toxic properties which include different organic compounds *e.g.* vitamins, flavonoids, alkaloids, *etc*. The trace elements play a very important role in the formation of these compounds. Also, the concentration of certain elements is a good indicator evidential about the origin of the samples.

This study was carried out to obtain information on the concentration of major, minor and trace elements in this type of material.

For our research we chose black and green tea leaves deriving from China (Yunnan black and green tea), India (Assam black and green tea) and Sri Lanka (Ceylon black and green tea). All samples were commercially available in Polish supermarkets and health food shops. Producers and exporters confirmed origin of samples. The samples were crushed to homogeneous fine powder, next weighed, homogeneous materials were put into polyethylene vials and were irradiated in the nuclear reactor TRIGA MARK II (Pavia, Italy) at a thermal neutron flux ($2x10^{12}$ n cm^{-2} s^{-1}) for 5 minutes, 1 hour and 30 hours, respectively. Irradiation time was appropriate to the half-lives of the activation products being measured. The mass of samples was dependent on irradiation time and was varied between 50 mg (for short irradiation) and 100 mg (for medium and long irradiation). The multielemental standards (Bovine Liver 1577A and Tomato Leaves 1573A) and blank were irradiated together with the samples. Certified reference material Tea Leaves (INCT-TL-1) was used as quality control standard

Table. Concentration range of some minor and trace elements in Yunnan black tea leaves.

Element	Content [mg/kg]	Element	Content [mg/kg]
Al	1053 ± 37	K	19442 ± 437
As	0.224 ± 0.088	La	0.564 ± 0.032
Ba	22.50 ± 1.08	Lu	0.009 ± 0.001
Br	9.81 ± 0.75	Mg	2113 ± 87
Ca	3481 ± 213	Mn	631.3 ± 13.2
Ce	0.580 ± 0.058	Na	9.81 ± 0.91
Cl	753.5 ± 35.5	Rb	144.0 ± 3.9
Co	0.222 ± 0.021	Sb	0.018 ± 0.05
Cr	2.55 ± 0.28	Sc	0.083 ± 0.003
Cs	1.74 ± 0.09	Tb	0.009 ± 0.001
Eu	0.018 ± 0.004	Yb	0.048 ± 0.007
Fe	199.8 ± 6.2	Zn	31.44 ± 3.77
Hf	0.048 ± 0.010		

to validate the analytical technique. All samples and reference materials were prepared in triplicate. The counting and measurement of samples was done at the University of Pavia (Laboratorio Energia Nucleare Applicata) with the aid of HPGe detectors (Ortec) with associated electronics, coupled to the multichannel analysers and spectroscopy software GammaVision 3.2. We determined 26 elements: Al, As, Au, Ba, Br, Ca, Ce, Cl, Co, Cr, Cs, Eu, Fe, Hf, K, La, Lu, Mg, Mn, Na, Rb, Sb, Sc, Tb, Yb, Zn. The elemental content for Yunnan black tea leaves is shown in Table. The main constituent elements of tea leaves were: Al, Ca, Cl, K, Mg, and Mn. Among the alkaline metals, Mg and Ca are the major essential elements and are present in all leaves studied. The concentration of several determined elements is the highest in Ceylon green tea. Because Al is one of the easily extracted elements (*ca*. 35%) and is suspected to have a role in developing Alzheimer's disease it is very important to determine Al content in black tea leaves. Its concentration was between 600 and 2000 ppm. Bromine is present in varying amounts in all the leaves analysed. Its concentration is in the range of 1.8 to 17 ppm. It has been found to be selectively accumulated in plants from soil. In all cases, the results obtained for As show bigger concentration in green than in black tea leaves (Fig.) – it is the effect of different procedures during the preparation of black and green tea leaves. The variation in the elemental concentration levels of tea leaves clearly showed the influence of the different soil conditions in which plants have grown.

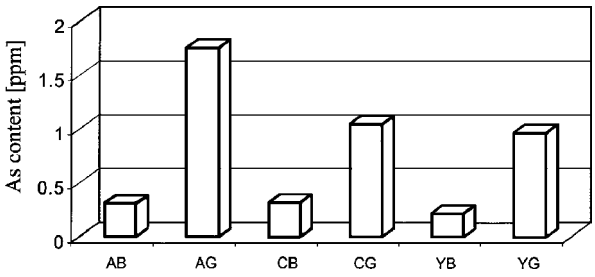

Fig. Concentration of As in tea leaves (AB – Assam black, AG – Assam green, CB – Ceylon black, CG – Ceylon green, YB – Yunnan black, YG – Yunnan green).

Generally, the observed differences in the concentration of these elements are attributed to factors such as the preferential absorbability of particular kinds of plant for the corresponding elements, the age of the plant, the mineral composition of the soil in which the plant grows, season of collection samples, as well as its ambient climatological conditions. Hence, there is an interest in tracing major, minor and trace elements in extracts obtained from tea leaves. We have shown that instrumental neutron activation analysis is a powerful analytical tool and can well serve for multielemental analysis of tea leaves. The data obtained from the study should prelude to detailed multielemental analysis of tea infusions. Although concentration of metals and other elements in beverages are generally low, they can make a significant contribution to dietary intake because of the potentially large quantities consumed.

POTENTIAL OF RADIOCHEMICAL NEUTRON ACTIVATION ANALYSIS AS A PRIMARY RATIO METHOD

Halina Polkowska-Motrenko, Bożena Danko, Rajmund Dybczyński

Primary methods of measurements (PMM) are very important elements of chemical metrological system. According to the definitions adopted by CCQM in 1998 [1]: A primary method of measurement is the method having the highest metrological qualities, whose operation can be completely described and understood, for which a complete uncertainty statement can be written down in terms of SI units. A primary direct method measures the value of an unknown without reference to a standard of the same quantity. A primary ratio method measures the value of the ratio of an unknown to a standard of the same quantity; its operation must be completely described by a measurement equation.

By this definition, primary methods result in SI unit-traceable values with the smallest combined uncertainties (representing the highest metrological quality). The use of PPM allows checking the accuracy of chemical results obtained by other (routine) methods of analysis. Isotope dilution mass spectrometry (IDMS) is the only trace analysis method indicated by CCQM as PMM. However, even PMMs are the methods that have only the potential to be primary methods. This means that the application, or rather realization of the method, is at least as important as the method itself. IDSM has some limitation, *i.e*. the method cannot be used in the case of monoisotopic elements. Hence, there is a need for other PMM, complementary to the IDMS.

Neutron activation analysis (NAA) has a very well recognized potential for accuracy. It has been shown that its instrumental mode can meet the requirements of a primary ratio method when the method operates under its favorable conditions [2-4]. We have shown lately that a high-accuracy radiochemical NAA (RNAA), in agreement with the concept developed in the Institute of Nuclear Chemistry and Technology (INCT), can also fulfil this definition [5] in a relatively easy case of Co determination in biological material. The aim of this work is to demonstrate that the definition can be also met in the case of less favorable conditions from the point of view of nuclear properties of the element. A method of Mo determination in biological materials has been used chosen as an example.

In this study, seven biological type certified reference materials (CRMs) were analyzed: Peach Leaves NIST 1547, Oyster Tissue NBS 1566, Virginia Tobacco Leaves CTA-VTL-2, Oriental Tobacco

Leaves CTA-OTL-1, Tea Leaves INCT-TL-1, Mixed Polish Herbs INCT-MPH-2 and Versieck's Serum. Samples (0.1-0.2 g) and standards (0.02-0.05 g) were placed in high purity polyethylene (PE) snap-cap containers of volume 0.5 and 0.22 cm^3, respectively (Faculteit Biologie, Vrije Universiteit, Amsterdam, the Netherlands) and firmly covered. Stock standard solutions of Mo and U were prepared from MoO_3 and U_3O_8 by weighing an appropriate amount of oxide, then dissolving in aqua regia (sp. purity) and in high purity HNO_3, respectively, then diluting to proper concentration with water and weighing the obtained solution. Standards of 5 μg Mo and 1 μg U were obtained by weighing aliquots of freshly prepared standard solution, dropped directly on the filter paper discs placed in a PE container and evaporating to dryness before encapsulation.

The calibrated microanalytical and analytical balances: Sartorius MC5, Precisa 40SM 200A and Satrorius BP221S were used.

In order to avoid contamination, all operations before irradiation were carried out using a laminar flow air cabinet equipped with an HEPA-filter (air class 100).

The package consisting of standards, samples and an empty PE container for the determination of residual blank was irradiated in the MARIA nuclear reactor for one hour at a neutron flux of $1x10^{14}$ n cm^{-2} s^{-1} and cooled for 4 days before processing.

Samples were digested under pressure in teflon digestion vessels using a microwave system (Plazmatronika, Poland) and a mixture of 3 cm^3 of concentrated HNO_3, 1 cm^3 of concentrated (30%) H_2O_2 and 1 cm^3 of concentrated (48%) HF. A three step procedure (5 min, 60% power; 5 min, 80% power and 15 min, 100% power – 100 W inside of digestion vessel; 24 atm) was used. Prior to digestion, a non-active carrier (50 μg of Mo of sp. purity) was added to the sample. After decomposition, the samples were converted into nitrates and subjected to the separation procedure as described previously [6].

To determine the residual blank, the interior of the empty PE container irradiated in the package was washed with the same amount of concentrated HNO_3, then the washings were processed in the same way as the samples, including microwave digestion.

Measurements were made using a gamma-ray spectrometer with an HPGe detector (Canberra), active volume 255 cm^3, well type, well diameter 16 mm and depth 40 mm, resolution 2.4 keV for the 1332.4 keV peak of ^{60}Co, relative efficiency 24%, with the GENIE-2000 Canberra Gamma Spectroscopy System. The same PE counting vessels were used for the samples and standards. The samples and standards had the same shape and matrix.

A high-accuracy RNAA method for Mo determination has been elaborated according to the concept developed in the INCT [7-9]. The concept was based on the definition of the definitive method given by Uriano and Gravatt [10]. The high-accuracy RNAA method is based on the combination of neutron activation with quantitative isolation of an indicator radionuclide in the stage of high radiochemical purity by column chromatography followed by gamma-spectrometric measurement. The method is designed and elaborated according to rules assuring high accuracy:

- All conditions should be optimized enabling selective isolation of an element with 100% yield confirmed by tracer experiments.
- All potential sources of errors starting from sampling and sample dissolution up to gamma-spectrometric measurements should be identified at stage of elaborating the method, and removed or appropriate corrective actions introduced into the procedure.
- Whenever possible, the colour of the ion in question (or its complex) added as a carrier should be used for visual control to safeguard against unexpected failure of the separation procedure.
- With each set of samples at least two standards should be irradiated, one of which is later on processed exactly as are the samples and the other is not. The specific activities of both standards should agree within predetermined limits.
- Residual blank resulting from the contact of the sample with a sample container should be measured in each series of determinations.
- The method should be universal, *i.e.* capable of being used without further modifications for the determination of analyte in all kinds of biological materials.

In principle, the method should be a single element one, while all parameters can be then optimized with respect to this particular element, as in the case of Co determination in biological materials [5]. In the less favorable case, also more than one element has to be taken into account. How-

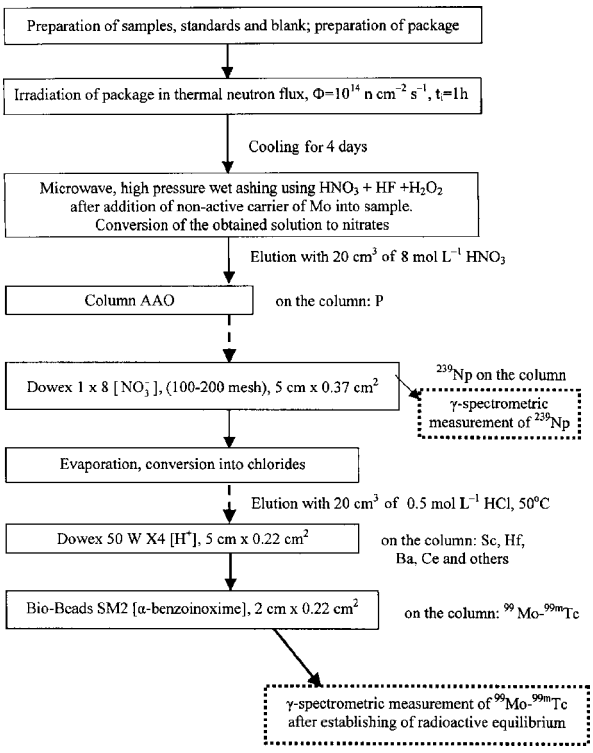

Fig.1. Schematic diagram of the high-accuracy RNAA method for determination of Mo in biological materials.

ever, the optimization has to be always preserved. Otherwise the method cannot be recognized as a high-accuracy one. In the case of Mo determination by the NAA method, Mo is determined by means of the reaction $^{98}Mo\ (n,\gamma)\ ^{99}Mo \xrightarrow{\beta} {}^{99m}Tc$. The same indicator nuclide is forming in the nuclear fission reaction $^{235}U\ (n,f)\ ^{99}Mo \xrightarrow{\beta} {}^{99m}Tc$. Hence, the contents of both elements, Mo and U in the sample, should be determined and correction for the interfering reaction (*i.e.* uranium fission) must be evaluated. A scheme of the elaborated method for the determination of Mo in biological materials, providing simultaneously information on interfering U, is presented in Fig.1. All stages of the method were very carefully studied [6,11,12]. Special attention was paid to reduce uncertainty values at all stages of the method.

The high-accuracy RNAA method is equipped with some classification criteria providing protection against making gross errors. The result has to fulfil all the criteria simultaneously to be accepted. The criteria are as follows:

- Visual control of the correctness of the separation procedure: in the retention stage on the chromatography columns the colour band of analyte should not travel more than 1/3 of the bed length.
- Small residual blank: the results were accepted if the correction for residual blank determined in a given run was below 5% of the analyte contents in analyzed sample.
- Agreement of standards: the results for a given series of samples were accepted if the normalized count rates of the two standards, one of which was processed in the same way as the samples and the other one was measured directly after dissolution, did not differ by more than 5% (after correcting for flux gradient, if any).
- The result for the certified material irradiated and analyzed together with the samples should be in agreement with the certified value.

Of course, there should be no indications, that something might go wrong during the analysis.

In the case of Mo determination by the RNAA method, the first criterion is not applicable, as the separated compounds are colourless.

NAA is fully described mathematically [13,14] and very well understood. In the case of RNAA when post-irradiation separations are carried out, the method is free from contamination, which can occur when using separations together with non-nuclear methods. Also, when the indicator nuclides are selectively and quantitatively isolated from the activated samples, the uncertainty of counting statistics and calculation of analytical peak areas in gamma-ray spectra are significantly reduced comparing with instrumental neutron activation analysis – INAA (low background, lack of spectral interferences). The other advantageous features are:

- performing the chemical operations under controlled conditions by addition of inactive carriers (freedom from trace and ultra-trace concentration behaviour),
- accurate yield determination by using of radiotracer or carrier budgeting.

In the relative standardization of the RNAA method, a standard of known mass of element W_{st} is irradiated together with the sample of known mass W_x, usually with a neutron flux monitor and counted under the same geometrical conditions using the same HPGe detector. In that case $M_x=M_{st}$, $\Theta_x=\Theta_{st}$, $\gamma_x=\gamma_{st}$, $S_x=S_{st}$, $\sigma_x=\sigma_{st}$ and $\varepsilon_x=\varepsilon_{st}$, the mass fraction c_m of the element to be determined (x) is given by the well known equation [14,15]:

$$\bullet. \bullet \frac{\bullet . \bullet .. \bullet .. \bullet ..}{\bullet .. \bullet . \bullet . \bullet . \bullet .} \qquad (1)$$

where: A_x – count rate of analytical gamma-ray of indicator nuclide; $A_x = N_p\, t_c^{-1}\ [s^{-1}]$; D – decay factor, $D=\exp(-\lambda t_d)$ (t_d – decay time); C – measurement factor, $C=(1-\exp(-\lambda t_m))/\lambda t_m$ (t_m – measurement time). The above equation is valid when the neutron flux gradient between sample and standard position is negligible or corrected, and neutron self-shielding is negligible for sample and standard.

In the case of the high-accuracy of the RNAA method $Y_x=1$, since the determined element is separated quantitatively.

The uncertainty budget, taking into account all possible sources of uncertainty, has been performed using GUM [16] and EURACHEM Guide [17]. As it has been pointed above NAA is very well understood and the sources of uncertainty have been established and discussed in the literature [2-5,15]. The sources of uncertainty can be grouped into four categories:

- preparation of the sample and standard,
- irradiation,
- gamma-ray spectrometric measurement,
- radiochemical separation.

A cause and effect diagram is provided in Fig.2 [17]. The standard uncertainties within particular categories connected with individual sources of uncertainty have been quantitatively evaluated [18]. The com-

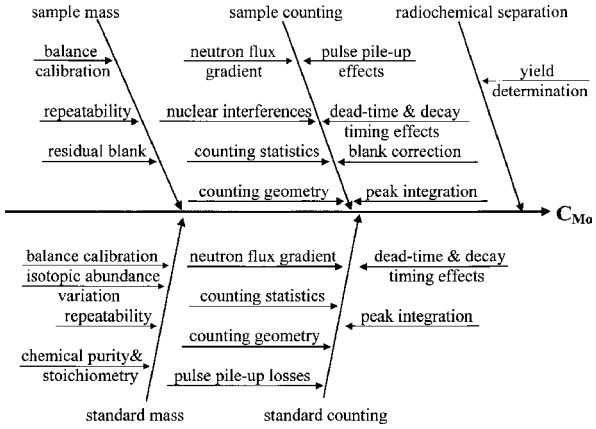

Fig.2. Cause and effect diagram for the determination of Mo in biological materials by RNAA method.

bined standard uncertainty was calculated according to uncertainty propagation law [16,17]. Since equation (1) contains only multiplication and division of quantities, the combined standard uncertainty can be calculated as a square root of the sum of the squares of relative standard uncertainties. The budget for the calculations of the combined uncertainty for Mo determination in two CRMs by the high-accuracy RNAA method is presented in

Table. Uncertainty budget for Mo determination in NIST 1547 Peach Leaves and INCT-MPH-2 Mixed Polish Herbs.

Source of uncertainty	Unit	NIST 1547 Peach Leaves		INCT-MPH-2 Mixed Polish Herbs	
		value	rel. std. uncertainty, u_i [%]	value	rel. std. uncertainty, u_i [%]
Mass of sample	mg	150	0.1	150	0.1
Mass of standard	mg	20	0.1	20	0.1
Residual blank	mg	0	0.1	0	0.1
Neutron flux gradient		1.00 ± 0.012	0.5	1.00 ± 0.012	0.5
Interfering reaction	ng	2	2.1	190	1.1
Neutron self-shielding/scattering			0.2		0.2
Sample counting statistics	Bq/counts	10 000	1.0	22 000	0.7
Standard counting statistics	Bq/counts	150 000	0.4	150 000	0.4
Counting positioning of sample			0.3		0.3
Counting positioning of standard			0.3		0.3
Pulse pile-up effect – sample			0.1		0.1
Pulse pile-up effect – standard			0.2		0.2
Peak calculation – sample			0.2		0.2
Peak calculation – standard			0.2		0.2
Radiochemical separation		1.00 ± 0.01	0.8	1.00 ± 0.01	0.8
Combined standard uncertainty, $u = \sqrt{\sum_i u_i^2}$			2.6		1.7

Mass fraction of Mo in NIST 1547 Peach Leaves: 58 ng g^{-1} ±3 ng g^{-1} (k=2); (NIST certified value: 60 ng g^{-1} ±8 ng g^{-1}).
Mass fraction of Mo in INCT-MPH-2 Mixed Polish Herbs: 543.5 ng g^{-1} ±18.5 ng g^{-1} (k=2); (INCT information value: 520 ng g^{-1}).

Table. As can be seen, the results are traceable to SI units. The combined standard uncertainty amounted to 2.6% in the case of very low Mo and typical U content in biological materials as for NIST 1547 Peach Leaves and 1.7% for analysis of biological material of higher Mo content INCT-MPH-2 Mixed Polish Herbs. In the much more favorable case like a high-accuracy RNAA method of Co determination in biological materials the combined standard uncertainty was evaluated to be 1.3% [5]. Values like those are characteristic of the methods of the highest metrological quality and are comparable with values characteristic of IDMS. Hence, the high-accuracy RNAA methods fulfil the CCQM definition of the primary ratio method of measurement.

This work was financially supported in part by the State Committee for Scientific Research – grant No. 03290/C.P06-6/2003.

References

[1]. BIPM proceedings of the 4th meeting of CCQM. Bureau International des Poids et Mesures (BIPM), Paris, France 1998, p.71
[2]. Tian W., Ni B., Wang P., Cao L., Zhang Y.: Accred. Qual. Assur., 6, 488 (2001).
[3]. Tian W., Ni B., Wang P., Cao L., Zhang Y.: Accred. Qual. Assur., 7, 7 (2002).
[4]. Bode P., De Nadai Fernandes E.A., Greenberg R.R.: J. Radioanal. Nucl. Chem., 245, 109 (2000).
[5]. Polkowska-Motrenko H., Danko B., Dybczyński R.: Anal. Bioanal. Chem., 379, 221 (2004).
[6]. Danko B., Dybczyński R.: J. Radioanal. Nucl. Chem., 216, 51 (1997).
[7]. Dybczyński R., Wasek M., Maleszewska H.: J. Radioanal. Nucl. Chem., 130, 365 (1989).
[8]. Dybczyński R., Danko B.: J. Radioanal. Nucl. Chem., 181, 43 (1994).
[9]. Polkowska-Motrenko H., Dybczyński R., Danko B., Becker D.A.: J. Radioanal. Nucl. Chem., 207, 401 (1996).
[10]. Uriano G.A., Gravatt C.C.: Crit. Rev. Anal. Chem., 6, 361 (1977).
[11]. Danko B., Łobiński R., Dybczyński R.: J. Radioanal. Nucl. Chem., 137, 145 (1995).
[12]. Danko B., Dybczyński R.: J. Radioanal. Nucl. Chem., 192, 117 (1995).
[13]. Simonits A., Moens L., De Corte F., De Wispeelaere A., Elek A., Hoste J.: J. Radioanal. Nucl. Chem., 60, 461 (1980).
[14]. Dybczyński R.: Chem. Anal. (Warsaw), 46, 133 (2001).
[15]. Kučera J., Bode P., Štěpánek V.: J. Radioanal. Nucl. Chem., 245, 115 (2000).
[16]. ISO Guide to the Expression of Uncertainty in Measurements. International Organization for Standardization, Geneva 1993.
[17]. EURACHEM-CITAC, Quantifying Uncertainty in Analytical Measurement. 2nd ed. EURACHEM, Teddington, England 2000.
[18]. Polkowska-Motrenko H., Danko B., Dybczyński R.: Potential of RNAA as a primary ratio method. Chem. Anal. (Warsaw), in press.

SPECIATION ANALYSIS OF INORGANIC SELENIUM AND TELLURIUM IN MINERAL WATERS BY ATOMIC ABSORPTION SPECTROMETRY AFTER SEPARATION BY SOLID PHASE EXTRACTION

Jadwiga Chwastowska, Witold Skwara, Elżbieta Sterlińska, Jakub Dudek, Leon Pszonicki

Natural concentration of selenium and tellurium in the environment is extremely low, however, the application of these elements in many industrial processes, such as manufacture of semiconductor materials, photoelectric cells, glass, pigments and pharmaceuticals and in metallurgy, causes their emission and local contamination of the surrounding areas. Since both the elements are toxic for animals and humans, it is necessary to test their concentration level in the environment. Selenium attracts particular attention since it plays a double role: as an essential nutrient in small concentration and as a toxic substance in higher concentration [1]. It is a component of the enzyme glutathione peroxidase [2] and a detoxifying agent playing an antagonistic role towards many heavy metals and others [3]. The serious problem is a very narrow range between selenium concentration playing a positive role in the organism and the concentration that becomes toxic. The recommended daily intake of selenium is 55 μg for women and 70 μg for men [4]. The maximum recommended concentration of selenium in drinking water is 10 μg l^{-1} [5].

In the natural samples selenium and tellurium can exist in various oxidation steps as -2, 0, +4 and +6. Moreover, owing to the microbiological activity both elements can be transformed into organometalloid compounds with consequent modification in their transport pattern and toxicological behaviour [3]. The inorganic forms in the oxidation steps +4 and +6 are most common and these forms are usually being determined. Since the concentration of both elements is very low the most sensitive analytical methods as mass spectrometry with inductively coupled plasma (ICP-MS), optical emission spectrometry with ICP atomization (ICP-OES), spectrofluorimetry, voltammetry and atomic absorption spectrometry with graphite furnace atomization (GF AAS) or hydride generation (HG AAS) are used for their determination. However, the lower determination limit of these methods is often insufficient for the analysis of environmental samples and preconcentration of the analytes is required. In the case of speciation analysis the preconcentration process is usually hyphened with separation of individual chemical forms of the element to be determined. The preconcentration and separation methods used most frequently for selenium and tellurium are various chromatographic techniques, solvent extraction, solid phase extraction and capillary electrophoresis. Application of all these methods is discussed in reviews [1,3].

The aim of the presented work was the investigation and application for speciation analysis of

selenium and tellurium in mineral waters of two chelating sorbents with thiol groups. One of them, proposed and prepared by us [6], is a dithizon sorbent obtained by immobilization of dithizon on the solid bed (methyl polymethacrylic ester). The second one is "thiol cotton" obtained by the fixation of thioglycolic acid on the cotton gauze according to Mu-qing Yu *et al*. [7]. For each of the sorbents there were estimated the sorption efficiency of Se(IV) and Te(IV) as a function of the solution acidity, amount of the sorbent in the column, optimum flow rate, type and amount of eluent and the separation effectiveness of Se(IV) from Se(VI) and Te(IV) from Te(VI). On the basis of the obtained data there were prepared two procedures for separation and speciation analysis; one for selenium and the second for selenium and tellurium.

The investigation showed that the dithizon sorbent reacts quantitatively with Se(IV) in a large range from 0.5 to 4 N of HCl concentration and in the total range the kinetic of the process is very good. For tellurium, the curve of sorption is untypical and the kinetic of the process is unsatisfactory. Therefore, it was assumed that the dithizon sorbent may be applied only for separation of selenium. Since only Se(IV) may be separated in this way, the total analytical procedure is composed of two steps. In the first step, 500 ml of a water sample is acidified with HCl to pH=0 and passed through the column with the sorbent (column diameter – 4 mm, sorbent amount – 0.2 g). The adsorbed Se(IV) is eluted with 2 ml of concentrated HNO_3, diluted to 10 ml and determined by AAS. In the second step, the total inorganic selenium is reduced in the 500 ml sample of the same water to Se(IV) and then the sample is treated in the same way as in the first step. The obtained result represents the concentration of total selenium. The concentration of Se(VI) is calculated as the difference of the two results.

The reduction of Se(VI) to Se(IV) must be carried out under carefully selected condition since a part of it may be reduced to elemental selenium and lost. We tested concentrated HCl, hydroxylamine, $TiCl_3$ and KBr as reducing agents. Titanium chloride was found to be the best one and for it the optimum reduction conditions were defined.

The correctness of the separation procedure was tested by determination of the known amount of both forms of selenium added to the sample of synthetic water, with the composition similar to the natural river water, and to the natural mineral water. In both cases the recovery varied in the range from 95 to 102%.

The simultaneous separation of selenium and tellurium is carried out using "the thiol cotton" sorbent. It demonstrates very good sorption properties for Se(IV) and Te(IV) in a large range from 0.3 to 6 M HCl, whereas the forms of both elements in the oxidation degree six pass completely through the column. Moreover, this sorbent is stable during a long time and shows very good kinetic of the sorption process. Under the conditions of our experiments the total sorption takes place at the column flow rate up to 10 ml min^{-1}. The accepted conditions of separation and determination of Se(IV) and Te(IV) and the sum of Se(IV) and Se(VI) and the sum of Te(IV) and Te(VI) were the same as those accepted for the procedure with the dithizon sorbent with one exception. The elution of analytes from the column was carried out not with concentrated HNO_3, but with 1% solution of KJO_3 in 2 M HCl. The recovery of the added known amounts of both forms of selenium and tellurium was tested in the same way as it was described above and it was also in the range from 95 to 102%.

The species of selenium or selenium and tellurium separated by both the described separation procedures were determined either by GF AAS using a $Mg(NO_3)_2$ modifier or by HG AAS after reduction by 1% $NaBH_4$ solution in 1% NaOH.

Absorbance was measured for the spectral lines: selenium – 196.0 nm and tellurium – 204.3 nm.

The lower detection limits for 500 ml water samples determined by GF AAS method were 0.2 ng l^{-1} for selenium and 0.1 ng l^{-1} for tellurium. For the HG AAS method these limits were 0.02 and 0.01 ng l^{-1}, respectively.

References

[1]. Pyrzyńska K.: Chem. Anal. (Warsaw), 40, 677 (1995).
[2]. Rotruck J., Pope A., Ganther H., Swanson A., Hafeman D., Hoekstra W.: Science, 179, 588 (1973).
[3]. D'Ulivo A.: Analyst, 122, 117R (1997).
[4]. Levander A.O.: Amer. Diet. Assoc., 91, 1572 (1991).
[5]. Drinking Water and Health, Recommendation of the National Academy of Sciences. Environmental Protection Agency, Federal Register, 42, 3573 (1977).
[6]. Chwastowska J., Skwara W., Sterlińska E., Pszonicki L.: Talanta, 64, 224 (2004).
[7]. Mu-qing Yu, Gui-qin Liu, Qinhan Iin: Talanta, 30, 265 (1983).

EVALUATION OF AIR POLLUTION AT THREE URBAN SITES IN POLAND USING INAA

Zygmunt Szopa, Rajmund Dybczyński, Krzysztof Kulisa, Maria Bysiek[1/], Małgorzata Biernacka[1/], Sławomir Sterliński[1/]

[1/] Central Laboratory for Radiological Protection, Warszawa, Poland

Introduction

Monitoring and evaluating of air pollution has become a matter of urgent concern in many countries worldwide, particularly in big cities of the industrial areas. The reason is that the growing air pollution affects the environment, and, therefore, may cause not only economic problems but also severe problems to public health [1-4]. The econ-

omic problems are caused by significant reduction of visibility and affecting regional climate, which results, *e.g.* in increased number of vehicle accidents, reduction of agriculture production and losses for tourism. High air pollution, particularly during regional haze episodes, results in increased occurrence of respiratory diseases [3-5].

Air pollution is caused by many different components. Among them sulphur dioxide, carbon monoxide, nitrogen oxides, reactive hydrocarbon compounds, and airborne particulate matter (APM) are considered to be the most hazardous ones. APM consists of particles of different sizes. Its size frequency distribution shows two maxima at about 0.2 and 10 μm [1-5]. APM may be classified according to the particle size or to source of origin. Roughly, particles of a size not exceeding 2 μm are coming from combustion processes or gas-to-particle conversion, while those larger than 2 μm – from mechanical ones, like soil erosion or incomplete combustion [1-4]. The APM size has an adverse effect on human health, *i.e.* the smaller the particles are, the deeper is the penetration into the lungs [4,5]. For collection and characterization of APM, different samplers are used. The simplest method is a collection of total suspended particulate matter (TSP) without any size selection. The other samplers (like *e.g.* samplers with physical/virtual impactor stages, samplers using centrifugal forces, stacked filter units or personal samplers) differentiate the particle size in various ways so as to enable analyzing APM fractions of a particular size [3-5]. Recently, a part of scientific interest has been paid to other kinds of air pollution indicators, *i.e.* biomonitors like mosses, lichens and even tree--barks. They obtain their nutrients mainly from the atmosphere and thus they are already "in place" of the sampling sites and can be obtained almost "for free" [6,7].

A variety of analytical techniques are used for monitoring of air pollution. Among them, the nuclear and nuclear-related techniques play the leading role [8,9]. These techniques have characteristics that make them suitable or even unique for conducting non-destructive, multi-element analyses of samples of very low masses like APM on filters or biomonitors [4,8]. Due to the fact that APM from different sources is composed of different mixtures of elements in different proportions, the elemental patterns they form are characteristic like a fingerprint for the particular sources. Their identification is twofold, *i.e.* either statistical methods can be used to estimate the contribution of air pollutant source or the APM element content can be combined with meteorological data on direction and speed of air masses movement at a specific site [3-5,10,11].

The aim of this work was to demonstrate the ability of instrumental neutron activation analysis – INAA (using thermal neutron flux and followed by simple gamma-ray spectra measurement) to be used to the analysis of APM collected on filters which are normally employed for routine monitoring of airborne radioactivity in Poland. It has been exemplified by analyses of APM samples collected in 1996 at 3 different urban sites in Poland. This method enables routine content determination of 26 elements. Results have been evaluated so as to show similarities and differences in content level depending on the collection site and period of collection. Its reliability has been checked by analyses of two certified reference materials (CRMs), similarly as in the previous paper [12].

Experimental

A general scheme of the INAA procedure has been shown in Fig.1. It consists of four main stages:

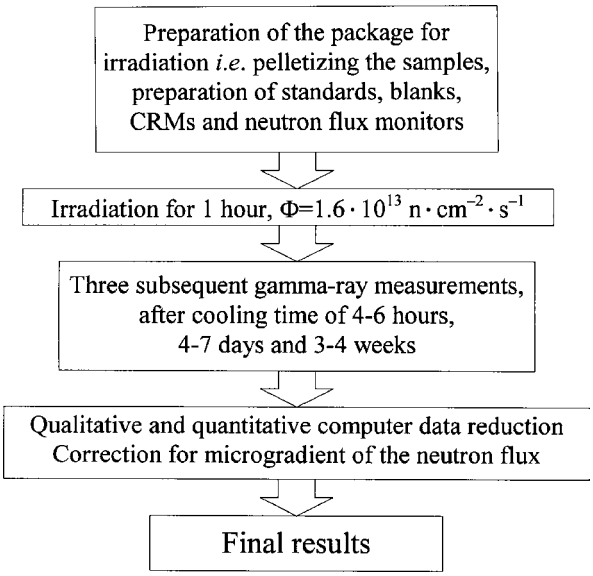

Fig.1. General scheme of the INAA procedure used for APM analyses.

- sample preparation,
- irradiation in a nuclear reactor,
- acquisition of gamma-ray spectra,
- computer interpretation and evaluation of the measured spectra and calculation of the results after final correction according to the measured activity of the neutron flux monitors.

Samples, standards, neutron flux monitors and CRMs

The APM samples deposited on a filter material have been taken from three stations (Gdynia, Warsaw and Cracow) of the Polish network of the high volume aerosol sampling stations of ASS-500 type. Since 1992, the network has been used for monitoring radionuclide concentrations in ground--level air in Poland [13]. The details on sample, CRM and blank preparation as well as composition of standards and their preparation will be published elsewhere [14].

Irradiation

A typical package ready for irradiation consisted of 18-20 samples, 6 mixed standards and 8 Au monitors uniformly distributed along the package length. Two CRMs have been included into each package in order to control the accuracy of the analyses as well as one pure filter material tablet to control the blank. Such package has been irradiated in the nuclear reactor MARIA at Świerk at a thermal neutron flux density of 1.6×10^{13} n·cm^{-2}·s^{-1} ($\Phi_{fast}/\Phi_{th}=0.005$) for 1 hour and cooled for *ca.* 4-6 hours.

Gamma-ray spectra measurement, interpretation and calculation of results

Gamma-ray spectra of all samples, standards, CRMs, blanks and Au monitors have been measured with the aid of a high-resolution spectrometer (HPGe coaxial ORTEC detector with the active volume of 213 cm^3 coupled *via* ORTEC analog line with the "plug-in" type multichannel analyser TUKAN-2 installed into and controlled by PC). All irradiated objects have been subsequently measured in three periods shown in Fig.1. The spectrometer has been calibrated so (*ca*. 0.5 keV per channel) as to enable the spectra measurement in the range from 60 keV to 2 MeV.

For qualitative and quantitative evaluation of the spectra the SAWAP-PC computer program has been used [15]. The element contents have been calculated using the well-known formula for comparative neutron activation analysis (NAA) [9]. Finally, the quantitative results have been obtained by a further correction for the microgradient of the neutron flux observed along the irradiated package as the specific activity of the Au monitors indicate [12].

Results and discussion

The filter samples came from the 1996-year collection, from three different collection sites located in the proximity of three Polish cities. Warsaw, Cracow and Gdynia were chosen to represent the central, southern and northern part of Poland, respectively. For each collection site, 2-3 samples coming from each month have been analyzed. The only exception was for July and August where only 1 sample was available for analyses by INAA. This makes 27 samples analyzed by INAA altogether at each collection site. Each irradiated sample was independently measured 2-3 times, so that there have been 64 independent measurements.

Element concentrations at the particular sites for the whole 1996 year

The results for the whole year (*i.e*. the results not apportioned to months) at each collection site will be published elsewhere [15]. Some of the results for chosen elements, *i.e*. for As, Cr, La, Na, Sb and Yb – at the three collection sites – have been presented in the form of multiple box-and-whisker plots in Fig.2. The similarities and differences between the data subsets can easily be observed when they are placed in the same Fig. For example, the apparently higher As and Cr concentration at Cracow site than at the other sites, and almost similar for the two other sites. As it could be expected, the elevated levels of As and Cr at Cracow site are characteristic of the neighbourhood of metallurgy centre (Nowa Huta) as it was observed in other papers [3-5]. Another example concerns Na and Sb concentrations at Gdynia site, which are apparently higher than at the other (Cracow and Warsaw) sites. Again, the elevated Na level at Gdynia site is characteristic of the sea neighbourhood [1,3-5].

Monthly changes of elemental concentrations

The INAA method applied for this task is sensitive enough not only to monitor the element content in APM associated with the collection site, but also to watch monthly changes in the element content at a particular site. As one example, the average element content in APM, which was gathered on the filters in March 1996 is shown in Fig.3. The elements are roughly ordered in ascending order of concentration, from trace elements (Au, Lu, Tb, *etc*.) to major constituents (*e.g*. Na, K and Fe), which occur at percent level. Significantly higher concentrations for Na, Ba, Co, Sb and Au are at Gdynia site, a part of which could come from the sea spray [1,3-5]. At Cracow site, the higher concentration level for Cr and As could indicate

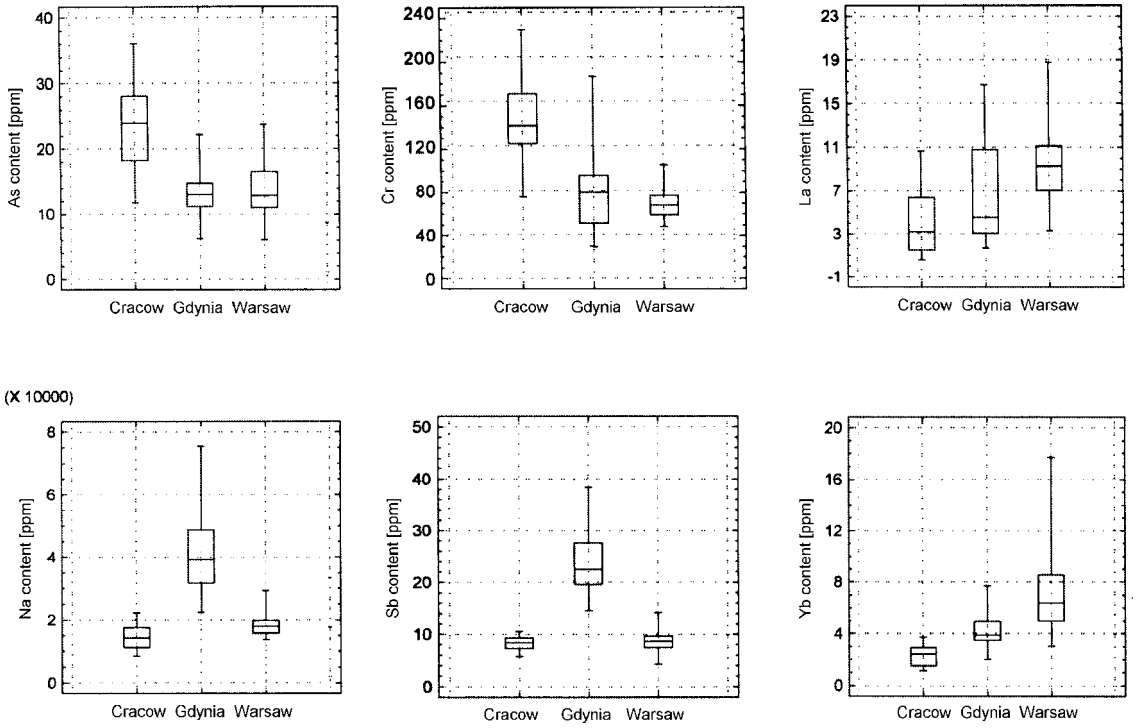

Fig.2. Multiple box-and-whisker plots for concentrations of As, Eu, La, Na, Sb and Yb at Cracow, Gdynia and Warsaw collection sites observed during 1996.

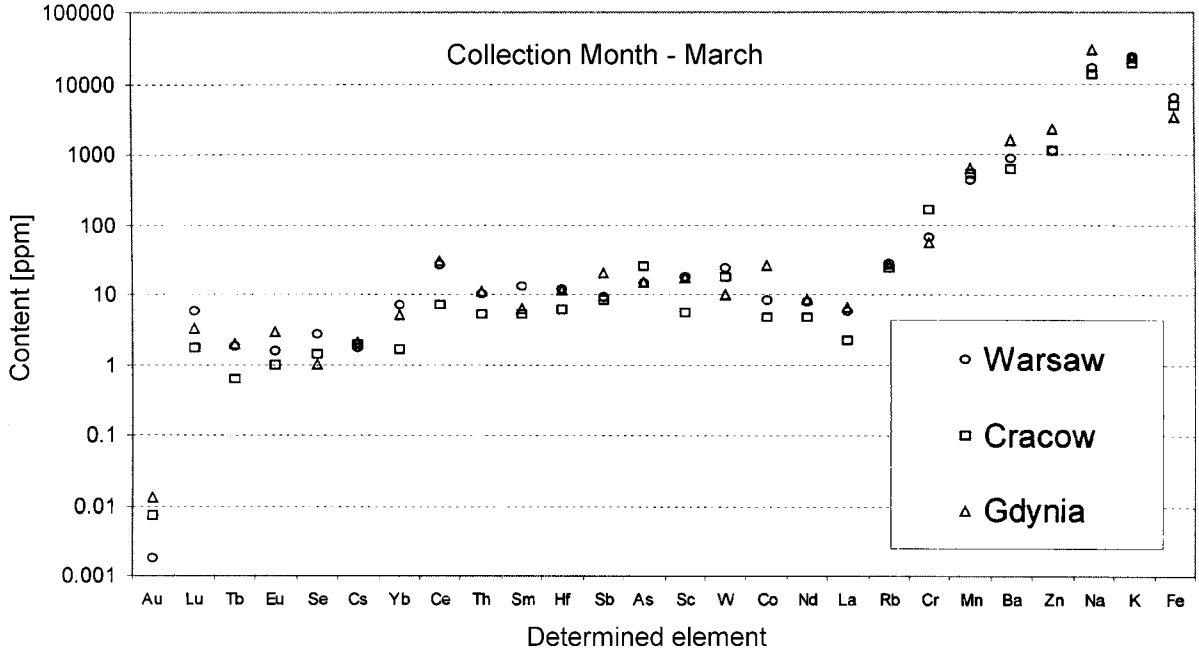

Fig.3. Average content of 26 elements in APM collected in March 1996 for three different collection sites.

the neighbourhood of metallurgy centre (Nowa Huta). The higher concentrations for Se, Fe and W at Warsaw site could be associated with coal combustion, motor vehicles and steel industry [3,5].

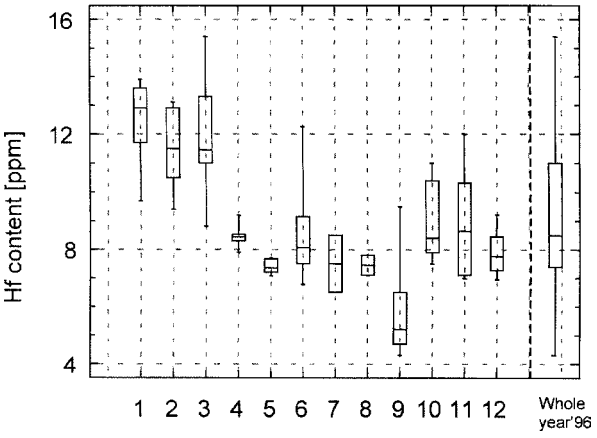

Fig.4. The range of Hf results for each month and for the whole year at Warsaw site.

Another example is shown in Fig.4. This is the Hf concentration in APM at Warsaw site apportioned to collection months (from January – 1 to December – 12). At the same graph, the Hf distribution for the whole year has been shown. One can clearly see how the particular month distribution contributes to the pattern of the whole year and how the concentrations have been changing from month to month. This could be useful for long term evidence particularly for the indication of pollution level if a haze episode happens.

Enrichment factors

The so called "enrichment factors" (EF) have been calculated [12]. These factors are used for comparison of relative concentrations of determined elements with respect to some macroconstituent (in our case – Fe), with analogous values characterizing the average composition of the lithosphere [16].

As an example, the EFs derived in this way for the average spring 1996 results at the three investigated sites have been shown in Fig.5. For the majority of the determined elements they do not exceed the value of 10, what means that the soil-derived elements (those for which the EFs are closer to 1) and the anthropogenic ones (of higher EF values) are mixed in APM [5]. Generally, the EFs for the

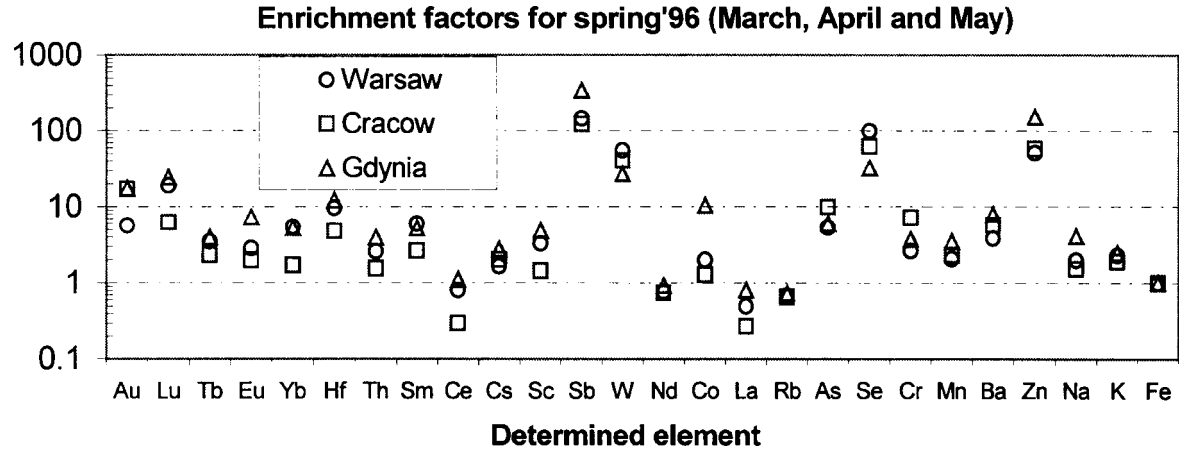

Fig.5. Comparison of enrichment factors for spring 1996 at Warsaw, Cracow and Gdynia sites.

three investigated sites form rather similar patterns, though their values differ much in some cases like for Sb, Co, Se, Cr and Zn. Some elements like Sb, W, As, Se and Zn are highly concentrated in APM when compared with their occurrence in the Earth's crust. This shows their anthropogenic occurrence in APM. Elements like W and Zn are mainly associated with the steel industry and may come from Polish as well as from the neighbouring countries' sources. The other ones like Sb, As and Se are mainly associated with coal combustion and motor vehicle exhausts [1,3-5].

This could be explained by the fact that over 80% of energy production in Poland come from coal burning and that in the neighbourhood of the Polish big cities, power/heating plants are located. It is perhaps worth to conclude that high EFs for the same elements has also been observed by the authors when analyzing fly ashes coming from Polish power plants [12].

The method reliability

A significant analytical problem encountered in the analysis of APM collected on filters may arise from a blank, *i.e*. filter itself [5,15,17]. It may contain some elements at measurable levels (roughly from one tenth up to one third) of the content of these elements in APM. In this work, it was the case for Yb, Cs, Sc, Sb, Rb, and As. For Br, the relatively high and changeable content of this element in filters has made its quantitative determination unreliable.

Analyzing two CRMs along with the APM analyses has assessed the method reliability. Unfortunately, CRMs of the same or similar matrix like APM have not been available. Therefore, two others, well known CRMs of geological/environmental origination namely SOIL-5 (International Atomic Energy Agency – IAEA) and CTA-FFA-1 (Institute of Nuclear Chemistry and Technology – INCT) have been analyzed in course of the present work. Generally, the results showed a good or at least satisfactory agreement between them. Additionally, the agreement of K results, which have been obtained on the one hand using INAA at the INCT and on the other hand, using the ^{40}K measurements within ASS-500 network at the Central Laboratory for Radiological Protection, confirms the method reliability.

References

[1]. Boubel R.W., Fox D.L., Turner B.: Fundamentals of Air Pollution. 3rd edition. Academic Press, London 1994.
[2]. Seinfeld J.H., Pandis S.N.: Atmospheric Chemistry and Physics: From Air Pollution to Climate Change. John Wiley & Sons, 1997.
[3]. Environmental Development. IAEA Bull., 38, 2 (1996).
[4]. Air Pollution and Its Trends. UNDP/RCA/IAEA Project RAS/97/030/A/01/18, 1997.
[5]. IAEA/ANL Interregional Training Course on Nuclear Related Analytical Techniques in Air Pollution Monitoring and Research. Lectures. Argonne National Laboratory, Argonne, USA 1993.
[6]. Steinnes E., Rambaek J.P., Hanssen J.E.: Chemosphere, 25, 735 (1992).
[7]. Kuik P., Wolterbeek H.Th.: Water, Air, Soil Pollut., 84, 323 (1995).
[8]. Compendium of Methods for Determination of Inorganic Compounds in Ambient Air. Center for Environmental Research Information, U.S. Environmental Protection Agency, June 1999.
[9]. Dybczyński R.: Chem. Anal. (Warsaw), 46, 133 (2001).
[10]. Barnett V., Turkman K.F.: Statistics for the Environment. Vol.3. Pollution Assessment and Control. John Wiley & Sons, 1997.
[11]. Hopke P.K., Gladney E.S., Gordon G.E., Zoller W.H., Jones A.G.: Atmos. Environ., 10, 1015 (1976).
[12]. Szopa Z., Dybczyński R., Kulisa K., Sterliński S.: Chem. Anal. (Warsaw), 39, 497 (1994).
[13]. Bysiek M., Biernacka M., Jagielak J.: Zanieczyszczenie promieniotwórcze przyziemnego powietrza atmosferycznego w Polsce w 1998 roku. Centralne Laboratorium Ochrony Radiologicznej, Warszawa, 2000, Raport CLOR Nr 142, in Polish.
[14]. Szopa Z., Dybczyński R., Kulisa K., Bysiek M., Biernacka M., Sterliński S.: The use of INAA for the evaluation of air pollution at three urban sites in Poland. Chem. Anal. (Warsaw), 49 (2004), in print
[15]. Szopa Z., Dybczyński R.: Simple PC software for routine analysis of gamma-ray specta. In: INCT Annual Report 2000. Institute of Nuclear Chemistry and Technology, Warszawa 2001, p.70.
[16]. Heide F., Wlotzka F.: Meteorites, Messengers form Space. Springer-Verlag, Berlin 1995.
[17]. Bem H., Gallorini M., Rizzio E., Krzemińska M.: Environ. Int., 29, 421 (2003).

CENTRAL EUROPEAN CRYSTAL GLASS OF THE FIRST HALF OF THE 18th CENTURY

Jerzy Kunicki-Goldfinger, Joachim Kierzek, Piotr Dzierżanowski[1/], Aleksandra J. Kasprzak[2/]

[1/] Faculty of Geology, Warsaw University, Poland
[2/] National Museum in Warsaw, Poland

Since 1998, a project of investigation into 18th century central European vessel glass has been underway. Physicochemical analysis has been carried out, as well as stylistic analysis of over 1000 objects of different provenience. A scheme of the whole project has been built on three main steps and had been already discussed in a previous paper [1]. These steps are historical studies, non-destructive examination of the vessels, and quantitative chemical analysis of the samples taken from selected objects. Some preliminary results of the energy dispersive X-ray spectrometry analysis (EDXRF) had been already discussed [2,3]. Hereunder, some further results in regard to the electron probe microanalysis (EPMA) of the selected samples will be taken over, and we want to focus on the characteristics of *crystal glass* which were recognized among the glass manufactured in cer-

tain places in central Europe during the first half of the 18th century.

In the 17th century, in some centers of northern Europe, new technologies of colourless glass were experimented with. It was the consequence of science development of that time, and the migration of glassworkers that caused the spread of technological innovations. In some glasshouses, new types of furnace construction, new kinds of fuel (coal), new raw materials, batches, and so on, appeared. Many written historical documents may direct our attention to certain territories, and information, revealed in recent years, might lead us to the statement that most of the late 17th and early 18th century luxury colourless glass in almost all of Europe, including English lead-crystal, could have their technological roots somewhere on the French and Dutch borderland. However, few results of the chemical analyses of these glasses have been known to clearly support such statement up to now.

The significant changes in the glass technology can be observed already in the earliest 60s in the Netherlands, Netherlands/French borderlands and almost immediately on the British islands; in the 70s, among other things, also in central Europe [4-6]. Louis le Vasseur d'Ossimont (1629-1689), French native, was probably the first and most important glassworker known to us, who transferred new technology of *crystal glass* to central Europe. He appeared in Bohemia in Buquoy service in 1673 and established a glasshouse in Nové Hrady (Gratzen) [7,8]. The lists of raw materials used by him there (which included, among other things, quarz pebbles, saltpeter, arsenic, borax, chalk, wine stone) were characteristic of *crystal glass* batch. This set of raw materials appeared in Nové Hrady at the same time when Johann Kunckel published *crystal glass* recipe in "Ars vitraria experimentalis" [9]. At present, it is very difficult to state where and when this new batch appeared first in central Europe. But what is obvious, in the light of documents as well as of the results of the chemical analyses of glasses discussed below, is that these raw materials were characteristic of *crystal glass* in the last quarter of the 17th century and the 1st half of the 18th century, as well. This glass formulation has been practiced in very limited number of glasshouses. One important improvement of this batch, the addition of lead compounds, was probably of slightly later origin. Although, what has been already shown on the example of the 18th century glasses, intentionally introduced lead in central European glass can already be observed in items dating around 1700 [10]. This date might well become earlier in the future when more 17th century *crystal glass* wares are examined.

Almost till the end of the 17th century this new glass formulae competed with Venetian *cristallo* that had been dominant up to that time. This period saw the decline of soda-ash colourless glass as well as the end of the dominance of *façon de Venice* in the market of the luxury tableware. At the turn of the 17th century in Europe, at least three main glass formulae for luxury colourless vessels were being developed separately: *crystal glass* – developed probably somewhere on the French-Netherlands borderlands, *chalk glass* – credited to Michael Müller (1639-1709) in Bohemia, and *lead-crystal glass* – ascribed traditionally to George Ravenscroft (1618-1681) in England. The first two mentioned quickly spread over the continent. But if *chalk glass* (later called *Bohemian glass*, too) became the really "popular" one; the manufacturing of *crystal glass* was characteristic of only a limited number of glasshouses that mainly run under royal, ducal or aristocratic patronage. Michael Vickers writes "No longer were kings and princes the arbiters of taste, but this role was increasingly played by the middle classes of Europe and America. The eighteenth century witnessed these important changes" [11]. He writes in relation to the changing role of rock crystal and glass. It also seems true, however, in regard to the differentiation of *crystal glass* as a most valuable metal at this time, and *chalk glass* as a cheaper one; but enough good to fulfil the new baroque taste, which expressed itself in frequently dense rich decoration. This decoration occasionally could even be used on metal of imperfect quality. Nevertheless, this simplified history of baroque glass technology in northern Europe nowadays seems not entirely accurate. Firstly, chalk was already in usage in western Europe in time of Michael Müller; and secondly, lead compounds were used for colourless metal in the continent probably independently of the influence of English technology. Tracing the succeeding steps of the introduction of the new raw materials has, until now, been very puzzling.

The terminological context of this *crystal glass* is no less complicated. It is not the intention of the authors to discuss this problem here, but at least two of its aspects need be highlighted. The first one concerns the differentiation between the original technological terms and the terms introduced to the professional literature by art historians during the last two centuries. A term *Bohemian crystal* constitutes one of such examples – whereas *crystal glass* was manufactured in Bohemia only in a few glasshouses in the last quarter of the 17th century and then probably not before the middle of the 18th century [5]. The second one concerns the different semantic connotations of the term *crystal glass*, which were sometimes simultaneously used even in historical times. The term *crystal* derives from Greek *Krystallo* denoting glass that resembles rock crystal, a material that belonged to one of the most precious ones [12]. Therefore, a quality of metal constituted an important feature when one used the term *crystal glass*. On the other hand, this high quality glass was used to imitate very expensive, rare and frequently richly decorated wares made of rock crystal [13]. Put simply, glass ware resembled more expensive rock crystal ware. The type, shape and decoration of the ware was as valuable a feature as the quality of its metal. David Jacoby in his article about the raw materials used in Venice and Terraferma writes according the term *cristallino*: "We may safely assume that once this material [*glass*] had been improved, a specific type of vessel was designed to be exclusively made of it so as to high-

light its particular features. As a result, the term *crsitallino*, first applied to the material, was later used to designate the mold and the vessel related to it. There was thus a direct link between the type of material used and the specific shape given to the finished luxury product. This relationship was similar, say, to that existing between the particular features of the glass from which vessels were made and the choice of specific cutting designs and techniques used for their decoration" [14]. Although, according to Venetian *cristallo,* W. Patrick McCray calls our attention towards some statements by the Renaissance persons (15th-17th centuries) "regarding what was desired in terms of glass quality (the *material* and not the form)" [15]. The phenomenon of understanding the term *crystal glass* as a certain type of vessel or/and certain type of its decoration, seems to return in the 18th century or even at the turn of 17th century. It cannot be excluded that this phenomenon was influenced by the change of "good taste" in that time, as strongly underlined by Michael Vickers [11]. Numerous 18th century glasshouses were called *crystal glasshouses,* and the term *crystal glass* was widely applied towards the certain types of vessels frequently very rich decorated but manufactured with the use of cheaper *chalk glass*. The susceptibility of glass for applying fashionable decoration constituted more important feature than quality of the metal. In the discussion below, the term *crystal glass* will only concern the special kind of metal.

According to known sources, in the 1670s in central Europe, *crystal glass* was manufactured only in a few glasshouses in Bohemia (Buquoy glass) and Brandenburg. At the beginning of the 18th century, *crystal glass* seemed to survive in central Europe only in some German and Polish glasshouses – on the territories, where luxury glass production was still maintained mainly by the royal and aristocracy courts. The Polish-Saxon Union (1697-1763) was of a certain importance in this process, too [16].

In central Europe in the first half of the 18th century, three main types of colourless vessel glass – *crystal*, *white (chalk)* and *ordinary* – were manufactured. They corresponded to the former Venetian glass types: *cristallo, vitrum blanchum* and *vetro communale* [17].

Vetro communale, as most ordinary glass might be compared with *forest glass. Ordinary glass* was their successor. It was melted as a rule with the use of four basic raw materials (sand, lime, potash and pyrolusite) and, excepting of pyrolusite, these raw materials were gained from local, easily accessible sources. We can recognize such glass on the basis of a few qualities. The absence of arsenic is the first one, assumed obviously that the element was not introduced with a cullet, and the high content of glass contaminations constitutes no less important feature of the metal.

White glass might be considered as a successor of *vitrum blanchum*. There were multicomponent batches used for its production and the raw materials were better selected and purified. Chalk was used in place of lime stone; potash was partly replaced by saltpeter; the quality of the sand constituted a very important feature. Pyrolusite remained the main decolourizing agent. Beside saltpeter, there were applied new raw materials: arsenic and wine stone. The saltpeter/potash ratio as well as the whole batches differentiated each other depending on the glasshouse and glassmaking tradition.

Crystal glass production required the best quality raw materials, but obviously in this regard, particular glasshouses differed from one another, too. The *crystal glass* batch distinguished itself also in certain other qualities. The saltpeter/potash ratio was much higher than in the case of *white glass* batch or potash could even be completely replaced by saltpeter. The saltpeter/chalk ratio was also higher than for *white glass*. On the basis of chemical analysis, we are not able to distinguish the fraction of potassium introduced with saltpeter from the fraction introduced with potash and wine stone which also constituted a source of the element. Considering only dependence of the concentration of alkaline and alkaline earths oxides in glass, the differentiating of *white* and *crystal* ones is possible in most cases, but not always. Figure well illustrates the technological relationship between *vitrum blanchum* and *white glass* as well as between *cristallo* and *crystal glass*. Considering *vitrum blanchum* manufactured in other places than Venice, even in northern Europe, this scatter plot does not undergo significant changes. Only for the sum of alkaline oxides ($Na_2O + K_2O$), a contribution of Na_2O and K_2O

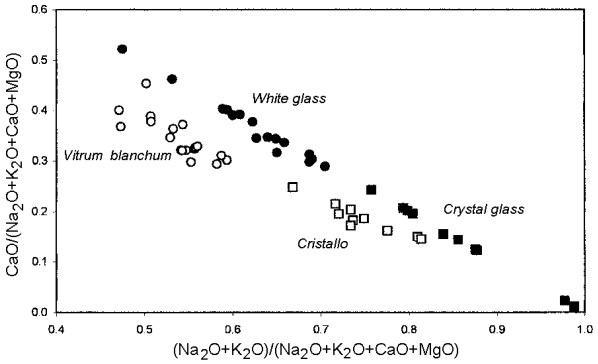

Fig. Scatter plot for Venetian soda-ash glass (*vitrum blanchum*, *cristallo*) [18] and 18th century central European potassium glass (*white*, *crystal*) (own results).

changes respectively to the type of applied ash. Now we can easily observe that *white glass* constitute continuation of northern *vitrum blanchum* manufactured frequently with the use of mixed alkaline ashes or even noticeable potash-ash. The same concerns *crystal glass*. In this case, *salicornia* was replaced mainly by saltpeter and the sodium contribution to this sum of alkaline oxides appears almost insignificant. But the overall ratio of alkaline and alkaline earths oxides remains the same. Due to the possible overlapping of regions characteristic of *crystal* and *white glass* when the alkaline oxides/alkaline earths oxides ratio is considered, the As_2O_3/CaO ratio constitutes a better and more convenient technological indicator. Firstly, the proportion of arsenic is related (in many cases) to the proportion of saltpeter due to the technological requirements. Secondly, there is easier to estimate arsenic than potassium content in the glassware by the use of

non-destructive methods (like EDXRF). The next important feature that discriminates *crystal glass* is boron presence in the glass. We are not fully convinced whether borax was used exclusively for *crystal glass* production. It is difficult to detect boron by the analytical methods commonly applied to baroque glass analysis or their detection limits for boron are not sufficient. But, as till now, both still scarcities of written sources and of the results of chemical analyses confirm the boron presence only in *crystal glass*.

Having distinguished the main glass formulations, it is important to underline that among *crystal* and *white glasses*, there were found glasses which contained also lead [10]. For *white glass* only some of the items examined contained lead and its highest concentration reached about 2%wt. It was impossible to distinguish *white glasses* with intentionally and accidentally (*e.g.* with cullet) introduced lead. Among *crystal glasses*, most of them contained lead and it was possible to distinguish unleaded from leaded items. This is surely influenced by the better technological regime and the greater care taken when *crystal glass* was manufactured. For the leaded *crystal glass*, the PbO concentration exceeded ~0.4%wt. and reached in certain cases almost 13%wt. The overlapping of these PbO concentration ranges (~0.4-~2%) means that knowledge about lead concentration does not constitute always a differentiating feature for *white* and *crystal* formulation. Although, when the PbO content is really high (much higher than 2%), it may be assumed that the examined glass is made of *crystal* metal (although, further results might change these ranges). We have found only one unleaded glass sample among all *crystal glass* samples analyzed by the use of EPMA, but a few more were found by the use of EDXRF. Supported by these results, we want to verify some of our previous conclusions [1-3] and to state that most of *crystal glasses* melted in the 1st half of the 18th century in central Europe contain lead, but some of them do not. Among leaded *crystal glass*, the highest PbO concentration was found in the case of glass medallions on the Dresden (or Naliboki) goblets (<13%), and in the case of goblets made in Altmünden and Dresden (<11%). For examined Naliboki and Zechlin glasses, PbO content did not exceed 6%, and for Potsdam glass – 3%. It should be emphasized once again, that if leaded *crystal* was manufactured for the whole first half of the 18th century, the examined unleaded *crystal glasses* originated only from the beginning of the century.

The following glasshouses were found to produce *crystal glass* (regardless to the lead compounds usage) in the 1st half of the 18th century: Potsdam (since 1737 – Zechlin), Altmünden, Dresden, Naliboki (since 1722), and Bielany (since ~1710). Till now, for Bielany factory, only certain written sources (list of imported raw materials) allow us to include it to this register of glasshouses. No glass manufactured in Bielany has been recognized as till now.

Experimental details: Analyses by wavelength dispersive spectrometry in the EPMA system were carried out using Cameca SX-100 with three simultaneously working spectrometers (PET, LIF, TAP crystals and PC2 for boron) at the Electron Microprobe Laboratory (Faculty of Geology, Warsaw University). The measurements conditions were as follows:

- for main constituents: 15 kV, 6 nA, beam diameter – 20 μm, counting time – 20 s for each element;
- for minor and trace constituents (with fixed concentration of main constituents): 20 kV, 100 nA, beam diameter – 80 μm, counting time – 20-60 s;
- for boron (with fixed concentration of main and minor constituents): 5 kV, 100 nA, beam diameter – 20 μm, counting time – 20 s.

Standards were oxides and minerals. Corning C, D and NIST 610, 612 were used as secondary standards. There was good agreement between the EDXRF and EPMA results according to the most of the examined elements. For example, the correlation coefficient (R) for PbO concentration analysed by both the systems amounted to 0.9952 (n=12). Although some small discrepancies have been also found. They are discussed in the mentioned above forthcoming article.

The authors express their gratitude to the Boards of Museums who made the vessels available for examination: National Museums (Kraków, Poznań, Warszawa, Wrocław), Royal Castle in Warsaw, Wilanów Museum Palace, District Museum in Tarnów, and Historical Museum of Warsaw.

The research was partly supported by the State Committee for Scientific Research – grant No. 2 H01E 008 25.

References

[1]. Kunicki-Goldfinger J.J., Kierzek J., Kasprzak A.J., Małożewska-Bućko B.: Analyses of 18th century central European colourless glass vessels. In: Annales du 15e Congrès de l'Association Internationale pour l'Histoire du Verre (New York – Corning 2001). AIHV, Nottingham 2003, pp.224-229.

[2]. Kunicki-Goldfinger J.J., Kierzek J., Kasprzak A.J., Małożewska-Bućko B.: X-Ray Spectrom., 29, 310-316 (2000).

[3]. Kunicki-Goldfinger J.J., Kierzek J., Kasprzak A.J., Małożewska-Bućko B.: Non-destructive examination of 18th century glass vessels from central Europe. In: Proceedings of the 6th International Conference on Non-Destructive Testing and Microanalysis for the Diagnostics and Conservation of the Cultural and Environmental Heritage (Rome 1999). Italian Society for Non-destructive Testing Monitoring Diagnostics (Brescia) and Central Institute for Restoration (Rome), Rome 1999, Vol.2, pp.1539-1552.

[4]. Francis P.: Apollo, February, 47-53 (2000).

[5]. Buquoy Glass in Bohemia 1620-1851. Buquoyské sklo v Čechách 1620-1851. [Katalog]. Uměleckoprůmyslove Museum v Praze, Prague 2001, in Czech.

[6]. Brain C.: Glass Technol., 43C, 357-360 (2002).

[7]. Drahotová O.: J. Glass Stud., 23, 46-55 (1981).

[8]. Drahotová O.: Vznik buquoyského křišťálového skla v poslední čtvrtině 17. století. In: Buquoy Glass in Bohemia 1620-1851. Buquoyské sklo v Čechách 1620-1851. [Katalog]. Uměleckoprůmyslove Museum v Praze, Prague 2001, pp.13-16, in Czech.

[9]. Kunckel J. [Johannis Kunckelii]: Ars vitraria experimentalis oder Vollkommene Glasmacher-Kunst. 1679 – 1st edition; 1689 – 2nd edition, in German.

[10]. Kunicki-Goldfinger J.J., Kierzek J., Kasprzak A.J., Dzierżanowski P., Małożewska-Bućko B.: Lead in central European 18th century colourless vessel glass. In: Archäometrie und Denkmalpflege. Kurzberichte 2003 (Berlin). Berlin 2003, pp.56-58.
[11]. Vickers M.: Antiquity and utopia: the paradox in glass studies. In: The Prehistory & History of Glassmaking Technology. Ed. P. McCray. The American Ceramic Society, Westrville, OH, USA 1998, pp.17-31. Series: Ceramic and Civilization. Vol.VIII.
[12]. Stern E.M.: J. Roman Archaeol., 10, 192-206 (1997).
[13]. Vickers M.: J. Roman Archaeol., 9, 48-65 (1996).
[14]. Jacoby D.: J. Glass Stud., 35, 65-90 (1993).
[15]. McCray W.P.: Glassmaking in Renaissance Venice. The Fragile Craft. Aldershod, Ashgate 1999.
[16]. Kunicki-Goldfinger J.J., Kierzek J., Kasprzak A.J.: Some features of the 18th century glass technology used in central Europe (Saxony, Brandenburg, Poland). In: Archäometrie und Denkmalpflege. Kurzberichte 2000 (Dresden). Eds. G. Schulze, I. Horn. Mensch & Buch Verlag, Berlin 2000, pp.107-109.
[17]. Moretti C., Toninato T.: Rivista della Stazione Sperimentale del Vetro, 1, 31-40 (1987), in Italian.
[18]. Veritá M.: Rivista della Stazione Sperimentale del Vetro, 1, 17-29 (1985), in Italian.

ELECTRICAL PARAMETERS OF POLYPYRROLE NANOTUBULES DEPOSITED INSIDE TRACK-ETCHED MEMBRANE TEMPLATES

Marek Buczkowski, Danuta Wawszczak, Wojciech Starosta

Polypyrrole (PPy) – an electrically conducting polymer seems to be a very interesting material for nanotechnology [1,2]. In such case, it is necessary to know its electrical parameters. In the accessible literature there are differences in such data [3,4]. Because of this the present work was undertaken to measure electrical parameters of PPy nanotubules deposited in track-etched membrane (TM) templates – as resistivity and temperature dependence on resistance.

In order to get samples, a synthesis of PPy nanotubules was carried out in TMs (from the Joint Institute for Nuclear Research – JINR, Dubna, Russia) made of a 10 μm thick poly(ethylene terephthalate) (PET) film. For the synthesis, aqueous solution: 0.1 M pyrrole and 0.3 M $FeCl_3$ (III) as oxidant, have been taken [5,6].

Table. Parameters of membrane templates and nanotubules inside pores.

Number	Pore size in membrane template [μm]	Pore density [cm^{-2}]	Thickness of nanotubules walls [nm]	Resistance [Ω]	Resistivity [Ω cm]
1	0.2	$6.0x10^8$	40	58	$3.50x10^5$
2	0.2	$6.0x10^8$	70	25	$2.04x10^5$
3	1.3	$7.5x10^6$	85	68	$1.11x10^4$
4	1.3	$7.5x10^6$	195	19	$0.68x10^4$

For getting samples without necessity of cutting out the prepared membranes, a special matrix has been used. This matrix gave ready disc samples with

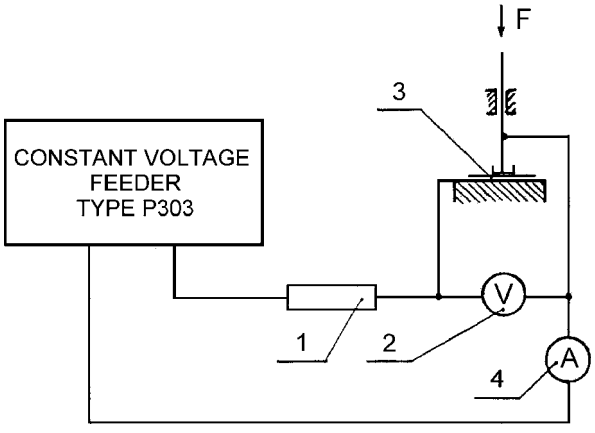

Fig.1. A scheme of measuring set-up for determining nanotubule resistances in TMs templates: 1 – matching resistor, 2 – digital voltmeter, 3 – sample, 4 – miliammeter.

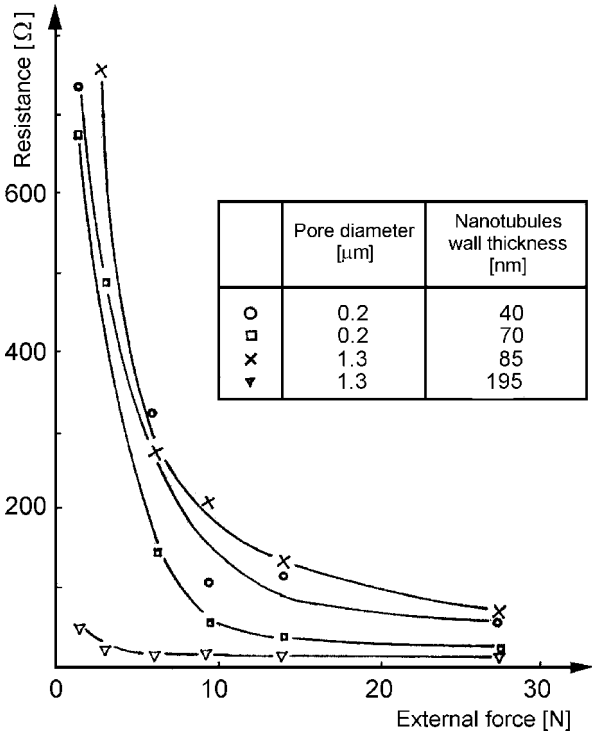

Fig.2. Dependence of resistance of TMs samples with deposited nanotubules upon outer force applied to the sample.

a diameter of 25 mm. For measurements, four types of deposited nanotubules have been taken with parameters described on the left side of Table.

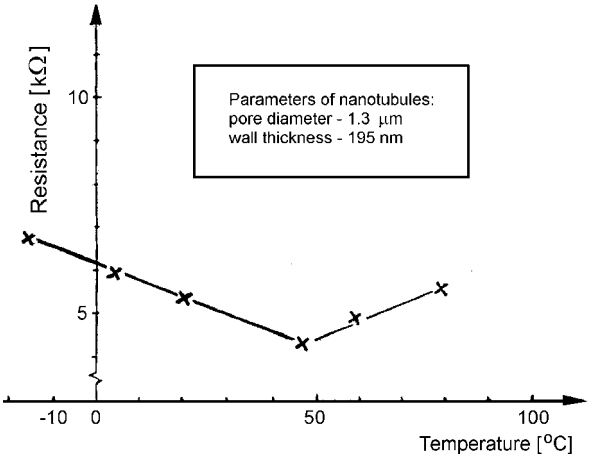

Fig.3. Dependence of resistance of a TM sample with deposited nanotubules upon outer temperature.

Resistance of the above samples was measured in a set-up whose scheme is given in Fig.1. A sample (3) with the diameter 25 mm was put between two metal plates (upper round plate was movable) and its resistance was determined at a given force (F) by measurement of voltage (2) and current (4). At properly big forces, resistances have been stabilized as it is given in Fig.2. Measured resistances and calculated resistivities for four types of samples with nanotubules are given in the right part of Table.

So, it was found that the resistivity of nanotubules depends on their outer diameter. Mean value of the resistivity was equal to 2.8×10^5 Ω cm at outer diameter 200 nm and 0.9×10^4 Ω cm at outer diameter 1300 nm.

In the second part of the work, the temperature dependence on resistance, for samples with PPy nanotubules, has been determined. For a sample with nanotubules of the wall thickness 195 nm, deposited inside the membrane template with 1.3 μm pore size, such dependence is given in Fig.3. For this sample (surface 10x10 mm^2), the initial value of resistance at room temperature (20°C) was equal to 5.4 kΩ. In the range of temperatures between -16 and +45°C, the change of resistance had linear characteristic with a negative proportional coefficient.

References

[1]. Huczko A.: Appl. Phys., A70, 365-376 (2000).
[2]. Whang Y.F. *et al.*: Synth. Met., 45, 151 (1991).
[3]. Park J.G. *et al.*: Appl. Phys. Lett., 81, 24, 4625-4627 (2002).
[4]. Rane S., Beaucage G.: Polymer Data Handbook by Oxford University Press. 1999, pp.810-813.
[5]. Martin C.R. *et al.*: Synth. Met., 57, 3766 (1991).
[6]. Zhitariuk N.I. *et al.*: Nucl. Instrum. Meth. Phys. Res. B, 105, 204-207 (1995).

SYNTHESIS AND ELECTROCHEMICAL CHARACTERIZATION OF $Li_{1.1}V_3O_8$ BY COMPLEX SOL-GEL PROCESS

Andrzej Deptuła, Tadeusz Olczak, Wiesława Łada, Matthieu Dubarry[1/], Aurélie Noret[1/], Dominique Guyomard[1/], Rita Mancini[2/]

[1/] Institut des Matériaux Jean Rouxel, Nantes, France

[2/] Italian Agency for the New Technologies, Energy and Environmental (ENEA), C.R.E Casaccia, Rome, Italy

Lithium vanadium oxide, $Li_{1+\alpha}V_3O_8$ ($\alpha \approx 0.1$-0.2) has been intensively studied for the past 20 years for its attractive electrochemical properties. Indeed, it provides a fair energy density and a good capacity retention. $Li_{1+\alpha}V_3O_8$ could be prepared by several routes. One interesting synthesis technique consisted in the annealing at a temperature higher than 300°C of a gel precursor obtained from the reaction of V_2O_5 and $LiOH,H_2O$ at 50°C under N_2 [1-3].

The goal of this work was to use a new [4] variant of sol-gel process named Complex Sol-Gel Process (CSGP) to synthesize $Li_{1.1}V_3O_8$. The main feature in this process is the application of a very strong complexing agent (ascorbic acid – ASC) for the preparation of sols. This procedure successfully was applied to the synthesis of $Li_xMn_2O_{4\pm\delta}$ spinels [5,6], $LiNi_xCo_{1-x}O_2$ layered oxides [6,7] and also $LiCoO_2$ doped with inert Al, Ti, Si oxides [8].

A flowchart of the preparation procedures is shown in Fig. 1. Commercial NH_4VO_3 (Aldrich No. 39,812-8, determined content in INCT 0.432 g of V in 1 g of reagent) was dissolved in water and after addition of ASC immediately introduced to a reservoir of Rotavapor equipment (Büchi, Switzerland).

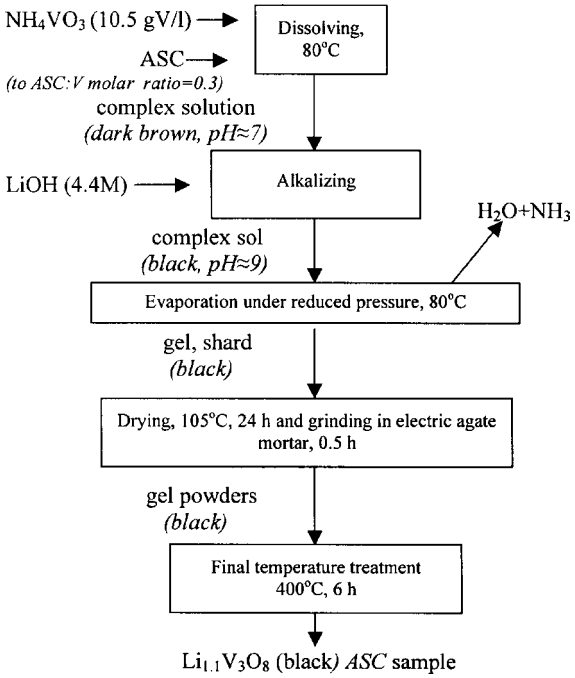

Fig.1. Flow chart for preparation of $Li_{1.1}V_3O_8$.

Concentrated LiOH was slowly (several minutes for quantity of 1 l of starting solution) sucked into the reservoir. For the evaluation of results the process was repeated without addition of ASC.

A chemical treatment of sample with concentrated HNO_3 and H_2O_2 (1 ml of each reagent on 1 g of powder) is also applied in order to remove traces of ASC in the sample; the obtained slip was dried at 105°C for 24 h (*ASC retreated* sample).

Three samples have been chosen: *no ASC* sample as a reference, *ASC* sample and *ASC retreated* sample. All of them were heated slowly until 400°C and socked 6 h before tests. Another sample was prepared by classic sol-gel route [9] and annealed at 400°C, noted SG400 was also added to some tests as reference.

All thermal treatments were performed in a programmed Carbolite furnace type CSF 1200. The X-ray diffraction (XRD) records were obtained using a Θ/2Θ SIEMENS D5000 diffractometer with a linear MOXTEK detector and a Θ/Θ SIEMENS D5000 diffractometer with a linear PSD detector. Fourier transformed analysis (FITR) was performed on a GX Spectrometer Perkin Elmer using potassium bromide pellet technique. Thermal analysis (TG – thermogravimetry, DTA – differential thermal analysis) was carried out using a Hungarian MOM Derivatograph. Scanning electron microscopy (SEM) images were obtained from a GEOL 6400 microscope. Electrochemical measurements were achieved with a Mac-Pile controller using Swagelok type cells. The composite electrode was coated with Al discs from a mixture of 85% of LiV_3O_8, 10% of C super P and 5% of PVDF. EC:DMC(2:1)+1 M $LiPF_6$ (from Merck) and was used as the electrolyte. Galvanostatic cyclings were obtained using a current that corresponds to the insertion-desinsertion of 1 Li/2.5 h and 1 Li/5 h, respectively from 3.7 to 2 V.

We observed that the yellow colour solution, after addition of ASC, changed into dark brown

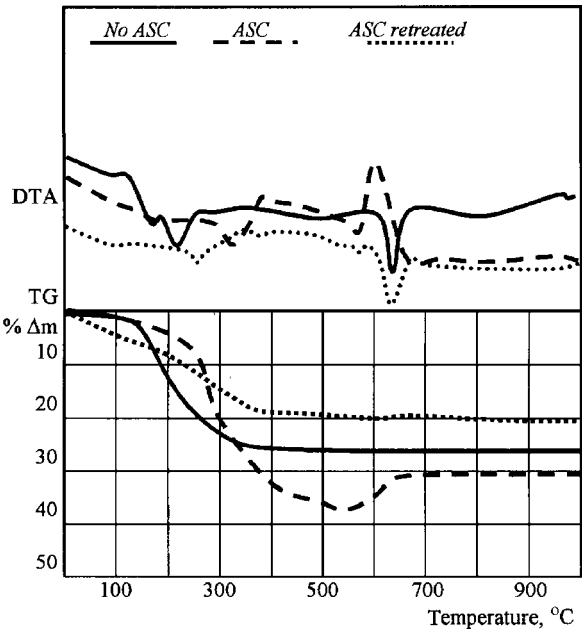

Fig.2. Thermal analysis of $Li_{1.1}V_3O_8$ gels dried for 24 h at 105°C.

what indicates reduction of V^{5+} to V^{4+}. We confirmed indirectly this observation by thermal analysis of samples shown in Fig.2.

We observed that for sample *no ASC*, after removal of chemically bonded H_2O and presumably remaining NH_3 (endotherms at 180 and 220°C) weight stabilization takes place at 370°C. The DTA complex behaviour of the sample before weight stabilization may be associate also with different phase transformation between particular $Li_{1+\alpha}V_3O_8$ hydrates. From DTA curve, we observed at 620°C endotherm connected with melting of the sample. Completely different thermal decomposition was observed for sample *ASC* in which preparation ASC was employed. Evidently higher weight loss – than in the former sample (oxidation of organics besides removal of H_2O and NH_3) – is observed till 550°C. Starting from this temperature increasing of weight is observed. This can be attributed only to reoxidation of V^{4+} species to V^{5+} final compound $Li_{1.1}V_3O_8$. Weight increasing roughly corresponds to reoxidation of hypothetic composition $Li_{1.1}V_3^{4+}O_{6.55}$ into the final product. Reoxidation is accompanied by an exothermic effect at 600°C which completely masked endotherm accompanied by melting. We observed visually melting of samples in this temperature region.

Because XRD patterns (Fig.3) of *ASC* indicated that some V^{4+} species are still observed – in contrast to *no ASC* sample and SG400 samples. This reduction implies a change in the structure of $Li_{1+\alpha}V_3O_8$ in β-$Li_xV_2O_5$.

As can be observed from XRD patterns of the *ASC retreated* sample, the retreatment is not efficient in the formation of pure $Li_{1.1}V_3O_8$, but leads to two impurities $LiVO_3$ and V_2O_5. Consequently, it seems that formation of stable biphasic composition with a small quantity of V^{4+} species is an intrinistic result of application of CSGP.

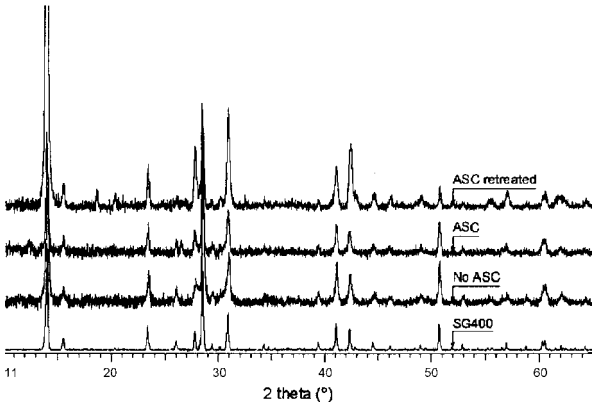

Fig.3. XRD patterns of *ASC retreated*, *ASC, no ASC* and SG400 samples.

ASC retreated sample presents impurity peaks at 18°, related to $LiVO_3$ and 20° related to V_2O_5. *ASC sample* presents an impurity peak at 10° related to β-$Li_xV_2O_5$.

SEM study (Fig.4) also shows differences between the 4 samples: *no ASC* sample presents a morphology close to the one observed for classical $Li_{1+\alpha}V_3O_8$ SG400. *ASC* sample presents large porous polycrystalline grains and *ASC retreated*

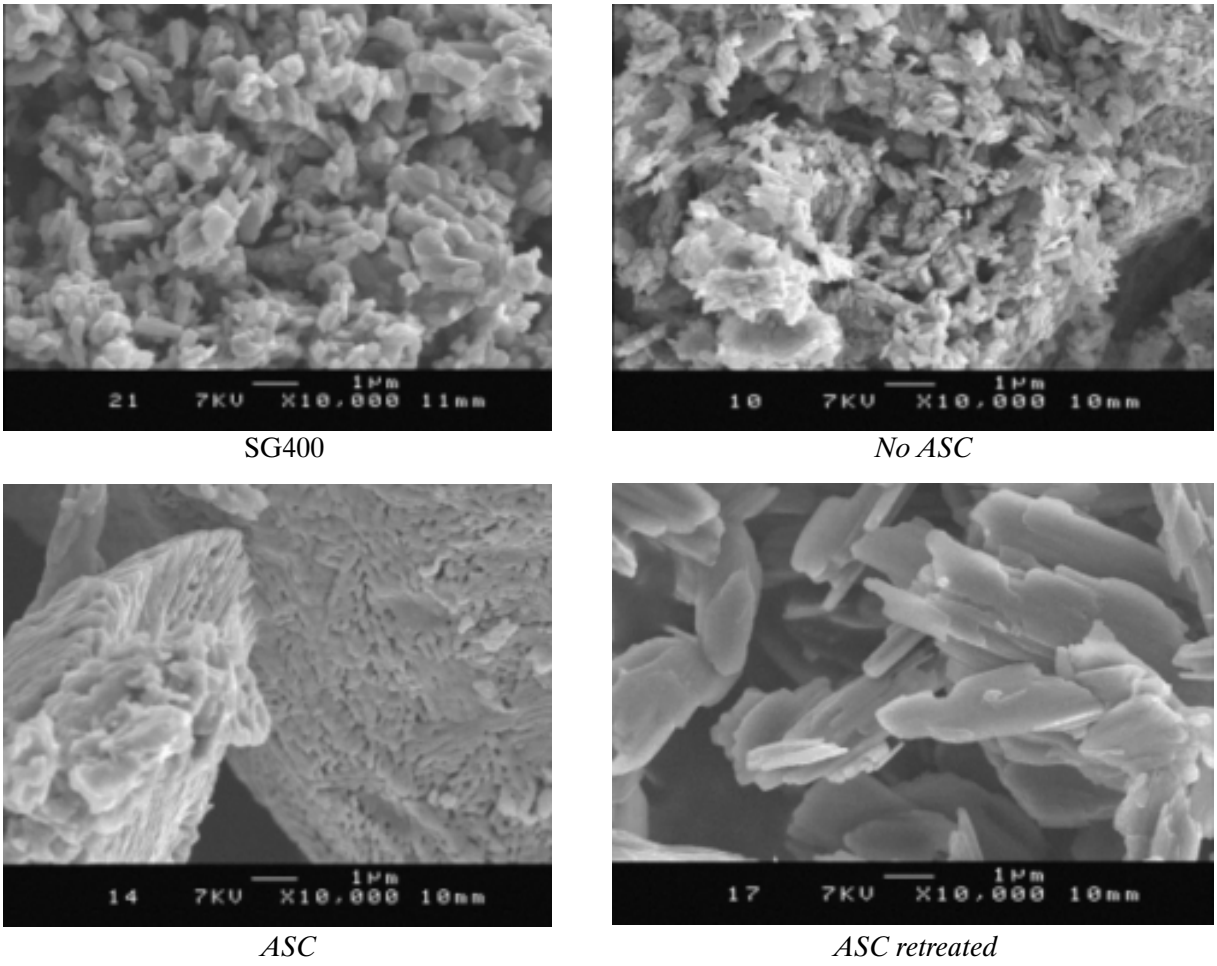

SG400 *No ASC*

ASC *ASC retreated*

Fig.4. SEM pictures of *no ASC*, *ASC*, *ASC retreated* and SG400 samples.

sample – large (3x6 μm) platelets; such morphologies have never been observed before for heat treated $Li_{1+\alpha}V_3O_8$ to our knowledge.

FITR spectra of the studied samples presented in Fig.5, are very similar and did not point out on the significant difference in indicated bonds arrangement. Practically there are two slight differences. One is a small band at 974 cm^{-1} (in other

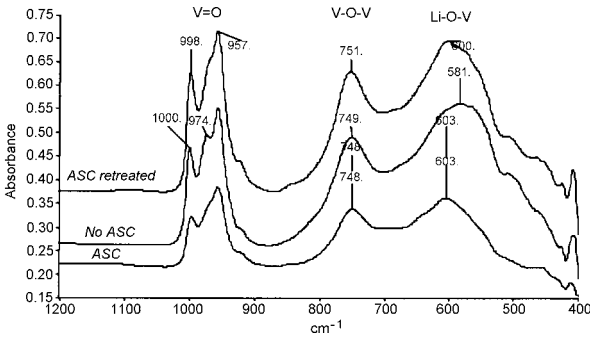

Fig.5. FITR spectra of $Li_{1.1}V_3O_8$ samples heated for 6 h at 400°C.

spectra only shoulders on principal bands are observed). According to work [10], existence of this band indicates on more crystalline structure of compound what can suggest a better crystalline structure. The second is shifting of Li-O-V frequencies to red, what means that O-V bond is shorter with the consequences of electronic structure exposed to Li. It seems that this phenomenon could explain better electrochemical performance materials synthesized by CSGP. It is worth of noting that lack of the bands at 875 cm^{-1}, which is very specific for carbonates (ν_2), indicated that decomposition of this organic precursors proceeds without formation of carbonates similarly as for $LiCoO_2$ and $LiMn_2O_4$ synthesized also by CSGP [6,7].

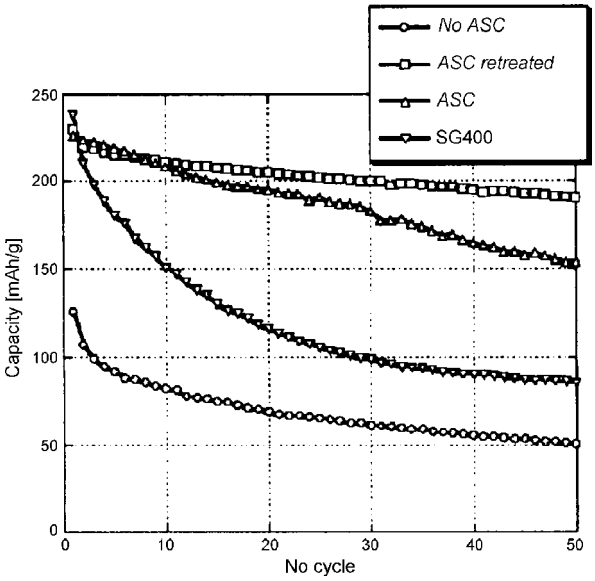

Fig.6. Variation of capacity, expressed in mAh/g, recorded during galvanostatic cycling at 1 Li/2.5 h in discharge and 1 Li/5 h in charge for the four studied samples.

It was rather surprising to observe that these materials have definitely better electrochemical properties (Fig.6) than those prepared without ASC additive which exhibit the well defined monophasic $Li_{1.1}V_3O_8$ (Fig.3) structure. In former works or work of some of the present authors [10], it has been observed the influence of morphology on electrochemical properties of similar to this compound prepared by another variant of sol-gel process. However, it seems that there are not significant differences which could explain this observed phenomenon.

The incremental capacity *vs*. voltage curve in the first cycle (Fig.7) shows that the main differences between all samples is the intensity of the peak at

All those observation indicate that the observed differences in the studied physicochemical parameters (except Li-V-O bond in FITR spectra) cannot explain definitely the reason of excellent electrochemical performance of the samples prepared by CSGP. One of the suggestion can be the existence of the second phase presumably created during reoxidation process. In former work of some of the present authors [11,12] concerning sinterability in the systems ZrO_2-(CaO, Y_2O_3 or CeO_2) definitely higher sinterability for CeO_2 doped samples was observed. This observation has been attributed to the ability of Ce to change the valency by reduction of Ce^{4+} to Ce^{3+} by carbon impurities and subsequently reoxidation to the initial valency.

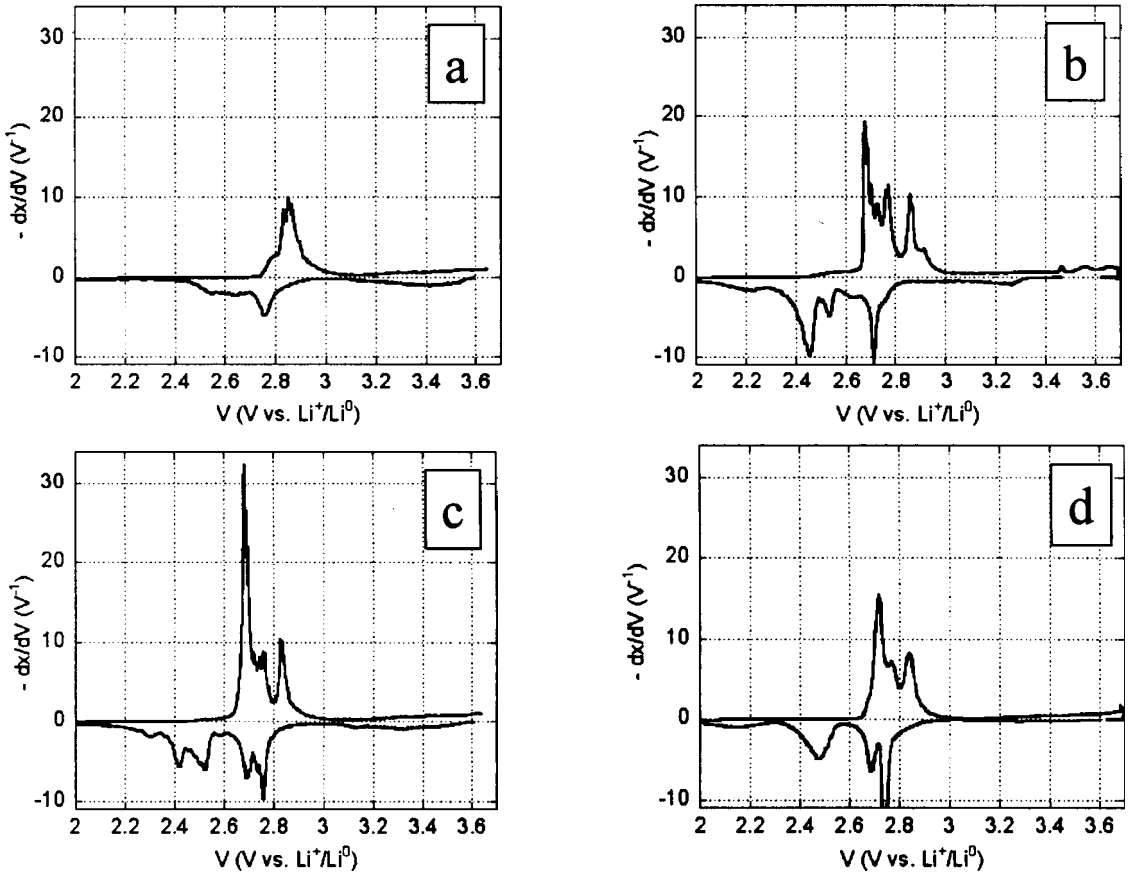

Fig.7. Incremental capacity *vs*. voltage curves, obtained from voltage *vs*. composition data for (a) *no ASC*, (b) *ASC*, (c) *ASC retreated* and (d) SG400 samples.

2.6 V, corresponding to a two-phase process. The peak is intense for *ASC retreated* sample (Fig.7c) and there is no trace of impurities (V_2O_5 is normally active in this range of potential). Classic SG400 (Fig.7d) and *ASC* (Fig.7b) samples gave the same behavior in the first cycle with one difference, the reduced β-$Li_xV_2O_5$ is active and responsible for the peaks at high potential, another study to be published also shows that the presence of the reduced phase seems to increase the cyclability of $Li_{1+\alpha}V_3O_8$ prepared at low temperature. Surprisingly, the phase transition do not occur in the *no ASC* sample (Fig.7a), that is why the capacity is lower than for other samples, this has already been observed for a $Li_{1+\alpha}V_3O_8$ gel prepared in another way, but the reason of the freezing of the phase transition had not been identificated yet.

Other studied parameters (specific surface area, XRD structure, particle size) were not connected with the observed improving of sinterability.

References

[1]. Pistoia G.: J. Electrochem. Soc., 137, 2365 (1990).
[2]. West A.C.: J. Electrochem. Soc., 143, 820 (1996).
[3]. Saidi M.Y.: Mat. Res. Soc. Symp. Proc., 139, 201 (1995).
[4]. Deptuła A., Łada W., Olczak T., Lanagan M., Dorris S.E., Goretta K.C., Poeppel R.B.: Method of preparing of high temperature superconductors. Polish Patent No. 172618.
[5]. Deptuła A., Łada W., Croce F., Appetecchi G.B., Ciancia A., Giorgi L., Brignocchi A., Di Bartolomeo A.: New Materials for Fuel Cell and Modern Battery Systems. Eds. O. Savadogo, P.R. Roberge. Polytechnique de Montreal, Montreal 1997, p.732.

[6]. Deptuła A., Olczak T., Łada W., Croce F., Giorgi L., Di Bartolomeo A., Brignocchi A.: J. Sol-Gel Sci. Technol., 26, 201-206 (2003).
[7]. Deptuła A., Olczak T., Łada W., Croce F., D'Epifanio A., Di Bartolomeo A., Brignocchi A.: J. New Mater. Electrochem. Syst., 6, 39-44 (2003).
[8]. Choblet A., Shiao H.C., Lin H.-P., Salomon M., Manivannan V.: Electrochem. Solid-State Lett., 4 (6) A65-A67 (2001).
[9]. Urca A.Š., Orel B., Drazie G., Pihlar B.: J. Electrochem. Soc., 146, 232 (1999).
[10]. LeGal La Salle A., Verbaere A., Deschamps M., Lascaud S., Guyomard D.: J. Mater. Chem., 13, 921-927 (2003).
[11]. Deptuła A., Carewska M., Olczak T., Łada W., Croce F.: J. Electrochem. Soc., 140, 2294 (1993).
[12]. Deptuła A., Carewska M., Olczak T., Di Bartolomeo A.: Developments in Processing of Advanced Ceramics. Ed. C. Galssi. C.N.R.-IRTEC, Faenza 1995, Vol.2, p.301.

A NEW COMPLEX METHOD OF SAXS DATA ANALYSIS IN THE CASE OF MONOSACCHARIDE GELS

Helena Grigoriew

SAXS (small angle X-ray scattering) study of gel structure is treated as a very efficient method. The monotonously decreased SAXS curve of scattered primary X-ray beam is very influenced by nanostructure of the studied material that is visible as a change of the curve shape. The main method of the SAXS measurement elaboration was its presentation on a log-log scale and/or a comparison of the SAXS curve with the intensity curve calculated from a chosen fragment of the studied material crystal. The last way was not a univocal possibility.

The monosaccharide gels are new materials discovered a few years ago. It is not clear why so small molecules, not able to join themselves with strong bonds and soluble in non-active organic solvents, can form a very extended structure. The scanning electron microscopy (SEM) study of these gels, after their drying (xerogels), showed fibrous superstructures, but drying probably changes these soft gel nanostructures. A study to evaluate the SAXS curve of these gels was not performed as yet, so all problems of their structure is still open.

The SAXS measurements of α-galactose-based gels were carried out [1] in the frame of present work, on a Hasylab-DESY synchrotron using time-resolved mode. The mode makes it possible to detect SAXS curves during process of gelation, *vs.* time, from sol state to wholly formed gel.

I established a complex way of treatment of the monosaccharide gel SAXS measurements that comprises some methods and makes it possible the discovery of these nanostructure materials. The methods are: fractal analysis, determination of gyration radius, Fourier transform results in distance distribution function, and dummy atom model simulation. This complex way can be applied for the analysis of both sol and gel, independently of the degree of their nanostructure development and its ordering.

This complex method was applied to the elaboration of all SAXS curves obtained from the time-resolved mode. Surprisingly, it occurred that during the gelation process of this material in the range 3th and 4th measurements, all found parameters quickly change their values (Table). For example: the size of aggregate, R_g, decreased, not increased as it can be expected, and at the same time mass fractal dimension increased and fractal surface appeared, *i.e.* the phase transition in amorphous state has taken place.

Table. Structural parameters *vs.* time of gelation.

Number of measurement	Maximum SAXS intensity	Mass fractal dimension, d_m	Surface fractal dimension, d_s	Radius of gyration, R_g [nm]
1	164	1.57		18.45
2	168	1.56		18.33
3	181	1.79		17.72
4	550	1.79	2.90	14.88
5	919	1.77	2.47	14.60
6	1032	1.80	2.43	14.70
10	1157	1.84	2.29	14.56
20	1338	1.81	2.19	14.69

All results made it possible to get some conclusions about the nanostructure material and the way of it change during the process of gelation:

- In the sol state – the fractal type structure exists. Aggregates are of rounded, disk-like shape, formed by loose net of chains (probably built of molecules joined by hydrogen bonds).
- The structural transition causing the rapid change of the aggregate size, shape and density takes place. The aggregate become smaller, denser and of irregular cylinder-like shape.
- The aggregation process is continued after the

transition to the complete formation of the gel structure.
- The process of gelation is of DLCCA (diffusion--limited cluster-cluster aggregation) type.

Further investigations are in progress disposing to elaborate a complex way of SAXS data treatment. It is possible to find the nanostructure in a number of soft, organic gels and sols. That collection should make it possible to generalize these gel nanostructures.

References

[1]. Grigoriew H., Luboradzki R., Cunis S.: Langmuir, 20, 7374-7377 (2004).

CRYSTAL CHEMISTRY OF COORDINATION COMPOUNDS WITH HETEROCYCLIC CARBOXYLATE LIGANDS. PART XLIX. THE CRYSTAL AND MOLECULAR STRUCTURE OF AN IONIC CALCIUM(II) COMPLEX WITH PYRAZINE-2,3-DICARBOXYLATE AND WATER LIGANDS

Wojciech Starosta, Janusz Leciejewicz

Crystals of *catena*-[(tetraqua-O)(μ-hydrogen pyrazine-2,3-dicarboxylato-N,O,-N',O')calcium(II)] chloride contain molecular ribbons composed of polycations $\{Ca[H(2,3\text{-}PZDC](H_2O)_4\}_n^+$ and chloride anions (Fig.1). Two adjacent calcium(II) atoms are bridged by a ligand molecule which uses both its N,O bonding moieties. One of the carboxylic groups retains its hydrogen atom which takes part in a short intramolecular hydrogen bond of 2.378(2) Å. The coordination polyhedron around the calcium(II) atom is a distorted pentagonal bipyramid with two apices on one side of the equatorial plane and one apex on the other side. Chloride anions are located in the interstitial space between the ribbons. Figure 2 shows the structural unit with atom labelling scheme.

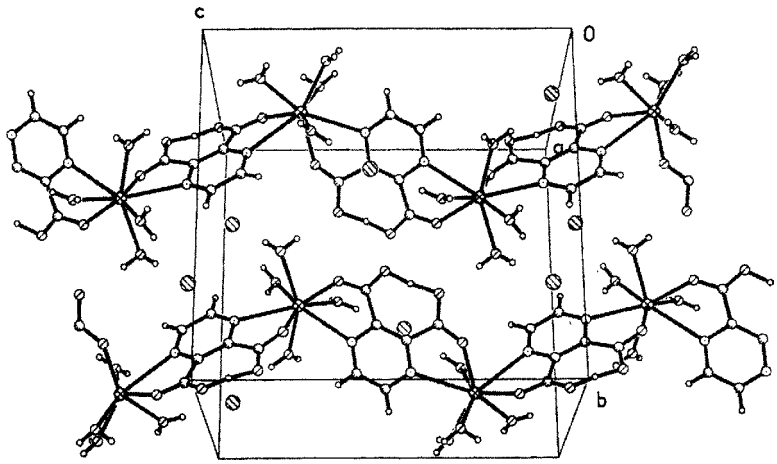

Fig.1. The alignment of the molecular ribbons in the structure of $Ca[H(2,3\text{-}PZDC)](H_2O)_4^+Cl^-$.

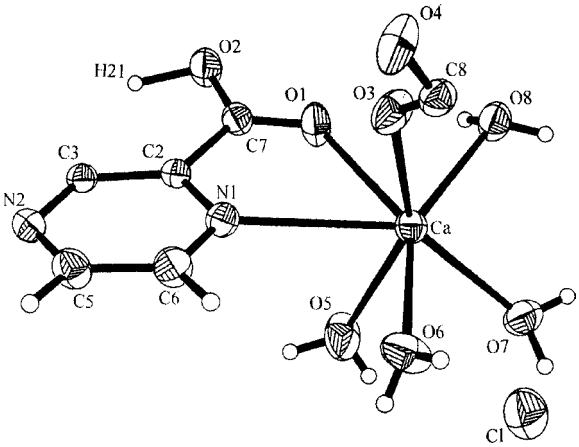

Fig.2. A structural unit of $Ca[H(2,3\text{-}PZDC)](H_2O)_4^+Cl^-$ with atom numbering scheme. Non-hydrogen atoms are shown as 50% probability elipsoids.

X-ray diffraction data collection was carried out on a KUMA KM4 four circle diffractometer at the Institute of Nuclear Chemistry and Technology. Structure solution and refinement was performed using SHELXL programme package.

References

[1]. Part XLIII. Leciejewicz J., Ptasiewicz-Bąk H., Premkumar T., Govindarajan S.: Crystal structure of a lanthanum(III) complex with pyrazine-2-carboxylate and water ligands. J. Coord. Chem., 57, 97 (2004).
[2]. Part XLIV. Starosta W., Ptasiewicz-Bąk H., Leciejewicz J.: The crystal structure of a novel calcium(II) complex with pyrazine-2,6-dicarboxylate. J. Coord. Chem., 57, 167 (2004).
[3]. Part XLV. Premkumar T., Govindarajan S., Starosta W., Leciejewicz J.: Pyrazine-2,3-dicarboxylic acid. Acta Crystallogr., E60, o1305 (2004).
[4]. Part XLVI. Gryz M., Starosta W., Leciejewicz J.: The crystal structure of an ionic hydrazinium magnesium(II) complex with pyridazine-3,6-dicarboxylate and water ligands. J. Coord. Chem., 57, 917 (2004).
[5]. Part XLVII. Gryz M., Starosta W., Leciejewicz J.: Diaqua-*trans*-bis(pyridazine-3-carboxylato-κ^2O,N)zinc(II). Acta Crystallogr., E60, m1481 (2004).

[6]. Part XLVIII. Starosta W., Leciejewicz J.: Pyridazine-3,6-dicarboxylic acid monohydrate. Acta Crystallogr., E60, o2219 (2004).

[7]. Part XLIX. Starosta W., Leciejewicz J.: The crystal structure of Ca(II) (pyrazine-2,3-dicarboxylate) tetrahydrate chloride. J. Coord. Chem., 57, 1151 (2004).

CRYSTAL CHEMISTRY OF COORDINATION COMPOUNDS WITH HETEROCYCLIC CARBOXYLATE LIGANDS. PART L. THE CRYSTAL AND MOLECULAR STRUCTURE OF A ZINC(II) COMPLEX WITH PYRAZINE-2,3-DICARBOXYLATE AND WATER LIGANDS

Michał Gryz[1/], Wojciech Starosta, Janusz Leciejewicz

[1/] Office for Registration of Medicinal Products, Medical Devices and Biocides, Warszawa, Poland

The structure of dihydronium [*catena*–bis(μ-pyrazine-2,3-dicarboxylato-N,O,O')zinc(II)] complex $[2(H_3O)^+]_n[Zn(2,3\text{-}PZDC)_2]_n^{2-}$ is composed of polyanionic ribbons of zinc(II) ions linked by double bridging (2,3-PZDC) ligand molecules (Fig.1). Each ligand uses a N,O bonding moiety formed by one carboxylic group [Zn-O 2.071(2) Å; Zn-N 2.184(2) Å] and an monodentate oxygen atom belonging to the other carboxylate group [Zn-O 2.092(2) Å]. The coordination around the zinc(II) ion is strongly distorted octahedral. Figure 2 shows a structural unit of this compound. Hydronium cations $(H_3O)^+$ link the ribbons *via* hydrogen bonds.

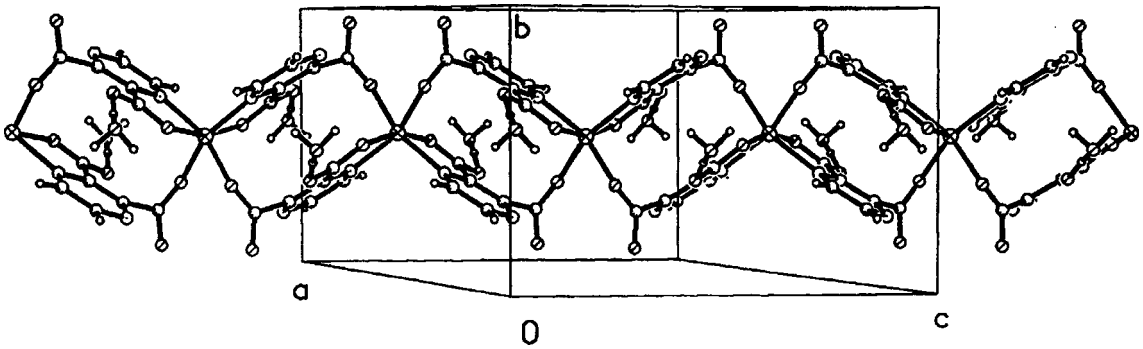

Fig.1. The packing diagram of the $[2(H_3O)^+]_n[Zn(2,3\text{-}PZDC)_2]_n^{2-}$ structure. Broken lines indicate hydrogen bonds. For clarity, only two ribbons are shown.

X-ray diffraction data collection was carried out on a KUMA KM4 four circle diffractometer at the Institute of Nuclear Chemistry and Technology. Structure solution and refinement was performed using SHELXL programme package.

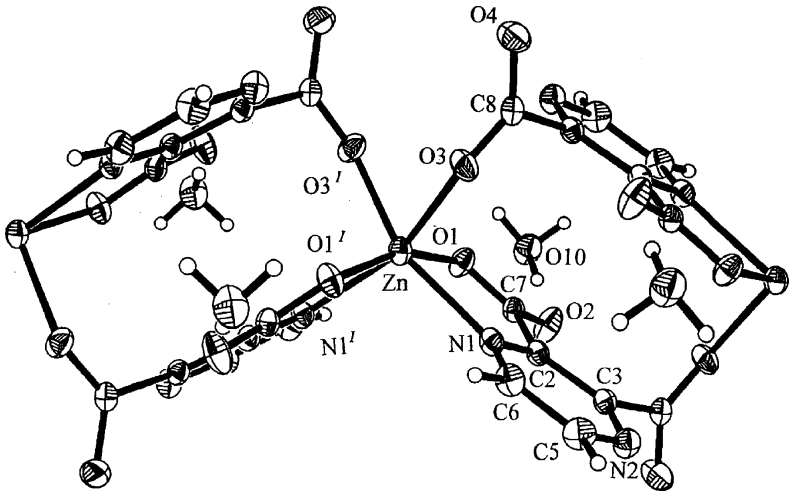

Fig.2. $(H_3O)_2^+[Zn(2,3\text{-}PZDC)_2]^{2-}$ structural unit with atom numbering scheme. Hydrogen atoms attached to the pyrazine ring are not shown. The non-hydrogen atoms are represented by 50% probability ellipsoids.

CRYSTAL CHEMISTRY OF COORDINATION COMPOUNDS WITH HETEROCYCLIC CARBOXYLATE LIGANDS. PART LI. THE CRYSTAL AND MOLECULAR STRUCTURE OF AN IONIC CALCIUM(II) COMPLEX WITH PYRAZINE-2,3-DICARBOXYLATE NITRATE AND WATER LIGANDS

Wojciech Starosta, Janusz Leciejewicz

The structure of *catena*-[tris(aquo-O)(nitrato-O,O')(μ-hydrogen pyrazine-2,3-dicarboxylato-O,N,-O'N')calcium(II)] [tetra(aquo-O)(μ-hydrogen pyrazine-2,3-dicarboxylato-O,N,-O'N')calcium(I)] nitrate, $\{Ca[H(2,3\text{-}PZDC)](H_2O)_3(NO_3)\}\{Ca[H(2,3\text{-}PZDC)](H_2O)_4\}^+(NO_3)^-$ is composed of molecular ribbons in which calcium atoms are bridged by both N,O bonding moieties of singly deprotonated ligand molecules (Figs.1 and 2). Hydrogen atom donated by one of the carboxylic group is linked by a short intramolecular hydrogen

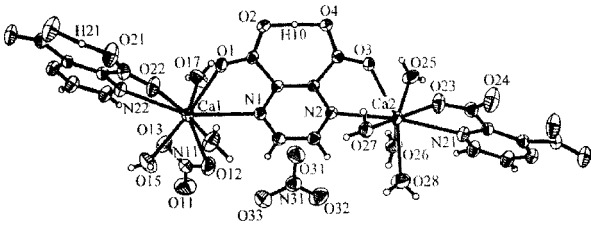

Fig.1. $\{Ca[H(2,3\text{-}PZDC)](H_2O)_3(NO_3)\}\{Ca[H(2,3\text{-}PZDC)](H_2O)_4\}^+(NO_3)^-$ molecular unit with atom labelling scheme. The non-hydrogen atoms are shown at 50% probability level. For clarity, pyrazine ring hydrogen atoms are not marked.

bond of 2.37 Å to an oxygen atom of the second carboxylic group of the same ligand molecule. Two crystallographically independent calcium(II) ions exhibit different coordination modes. One is coordinated by two bonding moieties of the bridging ligand molecules, three water oxygen atoms and two oxygen atoms of a nitrate ligand. The other calcium ion is chelated by two bonding moieties donated by the bridging ligand molecules and four water oxygen atoms forming a positively charged assembly with a nitrate anion located nearby. The coordination polyhedron of the first calcium ion is a strongly deformed bicapped pentagonal bipyramid with nine coordinated atoms, in the case of the second calcium ion – also a strongly deformed pentagonal bipyramid with one apex on one side of the equatorial plane and two apices on the other. Coordinated water oxygen atoms act as donors in a hydrogen bond network.

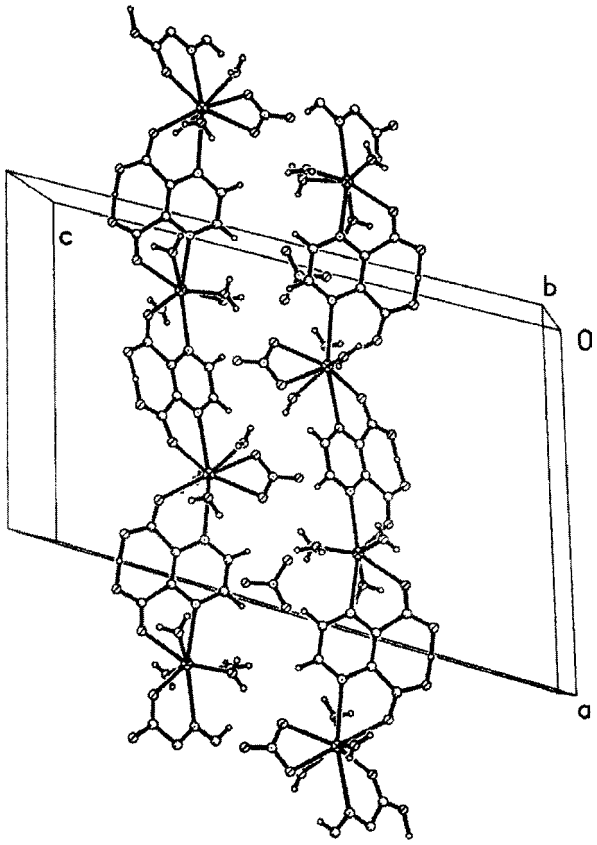

Fig.2. The alignment of molecular chains in repect to the unit cell in the structure of $\{Ca[H(2,3\text{-}PZDC)](H_2O)_3(NO_3)\}\{Ca[H(2,3\text{-}PZDC)](H_2O)_4\}^+(NO_3)^-$. For clarity, only two chains are shown.

CRYSTAL CHEMISTRY OF COORDINATION COMPOUNDS WITH HETEROCYCLIC CARBOXYLATE LIGANDS. PART LII. THE CRYSTAL AND MOLECULAR STRUCTURE OF A CALCIUM(II) COMPLEX WITH PYRAZINE-2,3-DICARBOXYLATE AND WATER LIGANDS

Wojciech Starosta, Janusz Leciejewicz

The structure of di(aquo-O)(pyrazine-2,3-dicarboxylato-N,O; -O',O'')calcium(II) hydrate: $Ca(2,3\text{-}PZDC)(H_2O)_2{\cdot}H_2O$ contains molecular sheets in which calcium(II) ions are bridged by the carboxylate groups of the ligand molecules. Two bridging paths are operating. In the first, a N,O bonding moiety is formed by a hetero-ring nitrogen atom and the nearest to it carboxylate oxygen atom and both oxygen atoms of the second carboxylic group are active. The second path is formed by the other oxygen atom belonging to the carboxylic group involved in the N,O bonding moiety and an oxygen atom from the second carboxylic group. The latter atom acts as bidentate. A two dimensional molecu-

lar pattern is formed (Fig.1). Each calcium(II) ion is also coordinated by two water oxygen atoms com-

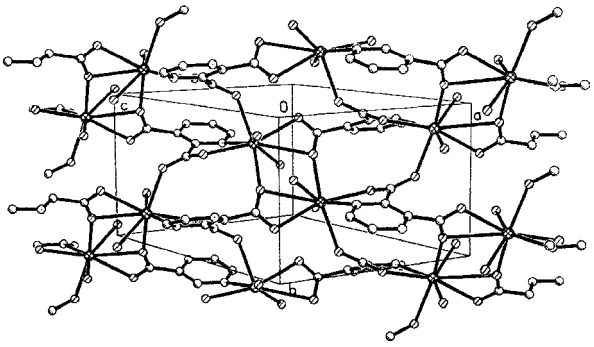

Fig.1. A fragment of a molecular sheet in the structure of $Ca(2,3\text{-}PZDC)(H_2O)_2 \cdot H_2O$.

pleting the number of coordinated atoms to eight. The coordination polyhedron is a distorted pentagonal bipyramid with an oxygen atom at the apex on one side of the equatorial plane and two oxygen

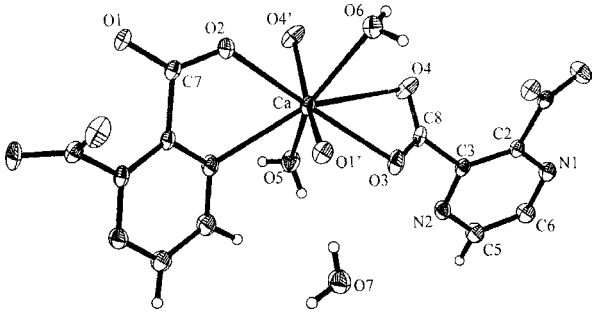

Fig.2. The structural unit of $Ca(2,3\text{-}PZDC)(H_2O)_2 \cdot H_2O$ with atom labelling scheme. The non-hydrogen atoms are shown as 50% probability ellipsoids.

atoms at the apices below it. Figure 2 shows the structural unit of the title compound.

X-ray diffraction data collection was carried out on a KUMA KM4 four circle diffractometer at the Institute of Nuclear Chemistry and Technology. Structure solution and refinement was performed using SHELXL programme package.

CRYSTAL CHEMISTRY OF COORDINATION COMPOUNDS WITH HETEROCYCLIC CARBOXYLATE LIGANDS. PART LIII. THE CRYSTAL AND MOLECULAR STRUCTURE OF A COPPER(II) COMPLEX WITH PYRAZINE-2,6-DICARBOXYLATE AND CHLORIDE LIGANDS

Wojciech Starosta, Janusz Leciejewicz

The crystals of *catena*-dichloro-(dihydrogen pyrazine-2,6-dicarboxylato-O,O',N,-N') copper(II) dihydrate contain molecular chains in which two adjacent copper(II) ions are bridged by a fully protonated pyrazine-2,6-dicarboxylic acid molecule which uses for bridging its O,O,N bonding moiety on one side and a single hetero-ring nitrogen atom on the other. Two chloride ions in axial position complete the coordination around the metal ion to octahedral with bond distances: Cu-N1 2.028(1) Å, Cu-N2 2.006(1) Å, Cu-Cl 2.28(1) Å and Cu-O2 2.446(2) Å (Fig.1). Copper(II) ions are located in the centre of symmetry and are coplanar with the

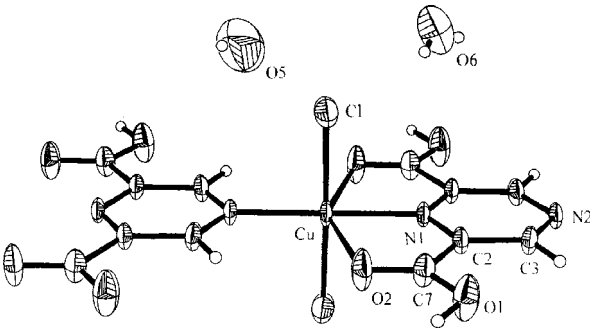

Fig.1. A structural unit of $Cu[H_2(2,6\text{-}PZDC)](Cl)_2 \cdot 2H_2O$ with atom numbering scheme. Non-hydrogen atoms are shown as 50% probability elipsoids.

ligand acid molecule forming flat molecular chains propagating in the direction of the X-axis (Fig.2). To maintain charge balance, the ligand acid molecule remains fully protonated. Its hydrogen atoms

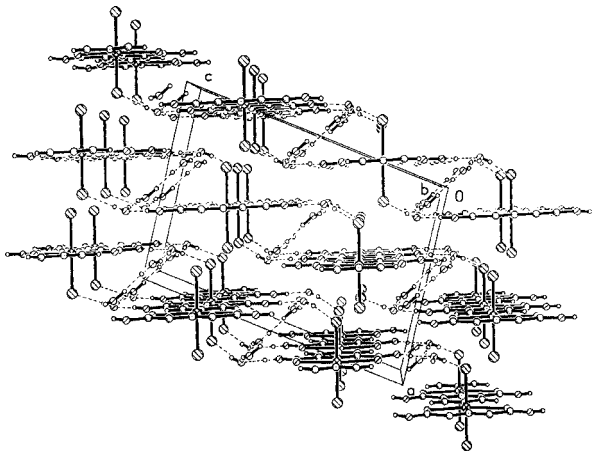

Fig.2. The alignment of molecular chains in the structure of $Cu[H_2(2,6\text{-}PZDC)](Cl)_2 \cdot 2H_2O$. For clarity, only two chains are shown.

attached to the non-coordinated carboxylate oxygen atoms participate in fairly short hydrogen bonds of 2.511(2) Å to solvation water molecules O6. In turn, the latter act as donors in the bonds to the coordinated chlorine atoms in adjacent chains. The O6 and O5 solvation water molecules form pairs being linked by hydrogen bonds of 2.812(2) Å.

X-ray diffraction data collection was carried out on a KUMA KM4 four circle diffractometer at the Institute of Nuclear Chemistry and Technology. Structure solution and refinement was performed using SHELXL programme package.

RADIOBIOLOGY

INTERACTION OF DINITROSYL IRON COMPLEXES WITH DNA

Hanna Lewandowska, Marcin Kruszewski

Dinitrosyl iron (I) complexes (DNIC) are important factors in NO-dependent regulation pathways in the cell [1,2]. In general, there appear to be two main binding sites for Fe-NO complex in proteins: (i) sulphur (II)-containing ligands, such as thiols and inorganic sulphur clusters, and (ii) imidazole rings present in residues such as histidine or purines; particular case are pyrrole rings of prosthetic groups, when NO binds to haem iron.

We examined dinitrosyl iron interactions with DNA, choosing two ligands, each representing one characteristic site of dinitrosyl iron binding to proteins. Glutathione is a low-molecular thiol compound ubiquitous in all kinds of cells and displaying a wide range of biological activities, among others playing part in detoxification and radical scavenging and also acting as a reductant. Dinitrosyl-dithiol iron (II) complexes are well characterised species in which iron is chelated by two S^{-2} atoms and two NO molecules. Charge of this complex is (-1) and iron is in formal (+1) oxidation state [3]. Histidine is an amino acid whose imidazole ring has been shown to be responsible for DNIC formation in non-thiol proteins. In the case of histidine, iron is coordinated to the N7 atom of imidazole ring.

To investigate the influence of ferrous complexes on DNA, we used circular dichroism. Formation of complexes was monitored by UV-VIS spectroscopy, infrared spectroscopy and NMR (nuclear magnetic resonance). Complexes of iron with histidine and glutathione were obtained. We examined the dependence of pH and ionic strength on DNA-Fe complex formation, comparing it to the effect of hydrated Fe^{2+} ion on DNA. In particular, influence of increasing amounts of Fe^{2+} ions on DNA was investigated by circular dichroism (CD) spectroscopy in different pH and ionic strength conditions.

The CD spectra of DNA 1.0×10^{-4} M, in the presence of increasing amounts of $FeSO_4$ and $Fe(NO)_2$ are shown in Fig.1. The right band of the DNA spectrum is monotonously decreased with increasing $FeSO_4$ concentration. This effect is completely suppressed at pH 7 (not shown); increasing ionic strength also eliminates this effect gradually. The small decrease in the intensity of the right band of the CD spectrum of DNA, upon addition of Fe^{2+} up to 1:1 molar ratio indicates that the interaction between the metal complex and DNA induces only slight modifications to the native conformation of DNA. Disappearance of this effect at pH 7 illustrates that observed effect comes from an external electrostatic binding interaction, between the Fe^{2+} cation and the negatively charged phosphate groups of DNA.

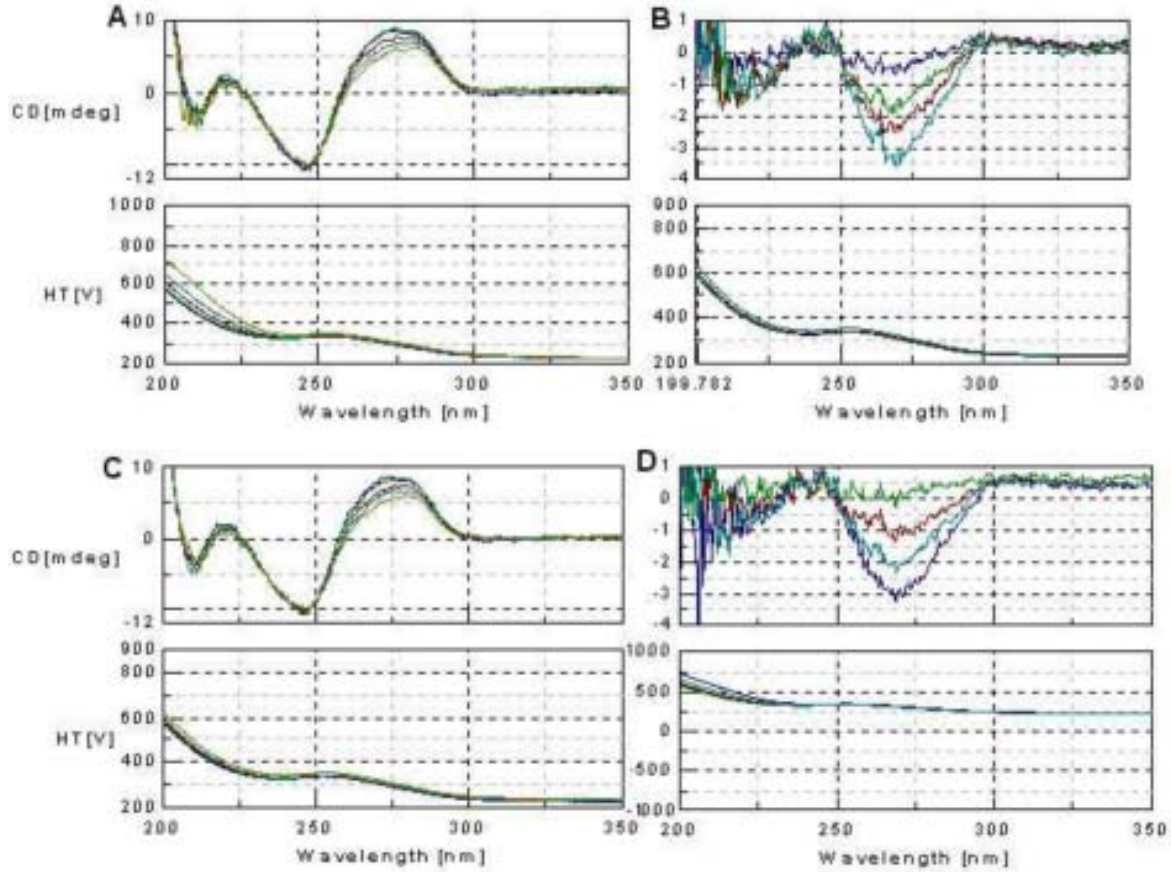

Fig.1. A – CD spectra of DNA (189 μM), in the presence of increasing amounts of $FeSO_4$, phosphate buffer 10 mM, pH 6. B – differences between spectrum of pure DNA and DNA at increasing concentrations of $FeSO_4$. C – CD spectra of DNA 1.0×10^{-4} M, in the presence of increasing amounts of $Fe(NO)_2$, phosphate buffer 10 mM, pH 6. D – differences between spectrum of pure DNA and DNA at increasing concentrations of $Fe(NO)_2$.

At pH 7 iron (II) is present in the solution in the form of $Fe(OH)_2$, and therefore, is no longer attracted to DNA. Influence of ionic strength supports this explanation. Similar spectra were found by Silvestri *et al*. [4] for iron (Salen) complexes and also attributed to ionic interaction. This kind of CD DNA spectrum change was previously reported also by Baase and Johnson [5]; correlation with crystallographic data allowed these authors to attribute these changes to the change in the number of base pairs per turn of DNA helix.

Supported by the State Committee for Scientific Research (KBN) statutory grant for the INCT.

References

[1]. De Maria F., Pedersen J.Z., Caccuri A.M., Antonini G., Turella P., Stella L., Lo Bello M., Federici G., Ricci G.: J. Biol. Chem., 278, 42283-42293 (2003).
[2]. Turella P., Pedersen J.Z., Caccuri A.M., De Maria F., Mastroberardino P., Lo Bello M., Federici G., Ricci G.: J. Biol. Chem., 278, 42294-42299 (2003).
[3]. Vanin A.F., Papina A.A., Serezhenkov V.A., Koppenol W.H.: Nitric Oxide, 10, 60-73 (2004).
[4]. Silvestri A., Barone G., Ruisi G., Lo Giudice M.T., Tumminello S.: Inorg. Biochem., 98, 589-594 (2004).
[5]. Baase W.A., Johnson C. Jr.: Nucleic Acids Res., 6, 797-814 (1979).

IRON REGULATORY PROTEIN 1 ACTIVITIES AND PROTEIN LEVEL ARE DECREASED IN THE LIVERS OF SUPEROXIDE DISMUTASE 1 KNOCKOUT MICE

Paweł Lipiński[1/], Rafał Starzyński[1/], Teresa Bartłomiejczyk, Marcin Kruszewski

[1/] Institute of Genetics and Animal Breeding, Polish Academy of Sciences, Jastrzębiec, Poland

The use of molecular oxygen as the terminal electron acceptor in oxidative phosphorylation involves interaction with iron atoms located in the catalytic centers of various enzymes. However, the ability of iron to react with superoxide anion and hydrogen peroxide leads to the generation of hydroxyl radical, which is highly destructive in biological systems. Therefore, the cells are equipped with protective enzymes, which destroy superoxide anion and hydrogen peroxide [1] and control the metabolism of iron [2]. One such enzyme is superoxide dismutase (SOD). Its deficiency promotes oxidative damage. Since exposure to ionising radiation also is a source of oxidative stress, understanding of relations between reactive oxygen species and iron metabolism contributes to the knowledge of the cellular response to irradiation.

One biological consequence of superoxide anion presence in the cytoplasm is inactivation of the cytosolic counterpart of mitochondrial aconitase, known as iron regulatory protein 1 (IRP1). Apart from its ability to convert citrate to *iso*-citrate, IRP1 in its apo-form binds to iron-responsive elements (IRE) in the untranslated regions of mRNAs coding for proteins involved in iron metabolism; thus, IRP1 contributes to the control of the cellular homeostasis of this metal [2].

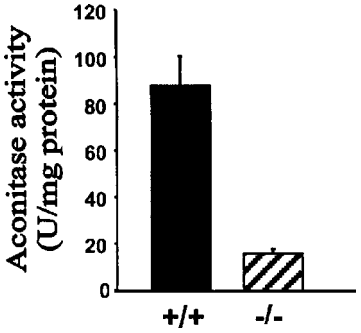

Fig.1. Aconitase activity in liver cell extracts measured according to [3]. Mean values ± SD from 6 mice wild type (+/+) or SOD1 knockouts (–/–).

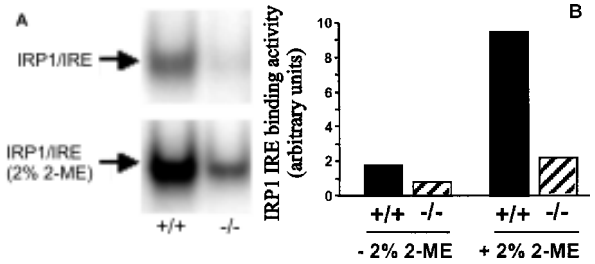

Fig.2. A: IRE-binding activity of IRP1, representative EMSA analysis. B: Radioactivity of ^{32}P (from ^{32}P-labelled H-ferritin IRE probe) associated with IRE-IRP1 complexes from extracts untreated or treated with 2% mercaptoethanol (ME). Mean values ± SD from 6 mice wild type (+/+) or SOD1 knockouts (–/–).

Here, we report results of experiments carried out on livers of $SOD1^{-/-}$ mice; these mice lack Cu,Zn-SOD, an enzyme which acts to reduce the concentration of superoxide anion mainly in cytosol [3]. Aconitase activity was measured spectrophotometrically according to [4]. IRE-binding activity of IRP1 was estimated by EMSA (electrophoretic mobility shift assay) using liver cytosolic extracts from wild type or SOD knockout mice. IRP1 levels were analysed by Western blotting and quantified with a Molecular Imager Quantity One (Biorad).

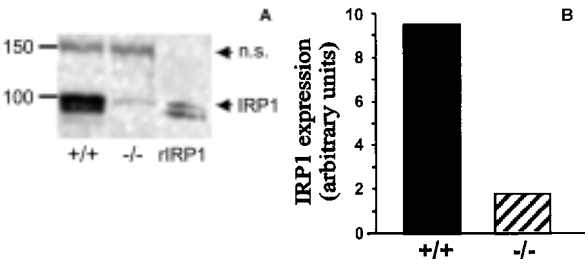

Fig.3. A: IRP1 levels analysed by Western blotting. B: Quantification of the Western blots, plotted in arbitrary units. Mean values ± SD from 6 mice wild type (+/+) or SOD1 knockouts (–/–).

We show (Figs.1-3) that in liver cells, not only aconitase activity is inhibited, but also the level of IRP1 protein is markedly lowered. IRP1 down-regulation in $SOD^{-/-}$ mice points to the existence of a new control mechanism that maintains a correct balance between iron and oxygen-derived free radicals.

Supported by the State Committee for Scientific Research (KBN) statutory grant for the INCT.

References

[1]. Fridovich I.: J. Biol. Chem., 272, 18515-18517 (1997).
[2]. Hentze M.W., Muckenthaler M.U., Andrews N.C.: Cell, 117, 285-297 (2004).
[3]. Matzuk M.M., Dionne L., Guo Q., Kumar T.R., Lebowitz R.M.: Endocrinology, 139, 4008-4011 (1998).
[4]. Drapier J.C., Hibbs J.B. Jr.: Methods Enzymol., 269, 26-36 (1996).

CHROMOSOMAL ABERRATIONS, SISTER CHROMATID EXCHANGES AND SURVIVAL IN HOMOLOGOUS RECOMBINATION REPAIR DEFICIENT CL-V4B CELLS (Rad51C MUTANTS) EXPOSED TO MITOMYCIN C

Andrzej Wójcik[1,2], Lubomir Stoilov[3], Irena Szumiel[1], Randy Legerski[4], Günter Obe[5]

[1] Institute of Nuclear Chemistry and Technology, Warszawa, Poland
[2] Institute of Biology, Świętokrzyska Academy, Kielce, Poland
[3] Department of Molecular Genetics, Institute of Genetics, Sofia, Bulgaria
[4] Department of Molecular Genetics, The University of Texas M.D. Anderson Cancer Center, Houston, USA
[5] Institute of Genetics, University of Duisburg-Essen, Essen, Germany

DNA interstrand crosslinks (ICL) pose a major problem for the cell during replication and transcription. The mechanisms of repair of ICL in mammalian cells are presently a topic of intense research.

Rad51C mutated CL-V4B cells [5] and wt cells V79B were exposed to different doses of MMC. The analysed endpoints included chromosomal aberrations, clonogenic cell survival and SCE.

Table. Chromosomal aberrations (per 100 cells) and percent aberrant cells in CL-V4B and V79B cells exposed to MMC. Results are the means and standard deviations of data from 3 independent experiments.

MMC dose [μM]	CL-V4B cells		V79B cells	
	Total aberrations	% aberrant cells	Total aberrations	% aberrant cells
0	1.7 ± 1.3	1.3 ± 1.2	0.3 ± 0.6	0.3 ± 0.6
0.1	40.0 ± 18.2*	21.3 ± 8.5*	0.7 ± 1.2	0.7 ± 1.2

* difference significant at $p<0.05$.

The major pathway of ICL repair appears to be homologous recombination repair (HRR) involving generation of a double strand break at the ICL and a subsequent recombination event with a homologous strand [1,2]. Recent data indicate that recombination independent pathways also exist [3].

Crosslinking agents such as mitomycin C (MMC) are extremely potent inducers of sister chromatid exchanges (SCE). It was estimated that they triple the SCE frequency with one thousandth the concentration required for inducing the same effect with monofunctional alkylating agents. This clearly points towards the ICL as the major lesion responsible for SCE.

Cells deficient in HRR are very sensitive to crosslinking agents (reviewed in [2]). It has been reported that MMC-induced SCE in the chicken B lymphocyte line DT40, mutated to obtain cells deficient in various genes involved in HRR, is lower than in the wild type (wt) line [4]. In the CL-V4B cells, which contain a mutated Rad51C paralog, no MMC-induced SCE can be observed in M1 [5]. These findings suggest that SCE are mediated by HRR [4].

MMC-induced SCE were analysed in the first (M1) and second (M2) post-treatment mitoses.

The analysis of chromosomal aberrations and survival confirmed that CL-V4B cells are very sensitive to MMC due to induction of ICL (Table).

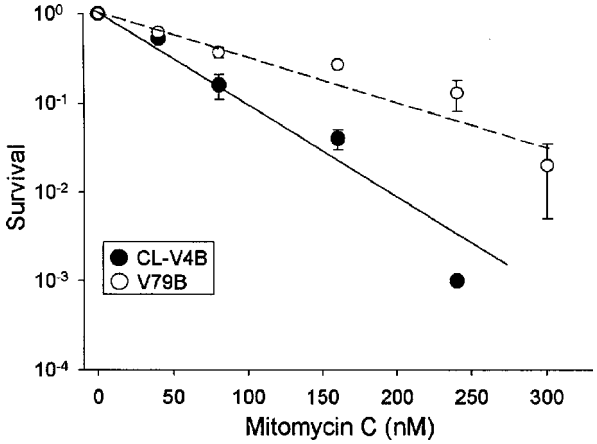

Fig.1. Clonogenic survival of CL-V4B and V79B cells following treatment with MMC. Error bars represent standard deviations from mean values of three independent experiments.

The survival of CL-V4B cells treated with MMC was lower than that of wt cells (Fig.1) but distinctly higher than reported by Godthelp *et al.* [5], possibly due to different culture conditions. The mutant cells showed the same frequencies of MMC-induced SCE as the wt cells (Fig.2). So, mutation in Rad51C did not affect SCE formation after MMC treatment. Additionally, while the wt cells showed the same frequency of MMC-induced SCE in M1 and M2, in CL-V4B cells somewhat more SCE were observed in M2 than M1 (Fig.2). This suggests that in Rad51C mutants ICL induced by MMC are either not removed completely or are transformed into another form of damage, which persists until the next cell cycle. Hence, SCEs may represent a mechanism to bypass MMC-induced ICL without their removal.

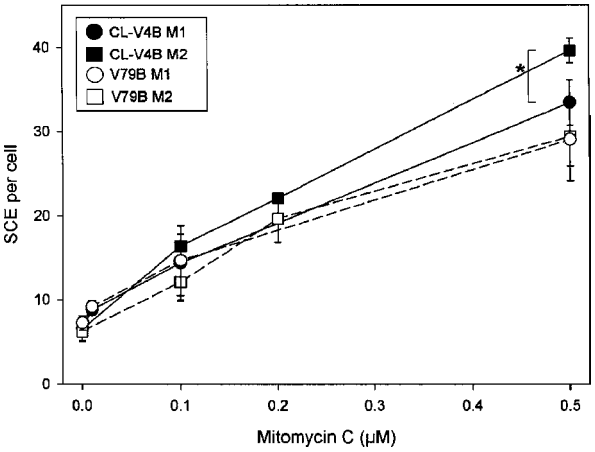

Fig.2. SCEs in first and second mitoses (M1 and M2) following treatment with MMC. Twenty cells were scored per point in each experiment. Error bars represent standard deviations from mean values of three independent experiments. * – difference significant at $p<0.05$ (two-sided, unpaired Student's *t*-test).

Supported by the State Committee for Scientific Research (KBN) statutory grant for the INCT.

References

[1]. McHugh P.J., Spanswick V.J., Hartley J.A.: Lancet Oncol., 2, 483-490 (2001).
[2]. Legerski R.J., Richie C.: Cancer Treat. Res., 112, 109-128 (2002).
[3]. Zheng H., Wang X., Warren A.J., Legerski R.J., Nairn R.S., Hamilton J.W., Li L.: Mol. Cell. Biol., 23, 754-761 (2003).
[4]. Sonoda E., Sasaki M.S., Morrison C., Yamaguchi-Iwai Y., Takat M., Takeda S.: Mol. Cell. Biol., 19, 5166-5169 (1999).
[5]. Godthelp B.C., Wiegant W.W., van Duijn-Goedhart A., Schaerer O.D., van Buul P.P.W., Kanaar R., Zdzienicka M.Z.: Nucleic Acids Res., 30, 2172-2182 (2002).

COMPARISON OF SISTER CHROMATID EXCHANGE INDUCTION IN Rad51C MUTANTS TREATED WITH MITOMYCIN C OR UVC

Andrzej Wójcik[1,2/], Lubomir Stoilov[3/], Irena Szumiel[1/], Randy Legerski[4/], Günter Obe[5/]

[1/] Institute of Nuclear Chemistry and Technology, Warszawa, Poland
[2/] Institute of Biology, Świętokrzyska Academy, Kielce, Poland
[3/] Department of Molecular Genetics, Institute of Genetics, Sofia, Bulgaria
[4/] Department of Molecular Genetics, The University of Texas M.D. Anderson Cancer Center, Houston, USA
[5/] Institute of Genetics, University of Duisburg-Essen, Essen, Germany

The mechanisms of sister chromatid exchanges (SCEs) are not known. Cytologically, it is evident that SCE involves a recombination mechanism between sister chromatids. Available data indicate that SCEs arise during S-phase, and it was suggested that the SCE-initiating event is a hindrance of DNA replication by DNA damage [1,2]. A lesion that poses a major problem for the cell during replication is the DNA interstrand crosslink (ICL). One hypothesis is that SCE is a manifestation of Rad51--dependent homologous recombination repair. In order to test this hypothesis, we have compared the frequencies of SCEs induced by mitomycin C (MMC) and 254 nm ultraviolet radiation (UVC) in wild type (wt) V79B and the Rad51C-deficient CL-V4B cells.

In the present study, CL-V4B (mutated in Rad51C) and V79B cells were prelabelled with BrdU for one cell cycle and treated with different doses of MMC. In addition to MMC, we compared the SCE frequencies following exposure of both cell lines to 254 nm UVC. Along with pre-labelling cells with BrdU, the cells were prelabelled with biotin-16-2´-deoxyuridine-5´-triphosphate (biotin-dUTP) in order to exclude the impact of BrdU on the formation of DNA lesions by UVC [3].

SCEs were analysed in the first (M1) and second (M2) post-treatment mitoses. As shown in Fig.1, in M1 MMC induced the same frequencies of SCEs in CL-V4B and V79B cells, while the UVC-induced SCE frequencies were lower in CL-V4B than V79B cells. Following exposure to UVC, less SCEs were observed in CL-V4B than in V79B cells, irrespective of whether cells were prelabelled with BrdU or biotin-dUTP. We have shown recently that the strong sensitizing effect of BrdU towards UVC-induced SCEs may be due to ICL formation [3]. ICLs presumably arise as a result of the formation of bromine atoms and uracilyl radicals in BrdU-prelabelled cells following exposure to UVC. Biotin-dUTP lacks a halogen atom which dissociates upon exposure to UVC. Therefore, it can be assumed that SCEs that arise after exposure to UVC of cells prelabelled with this thymidine analogue are formed by cyclobutane pyrimidine dimers and (6-4) photoproducts. These lesions are efficiently

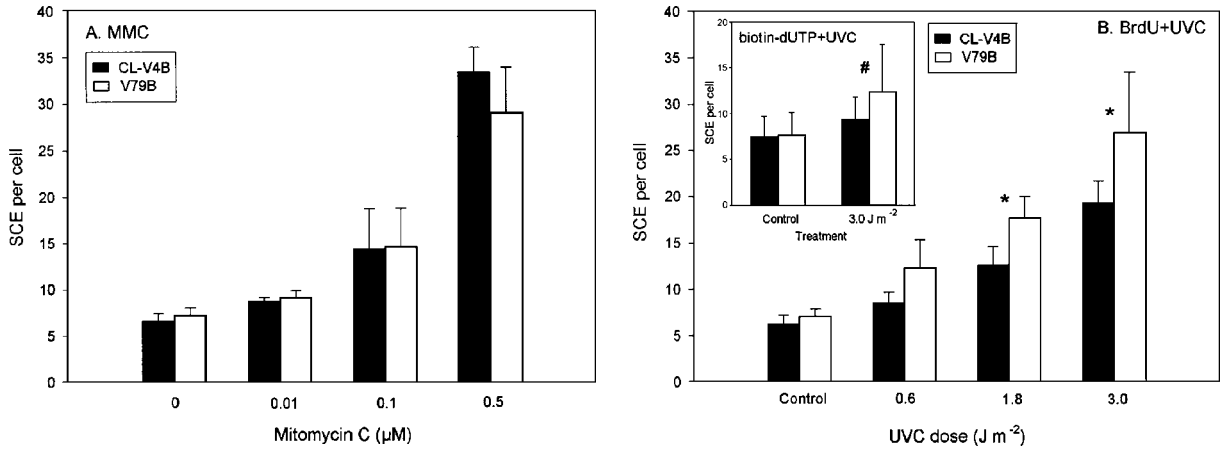

Fig.1. SCEs in first mitosis (M1) following treatment of CL-V4B and V79B cells with: A – MMC and B – BrdU+UVC. Twenty cells were scored per point in each experiment. Error bars represent standard deviations from mean values of three independent experiments (inset: treatment with biotin-dUTP+UVC; standard deviations from a single set of data). * – difference significant at $p<0.05$, two-sided, paired Student's *t*-test; # – difference significant at $p<0.05$, two-sided, unpaired Student's *t*-test.

removed by nucleotide excision repair. The reduced frequency of UVC-induced SCEs in CL-V4B cells could either be due to enhanced removal of photoproducts before the damaged DNA is replicated or due to reduced SCE formation by this type of damage.

This conclusion is not incompatible with the results of the MMC-induced SCE experiments because it is known that multiple recombination pathways exist which can lead to SCE formation [4]. Which pathway is triggered may depend on the type of DNA lesion, as recently suggested [5]. Also, it is not totally certain that the reduced SCE frequencies following exposure to UVC are a consequence of the Rad51C deficiency. CL-V4B cells may have other deficiencies apart from the mutated *Rad51C* gene. Thus, the genetic defect that may be responsible for the reduced SCE frequencies following exposure to UVC is somewhat uncertain.

As shown in the preceding report [6], mutation in Rad51C did not affect SCE formation after MMC treatment. Additionally, while the wt cells showed the same frequency of MMC-induced SCE in M1 and M2, in CL-V4B cells somewhat more SCE were observed in M2 than M1. This suggests that in Rad51C mutants ICL induced by MMC are either not removed completely or are transformed into another form of damage, which persists until the next cell cycle. In conclusion, our results indicate that homologous recombination repair is not involved in the SCEs induced by the DNA interstand-crosslinking agent MMC. In accordance with the model of Shafer [7], we suggest that SCEs may represent a mechanism to bypass an ICL during DNA replication.

Supported by the State Committee for Scientific Research (KBN) statutory grant for the INCT.

References

[1]. Latt S.: Ann. Rev. Genet., 15, 11-55 (1981).
[2]. Ishii Y., Bender M.A.: Mutat. Res., 79, 19-32 (1980).
[3]. Wojcik A., von Sonntag C., Obe G.J.: Photochem. Photobiol., 69, 139-144 (2003).
[4]. Dillehay L.E., Jacobson-Kram D., Williams J.R.: Mutat. Res., 215, 15-23 (1989).
[5]. Rothfuss A., Grompe M.: Mol. Cell. Biol., 24, 123-134 (2004).
[6]. Wójcik A., Stoilov L., Szumiel I., Legerski R., Obe G.: Chromosomal aberrations, sister chromatid exchanges and survival in homologous recombination repair deficient CL-V4B cells (Rad51C mutants) exposed to mitomycin C. In: INCT Annual Report 2004. Institute of Nuclear Chemistry and Technology, Warszawa 2005, pp.107-108.
[7]. Shafer D.A.: Hum. Genet., 39, 177-190 (1977).

REPAIR OF DNA DOUBLE STRAND BREAKS IN DIFFERENTIALLY RADIOSENSITIVE GLIOMA CELLS X-IRRADIATED AND TREATED WITH KINASE INHIBITOR PD 98059

Iwona Grądzka, Iwona Buraczewska, Barbara Sochanowicz, Irena Szumiel

Radiosensitisation caused by inhibition of cellular signalling has recently been subject of numerous studies. Signalling pathways are a potential target in cancer radiotherapy [1]. Of special interest are pathways initiated by EGFR (epidermal growth factor receptor). The signal is generated at the receptor that – upon ligand binding – acquires tyrosine kinase activity. The outcome of such signalling is activation of specific transcription factors and expression of specific genes, including those that code DNA repair enzymes.

The aim of this study was to determine the effect of signalling inhibition on double strand break (DSB) rejoining as well as to establish whether the DNA-PK-dependent repair system is the target of the signalling pathway initiated at the EGFR.

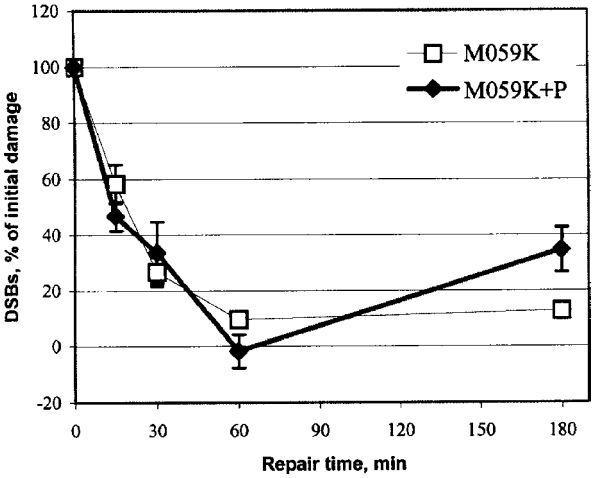

Fig.1. Effect of continuous treatment of M059 K cells with the MEK1/2 kinase inhibitor, PD 98059 (P, 20 μM) on DSB rejoining after X-irradiation (10 Gy) as determined by PFGE. Data points are mean values ± SEM.

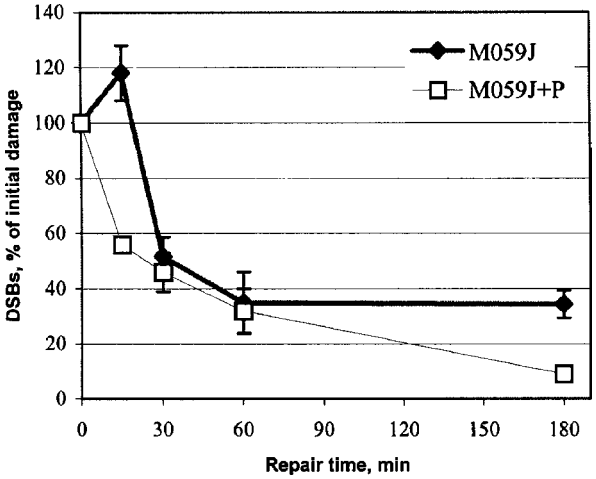

Fig.2. Effect of continuous treatment of M059 J cells with the MEK1/2 kinase inhibitor, PD 98059 (P, 20 μM) on DSB rejoining after X-irradiation (10 Gy) as determined by PFGE. Data points are mean values ± SEM.

Human glioma M059 cells [2], K (normal radiosensitivity) and J (radiosensitive, with defective DNA-PK catalytic subunit) were X-irradiated and treated with signalling inhibitor, PD 98059, specific for kinase MEK1/2. DSB rejoining was determined with pulse field gel electrophoresis (PFGE). M059 J cells are much more sensitive to X-radiation than M059 K cells; this correlates with lower initial DSB rejoining rate in the M059 J cell line as determined by PFGE (*cf.* Figs.1 and 2). M059 K cells are more sensitive to cell signalling inhibitor: PD 98059 as compared to M059 J cells. In contrast to the effects on cell survival, PD 98059 has little influence on DSB rejoining rate, with the exception of 3 h repair time for M059 cells, as shown in Fig.2. The apparent discrepancy between survival and DSB rejoining after combined PD+X-ray treatment may be due to PD effect on apoptosis.

Supported by the State Committee for Scientific Research (KBN) – grant No. 4 P05A 022 15.

References

[1]. Amorino G.P., Hamilton V.M., Valerie K., Dent P., Lammering G., Schmidt-Ullrich R.K.: Mol. Biol. Cell, 13, 2233-2244 (2002).

[2]. Allalunis-Turner M.J., Barron G.M., Day R.S. 3rd, Dobler K.D., Mirzayans R.: Radiat. Res., 134, 349-354 (1993).

REPAIR OF DNA DOUBLE STRAND BREAKS IN DIFFERENTIALLY RADIOSENSITIVE GLIOMA CELLS X-IRRADIATED AND TREATED WITH TYRPHOSTINE AG 1478

Iwona Grądzka, Iwona Buraczewska, Barbara Sochanowicz, Irena Szumiel

Signalling pathways are a potential target in cancer radiotherapy [1]. Of special interest are pathways initiated by EGFR (epidermal growth factor receptor) [2,3]. The signal is generated at the receptor that – upon ligand binding – acquires tyrosine kinase activity. The outcome of such signalling is activation of specific transcription factors and expression of specific genes, including those that code DNA repair enzymes.

We determined the effects of signalling inhibition by using tyrphostine AG 1478, specific for EGFR tyrosine kinase, which is activated both by the specific ligand, EGF, and X-rays [4]. The effects were examined on survival (not shown) and on double strand break (DSB) rejoining. In order to establish whether the DNA-PK-dependent repair system is the target of the signalling pathway initiated at the EGFR, we used two differentially radiosensitive cell lines, human glioma M059 [2]. Activity of DNA-PK (DNA-dependent protein

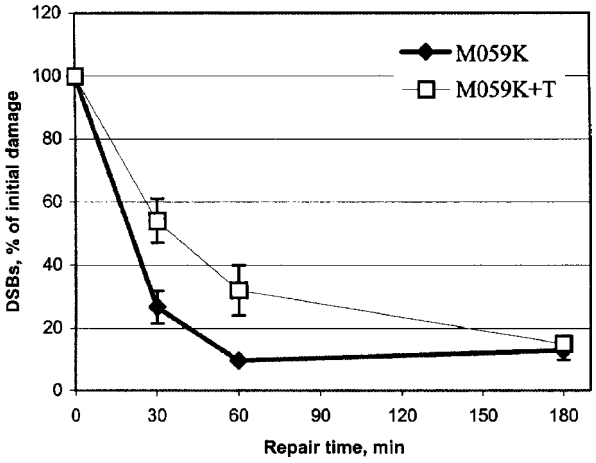

Fig.1. Effect of continuous treatment of M059 K cells with tyrphostine AG 1478 (T, 5 μM) on DSB rejoining after X-irradiation (10 Gy) as determined by PFGE. Data points are mean values ± SEM.

kinase) determines the function of the non-homologous rejoining of DSB (NHEJ), the main repair system of mammalian cells.

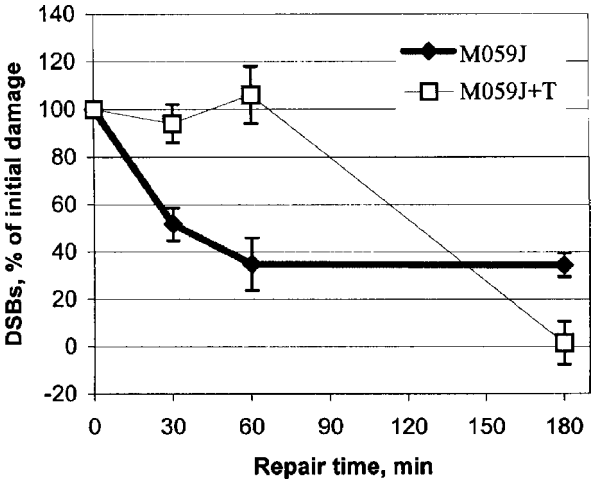

Fig.2. Effect of continuous treatment of M059 J cells with tyrphostine AG 1478 (T, 5 μM) on DSB rejoining after X-irradiation (10 Gy) as determined by PFGE. Data points are mean values ± SEM.

M059 K cells (normal radiosensitivity) and M059 J cells (radiosensitive, with defective DNA-PK catalytic subunit) were X-irradiated and treated with tyrphostine AG 1478. DSB rejoining was determined with pulse field gel electrophoresis (PFGE). M059 K cells are considerably more sensitive to tyrphostine AG 1478 than M059 J cells. This is explained by the difference in EGFR levels [5]. Tyrphostine AG 1478 has a marked influence on DSB rejoining rate (Figs.1 and 2) and the effect is considerably stronger in M059 J than in M059 K cells. Since M059 J cells with defective DNA-PK-dependent NHEJ so strongly respond to signalling inhibition, this observation suggests its preferential action on homologous recombination repair or DNA-PK independent non-homologous end-joining. The effect of tyrphostine AG 1478 on DSB rejoining is considerably stronger in M059 J than in M059 K cells. Since M059 J cells with defective DNA-PK-dependent NHEJ respond to signalling inhibition, this observation suggests its preferential action on homologous recombination repair or DNA-PK independent non-homologous end-joining (B-NHEJ according to the term proposed by Wang *et al.* [6]).

Supported by the State Committee for Scientific Research (KBN) – grant No. 4 P05A 022 15.

References

[1]. Amorino G.P., Hamilton V.M., Valerie K., Dent P., Lammering G., Schmidt-Ullrich R.K.: Mol. Biol. Cell, 13, 2233-2244 (2002).
[2]. Milas L., Mason K.A., Ang K.K.: Int. J. Radiat. Biol., 79, 539-545 (2003).
[3]. Sartor C.I.: Semin. Radiat. Oncol., 13, 22-30 (2003).
[4]. Allalunis-Turner M.J., Barron G.M., Day R.S. 3rd, Dobler K.D., Mirzayans R.: Radiat. Res., 134, 349-354 (1993).
[5]. Grądzka I., Sochanowicz B.: Epidermal growth factor receptor activation in X-irradiated glioma cells M059 K and M059 J. In: INCT Annual Report 2004. Institute of Nuclear Chemistry and Technology, Warszawa 2005, pp.111-112.
[6]. Wang H., Perrault A.R., Takeda Y., Qin W., Wang H., Iliakis G.: Nucleic Acids Res., 31, 5377-5388 (2003).

EPIDERMAL GROWTH FACTOR RECEPTOR ACTIVATION IN X-IRRADIATED GLIOMA CELLS M059 K AND M059 J

Iwona Grądzka, Barbara Sochanowicz

In studies concerning new potential targets in cancer radiotherapy of special interest are signalling pathways initiated by EGFR (epidermal growth factor receptor) [1,2]. The signal is generated at the receptor that – upon ligand binding – acquires tyrosine kinase activity. It is further transmitted through the MAPK/ERK (mitogen-activated protein kinase/extracellular signal-regulated kinase) pathway. EGF receptor also is activated by ionising irradiation [3], usually 1-5 Gy of X- or γ-rays. This is the dose range applied in cancer radiotherapy. The outcome of such signalling is activation of specific transcription factors and expression of specific genes, including those that code DNA repair enzymes.

To complete our studies on the effects of signalling inhibition on double strand break (DSB) rejoining in M059 cells [4], we determined the level of EGFR and its activation by X-rays. Human glioma M059 cells [5], K (normal radiosensitivity) and J (radiosensitive, with defective DNA-PK catalytic subunit) control and X-irradiated (10 Gy) served for preparation of extracts. EGFR was determined with ELISA.

ELISA kit for human EGFR (Biosource International, Inc., USA) was used. With the use of specific primary antibodies, polyclonal antibody against

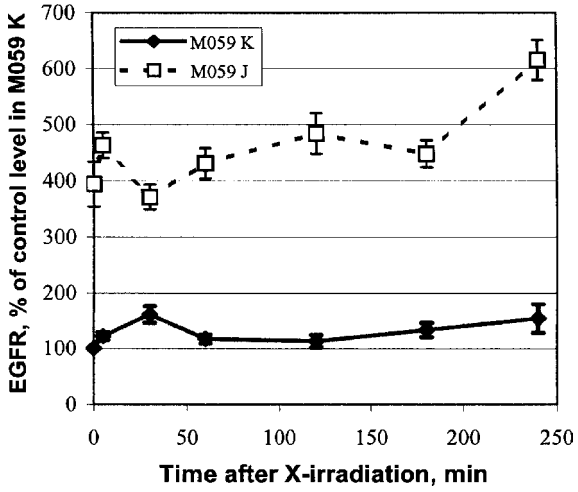

Fig.1. Change in the level of EGFR in M059 K and M059 J cells after irradiation with 10 Gy X-rays, determined with ELISA test. Data points are mean values ± SD.

human EGFR or anti-tyrosine 1068, it was possible to estimate the total EGFR or that activated in consequence of tyrosine 1068 phosphorylation, respectively.

Figure 1 shows that the basal level of the EGFR, determined by ELISA, is about 4 times higher in M059 J cells than that in M059 K cells. This explains the difference in sensitivity to tyrphostine AG 1478 between the cell lines examined (not shown). After X-irradiation, in both cell lines a bi-phasic increase in EGFR level takes place. In M059 J cells, the first maximum is seen after 5 min, followed by an increase up to 50% after 240 min. In M059 K cells, the first maximum is seen after 30 min, followed by a gradual increase, also up to 50% after 240 min.

Activation of the receptor was estimated from tyrosine 1068 phosphorylation. Figure 2 shows that after X-irradiation with 10 Gy the increase in tyrosine 1068 phosphorylation essentially follows the pattern of EGFR level increase: it takes place early only in M059 J cells, whereas the second increase, after about 2 h, is seen in both cell lines. Since the signal generated at the EGFR is, among others, targeted on DNA repair, the strong effect of EGFR inhibitor, tyrphostin AG 1478 on DSB rejoining in M059 J cells may be to some extent due to the high EGFR level in these cells.

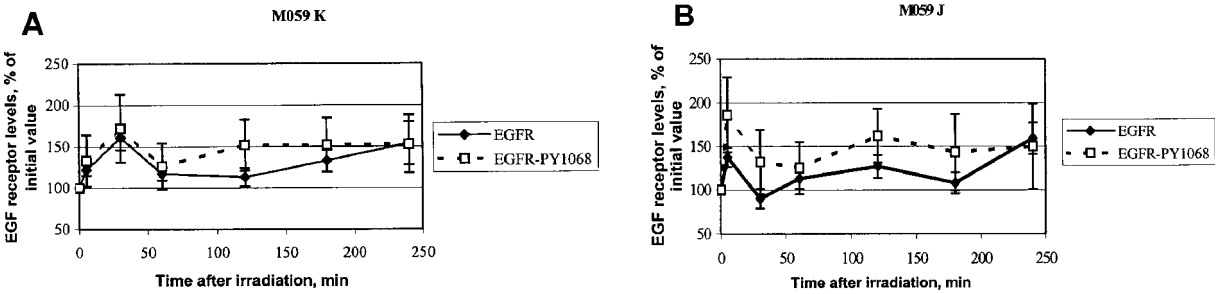

Fig.2. Change in tyrosine 1068 phosphorylation of the EGFR molecules in cell extracts from M059 K (A) and M059 J (B) cells after irradiation with 10 Gy X-rays, determined with ELISA test. Data points are mean values ± SD.

Supported by the State Committee for Scientific Research (KBN) – grant No. 4 P05A 022 15.

References

[1]. Milas L., Mason K.A., Ang K.K.: Int. J. Radiat. Biol., 79, 539-545 (2003).
[2]. Sartor C.I.: Semin. Radiat. Oncol., 13, 22-30 (2003).
[3]. Schmidt-Ullrich R.K., Mikkelsen R.B., Dent P., Todd D.G., Valerie K., Kavanagh B.D., Contessa J.N., Rorrer W.K., Chen P.B.: Oncogene, 15, 1191-1197 (1997).
[4]. Grądzka I., Buraczewska I., Sochanowicz B., Szumiel I.: Repair of DNA double strand breaks in differentially radiosensitive glioma cells X-irradiated and treated with tyrphostine AG 1478. In: INCT Annual Report 2004. Institute of Nuclear Chemistry and Technology, Warszawa 2005, pp.110-111.
[5]. Allalunis-Turner M.J., Barron G.M., Day R.S. 3rd, Dobler K.D., Mirzayans. R.: Radiat. Res., 134, 349-354 (1993).

NO EFFECT OF INHIBITION OF POLY(ADP-RIBOSYLATION) ON THE FREQUENCY OF HOMOLOGOUS RECOMBINATION. I. ENZYMATIC ASSAY

Maria Wojewódzka, Teresa Bartłomiejczyk, Marcin Kruszewski

Two main pathways for DNA double strand break (DSB) repair in mammalian cells are homologous recombination (HR) and nonhomologous end-joining (NHEJ). Participation of poly(ADP-ribose) polymerase-1 (PARP-1) in DSB repair has been long postulated, but it remains poorly defined [1]. On the other hand, $PARP^{-/-}$ cells and PARP-null knockout mice are hypersensitive to ionising radiation and alkylating agents. So, to our knowledge of the cellular response to ionising radiation one essential element is missing.

With the aim of explaining the role of poly(ADP-ribosylation) in repair of DSB, we investigated the frequency of spontaneous and X-ray induced HR in NHEJ-competent (Chinese hamster cell line CHO-K1) and NHEJ-deficient (xrs-6) cells lines. The latter is defective in DNA-PK-mediated DSB repair pathway due to the deficiency in Ku80 protein.

To study HR we used pLrec plasmid that carries two non-functional copies of a bacterial gene, *lacZ*, (β-galactosidase) in a tandem array [2]. The *lacZ* genes are divided by a selective marker gene, which provides resistance to the G418 antibiotic (gene *neo*). The cells were transfected with a linear plasmid by electroporation and the transfected clones were selected in the medium containing 500 μg/ml G418. The clones with a single plasmid copy and

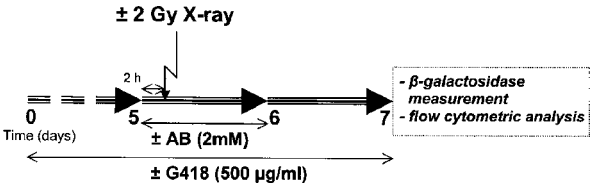

Fig. Experimental schedule for analysis of frequency of homologous recombination.

with two copies of *lacZ* were identified by Southern blotting and PCR.

To study the role of poly(ADP-ribosylation) in repair of spontaneous and X-ray induced DNA DSBs, the transfected cells of both lines were incubated with the PARP-1 inhibitor (2 mM 3-aminobenzamide, AB, 2 h, 37°C). The measure of HR was the frequency of clones with reconstituted *lacZ* gene, showing β-galactosidase activity. The experimental schedule is presented in Fig.

Table 1. Activity of β-galactosidase as a measure of X-ray induced recombination in clones of CHO-K1 cells transfected with a single copy of pLrec plasmid.

Clone	Treatment	G418	β-galactosidase activity U/g protein ± SD
N11	control	-	1.42 ± 0.63
	2 Gy	-	1.66 ± 0.61
	AB	-	1.63 ± 0.46
	2 Gy+AB	-	1.64 ± 0.65
	control	+	1.17 ± 0.59
	2 Gy	+	1.46 ± 0.67
	AB	+	1.53 ± 0.57
	2 Gy+AB	+	1.70 ± 0.27
TK15	control	-	1.51 ± 0.41
	2 Gy	-	1.87 ± 0.69
	AB	-	1.37 ± 0.27
	2 Gy+AB	-	1.43 ± 0.51
	control	+	1.40 ± 0.31
	2 Gy	+	1.58 ± 0.49
	AB	+	1.47 ± 0.26
	2 Gy+AB	+	1.56 ± 0.35

The fluorimetric β-galactosidase assay was performed according to Sanbrook *et al.* [3]. The results are summarized in Tables 1 and 2. As expected, in non-irradiated cells, release of the selective pressure (7 days without G418) significantly elevated the level of β-galactosidase activity, in comparison to that in cells cultured with G418. The data show that inhibition of PARP has no effect on recombination frequency. The next report [4] presents the results of parallel estimations carried out by flow cytometry, leading to the same conclusion. This lack of effect of poly(ADP-ribosylation) inhibition of recombination frequency is compatible with a recent report [5] which suggests that PARP is not a part of the HR repair system.

Supported by the State Committee for Scientific Research (KBN) – grant No. 3 P04A 036 24.

Table 2. Activity of β-galactosidase as a measure of X-ray induced recombination in clones of xrs6 cells transfected with a single copy of pLrec plasmid.

Clone	Treatment	G418	β-galactosidase activity U/g protein ± SD
S9	control	-	2.53 ± 0.56
	2 Gy	-	2.78 ± 0.38
	AB	-	2.67 ± 1.41
	2 Gy+AB	-	2.68 ± 0.44
	control	+	2.10 ± 0.69
	2 Gy	+	2.32 ± 0.60
	AB	+	2.19 ± 0.32
	2 Gy+AB	+	2.75 ± 0.87
S11	control	-	2.83 ± 0.66
	2 Gy	-	3.19 ± 0.48
	AB	-	2.97 ± 0.50
	2 Gy+AB	-	3.31 ± 1.03
	control	+	2.46 ± 1.04
	2 Gy	+	3.13 ± 0.25
	AB	+	2.76 ± 0.42
	2 Gy+AB	+	2.89 ± 0.34
S15	control	-	4.79 ± 0.69
	2 Gy	-	5.02 ± 0.72
	AB	-	4.29 ± 1.51
	2 Gy+AB	-	5.23 ± 0.73
	control	+	4.32 ± 2.12
	2 Gy	+	4.56 ± 0.51
	AB	+	5.37 ± 1.27
	2 Gy+AB	-	5.91 ± 0.52

References

[1]. Le Rhun Y., Kirkli J.B., Shah G.M.: Biochem. Biophys. Res. Commun., 245, 1-10 (1998).
[2]. Herzing L.B., Meyn M.S.: Gene, 137, 163-169 (1993).
[3]. Sanbrook J., Fritsch E.F., Maniatis T.: Molecular Cloning: A Laboratory Manual 2nd ed. Cold Spring Harbor Laboratory Press, Cold Spring Harbor 1989.
[4]. Wojewódzka M., Bartłomiejczyk T., Ołdak T., Kruszewski M.: No effect of inhibition of poly(ADP-ribosylation) on the frequency of homologous recombination. II. Flow cytometry. In: INCT Annual Report 2004. Institute of Nuclear Chemistry and Technology, Warszawa 2005, pp.114-115.
[5]. Schultz N., Lopez E., Saleh-Gohari N., Helleday T.: Nucleic Acids Res., 31, 4959-4964 (2003).

NO EFFECT OF INHIBITION OF POLY(ADP-RIBOSYLATION) ON THE FREQUENCY OF HOMOLOGOUS RECOMBINATION. II. FLOW CYTOMETRY

Maria Wojewódzka, Teresa Bartłomiejczyk, Tomasz Ołdak[1/], Marcin Kruszewski

[1/] Maria Skłodowska-Curie Memorial Cancer Center and Institute of Oncology, Warszawa, Poland

The preceding report of Wojewódzka *et al.* [1] presented a study carried out with the aim of explaining the role of poly(ADP-ribosylation) in repair of DNA double strand breaks (DSB). The frequency of spontaneous and X-ray induced homologous recombination (HR) in non-homologous end-joining (NHEJ)-competent (Chinese hamster cell line CHO-K1) and NHEJ-deficient (xrs-6) cells lines was estimated in transfectants containing pLrec plasmid that carries two non-functional copies of a bacterial gene, *lacZ*, (ß-galactosidase) in a tandem array [2]. The *lacZ* genes are divided by a selective marker gene, which provides resistance to the G418 antibiotic (gene *neo*). The cells were transfected with a linear plasmid by electroporation and the transfected clones were selected in the medium containing 500 µg/ml G418. The experimental schedule was presented in [1].

Table 1. Frequency of spontaneous and induced recombination of *lacZ* genes in clones of CHO-K1 cells transfected with single copy of pLrec (rate of conversion to LacZ(+) expressed as event/cell generation).

Clone	Treatment	G418	Rate of conversion to LacZ(+) (event/cell generation)
N11	control	-	3.39 E-05
	2 Gy	-	4.60 E-05
	AB	-	5.10 E-05
	2 Gy+AB	-	5.46 E-05
	control	+	3.22 E-05
	2 Gy	+	4.35 E-05
	AB	+	5.18 E-05
	2 Gy+AB	+	4.69 E-05
TK15	control	-	2.40 E-04
	2 Gy	-	2.36 E-04
	AB	-	2.46 E-04
	2 Gy+AB	-	2.32 E-04
	control	+	2.25 E-04
	2 Gy	+	2.08 E-04
	AB	+	2.17 E-04
	2 Gy+AB	+	2.34 E-04

To assess the number of LacZ expressing cells, the following procedure for flow cytometry (FACS) sorting of LacZ containing cells based on cleavage of a fluorescent substrate (fluorescein di-β-D-galactopyranoside, FDG) by β-galactosidase was used, as originally described by Nolan *et al.* [3]. Exponentially growing cells were treated with trypsin (0.25% in phosphate buffered saline) until they could be removed from the plate with mild agitation. Cells were counted and brought to $5x10^6$ per ml in MEM medium containing 2% (vol/vol) foetal calf serum. Number of β-galactosidase cells was estimated according to the following protocol: 100 µl of cell suspension was added to a 5-ml polystyrene tube and brought to 37°C in a water bath for 5 min. The cell suspension was mixed gently but thoroughly

Table 2. Frequency of spontaneous and induced recombination of *lacZ* genes in clones of xrs6 cells transfected with a single copy of pLrec (rate of conversion to LacZ(+) expressed as event/cell generation).

Clone	Treatment	G418	Rate of conversion to LacZ(+) (event/cell generation)
S9	control	-	4.11 E-03
	+2 Gy	-	5.17 E-03
	+AB	-	4.69 E-03
	+2 Gy+AB	-	5.17 E-03
	control	+	3.58 E-03
	+2 Gy	+	4.93 E-03
	+AB	+	3.19 E-03
	+2 Gy+AB	+	5.66 E-03
S11	control	-	6.46 E-03
	+2 Gy	-	8.23 E-03
	+AB	-	8.24 E-03
	+2 Gy+AB	-	8.53 E-03
	control	+	3.62 E-03
	+2 Gy	+	4.18 E-03
	+AB	+	6.12 E-03
	+2 Gy+AB	+	6.03 E-03
S15	control	-	1.17 E-03
	+2 Gy	-	1.31 E-03
	+AB	-	1.09 E-03
	+2 Gy+AB	-	1.44 E-03
	control	+	1.11 E-03
	+2 Gy	+	1.15 E-03
	+AB	+	1.00 E-03
	+2 Gy+AB	-	1.26 E-03

with 100 μl of 2 mM FDG pre-warmed to 37°C and immediately placed in 37°C water bath for exactly 1 min. FDG loading was terminated by addition of 1800 μl ice-chilled incubation medium and 1 μM propidium iodide. The cells were kept on ice for 60 min until viewed by FACS analysis.

The results, presented in Tables 1 and 2, are in agreement with the previously described enzymatic activity determinations. They show that there is no effect of poly(ADP-ribosylation) inhibition on recombination frequency in this experimental model. This result is compatible with those of other authors [4], who show that poly(ADP-ribose) polymerase (PARP) is not directly engaged in HR repair. Nevertheless, as discussed in [4,5], there are numerous data on the anti-recombinogenic role of PARP. Hence, inhibition of poly(ADP-ribosylation) should have a pro-recombinogenic effect. This, however, was not observed in our experimental system, where the substrate was the plasmid incorporated into the host cell genome. A possible reason for this is the p53 mutation in CHO and xrs6 cells [6], whereas the effect of PARP on DSB repair depends on wild type p53, as shown by Susse *et al*. [5].

Supported by the State Committee for Scientific Research (KBN) – grant No. 3 P04A 036 24.

References

[1]. Wojewódzka M., Bartłomiejczyk T., Kruszewski M.: No effect of inhibition of poly(ADP-ribosylation) on the frequency of homologous recombination. I. Enzymatic assay. In: INCT Annual Report 2004. Institute of Nuclear Chemistry and Technology, Warszawa 2005, pp.112-113.
[2]. Herzing L.B., Meyn M.S.: Gene, 137, 163-169 (1993).
[3]. Nolan G.P., Fiering S., Nicolas J.F., Herzenberg L.A.: Proc. Natl. Acad. Sci. USA, 85, 2603-2607 (1988).
[4]. Schultz N., Lopez E., Saleh-Gohari N., Helleday T.: Nucleic Acids Res., 31, 4959-4964 (2003).
[5]. Susse S., Scholz C.J., Burkle A., Wiesmuller L.: Nucleic Acids Res., 32, 669-680 (2004).
[6]. Lee H., Larner J.M., Hamlin J.L.: Gene, 184, 177-183 (1997).

ADAPTIVE RESPONSE: STIMULATED DNA REPAIR OR DECREASED DAMAGE FIXATION?

Irena Szumiel

The usual definition of the adaptive response says that this is a cellular response whereby a mild stress stimulus (called adaptive or priming) applied before a challenge treatment with a DNA damaging agent causes a decrease in the detrimental effects of that treatment. Many experimental results suggest that the priming stimulus is the source of signalling which eventually leads to expression of the adaptive response. Then, the "primed" cell is for a certain time able to respond to the challenge dose by an increased recovery, as compared to the control one. An essential part of the adaptive response is generation or receipt and transmission of a signal which is the direct cause of initiation of a cellular response that diminishes the effects of DNA damage.

The often accepted view that DNA repair is stimulated in the "primed" and challenged cell is not supported by consistent data on increase in the rate of repair or altered level of initial damage (*e.g.* [1-3]). So, the emphasis is now shifted towards fidelity of repair rather than its stimulation, as in the more recent studies of Sasaki *et al.* [4]. These authors, however, did not identify the molecular mechanism of the fidelity increase. The hypothesis which I present does not contradict that of Sasaki *et al.* [4], but rather redefines it. Instead of ascribing the radioadaptation to DNA repair stimulation or repair fidelity increase, I interpret the experimental results in terms of decreased damage fixation. This idea derives from the transcription-based model of damage fixation of Radford [5].

Taking into account the abrogation of radioadaptation by poly(ADP-ribosylation) inhibitors applied simultaneously with the challenge dose and the fact that adaptation is revealed as a decrease in chromosomal aberration frequency, one can apply to the adaptive response the same arguments as those that support the fixation model of Radford [5]. According to it, double strand break (DSB) fixation takes place in transcriptional factories due to cooperation of two molecules of topoisomerase I. In result, an exchange event takes place, bringing

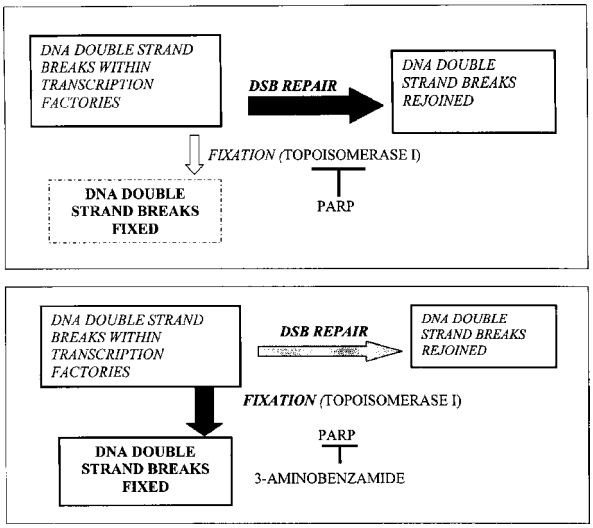

Fig. Competition between DSB repair and fixation in transcription factories, according to the model of Radford [5].

about chromosomal aberration. There is a competition between repair and fixation (Fig.); poly(ADP-ribose) polymerase (PARP)-effected inhibition of topoisomerase I prevents damage fixation whereas PARP inhibitor, 3-aminobenzamide promotes it. In conclusion, adaptive response (at least in part) is due to diminished fixation of DSBs in the transcription factories by the mechanism proposed by Radford [5].

Supported by the State Committee for Scientific Research (KBN) statutory grant for the INCT.

References

[1]. Wójcik A., Sauer C., Zolzer F., Bauch T., Muller W.U.: Mutagenesis, 11, 291-297 (1996).
[2]. Ikushima T., Aritomi H., Morisita J.: Mutat. Res., 358, 193-198 (1996).
[3]. Wojewódzka M., Kruszewski M., Szumiel I.: Int. J. Radiat. Biol., 71, 245-252 (1997).
[4]. Sasaki M.S., Ejima Y., Tachibana A., Yamada T., Ishizaki K., Shimizu T., Nomura T.: Mutat. Res., 504, 101-118 (2002).
[5]. Radford I.R.: Int. J. Radiat. Biol., 78, 1081-1093 (2002).

NUCLEAR TECHNOLOGIES
AND
METHODS

PROCESS ENGINEERING

INFRARED SPECTRA OF SO_2 DISSOLVED IN POLAR SOLVENTS: WATER, METHANOL, NITROBENZENE

Agnieszka Mikołajczuk, Czesława Paluszkiewicz[1/], Andrzej G. Chmielewski

[1/] Jagiellonian University, Kraków, Poland

Most of the data concerning SO_2 solubility in water and organic solvents are published in the process and environmental engineering journals. This is due to the fact that SO_2 absorption is the most often applied technology for the flue gas and industrial off gases desulfurisation.

The idea of using organic solvents for SO_2 adsorption is not very new. The process applying dimethylaniline has already been patented in 1940 [1]. The process using tetraethyleneglycol dimethyl ether as a solvent has been commercialized recently [2]. In 1997 new solvents: N-methylpyrrolidone (NMP) and N,N-(dimethylpropylene)urea (DMPU) for SO_2 adsorption were investigated [3]. The infrared (IR) spectra showed that two stretching bands of the SO_2 are observed at 1323 and 1146 cm^{-1} in a 1:1 SO_2-NMP mixture and at 1321 and 1144 cm^{-1} in a SO_2-DMPU mixture, while these bands are found at 1344 and 1145 cm^{-1} SO_2 in noncomplexing CCl_4.

Water is used for removal of SO_2 from outlet gases [2]. On the basis of an empirical model, the solubility of a reactive gas (SO_2) in water might be represented by the following equilibrium processes [4]:

Gas molecules
Gaseous phase
⇑
⇓

Liquid phase	Liquid phase	Liquid phase
Gas molecules ⇐⇒	Gas molecules ⇐⇒	Ionic species
(unreacted form)	(reacted but undissociated)	

The equilibrium between the unreacted gas molecules in water and those in the gaseous phase exists in the gas-liquid interference (described by Henry's law). In the liquid phase, two successive equilibrating processes occur. In developing of the empirical model, any change in the water structure is neglected. The gases under consideration react with water and the reaction products undergo ionic dissociation.

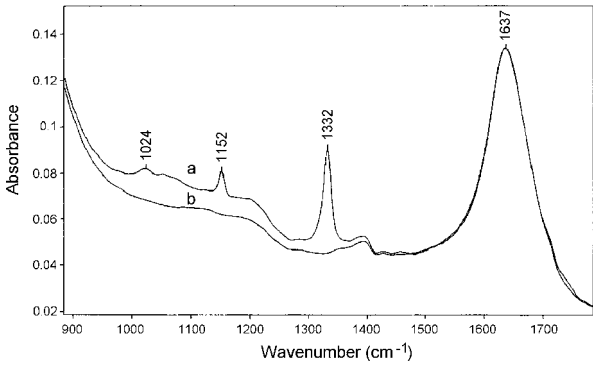

Fig.1. Stretching bands of SO_2: (a) in water, (b) spectra of pure water.

The solubility of SO_2 in nitrobenzene is higher than in water and lower than in methanol. Solubility of SO_2 decreases with the temperature rise. The process of SO_2 sorption in water is defined as [4]:

$$SO_{2(g)} \Leftrightarrow SO_{2(l)} \quad (1)$$

$$SO_{2(l)} + H_2O \Leftrightarrow H_2SO_3 \quad (2)$$

$$H_2SO_3 + H_2O \Leftrightarrow H_3O^+ + HSO_3^- \quad (3)$$

$$HSO_3^- + H_2O \Leftrightarrow H_3O^+ + SO_3^{-2} \quad (4)$$

Obviously, an increase in pH of the solution would shift the equilibrium processes to the right side of equation (3). For pH≤5.5, reaction (4) may be neglected, and the sorption process is described by equations (1)-(3) because the pH is lower than 5.5. For methanol and nitrobenzene, we do not know precisely what kind of structures is formed in these solution after SO_2 dissolution.

The characteristic bands of the solvents and SO_2 were identified with IR. The recorded spectra are shown in Figs.1-3 (solvents were saturated with SO_2).

Two stretching bands of SO_2 are observed at 1332 and 1152 cm^{-1} in the water (Fig.1), and at 1332 and 1150 cm^{-1} in methanol (Fig.2), and one stretching band at 1146 cm^{-1} in the nitrobenzene (Fig.3). The spectrum of pure nitrobenzene is quite com-

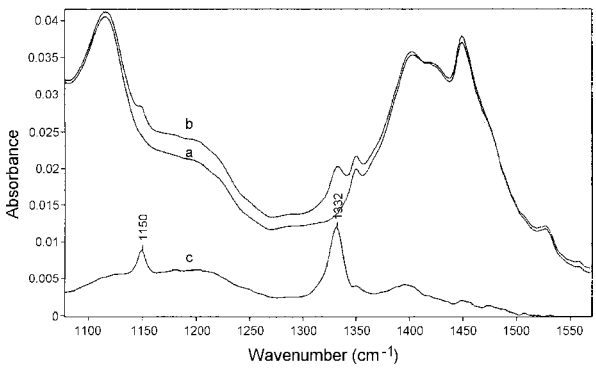

Fig.2. Stretching bands of SO_2: (a) spectra of pure methanol, (b) in methanol, (c) result subtraction spectra (b-a).

plicated and only one stretching band of SO_2 was found.

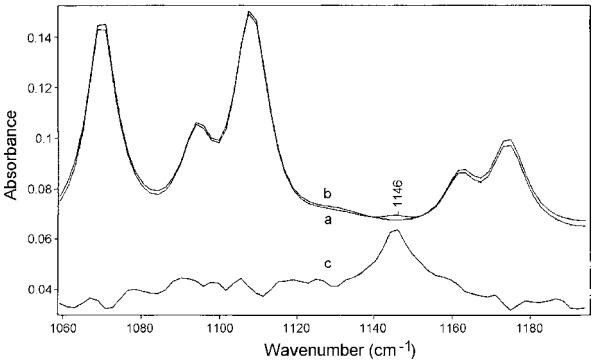

Fig.3. Stretching bands of SO_2: (a) spectra of pure nitrobenzene, (b) in nitrobenzene, (c) result subtraction spectra (b-a).

The stretching band observed at 1024 cm^{-1} (Fig.1), showed that the dissociation product of H_2SO_3 (according to equations (1)-(3)) in the water solution was observed.

The IR spectra for SO_2 saturated solvents were measured. The stretching bands of SO_2 were observed for three spectra of solvents saturated with SO_2.

For SO_2 dissolved in water, the stretching bands of SO_2 and also the product of SO_2 sorption were observed. For methanol and nitrobenzene, only the stretching bands of SO_2 were observed.

This work was supported by the State Committee for Scientific Research (KBN) – grant No. 4 T09A 039 24.

References

[1]. Gleason G.H., Montclair N.J., Loonam A.C.: U.S. Patent No. 21.106.453.
[2]. Heisel M., Bellani A.: Gas Sep. Purif., 5, 111 (1991).
[3]. van Dam M.H.H., Lamine A.S., Roizard D., Lochon P., Roizard C.: Ind. Eng. Chem. Res., 36, 4628 (1997).
[4]. Islam M.A., Kalam M.A., Khan M.R.: Ind. Eng. Chem. Res., 39, 2627 (2000).

DETERMINATION OF SULFUR ISOTOPE RATIO IN COAL COMBUSTION PROCESS

Małgorzata Derda, Andrzej G. Chmielewski

Worldwide energy production is and will be for the next future based on fossil fuels combustion. While oil and fuel will be exhausted in the next 50-60 years, the coal reserves will retain for the next 200-300 years. In some countries like Poland, over 90% of electricity is produced using coal combustion. Unfortunately, coal and heavy oil combustion lead to emission of vast quantities of sulfur dioxide and other pollutants. Environmental acidification through dry and wet deposition (acidic rain) results from these emissions [1].

There are not known other methods beside sulfur isotope ratio measurements to investigate the fate of anthropogenic sulfur in the atmosphere and environment. Some scientists discussed in their papers [2-5] regional and seasonal changes of sulfur isotope composition and the possibility of using of sulfur isotope ratios to determine anthropogenic sulfur signals. They allow to identify the source of sulfate in different regions [6,7] even from single sources [8].

Querol [9] reported the possibility of using stable sulfur isotopic ratio for the identification of sources of atmospheric sulfur compounds. Sulfur isotope analyses were carried out for bedrock and sediment samples, surface and groundwater, wet-only and total deposition, total suspended particles and sulfur dioxide emitted from power plants in Spain. Due to the hazardous effects of sulfur dioxide emissions on the environment and human health, the emission control technologies have been introduced. Sulfur content can be reduced before combustion by physical, chemical, or biological coal cleaning [10,11]. However, this technology reduces the sulfur mostly contained in the pyrite forms. Therefore, most often the flue gas desulfurization (FGD) technologies are used. The most popular is wet FGD process, using lime or limestone water suspension for sulfur dioxide absorption [12]. Other technologies in which simultaneously sulfur dioxide and nitrogen oxides are removed is applied and byproduct as fertilizer are being implemented as well [13]. Due to the chemistry of the process [14], change in the sulfur isotope ratio in sulfur dioxide emitted to the atmosphere can be expected.

The results of investigation concerning changes of sulfur isotope ratio along lignite combustion process from the Electric Power Station (EPS) Bełchatów were presented earlier [15]. The changes of sulfur isotopic ratio in the desulfurization process were investigated for the EPS Bełchatów which is applying "wet" lime stone technology in which gypsum is produced as by-product. The flue gas is purified in an absorber by a suspended limestone water solution flowing in the counter-current to the gas. Sulfur dioxide, contained in the flue gas, reacts with calcium bicarbonate, the main component of the limestone, existing in the absorber in the form of a solution, the product originating from this reaction is calcium sulfite. After oxidation and crystallization, gypsum is obtained. The gypsum is removed by filtration as by-product in desulfurization process.

Sulfur dioxide from the outlet gas was absorbed in hydrogen peroxide solution [16]. The sulfate ions produced in this way were quantitatively recovered as barium sulfate by precipitation with barium chloride solution [17].

Sulfur isotope composition is presented in the usual $\delta^{34}S$ notation as parts per thousand enrichment or depletion in the abundance of ^{34}S relative to the CDT (Canyon Diablo Troilite) standard [18]. Sul-

fur isotope compositions were determined on a DELTA plus FINNIGAN mass spectrometer with precision 0.3‰.

Table. $\delta^{34}S$ for gases in the desulfurization process from the EPS Bełchatów.

$\delta^{34}S$ [‰]$_{CDT}$			
Inlet (SO_2)	Product	Outlet (SO_2)	α
1.56 ± 0.03	2.29 ± 0.03 ($CaSO_4$ x $2H_2O$)	-4.03 ± 0.03	0.994

The obtained results from installation are presented in Table. Additionally, the fractionation factor (α) was calculated. During the desulfurization process, a fractionation of sulfur isotopes occurs. Sulfur in the outlet gases is depleted in the heavy isotope and the byproduct from this process is enriched in the isotope ^{34}S (fractionation factor is lower than 1). This fractionation may suggest that the main process runs in heterogenic conditions (gas-liquid). Therefore, most likely equilibrium and kinetic processes are responsible the sulfur isotopes fractionation. The condensed phase (lignite, solid) is enriched in heavier isotope [19].

The sulfur isotope ratio can be used as a marker of anthropogenic sulfur in the environment. However, introduction of desulfurization units has changed isotopic ratio of sulfur in the outlet gas streams. Normally, sulfur dioxide remaining in this flue gas is depleted in the heavy isotope ^{34}S. This phenomenon should be taken into account during preparing sulfur balance for the country and the region.

References

[1]. Chmielewski A.G.: Environmental effects of fossil fuel combustion. In: Encyclopedia of Life Support Systems [EOLSS]. Eolss Publishers, Oxford 2002, www.eolss.net.

[2]. Zhao F.J., Spiro B., Poulton P.R., McGrath S.P.: Environ. Sci. Technol., 32, 2288-2291 (1998).

[3]. Krouse H.R., Grinenko V.A.: Stable Isotopes in the Assessment of Natural and Anthropogenic Sulfur in the Environment. John Wiley & Sons Ltd., 1991.

[4]. Mukai H., Tanaka A., Fujii T., Zeng Y., Hong Y., Tang J., Guo S., Xue H., Sun Z., Zhou J., Xue D., Zhao J., Zhai G., Gu J., Zhai P.: Environ. Sci. Technol., 36, 1054-1071 (2001).

[5]. Novak M., Jackova I., Prechova E.: Environ. Sci. Technol., 35, 255-260 (2001).

[6]. Mast M.A., Turk J.T., Ingersoll G.P., Clow D.W., Kester C.L.: Atmos. Environ., 35, 19, 3303-3313 (2001).

[7]. Thompson A., Bottrell S.: Environ. Pollut., 101, 2, 201-207 (1998).

[8]. Prietzel J., Mayer B., Legge A.H.: Environ. Pollut., 132, 1, 129-144 (2004).

[9]. Querol X., Alastuey A., Chaves A., Spiro B., Planta F., Lopez-Soler A.: Atmos. Environ., 34, 333-345 (2000).

[10]. Andrews G.F., Noah K.S.: Fuel Process. Technol., 52, 247-266 (1997).

[11]. Rubiera F., Arenillas A., Martinez O., Moran A., Fuente E., Pis J.J.: Environ. Sci. Technol., 33, 476-481 (1999).

[12]. Srivastava R.K., Jozewicz W., Singer C.: Environ. Prog., 20, 4, 219-227 (2001).

[13]. Chmielewski A.G., Iller E., Tymiński B., Zimek Z., Licki J.: Modern Power Systems, 5, 53-54 (2001).

[14]. Chmielewski A.G., Wierzchnicki R., Derda M., Mikołajczuk A.: Nukleonika, 47, 67-68 (2002).

[15]. Derda M., Chmielewski A.G.: Determination of sulfur isotope ratio in coal combustion process. In: INCT Annual Report 2003. Institute of Nuclear Chemistry and Technology, Warszawa 2004, pp.110-111.

[16]. Determination of Sulfur Dioxide Emissions from Stationary Sources. Federal EPA Method, 2000.

[17]. Hałas S., Jasionowski M., Peryt T.M.: Prz. Geol., 44, 10 (1996).

[18]. Hoefs J.: Stable Isotope Geochemistry. Springer, Germany 1997.

[19]. Chmielewski A.G., Wierzchnicki R., Mikołajczuk A., Derda M.: Nukleonika, 47, 69-70 (2002).

BRIEF COST ANALYSIS OF ELECTRON BEAM FLUE GAS TREATMENT METHOD

Andrzej Pawelec, Bogdan Tymiński

The sulfur and nitrogen oxides emission is one of the most important problems during the fossil fuels combustion. Various methods of SO_2 and NO_x removal from flue gases have been developed, but commonly it is realised in two separate installations. Therefore, various research have been undertaken in order to develop a method for simultaneous pollutants removal from flue gases. Although various pilot plants have been constructed up to now, only electron beam process have been implemented on industrial scale.

The industrial installation for electron beam flue gas treatment was constructed in the Electric Power Station (EPS) Pomorzany in Szczecin [1,2]. After the start-up period, the installation was put into routine operation at the beginning of 2004. During the preliminary exploitation, the installation has proved its ability to simultaneous removal of pollutants with high efficiency reaching 70% for NO_x and 95% for SO_2. From the technological point of view, the installation is competitive with conventional flue gas treatment methods. According to previous predictions, such a method should also be economically competitive. Therefore, the investment and operational cost evaluation based on the data obtained during construction and exploitation of the Pomorzany plant was made.

The total cost of retrofit electron beam flue gas treatment plant of capacity of 300 000 Nm^3/h (corresponding to 130-150 MW_e electric power plant) is predicted for 21 million USD. So calculated unit investment cost is about 160 USD per 1 kW of installed power. This figure should be much lower in the case of newly built plants (up to 30-50%). On the other hand, the enlargement of the plant size, although rising the total costs, shall considerably

reduce the unit investment cost. According to the literature [3], on increasing the plant size from 130 to 250 MW_e the unit cost shall reduce from 160 to 140 USD/kW_e. Summing up, the investment cost of retrofit installation should not exceed 140-160 USD/kW_e, while the cost of a newly built plant may be even lower than 100 USD/kWe.

The investment costs strongly depend on local conditions as labour and equipment cost, ground prices, *etc*. The same concerns operational costs, that depend mostly on electricity and ammonia prices and local legislation towards pollutant emission. With low NO_x removal needs, the required dose and electricity consumption lowers rapidly that also lowers total operational costs. According to the data obtained at the Pomorzany flue gas treatment plant, the mean annual operational cost of the plant is 7000-7500 USD/MW_e. A comparison of the investment and operational cost with the conventional methods is presented in Table.

Table. The costs of various emission control methods for a retrofit 120 MW_e unit.

Emission control method	Investment cost [USD/kW_e]	Annual operational cost [USD/MW_e]
Wet flue gas desulfurisation (Wet FGD)	120	3000
Selective catalytic reduction (SCR)	110	4600
Wet FGD + SCR	230	7600
Electron beam flue gas treatment	**160**	**7350**

The conclusion of this brief report of cost evaluation of electron beam flue gas treatment method is, that the process is economically competitive with conventional ones in the cases, where removing of both SO_2 and NO_x is needed. With further development of this technique both the investment and operational costs shall decrease and the method should be economically attractive.

References

[1]. Chmielewski A.G., Iller E., Zimek Z., Licki J.: Radiat. Phys. Chem., 40, 4, 321-325 (1992).
[2]. Chmielewski A.G., Iller E., Tymiński B., Zimek Z., Licki J.: Modern Power Systems, 53-54 (May 2001).
[3]. Jackowski Z., Chmielewski A.G., Zimek Z.: Optimisation of irradiation chamber for electron-beam flue-gas treatment in application for large steam boilers. In: Environment applications of ionizing radiation. John Wiley and Sons, New York 1998, pp.167-195.

BOUNDARY LAYER PHENOMENA IN FILTRATION UNITS FOR RADIOACTIVE WASTE PROCESSING

Grażyna Zakrzewska-Trznadel, Marian Harasimowicz

Ultrafiltration (UF) membranes are susceptive to fouling which usually occurs when original industrial wastes containing particles, colloids, macromolecules, emulsions, *etc*., are filtered. Filtration of radioactive solutions containing radioactive compounds bound with suspensions or macromolecules results in deposition of colloids or suspended matter on/in the membrane, which is followed by a continuous flux decline. The cake formed in that way, *e.g*. some kind of a secondary membrane layer is characterised by different permeation parameters than UF membrane. This layer gives an additional resistance to the mass transfer resulted in flux decline, but sometimes in separation improvement, as was observed in some experiments. The filtration through a membrane covered with a layer of foulants may cause an additional retention of the complexes of macromolecule-radioisotope, which passed the membrane before, because too small size of the complex in relation to the membrane pore size. However, a flux decline is always considered as a negative phenomenon, diminishing the performance of the membrane. The negative impact of the fouling should be minimised by all available means, as pre-treatment of the feed solution, a control of hydrodynamic conditions in the module or adequate cleaning procedures.

The ceramic membranes applied in the experiments were in nanofiltration (NF) and UF pore size range. Such membranes used for filtration of the solutions containing the molecules of radioisotopes and their complexes with chelating polymers or suspensions of cyanoferrates usually are subjected to polarisation and fouling. The experiments showed that membrane operation in a short time resulted in flux decline caused by concentration polarisation. This is especially visible for membranes 15 kD and 50-100 nm pore size range, as was demonstrated in Fig. The figure shows the re-

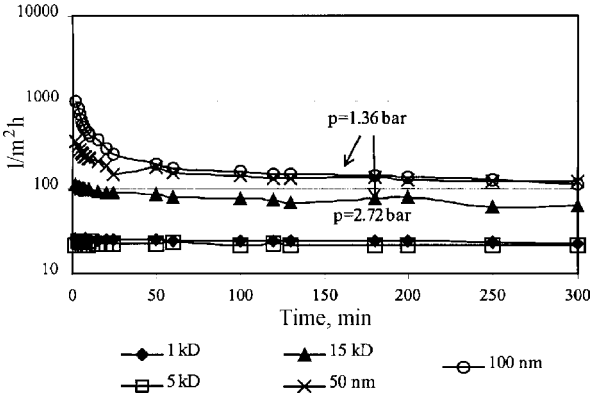

Fig. Flux *vs*. time for UF and NF membranes.

sults of 5-hour filtration of tap water of specific conductivity ~600 μS/cm. During the first 30 minutes of experiment for the membranes 100, 50 nm and 15 kD, a significant decrease in the flux was observed. It was caused by accumulation of the species, which always takes place near the membrane surface due to selectivity of the membrane. The water used in experiments contained some dissolved compounds, mainly mono- and bivalent ions (especially high concentration of Mg^{2+} – 33.4 mg/dm^3 and Ca^{2+} – 55.4 mg/dm^3 as well as SO_4^{2-} – 137.9 mg/dm^3), but also some amount of iron (0.1 mg/dm^3). As the experiments showed, the membrane always retained some part of multivalent cations and anions. These species are accumulated near the membrane causing the flux decline at the beginning of each experiment. When the steady-state conditions were attained a further decrease in flux was not observed; the flux was stable in time of experiment for all the membranes. This flux decline caused by concentration polarisation occurred after each cleaning procedure – the membrane needed some time to reach stable conditions of filtration. The time to reach stable permeate flux was different for UF and NF membranes: for UF it was less than 1 hour, while for NF membranes only 10-15 minutes. The effect of polarisation for UF process is more remarkable as UF membranes are characterised by high permeate fluxes. It is dependent on the flux and mass transfer coefficient or diffusion coefficient, which is generally low for macromolecular compounds. The relation between the polarisation effect can be expressed by equation:

$$\frac{c_m - c_p}{c_b - c_p} = \exp\left(\frac{J_v}{k}\right) = \exp\left(\frac{J_v\ \delta}{D}\right)$$

where: c_m – concentration at membrane surface, c_b – concentration in bulk solution, c_p – concentration in permeate, D – diffusion coefficient, J_v – permeate flux, k – mass transfer coefficient, δ – polarisation layer thickness.

All membranes exhibited good performance during the 5-hour operation; after reaching a steady state, the flux was almost constant as a function of time.

In experiments, when the real solutions of radioisotopes were treated in membrane-complexation process a continuous flux decline, caused by membrane fouling was observed. In several hours of operation, the flux can decrease even by 70-80% that corresponds with membrane blockage. To avoid clogging, the membrane cleaning is necessary. After cleaning the membranes behaved as before the filtration tests, or sometimes even better (higher fluxes, slight elongation of operation time before subsequent washing). Different cleaning procedures were tested.

APPLICATION OF MEMBRANE METHODS FOR SEPARATION OF GAS MIXTURES IN SYSTEMS GENERATING ENERGY FROM BIOGAS

Marian Harasimowicz, Grażyna Zakrzewska-Trznadel, Andrzej G. Chmielewski

In the first part of the project No. 4 T09C 041 24, which was realized in 2003, a laboratory-scale unit (Fig.) was constructed and the experiments with the use of different gas mixtures: CH_4+CO_2, $CH_4+CO_2+H_2S$, CO_2+N_2 and CH_4+N_2 were completed [1-3]. At present, the experiments dealing with separation of CH_4+CO_2 mixtures, concentration of CH_4 from 4.8 to 94.4%, using capillary polyimide GS (gas separation) membrane [4,5] mounted in A-2 pressure vessel were carried out. For that purpose, a low-pressure membrane has been prepared by UBE Industries Ltd. (Japan). Gas mixture delivered to the module under a pressure of 5-8 bar is separated in two streams: permeate – composed of the gases penetrating across the membrane material (high CO_2 concentration), and retentate – a mixture of gases retained by the membrane (high CH_4 concentration). The separation efficiency of the membrane was examined in the following conditions: feed pressure – 6.0 bar; feed flow, Q_F – from 0.184 (pure CO_2) to 0.06 Nm^3/h (pure CH_4); permeate flow, Q_P – from 0.134 to 0.01 Nm^3/h at 0 pressure; retentate flow, Q_R – 0.05 Nm^3/h at a pressure of 5.8 bar. The temperature of all gas streams was 40°C.

The influence of partition coefficient of the stream $k_S=Q_P/Q_R$ on CH_4 concentration in the retentate and permeate was observed. For the feed mixture CH_4:CO_2=1:1 and k_S=0.25, 0.70, 1.00, 1.20, the following concentration of CH_4 in the retentate stream was obtained: 60.30, 79.93, 89.50, 94.12%. The highest CH_4 concentration received with this kind of the membrane was 94.40%. The concentrations of CH_4 in permeate stream were as follows: 4.62, 7.53, 10,45, 13.33%. This stream can be delivered to a final purifying stage, where more than 95% of CO_2 is absorbed in amine solution, and a methane-rich gas is mixed with the retentate. By this way a high-methane fuel gas can be obtained from biogas in the membrane-absorption hybrid process.

The results of laboratory-scale experiments became the basis for the elaboration of biogas processing technology with GS low-pressure polyimide capillary membranes produced by UBE. Feasibility study for a pilot-plant construction (two-stage system with permeate stream recovery) with a capacity of ca. 120 Nm^3/h of high-methane fuel gas (CH_4 concentration about 94%) was performed and total cost of a such plant was evaluated.

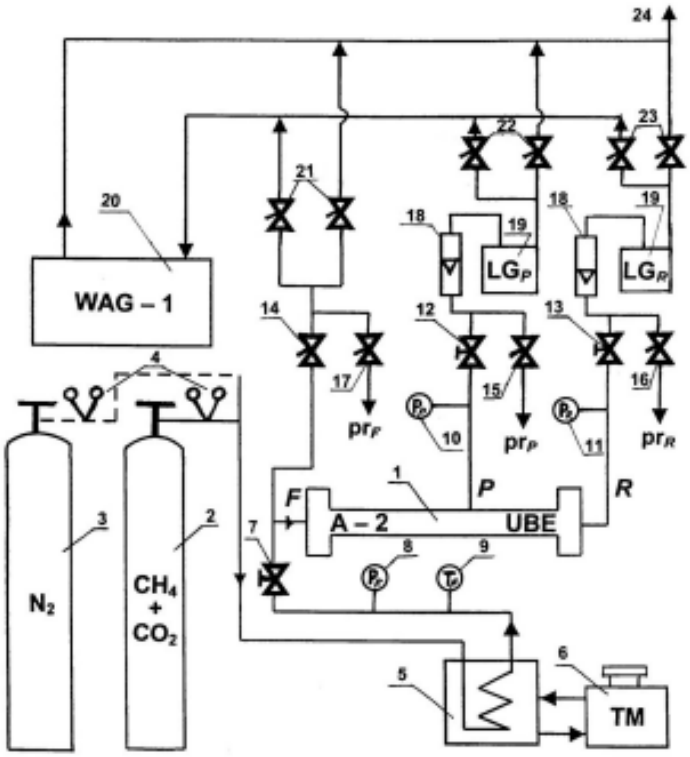

Fig. A scheme of laboratory-scale unit for investigation of gas mixture separation process on A-2 (UBE) module with capillary polyimide low-pressure membrane: 1 – A-2 module; 2, 3 – pressure bottles with gas mixtures CH_4+CO_2 and N_2; 4 – pressure reduction valves; 5, 6 – heater/cooler and temperature regulator; 7 – feed flow control valve; 8, 9 – manometer, thermometer on feed track; 10, 11 – manometers on permeate and retentate tracks; 12, 13, 14 – needle valves; 15, 16, 17 – sample collection valves; 18 – gas-flowmeters; 19 – gas volume counters; 20 – gas mixture spectrometric analyzer; 21, 22, 23 – cut-off valves; 24 – to vent shaft; pr_F, pr_P, pr_R – samples of feed, permeate and retentate; F, P, R – feed, permeate and retentate streams.

References

[1]. Harasimowicz M., Zakrzewska-Trznadel G., Chmielewski A.G.: Enrichment of biogas to 90-95% of CH_4 using GS membranes. In: Proceedings of the Conference "PERMEA 2003", Tatranské Matliare, Slovakia, 7-11 September 2003, p.171.

[2]. Harasimowicz M., Zakrzewska-Trznadel G., Mikołajczuk A., Chmielewski A.G.: Methane enrichment of CH_4+CO_2 mixture on 2-stage GS membrane module system with circulation stream and chemical final purification. In: Proceedings of the Conference "ARS SEPARATORIA 2004", Złoty Potok, Poland, 10-13 June 2004, pp.187-189.

[3]. Harasimowicz M., Zakrzewska-Trznadel G., Chmielewski A.G.: Monografie Komitetu Inżynierii Środowiska PAN, 22, 429-433 (2004), in Polish.

[4]. Robeson L.M.: Curr. Opin. Solid State Mater. Sci., 4, 549-552 (1999).

[5]. Gas separation for the oil and gas industries – UBE CO_2 separation membrane. UBE Technical Bulletin (2003).

JUICE AUTHENTICITY CONTROL BY STABLE ISOTOPE MEASUREMENTS

Ryszard Wierzchnicki, Małgorzata Derda, Agnieszka Mikołajczuk

There are two kinds of juices in the commercial market: fresh juices and juices made from the concentrate. Both methods of production are permissible, but it is obligatory to correctly label the products. The label should inform about the juice composition and the method of production. The fresh juice is received by squeezing fresh fruits, whereas the recreated juices are obtained by watering of juice concentrate. It is important to distinguish the two kinds of products because of price difference. Fresh juice is more expensive and more requested by consumers. However, it is difficult to notice the difference between these juices by application of conventional chemical methods.

The aim of the study was to recognize the method of juice production on the basis of $^{18}O/^{16}O$ isotope composition of water from fruit (vegetable) juice. This is possible due to the different isotope composition of oxygen in tap water and in water from the fruit (vegetable).

The first stage of the study was the preparation of tomato juices from fresh domestic tomatoes. The water from these juices was distilled (by lyophilization) and after that the oxygen stable isotope composition was measured in the obtained water. In the same way, samples of water from commercial juices were prepared. An example of the results of oxygen isotope composition for differ-

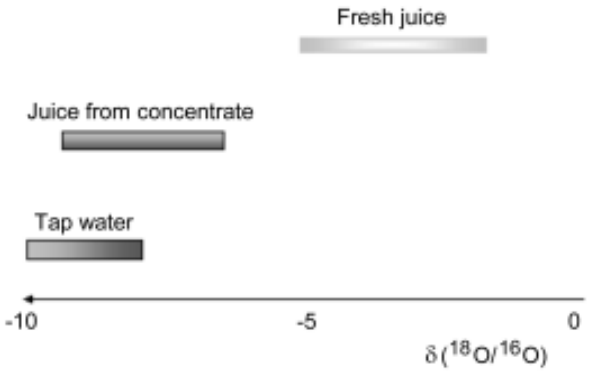

Fig. Oxygen isotope composition of tomato juice.

ent commercial tomato juices and fresh juices is shown in Fig.

The implementation of the new method of juice identification to the laboratory practice is not complicated. A basis for correct results is a good vacuum distillation of water from juice sample. For this purpose, a typical Rittenberg glass device was used. The process of oxygen measurements is automatic and computer controlled and has two additional advantages: simple sample preparation and not time-consuming. The set of Delta^{plus} spectrometer (ThermoFinnigan, Germany) associated with a sample preparation unit GasbenchII (ThermoFinnigan, Germany) used for the measurements gives a good precision and repeatability of results.

In summary, the importance and usefulness of the proposed method for the tomato juice were demonstrated. In the future work, the method will be tested for other kinds of fruit and vegetable juices.

WATER ISOTOPE COMPOSITION AS A TRACER FOR THE STUDY OF MIXING PROCESSES IN RIVERS. PART I. PRELIMINARY STUDIES

Andrzej Owczarczyk, Ryszard Wierzchnicki

This work is aiming at using the naturally existing differences in the isotope ratios $^{18}O/^{16}O$ and D/H of waters, to investigate the transport and accompanying dispersion processes as well as mixing of various waters in the tributary-receiver system. The originating differences in isotope composition of water are determined by isotope ratio mass spectrometry.

Preliminary studies were undertaken on the use as a tracer – the naturally existing differences in isotope composition of waters of a tributary and a receiver to follow and to describe dispersion and mixing processes in natural waters. Included also is the description of transport and dispersion of pollutants introduced into the receiver by the tributary. Conventional studies of this type require introducing into the studied system of large amount of an external tracer in the form, for example, of radionuclides, fluorescent dyes, *etc*. Such studies have been performed in the Institute of Nuclear Chemistry and Technology in the years 1970-1990, usually on a local scale, in the system discharge of pollutants-river. The recent rigorous environmental regulations practically excluded in the whole world the use of these conventional tracer methods. The application of naturally existing tracer, which are the differences in isotope composition of stable oxygen and hydrogen isotopes in waters of the examined system, gives the possibility to study the transport and mixing processes well as verification in natural conditions of mathematical model describing the studied phenomena.

Results of these studies should allow verifying the proposed mathematical model. They could also be a basis permitting to forecast the dispersion of pollutants and to evaluate the space-time scale of ecological hazard, for example, for potable water intakes appearing in the area of their interaction.

We propose to carry out studies on large hydrological systems as, for instance, river-lake or tributary-receiving river.

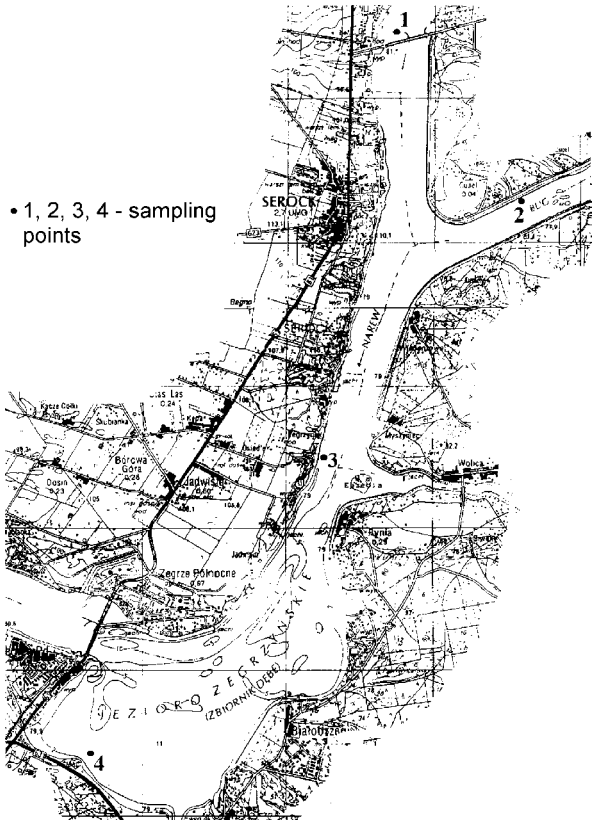

Fig. Localization of sampling points.

The real localization concerns the following system: the Bug and Narew rivers-the Zegrzyn Lake and the Bugo-Narew River-the Vistula River.
The intended studies include mathematical modeling which describes mass transport in both systems and two field sessions (separately for each

Table. Hydrogen isotope composition $\delta(D/^{1}H)$ in selection points of river water in 2004.

Month	1 – Narew River	2 – Bug River	3 – Zegrzyn Lake	4 – Zegrzyn Lake
January	-71.3	-77	-71.8	
February	-66.8	-71.5	-68.2	-69.5
March	-73.4	-77.1	-73.1	-75
April	-67.6	-71.1	-68.6	-70.3
May	-66.4	-68	-66.1	-66.1
June	-65	-67.5	-65.9	-65.6
July	-64.5	-66.9	-64.7	-65.2
August	-65.6	-68.3	-66.8	-67.5
September	-65.1	-68.3	-66.4	-66.7
October	-64.9	-69.8	-66.6	-66.4

selected hydrological systems) performed in two consecutive steps in order to investigate real transport and mixing processes of waters.
Measurements of the stable isotope ratios $^{18}O/^{16}O$ and D/H are carried out according to the earlier designed net of measuring points in the field.

The preliminary results of isotope ratio measurements in selected points of hydrological system (Fig.) have been presented in Table. Observed differences of water isotope composition in the Narew and Bug rivers are sufficient for application of this parameter as a tracer for study of the mixing process of rivers below their connection point.

This work was supported by the State Committee for Scientific Research (KBN) – grant No. 3 T09D 087 26.

TRACER AND CFD METHODS FOR INDUSTRIAL INSTALLATION INVESTIGATIONS

Jacek Palige, Andrzej Owczarczyk, Andrzej Dobrowolski, Sylwia Ptaszek

Actually, two methods are used for investigations of industrial flow installations or processes: residence time distribution (RTD) technique and computational fluid dynamics (CFD). The RTD is well established methodology [1]. On the basis of measured (in tracer experiment) RTD function, a model

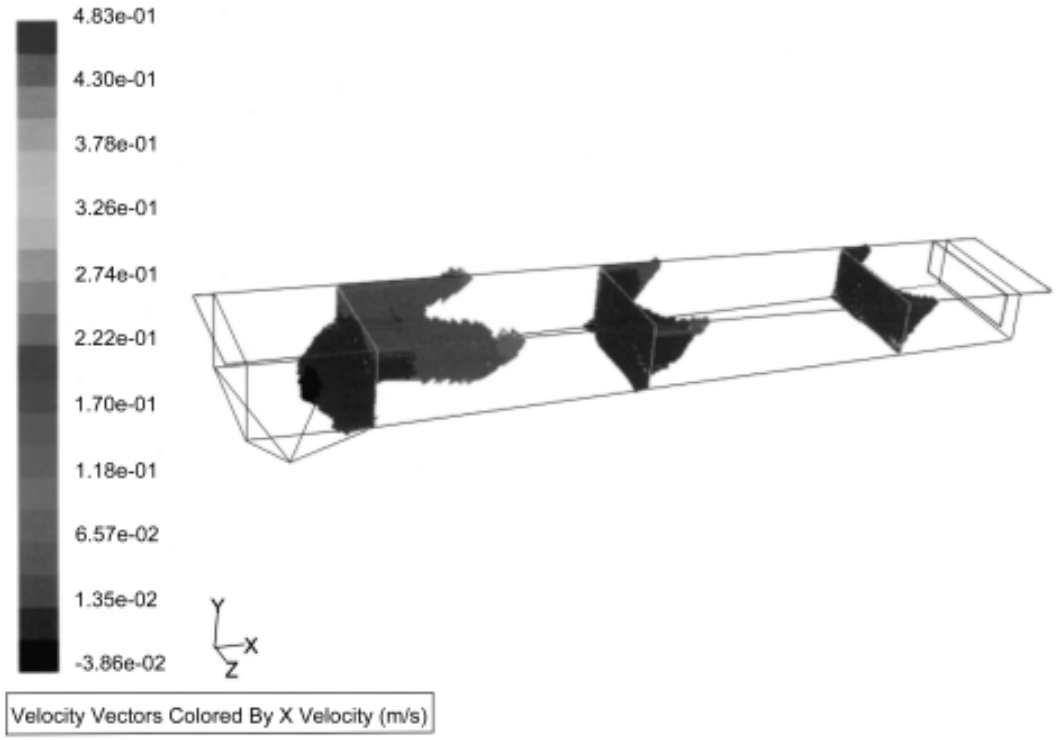

Fig.1. Geometry and liquid phase velocity profiles in an industrial rectangular settler.

of flow structure in the unit under investigation can be proposed. The numerical simulation of complex system by CFD is a new powerful tool for processes visualization.

Unfortunately, the RTD function can be described by several different models consisting of combinations and different connections of such elementary units as: perfect mixers, plug flow, transportation delay, recycle loop, backmixing, *etc*.
The CFD method gives a possibility to localize and visualize flow pattern inside the system, so the validation of proposed models can be made.
Both the RTD and CFD methods are complementary. The usefulness of these techniques was checked in large scale laboratory tests of flow installation (model of wastewater settler) [2,3]. A satisfactory agreement of data obtained by both methods was observed.

In this paper, the results of similar investigations carried out for an industrial rectangular settler of activated sludge sedimentation are presented.
Volume of the unit under investigation was V=1050 m^3, the flow rate of wastewater – Q=150 m^3/h. The input and output of sewage in a settler was realized by overflow. Using the professional software of CFD the flow structure, velocity field and profiles in selected cross sections of the settler were determined. The results of calculations are presented in Fig.1. The back flow in the bottom region of the settler is observed. Using the Lagrange technique (observations of fluid particles trajectories), a numerical RTD function was calculated.

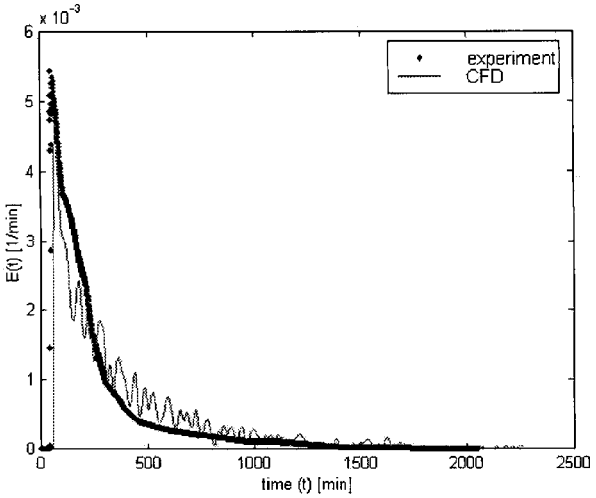

Fig.2. Comparison of experimental and numerical RTD functions obtained for a rectangular sediment settler.

The experimental RTD function was measured in tracer experiment using fluoresceine as a tracer of liquid phase. Comparison of experimental and numerical RTD functions is presented in Fig.2.

On the basis of data obtained by the CFD method and some technological observations, the model of flow in an industrial settler is proposed (Fig.3).

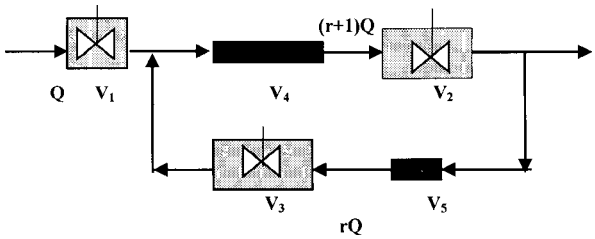

Fig.3. Model of liquid phase flow in a settler: V_1=7 m^3, V_2=440 m^3, V_3=395 m^3 – volumes of perfect mixing units; V_4=124 m^3, V_5=22 m^3 – volumes of plug flow units; r=0.15 – back flow rate; Q – liquid flow rate.

Comparison of the experimental and model RTD functions is presented in Fig.4. Good agreement between both curves is observed.

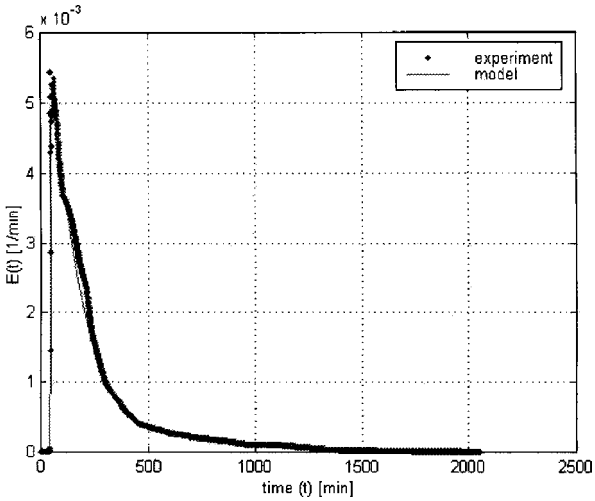

Fig.4. Comparison of experimental and model RTD functions for a sediment settler.

The obtained data confirm the usefulness of both, tracer and CFD, techniques for investigation of flow installations. Parallel application of the tracer and CFD methods permits on reciprocal validation of data obtained by both techniques.

References

[1]. Thyn J., Zitny R., Kluson J., Cechak T.: Analysis and diagnostics of industrial processes by radiotracers and radioisotope sealed sources. CVUT, Praha 2000.
[2]. Palige J., Owczarczyk A., Dobrowolski A., Chmielewski A.G., Ptaszek S.: Inż. i Ap. Chem., 4s, 72-75 (2003), in Polish.
[3]. Palige J., Owczarczyk A., Dobrowolski A., Chmielewski A.G., Ptaszek S.: Inż. i Ap. Chem., 5s, 151-152 (2003), in Polish.

MATERIAL ENGINEERING, STRUCTURAL STUDIES, DIAGNOSTICS

APPLICATION OF BULK ANALYTICAL TECHNIQUE – PGAA FOR STUDYING IRON METALLURGY SLAGS, ORE AND ARTEFACTS

Zsolt Kasztovszky[1/], Ewa Pańczyk, Władysława Weker[2/]

[1/] Institute of Isotope and Surface Chemistry, Chemical Research Centre, Budapest, Hungary
[2/] National Archeological Museum, Warszawa, Poland

In the course of the archaeological research (excavations) in Mazovia, to the west of Warsaw, a vast ironmaking region was discovered in 1967. It is estimated that the total number of furnaces in the region (area of 300 km^2 – Brwinów, Pruszków, Pęcice) probably numbered 100 000 – 150 000. Maximum production was achieved in the Roman-Barbarian Period (1st to 2nd centuries AD). The slag-pit furnaces were fed with local bog ores.

The smelting of ores is almost invariably related to the formation of slags, because slags act as collectors for impurities introduced into the smelting process. Slag analysis thus has the potential for revealing important information about the metallurgical technology. This technological information is important for establishing the context and scale of production of iron artefacts in ancient Poland [1].

The art and technique of ancient iron smelting in slag-pit furnaces, man's original method for winning metallic iron from its ore, has been largely lost in recent centuries. Many reconstructions of this technique have been attempted by archaeologists in the last 50 years [2]. These experimental smelts have tended to be rather disappointing in terms of the production of usable iron; nonetheless, many conclusions have been drawn from this work. Our primary goal was to smelt iron of sufficient quantity and quality, and to explore the process for a deeper understanding of iron production and distribution in antiquity.

Table 1. Chemical composition of bog iron in Poland – analytical method PGAA.

Element	Ore, product and slag – Rakszawa				Ore and product – Chorzele	
	ORE2	Roasted	IRON1	SLA3	Roasted	IRON7
	c% el/el					
B	0.002845	0.004593		0.00235	0.001218	3.25E-05
Na	0.62644			0.59496		
Al	2.481618	1.593409		2.376294	0.592094	
Si	40.01055	22.5588		33.74277	8.719373	
P			3.691281	2.28363	3.169151	3.545599
S					0.298987	0.10196
Cl					0.014419	0.006505
K	1.184573	1.846757		0.859582	0.171358	0.038389
Ca	4.013675	9.100188		0.688826	3.317972	0.148829
Ti	0.435308	0.144684		0.178788	0.032388	0.010794
Mn	14.24406	4.74582	15.71211	1.137574	0.372215	0.031574
Fe	36.99927	60.00548	80.53422	58.13245	83.31082	96.11632
Co			0.062397			
Sm	0.000759			0.000661		
Gd	0.000897	0.000271		0.000761		

Table 2. Chemical composition of bog iron ore after sieving.

	ORE11	ORE12	ORE13	ORE14	ORE15	ORE16	ORE17	ORE18	ORE19	ORE20	ORE21	ORE22	ORE23
Size of grain [mm]	>0.75	>1.2	>=0.75	>0.6	>0.49	>0.38	>0.3	>0.25	>0.2	>0.15	>0.1	>0.075	>0.06
Element	c% el/el												
B	0.00412	0.003649	0.003578	0.003848	0.003781	0.003994	0.004078	0.004521	0.004813	0.005298	0.006761	0.007096	0.007716
Na	1.071196				0.744947	1.145441	1.004881	1.560014	0.927536	2.813669			
Al	3.451308	3.736447	2.978499	5.767298	3.305274		4.012555	3.924189		4.066451	3.775672	3.1979	5.007714
Si	36.58437	33.3871	34.15583	35.8034	39.16056	42.41622	38.92991	43.91736	47.08168	49.78298	53.2189	53.267	50.99586
P		2.546826	2.710617	3.153743	2.578096		2.850344						
S													
Cl	0.822174	0.778042	0.676454	0.383306	0.242882	1.057682	0.711069	0.794459	0.655766	2.754597	0.941897	0.63368	0.53434
K	1.730395	1.304292	1.3365	1.394623	1.527534	1.383803	1.414027	1.562759	1.686705	1.784989	1.95491	2.150665	2.93739
Ca	2.933783	3.18085	3.125266	2.865877	2.974287	3.229209	4.419429	2.940707	3.222527	2.886085	3.261043	3.368803	3.161832
Ti	0.335858	0.404028	0.305729	0.304979	0.380223	0.638205	0.460639	0.545933	0.641261	0.385993	0.530718	0.699364	0.90925
Mn	6.363666	6.135541	6.453772	6.767827	6.506394	7.228881	7.303549	8.083364	8.248981	8.304647	9.473336	9.358181	9.46609
Fe	46.70227	48.52248	48.25301	43.55438	42.57532	42.89586	38.88882	36.66631	37.53034	27.21457	26.83595	27.31644	26.97888
Co													
Sm	0.000378	0.000341	0.000323	0.000313	0.0003	0.000286	0.00029			0.000308	0.000338	0.000383	0.00041
Gd	0.000479	0.000399	0.000427	0.000411	0.000402	0.000411	0.000411	0.00039	0.000389	0.000415	0.000472	0.000484	0.000514

The evidence from the mines suggests that all available bog iron ore was taken and used. First, it would be beneficiated (crushed an concentrated) by removing as much as possible of the gangue (waste rock). This could be done either by washing swirling the crushed material in water and letting the denser ore separate out or by simply picking out the richest mineral manually. To smelt the metal, the ore would be first have been roasted within the temperature range of 500-800°C to make it more friable and to convert any minerals (carbonates, sulphides or chlorides) to oxides. The enriched ore would then have been smelted in a bloomery furnace.

Iron was obtained directly from its ore within a single metallurgical process in a heart by reduction of the ore with charcoal which simultaneously served as a fuel.

The melting point of pure iron is 1540°C. Even by Roman times bloomery furnaces were not producing heat much over 1200°C. Bloomery iron did not involve the iron turning to the liquid state. Instead, it was a solid state conversion requiring chemical reduction of the ore. Ore was placed in a pit and mixed in a hot charcoal fire. Air was forced into the dome covered structure *via* bellows through a fireproof clay nozzle called a tuyere. After a sustained temperature of 1100-1200°C, liquid slag (oxidised non-metallics) penetrated the pores down and fell to the bottom leaving the spongy mass containing the iron. Holes forming the sponge texture were a result of the removal of the non-metallics impurities when the slag melted out.

The bloomery furnaces were always necessarily quite small: typical dimensions would be about 1.5 m tall with an internal diameter of about 50 cm. There are good technical reasons for such a small size of the individual furnaces. Air supply was one of the major constraints; if the furnace volume was larger then it was impossible to supply manually enough air to maintain the necessary temperatures.

Thus the early historical production process differed from the blast-furnace process in use nowadays, as iron was produced in direct process in the solid state and the slag liquified.

Slag fulfills two physical functions in a furnace: protection and transportation. Molten slag coats and protects reduced iron particles from reoxidation and carbonisation. Both protection and transportation require a liquid, free-running slag. The fluidity of the slag is a function both of its chemistry and temperature. Although the slags appear amorphous and uninformative, they are in fact a complex interacting systems of various crystalline minerals and glassy phases. Many of the minerals only form under quite specific conditions, and their identification and analysis, principally by scanning electron microscopy (SEM) and X-ray diffraction (XRD), can reveal much of the temperature and reducing conditions within the furnace. The bulk analysis of the slags, together with the identification of the minerals present, enable the chemistry, thermodynamics and efficiency of the process to be reconstructed.

Our first trials provided us with a valuable experience, but produced only the most pitiable examples of iron lumps. We attempted to deal with these problems by reducing both the fuel:ore ratio, and lowering the airflow and temperature, with disappointing results. The ore in this trial was our local bog ore with different iron contents from bog

Table 3. Chemical composition of bog iron ore after washing and sieving.

	ORE111	ORE112	ORE113	ORE114	ORE115	ORE116
Size of grain [mm]	0.06	0.102	0.075	<0.06	>0.075	0.15
Element	c% el/el					
B	0.008922	0.008509	0.008862	0.009034	0.006255	0.008802
Na	2.302044	1.121506	1.050139	1.511068	0.976348	
Al		5.357504	4.923862	4.95099	3.816995	5.488688
Si	52.9562	50.00307	50.40772	53.14214	69.10386	46.07704
P						
S						
Cl	0.63751	0.70355	0.664487	0.486551	0.284543	1.678677
K	2.653438	2.413196	2.423075	2.659867	2.359763	2.340581
Ca	4.042358	3.845684	3.918397	3.367239	1.733573	4.14504
Ti	0.561439	0.593748	0.517069	0.700938	0.470382	0.889727
Mn	10.1036	9.691022	9.68697	8.797393	5.15977	11.48238
Fe	26.73344	26.26169	26.39887	24.37363	16.08783	27.8882
Co						
Sm	0.000467			0.000507	0.000296	0.000362
Gd	0.000581	0.000515	0.000544	0.000643	0.000388	0.0005

Table 4. Composition of experimental slags – method PGAA.

	SLA1	SLA2	SLA33	SLA6	SLA7	SLA8	SLA9	SLA10
Element	c% el/el							
B	0.004997	0.004623	0.004832	0.002615	0.004103	0.001997	0.002339	0.00372
Na	0.064408							
Al			1.178934					0.469964
Si	19.4961	17.26569	16.88526	13.81824	17.68517	9.266886	12.56741	13.52937
P	2.707275	3.288353	2.980674	2.328626	2.818836	2.041433	2.219448	3.024368
S				0.142482	0.127723			
Cl								0.096596
K	1.264562	1.258678	1.307747	0.587635	1.152863	0.488882	0.453708	0.732912
Ca	4.647395	4.506834	4.636327	2.862201	4.196719	2.529265	2.87418	4.396486
Ti	0.133941	0.113901	0.128258	0.056435	0.099742	0.048548	0.045808	0.047322
Mn	1.625203	1.552447	1.500036	1.443747	1.78702	1.470789	1.41719	1.708313
Fe	70.05579	72.00915	71.37761	78.75785	72.12752	84.15206	80.41977	75.99077
Co								
Sm	0.00014	0.000139	0.000129	6.15E-05	0.000121	5.21E-05	6.28E-05	7.17E-05
Gd	0.000192	0.000177	0.000196	0.000101	0.00018	8.28E-05	8.52E-05	0.000113

ore: Brwinów (28.6% Fe), Chorzele (43.7% Fe) and Rakszawa (about 38% Fe).

The ore must be dressed carefully by hand-picking and washing, leaving less iron – rich pieces aside. It was roasted in a fire, and then broken up until the pieces ranged from 1-2 cm to fines. The next steps of dressing ore were sieving and flotation. After all these operations the results of smelting process were still disappointing. The question is about ancient methods of enriched bog iron ore.

The relationship between the chemical composition (especially at trace levels) of elements present in metal finding and the period and the ore where these findings belong, would enable us to work out chronological groupings.

The site provided enough material for an extensive analysis such as bog iron ore, slag, slagblocks and fragments of furnace. We carried out elemental analysis by means of a PGAA (prompt gamma activation analysis) analytical method. PGAA is a multicomponent analytical method, *i.e.* all the chemical elements can be detected with different sensitivities. In principle, it is possible to determine both the major and the trace elements simultaneously, though the detection limits are matrix-dependent. The measurements do not require sample preparation; they give prompt results. It allows for determining such elements as: H, B, N, Si, Ca, Cd, Gd, Pb and Bi, the analysis of which with the instrumental neutron activation analysis (INAA) method is difficult or almost impossible. On the other hand, the sensitivity of the PGAA method is lower than the INAA method by a few orders of magnitude. Moreover, usually after some days of cooling (*i.e.* decay of radioactive products) the same identical sample can be returned to the user.

PGAA is based on the detection of gamma-ray photons, which are emitted after the capture of thermal or subthermal neutrons into the atomic nuclei,

Table 5. Composition of ancient slags – method PGAA (Brwinów).

	SLA41	SLA43	SLA44	SLA48
Element	c% el/el			
B	0.004028	0.002702	0.004309	0.002099
Na				
Al				0.773157
Si	19.45592	16.34909	13.74093	13.49859
P	3.839959	4.37883		1.161344
S			0.110485	
Cl	0.003045			0.004855
K	0.974574	0.65318	1.217156	0.455521
Ca	3.533646	2.451395	4.184282	2.501455
Ti	0.094488	0.054389	0.068296	0.148695
Mn	1.983828	2.236292	2.307618	2.196033
Fe	70.11031	73.87398	78.36678	79.25794
Co				
Sm	8.86E-05	5.82E-05	6.65E-05	0.000136
Gd	0.000111	8.19E-05	8.37E-05	0.000176

i.e. the (n,γ) reaction. The photons energies range between 50 keV and 11 MeV and are characteristic of a given element. The element identification

is based on the precise determination of gamma photon energies and intensities.

The PGAA measurements were performed at the Institute of Isotope and Surface Chemistry, Chemical Research Center (Budapest, Hungary). For PGAA analysis purposes, a guided cold neutron beam, obtained from the 10 MW Budapest Research Reactor, was used [3]. The thermal neutrons, which exit the reactor core, are cooled by a liquid hydrogen cell down to 16 K. Consequently, the achieved thermal equivalent neutron flux was $5 \cdot 10^7$ cm^{-2}s^{-1}. The size of the neutron beam was restricted to 1×1 cm^2 area. The investigated samples ore, slags and iron artefacts were packed in thin teflon (FEP) films, and were placed in a well-defined position of the sample holder chamber. The mass of the investigated samples varied between 0.12-12 g.

The emitted gamma photons were detected with a complex HPGe-BGO detector system in Compton-suppression mode; the signals were processed with a multichannel analyser. The spectra were evaluated with Hypermet-PC software; the element identification was performed on the basis of our prompt-gamma element library [4].

The peaks of interest were fitted by Hypermet-PC and mass ratios were calculated. The combined standard uncertainties of the mass ratios depend on the uncertainty of the counting statistics, the uncertainty of efficiency function and the uncertainty of k_0 factors. The most dominating of them is the uncertainty of counting statistics. The measurement time for one individual coin varied between 460 s-24 h.

Chemical composition of bog iron ore, ancient iron products, and slags from Chorzele and Rakszawa are listed in Table 1. The results of the chemical analysis of the ore after sieving and washing are presented in Tables 2 and 3. Composition of the ancient slags and from our experiments is shown in Tables 4 and 5.

The Mn content of Chorzele and Rakszawa ores varies from 0.37 to 14.2%, respectively.

The Ca content is mainly below 10%. Si and Al are comparable in the ores and the slags and range from 40 to 8.7% and 2.5 to 0.6%, respectively. The slags contain up to 80% Fe and up to 2% Mn. The percentage of Fe present in the slags is still quite high, as could be expected from the mineralogical composition of the main component. The Fe content of the ore found in the settlement is, however, lower than of the slags (Tables 2-5). Because of the low Fe content in the ore, the analysed pieces cannot be characteristic of the ore used for the ancient production. The main problem connected with methods of enriching ores in ancient times still is unresolved. The main focus of our work is to continue to obtain iron as thoroughly as possible. We also hope to achieve more specific experiments in enriched ore and to apply our experience to other types of ore, including goethite and hematite.

References

[1]. Weker W.: Proces dymarski – teoria i praktyka. Hutnictwo Świętokrzyskie oraz inne centra i ośrodki metalurgii żelaza na ziemiach polskich. Kielce 2002, pp.199-202, in Polish.

[2]. Tylecote R.F., Adams R.: Experiments on iron smelting. In: Archeologie Experimental T1 – Le Feu. Actes du Colloque International "Experimentation en archeologie: Bilan et perspectives", Archeodrome de Beaune, France, 6-9 April 1988. Paris 1991, pp.123-128.

[3]. Révay Zs., Molnár G.L.: Radiochim. Acta, 91, 361-369 (2003).

[4]. Révay Zs., Belgya T., Kasztovszky Zs., Weil J.L., Molnár G.L.: Nucl. Instrum. Meth. Phys. Res. B, 213, 385 (2004).

TITANIUM DIOXIDE AND OTHER MATERIALS COATED WITH SILICA-QUATERNARY ALKYLAMMONIUM COMPOUNDS FOR USING IN BUILDING INDUSTRY AND ENVIRONMENT PROTECTION

Andrzej Łukasiewicz, Dagmara K. Chmielewska, Lech Waliś

Silica biocides based on water glass and quaternary N-alkylammonium salts (SiO_2-QAC) were elaborated previously [1,2], by precipitation them with H_2SO_4 from water glass (WG) and QAC. These water-insoluble biocides show fungicidal, bactericidal and algae destroying activity when added to water, or mixed with paints or building mortars. Biocides can contain structurally bonded carriers such as, *e.g.* TiO_2 or dolomite. Titanium dioxide is of special interest because of its properties useful for the building industry and environmental protection. Its ability to kill bacteria by absorbed UV light is known.

We have found that SiO_2-QAC materials absorb UV light similarly to TiO_2. Combined with TiO_2 they can show a synergism of UV effects.

Unfortunately, SiO_2-QAC biocides, with and without a carrier show a weak ability to disperse in commercial resins. This distinctly limits their practical use.

We elaborated, therefore, a modified technology for obtaining SiO_2-QAC biocides, especially containing TiO_2 and other materials with good ability to disperse in resins and building mortars. The technology is based on the observed ability of WG-QAC salts to coate under suitable conditions TiO_2, dolomite and other materials. The salt is formed by exchange of Na^+ cation in $Si(ONa)_n$ salt by QAC^+ cation:

$$Si(ONa)_n + QAC + Cl^- \rightarrow Si(ONa)_{n-1}QAC \quad (+NaCl)$$

Coated material is stabilised by adding H_2SO_4.

Benzalkonium chloride was used as QAC in our experiments.

Elaborated materials (TiO_2 and dolomite) coated with silica-benzalkonium salt show the following properties:
- disperse well in resins and mortars;
- absorb UV light (absorbed light reduces Ag^+);
- show high affinity for anions, among others for acidic dyes (can be used for obtaining colour pigments).

Technological details are omitted in this communication because of patenting procedures.

References

[1]. Łukasiewicz A., Chmielewska D., Waliś L., Rowińska L.: Pol. J. Chem. Technol., 5, 4, 20-22 (2003).
[2]. Łukasiewicz A., Krajewski K., Waliś L., Chmielewska D., Rowińska L.: Sposób otrzymywania nowych materiałów aktywnych biocydowo. Patent application P.357356.

SCANNING ELECTRON MICROSCOPY INVESTIGATIONS OF POLYCARBONATE TRACK-ETCHED MEMBRANES

Bożena Sartowska, Oleg Orelovitch[1/], Pavel Apel[1/]

[1/] Flerov Laboratory of Nuclear Reaction, Joint Institute for Nuclear Research, Dubna, Russia

Track-etched membranes can be used as the templates for synthesis of nano- and microstructural materials [1]. It is important – for these applications – to obtain pores with well defined sizes and geometry. It is stated in the literature that pores are often tapered towards the membrane surface [2,3]. This could be an important feature when the membrane is applied as a template.

Polycarbonate films with thickness of 10 μm were used in the experiments. The membranes were produced in the Centre of Applied Physics of Joint Institute for Nuclear Research (Dubna, Russia) by irradiation with Kr ions (250 MeV) and etched in 6 M NaOH.

To understand details of the production process, we need to investigate membranes parameters. Scanning electron microscope (SEM) is a very useful tool for this task. The surface of membrane was observed to define main membrane parameters – diameter and density of pores. Fractures were investigated to observe the shape of pores and to obtain detailed data on the membrane structure.

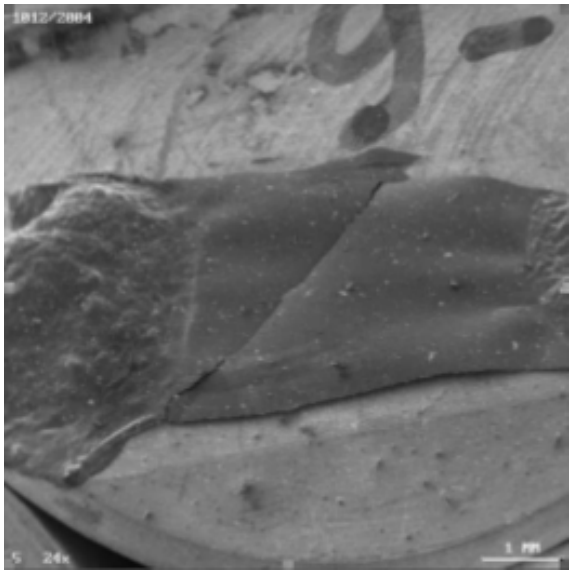

Fig.1. View of the sample of track-etched polycarbonate membrane after UV irradiation.

To observe these kinds of small objects, we need to use non-standard preparation procedure of samples. According to our previous experiments, the UV irradiation is a good way to obtain high brittleness of material [4]. Samples were irradiated by UV during several hours and then material becomes very brittle. Figure 1 presents a view of the investigated sample. Cracks through the material can be seen. The fracture line is not oriented in any direction; the crushed parts of membrane can be distinguished. The samples were fixed using conductive glue (Quick Drying Silver Paint, Agar Scientific Ltd.). The surfaces were coated with a thin layer of metal to reduce the charging which takes place during SEM observations. They were covered with a thin layer (less than 10 nm) of gold using a vacuum evaporator JEE-4X (JEOL, Japan). A special facility inside the bell was used to diminish the influence of overheating of the membrane surface. This condition allows us to protect the sample from heat destruction and to keep real parameters of objects during the covering process in a vacuum evaporator [5].

Observations were carried out using SEMs: JSM 840 (JEOL, Japan), DSM 942 (Zeiss, Germany) and LEO 1530 GEMINI (Zeiss, Germany) with low accelerating voltage. Figure 2 presents surface morphology of polycarbonate membrane. Average pore diameter measured by the use of SEM was 30 nm. In majority they have a round shape. Multiple pores can be seen. Counted pore density is $2x10^9$ cm^{-2}.

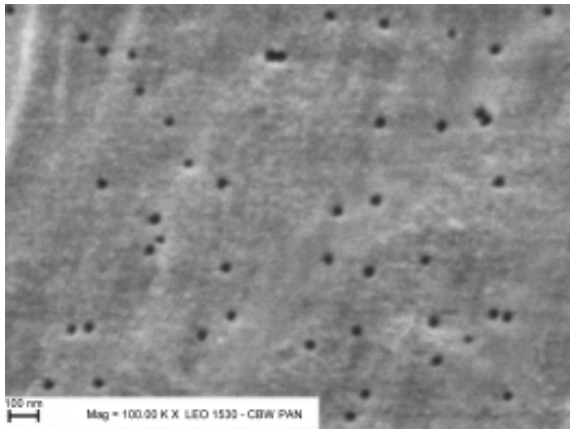

Fig.2. Surface of PC investigated track-etched membrane.

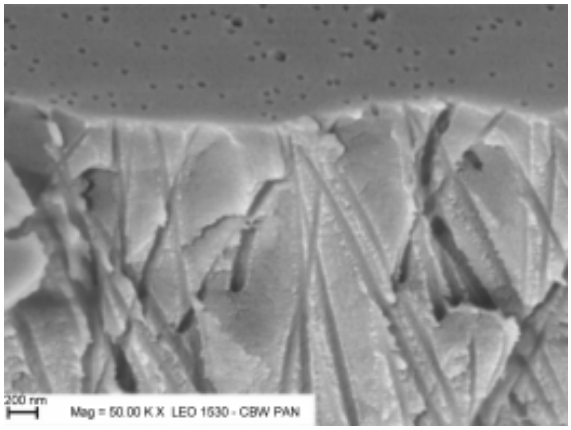

Fig.3. Fracture through the PC investigated track-etched membrane.

Figure 3 shows the fracture through the polycarbonate membrane. It can be seen that pore channels are not perfect cylinders along the whole length. Pores are tapered towards the end on channels. The diameter of inner part of pores is bigger than the pores diameter on the surface and it was estimated as 60.0 nm. Pores were not parallel, their directions are not perpendicular to the surface – they were randomly oriented.

In conclusions, observations with the use of the SEM give us new important information about the parameter and shape of small objects, in particular non-cylindrical, tapered pores in track-etched membranes. The investigations of the nanosized pores in polycarbonate membranes are still carried out. Results obtained from SEM observations and measurements allow us to plan the next parts of experiments.

Thanks to Dr. Adam Presz (Unipress, Warszawa) for help in SEM observations.

References

[1]. Spohr R.: Ion Tracks and Microtechnology. Principles and Applications. Vieweg, Braunschweig 1990, 272 p.
[2]. Schoenenberger C., Van der Zande B.M.I., Fokkink L.G.J., Henny L., Schmid M., Krueger M., Bachtold A., Huber R., Birk H., Staufer U.: J. Phys. Chem. B, 101, 5497-5503 (1997).
[3]. Apel P.Yu., Blonskaya I.V., Orelovitch O.L., Root D., Vutsadakis V., Dmitriev S.N.: Nucl. Instrum. Meth. Phys. Res. B, 209, 329-334 (2003).
[4]. Orelovitch O.L., Apel P.Yu.: Instrum. Exp. Tech., 44, 1, 111-114 (2001).
[5]. Goldstein I.J., Newbury D.E., Echlin P., Joy D.C., Romig A.D. Jr., Lyman C.E., Fiori C., Lifshin E.: Scanning Electron Microscopy and X-ray Microanalysis. A Text for Biologists, Material Scientists and Geologists. Plenum Press, New York and London 1992, 820 p.

SCANNING ELECTRON MICROSCOPY INVESTIGATIONS OF TRACKS INDUCED BY THE 5.5 MeV α PARTICLES IN PM-355 SOLID STATE NUCLEAR TRACK DETECTORS

Bożena Sartowska, Adam Szydłowski[1/], Marian Jaskóła[1/], Andrzej Korman[1/]

[1/] The Andrzej Sołtan Institute for Nuclear Studies, Świerk, Poland

Solid state nuclear track detectors (SSNTDs) are capable of proton, deuteron, α particles and heavy ions tracks recording and due to that are well suited to corpuscular diagnostics in hot plasma experiments. Many contemporary hot plasma facilities constitute of sources of very intensive fluxes of primary ions and nuclear reaction products which carry information about plasma properties. An important problem is to find convenient detectors of energetic, charged particles emitted from high temperature plasma, which make possible to measure their energy and to distinguish kind of projectiles. Modern solid state nuclear track detectors, especially of the PM-355 type, can be a good candidate to carry out such measurements.

Calibration measurements of charged projectiles tracks obtained in selected SSNTDs have been carried out for several years at the Sołtan Institute for Nuclear Studies (Świerk, Poland) [1,2]. Since the track diameter measurements enable the identification of the kind of projectiles [3], we have decided to extend our calibration experiments to an ion track depth analysis to measure energy of these particles.

Scanning electron microscope (SEM) is a very useful tool for investigations of developed ion tracks [4]. We are able to observe detector surface morphology, measure track diameter and determine track density. Furthermore, SEM is used for investigation of the etched-track intersection or fracture over the full length of the channel.

PM-355 (Pershore Ltd, the United Kingdom) detectors were irradiated by α particles with energy 5.5 MeV from a ^{241}Am source. Then the latent tracks in polymer detectors have been developed.

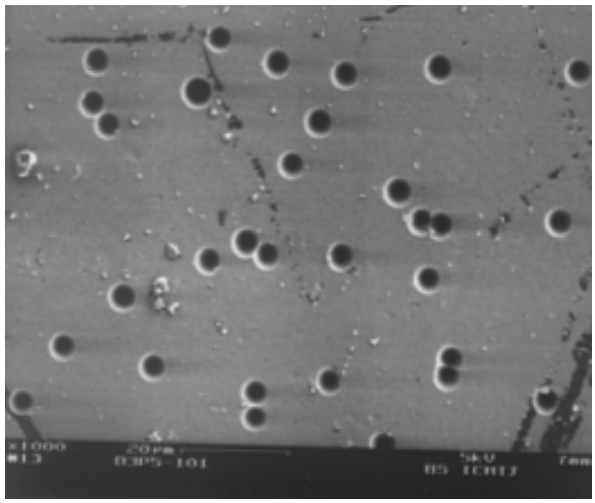

Fig.1. Surface morphology of PM-355 detector irradiated with 5.5 MeV α particles etched for 4 hours.

Chemical etching was performed in 6.25N NaOH at 70°C during various periods of time. Developed tracks were observed and measure using the SEM type DSM 942 (Zeiss, Germany). The PM-355 detectors surfaces were examined for the determination of the track diameter. Fractures of detectors were observed for the determination of the track depth. Samples were fixed with conductive glue (quick drying silver paint, Agar, the United Kingdom). Then they were coated with a thin – about 10 nm – layer of gold using a vacuum evaporator JEE-4X (JEOL, Japan) to protect the sample from heat destruction and to keep real parameters of the observed details [5,6].

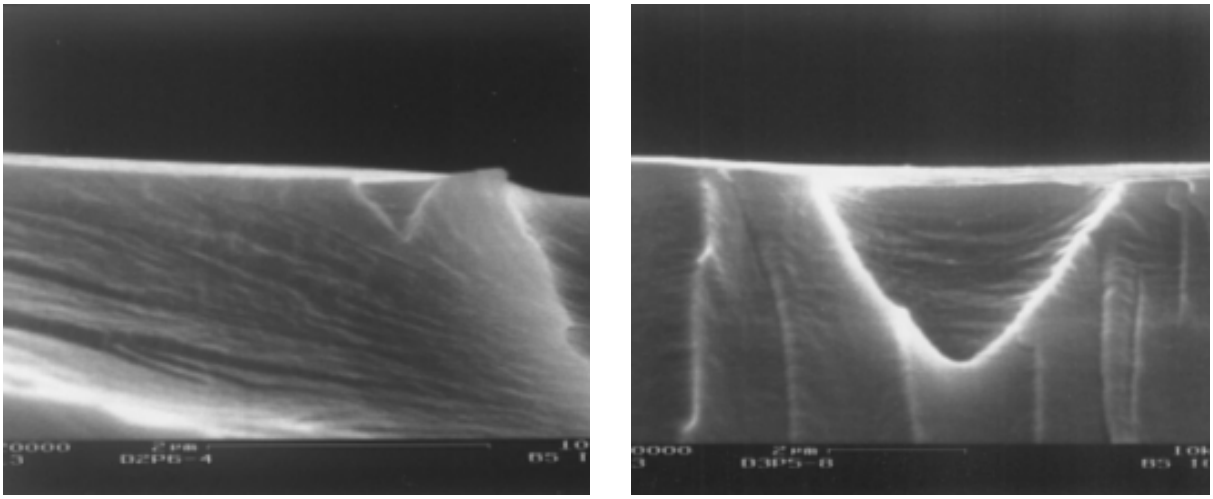

a b

Fig.2. Fracture of PM-355 detector irradiated with 5.5 MeV α particles etched for (a) 1 hour (magnification: 20 000x) and (b) 4 hours (magnification: 10 000x).

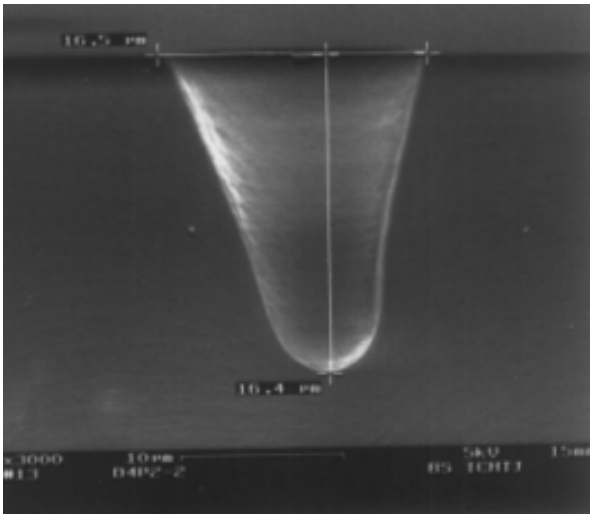

Fig.3. 5.5 MeV α particles track shape after 10 hours of etching.

In Figure 1, the surface of irradiated and etched detector is presented. Developed tracks became apparent. They are round in shape and randomly distributed. Results are consistent with data in our library set of calibration data. In Figure 2, the tracks in the PM-355 detector exposed to 5.5 MeV α particles were presented on the fracture of irradiated and etched detectors. Tracks of α particles have the cone shape. We found that the track depths are 0.39 and 4.54 μm for the etching time of 1 and 4 hours, respectively. After the sufficient etching time, the shape of tracks became roundish (Fig.3). One can notice that the rounding can be seen on the tip of the cone shape observed earlier. We can explain this phenomenon by the fact that the track length reached the region of an ion range in the detector material.

In conclusion, scanning electron microscopy was successively used for determination of the evolution of shape, diameter and track depth in the PM-355 solid state nuclear track detectors *vs*. etching time using the fracture technique for sample preparations. Track characteristics allow us to estimate the ion range in the detector material and to measure the full energy of projectile.

References

[1]. Sadowski M., Al-Mashhadani E.M., Szydłowski A., Czyżewski T., Głowacka L., Jaskóła M., Wieluński W.: Nucl. Instrum. Meth. Phys. Res. B, 86, 311-316 (1994).

[2]. Szydłowki A., Czyżewski T., Jaskóła M., Sadowski M., Korman A., Kędzierski J., Kretschmer W.: Radiat. Meas., 31, 257-260 (1999).

[3]. Szydłowski A., Banaszak A., Czyżewski T., Fijał I., Korman A., Sadowski M., Choiński J., Kretschmer W.: Response of the PM-355 Solid State Nuclear Track Detector to Energetic Sulphur Ions. In: Proceedings of the International Symposium Plasma, Warszawa, Poland, 19-21 September 2001, pp.36-38.

[4]. Vetter J.: Scanning, 16, 118-122 (1994).

[5]. Goldstein J.I., Newbury D.E., Echlin P., Joy D.C., Romig A.D. Jr., Lyman C.E., Fiori C., Lifshin E.: Scanning Electron Microscopy and X-ray Microanalysis, a Text for Biologists, Material Scientists and Geologists. Plenum Press, New York and London 1992, p.872.

[6]. Sartowska B., Orelovitch O.: SEM observations on the special type of particle track membranes. In: INCT Annual Report 2002. Institute of Nuclear Chemistry and Technology, Warszawa 2003, pp.138-139.

MODIFICATION OF THE NEAR SURFACE LAYER OF CARBON STEELS WITH INTENSE PLASMA PULSES

Bożena Sartowska[1/], Jerzy Piekoszewski[1,2/], Lech Waliś[1/], Jacek Stanisławski[2/], Lech Nowicki[2/], Michał Kopcewicz[3/], Adam Barcz[4/]

[1/] Institute of Nuclear Chemistry and Technology, Warszawa, Poland
[2/] The Andrzej Sołtan Institute for Nuclear Studies, Świerk, Poland
[3/] Institute of Electronic Materials Technology, Warszawa, Poland
[4/] Institute of Physics, Polish Academy of Sciences, Warszawa, Poland

Formation process, structure, features and the role of nitrogen expanded austenite in stainless steels are in a special interest of scientist in the surface engineering area [1-5]. It is documented that in the case of expanded austenite presence good corrosion resistance is maintained, while the mechanical properties increase. It is stated also in [2,3] that this phase can only be formed if iron, chromium and nickel are available in the system. In our previous experiments, using intense nitrogen plasma pulses, the phase nitrogen expanded austenite – γ_N was formed in carbon steels and even in pure iron [6].

The aim of this work was to investigate the surface layer of carbon steels after the modification process using intense short plasma pulses.

Carbon steels with different concentration of carbon were irradiated with five plasma (argon or nitrogen) intense (about 5 J/cm^2) short (μs range) pulses generated in a rod plasma injector (RPI) at the Andrzej Soltan Institute for Nuclear Studies [7]. Samples were characterised by: nuclear reaction analysis (NRA) $^{14}N(d,\alpha)^{12}C$ for determination of retained nitrogen dose; secondary ion mass spectroscopy (SIMS) for elemental profile measurements; conversion electron Mössbauer spectroscopy (CEMS) for quantitative analysis of identified phases and microhardness HV0.01 measurements.

Samples with the nitrogen retained dose of 1.2×10^{17} N/cm^2 were investigated. SIMS atomic concentration profiles show nitrogen distribution across the modified layer (Fig.1). An interesting correlation between the nitrogen profile and the initial carbon content in steels was observed. The nitrogen concentration reaches the value of 1/e of its maximum at the depths 250, 340 and 386 nm for Armco (0.03 wt.% C), steel 20 (0.28 wt.% C) and steel 45 (0.45 wt.% C), respectively. It means that nitrogen atoms diffused deeper into the steel when the initial carbon content is higher. It may be suggested that nitrogen diffusion in the liquid material is enhanced by the presence of carbon. Interactions of nitrogen and carbon were observed and reported in [4]. The presence of nitrogen enhances the activity of carbon and its diffusion. Carbon is very similar to nitrogen and could have similar behaviours in the liquid system, *i.e.* a synergic effect of simultaneous presence of carbon and nitrogen can be predicted. CEMS spectra obtained for the initial and modified with argon or nitrogen plasma pulses materials show the difference between these two sets of samples (Fig.2). The spectra of initial samples show six peaks characteristic of Zeeman pattern. In the case of argon modification of the steel samples, the peaks in the central part of spectrum appear. No changes are observed in the CEMS spectrum for Armco. In the case of nitrogen modification, the substantial changes in

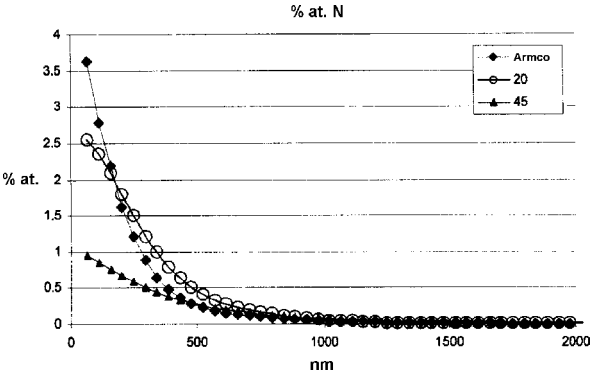

Fig.1. Nitrogen concentration profiles for Armco, steel 20 and steel 45 modified with nitrogen intense pulsed plasma beams.

a central part of CEMS spectra are observed for all samples including Armco (Fig.2). The intensities of the central peaks show the differences in austenitisation efficiency between argon and nitrogen modification processes.

In steels irradiated with argon phases α-Fe, γ-Fe and γ_C – carbon expanded austenite were found. In iron and steels irradiated with nitrogen phases, α-Fe, γ-Fe, γ_N – nitrogen expanded austenite, γ_C (except Armco) and ε – Fe_3N phases were found. Figure 3 shows the presence of paramagnetic phases detected in the modified layers. If there is a similar concentration of carbon or carbon plus nitrogen atoms, we observe more paramagnetic phases in the second case. The presence of 16 and 60% of paramagnetic phases were detected in the modified layer for steel 45 after argon modification (2.2 at.% C) and steel 20 after nitrogen modification (1.0 at.% C + 1.5 at.% N), respectively. Also the fraction of γ_C phase is lower for steel 45 irradiated with argon than for 20 steel irradiated with nitrogen. This again suggests the role of interactions between nitrogen and carbon, which facilitates the formation of expanded austenite when both nitrogen and carbon are present in the system.

Microhardness HV0.01 increased for all samples modified with nitrogen (Fig.4). A significant increase in HV0.01 was observed for one of the hardest initial material, *i.e.* steel 65. These results could be explained by the fact reported in [4] that nitrogen expanded austenite is harder than carbon ex-

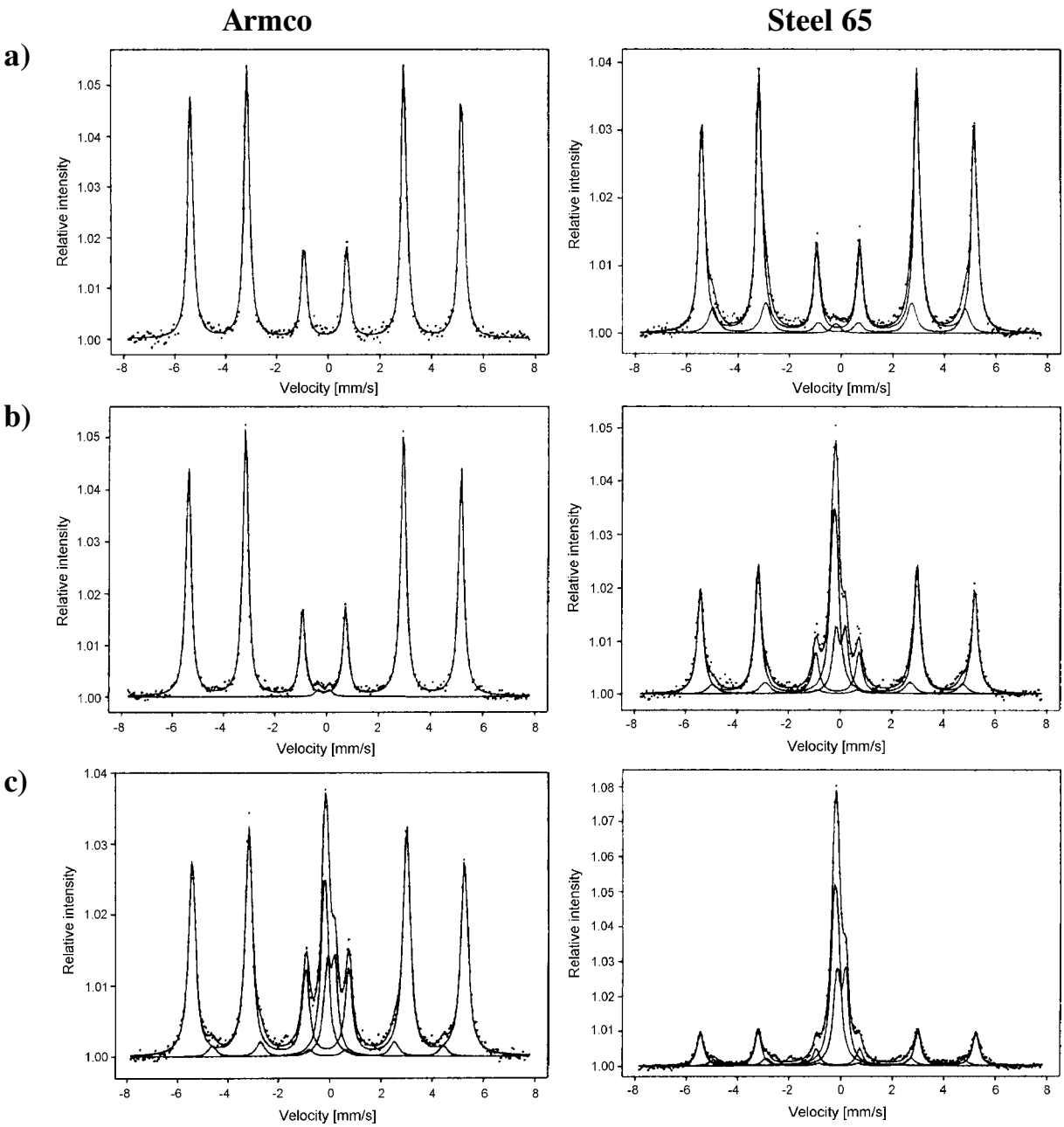

Fig.2. CEMS data for Armco and steel 65: (a) initial, modified with (b) argon and (c) nitrogen intense pulsed plasma beams.

panded austenite due to a larger deformation of the lattice by nitrogen atoms.

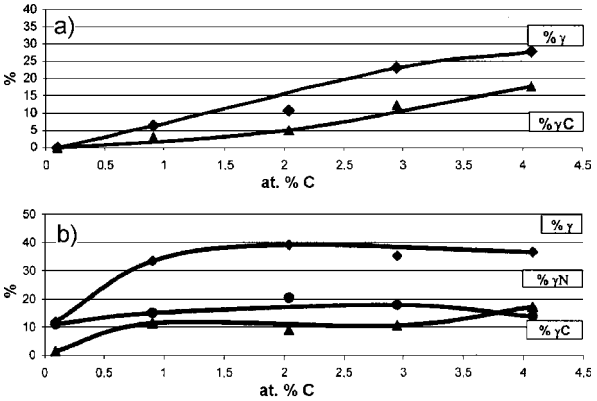

Fig.3. Fraction of paramagnetic phases after carbon steel modification with (a) argon and (b) nitrogen intense pulsed plasma beams.

In conclusions, paramagnetic phases were detected in the modified surface layers. Nitrogen was

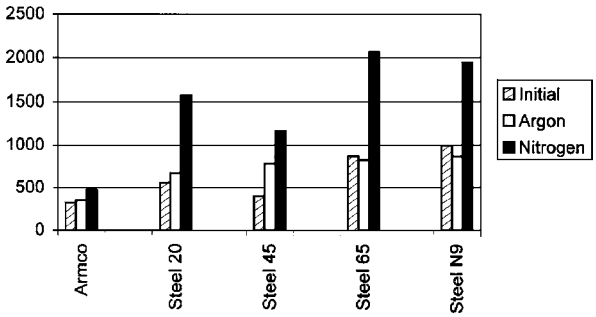

Fig.4. Changes of HV0.01 as a result of carbon steels modification with intense pulsed plasma beams.

detected to the depth depending on the carbon concentration in the initial material. The nitrogen expanded austenite – γ_N phase was found in the near

surface region of Armco and carbon steels in the case of nitrogen plasma modification despite of the absence of chromium and nickel in the system. A significant increase of microhardness was observed for the samples modified with nitrogen plasma, which can be explained by the presence of γ_N phase.

References

[1]. Williamson D.L., Oztruk O., Glick S., Wei R., Wilbur P.J.: Nucl. Instrum. Meth. Phys. Res. B., 59/60, 737-741 (1991).
[2]. Blawert C., Mordike B.L., Jirásková Y., Schneeweiss O.: Surf. Coat. Technol., 116-119, 189-198 (1999).
[3]. Jirásková Y., Svoboda M., Schneeweiss O.: Czech. J. Phys., 52A, 61-66 (2002).
[4]. Blawert C., Mordike B.L., Collins G.A., Short K.T., Jirásková Y., Schneeweiss O., Perina V.: Surf. Coat. Technol., 128-129, 219-225 (2000).
[5]. Gavriljuk V.G., Berns H.: High Nitrogen Steels. Structure, Properties, Manufacture, Applications. Springer-Verlag, Berlin Heilderberg 1999, 376p.
[6]. Sartowska B., Piekoszewski J., Waliś L., Kopcewicz M., Werner Z., Stanisławski J., Kalinowska J., Prokert F.: Vacuum, 70, 285-291 (2003).
[7]. Werner Z., Piekoszewski J., Szymczyk W.: Vacuum, 63, 701-708 (2001).

FORMATION OF SUPERCONDUTIVE MgB_2 REGIONS WITH THE USE OF ION IMPLANTATION AND PULSED PLASMA TREATMENT TECHNIQUE

Jerzy Piekoszewski[1,2/], Wojciech Kempiński[3/], Bartłomiej Andrzejewski[3/], Zbigniew Trybuła[3/], Lidia Piekara-Sady[3/], Jacek Kaszyński[3/], Jan Stankowski[3/], Zbigniew Werner[2,4/], Edgar Richter[5/], Friedrich Prokert[5/], Jacek Stanisławski[2/], Marek Barlak[2/]

[1/] Institute of Nuclear Chemistry and Technology, Warszawa, Poland
[2/] The Andrzej Sołtan Institute for Nuclear Studies, Świerk, Poland
[3/] Institute of Molecular Physics, Polish Academy of Sciences, Poznań, Poland
[4/] Institute of Physical Chemistry, Polish Academy of Sciences, Warszawa, Poland
[5/] Institut für Ionenstrahlphysik und Materialforschung, Forschungszentrum Rossendorf e.V., Dresden, Germany

Superconductive phase of inter-metallic MgB_2 compound discovered in 2001 by Nagamatsu *et al*. [1] has attracted a considerable interest due to its relatively high transition temperature T_C=39 K and potential application on an industrial scale. Study of this new material is conducted in two directions: development of fabricating and improving quality of solid MgB_2 and the same as above in the area of thin films formed on various substrates. Goal undertaken by the present authors is to verify the idea of a new approach in formation of supreconducting MgB_2 layers. It relies on growing such layer from liquid phase using ion implantation and intense pulse plasma treatment techniques. In our preliminary experiments [2], magnesium substrates were implanted with B^+ ions at energy of 100 keV and a dose of $5x10^{18}$ B/cm^2. Subsequent irradiation with 2 short (μs range) high-intensity pulsed hydrogen plasma pulses melted the near-surface layer of the substrate. Energy densities of pulses were 1.9 and 3.0 J/cm^2.

For detection of superconductivity, the magnetically modulated microwave absorption (MMMA) and four point probe (FPP) methods were used. In the samples irradiated with lower energy of pulses (1.9 J/cm^2), the MMMA signal was observed below 20 K. For higher energy (3.0 J/cm^2) the transition temperature was T_C=31 K. However, in both cases no macroscopic percolation chains occurred and MMMA signals in both cases were very weak.

In the present series of experiments, we extented the number of plasma pulses (2-4) and we also used argon as the working plasma which allows better control of the plasma generation process than in the hydrogen case. Boron implantation energy and dose were 80 keV and $3x10^{18}$ B/cm^2, respectively. Samples were characterized by MMMA, FPP, X-ray diffraction (XRD) and Rutheford backscattering (RBS) techniques. The most important information derived from the present results can be summarized as follows.

Careful examination of our XRD data (average taken over 5 samples) indicates that the *a* lattice constant decreased in the pulse-treated samples with respect to the as-implanted samples by $\Delta a/a$=-0.71%, whereas the *c* lattice constant increased by $\Delta c/c$=0.37%. According to theoretical predictions given by Wan [3], such changes should lead to an increased density of states near the Fermi level and, therefore, to an increased T_C as observed in our case. On the other hand, in [4] the highest value of the transition temperature T_C was observed for the sample, in which the *c* lattice constant (calculated from the MgB_2 002 peak position) had the smallest value with respect to the bulk data ($\Delta c/c$=-0.2%). However, some authors claim that T_C rises with lattice expansion [5-7]. Therefore, we feel it would be premature for us to deduce the superconducting properties from our experimental XRD result.

Figure presents the results of RBS measurements. It may be seen that in comparison to the spectrum of un-implanted sample (Mg), a pronounced valley centered at around channel 400 has appeared in the spectrum of as-implanted sample (a). This feature is associated with dilution of a

magnesium matrix with boron during implantation. The magnesium distribution after implantation exhibits a strange bimodal character, reflecting apparently the boron distribution. Such bimodal distributions in as-implanted samples were already reported in other cases although at the moment we see no explanation for this effect. Samples (b) and (c) were treated with 2 hydrogen plasma pulses with growing energy density (2 and 3 J/cm^2, respectively). It may be seen that the width of the valley (related to the width of the boron profile) grows with the pulse fluence. For sample (c), the boron profile seems to be spread over the greatest depth. On the other hand, the magnesium signal value at the minimum of the spectrum does not change significantly. Rough estimations based on SIMNRA simulations indicate that the magnesium content at the peak of boron profile amounts to no more than 15-25%. At the absence of other components of the surface layer, it means that the attained level of boron concentration is not less that 75-85% – far in excess of the stoichiometric composition of MgB_2. However, this excess of boron does not preclude the existence of MgB_2 phase, as evidenced by the XRD spectra (not shown here).

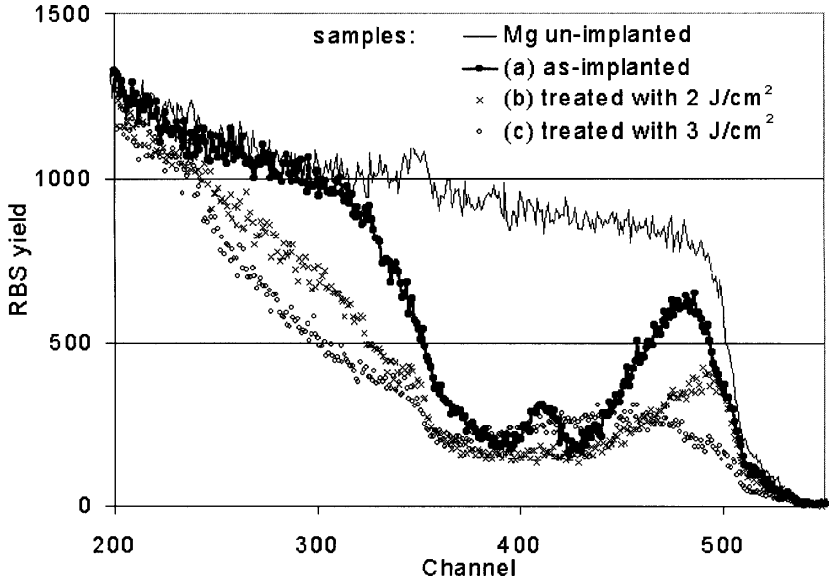

Fig. RBS spectra of: an un-implanted sample (Mg), as-implanted sample (a), sample (b) treated with 2 hydrogen plasma pulses of 2 J/cm^2 fluence, and sample (c) treated with 2 hydrogen plasma pulses of 3 J/cm^2 fluence.

The strongest MMMA signal hysteresis (higher by an order of magnitude with respect to samples (b) and (c)) has been obtained for the sample treated with 4 pulses of argon plasma at fluence of about 2 J/cm^2. However, T_C for that sample has a rather low value of about 12 K. This result demonstrates a possibility of creating a substantial amount of superconducting phase, with reduced T_C probably due to the lack of stoichiometry. Still no breakthrough occurred with respect to the macroscopic percolation of the superconductive regions.

We do not attribute special importance to the plasma pulse composition (hydrogen or argon). It is likely that rather the pulse energy and number of pulses determine the final result of the treatment. The highest T_C has been obtained for high-energy pulses, but the highest superconducting phase content has been obtained for the largest number of pulses, equivalent to a long diffusion time in the molten phase.

In further research, we plan to investigate effects of reduced ion implanted dose, increased pulse fluences and pulse multiplicity. We hope these treatment modifications help to spread and homogenize the superconducting phase.

The authors wish to thank Dr. R. Grötzschel (Forschungszentrum Rossendorf e.V.) for RBS measurements and Dr. W. Szymczyk (The Andrzej Sołtan Institute for Nuclear Studies) for his valuable assistance and comments.

References

[1]. Nagamatsu J., Nakagawa N., Muranaka T., Zenitani Y., Akimitsu J.: Nature, 410, 63-64 (2003).
[2]. Piekoszewski J., Kempiński W., Stankowski J., Richter E., Stanisławski J., Werner Z.: Superconductivity in MgB_2 thin films prepared by ion implantation and pulse plasma treatment. In: INCT Annual Report 2003. Institute of Nuclear Chemistry and Technology, Warszawa 2004, p.118.
[3]. Wan X., Dong J., Weng H., Xing D.Y.: www.cond-mat/0104216v3 (2001).
[4]. Yamazaki H., Hikita Y., Hori H., Takagi H.: Appl. Phys. Lett., 83, (18), 3740-3742 (2003).
[5]. Hur N., Scharma P.A., Guha S., Cieplak M.Z., Werder D.J., Horibe Y., Chen C.H., Choeng S.W.: Appl. Phys. Lett., 79, 4180-4183 (2001).
[6]. Tang J., Qin L.Ch., Matsushita A., Takano Y., Togano K., Kito H., Igara H.: Phys. Rev., 64, 132509-132511 (2001).
[7]. Neaton J.B., Perali A.: www.cond-mat/0104098v1 (2001).

EXPERIMENTAL EVIDENCE OF ATTRACTIVE INTERACTION BETWEEN THE NITROGEN ATOMS IN EXPANDED AUSTENITE FORMED IN IRON BY INTENSE NITROGEN PLASMA PULSES

Jerzy Piekoszewski[1,2/], Bożena Sartowska[2/], Lech Waliś[2/], Zbigniew Werner[1,3/], Michał Kopcewicz[4/], Friedrich Prokert[5/], Jacek Stanisławski[1/], Justyna Kalinowska[4/], Władysław Szymczyk[1/]

[1/] The Andrzej Sołtan Institute for Nuclear Studies, Świerk, Poland

[2/] Institute of Nuclear Chemistry and Technology, Warszawa, Poland

[3/] Institute of Physical Chemistry, Polish Academy of Sciences, Warszawa, Poland

[4/] Institute of Electronic Materials Technology, Warszawa, Poland

[5/] Institut für Ionenstrahlphysik und Materialforschung, Forschungszentrum Rossendorf e.V., Dresden, Germany

Several authors, *e.g.* [1,2], have shown that it is possible to nitride stainless steel in such a way that a metastable phase is formed in which nitrogen remains in solid solution, increasing the surface hardness and wear resistance without compromising the corrosion behaviour. This phase is referred to as a nitrogen-expanded austenite and is denoted as γ_N or S phase. Some of the authors, *e.g.* [3,4], claim that regardless of the processing used, the γ_N phase can only be formed if iron, chromium and nickel are available in the system, but the initial material needs not be of fcc (face centered cubic lattice) austenite structure. This finding has not been fully confirmed by other authors.

For example, it was demonstrated [5] that if nitriding is carried out with the use of high intensity nitrogen plasma pulses, the γ_N phase can be formed even in pure α-Fe – Armco.

On the other hand, in [6] it was shown that presence of γ_N also in carbon steels also improves their tribological properties. In the present work, we have undertaken the task to determine the character of the interaction between nitrogen atoms in γ_N phase formed in pure iron treated with high intensity nitrogen plasma pulses. In addition, the susceptibility of the lattice expansion in γ_N was considered. The choice of the pure Fe-N system is dictated by the fact that the influence of other elements in these interactions is avoided.

Armco samples were irradiated with 20 intense nitrogen plasma pulses. The duration of nitrogen plasma pulses is approximately 1 μs, and the energy density amounts to about 5 J/cm^2. Such pulses are capable to melt the surface layer of the substrate (1-2 μm) and to introduce a significant concentration of nitrogen into the molten layer. According to nuclear reaction analysis (NRA), the retained dose of nitrogen after 20 pulses was 5.5x10^{17} N/cm^2.

Apart from NRA, the samples were examined by X-ray diffraction (XRD) in grazing incident geometry (ω=2°) using CuK_α radiation and conversion electron Mössbauer spectroscopy (CEMS) methods. The thickness of the layer analysed by CEMS and XRD amounts to about 300 and 500 nm, respectively. From the NRA nitrogen profile we could deduce that in this range of thickness the analysed material contains from about 6.5 to 8.5 at.% of nitrogen.

The most important information derived from XRD data is summarised in Table. As it is seen, an expansion of the crystal lattice is confirmed [7,8]. However, the susceptibility for expansion of the lattice transformed to austenite from α-Fe by our pulse plasma treatment is smaller than in the case when the steel subjected to nitriding is originally of austenite type. It is clearly seen, when comparing, for example, the change of the lattice parameter in our case equal to about 2% with the value 2.9% observed in [8] for type 310 steel containing 8 at.% of nitrogen as in our case. This difference is certainly due to the difference in structure and composition of the initial materials, however the mechanism cannot be given at present.

The CEMS spectra were analysed by fitting various spectral components corresponding to the anticipated phases to the experimental data for both, the full and the reduced Doppler velocity scale. The results have shown that the majority of spectra represents austenitic phases γ_0 and γ_N, however small fractions of α, α' and α'' are also present. We believe that the signals corresponding to these fractions originate partly in the top layer of the sample where due to the low nitrogen concentration no

Table. XRD parameters of Armco sample after 20 pulses of nitrogen plasma.

(hkl)	2 Θ [deg]	FWHM [deg]	*a* [nm]	$(a-a_0)/a_0$ [%]	
				$a_0(1)$*	$a_0(2)$**
(200)	50.180	0.622	0.36332	2.056	1.29
(220)	73.652	0.838	0.36349	2.104	-
(311)	89.276	1.189	0.36361	2.138	-

* $a_0(1)$=0.356 nm extrapolated for pure austenit, after [7].

** $a_0(2)$=0.3587 nm for untreated 310 stainless steel, after [8].

complete α to γ transformation has occurred and partly in the deeper (>500 nm) layers where the nitrogen concentration is also low.

The values of the ratio $F\gamma_0/F\gamma_N$ fractions derived from the fitting procedure were used for semi-qualitative estimation of the character of the interaction between the nitrogen atoms present in the austenitic phases. To do this, we considered two models discussed first in [9].

In model A, we assume that the occupation of each of 6 octahedral sites occurs in the random way, *i.e.* there is no interaction between nitrogen atoms in the nearest neighbour positions of an iron atom. In model B, we assume, following [9], that strong repulsive forces act between both first- and second-nearest nitrogen atoms. So they tend to separate from each other.

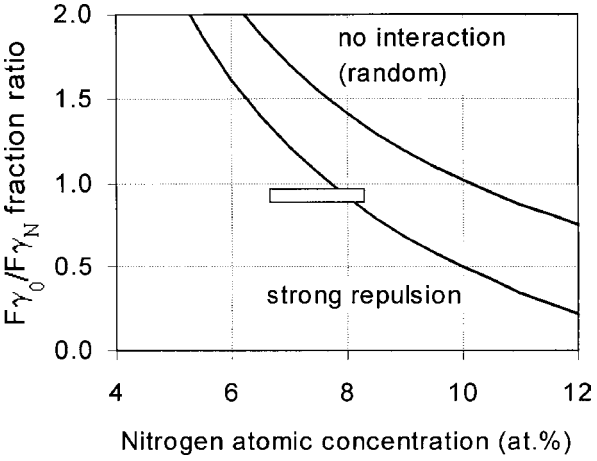

Fig. The box represents value of $F\gamma_0/F\gamma_N$ fraction ratio observed experimentally in Armco sample after 20 pulses of nitrogen plasma. The horizontal sides represent the range of experimentally measured concentrations, the vertical sides represent the estimated error of the $F\gamma_0/F\gamma_N$ fraction ratio. The solid lines show theoretical predictions assuming no interaction and strong repulsion between nitrogen atoms in nearest-neighbour positions.

In Figure, we depicted the calculated ratio of $F\gamma_0/F\gamma_N$ *vs.* nitrogen atomic concentration in the range of interest, *i.e.* from 4 to 12 at.% for cases A and B using the formulae given in [9]. Range of experimentally measured concentrations is represented by the horizontal sides of the box. The vertical sides represent the estimated error of the experimental $F\gamma_0/F\gamma_N$ fraction ratio. The position of the box has been established under the following assumptions: Firstly, we assume that all nitrogen atoms introduced into the sample are distributed in fcc structure. Such assumption seems to be justified by the fact that, according to Fe-N phase diagram, the nitrogen does not practically dissolve in the α-Fe phase. Secondly, we disregard the role of α' (martensite) and α'' ($Fe_{16}N_2$) phases since their fraction identified by CEMS analysis is very small. The length of the box on the nitrogen concentration scale is deduced from the analysis of the nitrogen concentration. As it is seen in Fig., the experimental result is definitely much closer to the data predicted by model B than by model A. Therefore, we conclude that strong repulsion forces act between both, the first and the second-nearest-neighbour nitrogen atoms in the fcc austenitic structure formed as a result of nitriding of pure iron by intense nitrogen plasma pulses.

We are grateful to Dr. L. Nowicki and Mrs. R. Ratajczak (The Andrzej Sołtan Institute for Nuclear Studies) for performing NRA measurements.

References

[1]. Blawert C., Mordike B.L., Jirásková Y., Schneeweiss O.: Surf. Eng., 15, 469 (1999).
[2]. Özturk O., Williamson D.L.: J. Appl. Phys., 77 (8), 3839 (1995).
[3]. Blawert C., Mordike B.L., Jirásková Y., Schneeweiss O.: Surf. Coat. Technol., 116-119, 1891 (1999).
[4]. Menthe E., Rie K.T., Schultze J.W., Simon S.: Surf. Coat. Technol., 74-75, 412 (1995).
[5]. Piekoszewski J., Langner J., Białoskórski J., Kozłowska B., Pochrybniak C., Werner Z., Kopcewicz M., Waliś L., Ciurapiński A.: Nucl. Instrum. Meth. Phys. Res., B80/81, 344 (1993).
[6]. Sartowska B., Piekoszewski J., Waliś L., Szymczyk W., Stanisławski J., Nowicki L., Ratajczak R., Kopcewicz M., Barcz A.: Modification of the near surface layer of carbon steels with intense argon and nitrogen plasma pulses. Vaccum, in press.
[7]. Gulaiev A.P.: Metalloviedenie. Izdatilestwo "Metallurgia", Moscow 1977, in Russian.
[8]. Saker A., Leroy Ch., Michel H., Frantz C.: Mater. Sci. Eng., A140, 702 (1991).
[9]. Oda K., Umezu K., Ino H.: J. Phys. Condens. Matter, 2, 10147 (1990).

PRETREATMENT OF AlN CERAMIC SURFACE PRIOR TO DIRECT BONDING WITH COPPER USING ION IMPLANTATION TECHNIQUE

Marek Barlak[1/], Wiesława Olesińska[2/], Jerzy Piekoszewski[1,3/], Marcin Chmielewski[2/], Jacek Jagielski[1,2/], Dariusz Kaliński[2/], Zbigniew Werner[1,4/], Bożena Sartowska[3/]

[1/] The Andrzej Sołtan Institute for Nuclear Studies, Świerk, Poland
[2/] Institute of Electronic Materials Technology, Warszawa, Poland
[3/] Institute of Nuclear Chemistry and Technology, Warszawa, Poland
[4/] Institute of Physical Chemistry, Polish Academy of Sciences, Warszawa, Poland

According to the recent literature, the direct bonding (DB) of ceramic substrates, especially aluminium nitride (AlN) to the conductor is considered as the most promising technique for electronic appli-

cations in high power density packing. In DB technique, the metal is joined immediately to the ceramics with only a very thin transition layer between metal-ceramic interface. In one of the pioneering works [1], it was shown that satisfactory results of AlN-Cu bonding can be achieved by addition of 1-1.5 at.% of oxygen as an active element to AlN-Cu system without intentional modification of surfaces of the joint components. Our previous, preliminary experiments with implanted titanium, iron and oxygen ions into AlN substrates were aimed at the replacement of the conventional process of thermal oxidation. The results obtained suggested that the best shear strength could be expected for relatively low energy of titanium ions [2]. In the present work, more systematic studies on this subject have been undertaken. Titanium, iron and oxygen ions were used at acceleration voltages of 15 and 70 kV in the dose range between 10^{16} and 10^{18} ions/cm^2. The metallic ions, *i.e.* titanium and iron, were implanted into commercial (Goodfellow) AlN substrates of 12x3x0.63 mm^3 with roughness of about R_a=0.1 μm, using MEVVA type TITAN implanter with direct beam, described in detail elsewhere [3]. Oxygen ions were implanted with non-mass separated beam in a home made semi-industrial implanter. In both cases to avoid overheating effects the samples were clamped onto a water-cooled stainless steel plate. The ion current densities were kept below 10 μA/cm^2, so the substrate temperature did not exceed 200°C. The metallic component of the joint, *i.e.* oxygen-free copper in the form of strips of 30x3x0.3 mm^3 was first annealed at 600°C for about 30-40 min in flowing nitrogen containing 1.5 ppm of oxygen. Subsequently, the copper component was oxidized in air at 380°C for 3 min. Following this preparatory procedure, the conventional DB process was performed and the resultant joints were examined with respect to their mechanical properties and microstructure. Figure 1 shows a dependence of the observed shear strength for different implantation conditions. The measured shear strengths were between 20 and 70 kG/cm^2 depending on implanted element, dose and energy. The implantation program started with higher dose range and since the best results were obtained for titanium ions the tests in lower dose range were continued only for this element. The following regularities can be inferred from these results:

- Oxygen implantation gives consistently better results than iron.
- For all elements, the lower energy of (15 kV) implantation leads to shear strength greater by a factor of about 2 than implantation at higher energy (70 kV).
- The best results are attained for titanium implantation with the optimum corresponding to a dose of 5x10^{16} cm^{-2}. The shear strength of such joints equal to about 70 kG/cm^2 exceeds by a factor of 5 the value (14 kG/cm^2) obtained using conventional isothermal oxidation AlN pretreatment process [2].
- For 70 kV, the shear strength is low and shows a weak dependence on ion dose. Searching for the reason of such distinct difference in behaviour of the joint, careful scanning electron microscopy (SEM) observations were performed on the fractured surfaces of both components of the joints.

The results of this inspection can be summarised as follows.

The strongest joints are of adhesive type over the entire surface. Over 90% of the copper surface in contact with the ceramics shows neither changes, nor inhomogeneities. The joint has a continuous and homogeneous structure. Only insignificant copper grooves are observed at the grain boundaries. They are associated with copper oxidation prior to the joining process. The ceramic surface has a homogeneous compact grain structure. The grain surfaces are covered homogeneously with nanoprecipitates. Small quantities of needle-shape precipitates are also present. An increase of titanium ion dose results in a growth of the number of needle-shape precipitates and in appearing of a new phase in the form of multifaceted crystals. On the other hand, an increase of both energy and dose of titanium ions gives rise to a growth of a grain-like phase.

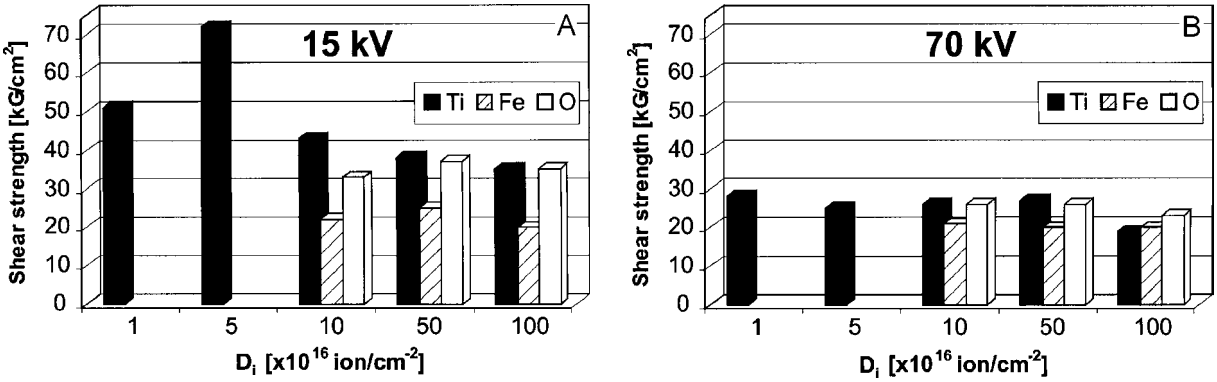

Fig.1. Summarized results of shear strength tests for various implantation conditions *i.e.* for 15 (A) and 70 kV (B) of acceleration voltage.

With regard to the other implanted ions, AlN/O-Cu joints are formed on no more that 30% of the surface. Copper ruptures together with the surface layer of the ceramic and the remaining copper surface exhibits deep surface morphology changes. Similar changes are observed at the AlN/Fe-Cu joint surfaces, the number of new phase precipitates being much greater than in the case of oxygen and the joint being with a laminar structure. Although as much as 60% of the surface is ruptured together

with the ceramic surface layer, these joints exhibit the lowest shear strength which means that the presence of iron atoms in the near surface layer of AlN deteriorates its mechanical toughness.

Both, iron and oxygen implantations, do not lead to substantial changes of the microstructures at the joint surfaces of ceramics and copper for different implantation conditions. Such effects are seen only for titanium.

In conclusions, ion implantation seems to be ideally suited for DB process. As it was shown, the optimised implantation process leads to much better results than a conventional process at a comparable processing time. The advantages of ion implantation include:

- potentially fast processing time, for instance, for ion beam intensities in the 100 mA range, the processing time would be of the order of minutes instead of tens of minutes in the conventional process;
- accuracy in creating an appropriate dopant content;
- flexibility in tailoring the desired distribution of the introduced atoms at nanometer depth range;
- ability to form non-equilibrium compounds.

References

[1]. Entezarian E., Drew R.: Mat. Sci. Eng., A212, 206, (1996).
[2]. Piekoszewski J., Olesińska W., Jagielski J., Kaliński D., Chmielewski M., Werner Z., Barlak M., Szymczyk W.: Solid State Phenom., 99-100, 231 (2004).
[3]. Bugaev S., Nikolaev A., Oks E., Schanin P., Yushkov G.: Rev. Sci. Instrum., 10, 3110 (1994).

NUCLEONIC CONTROL SYSTEMS AND ACCELERATORS

PRINCIPAL COMPONENT REGRESSION DATA PROCESSING IN RADON PROGENY MEASUREMENTS

Bronisław Machaj, Piotr Urbański

Random errors due to fluctuation of count rate originating from radon progeny disintegration, due to errors of air volume passed through an air filter and due to deposition errors, the accuracy of measurement and a minimum detectable concentration that can be measured are limited. The errors can be made lower by increasing airflow through the air filter, but this requires more energy and larger batteries that is in a portable gauge inconvenient. Much better solution is data processing that can decrease random errors. Principal component regression (PCR) is a processing method that is able to improve accuracy of a radon progeny monitor [1-2]. To investigate random error due to fluctuation of pulse count rate originating from disintegration of radon progeny, a computer program was developed for simulation of activity of radon progeny deposited on air filter [3]. Count rate corresponding to such activity was then randomized and such randomized count rate was PCR processed [4]. Investigations showed that random error could be made three times lower when the data were PCR processed comparing to readings without PCR processing. A further step in investigation of PCR processing for radon progeny monitor, presented here, were real measurements of radon progeny concentration in a radon chamber and their processing with the PCR method [5].

A series of 16 measurements, made with an RGR-40 radiometer [6], of radon progeny ^{218}Po, ^{214}Pb, ^{214}Po and PAE (potential alpha energy) concentration and corresponding to the 1 min mea-

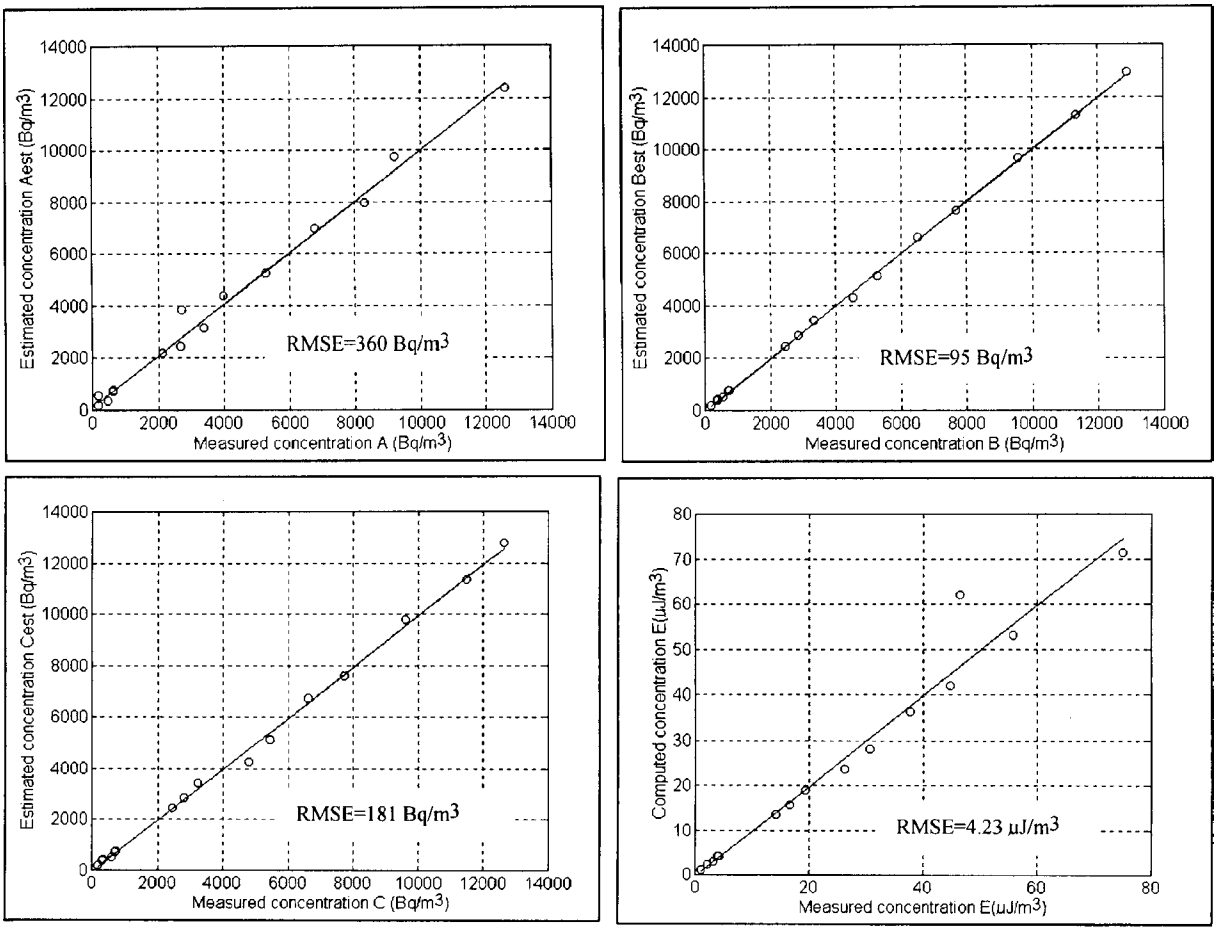

Fig. PCR estimated A_{est}, B_{est}, C_{est} and PAE_{est} concentration against measured concentration A (^{218}Po), B (^{214}Pb), C (^{214}Po), E (PAE) of radon progeny.

surement count rates were PCR processed. Estimated radon progeny concentration from PCR processing against the measured progeny concentration and root mean square error (RMSE) is shown in Fig. The RMSE that is a measure of random error due to pulse count fluctuation and other contributing random errors is: 360 Bq/m^3, 95 Bq/m^3, 181 Bq/m^3, and 4.23 μJ/m^3 for ^{218}Po, ^{214}Pb, ^{214}Po and PAE, correspondingly. RMSE for three interval model presented in [7] is: 469 Bq/m^3, 507 Bq/m^3, 285 Bq/m^3, and 4.35 μJ/m^3 for ^{218}Po, ^{214}Pb, ^{214}Po and PAE, correspondingly. On the average, the RMSE for ^{218}Po, ^{214}Pb and ^{214}Po is 2.7 times higher than for PCR processing. The slope of regression line for ^{218}Po and ^{214}Pb differs from unity by approximately 10% (the slope is 0.9 for ^{218}Po, and 1.08 for ^{214}Pb).

References

[1]. Martens H., Naes T.: Multivariate calibration. Wiley & Sons, Chichester 1991.
[2]. Rencher A.C.: Multivariate statistical interference and application. John Wiley & Sons, New York 1996.
[3]. Machaj B., Bartak J.: Nukleonika, 43, 2, 175-184 (1998).
[4]. Machaj B., Urbanski P.: Nukleonika, 47, 1, 39-42 (2002).
[5]. Machaj B., Urbanski P.: Nukleonika, 49, 3, 123-129 (2004).
[6]. Gierdalski J., Bartak J., Urbanski P.: Nukleonika, 38, 4, 27-32 (1993).
[7]. Thomas J.W.: Health Phys., 23, 783-789 (2001).

RADIATION SOURCE CONTROLLER KAI-2

Bronisław Machaj, Edward Świstowski, Jan Mirowicz

During production of medical radiation sources on production line, every 12 s a new capsule containing ^{131}I isotope is packed into a lead container. Packed in the lead container sources are then delivered to hospitals and clinics. To exclude the case when because of faulty operation of packing mechanism, the capsule with radiation source was not packed into the lead container, additional control of the containers leaving the production line is needed. Such control is ensured by the radiation source controller KAI-2. Block diagram shown in Fig. illustrates the principle of operation of the controller.

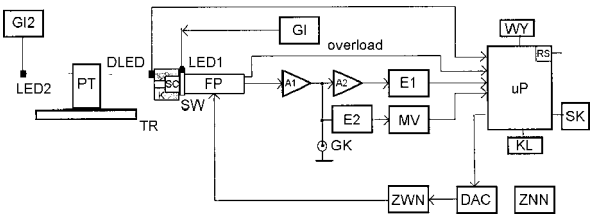

Fig. Block diagram of the controller: PT – source container with the source; TR – transport conveyor; K – collimator; LED1 – reference light pulse source; GI, GI2 – pulse generators; LED2 – IR light beam source; DLED – IR sensor; SC – NaI(Tl) scintillator; SW – lightguide; FP – photomulltiplier tube; A1, A2 – pulse amplifiers; E1 – discriminator of ^{131}I pulses; E2 – discriminator of LED1 pulses; MV – monovibrator; uP – microprocessor system; RS – serial port; WY – display; KL – keyboard; SK – control signals (ready, measurement, alarm); ZWN – high voltage power supply; ZNN – low voltage power supply; DAC – digit-to-analog converter; GK – control socket.

The container with the ^{131}I source in measuring position in front of the scintillation probe is sensed with an infrared (IR) light beam source and an IR sensor. Radiation collimator in front of the scintillation detector ensures that the radiation from the neighboring containers is not incident on scintillation detector. After amplification and shaping of the pulses originated from ^{131}I, the pulses are passed through pulse discriminator E1 and are counted by pulse counter under the control of microprocessors unit. Count rate, a few times higher than the background count rate, indicates that the source container is packed with the source. Counting time is fixed and is equal to 5 s. To handle the wide variation of radiation intensity in the span 1:300, dc current of the last dynode of photomultiplier tube (PMT) is measured that, at very high pulse count rate, produces an "overload" signal. For a very high count rate of paralyzing pulse measuring channel, the overload signal is an indicator of radiation source in the source container. To ensure stable operation of the scintillation detector, an automatic gain control circuit of PMT is used. Reference light pulses are generated by reference light emitting diode. The diode is coupled with the PMT by means of a lightguide. The PMT high voltage is increased or decreased as to get pulse amplitude originating from light emitting diode equal to discrimination level E2. In such a case, at the monovibrator output logic "1" is produced that is sensed by the microprocessor. The high voltage of the PMT is regulated by the microprocessor through digit-to-analog converter controlling high voltage power supply. The PMT gain is automatically controlled at the beginning of each counting interval.

Control of the containers is carried out in a closed loop cycle: PMT automatic gain control (1 s) – awaiting for the container in measuring position – count rate measurement (5 s) when the container in measuring position. Measured count rate is displayed, stored in the controller memory and is sent to an external computer by RS485 serial port. Alarm signal is generated in case when no source in the source container is detected. The controller is equipped with functions enabling check up proper operation of the controller and facilitating installation of the controller at production line.

GAMMA COUNTER LG-1

Bronisław Machaj, Jakub Bartak, Adrian Jakowiuk

Radioimmunoassay (RIA) analysis is widely used in medical laboratories in the process of diagnosis of illness of patients [1]. Large size laboratories employ for this purpose multi-well gamma counters [2] or gamma counters with automatic sample changing [3]. For medium size laboratories, a few well-type gamma counters seems sufficient [4]. For small size laboratories, a single well-type gamma counter is required and such a gamma counter with proper software has been developed. Block diagram of the counter illustrating the principle of operation is shown in Fig.

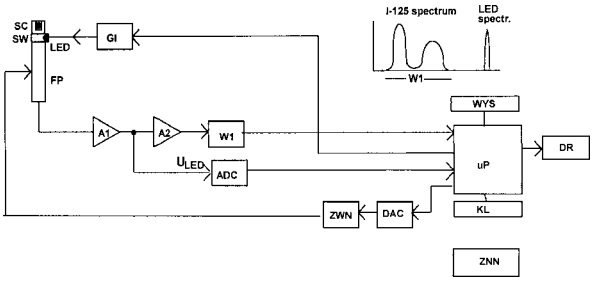

Fig. Block diagram of measuring channel of gamma counter: SC – well scintillator NaI(Tl); SW – lightguide; LED – light emitting diode; FP – photomultiplier tube; GI – pulse generator approximately 1000 p/s; A1, A2 – pulse amplifier; W1 – single channel analyzer; ADC – analog-to-digit converter for LED pulse measurement; ZNN – low voltage supply; ZWN – high voltage supply; DAC – digit-to-analog converter; WYS – LCD display; KL – keyboard; uP – microprocessor; DR – external printer; U_{LED} – LED pulse discrimination level.

^{125}I radiation of the analyzed sample is measured with an NaI(Tl) well scintillator. The pulses from a photomultiplier tube (PMT) after amplification and shaping in two pulse amplifiers are counted by a single channel analyzer under the control of a microprocessor system. The measured count rate is proportional to the activity of measured sample in the energy range 15-80 keV.

To ensure high stability of the measurement, an automatic gain control circuit is employed. Light emitting diode (LED) fixed in the lightguide and a pulse generator are used to produce reference light pulses for automatic gain control circuit of the PMT. During the gain control process, the pulse generator is activated and reference light pulses are generated. Immediately after the gauge is switched on, the microprocessor system starts to increase the PMT high voltage through a digit-to-analog converter, beginning from some minimum voltage. Simultaneously, pulse voltage originating from the reference light pulse is compared if it is not higher than the fixed LED pulse discrimination level. As soon as the pulse voltage becomes higher than the discrimination level, the increase of PMT voltage is stopped. Automatic gain control is carried out after the gauge is switched on. Additionally, when measurements of samples are carried out, the gain of the PMT is automatically checked at the beginning of each measuring cycle and, if needed, is automatically corrected.

To decrease the background due to natural radiation, the scintillator is shielded by a layer of lead. Pulse count rate originating from the measured radiation is proportional to the concentration of the determined substance in the investigated sample. Random error due to statistical fluctuations of ionizing radiation is kept to an acceptable level by selecting time of measurement (from 1/4 to 8 min). Random error connected with preparation of samples to be measured is decreased to an acceptable level by measuring two or three samples (vials) with the same concentration. Standard RIA or immunoradiometric assay (IRMA) includes the following steps: setting measuring parameters, measurements of reference samples, calibration curve computation, measurement of control samples, and at the end measurement of unknown samples. The software of the counter enables programming of all the steps of an analysis that is to be carried out. Digital processing of the measured pulse count rate matches two types of calibration curves:

- type RIA – Pulse count rate decreases against the substance concentration. Calibration curve: lin(A/Ao) *vs*. log(CONC);
- type IRMA – Pulse count rate increases against the substance concentration. Calibration curve: log(A/T) *vs*. log(CONC);

where: A – sample pulse count rate, Ao – pulse count rate at the concentration CONC=0 for curve RIA, T (TOTAL) – pulse count rate corresponding to the total activity of the sample. If repeated samples of the same concentrations are measured (two or three samples), the average count rate is taken in constructing the calibration curve. The results of calibrating measurements and the calibration curve, as well as the results of measurements of the control samples and unknown samples are printed on a computer (tractor) paper that makes a written document of the analysis performed.

References

[1]. Chard T.: Introduction to radioimmunoassay and related techniques. www.alibris.com/search/search.cfm.
[2]. Laboratory Technologies Instrumentation. www.labtechnic.com/productsservices/instrumentation.htm.
[3]. Packard cobra gamma counters. www.gmi-inc.com/Products/packard cobra.htm.
[4]. LG-4 gamma counter. www.zami.ajaksoft.com.pl/eng.htm.

APPLICATION OF ARTIFICIAL NEURON NETWORK FOR IMAGE ANALYSIS

Adrian Jakowiuk

During a morphologic analysis of an image with the use of Minkowski functionals, three functionals are obtained having the form of function [1]. On the basis of such functions, determination of variations between similar pictures is possible. Impossible is, however, classification of some objects existing on the picture to determined groups by means of some simple methods.

To analyze the functions obtained, the Counter Propagation (CP) neuron network was used [2]. The task of this neuron network is classification of elements existing in the analyzed picture. This is done on the basis of Minkowski functionals for each fragment of the picture.

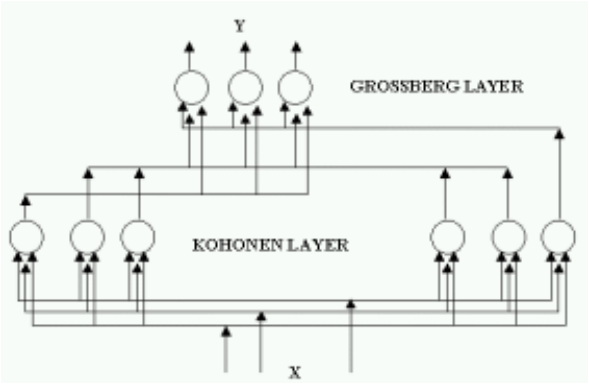

Fig.1. Diagram of CP neural network.

The CP network was created by Robert Hecht-Nielsen as a compilation of Kohonen and Grossberg network. The diagram of the CP network is shown in Fig.1. The network is called the transmitting counter network. Due to a simple principle of operation, functioning of the network is comparable to reading out of a result from a table. The operation of the network is not limited anyhow to such activity. Its input layer makes additionally an adaptive classification of input stimulus that enables for generalizing the accumulated experience. Additionally, the CP, similarly as all other networks, can be taught (trained), which allows for application of the network in a wide range of interesting applications.

Fig.2. Example of four text pictures (characters), each 100x100 pixels.

In order to check up if the selected type of neuron network will function properly in practice, a test software was developed, the task of which is:

- computation of Minkowski functionals for the picture,
- analysis of obtained functionals by means of neuron network.

Operation of the network was tested on the picture containing 26 characters of Latin alphabet. The pictures have 100x100 pixels resolution. The example characters are shown in Fig.2.

Minkowski functionals were computed for each of the pictures (characters) (A, L, X) and their com-

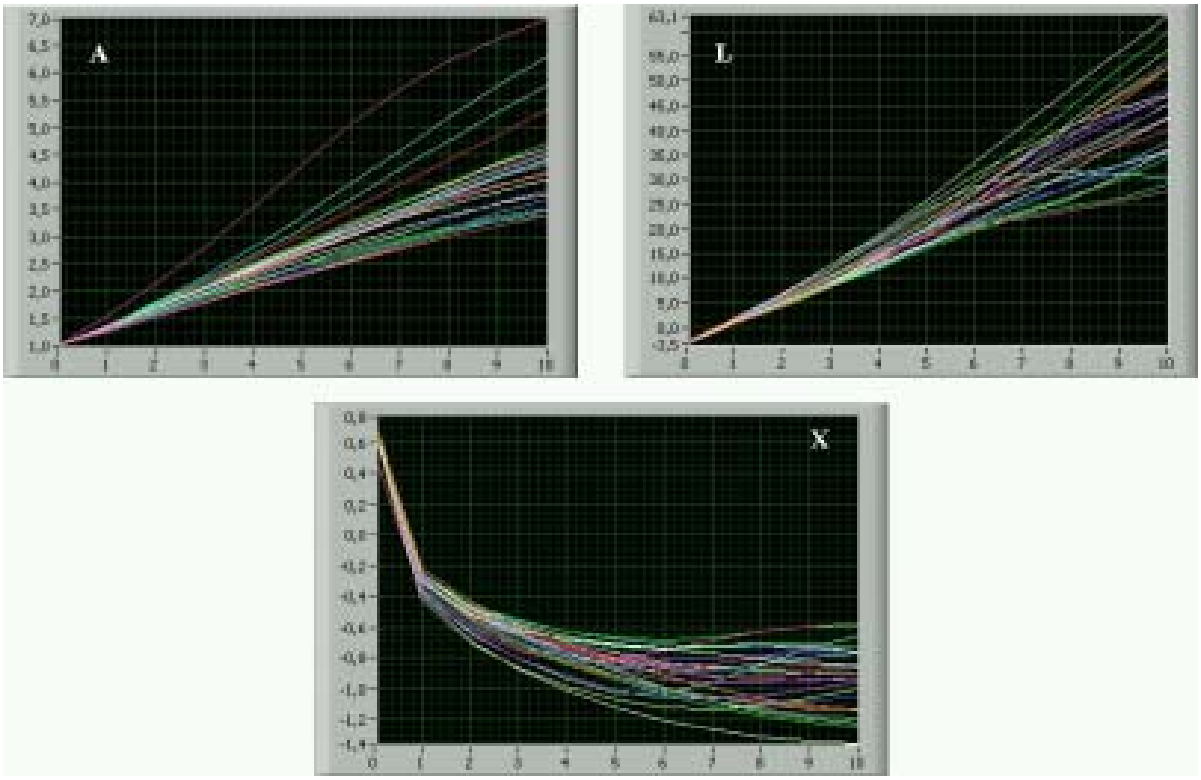

Fig.3. Obtained Minkowski functionals.

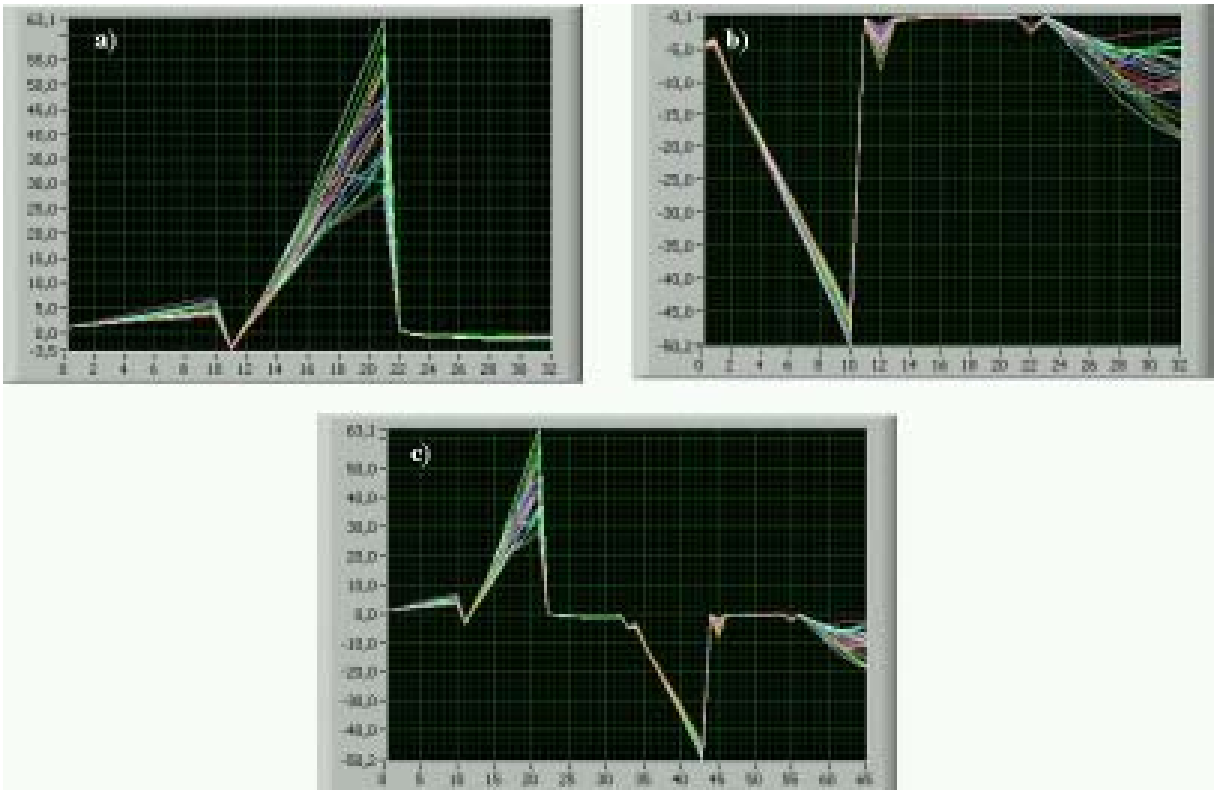

Fig.4. Vectors used for teaching the neuron network made from the variables: a) A, L, X; b) L/X, AL/X, LX/A; c) all functionals.

binations (L/X, AL/X, LX/A) [3]. The Minkowski functionals are shown in Fig.3.

To teach the neuron network, three combinations of the variables were used:

- vector made from Minkowski functional A, L and X (Fig.4a);
- vector made from Minkowski functionals combination, L/X, AL/X and LX/A (Fig.4b);
- all the functionals shown as one vector (Fig.4c).

The network was trained (taught) with the use of the following parameters:

- number of characters to be recognized – 26;

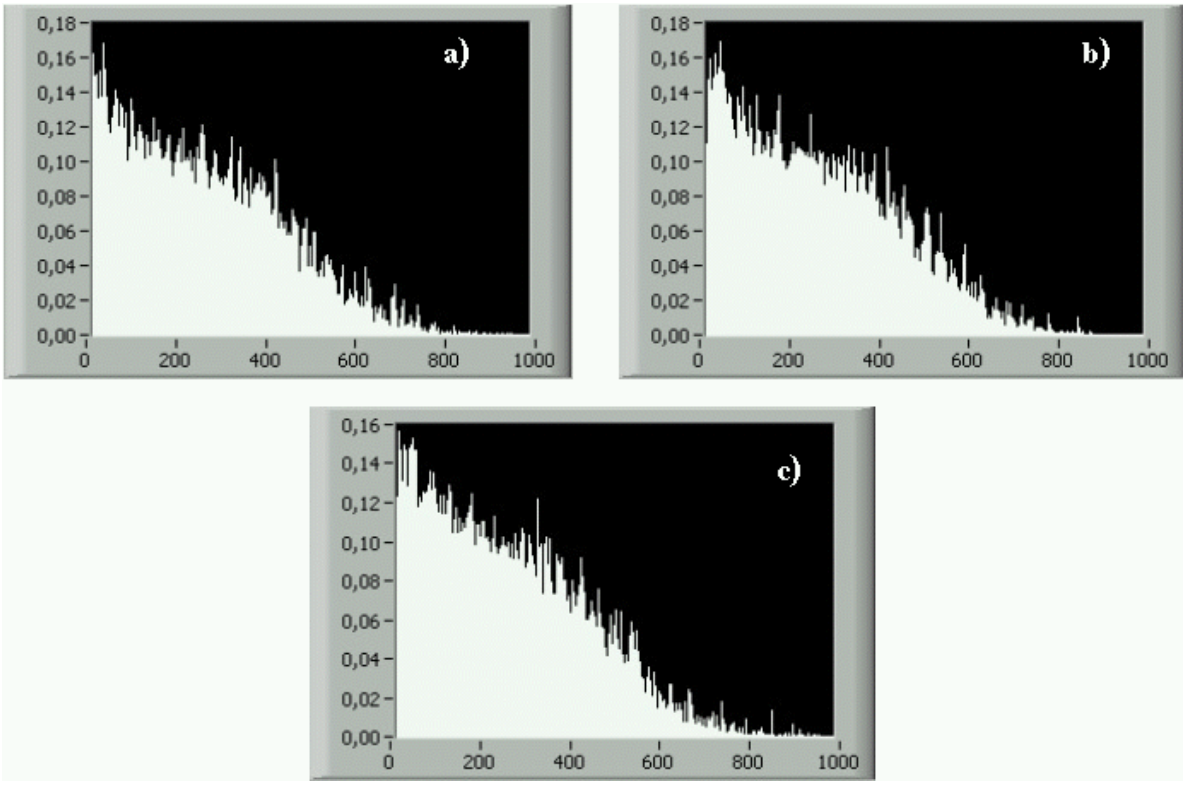

Fig.5. Speed of teaching of neuron network. X-axis shows number of steps, Y-axis – average MSE (mean squared error) for every 10 steps for the combination: a) A, L, X; b) L/X, AL/X, LX/A; c) all functionals.

- number of training steps – 1000;
- number of inputs:
  - for input vectors 1 and 2 – 33,
  - for vector 3 – 66;
- number of neurons in hidden layer (number of characters to be recognized multiplied by number of outputs from the network) – 416;
- number of neuron outputs – 16;
- initial training coefficient of the first layer – 0.7;
- initial training coefficient of the second layer – 0.3;
- activation function – linear.

The neuron network was taught successfully to recognize the characters at the use all the three training vectors. The diagrams showing the speed of teaching the neuron network are shown in Fig.5. In each of the cases, the neuron network was taught to recognize all the characters. The network was taught slightly quicker when the input vectors were values of the functionals A, L, X.

Use of selected neuron network for the analysis of elements existing in a picture is possible. For such a possibility, indicate the results of the tests of neuron network that were carried out. The network war taught (trained) to recognize the characters of Latin alphabet. Similar successful tests were also done for a dozen of selected characters of Japanese alphabet.

References

[1]. Michielsen K., De Raedt H.: Comp. Phys. Commun., 132, 94-103 (2000).
[2]. Tadeusiewicz R.: Sieci neuronowe, AOW, Warszawa 1993, p.65, in Polish.
[3]. Jakowiuk A.: Use of multivariate analysis to image processing. In: INCT Annual Report 2003. Institute of Nuclear Chemistry and Technology 2004, p.135.

KLYSTRON MODULATOR FOR "ELEKTRONIKA 10/10" ACCELERATOR

Zygmunt Dźwigalski, Zbigniew Zimek

Poor accelerator availability, instability of accelerator parameters and high cost of "Elektronika 10/10" accelerator exploitation are connected to the characteristics of microwave sources applied by the accelerator producers. A program of linear electron accelerator "Elektronika 10/10" upgrading towards higher technical and economical effectiveness, better operational characteristics suitable for radiation processing is proposed.

The objectives of the project are related to the replacement of a short live time magnetron, type MI470, of a microwave source (1.863 GHz) for a modern TH2158 klystron device operated at a frequency of 2.856 GHz according to European standards and adopting the accelerator section to the new source.

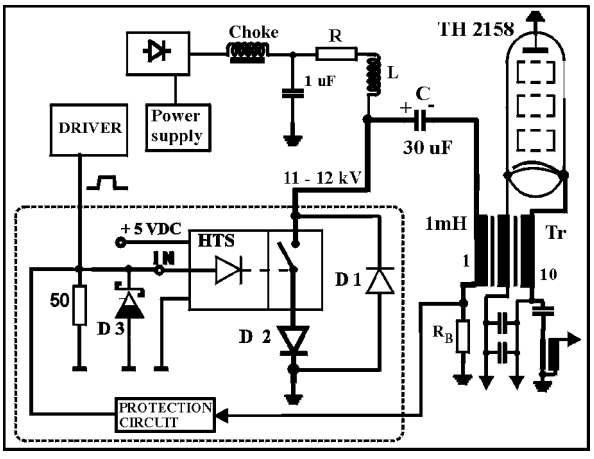

Fig.1. The electrical circuit of the modulator.

The main aim of this work is to ensure the pulse power supply stand-modulator for the klystron. The electrical circuit of the modulator with incomplete discharge of the energy storage capacitors is shown in Fig.1. The modulator was designed using the following assumptions:

- average real output power – about 40 kW,
- maximum operating voltage – 13 kV,
- maximum switching frequency (repetition frequency) – 400 Hz.

The basic klystron modulator parameters are given in Table 1. The basic elements of the klystron pulse modulator are: charging supply, bank of energy storage capacitors, on-off high voltage solid-state switch,

Table 1. Klystron modulator parameters.

Parameters	Value	Units
Klystron frequency	2.856	GHz
Klystron voltage (max)	122	kV
Klystron current (max)	91	A
Klystron efficiency (min)	45	%
Perveance	1.75-2x10^{-6}	A/V$^{1.5}$
Repetition frequency (max)	400	Hz
Modulator pulse width (max)	18	μs
Pulse voltage rise time (10-90)	1.5	μs
Pulse voltage fall time (10-90)	1.5	μs
Modulator capacity voltage (max)	13	kV
Step-up pulse transformer ratio	1:10	-
Flat top voltage deviation	<5	%

and pulse transformer. The modulator parameters were calculated using a simple model. The solid-state switch was modelled by using one closing and one opening switch. The non-linear klystron impedance is modelled as a linear resistor. The pulsed transformer is modelled as a linear transformer. The simulated example of the voltage shape on the klystron is shown in Fig.2.

It is known from technical documentation that perveance of the TH2158 klystron should be in the

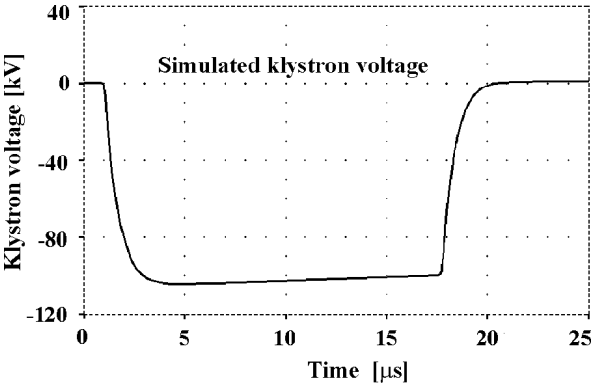

Fig.2. Simulated klystron voltage.

range from 1.75×10^{-6} to 2×10^{-6} A/V$^{1.5}$, according to the formula:

Klystron perveance = $(I_{klystron}/V_{beam\ voltage})^{1.5}$

The current klystron is between 60 and 70 A for 100-105 kV klystron beam voltage.

The stability and reproducibility of the RF pulses from klystron are very dependent on the modulator voltage flat top performance. It was, therefore, decided that the voltage drop on the klystron should be less than 5%. It is clear from the calculation that capacitance of the bank of modulator energy storage capacitors must be not less than 30 μF. The capacitors with the following parameters: 10 μF/15KVDC, 500 nH inductance, design life 100,000 hours plus, 0.003 dissipation factor, will be applied.

The modulator will be completed with tanked pulse transformer (pulse transformer, oil tank, klystron heater transformer, DC reset inductor, pulse current monitor, capacitive voltage divider, bypass capacitors).

The pulse transformer due to precision winding and construction techniques provides time to 1 μs (10-90) for a 18 μs pulse length.

The modulator will be using a commercial fast high voltage transistor switch, type HTS 181-160-FI, as the on-off switch operating at about 12 kV in the primary transformer circuit. The switch is protected by external diodes (D1 and D2), because the risk of current reversal exists. The switches are made up of a large number of a combination of classical bipolar transistors with the modern vertical MOSFET, lying parallel and in series, which are combined into a compact, low-inductance bank. A TTL-compatible control signal and a 5-volt auxiliary voltage is all that is required on the input side. We know that the proposed new solid-state devices offer a promise of higher efficiency and longer lifetimes [1-6] at a time when the availability of standard technologies is becoming questionable. The HTS 181-160-FI switch has low switching and on-state losses (only 500 W for 40 kW output power of the modulator). Then the efficiency of the switch is >98%. The basic switch parameters are given in Table 2.

Table 2. Parameters of the HTS 181-160-FI switch.

Parameters	Value	Units
Breakdown voltage	18	kV
Maximum reverse blocking voltage	540	V
Typical saturation voltage	82 ($0.1 \times I_{peak}$) 250 ($1 \times I_{peak}$)	V
Maximum peak current	1600 t_p < 100 μs	A
Maximum continuous frequency	500	Hz
Turn-on delay time	*ca.* 130	ns
Typical turn-on rise time	80 ($0.1 \times I_{peak}$) 180 ($1 \times I_{peak}$)	ns
Typical turn-off rise time	*ca.* 1 (resistive load)	μs
Switch natural capacitance	approx. 90	pF
Coupling capacitance	approx. 100	pF

References

[1]. Cook E.G.: Review of solid-state modulators. In: Proceedings of the XX International Linac Conference, Monterey, USA, 21-25 August 2000, pp.663-667.

[2]. Krasnykh A.: Analyses of klystron modulator approaches for NLC. In: Proceedings of the XX International Linac Conference, Monterey, USA, 21-25 August 2000, pp.772-774.

[3]. Gaudreau M.P.J., Casey J., Mulvaney J.M., Kempkes M.A.: Solid-state high voltage pulse modulators for high power microwave applications. In: Proceedings of the EPAC 2000, Vienna, Austria, 26-30 June 2000, pp.2361-2363.

[4]. Akemoto M., Chin Y.H., Sakamoto Y.: High-power klystron modulator using solid-state IGBT modules. In: Proceedings of the Second Asian Particle Accelerator Conference, Beijng, China, 17-21 September 2001, pp.618-620.

[5]. Pearce P., Sermeus L., Shen L.: A 50 Hz low-power solid-state klystron modulator. In: Proceedings of the European Pulsed Power Symposium, French German Research Institute, Saint Louis, France, 22-24 October 2002, pp.1-6.

[6]. Dolgov A., Kildisheva O.: Problems of Atomic Science and Technology, Series: Nuclear Physics Investigations, 42, 1, 66-68 (2004).

THE INCT PUBLICATIONS IN 2004

ARTICLES

1. **Ambroż H.B., Kemp T.J., Rodger A., Przybytniak G.**
   Ferric and ferrous ions: binding to DNA and influence on radiation-induced processes.
   Radiation Physics and Chemistry, 71, 1023-1030 (2004).

2. **Ambroż H.B., Kornacka E.M., Przybytniak G.K.**
   Influence of cysteamine on the protection and repair of radiation-induced damage to DNA.
   Radiation Physics and Chemistry, 70, 677-686 (2004).

3. **Barysz M., Leszczyński J., Bilewicz A.**
   Hydrolysis of the heavy metal cations: relativistic effects.
   Physical Chemistry Chemical Physics, 6, 4553-4557 (2004).

4. **Bik J.M., Rzymski W.M., Głuszewski W., Zagórski Z.P.**
   Electron beam crosslinking of hydrogenated acrylonitrile-butadiene rubber.
   KGK Kautschuk Gummi Kunststoffe, 57, 12, 651-655 (2004).

5. **Bilewicz A.**
   Ionic radii of heavy actinide(III) cations.
   Radiochimica Acta, 92, 69-72 (2004).

6. **Bilewicz A.**
   Sorption properties of stainless steel membranes impregnated with titanium dioxide sorbent.
   Nukleonika, 49, 4, 163-165 (2004).

7. **Bojanowska-Czajka A., Drzewicz P., Trojanowicz M.**
   Usuwanie zanieczyszczeń wód i ścieków przy użyciu promieniowania jonizującego (Application of ionizing radiation for removal of pollutants from water and wastes).
   Ekologia, 2, 8-9,28-29 (2004).

8. **Chajduk-Maleszewska E., Dybczyński R.**
   Selective separation and preconcentration of trace amounts of Pd on Duolite ES 346 resin and its use for the determination of Pd by NAA.
   Chemia Analityczna, 49, 281-297 (2004).

9. **Chajduk-Maleszewska E., Dybczyński R., Salvini A.**
   Oznaczanie zawartości wybranych pierwiastków w liściach herbaty za pomocą neutronowej analizy aktywacyjnej (Elemental analysis of the black and green tea leaves by instrumental neutron activation).
   Polish Journal of Human Nutrition and Metabolism, 31, Supplement 1, part II, 205-206 (2004).

10. **Cheblukov Yu.N., Didyk A.Yu., Hofman A., Semina V.K., Starosta W.**
    The influence of defect structure on the surface sputtering of metals under irradiation of swift heavy ion in the inelastic energy loss region.
    Nukleonika, 49, 1, 15-21 (2004).

11. **Chiarizia R., Jensen M.P., Borkowski M., Thiyagarajan P., Littrell K.C.**
    Interpretation of third phase formation in the Th(IV)-HNO_3, TBP-*n*-octane system with Baxter's "sticky spheres" model.
    Solvent Extraction and Ion Exchange, 22, 3, 325-351 (2004).

12. **Chiarizia R., Jensen M.P., Rickert P.G., Kolarik Z., Borkowski M., Thiyagarajan P.**
    Extraction of zirconium nitrate by TBP in *n*-octane: influence of cation type on third phase formation according to the "sticky spheres" model.
    Langmuir, 20, 10798-10808 (2004).

13. Chmielewski A.G., Licki J., Pawelec A., Tymiński B., Zimek Z.
Operational experience of the industrial plant for electron beam flue gas treatment.
Radiation Physics and Chemistry, 71, 441-444 (2004).

14. Chmielewski A.G., Sun Y.-X., Bułka S., Zimek Z.
Chlorinated aliphatic and aromatic VOC decomposition in air mixture by using electron beam irradiation.
Radiation Physics and Chemistry, 71, 437-440 (2004).

15. Chwastowska J., Skwara W., Sterlińska E., Dudek J., Pszonicki L.
Analiza specjacyjna chromu w wodach mineralnych (Speciation analysis of chromium in mineral waters).
Polish Journal of Human Nutrition and Metabolism, 31, Supplement 1, part I, 228-230 (2004).

16. Chwastowska J., Skwara W., Sterlińska E., Pszonicki L.
Determination of platinum and palladium in environmental samples by graphite furnace atomic absorption spectrometry after separation on dithizone sorbent.
Talanta, 64, 224-229 (2004).

17. Cieśla K., Rahier H., Zakrzewska-Trznadel G.
Interaction of water with the regenerated cellulose membrane studied by DSC.
Journal of Thermal Analysis and Calorimetry, 77, 279-293 (2004).

18. Cieśla K., Salmieri S., Lacroix M., Le Tien C.
Gamma irradiation influence on physical properties of milk proteins.
Radiation Physics and Chemistry, 71, 95-99 (2004).

19. Danilczuk M., Pogocki D., Lund A., Michalik J.
Interaction of silver atoms with ethylene in Ag-SAPO-11 molecular sieve: an EPR and DFT study.
Physical Chemistry Chemical Physics, 6, 1165-1168 (2004).

20. Danko B., Polkowska-Motrenko H., Ammerlaan M.J.J.
Oznaczanie zawartości pierwiastków śladowych w wybranych produktach żywnościowych za pomocą NAA (Determination of trace elements in the selected food products by NAA).
Polish Journal of Human Nutrition and Metabolism, 31, Supplement 1, part II, 201-202 (2004).

21. Drzewicz P., Nałęcz-Jawecki G., Gryz M., Sawicki J., Bojanowska-Czajka A., Głuszewski W., Kulisa K., Wołkowicz S., Trojanowicz M.
Monitoring of toxicity during degradation of selected pesticides using ionizing radiation.
Chemosphere, 57, 135-145 (2004).

22. Drzewicz P., Trojanowicz M., Zona R., Solar S., Gehringer P.
Decomposition of 2,4-dichlorophenoxyacetic acid by ozonation, ionizing radiation as well as ozonation combined with ionizing radiation.
Radiation Physics and Chemistry, 69, 281-287 (2004).

23. Dybczyński R., Danko B., Kulisa K., Chajduk-Maleszewska E., Polkowska-Motrenko H., Samczyński Z., Szopa Z.
Final certification of two reference materials for inorganic trace analysis.
Chemia Analityczna, 49, 143-158 (2004).

24. Dybczyński R., Danko B., Kulisa K., Maleszewska E., Polkowska-Motrenko H., Samczyński Z., Szopa Z.
Preparation and preliminary certification of two new Polish CRMs for inorganic trace analysis.
Journal of Radioanalytical and Nuclear Chemistry, 259, 3, 409-413 (2004).

25. Dybczyński R., Polkowska-Motrenko H.
Działalność IChTJ w zakresie zapewnienia jakości w analizie i jej związek z kontrolą żywności (The activity of the Institute of Nuclear Chemistry and Technology in the field of analytical quality assurance and its relevance to food analysis).
Polish Journal of Human Nutrition and Metabolism, 31, Supplement 1, part I, 234-235 (2004).

26. Filipiak P., Hug G.L., Carmichael I., Korzeniowska-Sobczuk A., Bobrowski K., Marciniak B.
Lifetimes and modes of decay of sulfur-centered radical zwitterions containing carboxylate and phenyl groups.
Journal of Physical Chemistry A, 108, 6503-6512 (2004).

27. Fuks L., Gniazdowska E., Mieczkowski J., Narbutt J., Starosta W., Zasępa M.
Structure and vibrational spectra of *fac*-$Re^{I}(CO)_3^+$ complex with *N*-methyl-2-pyridinecarbothioamide.
Journal of Organometallic Chemistry, 689, 4751-4756 (2004).

28. Gasińska A., Adamczyk A., Kojs Z., Szumiel I.
Are stromal fibroblasts from cervical tumors suitable to predict normal tissue radiation reaction?
Neoplasma, 51, 4, 285-292 (2004).

29. Głuszewski W.
Higienizacja i sterylizacja radiacyjna (Hygienization and radiation sterilization).
Hygeia, 28, 77-81 (2004).

30. Głuszewski W., Panta P.
Kontrola dozymetryczna promieniowania elektronowego (Dosimetric control of high energy EB).
Współczesna Onkologia, 8, 7, 342-346 (2004).

31. Grądzka I., Buraczewska I., Iwaneńko T., Sochanowicz B., Szumiel I.
Post-irradiation recovery in human glioma M059K cell line and its DNA-PK_{CS} deficient counterpart M059J: effect of signaling pathways inhibitors.
Central European Journal of Occupational and Environmental Medicine, 10, s62 (2004).

32. Grądzka I., Buraczewska I., Sochanowicz B., Szumiel I.
Radiosensitization of human glioma M059J and M059K cells by signaling pathways inhibitors: effects on DNA double-strand break repair and apoptosis.
European Journal of Biochemistry, 271, Supplement 1, 9 (2004).

33. Grigoriew H., Luboradzki R., Cunis S.
In situ studies of monosaccharide gelation using the small-angle X-ray scattering time-resolved method.
Langmuir, 20, 7374-7377 (2004).

34. Grigoriew H., Łukasiewicz A., Chmielewska D.K., Płusa M., Bernstorff S.
Structural change on the silica gel caused by its treatment with heavy metal complexes of aminoalcohols.
Polish Journal of Chemical Technologies, 6, 1, 14-16 (2004).

35. Grodkowski J., Mirkowski J., Płusa M., Getoff N., Popov P.
Pulse radiolysis of aqueous diphenyloxide.
Radiation Physics and Chemistry, 69, 379-386 (2004).

36. Gryz M., Starosta W., Leciejewicz J.
Diaqua-*trans*-bis(pyridazine-3-carboxylato-κ^2O,N)-zinc(II).
Acta Crystallographica E, 60, 1481-1483 (2004).

37. Harasimowicz M., Zakrzewska-Trznadel G., Chmielewski A.G.
Wykorzystanie metod membranowych w procesach wzbogacania biogazu w metan (Application of membrane methods for enrichment of biogas in methane).
Monografie Komitetu Inżynierii Środowiska PAN, 22, 429-433 (2004).

38. Jankowska A., Biesiaga M., Drzewicz P., Trojanowicz M., Pyrzyńska K.
Chromatographic separation of chlorophenoxy acid herbicides and their radiolytic degradation products in water samples.
Water Research, 38, 3259-3264 (2004).

39. Kałuska I., Lazurik V.T., Lazurik V.M., Popov G.F., Rogov Yu.V., Zimek Z.
Basic laws of boundaries effects for the absorbed dose distribution of electrons in the heterogeneous materials.
Journal of Kharkiv University, no. 619. Physical series: Nuclei, Particles, Fields, 1, 37-48 (2004).

40. Kałuska I., Lazurik V.T., Lazurik V.M., Popov G.F., Rogov Yu.V., Zimek Z.
Dose distribution in the heterogeneous materials irradiated by electron beams.
Problems of Atomic Science and Technology, no. 1. Series: Nuclear Physics Investigations, 42, 184-186 (2004).

41. Kciuk G., Mirkowski J., Bobrowski K.
Radiation-induced oxidation of enkephalins and their dipeptide fragments.
Europhysics Conference Abstracts, 28A, 78 (2004).

42. Kordyasz A.J., Bartoś B., Bilewicz A.
Simultaneous determination of ^{224}Ra and ^{226}Ra isotopes by measuring of emanated ^{220}Rn and ^{222}Rn using a 4-inch silicon epitaxial detector.
Chemia Analityczna, 49, 29-39 (2004).

43. Kruszewski M.
The role of labile iron pool in cardiovascular diseases.
Acta Biochimica Polonica, 51, 2, 471-480 (2004).

44. Kruszewski M.
The role of labile iron pool in induction of DNA damage and cellular response to oxidative stress.
European Journal of Biochemistry, 271, Supplement 1, 5 (2004).

45. Kruszewski M., Lewandowska H., Starzyński R.R., Bartłomiejczyk T., Iwaneńko T., Drapier J.-C., Lipiński P.
Labile iron pool, dinitrosyl iron complexes and nitric oxide genotoxicity.
Free Radical Biology and Medicine, 36, Supplement 1, s52 (2004).

46. Kulisa K.
The effect of temperature on the cation-exchange separations in ion chromatography and the mechanism of zone spreading.
Chemia Analityczna, 49, 665-689 (2004).

47. Lankoff A., Krzowski Ł., Głąb J., Banasik A., Lisowska H., Kuszewski T., Góźdź S., Wójcik A.
DNA damage and repair in human peripheral blood lymphocytes following treatment with microcystin-LR.
Mutation Research – Genetic Toxicology and Environmental Mutagenesis, 559, 131-142 (2004).

48. Leciejewicz J., Ptasiewicz-Bąk H., Premkumar T., Govindarajan S.
Crystal structure of a lanthanum(III) complex with pyrazine-2-carboxylate and water ligands.
Journal of Coordination Chemistry, 57, 2, 97-103 (2004).

49. Legocka I., Sadło J., Warchoł S., Przybytniak G.
Wpływ promieniowania jonizującego na poli(siloksanouretany) – materiału przeznaczonego do zastosowań biomedycznych (The influence of ionising radiation on poly(siloxaneurethanes) – material for biomedical applications).
Inżynieria Biomateriałów, 38-42, 197-198 (2004).

50. Legocka I., Zimek Z., Mirkowski K., Nowicki A.
Preliminary study on application of the PE filler modified by radiation.
e-Polymers. The Scientific e-only Polymer Journal, P_035[2004] < http://www.e-polymer.org >

51. Lewandowska H.
Rola wolnych rodników w organizmie (The role of free radicals in the human body).
Postępy Techniki Jądrowej, 47, 3, 20-27 (2004).

52. Lin Min, Kojima T., Peimel-Stuglik Z., Chen Yun-Dong, Cui Ying, Chen Ke-Sheng, Li Hua-Zhi, Xiao Zhen-Hong, Fabisiak S.
Dose inter-comparison studies for ^{60}Co gamma-ray and electron beam irradiation in the year 2002.
Nuclear Science and Techniques, 15, 3, 166-173 (2004).

53. Lund E., Gustafsson H., Danilczuk M., Sastry M.D., Lund A.
Compounds of ^{6}Li and natural Li for EPR dosimetry in photon/neutron mixed radiation fields.
Spectrochimica Acta A, 60, 1319-1326 (2004).

54. Łyczko K., Bilewicz A., Person I.
Stabilization of a subvalent oxidation state of bismuth in *N*,*N*-dimethylthioformamide solution: an EXAFS, UV-Vis, IR, and cyclic voltammetry study.
Inorganic Chemistry, 43, 22, 7094-7100 (2004).

55. Machaj B., Bartak J.
Fast measurement of radon concentration in water with Lucas cell.
Nukleonika, 49, 1, 29-31 (2004).

56. Machaj B., Urbański P.
Influence of aerosol concentration and multivariate processing on the indication of radon progeny concentration in air.
Nukleonika, 49, 3, 123-129 (2004).

57. Maddukuri L., Sommer S., Rahden-Staroń I., Kudła G., Wójcik A., Tudek B.
Hypersensitivity of *XPA* cells to genotoxic effects of lipid peroxidation product *trans*-4-hydroxy-2-nonenal.
European Journal of Biochemistry, 271, Supplement 1, 12 (2004).

58. Malec-Czechowska K., Stachowicz W.
Wykrywanie napromieniowanych przypraw w produktach spożywczych (Detection of irradiated spices in food products).
Polish Journal of Human Nutrition and Metabolism, 31, Supplement 1, part II, 206-207 (2004).

59. Michalik J., Sadło J., Prakash A., Kevan L.
ESR and ESEEM study of silver clusters in SAPO-17 and SAPO-35 molecular sieves.
Studies in Surface Science and Catalysis, 154, 1568-1575 (2004).

60. Migdał W., Tomasiński P.
Wykorzystanie promieniowania jonizującego do utrwalania artykułów rolno-spożywczych (Application of ionising radiation for preservation of food products).
Polish Journal of Human Nutrition and Metabolism, 31, Supplement 1, part I, 284-285 (2004).

61. Migdał W., Tomasiński P., Norwa I., Strupiechowski M.
System kontroli i rejestracji dawki akceleratorowej w procesie napromieniowania żywności (Control and monitoring system of eb dose in food irradiation process).
Polish Journal of Human Nutrition and Metabolism, 31, Supplement 1, part II, 208-209 (2004).

62. Misiak A., Kierzek J., Dudek J., Polkowska-Motrenko H., Bulska E., Halicz L.
Oznaczanie metali ciężkich i izotopów gamma-promieniotwórczych w materiałach roślinnych (Determination of heavy metals and gamma-ray emitters in plant materials).
Polish Journal of Human Nutrition and Metabolism, 31, Supplement 1, part II, 211 (2004).

63. Nartowska J., Sommer E., Pastewka K., Sommer S., Skopińska-Różewska E.
Anti-angiogenic activity of convallamaroside, the steroidal saponin isolated from the rhizomes and roots of *Convallaria majalis* L.
Acta Poloniae Pharmaceutica – Drug Research, 61, 4, 279-282 (2004).

64. Pawlukojć A., Leciejewicz J.
The dynamics of molecular dimers in the crystals of *m*-aminobenzoic acid studied by inelastic neutron scattering (INS), Raman, IR spectroscopy and DFT calculations.
Chemical Physics, 299, 39-45 (2004).

65. Pawlukojć A., Natkaniec I., Bator G., Grech E., Sobczyk L.
Inelastic neutron scattering studies on dichloro-1,4-benzoquinones.
Spectrochimica Acta A, 60, 2875-2882 (2004).

66. Piekoszewski J., Kempiński W., Stankowski J., Prokert F., Richter E., Stanisławski J., Werner Z.
Ion implantation and transient melting: a new approach to formation of superconducting MgB_2 phases.
Acta Physica Polonica A, 106, 6, 861-868 (2004).

67. Piekoszewski J., Olesińska W., Jagielski J., Kaliński D., Chmielewski M., Werner Z., Barlak M., Szymczyk W.
Ion implantated nanolayers in AlN for direct bonding with copper.
Solid State Phenomena, 99-100, 231-234 (2004).

68. Piekoszewski J., Sartowska B., Waliś L., Werner Z., Kopcewicz M., Prokert F., Stanisławski J., Kalinowska J., Szymczyk W.
Interaction of nitrogen atoms in expanded austenite formed in pure iron by intense nitrogen plasma pulses.
Nukleonika, 49, 2, 57-60 (2004).

69. Piekoszewski J., Stanisławski J., Baranowski J., Składnik-Sadowska E., Werner Z., Barlak M.
Optical measurements of the velocities of plasma pulses generated in the rod plasma injector.
Czechoslovak Journal of Physics, 54, Supplement C, c217-c222 (2004).

70. Pogocki D.
Mutation of the Phe^{20} residue in Alzheimer's amyloid β-peptide might decrease its toxicity due to disruption of the Met^{35}-cupric site electron transfer pathway.
Chemical Research in Toxicology, 17, 3, 325-329 (2004).

71. Pogocki D., Ghezzo-Schöneich E., Celuch M., Schöneich Ch.
Singlet oxygen-induced oxidation as benchmark of the conformational flexibility of Met-$(X)_n$-Met peptides.
Europhysics Conference Abstracts, 28A, 77 (2004).

72. Polkowska-Motrenko H., Danko B., Dybczyński R.
Metrological assessment of the high-accuracy RNAA method for determination of cobalt in biological materials.
Analytical and Bioanalytical Chemistry, 379, 221-226 (2004).

73. Polkowska-Motrenko H., Szopa Z., Dybczyński R.
Badanie biegłości: pierwiastki śladowe w korzeniu marchwi (Results of a proficiency test: trace elements in carrot's root).
Polish Journal of Human Nutrition and Metabolism, 31, Supplement 1, part II, 202-203 (2004).

74. Popov P., Getoff N., Grodkowski J., Zimek Z., Chmielewski A.G.
Steady-state radiolysis and product analysis of aqueous diphenyloxide in the presence of air and N_2O.
Radiation Physics and Chemistry, 69, 39-44 (2004).

75. Premkumar T., Govindarajan S., Starosta W., Leciejewicz J.
Pyrazine-2,3-dicarboxylic acid.
Acta Crystallographica E, 60, 1305-1306 (2004).

76. Pruszyński M., Bilewicz A.
Astat w chemii i medycynie (Astatine in chemistry and medicine).
Wiadomości Chemiczne, 58, 5-6, 404-425 (2004).

77. Rudawska-Frąckiewicz K., Siekierski S.
The effect of MX_4^- anions (M = Al, Ga, In, Tl; X = Cl, Br, I) on the structures of their tetra-*N*-butylammonium salts.
Journal of Coordination Chemistry, 57, 9, 777-784 (2004).

78. Sadło J., Michalik J., Yamada H., Michiue Y., Shimomura S.
New type of paramagnetic silver cluster in sodalite: Ag_8^{7+}.
Solid State Phenomena, 99-100, 213-216 (2004).

79. Samczyński Z., Dybczyński R.
Ion exchange behavior of cadmium, mercury, silver and zinc on Retardion 11A8 and Chelex 100 ion exchangers in ammonia medium and its application for radiochemical separations.
Microchimica Acta, 144, 103-114 (2004).

80. Sommer S., Buraczewska I., Wojewódzka M., Boużyk E., Szumiel I., Wójcik A.
Analysis of the frequencies of exchange type aberration in chromosomes 2, 8, and 14 in lymphocytes of seven donors by chromosome paintings.
Central European Journal of Occupational and Environmental Medicine, 10, s182-s183 (2004).

81. Stachowicz W., Malec-Czechowska K.
Identyfikacja napromieniowania żywności w Polsce (Detection of irradiated food in Poland).
Polish Journal of Human Nutrition and Metabolism, 31, Supplement 1, part I, 105-107 (2004).

82. Starosta W., Leciejewicz J.
The crystal structure of Ca(II) (pyrazine-2,3-dicarboxylate) tetrahydrate chloride.
Journal of Coordination Chemistry, 57, 13, 1151-1156 (2004).

83. Starosta W., Leciejewicz J.
Pyridazine-3,6-dicarboxylic acid monohydrate.
Acta Crystallographica E, 60, 2219-2220 (2004).

84. Starosta W., Ptasiewicz-Bąk H., Leciejewicz J.
The crystal structure of a novel calcium(II) complex with pyrazine-2,6-dicarboxylate.
Journal of Coordination Chemistry, 57, 2, 167-173 (2004).

85. Sun Y.-X., Chmielewski A.G.
1,2-Dichloroethylene decomposition in air mixture by using ionization technology.
Radiation Physics and Chemistry, 71, 433-436 (2004).

86. Szopa Z., Dybczyński R., Kulisa K., Bysiek M., Biernacka M., Sterliński S.
The use of INAA for the evaluation of air pollution at three urban sites in Poland.
Chemia Analityczna, 49, 915-928 (2004).

87. Szumiel I.
Efekt widza (The bystander effect).
Postępy Techniki Jądrowej, 47, 2, 17-21 (2004).

88. Szydłowski A., Banaszak A., Fijał I., Jaskóła M., Korman A., Sadowski M.J., Choiński J., Sartowska B.
Calibration and application of solid-state nuclear track detectors in spectroscopy of heavier ions of energy in few MeV/amu range.
Czechoslovak Journal of Physics, 54, Supplement C, c228-c233 (2004).

89. Szymczyk W., Werner Z., Piekoszewski J.
Differential thermocouples in megawatt plasma pulse measurements – computer simulations and preliminary results.
Review of Scientific Instruments, 75, 6, 2107-2110 (2004).

90. Trojanowicz M., Bojanowska-Czajka A., Drzewicz P.
Usuwanie zanieczyszczeń wód i ścieków przy użyciu promieniowania jonizującego (Application of ionizing radiation for removal of pollutants from water and wastes).
Ekologia dla Przedsiębiorstw (biuletyn), part 1, 3-5 (2004).

91. Trojanowicz M., Compagnone D., Gonçales C., Jońca Z., Palleschi G.
Limitations in the analytical use of invertase inhibition for the screening of trace mercury content in environmental samples.
Analytical Sciences, 20, 6, 899-904 (2004).

92. Trojanowicz M., Mulchandani A.
Analytical applications of planar bilayer lipid membranes.
Analytical and Bioanalytical Chemistry, 379, 347-350 (2004).

93. Trojanowicz M., Orska-Gawryś J., Surowiec I., Szostek B., Urbaniak-Walczak K., Kehl J., Wróbel M.
Chromatographic investigation of dyes extracted from Coptic textiles from the National Museum in Warsaw.
Studies in Conservation, 49, 115-130 (2004).

94. Varmenot N., Bergès J., Abedinzadeh Z., Scemama A., Strzelczak G., Bobrowski K.
Spectral, kinetic, and theoretical studies of sulfur-centered reactive intermediates derived from thioethers containing an acetyl group.
Journal of Physical Chemistry A, 108, 6331-6346 (2004).

95. Wierzchnicki R.
Oznaczanie składu izotopów stabilnych w kontroli autentyczności żywności (Stable isotope measurements for food authenticity control).
Polish Journal of Human Nutrition and Metabolism, 31, Supplement 1, part I, 238-239 (2004).

96. Wierzchnicki R., Derda M., Mikołajczuk A.
Kontrola autentyczności soków na podstawie składu izotopów stabilnych (Stable isotope composition for juice authenticity control).
Polish Journal of Human Nutrition and Metabolism, 31, Supplement 1, part II, 209-210 (2004).

97. Wiśniowski P., Bobrowski K., Carmichael I., Hug G.L.
Bimolecular homolytic substitution (S_H2) reactions with hydrogen atoms. Time-resolved electron spin resonance detection in the pulse radiolysis of α-(methylthio)acetamide.
Journal of the American Chemical Society, 126, 14468-14474 (2004).

98. Wojewódzka M., Buraczewska I., Sochanowicz B., Szumiel I.
The role of poly(ADP-ribosylation) in double strand break fixation in L5178Y and CHO cells.

Central European Journal of Occupational and Environmental Medicine, 10, s215-s216 (2004).

99. Wojewódzka M., Buraczewska I., Szumiel I.
Poly(ADP-ribosylation) affects DSB fixation in L5178Y and CHO cells.
European Journal of Biochemistry, 271, Supplement 1, 10 (2004).

100. Wojewódzka M., Kruszewski M., Sochanowicz B., Szumiel I.
Differential DNA double strand break fixation dependence on poly(ADP-ribosylation) in L5178Y and CHO cells.
International Journal of Radiation Biology, 80, 7, 473-482 (2004).

101. Woźniak A.
Osłony w złączach preizolowanych rur do podziemnych wodnych sieci ciepłowniczych (Covers for the connections of the pre-insulated pipes for the underground supply system of hot water).
Instal, 12, 39-41 (2004).

102. Wójcik A.
Naturalne tło promieniowania i zdrowie (Natural background radiation and health).
Postępy Techniki Jądrowej, 47, 4, 22-27 (2004).

103. Wójcik A., Bruckmann E., Obe G.
Insights into the mechanisms of sister chromatid exchange formation.
Cytogenetic and Genome Research, 104, 304-309 (2004).

104. Wójcik A., Gregoire E., Hayata I., Roy L., Sommer S., Stephan G., Voisin P.
Cytogenetic damage in lymphocytes for the purpose of dose reconstruction: a review of three recent radiation accidents.
Cytogenetic and Genome Research, 104, 200-205 (2004).

105. Wójcik A., Stoilov L., Szumiel I., Legerski R., Obe G.
BrdU and radiation-induced sisters chromatid exchangers (SCE): the role of interstrand crosslinks (ILC) and Rad51C.
Central European Journal of Occupational and Environmental Medicine, 10, s215 (2004).

106. Yamada H., Sadło J., Tamura K., Shimomura S., Turek J., Michalik J.
Electron paramagnetic resonance studies on silver atoms and clusters in regularly interstratified clay minerals.
Nukleonika, 49, 4, 131-136 (2004).

107. Zagórski Z.P.
Chemia radiacyjna eksploracji Marsa (Radiation chemistry of Mars exploration).
Postępy Techniki Jądrowej, 47, 2, 30-38 (2004).

108. Zagórski Z.P.
EB-crosslinking of elastomers, how does it compare with radiation crosslinking of other polymers?
Radiation Physics and Chemistry, 71, 261-265 (2004).

109. Zagórski Z.P.
Pół wieku sieciowania radiacyjnego polietylenu czyli pochwała nauki pozauczelnianej (Half a century of radiation crosslinking of polyethylene, an appraisal of science outside Academia).
Postępy Techniki Jądrowej, 47, 4, 10-16 (2004).

110. Zagórski Z.P.
Realnie o broniach jądrowych w Azji (Nuclear weapons in Asia: a reality approach).
Postępy Techniki Jądrowej, 47, 1, 32-38 (2004).

111. Zakrzewska-Trznadel G., Dobrowolski A.
Rozdzielanie trwałych izotopów tlenu w kaskadzie prostokątnej (Separation of stable isotopes of oxygen in square cascade).
Monografie Komitetu Inżynierii Środowiska PAN, 22, 421-427 (2004).

112. Zakrzewska-Trznadel G., Harasimowicz M.
Application of ceramic membranes for hazardous wastes processing: pilot plant experiments with radioactive solutions.
Desalination, 162, 191-199 (2004).

113. Zielińska B., Bilewicz A.
The hydrolysis of actinium.
Journal of Radioanalytical and Nuclear Chemistry, 261, 1, 195-198 (2004).

114. Ziółek M., Michalska A., Decyk P., Nowak I., Michalik J., Sadło J.
Alkali-resistance of MCM-41 mesoporous molecular sieves containing various T (Al, Si, Nb) elements.
Studies in Surface Science and Catalysis, 154, 439-445 (2004).

BOOKS

1. Przeszczep w walce z kalectwem. 40 lat bankowania i sterylizacji radiacyjnej tkanek w Polsce (Tissue grafts in the fight against cripplehood – 40 years of radiation sterilisation and tissue banking in Poland). Pod redakcją: A. Dziedzic-Gocławskiej, K. Ostrowskiego, J. Komendera, J. Michalika, W. Stachowicza.
Zakład Transplantologii i Centralny Bank Tkanek Akademii Medycznej, Warszawa 2004, 362 p.

CHAPTERS IN BOOKS

1. Bik J.M., Rzymski W.M., Zagórski Z.P., Głuszewski W.
Wpływ czynników strukturalnych na sieciowanie uwodornionego kauczuku butadienowo-akrylonitrylowego za pomocą promieniowania elektronowego (Influence of the chemical structure on the crosslinking of hydrogenated acrylonitrile-butadiene rubber by electron radiation).
In: Materiały polimerowe i ich przetwórstwo. Praca zbior. pod red. J. Koszkula i E. Bociągi. Wydawnictwa Politechniki Częstochowskiej, Częstochowa 2004, pp. 108-117.

2. Bobrowski K., Foryś M., Mayer J., Michalik J., Narbutt J., Zimek Z.
Chemia radiacyjna, chemia jądrowa i radiochemia (Radiation chemistry, nuclear chemistry and radiochemistry).
In: Misja chemii. Pod red. Bogdana Marcińca. Wydawnictwo Poznańskie, Poznań 2004, pp. 253-279.

3. Chmielewski A.G., Tymiński B., Pawelec A.
Radiacyjna metoda oczyszczania spalin – doświadczenia eksploatacyjne (Electron beam flue gas treatment method – operational experiences).
In: Emisje, zagrożenie, ochrona powietrza. Praca zbior. pod red. A. Musialik-Piotrowskiej i J.D. Rutkowskiego. Polskie Zrzeszenie Inżynierów i Techników Sanitarnych, Wrocław 2004, pp. 39-46.

4. Drzewicz P., Bojanowska-Czajka A., Trojanowicz M., Kulisa K., Nałęcz-Jawecki G., Sawicki J., Listopadzki E.
Degradacja pestycydu kwasu 2,4-dichlorofenoksyoctowego (2,4-D) w wodzie podczas napromieniowania γ w obecności nadtlenku wodoru (Degradation of herbicide 2,4-dichlorophenoxyacetic acid (2,4-D) in water by γ-radiation combined with H_2O_2).
In: Mikrozanieczyszczenia w środowisku człowieka. Pod red. M. Janosz-Rajczyk. Politechnika Częstochowska, Seria Konferencji 55. Wydawnictwa Politechniki Częstochowskiej, Częstochowa 2004, pp. 161-170.

5. Dybczyński R.
Confirmation of the common origin of two meteorites that fell in widely separated locations on the Earth.
In: Analytical applications of nuclear techniques. IAEA, Vienna 2004, pp. 19-23.

6. Kałuska I., Zimek Z.
Dozymetria procesu sterylizacji radiacyjnej, pomiar dawki pochłoniętej (Radiation sterilization dosimetry, the absorbed dose measurements).
In: Przeszczep w walce z kalectwem. 40 lat bankowania i sterylizacji radiacyjnej tkanek w Polsce. Pod red. A. Dziedzic-Gocławskiej, K. Ostrowskiego, J. Komendera, J. Michalika, W. Stachowicza. Zakład Transplantologii i Centralny Bank Tkanek Akademii Medycznej, Warszawa 2004, p. 119.

7. Kałuska I., Zimek Z.
Walidacja procesu sterylizacji radiacyjnej (Validation of radiation sterilization process).
In: Przeszczep w walce z kalectwem. 40 lat bankowania i sterylizacji radiacyjnej tkanek w Polsce. Pod red. A. Dziedzic-Gocławskiej, K. Ostrowskiego, J. Komendera, J. Michalika, W. Stachowicza. Zakład Transplantologii i Centralny Bank Tkanek Akademii Medycznej, Warszawa 2004, pp. 121-122.

8. Legocka I., Zimek Z., Mirkowski K., Nowicki A.

Influence of some additives to polypropylene on its properties under sterilization dose of e-beam.

In: Controlling of degradation effects in radiation processing of polymers. Internal report of the 1st RCM of the CRPF2.20.39 held in Vienna, 8-11 December 2003. IAEA, Vienna 2004, pp. 117-126.

9. Narbutt J., Czerwiński M.

Computational chemistry in modeling solvent extraction of metal ions.

In: Solvent extraction principles and practice. J. Rydberg, M. Cox, C. Musikas, G.R. Choppin (eds). 2nd ed., revised and expanded. Marcel Dekker, Inc., New York-Basel 2004, pp. 679-714.

10. Nichipor H., Dashouk E., Yacko S., Chmielewski A.G., Zimek Z.

Kinetics and mechanism of carbendazim transformation in water containing O_2 under the action of electron beam.

In: Report of the 2nd Research Coordination Meeting (RCM) on Remediation of Polluted Waters and Wastewater by Radiation Processing, Warsaw, Poland, 13-18 June 2004. IAEA, Vienna 2004, pp. 23-34.

11. Panta P.P.

Początki sterylizacji przeszczepów kostnych w Polsce promieniowaniem gamma z rdzenia wyłączonego reaktora jądrowego (Beginnings of human bone sterilization in Poland with gamma radiation from the core of a shutdown nuclear reactor).

In: Przeszczep w walce z kalectwem. 40 lat bankowania i sterylizacji radiacyjnej tkanek w Polsce. Pod red. A. Dziedzic-Gocławskiej, K. Ostrowskiego, J. Komendera, J. Michalika, W. Stachowicza. Zakład Transplantologii i Centralny Bank Tkanek Akademii Medycznej, Warszawa 2004, pp. 87-94.

12. Sadło J., Stachowicz W., Michalik J., Dziedzic-Gocławska A.

Ocena rozkładu dawki pochłoniętej w masywnym przeszczepie kostnym sterylizowanym wiązką elektronów 10 MeV (Evaluation of dose distribution in a massive bone graft sterilised with the beam of 10 MeV electrons).

In: Przeszczep w walce z kalectwem. 40 lat bankowania i sterylizacji radiacyjnej tkanek w Polsce. Pod red. A. Dziedzic-Gocławskiej, K. Ostrowskiego, J. Komendera, J. Michalika, W. Stachowicza. Zakład Transplantologii i Centralny Bank Tkanek Akademii Medycznej, Warszawa 2004, pp. 123-127.

13. Stachowicz W.

Zagadnienia techniczne sterylizacji przeszczepów tkankowych za pomocą promieniowania gamma i szybkich elektronów (Technical aspects of the sterilisation of tissue grafts with the use of gamma rays and fast electrons).

In: Przeszczep w walce z kalectwem. 40 lat bankowania i sterylizacji radiacyjnej tkanek w Polsce. Pod red. A. Dziedzic-Gocławskiej, K. Ostrowskiego, J. Komendera, J. Michalika, W. Stachowicza. Zakład Transplantologii i Centralny Bank Tkanek Akademii Medycznej, Warszawa 2004, pp. 95-104.

14. Stachowicz W., Michalik J., Sadło J., Ostrowski K., Dziedzic-Gocławska A.

Badania doświadczalne w bankowaniu tkanek (EPR study on radicals and paramagnetic centres evolued in skeleton tissues under the action of ionising radiation).

In: Przeszczep w walce z kalectwem. 40 lat bankowania i sterylizacji radiacyjnej tkanek w Polsce. Pod red. A. Dziedzic-Gocławskiej, K. Ostrowskiego, J. Komendera, J. Michalika, W. Stachowicza. Zakład Transplantologii i Centralny Bank Tkanek Akademii Medycznej, Warszawa 2004, pp. 301-308.

15. Trojanowicz M.

Summary of results and plans for further studies (Poland) presented by participants of 2nd Research and Coordination Meeting, Warsaw, Poland, June 13-18, 2004.

In: Report of the 2nd Research Coordination Meeting (RCM) on Remediation of Polluted Waters and Wastewater by Radiation Processing, Warsaw, Poland, 13-18 June 2004. IAEA, Vienna 2004, pp. 8-9.

16. Trojanowicz M., Drzewicz P., Nałęcz-Jawecki G., Gryz M., Sawicki J., Bojanowska-Czajka A., Głuszewski W., Kulisa K., Kozyra C., Listopadzki E.

Monitoring of toxicity and determination of products in degradation of selected pesticides using ionizing radiation.

In: Report of the 2nd Research Coordination Meeting (RCM) on Remediation of Polluted Waters and Wastewater by Radiation Processing, Warsaw, Poland, 13-18 June 2004. IAEA, Vienna 2004, pp. 76-94.

17. Werner Z., Szymczyk W., Piekoszewski J.

Ion implanted nanolayers in alloys and ceramic coatings for improved resistance to high-temperature corrosion.

In: Nanostructured thin films and nanodispersion strengthened coatings. A.A. Voevodin, D.V. Shtansky, E.A. Levashov, J.J. Moore (eds). NATO Science Series. II: Mathematics, Physics and Chemistry - Vol. 155. Kluwer Academic Publishers, Dordrecht 2004, pp. 193-202.

18. Zagórski Z.P., Głuszewski W.

Modyfikacja własności polimerów w procesie sterylizacji radiacyjnej (Modification of polymer properties in the process of radiation sterilization).

In: Przeszczep w walce z kalectwem. 40 lat bankowania i sterylizacji radiacyjnej tkanek w Polsce. Pod red. A. Dziedzic-Gocławskiej, K. Ostrowskiego, J. Komendera, J. Michalika, W. Stachowicza. Zakład Transplantologii i Centralny Bank Tkanek Akademii Medycznej, Warszawa 2004, pp. 347-349.

19. Zimek Z.

Akceleratory elektronów dla potrzeb bankowania tkanek (Electron accelerators for tissue banking).

In: Przeszczep w walce z kalectwem. 40 lat bankowania i sterylizacji radiacyjnej tkanek w Polsce. Pod red. A. Dziedzic-Gocławskiej, K. Ostrowskiego, J. Komendera, J. Michalika, W. Stachowicza. Zakład Transplantologii i Centralny Bank Tkanek Akademii Medycznej, Warszawa 2004, pp. 113-118.

REPORTS

1. INCT Annual Report 2003.

Institute of Nuclear Chemistry and Technology, Warszawa 2004, 202 p.

2. Grodkowski J.

Radiacyjna i fotochemiczna redukcja dwutlenku węgla w roztworach katalizowana przez kompleksy metali przejściowych z wybranymi układami makrocyklicznymi (Radiolytic and photochemical reduction of carbon dioxide in solution catalyzed by transition metal complexes with some selected macrocycles).

Instytut Chemii i Techniki Jądrowej, Warszawa 2004. Raporty IChTJ. Seria A nr 1/2004, 56 p.

3. Pogocki D.M.

Wewnątrzcząsteczkowe przemiany rodnikowe z udziałem utlenionego centrum siarkowego w modelowych związkach tioeterowych o znaczeniu biologicznym (Participation of oxidized sulfur center in intramolecular free radical processes in the model organic compounds of biological importance).

Instytut Chemii i Techniki Jądrowej, Warszawa 2004. Raporty IChTJ. Seria A nr 2/2004, 87 p.

4. Przybytniak G.

Rodniki powstające w DNA i jego nukleotydach pod wpływem promieniowania jonizującego (Radicals of DNA and DNA nucleotides generated by ionising radiation).

Instytut Chemii i Techniki Jądrowej, Warszawa 2004. Raporty IChTJ. Seria A nr 3/2004, 100 p.

5. Chmielewski A.G., Michalik J., Buczkowski M., Chmielewska D.K.

Ionizing radiation in nanotechnology.

Institute of Nuclear Chemistry and Technology, Warszawa 2004. Raporty IChTJ. Seria B nr 1/2004, 56 p.

6. Apel P.Yu., Błońska I.W., Orelovitch O.L., Akimenko S.N., Sartowska B., Dmitriev S.N.

Factors determining the pore shape in polycarbonate track membranes.

Joint Institute for Nuclear Research, Dubna. P18-2004-52, 12 p. (in Russian).

CONFERENCE PROCEEDINGS

1. Bonilla F.A., Ong T.S., Alcalá G., Skeldon P., Thompson G.E., Piekoszewski J., Ostapczuk A., Chmielewski A., Werner Z., Sartowska B., Stanisławski J., Richter E.

Corrosion of titanium surface-alloyed with nickel or nickel-molybdenum by high intensity pulsed beams in a simulated flue gas environment.

Ti-2003 science and technology. Proceedings of the 10th World Conference on Titanium held at the CCH-Congress Center Hamburg, Germany, 13-18.07.2003. G. Lütjering, J. Albrecht (eds). Wiley VCH Verlag, Weinheim 2004. Vol. II, pp. 891-898.

2. Chmielewski A.G., Pawelec A., Tymiński B., Zimek Z., Licki J.

Industrial applications of electron beam flue gas treatment.

Emerging applications of radiation processing. Proceedings of a technical meeting held in Vienna, 28-30.04.2003. IAEA, Vienna 2004. IAEA-TECDOC-1386, pp. 153-161.

3. Chmielewski A.G., Tymiński B., Pawelec A.

Usuwanie zanieczyszczeń z gazów emitowanych do atmosfery przy pomocy wiązki elektronów (Elimination of pollutants from gases emitted to atmosphere with the use of electron beam).

Ochrona powietrza w teorii i praktyce. IV Międzynarodowa konferencja naukowa. Zakopane, 25-27.10.2004. Red. J. Konieczny, R. Zarzycki. Instytut Podstaw Inżynierii Środowiskowej PAN, Zabrze 2004, pp. 73-80.

4. **Danko B.**
   High accuracy method for the determination of molybdenum content in bio-materials by RNAA.
   International Conference on Isotopic and Nuclear Analytical Method for Health and Environment. Vienna, Austria, 10-13.06.2003. Conference & Symposium Papers 22/CD. IAEA, Vienna 2004. IAEA-CN-103/021P, [13] p. (CD edition).

5. **Derda M., Chmielewski A.G.**
   Isotope ratio as a tracer for investigation of anthropogenic sulfur sources.
   TRACER 3: Tracers and Tracing Methods. Ciechocinek, Poland, 22-24.06.2004. Proceedings, pp. 92-95.

6. **Dłuska E., Zakrzewska-Trznadel G., Wroński S.**
   Couette-Taylor contractor for radioactive solutions filtration.
   Energy-efficient, cost-effective, and environmentally-sustainable systems and processes. Proceedings of the 17th International Conference on Efficiency, Costs, Optimization, Simulation and Environmental Impact of Energy and Process Systems ECOS 2004. Guanajuato, Mexico, 7-9.07.2004. R. Rivero, L. Monroy, R. Pulido, G. Tsatsaronis (eds). Instituto Mexicano del Petróleo, Mexico 2004. Vol. 1, pp. 137-145.

7. **Harasimowicz M., Zakrzewska-Trznadel G., Mikołajczuk A., Chmielewski A.G.**
   Methane enrichment of CH_4 + CO_2 mixture on 2-stage GS membrane module system with circulation stream and chemical final purification.
   "Ars Separatoria 2004": Proceedings of the XIX International Symposium on Physico-Chemical Methods of the Mixtures Separation. Złoty Potok n. Częstochowa, Poland, 10-13.06.2004, pp. 187-189.

8. **Korzeniowska-Sobczuk A., Mirkowski J., Hug G.L., Filipiak P., Bobrowski K.**
   Radiation induced oxidation of aromatic carboxylic acids containing the thioether group.
   Trombay Symposium on Radiation and Photochemistry (TSRP-2004). Mumbai, India, 8-12.01.2004. Vol. 1. Invited talks, IT-14, pp. 53-58.

9. **Kraś J., Waliś L., Myczkowski S., Pańczyk E.**
   Leakproof control of technological installations and underground pipelines using radioactive tracers as a contribution to the protection of the natural environment.
   TRACER 3: Tracers and Tracing Methods. Ciechocinek, Poland, 22-24.06.2004. Proceedings, pp. 253-259.

10. **Machaj B., Urbański P.**
    Influence of aerosol concentration and multivariate processing on indication of radon progeny concentration in air.
    International Conference on Isotopic and Nuclear Analytical Method for Health and Environment. Vienna, Austria, 10-13.06.2003. Conference & Symposium Papers 22/CD. IAEA, Vienna 2004. IAEA-CN-103/030P, [9] p. (CD edition).

11. **Mikołajczuk A., Wierzchnicki R., Chmielewski A.G.**
    Isotope effects for $^{34}S/^{32}S$ during dissolving process of SO_2 in polar solvents.
    "Ars Separatoria 2004": Proceedings of the XIX International Symposium on Physico-Chemical Methods of the Mixtures Separation. Złoty Potok n. Częstochowa, Poland, 10-13.06.2004, pp. 222-224.

12. **Mirkowski J., Smolik W., Brzeski P., Olszewski T., Radomski D., Szabatin R.**
    Software for sensor modelling in electrial capacitance tomography.
    3rd International Conference on Process Tomography in Poland. Łódź, Poland, 9-10.09.2004, pp. 106-110.

13. **Olszewski T., Kleczyński P., Brzeski P., Mirkowski J., Pląskowski A., Smolik W., Szabatin R.**
    Electrical capacitance tomograph designs.
    3rd International Conference on Process Tomography in Poland. Łódź, Poland, 9-10.09.2004, pp. 118-123.

14. **Palige J., Owczarczyk A., Dobrowolski A., Chmielewski A.G., Ptaszek S.**
    Applications of tracers and CFD methods for investigations of wastewater treatment installations.
    TRACER 3: Tracers and Tracing Methods. Ciechocinek, Poland, 22-24.06.2004. Proceedings, pp.129-137.

15. **Pańczyk E., Pytel K., Kalicki A., Rowińska L., Sartowska B., Waliś L.**
    Neutron-induced autoradiography in the study of Venetian oil paintings.
    Proceedings of the Enlargement Workshop on Neutron Measurements and Evaluations for Applications NEMEA. Budapest, Hungary, 5-8.11.2003. A.J.M. Plompen (ed.). IRMM, Geel [2004]. Report EUR 21100, pp. 6-9.

16. Pańczyk E., Waliś L.

Neutrons in art.

TRACER 3: Tracers and Tracing Methods. Ciechocinek, Poland, 22-24.06.2004. Proceedings, pp. 199-204.

17. Peimel-Stuglik Z., Skuratov V.A.

Heavy ion fluence measurements based on radiation effects generated in CTA foils.

Effects of radiation on materials: 21st International Symposium. M.L. Grossbeck, T.R. Allen, R.G. Lott, A.S. Kumar (eds). ASTM International, West Conshohocken, PA 2004. ASTM STP 1447, pp. 605-611.

18. Polkowska-Motrenko H.

Preliminary results of the characterization of the candidate mushroom reference material.

IAEA Interregional Training Course on Organizational, Reporting and Certifications Aspects of Proficiency Testing. Vienna, Austria, 8-19.03.2004, [12] p. (CD edition).

19. Polkowska-Motrenko H., Danko B., Dybczyński R.

Metrological assessment of the high-accuracy RNAA method of Co determination in biological materials.

International Conference on Isotopic and Nuclear Analytical Method for Health and Environment. Vienna, Austria, 10-13.06.2003. Conference & Symposium Papers 22/CD. IAEA, Vienna 2004. IAEA-CN-103/037, [8] p. (CD edition).

20. Sołtyk W., Dobrowolski A., Zimnicki R., Owczarczyk A.

Tracer investigation of ground water direction and flow velocity in the field of drainage system interaction.

TRACER 3: Tracers and Tracing Methods. Ciechocinek, Poland, 22-24.06.2004. Proceedings, pp. 169-173.

21. Stanisławski J., Piekoszewski J., Składnik-Sadowska E., Werner Z, Barlak M.

Spectral diagnostics of the interaction of plasma pulses with titanium substrate.

Proceedings of the 2nd German-Polish Conference on Plasma Diagnostics for Fusion and Applications. Cracow, Poland, 8-10.09.2004, [4] p.

22. Trojanowicz M.A., Drzewicz P., Bojanowska-Czajka A.

Chemical monitoring of the effectiveness of radiolytic degradation of organic pollutants in waters and wastes.

Proceedings of the 3rd SENSPOL Workshop: Monitoring in Polluted Environments for Integrated Water-Soil Management. Kraków, Poland, 3-6.06.2003. S. Alcock (ed.). [2004], pp. 63-70.

23. Tymiński B., Zwoliński K., Jurczyk R., Koronka A.

Rozkład katalityczny odpadów poliolefin z rozdestylowaniem produktów (Catalytic decomposition of polyolefine wastes with fractionation of products).

Dla miasta i środowiska – II Konferencja: Problemy unieszkodliwiania odpadów. Warszawa, Poland, 25.10.2004. Materiały konferencyjne, pp. 5-10.

24. Urbański P., Kowalska E., Jakowiuk A.

Multivariate techniques in processing data from radiometric experiments.

International Conference on Isotopic and Nuclear Analytical Method for Health and Environment. Vienna, Austria, 10-13.06.2003. Conference & Symposium Papers 22/CD. IAEA, Vienna 2004. IAEA-CN-103/031P, [12] p. (CD edition).

25. Urbański P., Mirowicz J., Owczarczyk A., Pieńkos P., Świstowski E., Machaj B.

Portable instrument for acquisition and processing data from radiometric experiments performed in the field and industrial conditions.

TRACER 3: Tracers and Tracing Methods. Ciechocinek, Poland, 22-24.06.2004. Proceedings, pp. 87-91.

26. Wierzchnicki R., Owczarczyk A., Sołtyk W.

Stable isotope composition of environmental water and food products as a tracer of origin.

TRACER 3: Tracers and Tracing Methods. Ciechocinek, Poland, 22-24.06.2004. Proceedings, pp. 229-231.

27. Woźniak A.

Osłony w złączach preizolowanych rur do podziemnych wodnych sieci ciepłowniczych (Covers for the connections of the pre-insulated pipes for the underground supply system of hot water).

VIII Forum Ciepłowników Polskich. Materiały 13. krajowej konferencji. Międzyzdroje, Poland, 13-15.09.2004, pp. 301-305.

28. Wójcik A., Cosset J.-M., Clough K., Gourmelon P., Bottolier J.-F., Trompier F., Stephan G., Sommer S., Wieczorek A., Słuszniak J., Kułakowski A., Góźdź S., Michalik J., Stachowicz W., Sadło J., Bulski W., Izewska J.

The radiological accident at the Bialystok Oncology Center: cause, dose estimation and patient treatment.

11th International Congress of the International Radiation Protection Association. Madrid, Spain, 23-28.05.2004. Full papers, [5] p. < http://www.irpa11.com/ >

29. Wójcik A., Stachowicz W., Michalik J.

Dozymetria biologiczna dla oceny dawki pochłoniętej (Biological dosimetry for estimation of absorbed dose).

VIII Jesienna Szkoła Fizyki Medycznej. Bydgoszcz, Poland, 12-13.10.2004, [9] p.

30. Wójcik A., Stoilov L., Obe G.

BrdU and radiation-induced sisters chromatid exchangers (SCE): the role of interstrand crosslinks (ILC) and Rad51C.

Proceedings of the 8th International Wolfsberg Meeting on Molecular Radiation Biology/Oncology 2004. M. Baumann, S. Bodis, E. Dikomey, H.P. Rodemann (eds). Wolfsberg Meeting Series. Poster Session Topic II, (PII.6), p. 51.

31. Zagórski Z.P.

Radiation chemistry of spurs in polymers.

Advances in radiation chemistry of polymers. Proceedings of a technical meeting held in Notre Dame, Indiana, USA, 13-17.09.2003. IAEA, Vienna 2004. IAEA-TECDOC-1420, pp. 21-31.

32. Zakrzewska-Trznadel G.

Membrane methods for processing of liquid radioactive waste.

Physical chemistry 2004. Proceedings of the 7th International Conference on Fundamental and Applied Aspects of Physical Chemistry. Belgrade, Serbia and Montenegro, 21-23.09.2004. A. Antić-Jovanović, S. Anić (eds). Vol. 1, pp. 419-425.

33. Zimek Z.

Accelerator technology for radiation processing: recent development.

Emerging applications of radiation processing. Proceedings of a technical meeting held in Vienna, 28-30.04.2003. IAEA, Vienna 2004. IAEA-TECDOC-1386, pp. 55-64.

34. Zimek Z.

Restrictions and limits of accelerator technology applied in industry and environment protection.

Emerging applications of radiation processing. Proceedings of a technical meeting held in Vienna, 28-30.04.2003. IAEA, Vienna 2004. IAEA-TECDOC-1386, pp. 78-84.

CONFERENCE ABSTRACTS

1. Banasik A., Lankoff A., Lisowska H., Kuszewski T., Góźdź S., Wójcik A.

Kinetyka naprawy uszkodzeń DNA w limfocytach krwi obwodowej człowieka po traktowaniu jonami glinu (Kinetics of repair of DNA damage in human peripheral blood lymphocytes after aluminium ion treatment).

XIII Zjazd Polskiego Towarzystwa Badań Radiacyjnych im. M. Skłodowskiej-Curie. Łódź, Poland, 13-16.09.2004. Materiały konferencyjne, P-21, p. 88.

2. Barlak M., Olesińska W., Piekoszewski J., Chmielewski M., Jagielski J., Kaliński D., Szymczyk W., Werner Z.

Ion implantation as a pre-treatment method of AlN substrate for direct bonding with copper.

5th International Conference: Ion Implantation and Other Applications of Ions and Electrons, ION 2004. Kazimierz Dolny, Poland, 14-17.06.2004, p. 80.

3. Bartłomiejczyk T., Wojewódzka M., Kruszewski M.

The effect of inhibition of PARP on the frequency of homologous recombination in CHO-K1 wild type and XRS-6 mutant cell line.

Gliwice Scientific Meeting 2004. Gliwice, Poland, 19-20.11.2004, p. 38.

4. Bartoś B., Bilewicz A.

Effect of crown ethers on the Sr^{2+}, Ba^{2+} and Ra^{2+} uptake on tunnel structure ion exchangers.

Advances in nuclear radiochemistry. Extended abstracts of papers presented at the Sixth International Conference on Nuclear and Radiochemistry (NRC-6), 29 August to 3 September 2004, Aachen, Germany. S.M. Qaim and H.H. Coenen (eds). Forschungszentrum Jülich GmbH, Institut für Nuklearchemie, Jülich 2004. Vol. 3, pp. 203-204.

5. Bik J.M., Rzymski W.M., Zagórski Z.P.

Sieciowanie i degradacja podczas napromieniania uwodornionego kauczuku nitrylowego (Crosslinking and degradation during the irradiation of hydrogenated nitrile rubber).

Materiały polimerowe – Pomerania-Plast 2004. Szczecin-Międzyzdroje, Poland, 2-4.06.2004. Streszczenia, pp. 59-61.

6. Bik J.M., Rzymski W.M., Zagórski Z.P., Głuszewski W.

Sieciowanie radiacyjne uwodornionego kauczuku butadienowo-akrylonitrylowego o odmiennej polarności (Radiation crosslinking of hydrogenated butadiene-acrylonitrile rubbers of diversified polarity).

XLVII Zjazd PTChem i SITPChem. Wrocław, Poland, 12-17.09.2004. Materiały zjazdowe, Vol. III, p. 919.

7. Bilewicz A.

Contraction of actinides 3+ ionic radii at the end of the serie.

Advances in nuclear radiochemistry. Extended abstracts of papers presented at the Sixth International Conference on Nuclear and Radiochemistry (NRC-6), 29 August to 3 September 2004, Aachen, Germany. S.M. Qaim and H.H. Coenen (eds). Forschungszentrum Jülich GmbH, Institut für Nuklearchemie, Jülich 2004. Vol. 3, pp. 57-59.

8. Bobrowski K., Pogocki D., Hug G.L., Marciniak B., Schöneich Ch.

Mechanistic studies of sulfur radical cation stabilization in cyclic and N-acetylated peptides containing methionine.

ISOFR 9th: International Symposium on Organic Free Radicals. Porto-Vecchio, France, 6-11.06.2004, p. P-10.

9. Bojanowska-Czajka A., Drzewicz P., Nałęcz-Jawecki G., Sawicki J., Kulisa K., Kozyra C., Trojanowicz M.

Determination of products and monitoring of toxicity during radiolytic treatment of industrial wastes from production of MCPA.

International Symposium: Analytical Forum 2004. Warsaw, Poland, 4-8.07.2004. Book of abstracts, p. 203.

10. Brzeski P., Mirkowski J., Olszewski T., Radomski D., Smolik W., Szabatin R.

Measurement effects in capacitance tomography.

3rd International Symposium on Process Tomography in Poland. Łódź, Poland, 9-10.09.2004, pp. 24-26.

11. Bułka S., Dźwigalski Z., Zimek Z.

LAE 10 accelerators as a part of pulse radiolysis experimental set.

VIII Electron Technology Conference – ELTE 2004. Stare Jabłonki, Poland, 19-22.04.2004. Book of extended abstracts, TP-3, pp. 384-385.

12. Chwastowska J., Skwara W., Sterlińska E., Dudek J., Pszonicki L.

Analiza specjacyjna arsenu, antymonu i selenu w wodach mineralnych i solankach (Speciation analysis of arsenic and antimony in mineral waters and brines).

Nowoczesne metody przygotowania próbek i oznaczania śladowych ilości pierwiastków. Materiały XIII Poznańskiego Konwersatorium Analitycznego. Poznań, Poland, 6-7.05.2004, p. 117.

13. Chwastowska J., Skwara W., Sterlińska E., Dudek J., Pszonicki L.

Problemy w analizie specjacyjnej chromu w wodach mineralnych (Problems in speciation analysis of chromium in mineral waters).

Konferencja: Zastosowanie metod AAS, ICO-AES i ICP-MS w analizie środowiskowej. Łódź, Poland, 8-9.12.2004, P-9, p. 31.

14. Cieśla K., Diduszko R.

Polyester films modified by chemical compositions and physical treatment studied by X-ray diffraction methods.

The Sixth International Conference: X-Ray Investigations of Polymer Structure – XIPS'2004. Bielsko-Biała, Poland, 8-11.12.2004. Programme, p. PI/5.

15. Cieśla K., Eliasson A.Ch.

Influence of gamma irradiation on the amylose-lipid complex studied by DSC.

XII International Starch Convention Cracow-Moscow. Cracow, Poland, 14-18.06.2004, p. 103.

16. Danko B., Dybczyński R., Kulisa K., Samczyński Z.

Ion exchange analytical scheme for selective and quantitative separation of the lanthanides from biological materials.

Euroanalysis XIII. European Conference on Analytical Chemistry. Salamanca, Spain, 5-10.09.2004. Book of abstracts, p. PS2-278.

17. Danko B., Dybczyński R., Kulisa K., Samczyński Z.

Jonitowa metoda ilościowego i selektywnego wydzielania frakcji lantanowców z materiałów pochodzenia biologicznego (Ion exchange method for quantitative and selective isolation of the lanthanides from biological materials).

XLVII Zjazd PTChem i SITPChem. Wrocław, Poland, 12-17.09.2004. Materiały zjazdowe, Vol. I, p. 332.

18. Dębowska R., Eris I., Iwaneńko T., Kruszewski M., Wojewódzka M.

Repair of UV- and X-radiation induced DNA damage in folacin-treated primary human fibroblasts.

4th DNA Repair Workshop. Smolenice, Slovakia, 2-5.05.2004. Book of abstracts, p. 62.

19. Dybczyński R.

The position of NAA among the methods of inorganic trace analysis in the past and now.

NEMEA-2 Workshop: Neutron Measurements, Evaluations and Applications. Bucharest, Romania, 20-23.10.2004. Book of abstracts, pp. 13-14.

20. Dybczyński R.

The significance of reference materials and definitive methods for quality assurance in inorganic trace analysis and its relation to environmental pollution.

Conference on Bioaccumulation of Radionuclides and Heavy Metals – as a Marker of Environmental Contamination. Kazimierz Dolny upon Vistula, Poland, 26-28.09.2004. Book of abstracts, pp. 17-18.

21. Dybczyński R., Polkowska-Motrenko H.

Działalność i osiągnięcia Instytutu Chemii i Techniki Jądrowej w dziedzinie zapewnienia jakości w nieorganicznej analizie śladowej (The activity and achievements of the Institute of Nuclear Chemistry and Technology in the field of quality assurance in inorganic analysis).

Ogólnopolska konferencja naukowa: „Jakość w chemii analitycznej". Warszawa, Poland, 25-26.11.2004, p. 7.

22. Filipiak P., Hug G.L., Bobrowski K., Carmichael I., Marciniak B.

Direct and sensitized photochemistry of aromatic carboxylic acids containing the thioether group. Steady--state and laser flash photolysis studies.

ISOFR 9th: International Symposium on Organic Free Radicals. Porto-Vecchio, France, 6-11.06.2004, p. P-57.

23. Filipiak P., Kozubek H., Marciniak B., Hug G.L., Korzeniowska-Sobczuk A., Bobrowski K.

Photoinduced oxidation of aromatic carboxylic acids containing the thioether group.

3rd Trivandrum International Symposium on Recent Trends in Photochemical Sciences. Trivandrum, India, 5-7.01.2004. Abstracts, L-20, p. 22.

24. Filipiuk D., Fuks L., Majan M.

Transition metal complexes with uronic acids.

XXVII European Congress on Molecular Spectroscopy. Kraków, Poland, 5-10.09.2004. Book of abstracts, P5-6, p. 287.

25. Fuks L., Gniazdowska E., Mieczkowski J., Narbutt J., Starosta W., Zasępa M.

fac-$RE^{I}(CO)_3^+$ complexes with N,S-bidentate ligands.

ISBOMC'04: Second International Symposium on Bioorganometallic Chemistry. Zurich, Switzerland, 14-17.07.2004. Program and book abstracts, P-28, p. 82.

26. Fuks L., Kołodziejski W., Sadlej-Sosnowska N., Samochocka K.

Spectroscopic and quantum chemical studies of palladium(II) and platinum(II) thiourea chlorides in the solid state.

XXVII European Congress on Molecular Spectroscopy. Kraków, Poland, 5-10.09.2004. Book of abstracts, P2-2, p. 199.

27. Fuks L., Sadlej-Sosnowska N., Samochocka K., Starosta W.

Quantum chemical and structural studies of the palladium(II) and platinum(II) thiourea chlorides.

ISBOMC'04: Second International Symposium on Bioorganometallic Chemistry. Zurich, Switzerland, 14-17.07.2004. Program and book abstracts, P-27, p. 81.

28. Głuszewski W., Panta P., Zimek Z.

Kontrola dozymetryczna procesów sterylizacji i higienizacji radiacyjnej (Dosimetric control in radiation sterilization processes).

7. Spotkanie Inspektorów Ochrony Radiologicznej. Dymaczewo Nowe, Poland, 1-4.06.2004. Streszczenia referatów oraz materiały konferencyjne, pp. 27-28.

29. Głuszewski W., Zagórski Z.P.

Chemia radiacyjna materiału polimerowego PP/PS (Radiation chemistry of polymeric material PP/PS).

XIII Zjazd Polskiego Towarzystwa Badań Radiacyjnych im. M. Skłodowskiej-Curie. Łódź, Poland, 13-16.09.2004. Materiały konferencyjne, p. 64.

30. Głuszewski W., Zagórski Z.P.

Zjawiska ochronne w chemii radiacyjnej polimerów (Protective phenomena in radiation chemistry of polymers).

ChemSession'04: I Warszawskie seminarium doktorantów chemików. Warszawa, Poland, 14.05.2004. Streszczenia, P-24, p. 37.

31. Grądzka I., Buraczewska I., Iwaneńko T., Sochanowicz B., Szumiel I.

Post-irradiation recovery in human glioma M059K cell line and its DNA-PK_{CS} deficient counterpart M059J: effect of signaling pathways inhibitors.

European Radiation Research 2004: the 33rd Annual Meeting of the European Society for Radiation Biology. Budapest, Hungary, 25-28.08.2004, p. 109.

32. Grądzka I., Buraczewska I., Sochanowicz B., Szumiel I.

Promieniouczulanie komórek ludzkiego glejaka M059 przez inhibitory szlaków sygnałowych czynników wzrostu: wpływ na naprawę podwójnoniciowych pęknięć DNA (Radiosensitization of human glioma M059 cells by grown factor receptors inhibitors: effects on double-strand break repair).

XIII Zjazd Polskiego Towarzystwa Badań Radiacyjnych im. M. Skłodowskiej-Curie. Łódź, Poland, 13-16.09.2004. Materiały konferencyjne, P-24, p. 91.

33. Gryz M., Starosta W., Leciejewicz J.

The crystal and molecular structure of a magnesium(II) complex with pyridazine-3,6-dicarboxylate and water ligands.

46th Polish Crystallographic Meeting. Wrocław, Poland, 24-25.06.2004, A-27, p. 67.

34. Gryz M., Starosta W., Leciejewicz J.

Doubly bridged molecular ribbons in the structure of an ionic complex hydronium zinc(II) pyrazine-2,3-dicarboxylate.

46th Polish Crystallographic Meeting. Wrocław, Poland, 24-25.06.2004, A-26, p. 66.

35. Kałuska I., Zimek Z.

Dose setting procedures for radiation sterilization.

NATO Advanced Research Workshop on Radiation Inactivation of Bioterrorism Agents. Budapest, Hungary, 7-9.03.2004, [1] p.

36. Kapka L., Anderson D., Kruszewski M., Siwińska E., Ołdak T., Mielżyńska D.

DNA damage in children exposed to lead.

Gliwice Scientific Meeting 2004. Gliwice, Poland, 19-20.11.2004, p. 49.

37. Koczoń P., Kalinowska M., Lewandowska H., Świsłocka R., Piekut J., Borawska M., Lewandowski W.

Spectroscopic study of selected metal picolinates and benzoates.

RISBM 2004: International Bunsen Discussion Meeting "Raman and IR spectroscopy in biology and medicine". Jena, Germany, 29.02.-02.03.2004., D16, p. 104.

38. Kornacka E.M.

Niskotemperaturowa radioliza DNA w obecności tioalkoholi (Low temperature radiolysis of DNA with thioalcohols).

XIII Zjazd Polskiego Towarzystwa Badań Radiacyjnych im. M. Skłodowskiej-Curie. Łódź, Poland, 13-16.09.2004. Materiały zjazdu, p. 21.

39. Król M., Derezińska E., Sommer S., Buraczewska I., Lankoff A., Banasik A., Lisowska H., Kuszewski T., Góźdź S., Wójcik A.

Częstość popromiennych mikrojąder w limfocytach krwi obwodowej kobiet w zależności od miesięcznego rytmu biologicznego (Frequency of radiation-induced micronuclei in peripheral blood lymphocytes of women in dependence of menstruation rhythm).

XIII Zjazd Polskiego Towarzystwa Badań Radiacyjnych im. M. Skłodowskiej-Curie. Łódź, Poland, 13-16.09.2004. Materiały konferencyjne, p. 44.

40. Kruszewski M.

Uszkodzenia DNA wywołane przez promieniowanie jonizujące i ich naprawa (DNA lesions generated by ionising radiation and their repair).

ChemSession'04: I Warszawskie seminarium doktorantów chemików. Warszawa, Poland, 14.05.2004. Streszczenia, W-3, p. 9.

41. Kruszewski M., Iwaneńko T., Ołdak T., Gajkowska A., Jastrzewska M., Machaj E.K., Pojda Z.

Popromienne uszkodzenia DNA w proliferujących i nieproliferujących ludzkich komórkach $DC34^+$ (X-ray induced DNA damage in proliferating and non-proliferating human $CD34^+$ cells).

XIII Zjazd Polskiego Towarzystwa Badań Radiacyjnych im. M. Skłodowskiej-Curie. Łódź, Poland, 13-16.09.2004. Materiały konferencyjne, p. 38.

42. Kruszewski M., Lewandowska H., Starzyński R.R., Bartłomiejczyk T., Iwaneńko T., Drapier J.-C., Lipiński P.

The role of labile iron pool and dinitrosyl iron complexes in nitric oxide genotoxicity.

Summer Meeting SFRR-Europe 2004 "Reactive oxygen species and antioxidants". Łódź, Poland, 2-5.07.2004. Abstracts, p. 180.

43. Kulisa K., Dybczyński R.

Wpływ temperatury na proces rozdzielania kationów w chromatografii jonów (Effect of temperature on cation-exchange separations in ion chromatography).

Nowoczesne metody przygotowania próbek i oznaczania śladowych ilości pierwiastków. Materiały XIII Poznańskiego Konwersatorium Analitycznego. Poznań, Poland, 6-7.05.2004, p. 104.

44. Lankoff A., Carmichael W.W., Dziga D., Banasik J.A., Lisowska H., Kuszewski T., Białczyk J., Piorun I., Wójcik A.

Kinetyka naprawy pojedynczo (SSB)- i podwójnoniciowych (DSB) pęknięć DNA w limfocytach ludzkich napromienianych promieniowaniem jonizującym i traktowanych mikrocystyną-LR (Kinetics of single (SSB) and double (DSB) strand breaks in human lymphocytes irradiated with ionising radiation and treated with microcystin-LR).

XIII Zjazd Polskiego Towarzystwa Badań Radiacyjnych im. M. Skłodowskiej-Curie. Łódź, Poland, 13-16.09.2004. Materiały konferencyjne, P-26, p. 93.

45. Leciejewicz J., Starosta W., Premkumar T.

Crystal structure of an ionic thorium(IV) complex with pyridazine-2-carboxylate ligand.

46th Polish Crystallographic Meeting. Wrocław, Poland, 24-25.06.2004, A-42, p. 86.

46. Legocka I., Kostrzewa M., Mirkowski K.

Modification of polyethylene for obtaining PE films with increased surface and mechanical properties.

III Polish-Ukrainian Conference: Polymers of Special Application. Radom, Poland, 15-18.06.2004. Abstracts, p. 86.

47. Legocka I., Kostrzewa M., Mirkowski K., Nowicki A.

Modification of polypropylene to improve stabilization under irradiation with sterilization dose.

III Polish-Ukrainian Conference: Polymers of Special Application. Radom, Poland, 15-18.06.2004. Abstracts, p. 87.

48. Legocka I., Kozakiewicz J., Sadło J., Warchoł S., Kostrzewa M.

Using of poly(siloxaneurethanes) as medical scaffolds for tissue engineering.

III Polish-Ukrainian Conference: Polymers of Special Application. Radom, Poland, 15-18.06.2004. Abstracts, p. 106.

49. Legocka I., Lempert M., Warchoł S., Sadło J., Kozakiewicz J., Przybylski J.

Influence of radiation sterilization process on properties of poly(siloxaneurethanes) used as scaffolds for tissue engineering.

E-MRS 2004 Fall Meeting. Warsaw, Poland, 6-10.09.2004. Book of abstracts, B-16, p. 70.

50. Legocka I., Zimek Z., Mirkowski K., Nowicki A.

Preliminary study on application of PE filler modified by radiation.

E-MRS 2004 Fall Meeting. Warsaw, Poland, 6-10.09.2004. Book of abstracts, G-21, p. 215.

51. Lewandowska H., Samochocka K., Kruszewski M., Fuks L.

New antitumour derivative of *cis*-platinum: structure and biological activity of Pt(II) complex with methyl 3,4-diamino-2,3,4,6-tetradeoxy-α-L-lyxo-hexopyranoside.

Gliwice Scientific Meeting 2004. Gliwice, Poland, 19-20.11.2004, p. 55.

52. Lisowska H., Lankoff A., Banasik A., Padjas A., Wieczorek A., Kuszewski T., Góźdź S., Wójcik A.

Częstość aberracji chromosomowych w limfocytach krwi obwodowej pacjentów z nowotworem krtani (Frequency of chromosomal aberrations in peripheral blood lymphocytes of patients with larynx cancer).

XIII Zjazd Polskiego Towarzystwa Badań Radiacyjnych im. M. Skłodowskiej-Curie. Łódź, Poland, 13-16.09.2004. Materiały konferencyjne, P-27, p. 94.

53. Michalik J., Sadło J., Danilczuk M., Jong-Sung Yu, Kevan L.

Stabilization of cationic silver clusters in ZK-4 zeolite.

4th Asia Pacific EPR/ESR Symposium. Bangalore, India, 21-25.11.2004. Conference program and abstracts, p. 47.

54. Michalik J., Sadło J., Kevan L.

ESR and ESEEM study of silver clusters in SAPO-17 and SAPO-35 molecular sieves.

Abstracts of the 14th International Zeolite Conference. Cape Town, South Africa, 25-30.04.2004. E. van Steen, L.H. Callanan, M. Claeys (eds), pp. 589-590.

55. Narbutt J., Krejzler J.

Kinetics of hydrolysis and partition constants of neutral metal chelates as radiotracers. Solvent extraction of tris(thenoyltrifluoroacetonate)thallium(III).

Advances in nuclear radiochemistry. Extended abstracts of papers presented at the Sixth International Conference on Nuclear and Radiochemistry (NRC-6), 29 August to 3 September 2004, Aachen, Germany. S.M. Qaim and H.H. Coenen (eds). Forschungszentrum Jülich GmbH, Institut für Nuklearchemie, Jülich 2004. Vol. 3, pp. 474-476.

56. Narojczyk J., Werner Z., Piekoszewski J.

The effect of nitrogen implantation on the lifetime of cutting tools made of SK5M tool steel.

5th International Conference: Ion Implantation and Other Applications of Ions and Electrons, ION 2004. Kazimierz Dolny, Poland, 14-17.06.2004, p. 66.

57. Ołdak T., Iwaneńko T., Kruszewski M., Gajkowska A., Jastrzewska M., Machaj E.K., Pojda Z.

Naprawa popromiennych uszkodzeń DNA w proliferujących i nieproliferujących ludzkich komórkach $CD34^+$ (Repair of the radiation-induced DNA lesions in proliferating and non-proliferating human cells $CD34^+$).

XIII Zjazd Polskiego Towarzystwa Badań Radiacyjnych im. M. Skłodowskiej-Curie. Łódź, Poland, 13-16.09.2004. Materiały konferencyjne, P-28, p. 95.

58. Owczarczyk A., Dobrowolski A.

Application of tracers for transport investigations in unregulated rivers.

Isotope hydrology and integrated water resources management. International symposium held in Vienna, 19-23.05.2003 organized by the International Atomic Energy Agency and the Association of Hydrogeologists in cooperation with the International Association of Hydrological Sciences. Conference & Symposium Papers 23/P. IAEA, Vienna 2004, pp. 381-382.

59. Padjas A., Lankoff A., Banasik A., Lisowska H., Wieczorek A., Kuszewski T., Góźdź S., Wójcik A.

Analiza osobniczej promieniowrażliwości na podstawie uszkodzeń w limfocytach krwi obwodowej: porównanie różnych metod (Analysis of the individual radiation sensitivity on the basis of damage in peripheral blood lymphocytes: comparison of methods).

XIII Zjazd Polskiego Towarzystwa Badań Radiacyjnych im. M. Skłodowskiej-Curie. Łódź, Poland, 13-16.09.2004. Materiały konferencyjne, P-31, p. 98.

60. Panta P.P., Głuszewski W.

Ciepło właściwe najważniejszych grafitów, stosowanych w kalorymetrii wiązek elektronowych, i jego wpływ na dokładność pomiarów dużych dawek (The specific heat selected graphites used in calorimetry of electron beam and its influence on accuracy of measurements of large doses).

XIII Zjazd Polskiego Towarzystwa Badań Radiacyjnych im. M. Skłodowskiej-Curie. Łódź, Poland, 13-16.09.2004. Materiały konferencyjne, p. 65.

61. Pańczyk E., Kalicki A., Rowińska L., Waliś L.

Provenance studies of lead white of the 15th-18th century Venetian paintings by instrumental neutron activation analysis.

34th International Symposium on Archaeometry. Zaragoza, Spain, 3-7.05.2004. Program and abstracts, S4P37, [1] p.

62. Pańczyk E., Waliś L.

Applications of neutron activation analysis to identification of works of art.

NEMEA-2 Workshop: Neutron Measurements, Evaluations and Applications. Bucharest, Romania, 20-23.10.2004. Book of abstracts, p. 30.

63. Piekoszewski J., Kempiński W., Andrzejewski B., Trybuła Z., Piekara-Sady L., Kaszyński J., Stankowski J., Richter E., Stanisławski J., Werner Z.

Superconductivity of MgB_2 thin films prepared by ion implantation and pulsed plasma treatment.

5th International Conference: Ion Implantation and Other Applications of Ions and Electrons, ION 2004. Kazimierz Dolny, Poland, 14-17.06.2004, p. 22.

64. Pogocki D., Ghezzo-Schöneich E., Celuch M., Bobrowski K., Schöneich Ch., Hug G.L.

Singlet oxygen and hydroxyl radical induced oxidation as benchmarks of the conformational flexibility of Met-$(X)_n$-Met peptides.

RADAM'04: Radiation Damage in Biomolecular Systems. Lyon, France, 24-27.06.2004, [1] p.

65. Polkowska-Motrenko H.

Preparation of reference materials.

Workshop: Speciation Analysis – Reference Materials. Warsaw, Poland, 17.02.2004. Abstracts, p. 7.

66. Polkowska-Motrenko H., Danko B., Dybczyński R.

Potential of RNAA as a primary ration method.

11th International Conference: Modern Trends in Activation Analysis. Guildfort, United Kingdom, 20-25.06.2004. Programme and abstracts, M277, p. 199.

67. Polkowska-Motrenko H., Szopa Z., Dybczyński R.

Test biegłości „Rośliny 1" dla laboratoriów oznaczających metale w żywności (Proficiency test "PLANT 1" for laboratories which determine metals in foodstuff).

Nowoczesne metody przygotowania próbek i oznaczania śladowych ilości pierwiastków. Materiały XIII Poznańskiego Konwersatorium Analitycznego. Poznań, Poland, 6-7.05.2004, p. 125.

68. Polkowska-Motrenko H., Szopa Z., Dybczyński R.

Testy biegłości rośliny dla laboratoriów oznaczających metale w żywności (Proficiency tests "Plants" for the laboratories determining metals in food).

Ogólnopolska konferencja naukowa: „Jakość w chemii analitycznej". Warszawa, Poland, 25-26.11.2004, p. 34.

69. Pruszyński M., Bilewicz A., Wąs B., Petelenz B.

Use of metal-^{211}At complexes as a new method for preparation of astatine radiopharmaceuticals.

Advances in nuclear radiochemistry. Extended abstracts of papers presented at the Sixth International Conference on Nuclear and Radiochemistry (NRC-6), 29 August to 3 September 2004, Aachen, Germany. S.M. Qaim and H.H. Coenen (eds). Forschungszentrum Jülich GmbH, Institut für Nuklearchemie, Jülich 2004. Vol. 3, pp. 440-442.

70. Przybytniak G.

Radiation damage in the DNA.

3rd Workshop of the COST Chemistry Action D27: Prebiotic chemistry and early evolution. Heraklion, Greece, 30.09.-3.10.2004, [1] p.

71. Przybytniak G.

Stabilizacja anionorodników w DNA i jego nukleotydach (Stabilization of radicals anions in DNA and its nucleotides).

XIII Zjazd Polskiego Towarzystwa Badań Radiacyjnych im. M. Skłodowskiej-Curie. Łódź, Poland, 13-16.09.2004. Materiały zjazdu, p. 20.

72. Samczyński Z., Dybczyński R.

Rozdzielanie niektórych pierwiastków przejściowych na jonitach Retardion 11 A8 i Chelex 100 w środowiskach amoniakalnych (Separation of same transition elements on Ratardion 11 A8 and Chelex 100 ion exchange resins in ammoniacal media).

XLVII Zjazd PTChem i SITPChem. Wrocław, Poland, 12-17.09.2004. Materiały zjazdowe, Vol. I, p. 336.

73. Sartowska B., Piekoszewski J., Waliś L., Szymczyk W., Stanisławski J., Nowicki L., Kopcewicz M., Barcz M., Prokert F.

Modification of the near surface layer of carbon steels with intense argon and nitrogen plasma pulses.

5th International Conference: Ion Implantation and Other Applications of Ions and Electrons, ION 2004. Kazimierz Dolny, Poland, 14-17.06.2004, p. 39.

74. Sommer S., Buraczewska I., Wojewódzka M., Bożyk E., Szumiel I., Król M., Kasprzycka J., Wójcik A.

Zróżnicowane częstości popromiennych aberracji chromosomowych w chromosomach 2, 8 i 14 w limfocytach krwi obwodowej siedmiu dawców (Differential frequency of radiation-induced chromosomal aberration in chromosome 2, 8, and 14 in peripheral blood lymphocytes of seven donors).

XIII Zjazd Polskiego Towarzystwa Badań Radiacyjnych im. M. Skłodowskiej-Curie. Łódź, Poland, 13-16.09.2004. Materiały konferencyjne, P-29, p. 96.

75. Sommer S., Buraczewska I., Wojewódzka M., Bożyk E., Szumiel I., Wójcik A.

Analysis of the frequencies of exchange type aberration in chromosomes 2, 8, and 14 in lymphocytes of seven donors by chromosome paintings.

European Radiation Research 2004: the 33rd Annual Meeting of the European Society for Radiation Biology. Budapest, Hungary, 25-28.08.2004, p. 262.

76. Sommer S., Buraczewska I., Wójcik A.

Szybka dozymetria biologiczna w przypadkach masowego narażenia na promieniowanie jonizujące (Fast biological dosimetry cases of a mass radiobiological casualty).

Międzynarodowa konferencja naukowo-techniczna: Ochrona człowieka i środowiska naturalnego przed skażeniami. Warszawa, Poland, 2-4.06.2004, [1] p.

77. Starosta W., Leciejewicz J.

Crystal structures of three calcium(II) complexes with pyrazine-2,3-dicarboxylate ligand.

46th Polish Crystallographic Meeting. Wrocław, Poland, 24-25.06.2004, A-75, p. 130.

78. Szopa Z., Kulisa K., Dybczyński R.

Analiza materiałów opakowaniowych metodą instrumentalnej neutronowej analizy aktywacyjnej (INAA analysis of packing materials).

Nowoczesne metody przygotowania próbek i oznaczania śladowych ilości pierwiastków. Materiały XIII Poznańskiego Konwersatorium Analitycznego. Poznań, Poland, 6-7.05.2004, p. 89.

79. Trojanowicz M.A., Drzewicz P., Bojanowska-Czajka A., Nałęcz-Jawecki G., Sawicki J., Gryz M., Wołkowicz S.

Monitoring of toxicity during degradation of selected pesticides using ionizing radiation.

SETAC Europe 14th Annual Meeting: A Pan-European perspectives. Prague, Czech Republic, 18-22.04.2004. Abstracts, p. 97.

80. Tymiński B., Zwoliński K., Chmielewski A.G.

Badanie katalitycznego rozkładu polietylenu z rozdestylowaniem produktów rozkładu (Catalytic decomposition of polyethylene with fractionation of products by distillation).

XIII Środkowoeuropejska Konferencja ECOpole'04. Jamrozowa Polana – Hradec Králové, 21-23.10.2004. Streszczenia wystąpień, [1] p.

81. Wierzchnicki R., Derda M., Mikołajczuk A.

Stable isotope composition of food from different regions of Poland.

International Conference on Isotopic and Nuclear Analytical Method for Health and Environment. Vienna, Austria, 10-13.06.2003. Conference & Symposium Papers 22/CD. IAEA, Vienna 2004. IAEA-CN-103/037, [1] p. (CD edition).

82. Wiśniowski P., Bobrowski K., Filipiak P., Carmichael I., Hug G.L.

β-Scission of α-thioalkyl radicals. Time-resolved ESR detection in the pulse radiolysis of α-(alkylthio)-substituted acetamide, acetic acid, and acetone.

Trombay Symposium on Radiation and Photochemistry (TSRP-2004). Mumbai, India, 8-12.01.2004. Vol. 1. Invited talks, IT-13, p. 52.

83. Wojewódzka M., Bartłomiejczyk T., Buraczewska I., Zakierska I., Kruszewski M.

Częstość spontanicznej i indukowanej promieniowaniem rekombinacji homologicznej w dwóch liniach komórkowych różniących się zdolnością do napraw DSB (Frequency of spontaneous and radiation-induced homologous recombination in two cell lines differing in capacity to repair DSB).

XIII Zjazd Polskiego Towarzystwa Badań Radiacyjnych im. M. Skłodowskiej-Curie. Łódź, Poland, 13-16.09.2004. Materiały konferencyjne, P-22, p. 89.

84. Wojewódzka M., Bartłomiejczyk T., Kruszewski M.

Does inhibition of PARP change the frequency of homologous recombination?

DNA Repair 2004. 8th Meeting of the German DNA Repair Network. Ulm, Germany, 28.09.-1.10.2004, p. 173.

85. Wojewódzka M., Buraczewska I., Sochanowicz B., Szumiel I.

The role of poly(ADP-ribosylation) in double strand break fixation in L5178Y and CHO cells.

European Radiation Research 2004: the 33rd Annual Meeting of the European Society for Radiation Biology. Budapest, Hungary, 25-28.08.2004, p. 302.

86. Wójcik A.

Do interindividual differences in lymphocyte chromosome radiosensitivity exist?

Gliwice Scientific Meeting 2004. Gliwice, Poland, 19-20.11.2004, p. 36.

87. Wójcik A., Cosset J.-M., Clough K., Gourmelon P., Bottolier J.-F., Stephan G., Sommer S., Wieczorek A., Słuszniak J., Kułakowski A., Góźdź S., Michalik J., Stachowicz W., Sadło J., Bulski W., Izewska J.

The radiological accident at the Bialystok Oncology Center: cause, dose estimation and patient treatment.

11th International Congress of the International Radiation Protection Association. Madrid, Spain, 23-28.05.2004. Abstracts, p. 305.

88. Wójcik A., Stoilov L., Szumiel I., Legerski R., Obe G.

BrdU and radiation-induced sisters chromatid exchangers (SCE): the role of interstrand crosslinks (ILC) and Rad51C.

European Radiation Research 2004: the 33rd Annual Meeting of the European Society for Radiation Biology. Budapest, Hungary, 25-28.08.2004, p. 301.

89. Zagórski Z.P.

Chemia radiacyjna eksploracji Marsa (Radiation chemistry of Mars exploration).

XIII Zjazd Polskiego Towarzystwa Badań Radiacyjnych im. M. Skłodowskiej-Curie. Łódź, Poland, 13-16.09.2004. Materiały konferencyjne, p. 27.

90. Zagórski Z.P., Przybytniak GK., Głuszewski W.

Irreversible, radiation induced dehydrogenation of organic matter.

3rd Workshop of the COST Chemistry Action D27: Prebiotic Chemistry and Early Evolution. Heraklion, Greece, 30.09.-3.10.2004, [1] p.

91. Zakrzewska-Trznadel G.

Stable isotopes – some comments on new fields of applications.

The 12th International Symposium on Laser Spectroscopy. Daejeon, Korea, 4-5.11.2004. Program and abstracts. Vol. 12, no. 1, p. 18.

92. Zakrzewska-Trznadel G., Dobrowolski A.

Permeation cascades for separation of oxygen isotopes.

Euromembrane 2004. Hamburg, Germany, 28.09.-1.10.2004. Book of abstracts, p. 642.

93. Zasępa M., Mieczkowski J., Narbutt J.

^{99m}Tc(I) tricarbonyl complexes with N-methylamides of picolinic and thiopicolinic acids.

Advances in nuclear radiochemistry. Extended abstracts of papers presented at the Sixth International Conference on Nuclear and Radiochemistry (NRC-6), 29 August to 3 September 2004, Aachen, Germany. S.M. Qaim and H.H. Coenen (eds). Forschungszentrum Jülich GmbH, Institut für Nuklearchemie, Jülich 2004. Vol. 3, pp. 427-429.

94. Ziółek M., Michalska A., Decyk P., Nowak I., Michalik J., Sadło J.

Alkali-resistance of MCM-41 mesoporous molecular sieves containing various T (Al, Si, Nb) elements.

Abstracts of the 14th International Zeolite Conference. Cape Town, South Africa, 25-30.04.2004. E. van Steen, L.H. Callanan, M. Claeys (eds), pp. 214-215.

SUPPLEMENT LIST OF THE INCT PUBLICATIONS IN 2003

ARTICLES

1. Bik J., Zagórski Z.P., Rzymski W.M., Głuszewski W.

Radiacyjne sieciowanie elastomeru butadienowo-akrylonitrylowego (Radiation crosslinking of butadiene-acrylonitrile elastomer).

Prace Naukowe Instytutu Technologii Organicznej i Tworzyw Sztucznych Politechniki Wrocławskiej, Vol. 52, Seria: Konferencje, 147-150 (2003).

2. Chmielewski A.G., Wierzchnicki R., Derda M., Mikołajczuk A., Zakrzewska-Trznadel G.
Application of stable isotopes in environmental studies and in food authentication.
Studia Universitatis Babeş-Bolyai, Physica, Special issue, 1, XLVIII, 119-124 (2003).

3. Michalik J.
Trudne lata chemii jądrowej (Difficult years of nuclear chemistry).
Przegląd Techniczny, 22, 6-7 (2003).

4. Rudawska K., Ptasiewicz-Bąk H.
The crystal structures of tetra-*n*-butylammonium salts of $GaCl_4^-$, $GaBr_4^-$ and GaI_4^-.
Journal of Coordination Chemistry, 56, 18, 1567-1574 (2003).

5. Sartowska B., Piekoszewski J., Waliś L., Kopcewicz M., Werner Z., Stanisławski J., Kalinowska J., Prokert F.
Phase changes in steels irradiated with intense pulsed plasma beams.
Vacuum, 70, 285-291 (2003).

6. Stanisławski J., Baranowski J., Piekoszewski J., Składnik-Sadowska E., Werner Z.
Studies of interaction of plasma pulse with solid substrate as observed by optical spectroscopy.
Plasma Physics and Controlled Fusion, 45, 1121-1126 (2003).

7. Zakrzewska-Trznadel G., Chmielewski A.G., Miljević N., Van Hook A.
Separation of hydrogen and oxygen isotopes by membrane method.
Studia Universitatis Babeş-Bolyai, Physica, Special issue, 1, XLVIII, 39-46 (2003).

CONFERENCE PROCEEDINGS

1. Chmielewski A.G., Sun Y.-X., Bułka S., Zimek Z.
Volatile organic compounds treatment by using ionization technology.
4th International Conference of PhD Students. Miskolc, Hungary, 11-17 August 2003. Engineering sciences. Vol. II, pp. 47-53.

2. Chmielewski A.G., Tymiński B., Zimek Z., Pawelec A., Licki J.
Industrial plant for flue gas treatment with high power electron accelerators.
Application of accelerators in research and industry. 17th International Conference on the Application of Accelerators in Research and Industry. Denton, Texas, 12-16.11.2002. J.L. Duggan, I.L. Morgan (eds). AIP Conference Proceedings. Vol. 680. American Institute of Physics, Melville, New York 2003, pp. 873-876.

3. Zagórski Z.P.
Radiation chemistry of spurs in polymers.
Report of the Consultants Meeting on Advances in Radiation Chemistry of Polymers. Notre Dame, Indiana, USA, 13-17.09.2003. IAEA, Vienna 2003, pp. 36-45.

NUKLEONIKA
INTERNATIONAL JOURNAL OF NUCLEAR RESEARCH

CONTENTS OF No. 1/2004

CONTENTS OF No. 2/2004

CONTENTS OF No. 3/2004

Proceedings of the International Conference on Isotopic and Nuclear Analytical Techniques for Health and Environment, 10-13 June 2003, Vienna, Austria

CONTENTS OF No. 4/2004

SUPPLEMENT No. 1/2004

Proceedings of the International Conference "Bioaccumulation of Radionuclides and Heavy Metals – as a Marker of Environmental Contamination", 26-28 September 2004, Kazimierz Dolny upon Vistula, Poland

6. A simple and quick model to study uptake and transfer of radionuclides and heavy metals from mycelium to the fruitbody of saprophytic edible fungi
   J.L. Manjón, P.L. Urban, G. Bystrzejewska-Piotrowska
7. ^{137}Cs content in mushrooms from localities in eastern Slovakia
   A. Čipáková
8. Platinum uptake by mustard (*Sinapis alba* L.) and maize (*Zea mays* L.) plants
   J. Kowalska, M. Asztemborska, G. Bystrzejewska-Piotrowska
9. Uptake and distribution of caesium and its influence on the physiological processes in croton plants (*Codiaeum variegatum*)
   G. Bystrzejewska-Piotrowska, M. Jeruzalski, P.L. Urban
10. Analytical evaluation of the iron transfer from cigarette tobacco to human body
    M. Herman, P. Kościelniak
11. Application of probiotics in the xenobiotic detoxification therapy
    P.L. Urban, R.T. Kuthan

SUPPLEMENT No. 2/2004

Proceedings of the 2nd Warsaw Meeting on Particle Correlations and Resonances in Heavy Ion Collisions, 15-18 October 2003, Warsaw, Poland

1. Foreword
   J. Pluta
2. Correlation femtoscopy
   R. Lednický
3. Stable Bose-Einstein correlations
   T. Csörgő, S. Hegyi, W.A. Zajc
4. Understanding of the freeze-out in ultra-relativistic heavy-ion collisions
   B. Tomášik
5. BEC for photons and neutral pions
   O.V. Utyuzh, G. Wilk
6. Single particle spectra from information theory point of view
   F.S. Navarra, O.V. Utyuzh, G. Wilk, Z. Włodarczyk
7. Some new aspects of femtoscopy at high energy
   A.V. Stavinskiy, K.R. Mikhailov, A.V. Vlassov, B. Erazmus, G. Renault
8. Sum rule of the correlation function
   S. Mrówczyński, R. Maj
9. How to model BEC numerically?
   O.V. Utyuzh, G. Wilk, Z. Włodarczyk
10. Modeling Bose-Einstein correlations in heavy ion collisions at RHIC
    M. Bysterský
11. Pion entropy and phase space density in RHIC collisions
    J.G. Cramer for the STAR Collaboration
12. Buda-Lund hydro model and the elliptic flow at RHIC
    M. Csanád, T. Csörgő, B. Lörstad, A. Ster
13. A hint at quark deconfinement in 200 GeV Au+Au data at RHIC
    M. Csanád, T. Csörgő, B. Lörstad, A. Ster
14. Non-identical strange particle correlations in Au+Au collisions at $\sqrt{s_{NN}}=200$ GeV from the STAR experiment
    G. Renault for the STAR Collaboration
15. Alternative size and lifetime measurements for RHIC
    S. Pratt
16. Pion interferometry in Au+Au collisions at $\sqrt{s_{NN}}=200$ GeV
    M. López Noriega for the STAR Collaboration
17. Azimuthally-sensitive interferometry and the source lifetime at RHIC
    M.A. Lisa for the STAR Collaboration
18. Non-identical particle correlations in STAR
    M. Janik, A. Kisiel, P. Szarwas for the STAR Collaboration

SUPPLEMENT No. 3/2004

Proceedings of the All-Polish Seminar on Mössbauer Spectroscopy OSSM'04, 6-9 June 2004, Wisła, Poland

Information

INSTITUTE OF NUCLEAR CHEMISTRY AND TECHNOLOGY
NUKLEONIKA
Dorodna 16, 03-195 Warszawa, Poland
phone: (+4822) 811-30-21 or 811-00-81 int. 14-91; fax: (+4822) 811-15-32;
e-mail: nukleon@orange.ichtj.waw.pl
Abstracts and full texts are available on-line at http://www.ichtj.waw.pl/ichtj/general/nukleon.htm

THE INCT PATENTS AND PATENT APPLICATIONS IN 2004

PATENTS

1. Nowe środki do barwienia drewna i innych materiałów celulozowych o własnościach grzybobójczych (New fungicidal agents for colouring wood and other cellulose materials)
   A. Łukasiewicz, L. Waliś, B. Sartowska
   Polish Patent No. 186919
2. Sposób usuwania tlenków azotu z przemysłowych gazów odlotowych (Method for removal of nitrogen oxides from industrial flue gases)
   A.G. Chmielewski, Z. Zimek, J. Licki
   Polish Patent No. 187980

PATENT APPLICATIONS

1. Sposób metalizowania tkanin z włókien meta-aramidowych (Method for metallization of textures from meta-aramid fibres)
   A. Łukasiewicz, D. Chmielewska, L. Waliś, J. Michalik
   P.368010
2. Dozymetr alaninowo-polimerowy (Alanine-polymer dosimeter)
   Z. Stuglik
   P.371860

CONFERENCES ORGANIZED AND CO-ORGANIZED BY THE INCT IN 2004

1. 2nd RESEARCH COORDINATION MEETING OF THE INTERNATIONAL ATOMIC ENERGY AGENCY "REMEDIATION OF POLLUTED WATERS AND WASTEWATERS BY RADIATION PROCESSING", 14-18 JUNE 2004, WARSZAWA, POLAND

Organized by the Institute of Nuclear Chemistry and Technology and International Atomic Energy Agency

Organizing Committee: Prof. M. Trojanowicz, Ph.D., D.Sc., Prof. A.G. Chmielewski, Ph.D., D.Sc., R. Janusz, M.Sc., A. Bojanowska-Czajka, M.Sc., P. Drzewicz, M.Sc.

LECTURES

- Radiation processing of secondary effluents from municipal wastewater treatment plants
  P. Gehringer (ARC Seibersdorf Research GmbH, Austria)
- Present status of wastewater treatment in Brazil and economic analysis of mobile electron beam facility
  M.H.O. Sampa (Radiation Technology Centre, IPEN, Sao Paulo, Brazil)
- Radiation decontamination of municipal wastewater in pilot plant using electron beam accelerator
  T. Ramirez (National Polytechnic School, Quito, Ecuador)
- High-energy radiation treatment of wastewater containing textile dye
  E. Takacs (Institute of Isotopes and Surface Chemistry, Hungarian Academy of Sciences, Budapest, Hungary)
- Remediation of drinking water and wastewater by irradiation
  H. Amro (Ministry of Water and Irrigation, Amman, Jordan)
- Gamma sources based on europium
  R. Kuznetsov (FSUE "SSC RF RIAR", Dimitrovgrad, Russia)
- Impact of ionizing radiation on slaughterhouse wastewater
  M.L.C. Bothelo (Nuclear and Technological Institute, Sacavém, Portugal)
- Reuse of effluent from municipal sewage plant. EB and biological treatment of hazardous wastewater containing explosives
  B. Han (EB-TECH Co. Ltd., Daejong, Korea)
- The degradation of some pesticides and Apollofix dyes by γ-irradiation
  D. Solpan (Hacettepe University, Ankara, Turkey)
- Mechanism of destruction of MTBE
  W. Cooper (University of North Carolina-Wilmington, USA)
- Kinetics and mechanism of carbendazim transformation in water containing oxygen under action of electron beam
  G. Nichipor (National Academy of Sciences of Belarus, Minsk-Sosny, Belarus)
- Radiolytic degradation of selected chlorophenoxy acid pesticides in waters and industrial wastes
  M. Trojanowicz (Institute of Nuclear Chemistry and Technology, Warszawa, Poland)

2. PREPARATION OF A TECHNICAL DOCUMENT ON RADIOTRACERS AND LABELLING COMPOUNDS FOR APPLICATIONS IN INDUSTRY AND ENVIRONMENT – IAEA CONSULTANTS MEETING, 16-19 JUNE 2004, WARSZAWA, POLAND

Organized by the International Atomic Energy Agency and Institute of Nuclear Chemistry and Technology

SCIENTIFIC PART

- Radioisotope tracer applications in industry – an overview
  A.S. Hills (Nuclear Energy Corporation of South Africa, South Africa)
- Radiotracers for industrial applications – problems and difficulties faced by developing countries
  I. Khan (Pakistan Institute of Nuclear Science and Technology, Islamabad, Pakistan)
- Methodological aspects of the radiotracers use
  J. Palige (Institute of Nuclear Chemistry and Technology, Warszawa, Poland)

- Industrial radiotracers – ideal needs contra present availability
  T. Bjørnstad (Institute for Energy Technology, Kjeller, Norway)

PRACTICAL PART

Visit to the Radioisotope Centre POLATOM (Świerk, Poland)

3. INTERNATIONAL SYMPOSIUM ON ADVANCED OXIDATION TECHNOLOGIES FOR WASTEWATER TREATMENT, 18 JUNE 2004, WARSZAWA, POLAND

Organized by the International Atomic Energy Agency; Faculty of Chemical and Process Engineering, Warsaw University of Technology; Institute of Nuclear Chemistry and Technology

Organizing Committee: M. Obrębska, Ph.D., Prof. A. Biń, Ph.D., D.Sc., Prof. M. Trojanowicz, Ph.D., D.Sc., Prof. A.G. Chmielewski, Ph.D., D.Sc.

LECTURES

Session I

Chairman: Prof. A.G. Chmielewski, Ph.D., D.Sc. (Warsaw University of Technology; Institute of Nuclear Chemistry and Technology, Warszawa, Poland)

- Wastewater reuse in Jordan – policy and prospective
  H. Amro (Ministry of Water and Irrigation, Amman, Jordan)
- A proposed free radical-mechanism for the destruction of methyl *t*-butyl ether (MTBE) in water
  W. Cooper (University of North Carolina-Wilmington, USA)
- Advanced oxidations processes involving ozone
  A.K. Biń (Warsaw University of Technology, Poland)
- Biodegradation tests
  J. Zieliński (Institute of Organic Chemistry, Warszawa, Poland)

Session II

Chairman: Prof. A. Biń, Ph.D., D.Sc. (Warsaw University of Technology, Poland)

- Radiation processing of secondary effluents from municipal wastewater treatment plants
  P. Gehringer (ARC Seibersdorf Research GmbH, Austria)
- Microbiological aspects in wastewater
  M.L.C. Bothelo (Nuclear and Technological Institute, Sacavém, Portugal)
- Electron beam treatment of industrial wastewater – treatment by ionising radiation
  B. Han (EB-TECH Co. Ltd., Daejong, Korea)
- Wet oxidation of sludge
  R. Zarzycki (Technical Universty of Łódź, Poland)

4. CONFERENCE ON TRACERS AND TRACING METHODS, 22-24 JUNE 2004, CIECHOCINEK, POLAND

Organized by the Institute of Nuclear Chemistry and Technology; Faculty of Process and Chemical Engineering, Warsaw University of Technology; Laboratoire des Sciences du Génie Chimique; International Atomic Energy Agency

Organizing Committee: Jacek Palige, Ph.D., Dorota Korniszewska, Sylwia Ptaszek, M.Sc., Ewa Godlewska-Para, M.Sc., Piotr Grzybowski, Ph.D., Wojciech Orciuch, Ph.D.

LECTURES

A. Fundamental development

RTD and tracer methodology

- Application of test reactions to study mixing on the molecular scale
  J. Bałdyga (Warsaw University of Technology, Poland)
- Application of QMOM to simulate transient tracer and crystal size distributions
  J. Bałdyga (Warsaw University of Technology, Poland), W. Orciuch (Warsaw University of Technology, Poland)
- Reactive mixing in stirred tanks
  J. Bałdyga (Warsaw University of Technology, Poland), Ł. Makowski (Warsaw University of Technology, Poland)

- Tracer investigation of processes under variable flow
  L. Furman (AGH University of Science and Technology, Kraków, Poland), J.-P. Leclerc (CNRS, Nancy, France), Z. Stęgowski (AGH University of Science and Technology, Kraków, Poland)
- Advances in flow mapping of multiphase systems by radioactive techniques
  M.P. Dudukovic (Washington University, St. Louis, USA)
- The non-stationary two-phase flow evaluation by radioisotopes
  L. Petryka (AGH University of Science and Technology, Kraków, Poland), M. Zych (AGH University of Science and Technology, Kraków, Poland), R. Murzyn (AGH University of Science and Technology, Kraków, Poland)

RTD methodology and Computational Fluid Dynamics (CFD)

- Mixing and RTD in tanks: radiotracer experiments and CFD simulations
  A.R. Thatte (University of Mumbai, India), A.W. Patwardhan (University of Mumbai, India), H.J. Pant (Bhabha Atomic Research Centre, Mumbai, India), V.K. Sharma (Bhabha Atomic Research Centre, Mumbai, India), Gursharan Singh (Bhabha Atomic Research Centre, Mumbai, India), Ph. Berne (CEA, Grenoble, France)
- PIV, radiotracers and CFD for flow anomalies
  P. Houdek (Czech Technical University in Praque, Czech Republic), I. Reitspiesová (Czech Technical University in Praque, Czech Republic), R. Žitný (Czech Technical University in Praque, Czech Republic), J. Thýn (Czech Technical University in Praque, Czech Republic)
- Tracer dispersion – experiment and CFD
  R. Žitný (Czech Technical University in Praque, Czech Republic)
- Computational Fluid Dynamics (CFD) simulation for solid flow and selection in a hydrocyclone
  E. Nowak (AGH University of Science and Technology, Kraków, Poland), Z. Stęgowski (AGH University of Science and Technology, Kraków, Poland)
- Dynamical features extracted from the solid circulation trajectories in gas-liquid-solid fluidized bed
  M. Cassanello (Universidad de Buenos Aires, Argentina), F. Larachi (Laval University, Canada), J. Chaouki (École Polytechnique, Montreal, Canada)

New tracers and detectors

- Simplified SPECT camera for fluid flow monitoring
  L. Furman (AGH University of Science and Technology, Kraków, Poland), T. Prus (AGH University of Science and Technology, Kraków, Poland)
- Molecular imprinting, a valuable tool for tracer analysis?
  C. Galdiga (Institute for Energy Technology, Kjeller, Norway), T. Bjørnstad (Institute for Energy Technology, Kjeller; University of Oslo, Norway)
- Industrial radionuclide generators – status and perspectives
  T. Bjørnstad (Institute for Energy Technology, Kjeller; University of Oslo, Norway)
- New technologies for production of radiopharmaceuticals and other medical preparations
  Z. Bazaniak (Radioisotope Centre POLATOM, Świerk, Poland), E. Iller (Radioisotope Centre POLATOM, Świerk, Poland), R. Mikołajczak (Radioisotope Centre POLATOM, Świerk, Poland)
- Portable instrument for acquisition and processing data from radiometric experiments performed in the field and industrial conditions
  P. Urbański (Institute of Nuclear Chemistry and Technology, Warszawa, Poland), J. Mirowicz (Institute of Nuclear Chemistry and Technology, Warszawa, Poland), A. Owczarczyk (Institute of Nuclear Chemistry and Technology, Warszawa, Poland), J. Pieńkos (Institute of Nuclear Chemistry and Technology, Warszawa, Poland), E. Świstowski (Institute of Nuclear Chemistry and Technology, Warszawa, Poland), B. Machaj (Institute of Nuclear Chemistry and Technology, Warszawa, Poland)
- Isotope ratio as a tracer for investigation of anthropogenic sulphur sources
  M. Derda (Institute of Nuclear Chemistry and Technology, Warszawa, Poland), A.G. Chmielewski (Institute of Nuclear Chemistry and Technology, Warszawa; Warsaw University of Technology, Poland)

B. Industrial applications

Environment

- Industrial applications of radiotracer and sealed source technology promoted by IAEA
  J.-H. Jin (International Atomic Energy Agency, Vienna, Austria), J. Thereska (International Atomic Energy Agency, Vienna, Austria)
- Overview of radiotracer experiments for better understanding of wastewater and water treatment plants in Lima (Peru)
  C.S. Calvo (Nuclear Energy Peruvian Institute – IPEN, Lima, Peru), G. Maghella (Nuclear Energy Peruvian Institute – IPEN, Lima, Peru), E. Mamani (Nuclear Energy Peruvian Institute – IPEN, Lima, Peru), Ph. Berne (CEA, Grenoble, France), P. Brisset (CEA, Saclay, France), J.-P. Leclerc (CNRS, Nancy, France)

- Radiotracer study on the efficiency of a cylindrical 2-stage anaerobic sludge digester
  S.-H. Jung (Korea Atomic Energy Research Institute, Daejon, Korea), J.-H. Jin (Korea Atomic Energy Research Institute, Daejon, Korea), J.-B. Kim (Korea Atomic Energy Research Institute, Daejon, Korea)
- RTD measurements in an aerated sludge channel reactor: influence of the geometrical and operating parameters
  O. Potier (CNRS, Nancy, France), J.-P. Leclerc (CNRS, Nancy, France), M.-N. Pons (CNRS, Nancy, France)
- Applications of tracers and CFD methods for investigations of wastewater treatment installations
  J. Palige (Institute of Nuclear Chemistry and Technology, Warszawa, Poland), A. Owczarczyk (Institute of Nuclear Chemistry and Technology, Warszawa, Poland), A. Dobrowolski (Institute of Nuclear Chemistry and Technology, Warszawa, Poland), A.G. Chmielewski (Institute of Nuclear Chemistry and Technology, Warszawa; Warsaw University of Technology, Poland), S. Ptaszek (Institute of Nuclear Chemistry and Technology, Warszawa, Poland)
- Influence of fluid structure upon the shape of RTD curve at a sugar crystallizer
  J. Griffith (Cuban Institute of Sugar Research, Havana, Cuba), J.I. Borroto (Institute of Applied Technologies and Sciences, Havana, Cuba), J.-P. Leclerc (CNRS, Nancy, France)

Geology, hydrogeology and oil field applications

- Investigation of the transport behaviour of selected organic compounds at the electrochemical remediation of contaminated soils
  T. Jentsch (Fraunhofer Institute for Nondestructive Testing, Dresden, Germany)
- The role of radiotracers in petroleum exploration and production
  T. Bjørnstad (Institute for Energy Technology, Kjeller; University of Oslo, Norway)
- Use of tracer tests to evaluate hydraulic properties of constructed wetlands
  P. Wachniew (AGH University of Science and Technology, Kraków, Poland), P. Czupryński (AGH University of Science and Technology, Kraków, Poland), P. Małoszewski (GSF, Institute of Hydrology, Neuherberg, Germany)
- Development of multitracer methology for the characterization of petroleum reservoirs
  E.H.T. Pereira (Center for Development of Nuclear Technology, Belo Horizonte, Brazil), R.M. Moreira (Center for Development of Nuclear Technology, Belo Horizonte, Brazil), A.M.F. Pinto (Center for Development of Nuclear Technology, Belo Horizonte, Brazil), D.L. Floresta (Center for Development of Nuclear Technology, Belo Horizonte, Brazil)
- Tracer investigation of ground water direction and flow velocity in the field of drainage system interaction
  W. Sołtyk (Institute of Nuclear Chemistry and Technology, Warszawa, Poland), A. Dobrowolski (Institute of Nuclear Chemistry and Technology, Warszawa, Poland), R. Zimnicki (Institute of Nuclear Chemistry and Technology, Warszawa, Poland), A. Owczarczyk (Institute of Nuclear Chemistry and Technology, Warszawa, Poland)
- Application of artificial neural networks for modeling of water transport in the Danube catchment
  M. Zimnoch (AGH University of Science and Technology, Kraków, Poland), K. Różański (AGH University of Science and Technology, Kraków, Poland), W. Chmura (AGH University of Science and Technology, Kraków, Poland), M. Mikołajczak (AGH University of Science and Technology, Kraków, Poland), D. Rank (Institute of Geology, Vienna, Austria)

Civil engineering, mineral engineering and metallurgy applications

- Airflow characterization of an experimental chamber for investigations on indoor air purification
  G. Bulteau (Centre Scientifique et Technique du Bâtiment, Nantes, France), A. Lakel (Centre Scientifique et Technique du Bâtiment, Nantes, France), A. Subrenat (CNRS, Nantes, France), P. Le Cloirec (CNRS, Nantes, France)
- Radon as indicator for radiation quality indoor air
  Z.A. Kovtun (Tomsk Polytechnic University, Russia), V.S. Yakovleva (Tomsk Polytechnic University, Russia), V.P. Borisov (Tomsk Polytechnic University, Russia), V.D. Karataev (Tomsk Polytechnic University, Russia)
- Multitracer method of diffusion measurement in chromium-manganese steels
  J. Dudała (AGH University of Science and Technology, Kraków, Poland), Z. Stęgowski (AGH University of Science and Technology, Kraków, Poland), J. Gilewicz-Wolter (AGH University of Science and Technology, Kraków, Poland)
- Neutrons and art
  E. Pańczyk (Institute of Nuclear Chemistry and Technology, Warszawa, Poland), L. Waliś (Institute of Nuclear Chemistry and Technology, Warszawa, Poland)
- Investigating the radon flux density from the earth surface using different techniques
  Z.A. Kovtun (Tomsk Polytechnic University, Russia), V.S. Yakovleva (Tomsk Polytechnic University, Russia), V.P. Borisov (Tomsk Polytechnic University, Russia)

Food engineering and bio-engineering

- Tracer measurement of residence time distributions of the liquid flow inside a photo-reactor
  R.M. Moreira (Center for Development of Nuclear Technology, Belo Horizonte, Brazil), A.M.F. Pinto (Center for Development of Nuclear Technology, Belo Horizonte, Brazil), B.G. Batista (Center for Development of Nuclear Technology, Belo Horizonte, Brazil), C.V.P. Alves (Federal University of Minas Gerais, Belo Horizonte, Brazil)
- Analysis of the electrostatic precipitation of particles and drops in a smoking process of seafood products
  J. Bellier (École Normale Supérieure de Lyon, France), C. Solliec (CNRS, Nantes, France), M. Pavageau (CNRS, Nantes, France), R. Baron (Ifremer, Nantes, France)
- Characterization of the light availability in a photobioreactor by coupling microalgae trajectories prediction with a light attenuation model
  L. Pottier (CNRS, Nantes, France), J. Pruvost (CNRS, Nantes, France), J. Legrand (CNRS, St. Nazaire, France)
- Stable isotope composition of environmental water and food products as a tracer of origin
  R. Wierzchnicki (Institute of Nuclear Chemistry and Technology, Warszawa, Poland), A. Owczarczyk (Institute of Nuclear Chemistry and Technology, Warszawa, Poland), W. Sołtyk (Institute of Nuclear Chemistry and Technology, Warszawa, Poland)

Material engineering

- Numerical simulation of homogenization time measurement by probes with different volume size
  J. Thýn (Czech Technical University in Prague, Czech Republic), M. Nový (Czech Technical University in Prague, Czech Republic), M. Moštěk (Prague Institute of Chemical Technology, Czech Republic), R. Žitný (Czech Technical University in Prague, Czech Republic), M. Jahoda (Prague Institute of Chemical Technology, Czech Republic)
- *In situ* measurement of diffusivity
  Ph. Berne (CEA, Grenoble, France), J. Pocachard (CEA, Grenoble, France)
- Measurement of diffusion coefficients in porous grains by column experiments: influence of the size distribution
  Ph. Berne (CEA, Grenoble, France), I. Landry (CEA, Grenoble, France), R. Gouaty (Laboratoire d'Annecy-le-Vieux de Physique des Particules, France)
- Leakproof control of technological installations and underground pipelines using radioactive tracers as a contribution to the protection of the natural environment
  J. Kraś (Institute of Nuclear Chemistry and Technology, Warszawa, Poland), L. Waliś (Institute of Nuclear Chemistry and Technology, Warszawa, Poland), S. Myczkowski (Institute of Nuclear Chemistry and Technology, Warszawa, Poland), E. Pańczyk (Institute of Nuclear Chemistry and Technology, Warszawa, Poland)
- The introduction of the Euro: did the tracer community miss something?
  Ph. Berne (CEA, Grenoble, France)
- Study of wear in piston ring of a vehicle engine using thin layer activation technique
  I.H. Khan (Pakistan Institute of Nuclear Science and Technology, Islamabad, Pakistan), J.-H. Jin (International Atomic Energy Agency, Vienna, Austria), G. Wallace (Institute of Geological and Nuclear Sciences Limited, Lower Hutt, New Zealand), M. Farooq (Pakistan Institute of Nuclear Science and Technology, Islamabad, Pakistan), Ghiyas-ud-Din (Pakistan Institute of Nuclear Science and Technology, Islamabad, Pakistan), S. Gul (Pakistan Institute of Nuclear Science and Technology, Islamabad, Pakistan), R.M. Qureshi (Pakistan Institute of Nuclear Science and Technology, Islamabad, Pakistan)

Chemical engineering

- Investigation of flow behavior of coal/ash particles in an advanced pressurized fluidized bed gasifier (APFBG) using radiotracer technique
  H.J. Pant (Bhabha Atomic Research Centre, Mumbai, India), V.K. Sharma (Bhabha Atomic Research Centre, Mumbai, India), Gursharan Singh (Bhabha Atomic Research Centre, Mumbai, India), M. Vidhya Kamadu (Bharat Heavy Electricals Limited, Vikashnagar, Hyderabad, India), S.G. Prakash (Bharat Heavy Electricals Limited, Vikashnagar, Hyderabad, India), S. Krishanamoorthy (Bharat Heavy Electricals Limited, Vikashnagar, Hyderabad, India), N.V.S. Ramani (Bharat Heavy Electricals Limited, Vikashnagar, Hyderabad, India), R.R. Sonde (Heavy Water Board, Vikaram Sarabhai Bhawan, Anushaktinagar, Mumbai, India)
- Radiotracer study in a bubble column reactor (visbreaker)
  H.J. Pant (Bhabha Atomic Research Centre, Mumbai, India), V.K. Sharma (Bhabha Atomic Research Centre, Mumbai, India), Gursharan Singh (Bhabha Atomic Research Centre, Mumbai, India), R. Kulkarni (University Institute of Chemical Technology, Matunga, Mumbai, India), A.B. Pandit (University Institute of Chemical Technology, Matunga, Mumbai, India), M.M. Kumar (Indian Institute of Petroleum, Dehradun, India), Ph. Berne (CEA, Grenoble, France)

- Radioactive tracer studies in bubble column for dimethyl ether (DME) synthesis
  P. Chen (Washington University, St. Louis, USA), M.P. Dudukovic (Washington University, St. Louis, USA), P. Gupta (MEMC Electronic Materials, Inc., St. Peters, USA), B.A. Toseland (Air Products and Chemicals, Inc., Lehigh Valley, USA)
- Online measurements of liquid carry-over from scrubbers by using radioactive tracers
  A. Haugan (Institute for Energy Technology, Kjeller, Norway), S. Hassfjell (Institute for Energy Technology, Kjeller, Norway), A. Finborud (Mator, Porsgrunn, Norway)
- Visualization of flows in a liquid layer with the active interface
  T.R. Sosnowski (Warsaw University of Technology, Poland)
- Compartmental analysis of results of (radio)tracer experiments in non-living systems in steady state
  Z.I. Kolar (Delft University of Technology, the Netherlands)

5. II KONGRES „ŻYWNOŚĆ, ŻYWIENIE A ZDROWIE W POLSCE ZINTEGROWANEJ Z UNIĄ EUROPEJSKĄ" (2nd CONGRESS "FOOD, NUTRITION AND HEALTH IN POLAND INTEGRATED WITH EUROPEAN UNION", 23-26 JUNE 2004, WARSZAWA, POLAND

Organized by the National Food and Nutrition Institute, Polish Federation of Food Industry, Warsaw Agricultural University, National Institute of Hygiene, Institute of Plant Protection, Research Institute of Medicinal Plants, Institute of Nuclear Chemistry and Technology, Central Laboratory for Radiological Protection, National Veterinary Research Institute.

Board of Scientific Committee: Mirosław Jarosz (Congress President and Chair of Scientific Committee), Stanisław Berger, Andrzej Blikle, Jan Dzieniszewski, Krystyna Gutkowska, Longina Kłosiewicz-Latoszek, Jan K. Ludwicki, Przemysław Mrozikiewicz, Stefan Pruszyński, Włodzimierz Sekuła, Sławomir Sterliński, Bruno Szczygieł, Wiktor B. Szostak, Lucjan Szponar, Lech Waliś, Tadeusz Wijaszka

OPENING SESSION

PLENARY SESSIONS

Session I: Profilaktyka chorób niezakaźnych żywieniowozależnych (Prevention of noncommunicable diet related diseases)

Session II: Niedożywienie szpitalne i standardy żywienia w szpitalach zgodnie z wytycznymi UE (Malnutrition in hospitalised patients and standards for nutrition in hospitals according to EU guidelines)

Session III: Strategia bezpieczeństwa żywności (Food safety strategy)

Session IV: Rynek i konsumpcja żywności (The market and food consumption)

PROBLEM SESSIONS

Session 1: Żywienie populacji w aspekcie zagrożenia chorobami układu krążenia (Dietary habits of population in relation to risk of cardiovascular diseases)

Session 2: Sposób żywienia różnych populacji polskich (Dietary habits of different Polish population)

Session 3: Leczenie żywieniowe (Diet therapy)

Session 4A: Ustawodawstwo żywnościowe. Cz.1 (Food law. Part 1)

Session 5A: Bezpieczeństwo żywności. Cz.1 (Food safety. Part 1)

INCT presentations

- Identyfikacja napromieniowania żywności w Polsce (Detection of irradiated food in Poland)
  W. Stachowicz (Institute of Nuclear Chemistry and Technology, Warszawa, Poland), K. Malec-Czechowska (Institute of Nuclear Chemistry and Technology, Warszawa, Poland), K. Lehner (Institute of Nuclear Chemistry and Technology, Warszawa, Poland)

Session 6: Uwarunkowania zachowań konsumentów na rynku żywności (Determination of consumers behaviours at the food market)

Session 7: Żywienie a żywieniowozależne choroby niezakaźne (Nutrition and noncommunicable diet related diseases)

Session 8: Żywienie w szpitalach (Nutrition in the hospitals)

Session 4B: Ustawodawstwo żywieniowe. Cz. II (Food law. Part II)

Session 5B: Bezpieczeństwo żywności. Cz. II (Food safety. Part II)

Session 9: Wpływ czynników ekonomicznych i społecznych na spożycie żywności (The impact of economic and social factors on the food consumption)

Session 10A: Suplementy diety i żywność funkcjonalna. Cz. I (Food supplements and functional food. Part I)

Session 11: Wybrane zagadnienia dietetyczne (Selected dietetic topics)

Session 12A: Urzędowa kontrola żywności i monitoring. Cz. I (Official food control and monitoring. Part I)

Session 13: Metody analityczne w badaniu żywności (Analytical methods used in food tests)

INCT presentations

- Analiza specjacyjna chromu w wodach mineralnych (Speciation analysis of chromium in mineral waters)
  J. Chwastowska (Institute of Nuclear Chemistry and Technology, Warszawa, Poland), W. Skwara (Institute of Nuclear Chemistry and Technology, Warszawa, Poland), E. Sterlińska (Institute of Nuclear Chemistry and Technology, Warszawa, Poland), J. Dudek (Institute of Nuclear Chemistry and Technology, Warszawa, Poland), L. Pszonicki (Institute of Nuclear Chemistry and Technology, Warszawa, Poland)
- Działalność IChTJ w zakresie zapewnienia jakości w analizie i jej związek z analizą żywności (The activity of the Institute of Nuclear Chemistry and Technology in the field of analytical quality assurance and its relevance to food analysis)
  R. Dybczyński (Institute of Nuclear Chemistry and Technology, Warszawa, Poland), H. Polkowska-Motrenko (Institute of Nuclear Chemistry and Technology, Warszawa, Poland)
- Oznaczanie składu izotopów stabilnych w kontroli autentyczności żywności (Stable isotope measurements for food authenticity control)
  R. Wierzchnicki (Institute of Nuclear Chemistry and Technology, Warszawa, Poland)

Session 10B: Suplementy diety i żywność funkcjonalna. Cz. II (Food supplements and functional food. Part II)

Session 14: Znaczenie dietetyki w leczeniu chorób żywieniowozależnych (Significance of dietetics in therapy of diet related diseases)

Session 12B: Urzędowa kontrola żywności i monitoring. Cz. II (Official food control and monitoring. Part II)

Session 15: Technologia i jakość żywności (Technology and food quality)

INCT presentations

- Wykorzystanie promieniowania jonizującego do utrwalania artykułów rolno-spożywczych (Application of ionising radiation for preservation of food products)
  W. Migdał (Institute of Nuclear Chemistry and Technology, Warszawa, Poland), P. Tomasiński (Institute of Nuclear Chemistry and Technology, Warszawa, Poland)

POSTER SESSIONS

Session 1: Ocena sposobu żywienia (Assessment of dietary habits)

Session 2: Niezakaźne choroby żywieniowozależne (Noncommunicable diet related diseases)

Session 3: Sposób żywienia (Dietary habits)

Session 4: Dietetyka (Dietetics)

Session 5: Bezpieczeństwo żywności (Food safety)

Session 6: Technologia i jakość żywności (Technology and food quality)

Session 7: Metody analizy żywności (Methods of food analyses)

INCT presentations

- Oznaczanie zawartości pierwiastków śladowych w wybranych produktach żywnościowych za pomocą NAA (Determination of trace elements in the selected food products by NAA)
  B. Danko (Institute of Nuclear Chemistry and Technology, Warszawa, Poland), H. Polkowska-Motrenko (Institute of Nuclear Chemistry and Technology, Warszawa, Poland), M.J.J. Ammerlaan (Delft University of Technology, the Netherland)
- Badanie biegłości: pierwiastki śladowe w korzeniu marchwi (Results of a proficiency test: trace elements in carrot's root)
  H. Polkowska-Motrenko (Institute of Nuclear Chemistry and Technology, Warszawa, Poland), Z. Szopa (Institute of Nuclear Chemistry and Technology, Warszawa, Poland), R. Dybczyński (Institute of Nuclear Chemistry and Technology, Warszawa, Poland)
- Oznaczanie zawartości wybranych pierwiastków w liściach herbaty za pomocą neutronowej analizy aktywacyjnej (Elemental analysis of the black and green tea leaves by instrumental neutron activation analysis)
  E. Chajduk-Maleszewska (Institute of Nuclear Chemistry and Technology, Warszawa, Poland), R. Dybczyński (Institute of Nuclear Chemistry and Technology, Warszawa, Poland), A. Salvini (University of Pavia, Italy)
- Wykrywanie napromieniowanych przypraw w produktach spożywczych (Detection of irradiated spices in food products)
  K. Malec-Czechowska (Institute of Nuclear Chemistry and Technology, Warszawa, Poland), W. Stachowicz (Institute of Nuclear Chemistry and Technology, Warszawa, Poland)
- System kontroli i rejestracji dawki akceleratorowej w procesie napromieniowania żywności (Control and monitoring system of EB dose in food irradiation process)

W. Migdał (Institute of Nuclear Chemistry and Technology, Warszawa, Poland), P. Tomasiński (Institute of Nuclear Chemistry and Technology, Warszawa, Poland), I. Norwa (Institute of Nuclear Chemistry and Technology, Warszawa, Poland), M. Strupiechowski (Institute of Nuclear Chemistry and Technology, Warszawa, Poland)

- Kontrola autentyczności soków na podstawie składu izotopów stabilnych (Stable isotope composition for juice authenticity control)
  R. Wierzchnicki (Institute of Nuclear Chemistry and Technology, Warszawa, Poland), M. Derda (Institute of Nuclear Chemistry and Technology, Warszawa, Poland), A. Mikołajczuk (Institute of Nuclear Chemistry and Technology, Warszawa, Poland)
- Oznaczanie metali ciężkich i izotopów gamma-promieniotwórczych w materiałach roślinnych (Determination of heavy metals and gamma-ray emitters in plant materials)
  A. Misiak (Institute of Nuclear Chemistry and Technology, Warszawa, Poland), J. Kierzek (Institute of Nuclear Chemistry and Technology, Warszawa, Poland), J. Dudek (Institute of Nuclear Chemistry and Technology, Warszawa, Poland), H. Polkowska-Motrenko (Institute of Nuclear Chemistry and Technology, Warszawa, Poland), E. Bulska (Warsaw University, Poland), L. Halicz (Geological Survey of Israel, Israel)

Session 8: Rynek i konsumpcja żywności (Market and food consumption)

6. II KONFERENCJA „PROBLEMY UNIESZKODLIWIANIA ODPADÓW" (II CONFERENCE ON PROBLEMS OF WASTE DISPOSAL), 25 OCTOBER 2004, WARSZAWA, POLAND

Organized by the Faculty of Process and Chemical Engineering, Warsaw University of Technology; Plant for Utilization of Solid Municipal Wastes (Warszawa); Institute of Nuclear Chemistry and Technology; Gdańsk University of Technology

Organizing Committee: M. Obrębska, Ph.D., S. Sobera-Madej, M.Sc.

LECTURES

Session A1

Chairman: Prof. A.G. Chmielewski, Ph.D., D.Sc. (Warsaw University of Technology; Institute of Nuclear Chemistry and Technology, Warszawa, Poland)

- Właściwości technologiczne odpadów komunalnych Warszawy (Technological properties of municipal wastes of Warsaw)
  K. Skalmowski (Warsaw University of Technology, Poland), K. Wolska (Warsaw University of Technology, Poland)
- Rozkład katalityczny odpadów poliolefin z rozdestylowaniem produktów (Catalytic decomposition of olefin wastes with separation of products by distillation)
  B. Tymiński (Institute of Nuclear Chemistry and Technology, Warszawa, Poland), K. Zwoliński (Institute of Nuclear Chemistry and Technology, Warszawa, Poland), R. Jurczyk (Institute of Nuclear Chemistry and Technology, Warszawa, Poland), A. Koronka (Institute of Nuclear Chemistry and Technology, Warszawa, Poland)
- Termiczne przekształcanie biomasy wydzielonej z odpadów komunalnych (Thermal transformation of biomass separated from municipal wastes)
  U. Kruszewska (Warsaw University of Technology, Poland)
- Produkcja betonów z zastosowaniem mineralnych odpadów przemysłowych o właściwościach pucolanowych (Production of concrete with the use of industrial mineral wastes of pozzolana properties)
  A. Duber (The Agricultural University of Wrocław, Poland), A. Pawłowski (The Agricultural University of Wrocław, Poland)

Session B1

Chairman: J. Kaznowski, M.Sc. (Consultant Engineering Office, Warszawa, Poland)

- Gospodarka odpadami w świetle obowiązujących przepisów (Waste management in the light of obligatory rules)
  M. Szymborska (Ministry of the Environment, Warszawa, Poland)
- Wpływ założeń KPGO na potencjalne możliwości pozyskiwania biogazu ze składowisk odpadów komunalnych (Effect of KPGO foredesigns on the possibility of obtaining of biogas from storage yards of municipal wastes)
  A. Pawłowski (The Agricultural University of Wrocław, Poland), K. Lejcuś (The Agricultural University of Wrocław, Poland)
- Pozwolenie zintegrowane – od wniosku do decyzji – na przykładzie ZUSOK (Integreted permission – from inference to decision. Plant for Utilization of Solid Municipal Wastes (ZUSOK) as example)
  S. Sochan (Plant for Utilization of Solid Municipal Wastes, Warszawa, Poland)

- Możliwości finansowania inwestycji proekologicznych, w tym gospodarki odpadami (Financing possibilities of proecological investments including waste management)
  M. Wagner (Eko-Efekt Sp. z o.o., Warszawa, Poland)

Session A2

Chairman: Prof. B. Kawalec-Pietrenko, Ph.D., D.Sc. (Gdańsk University of Technology, Poland)

- Instalacje termicznego przekształcania odpadów w systemach gospodarki odpadami komunalnymi – bariery i perspektywy wdrożenia (Installations of thermal transformation of wastes in the management of municipal wastes – barriers and perspectives of implementation)
  T. Pająk (AGH University of Science and Technology, Kraków, Poland)
- Zastosowanie unieruchomionych mikroorganizmów na cząsteczkach stałych do biodegradacji alkoholi o krótkim łańcuchu węglowym (Use of microorganisms fixed on solid molecules to the biodegradation of alcohols of short carbon chain)
  B. Kawalec-Pietrenko (Gdańsk University of Technology, Poland), M. Łazarczyk (Gdańsk University of Technology, Poland)
- Usuwanie błękitu metylenowego z wody przez sorbenty z biomasy (Removal of methylene blue from water by sorbents from biomass)
  K. Bratek (Wrocław University of Technology, Poland), W. Bratek (Wrocław University of Technology, Poland), E. Turkot (Wrocław University of Technology, Poland)

Session B2

Chairman: A. Zielińska, M.Sc. (Prochem S.A., AMZ Consulting, Warszawa, Poland)

- Możliwe kierunki rozwoju ZUSOK w świetle gospodarki odpadami w m.st. Warszawie (Possible trends in the development of the Plant for Utilization of Solid Municipal Wastes in the light of the waste management in Warsaw)
  J. Naumienko (Plant for Utilization of Solid Municipal Wastes, Warszawa, Poland)
- Biogazowanie rolnicze szansą na utylizację wybranych odpadów komunalnych (Agricultural biogas as a chance to utilize selected municipal wastes)
  J. Cebula (The Silesian University of Technology, Gliwice, Poland)
- Mogilniki – zagrożenie środowiska naturalnego (Burial grounds – hazard to the natural environment)
  R. Marcjoniak (The Agricultural University of Wrocław, Poland)

Session A3

Chairman: T. Pająk, Ph.D. (AGH University of Science and Technology, Kraków, Poland)

- Zastosowanie reakcji Fentona w oczyszczaniu ścieków farmaceutycznych (Use of Fenton reaction in the purification of pharmaceutical wastes)
  S. Sobera-Madej (Warsaw University of Technology, Poland), A. Biń (Warsaw University of Technology, Poland)
- Zastosowanie wybranych metod pogłębionego utleniania do rozkładu fipronilu oraz jego zniszczenia w wodnych roztworach (Use of selected methods of deepening oxidation for the decomposition of fipronil and its destruction in aqueous solutions)
  M. Miśkiewicz (Warsaw University of Technology, Poland), A. Biń (Warsaw University of Technology, Poland)
- Termiczny rozkład struktury azbestu na przykładzie eternitu (Thermal decomposition of asbestos structure – eternit as example)
  A. Poniatowska (Warsaw University of Technology, Poland)

Session B3

Chairman: M. Obrębska, Ph.D. (Warsaw University of Technology, Poland)

- Przyczyny i efekty wykonania w ZUSOK instalacji do deodoryzacji nieprzyjemnych zapachów (Reasons and deodorization effects of the installation in the Plant for Utilization of Solid Municipal Wastes – Warszawa)
  K. Stańczak (Plant for Utilization of Solid Municipal Wastes, Warszawa, Poland)
- Perspektywy odzysku energii z odpadów w Warszawie (Perspectives for energy recovery from wastes in Warsaw)
  J. Kaznowski (Consultant Engineering Office, Warszawa, Poland)

PRACTICAL PART

Visit to the Plant for Utilization of Solid Municipal Wastes in Warsaw.

7. KICK-OFF WORKSHOP ON THE PROJECT "CHEMICAL STUDIES FOR DESIGN AND PRODUCTION OF NEW RADIOPHARMACEUTICALS (POL-RAD-PHARM)" WITHIN THE EU PROGRAMME MARIE CURIE HOST FELLOWSHIPS FOR TRANSFER OF KNOWLEDGE (ToK), 4-6 DECEMBER 2004, WARSZAWA, POLAND

Organized by the Institute of Nuclear Chemistry and Technology

Organizing Committee: Prof. J. Narbutt, Ph.D., D.Sc., E. Gniazdowska, Ph.D., L. Fuks, Ph.D., Assoc. Prof. A. Bilewicz, Ph.D., D.Sc.

SCIENTIFIC PART

Session I. Introductory session

- Opening of the Workshop
  J. Narbutt (Institute of Nuclear Chemistry and Technology, Warszawa, Poland)
- Institute of Nuclear Chemistry and Technology and the Department of Radiochemistry
  J. Narbutt (Institute of Nuclear Chemistry and Technology, Warszawa, Poland)
- Institute of Nuclear Chemistry and Technology – Department of Analytical Chemistry
  H. Polkowska-Motrenko (Institute of Nuclear Chemistry and Technology, Warszawa, Poland)
- Features and objectives of the Programme Marie Curie Host Fellowships for Transfer of Knowledge. Project managing
  L. Fuks (Institute of Nuclear Chemistry and Technology, Warszawa, Poland)

Session II. INCT research programmes relevant to the ToK project

- Tricarbonyltechnetium(I) complexes
  J. Narbutt (Institute of Nuclear Chemistry and Technology, Warszawa, Poland), M. Zasępa (Institute of Nuclear Chemistry and Technology, Warszawa, Poland)
- Rhenium(VI) complexes with dendritic ligands
  E. Gniazdowska (Institute of Nuclear Chemistry and Technology, Warszawa, Poland)
- Radionuclides for nuclear medicine
  A. Bilewicz (Institute of Nuclear Chemistry and Technology, Warszawa, Poland), M. Pruszyński (Institute of Nuclear Chemistry and Technology, Warszawa, Poland)
- Analytical methods of purity control
  H. Polkowska-Motrenko (Institute of Nuclear Chemistry and Technology, Warszawa, Poland)

Session III. Other Polish research programmes relevant to the ToK project

- Activities of the Radioisotope Centre POLATOM
  R. Mikołajczak (Radioisotope Centre POLATOM, Świerk, Poland)
- Activities of the Isotope Laboratory in the Department of Nuclear Physical Chemistry (in co-operation with the Cyclotron Group), Institute of Nuclear Physics, Polish Academy of Sciences
  B. Petelenz (The Henryk Niewodniczański Institute of Nuclear Physics, Polish Academy of Sciences, Kraków, Poland)
- Activities of the Department of Radiobiology, Institute of Nuclear Chemistry and Technology
  M. Kruszewski (Institute of Nuclear Chemistry and Technology, Warszawa, Poland)

Session IV. Foreign partners' research programmes relevant to the ToK project

- Activities of the Institute of Inorganic Chemistry, University of Zürich
  R. Alberto (University of Zürich, Switzerland)
- Activities of the Centre for Radiopharmaceutical Science, Paul Scherrer Institute
  R. Schibli (Paul Scherrer Institute, Villigen, Switzerland)
- Activities of the Institute of Bioinorganic and Radiopharmaceutical Chemistry, FZ Rossendorf
  H.-J. Pietzsch (Forschungszentrum Rossendorf e.V., Dresden, Germany)
- Activities of the Radiation Protection Department, Nuclear and Technological Institute
  M. Neves (Nuclear and Technological Institute, Sacavém, Portugal)
- Activities of the Institute of Nuclear Chemistry, Chalmers University of Technology
  G. Skarnemark (Chalmers University of Technology, Göteborg, Sweden)
- Activities of the Institute of Nuclear Chemistry, Johannes Gutenberg University, Mainz
  F. Rösch (Johannes Gutenberg University, Mainz, Germany)

Technical visits to the Institute of Nuclear Chemistry and Technology and to the Radioisotope Centre POLATOM.

Ph.D./D.Sc. THESES IN 2004

Ph.D. THESES

1. Marek Danilczuk, M.Sc.

   Badania EPR paramagnetycznych produktów radiolizy stabilizowanych w sitach molekularnych: małe rodniki i nanocząsteczki metaliczne (Paramagnetic products of radiolysis stabilized in molecular sieves: small radicals and metallic nanoparticles)

   supervisor: Prof. Jacek Michalik, Ph.D., D.Sc.

   Institute of Nuclear Chemistry and Technology, 16.12.2004

2. Kinga Frąckiewicz, M.Sc.

   Tetrabutyloamoniowe sole tetrahalogeno kompleksów pierwiastków grupy 13. Struktura kryształów i wtórna periodyczność (Tetrabutylammonium salts of tetrahalogeno complexes of the Group 13 elements. Crystal structure and secondary periodicity)

   supervisor: Prof. Sławomir Siekierski, Ph.D.

   Institute of Nuclear Chemistry and Technology, 16.12.2004

3. Agnieszka Mikołajczuk, M.Sc.

   Równowagowe efekty izotopowe siarki ($^{34}S/^{32}S$) w wybranych układach dwufazowych zawierających SO_2 (Equilibrium isotope effects of sulphur ($^{34}S/^{32}S$) in selected two phase systems containing SO_2)

   supervisor: Prof. Andrzej G. Chmielewski, Ph.D., D.Sc.

   Institute of Nuclear Chemistry and Technology, 17.06.2004

4. Barbara Zielińska, M.Sc.

   Wpływ efektu relatywistycznego na własności hydrolityczne kationów ciężkich pierwiastków (Influence of relativistic effect on hydrolytic properties of heavy element cations)

   supervisor: Assoc. Prof. Aleksander Bilewicz, Ph.D., D.Sc.

   Institute of Nuclear Chemistry and Technology, 23.09.2004

D.Sc. THESES

1. Jan Grodkowski, Ph.D.

   Radiacyjna i fotochemiczna redukcja dwutlenku węgla w roztworach katalizowana przez kompleksy metali przejściowych z wybranymi układami makrocyklicznymi (Radiolytic and photochemical reduction of carbon dioxide in solution catalyzed by transition metal complexes with some selected macrocycles)

   Institute of Nuclear Chemistry and Technology

2. Dariusz Mirosław Pogocki, Ph.D.

   Wewnątrzcząsteczkowe przemiany rodnikowe z udziałem utlenionego centrum siarkowego w modelowych związkach tioeterowych o znaczeniu biologicznym (Participation of oxidized sulfur center in intramolecular free radical processes in the model organic compounds of biological importance)

   Institute of Nuclear Chemistry and Technology

EDUCATION

Ph.D. PROGRAMME IN CHEMISTRY

The Institute of Nuclear Chemistry and Technology holds a four-year Ph.D. degree programme for graduates of chemical, physical and biological departments of universities, for graduates of medical universities and to engineers in chemical technology and material science.

The main areas of the programme are:

- radiation chemistry and biochemistry,
- chemistry of radioelements,
- isotopic effects,
- radiopharmaceutical chemistry,
- analytical methods,
- chemistry of radicals,
- application of nuclear methods in chemical and environmental research, material science and protection of historical heritage.

The candidates accepted for the aforementioned programme can be employed in the Institute. The candidates can apply for a doctorial scholarship. The INCT offers accommodation in 10 rooms in the guesthouse for Ph.D. students not living in Warsaw.

During the four-year Ph.D. programme the students participate in lectures given by senior staff from the INCT, Warsaw University and the Polish Academy of Sciences. In the second year, the Ph.D. students have teaching practice in the Chemistry Department of Warsaw University. Each year the Ph.D. students are obliged to deliver a lecture on topic of his/her dissertation at a seminar. The final requirements for the Ph.D. programme graduates, consistent with the regulation of the Ministry of National Education and Sport, are:

- submission of a formal dissertation, summarizing original research contributions suitable for publication;
- final examination and public defense of the dissertation thesis.

In 2004, the following lecture series were organized:

- "Selected problems of analytical chemistry" – Prof. Marek Trojanowicz, Ph.D., D.Sc. (Institute of Nuclear Chemistry and Technology);
- "Thermodynamics" – Prof. Robert Hołyst, Ph.D., D.Sc. (Institute of Physical Chemistry, Polish Academy of Sciences).

Most of the students expand their knowledge during a short or long training in numerous renowned European research centres, *e.g.* European Institute of Transuranium Elements (Karlsruhe, Germany), Philips Cyclotron in Paul Scherrer Institute (Switzerland), Gent University (Belgium), Orsay University (France), Mainz University (Germany), *etc*.

The qualification interview for the Ph.D. programme takes place in the mid of October. Detailed information can be obtained from:

- Head: Assoc. Prof. Aleksander Bilewicz, Ph.D., D.Sc.
  (phone: (+4822) 811-30-21 ext. 15-98, e-mail: abilewic@ichtj.waw.pl);
- Secretary: Dr. Ewa Gniazdowska
  (phone: (+4822) 811-30-21 ext. 15-96, e-mail: studium@ichtj.waw.pl).

TRAINING OF STUDENTS

Institution	Country	Number of participants	Period
International Atomic Energy Agency	Algeria	1	2 months
		2	1 month

Institution	Country	Number of participants	Period
International Atomic Energy Agency	Syria	1	2 weeks
		1	3 months
International Atomic Energy Agency	Tunisia	2	2 months
Maria Curie-Skłodowska University	Poland	1	1.5 month
Technical School of Chemistry	Poland (Warszawa)	4	1 month
Warsaw University of Technology, Faculty of Chemistry	Poland	1	1 month
Warsaw University of Technology, Faculty of Materials Science and Engineering	Poland	3	1 month
Warsaw University of Technology, Faculty of Physics	Poland	1	1 month
		35	one-day practice

RESEARCH PROJECTS AND CONTRACTS

RESEARCH PROJECTS GRANTED BY THE STATE COMMITTEE FOR SCIENTIFIC RESEARCH IN 2004 AND IN CONTINUATION

1. **Multiphase flow dynamics determination by radiotracer and computational fluid dynamics (CFD) methods.**
   supervisor: Jacek Palige, Ph.D.
2. **Catalytic tubular reactor for olefine polymers cracking with distillation products of decomposition.**
   supervisor: Bogdan Tymiński, Ph.D.
3. **Tricarbonyl technetium(I) and rhenium(I) complexes with chelating ligands as radiopharmaceutical precursors.**
   supervisor: Prof. Jerzy Narbutt, Ph.D., D.Sc.
4. **Investigation of the mechanism of human glioma MO59 cells radiosensitisation by inhibitors of signal transduction pathways which are growth factors dependent: influence on DNA double-strand break rejoning and apoptosis.**
   supervisor: Iwona Grądzka, Ph.D.
5. **Neutron activation analysis and ion chromatography as a tool for reliable lanthanides determination in the biological and environmental samples.**
   supervisor: Bożena Danko, Ph.D.
6. **The chemical isotope effects of gallium, indium and thallium in ligand exchange and red-ox reactions.**
   supervisor: Wojciech Dembiński, Ph.D.
7. **Comparative analysis of telomere length, chromosomal aberration frequency and DNA repair kinetics in peripheral blood lymphocytes of healthy donors and cancer patients.**
   supervisor: Assoc. Prof. Andrzej Wójcik, Ph.D., D.Sc.
8. **Baroque glass in Polish collections (provenance verification).**
   supervisor: Jerzy Kunicki-Goldfinger, Ph.D.
9. **Application of membrane methods for separation of gas mixtures in the systems generating energy from biogas.**
   supervisor: Marian Harasimowicz, Ph.D.
10. **The role of PARP-1 in DNA double strand breaks repair.**
    supervisor: Maria Wojewódzka, Ph.D.
11. **Crystal chemistry of calcium complexes with azinedicarboxylate ligands.**
    supervisor: Prof. Janusz Leciejewicz, Ph.D., D.Sc.
12. **Hydrolysis of heavy element cations.**
    supervisor: Assoc. Prof. Aleksander Bilewicz, Ph.D., D.Sc.
13. **Sodium and silver clusters in gamma irradiated sodalites.**
    supervisor: Prof. Jacek Michalik, Ph.D., D.Sc.
14. **Paramagnetic products of radiolysis stabilized in molecular sieves: small radicals and metallic nanoparticles.**
    supervisor: Prof. Jacek Michalik, Ph.D., D.Sc.
15. **Equilibrium sulfur isotope effects ($^{34}S/^{32}S$) in selected SO_2 containing systems.**
    supervisor: Prof. Andrzej G. Chmielewski, Ph.D., D.Sc.
16. **Radiation induced decomposition of selected chlorinated hydrocarbons in gaseous phase.**
    supervisor: Prof. Andrzej G. Chmielewski, Ph.D., D.Sc.

17. **Oxidation of thioether by organic complexes of copper. Processes of potential importance for pathogenesis of some neurodegenerative diseases.**
supervisor: Assoc. Prof. Dariusz Pogocki, Ph.D., D.Sc.

18. **New methods of the study and reduction of fouling in processes of micro- and ultrafiltration of liquid radioactive waste.**
supervisor: Grażyna Zakrzewska-Trznadel, Ph.D.

19. **Modelling of the dispersion of pollutants and studying their transport in natural water receivers using stable isotopes as tracers.**
supervisor: Andrzej Owczarczyk, Ph.D.

20. **Influence of gamma irradiation on starch properties: starch interaction with water and lipids, starch-lipid films.**
supervisor: Krystyna Cieśla, Ph.D.

21. **Changes of sulphur isotope ratio in the products of coal combustion and flue gas desulphurization processes.**
supervisor: Prof. Andrzej G. Chmielewski, Ph.D., D.Sc.

22. **Process of nanostructure formation of small-molecule organic gels using synchrotron methods.**
supervisor: Assoc. Prof. Helena Grigoriew, Ph.D., D.Sc.

IMPLEMENTATION PROJECTS GRANTED BY THE STATE COMMITTEE FOR SCIENTIFIC RESEARCH IN 2004 AND IN CONTINUATION

1. **Polish certified reference materials: maize meal and soia flour for the quality control of laboratories analyzing food.**
06 PO6 2002C/05899
supervisor: Halina Polkowska-Motrenko, Ph.D.

RESEARCH PROJECTS ORDERED BY THE STATE COMMITTEE FOR SCIENTIFIC RESEARCH IN 2004

1. **Radiation processing application to modify and sterilize polymer scaffolds.**
PBZ-KBN-082/T08/2002
supervisor: Assoc. Prof. Izabella Legocka, Ph.D., D.Sc.

2. **Radiation processing application to form nanofillers with different structure including hybrid and functionalized.**
PBZ-KBN-095/T08/2003
supervisor: Zbigniew Zimek, Ph.D.

3. **Mutual interactions between nutritional components in steering of development of the intestinal immunological system.**
PBZ-KBN-093/P06/2003
supervisor: Assoc. Prof. Marcin Kruszewski, Ph.D., D.Sc.

IAEA RESEARCH CONTRACTS IN 2004

1. **Application of ionizing radiation for removal of pesticides from ground waters and wastes.**
12016/RO
principal investigator: Prof. Marek Trojanowicz, Ph.D., D.Sc.

2. **Radiation resistant polypropylene for medical applications and as component of structural engineering materials.**
12703/RO
principal investigator: Zbigniew Zimek, Ph.D.

3. **Electron beam for VOCs treatment emitted from oil combustion process.**
   13136/Regular Budget Fund
   principal investigator: Anna Ostapczuk, M.Sc.

IAEA TECHNICAL CONTRACTS IN 2004

1. **Accredited laboratory for the use of nuclear and nuclear-related analytical techniques.**
   POL/2/014
2. **Feasibility study for a sewage irradiationplant in Egypt.**
   RAF0014-91650L
3. **Complete three XRF analysers, model AF-30, for determination of ash in lignite in coal plant laboratory conditions through sample measurement.**
   MON 8005-84723G
4. **The method was made available, and the installations and instrumentations were delivered to control the tightness of underground pipelines.**
   TC RAF0014-90533L
5. **Report of final cost analysis of EPS Pomorzany electron beam flue gas treatment plant.**
   RER0016-87307D
6. **Material origin – proficiency test material for environmental analysis.**
   2003-5926-1

EUROPEAN COMMISSION RESEARCH PROJECTS IN 2004

1. **Research Training Network: Sulfur radical chemistry of biological significance: the protective and damaging roles of thiol and thioether radicals.**
   principal investigator: Prof. Krzysztof Bobrowski, Ph.D., D.Sc.
   RTN-2001-00096 under FP.5
2. **Advanced methods for environment research and control.**
   principal investigator: Grażyna Zakrzewska-Trznadel, Ph.D.
   MTKD-CT-2004-509226
3. **Chemical studies for design and production of new radiopharmaceuticals.**
   principal investigator: Prof. Jerzy Ostyk-Narbutt, Ph.D., D.Sc.
   MTKD-CT-2004-509224
4. **European research program for the partitioning of actinides from high active wastes issuing the reprocessing of spent nuclear fuels.**
   FP6-508854
5. **European cooperation in the field of scientific and technical research. COST D27 – Prebiotic chemistry and early evolution. Role of radiation chemistry in the origin of life on Earth.**
   supervisor: Prof. Zbigniew Zagórski, Ph.D., D.Sc.
6. **European cooperation in the field of scientific and technical research.** COST P9 – Radiation damage in biomolecular systems (RADAM). Mechanisms of radiation damage transfer in polypeptide molecules.
   supervisor: Prof. Krzysztof Bobrowski, Ph.D., D.Sc.

OTHER FOREIGN CONTRACTS IN 2004

1. **Laboratory scale experimental analysis of electron beam treatment of flue gases from combustion of liquid petroleum oils**
   Contract with King Abdulaziz City for Science and Technology, Atomic Energy Research Institute, Saudi Arabia
2. **Realization and delivery of nickel oxide electrodes coated with magnesium doped lithium cobaltite.**
   principal investigator: Andrzej Deptuła, Ph.D.
   ENEA, Italy

LIST OF VISITORS TO THE INCT IN 2004

1. **Alberto Roger**, University of Zürich, Switzerland, *03-05.12*.
2. **Al-Khateeb Shatha**, Atomic Energy Commission of Syria, Damascus, Syria, *01-14.01*.
3. **Amro Hasan**, Ministry of Water and Irrigation, Amman, Jordan, *17.06*.
4. **Asmus Klaus-Dieter**, University of Notre Dame, USA, *10-13.09*.
5. **Benamer Samah**, Centre de Recherche Nucléaire d'Alger, Algeria, *06.01-06.03*.
6. **Bernard Olivier**, France, *01.01-31.12.*
7. **Bjørnstad Tor**, Institute for Energy Technology, Norway, *15-21.06*.
8. **Boner Marcus**, Forschungszentrum Jülich, Germany, *13-14.01*.
9. **Bothelo M. Luisa Camelo**, Nuclear and Technological Institute, Sacavém, Portugal, *17.06*.
10. **Cardella Antonio**, Max Planck Institute, Germany, *18.11*.
11. **Chen Haiyan**, China Academy of Engineering Physics, China, *24.02-04.03*.
12. **Chmielewski Andrzej G.**, International Atomic Energy Agency, United Nations, *17.06*.
13. **Cooper William**, University of North Carolina-Wilmington, USA, *17.06*.
14. **Drapkin Valerij**, St. Petersburg Instruments Ltd., Russia, *31.05-05.06*.
15. **Einav Izaak**, International Atomic Energy Agency, United Nations, *23-25.10*.
16. **El-Motaium Rawia**, Egypt, *05-11.05*.
17. **Forstel Hilmar**, Forschungszentrum Jülich, Germany, *13-14.01*.
18. **Gehringer Peter**, ARC Seibersdorf Research GmbH, Austria, *17.06*.
19. **Goedecke Wolfgang**, University of Duisburg-Essen, Germany, *22.11*.
20. **Goncharowa Rosa**, Institute of Genetics and Cytology, National Academy of Sciences of Belarus, Belarus, *21-24.11*.
21. **Griffith Jose Martinez**, Instituto Cubano de Investigaciones Azucareras, Cuba, *20-21.06*, *25.06-03.07*.
22. **Gryzlov Anatolij**, State Research and Production Corporation TORIJ, Russia, *12.02-07.03*, *20-28.07*.
23. **Han Bumsoo**, EB-TECH Co. Ltd., Daejon, Korea, *17.06*.
24. **Hills Andries S.**, Nuclear Energy Corporation of South Africa, South Africa, *15-21.06*.
25. **Huang Wenfeng**, China Academy of Engineering Physics, China, *24.02-04.03*.
26. **Joon-Ha Jin**, International Atomic Energy Agency, United Nations, *15-21.06*.
27. **Kasztovszky Zsolt**, Institute of Isotope and Surface Chemistry, Hungary, *29.09-07.10*.
28. **Khan Iqbal Hussain**, Pakistan Institute of Nuclear Science and Technology, Pakistan, *15-21.06*.
29. **Kim Jo Chun**, Konkuk University, Korea, *02-03.08*.
30. **Knyazev Michail**, St. Petersburg Instruments Ltd., Russia, *31.05-05.06*.
31. **Kraiem Mokhtar**, Centre National des Sciences and Technologies Nucléaires, Tunisia, *31.08-31.10*.
32. **Kusnetsov R.A.**, FSUE "SSC RF RIAR", Russia, *17.06*.
33. **Larbi Youcef Soud Fatima**, Centre de Recherche Nucléaire d'Alger, Algeria, *06.02-07.03*.
34. **Lazurik Vladymir**, Kharkiv National University, Ukraine, *04-09.10*.
35. **Melo Rita**, Nuclear and Technological Institute, Sacavém, Portugal, *17.06*.
36. **Nacer Khodia Assia Boukrif**, Centre de Recherche Nucléaire d'Alger, Algeria, *06.02-07.03*.
37. **Neves Maria**, Nuclear and Technological Institute, Sacavém, Portugal, *03-06.12*.
38. **Nichipor Henrieta**, Institute of Radiation Physics and Chemistry Problems, National Academy of Sciences of Belarus, Belarus, *13-25.06*, *01-03.10*.

39. **Othman Yasser**, Atomic Energy Commission of Syria, Damascus, Syria, *03.05-01.08*.
40. **Panavas Romanas**, JSC Vilniaus Venta Semiconductors, Lithuania, *14-16.04*.
41. **Piacentini Mario**, University of Rome "La Sapienza", Italy, *25-27.04*.
42. **Pieszekhonov Vladymir**, State Research and Production Corporation TORIJ, Russia, *12.02-07.03*.
43. **Pietzsch Hans-Jurgen**, Kernforschungzentrum Rossendorf e.V., Germany, *03-06.12*.
44. **Pnina Einav**, Pasta Amore Corporation, Canada, *08-10.07*.
45. **Politovskij Fiodor**, State Research and Production Corporation TORIJ, Russia, *12.02-07.03*, *20-28.07*.
46. **Popov Genadij**, Kharkiv National University, Ukraine, *04-09.10*.
47. **Ramirez Trajano**, National Polytechnic School, Quito, Ecuador, *17.06*.
48. **Roberts P.B.**, International Atomic Energy Agency, United Nations, *12.08*.
49. **Roesch Frank**, University of Meinz, Germany, *04-06.12*.
50. **Sampa Maria Helena**, Radiation Technology Centre, IPEN, Sao Paulo, Brazil, *17.06*.
51. **Schibli Roger**, Swiss Federal Institute of Technology, Zürich, Switzerland, *03-05.12*.
52. **Skarnemark Gunar**, Chalmers University of Technology, Göteborg, Sweden, *03-06.12*.
53. **Solpan Dilek**, Hacettepe University, Ankara, Turkey, *17.06*.
54. **Tacas Erzsebe**t, Institute of Isotopes and Surface Chemistry, Budapest, Hungary, *17.06*.
55. **Trabelsi Mohamed Hedi**, Centre National des Sciences and Technologies Nucléaires, Tunisia, *31.08-31.10*.
56. **Valeika Lechas**, JSC Vilniaus Venta Semiconductors, Lithuania, *14-16.04*.
57. **Villavicencio Anna Lucia**, Institute of Energy Nuclear and Nuclear Research, Brazil, *26.10-02.11*.
58. **Watanabe Yujiro**, National Institute of Material Science, Japan, *20-26.10.*
59. **Yamada Hirohisa**, National Institute of Material Science, Japan, *20-26.10*.

THE INCT SEMINARS IN 2004

1. Prof. Ewa Bulska (Warsaw University, Poland)
   Ciekawe zastosowania ICP-MS: nowe wyzwania w chemii analitycznej (On the modern analytical chemistry with ICP-MS)
2. Dr. Wolfgang Goedecke (University of Duisburg-Essen, Essen, Germany)
   Involvement of the MRE11 - protein in double strand break repair and apoptosis
3. Dr. Jan Grodkowski (Institute of Nuclear Chemistry and Technology, Warszawa, Poland)
   Radiacyjna i fotochemiczna redukcja dwutlenku węgla w roztworach katalizowana przez kompleksy metali przejściowych z wybranymi układami makrocyklicznymi (Radiolytic and photochemical reduction of carbon dioxide in solution catalyzed by transition metal complexes with some selected macrocycles)
4. Hanna Lewandowska, M.Sc. (Institute of Nuclear Chemistry and Technology, Warszawa, Poland)
   Powstawanie, struktura i przemiany dinitrozylowych kompleksów żelaza w modelowych układach biologicznych (Formation, structure and interactions of dinitrosyl iron complexes in model biological systems)
5. Krzysztof Łyczko, M.Sc. (Institute of Nuclear Chemistry and Technology, Warszawa, Poland)
   Stopnie utlenienia metali w solwatach najcięższych pierwiastków bloku p (Metals oxidation states in solvates of heaviest p block elements)
6. Dr. Andrzej Pawlukojć (Joint Institute for Nuclear Research, Dubna, Russia)
   Zastosowanie rozpraszania neutronów termicznych w spektroskopii molekularnej (Thermal neutron scattering application in molecular spectroscopy)
7. Prof. Mario Piacentini (University of Rome “La Sapienza”, Italy)
   Study of the cultural heritage with transportable instrumentation
8. Dr. Dariusz Pogocki (Institute of Nuclear Chemistry and Technology, Warszawa, Poland)
   Utlenione centrum siarkowe oraz wewnątrzcząsteczkowe przemiany rodnikowe w modelowych związkach tioeterowych o znaczeniu biologicznym (Oxidized sulfur center and intramolecular free radical processes in the model organic compounds of biological importance)
9. Dr. Grażyna Przybytniak (Institute of Nuclear Chemistry and Technology, Warszawa, Poland)
   Rodniki nukleotydów i DNA inicjowane promieniowaniem jonizującym (DNA radicals and its nucleotides initiated by ionising radiation)
10. Assoc. Prof. Władysław M. Rzymski (Technical University of Łódź, Poland)
    Niekonwencjonalne sieciowanie elastomerów (Nonconventional crosslinking of elastomers)
11. Prof. Daniel William Tedder (Georgia Institute of Technology, USA)
    Efficient strategies for partitioning actinides from alkaline wastes
12. Prof. Zbigniew Zagórski (Institute of Nuclear Chemistry and Technology, Warszawa, Poland)
    Europejski program współpracy COST-D27 (European programme of cooperation: COST-D27)

LECTURES AND SEMINARS DELIVERED OUT OF THE INCT IN 2004

LECTURES

1. **Bobrowski K.**
   Radical processes during oxidation of cyclic peptides containing methionine.
   Radiation Chemistry Gordon Conference, Waterville, Maine, USA, 20-25.06.2004.
2. **Danilczuk M., Lund A., Shiotani M., Omori Y.**
   ESR characterization of TiO_2 photocatalysis.
   4th Meeting on Surface Active Sites & Emission Control Catalysis, Magdeburg, Germany, 11-14.05.2004.
3. **Kraś J.**
   Koncepcje izotopowej kontroli szczelności rurociągów podziemnych o średnicach przekraczających 800 nm wyposażonych w komory czyszczakowe (Conception of isotope control of underground pipelines with diameters above 800 nm, equiped with cleaning chambers).
   VII Krajowa Konferencja „Zarządzanie ryzykiem w eksploatacji rurociągów", Płock, Poland, 22.05.2004.
4. **Michalik J., Sadło J., Perlińska J., Yamada H.**
   Cationic metal clusters in nanoporous materials.
   23th International Symposium on Separation Chemistry, Kanzawa, Japan, 06-07.02.2004.
5. **Stachowicz W.**
   INCT faced to food safety.
   Seminar "Food Safety", Warszawa, Poland, 23.09.2004.
6. **Szumiel I.**
   Adaptive response: facts, signals and a hypothesis.
   Nordic Joint Meeting in Radiation Research, Uppsala, Sweden, 16-17.09.2004.
7. **Wójcik A.**
   Health effects of exposure to natural radiation.
   11th International Congress of the International Radiation Protection Association, Madrid, Spain, 23-28.05.2004.
8. **Wójcik A.**
   Wypadki w radioterapii (Accidents in radiotherapy).
   VIII Jesienna Szkoła Fizyki Medycznej, Bydgoszcz, Poland, 12-13.10.2004.
9. **Zakrzewska-Trznadel G.**
   Membranowa separacja substancji radioaktywnych (Membrane separation of radioactive substances).
   VI Letnia Szkoła Membranowa, Szklarska Poręba, Poland, 26-29.04.2004.
10. **Zakrzewska-Trznadel G.**
    Stable isotopes – some comments on new fields of application.
    International Symposium on Advanced Analytical Techniques and Applications, Daejeon, Korea, 05-08.11.2004.

SEMINARS

1. **Andrzej G. Chmielewski**
   Progress in radiation technologies.
   Institute of Nuclear Science and Technology, Dhaka, Bangladesh, 25.02.2004.

2. **Andrzej G. Chmielewski**
   Applications of radiation processing.
   Ghana Atomic Energy Commission, Accra, Ghana, 19.04.2004.

3. **Andrzej G. Chmielewski**
   General requirements for radiation facilities' design and construction (gamma radiation).
   Ghana Atomic Energy Commission, Accra, Ghana, 20.04.2004.

4. **Andrzej G. Chmielewski**
   General requirements for radiation facilities' design and construction (electron beam).
   Ghana Atomic Energy Commission, Accra, Ghana, 20.04.2004.

5. **Andrzej G. Chmielewski**
   General requirements for radiation facilities' design and construction (on-line systems).
   Ghana Atomic Energy Commission, Accra, Ghana, 21.04.2004.

6. **Andrzej G. Chmielewski**
   Radiation safety of gamma and electron beam irradiation facilities.
   Ghana Atomic Energy Commission, Accra, Ghana, 22.04.2004.

7. **Andrzej G. Chmielewski**
   Strategy concerning radiation technology implementation.
   Ghana Atomic Energy Commission, Accra, Ghana, 23.04.2004.

8. **Andrzej G. Chmielewski**
   Recent advances in radiation technology.
   Nuclear Research Center, AECS, Damascus, Syria, 19.05.2004.

9. **Andrzej G. Chmielewski**
   Recent progress in radiation technology.
   Vinca Institute of Nuclear Sciences**,** Belgrade, Serbia and Montenegro, 04.11.2004.

10. **Andrzej G. Chmielewski**
    Recent progress in radiation technology.
    Nuclear Research Center, AOI, Yazd, Iran, 02.12.2004.

11. **Andrzej G. Chmielewski**
    Progress in radiation processing of polymers (synthetic).
    Philippinian Nuclear Research Institute, Manila, the Philippines, 15.12.2004.

12. **Marcin Kruszewski**
    Test kometowy – nowa metoda oznaczania uszkodzeń DNA (Comet assay – new method of determination of DNA damages).
    Institute of Genetics and Animal Breeding, Polish Academy of Sciences, Jastrzębiec, Poland, 27.02.2004.

13. **Dariusz Pogocki**
    Stabilizacja kationorodników tioeterowych poprzez oddziaływanie z nukleofilami a cytotoksyczność białek patologicznych (Stabilization of thioether radical cations by interaction with nucleophylic agents *vs*. cytotoxicity of proteins).
    Technical University of Łódź, Poland, 08.03.2004.

14. **Dariusz Pogocki**
    Wewnątrzcząsteczkowe przemiany rodnikowe a neurotoksyczność β-amyloidu i białek prionowych (Intramolecular radical processes *vs*. neurotoxicity of β-amyloid and prion proteins).
    Polish Radiation Research Society, Łódź, Poland, 20.04.2004.

15. **Dariusz Pogocki**
    How α-helical Aβ could be a source of free radicals.
    University of Calgary, Canada, 13.05.2004.

16. **Irena Szumiel**
    Odpowiedź adaptacyjna – nowa hipoteza (Adaptive response – new hypothesis).
    Polish Radiation Research Society, Warszawa, Poland, 29.10.2004.

17. Andrzej Wójcik
Genetic basis of the immunological system. Introduction to immunology.
University of Duisburg-Essen, Germany, 07.01.2004.

18. Andrzej Wójcik
Genetic basis of the immunological system. Antibodies.
University of Duisburg-Essen, Germany, 14.01.2004.

19. Andrzej Wójcik
Biological dosimetry.
University of Duisburg-Essen, Germany, 15.01.2004.

20. Andrzej Wójcik
Genetic basis of the immunological system. Major histocompatibility complex.
University of Duisburg-Essen, Germany, 21.01.2004.

21. Andrzej Wójcik
Genetic basis of the immunological system. Maturation of lymphocytes.
University of Duisburg-Essen, Germany, 28.01.2004.

22. Andrzej Wójcik
Dozymetria biologiczna w trzech wypadkach radiacyjnych (Biological dosimetry in the case of three radiation accidents).
The Ludwik Rydygier Medical University in Bydgoszcz, Poland, 16.03.2004.

23. Andrzej Wójcik
Promieniowanie jonizujące i zdrowie (Jonizing radiation and health).
Mokotów University of III Age, Warszawa, Poland, 08.11.2004.

24. Grażyna Zakrzewska-Trznadel
Institute of Nuclear Chemistry and Technology – presentation of activities and projects.
Kyungnam University, Masan, Korea, 08.11.2004.

25. Grażyna Zakrzewska-Trznadel
Membranes in nuclear technology.
Korea Atomic Energy Research Institute, Daejeon, Korea, 09.11.2004.

AWARDS IN 2004

1. First degree group award for a paper "Radiosensitizing properties of novel hydroxydicarboxylatoplatinum (II) complexes with high or low reactivity with thiols: two modes action".

   XIII Meeting of the Polish Radiation Research Society, Łódź, Poland, 14.09.2004.

   Iwona Grądzka, Iwona Buraczewska, Irena Szumiel

2. Distinction for the merits of a poster „Oznaczanie zawartości pierwiastków śladowych w wybranych produktach żywnościowych za pomocą NAA" (Determination of trace elements in the selected food products by NAA).

   II Kongres „Żywność, żywienie a zdrowie w Polsce zintegrowanej z Unią Europejską", Warszawa, Poland, 23-26.06.2004.

   Bożena Danko, Halina Polkowska-Motrenko, Aneeke Ammerlaan (Delft University of Technology, the Netherlands)

3. First degree individual award of Director of the Institute of Nuclear Chemistry and Technology for presenting an innovatory approach in a series of papers to the formation of sulphuranyl oxides, using modern techniques of molecular modelling.

   Dariusz Pogocki

4. Second degree group award of Director of the Institute of Nuclear Chemistry and Technology for a series of papers concerning interdisciplinary studies on synthesis of platinum and palladium complex compounds and their biological activity of antitumor characteristics.

   Leon Fuks, Marcin Kruszewski, Elżbieta Boużyk, Hanna Lewandowska-Siwkiewicz

5. Third degree group award of Director of the Institute of Nuclear Chemistry and Technology for a series of papers on the formation of new materials using sol-gel technique enabling practical application of the obtained results.

   Andrzej Deptuła, Wiesława Łada, Tadeusz Olczak

6. Diploma of the social movement „Piękniejsza Polska" for the outstanding contribution to the development of Polish radiobiology.

   Irena Szumiel

INSTRUMENTAL LABORATORIES AND TECHNOLOGICAL PILOT PLANTS

I. DEPARTMENT OF NUCLEAR METHODS OF MATERIAL ENGINEERING

1. Laboratory of Materials Research

Activity profile: Studies of the structure and properties of materials and historical art objects. Determination of elemental content of environmental and geological samples, industrial waste materials, historic glass objects and other materials by energy dispersive X-ray fluorescence spectrometry using a radioisotope excitation source as well as a low power X-ray tube and using a 2 kW X-ray tube in total reflection geometry. Determination of radioactive isotope content in environmental samples and historical glass objects by gamma spectrometry.

- Scanning electron microscope

DSM 942, LEO-Zeiss (Germany)

Technical data: spatial resolution – 4 nm at 30 kV, and 25 nm at 1 kV; acceleration voltage – up to 30 kV; chamber capacity – 250x150 mm.

Application: SEM observation of various materials such as metals, polymers, ceramics and glasses. Determination of characteristic parameters such as molecule and grain size.

- Scanning electron microscope equipped with the attachment for fluorescent microanalysis

BS-340 and NL-2001, TESLA (Czech Republic)

Application: Observation of surface morphology and elemental analysis of various materials.

- Vacuum evaporator

JEE-4X, JEOL (Japan)

Application: Preparation of thin film coatings of metals or carbon.

- Gamma radiation spectrometer

HP-Ge, model GS 6020; Canberra-Packard (USA)

Technical data: detection efficiency for gamma radiation – 60.2%, polarization voltage – 4000 V, energy resolution (for Co-60) – 1.9 keV, analytical program "GENIE 2000".

Application: Neutron activation analysis, measurements of natural radiation of materials.

- Gamma spectrometer in low-background laboratory

EGG ORTEC

Technical data: HPGe detector with passive shield; FWHM – 1.9 keV at 1333 keV, relative efficiency – 92%.

- Total reflection X-ray spectrometer

Pico TAX, Institute for Environmental Technologies (Berlin, Germany)

Technical data: Mo X-ray tube, 2000 W; Si(Li) detector with FHWM 180 eV for 5.9 keV line; analysed elements: from sulphur to uranium; detection limits – 10 ppb for optimal range of analysed elements, 100 ppb for the others.

Application: XRF analysis in total reflection geometry. Analysis of minor elements in water (tap, river, waste and rain water); analysis of soil, metals, raw materials, fly ash, pigments, biological samples.

- X-ray spectrometer

SLP-10180-S, ORTEC (USA)

Technical data: FWHM – 175 eV for 5.9 keV line, diameter of active part – 10 mm, thickness of active part of detector – 5.67 mm.

Application: X-ray fluorescence analysis.

- Coulter Porometer II

Coulter Electronics Ltd (Great Britain)

Application: Pore size analysis in porous media.

- Vacuum chamber for plasma research

POLVAC Technika Próżniowa

Technical data: dimensions – 300x300 mm; high voltage and current connectors, diagnostic windows.

Application: Studies on plasma discharge influence on physicochemical surface properties of polymer films, particularly TEM (track-etched membranes).

2. Laboratory of Diffractional Structural Research

Activity profile: X-ray diffraction structural studies on metal-organic compounds originating as degradation products of substances naturally occurring in the environment. Röntgenostructural phase analysis of materials. Studies on interactions in a penetrant-polymer membrane system using small angle scattering of X-rays, synchrotron and neutron radiation. Studies of structural changes occurring in natural and synthetic polymers under influence of ionising radiation applying X-ray diffraction and differential scanning calorimetry.

- KM-4 X-ray diffractometer

KUMA DIFFRACTION (Poland)

Application: 4-cycle diffractometer for monocrystal studies.

- CRYOJET - Liquid Nitrogen Cooling System

Oxford Instruments

Application: Liquid nitrogen cooling system for KM-4 single crystal diffractometer.

- HZG4 X-ray diffractometer

Freiberger Präzisionsmechanik (Germany)

Application: Powder diffractometers for studies of polycrystalline, semicrystalline and amorphous materials.

- URD 6 X-ray diffractometer

Freiberger Präzisionsmechanik (Germany)

Application: Powder diffractometers for studies of polycrystalline, semicrystalline and amorphous materials.

3. Sol-Gel Laboratory of Modern Materials

Activity profile: The research and production of advanced ceramic materials in the shape of powders, monoliths, fibres and coatings by classic sol-gel methods with modifications – IChTJ Process or by CSGP (Complex Sol-Gel Method) are conducted. Materials obtained by this method are the following powders: alumina and its homogeneous mixtures with Cr_2O_3, TiO_3, Fe_2O_3, $MgO+Y_2O_3$, MoO_3, Fe, Mo, Ni and CaO, CeO_2, Y_2O_3 stabilized zirconia, β and β'' aluminas, ferrites, $SrZrO_3$, ceramic superconductors, type YBCO (phases 123, 124), BSCCO (phases 2212, 2223), $NdBa_2Cu_3O_x$, their nanocomposites, Li-Ni-Co-O spinels as cathodic materials for Li rechargeable batteries and fuel cells MCFC, $BaTiO_3$, $LiPO_4$, Li titanates: spherical for fusion technology, irregularly shaped as superconductors and cathodic materials, Pt/WO_3 catalyst. Many of the mentioned above systems, as well as sensors, type SnO_2, were prepared as coatings on metallic substrates. Bioceramic materials based on calcium phosphates (*e.g.* hydroxyapatite) were synthesized in the form of powders, monoliths and fibres.

- DTA and TGA thermal analyser

OD-102 Paulik-Paulik-Erdey, MOM (Hungary)

Technical data: balance fundamental sensitivity – 20-0.2 mg/100 scale divisions, weight range – 0-9.990 g, galvanometer sensitivity – $1x10^{-10}$ A/mm/m, maximum temperature – 1050°C.

Application: Thermogravimetric studies of materials up to 1050°C.

- DTA and TGA thermal analyser 1500

MOM (Hungary)

Technical data: temperature range – 20-1500°C; power requirements – 220 V, 50 Hz.

Application: Thermal analysis of solids in the temperature range 20-1500°C.

- Research general-purpose microscope

Carl Zeiss Jena (Germany)

Technical data: General purpose microscope, magnification from 25 to 2500 times, illumination of sample from top or bottom side.

- Metallographic microscope

EPITYP-2, Carl-Zeiss Jena (Germany)

Technical data: magnification from 40 to 1250 times.

Application: Metallographic microscope for studies in polarized light illumination and hardness measurements.

- Laboratory furnace

CSF 12/13, CARBOLITE (Great Britain)

Application: Temperature treatment of samples in controlled atmosphere up to 1500°C with automatic adjustment of final temperature, heating and cooling rate.

II. DEPARTMENT OF RADIOISOTOPE INSTRUMENTS AND METHODS

Laboratory of Industrial Radiometry

Activity profile: Research and development of non-destructive methods and measuring instruments utilizing physical phenomena connected with the interaction of radiation with matter: development of new methods and industrial instruments for measurement of physical quantities and analysis of chemical composition; development of measuring instruments for environmental protection purpose (dust monitors, radon meters); implementation of new methods of calibration and signal processing (multivariate models, artificial neural networks); designing, construction and manufacturing of measuring instruments and systems; testing of industrial and laboratory instruments.

- Multichannel analyser board with software for X and γ-ray spectrometry

Canberra

- Function generator

FG-513, American Reliace INC

III. DEPARTMENT OF RADIOCHEMISTRY

1. Laboratory of Coordination and Radiopharmaceutical Chemistry

Activity profile: Preparation of novel complexes, potential radiopharmaceuticals, *e.g.* derivatives of tricarbonyltechnetium(I) (^{99m}Tc) with chelating ligands mono- and bifunctional. Studying of their hydrophilic-lipophilic properties, structure and their interactions with peptides. Also rhenium(VI) complexes with dendrimeric ligands are synthesised and studied. Novel platinum and palladium complexes with organic ligands, analogs of *cis*platin, are synthesised and studied as potential anti-tumor agents. Solvent extraction separation of trivalent actinides from lanthanides is studied, directed towards nuclear waste treatment. Studies in the field of isotope chemistry of middle and heavy elements in order to find correlations between isotope separation factor and the structure of species which exchange isotopes in chemical systems, as well as to select the methods suitable for isotope enrichment. (For the research equipment, common for both Laboratories, see below.)

2. Laboratory of Heavy Elements

Activity profile: Studies on chemical properties of the heaviest elements: nobelium, rutherfordium, dubnium, element 112. Studies on the influence of relativistic effects on the chemical properties (oxidation state, hydrolytic properties, *etc*.). Synthesis and studies of p-block metal complexes in uncommon oxidation states *e.g.* Bi^{+}, Po^{2+}, Tl^{2+}. Elaboration of new methods for binding of ^{211}At to biomolecules. Studies on separation of Lu^{3+} from Yb^{3+} in order to obtain non-carrier added ^{177}Lu, ^{47}Sc, ^{103m}Rh and ^{105}Rh.

- Spectrometric set

ORTEC

Multichannel analyser, type 7150, semiconductor detector

Application: Measurements and identification of γ- and α-radioactive nuclides.

- Spectrometric set

TUKAN, IPJ (Świerk, Poland)

Multichannel analyser, type SILENA with a PC card type TUKAN

Application: Measurements and identification of γ-radioactive nuclides.

- Gas chromatograph

610, UNICAM (England)

Application: Analysis of the composition of mixtures of organic substances in the gas and liquid state.

- High Performance Liquid Chromatography system

Gradient HPLC pump L-7100, Merck (Germany) with γ-radiation detector, INCT (Poland)

Application: Analytical and preparative separations of radionuclides and/or various chemical forms of radionuclides.

- Capillary electrophoresis system

PrinCE Technologies with a UV-VIS detector (Bischoff Lambda 1010) and a radiometric detector Activity Gauge type Tc-99m (INCT, Poland)

Application: Analytical separation of various radiochemical and chemical species, in particular charged.

- UV-VIS spectrophotometer

DU 68, Beckman (Austria), modernized and computerized

Application: Recording of electronic spectra of metal complexes and organic compounds in solution. Analytical determination of the concentration of these compounds.

- FT-IR spectrophotometer

EQUINOX 55, Bruker (Germany)

Application: Measurements of IR spectra of metal complexes and other species in the solid state and in solution.

IV. DEPARTMENT OF NUCLEAR METHODS OF PROCESS ENGINEERING

1. Pilot Plant for Flue Gases Treatment

Activity profile: A pilot plant was installed for basic and industrial research on radiation processing application for flue gas treatment at the Electric-Power Station KAWĘCZYN.

- Two accelerators ELW-3A

Technical data: 50 kW power, 800 kV

- Analyser of gases

Model 17, Thermo Instrument (USA)

Application: Measurement of NO, NO_2, NO_x, NH_3 concentrations.

- Analyser 10AR (Shimadzu, Japan) with analysers NOA-305A for NO concentration determination and URA-107 for SO_2 determination
- Analysers of CO/CO_2, O_2

2. Laboratory for Flue Gases Analysis

Activity profile: Experimental research connected with elaboration of removal technology for SO_2 and NO_x and other hazardous pollutants from flue gases.

- Ultrasonic generator of aerosols

TYTAN XLG

- Gas chromatograph

Perkin-Elmer (USA)

- Gas analyser LAND

Application: Determination of SO_2, NO_x, O_2, hydrocarbons, and CO_2 concentrations.

- Impactor MARK III

Andersen (USA)

Application: Measurement of aerosol particle diameter and particle diameter distribution.

3. Laboratory of Stable Isotope Ratio Mass Spectrometry

Activity profile: Study of isotope ratios of stable isotopes in hydrogeological, environmental, medical and food samples.

- Mass spectrometer DELTA^{plus}

Finnigan MAT (Bremen, Germany)

Technical data: DELTA^{plus} can perform gas isotope ratio measurements of H/D, $^{13}C/^{12}C$, $^{15}N/^{14}N$, $^{18}O/^{16}O$, $^{34}S/^{32}S$.

Application: For measurements of hydrogen (H/D) and oxygen ($^{18}O/^{16}O$) in water samples with two automatic systems: H/Device and GasBench II. The system is fully computerized and controlled by the software ISODAT operating in multiscan mode (realtime). The H/Device is a preparation system for hydrogen from water and volatile organic compounds determination. Precision of hydrogen isotope ratio determination is about 0.5‰ for water. The GasBench II is a unit for on-line oxygen isotope ratio measurements in water samples by "continuous flow" techniques. With GasBench II, water samples (0.5 ml) can be routinely analyzed with a precision and accuracy of 0.05‰. The total volume of water sample for oxygen and hydrogen determination is about 2 ml.

- Elemental Analyzer Flash 1112 NCS

Thermo Finnigan (Italy)

Application: For measurement of carbon, nitrogen and sulfur contents and their isotope composition in organic matter (foodstuff and environmental samples).

- Gas chromatograph mass spectrometer

GC MS-QP 5050A, GC-17A, Shimadzu (Japan)

Technical data: capillary column – SPB 5, HP-5MS, SUPELCOWAX™-10

4. Radiotracers Laboratory

Activity profile: Radiotracer research in the field of: environmental protection, hydrology, underground water flow, sewage transport and dispersion in rivers and sea, dynamic characteristics of industrial installations and waste water treatment stations.

- Heavy lead chamber (10 cm Pb wall thickness) for up to $3.7x10^{10}$ Bq (1 Ci) radiotracer activity preparations in liquid or solid forms
- Field radiometers for radioactivity measurements
- Apparatus for liquid sampling

- Turner fluorimeters for dye tracer concentration measurements
- Automatic devices for liquid tracers injection
- Liquid-scintillation counter

Model 1414-003 "Guardian", Wallac-Oy (Finland)

Application: Extra low-level measurements of α and β radionuclide concentrations, especially for H-3, Ra-226, Rn-222 in environmental materials *e.g.* underground waters, surface natural waters; in other liquid samples as waste waters biological materials, mine waters, *etc*.

5. Membrane Laboratory

Activity profile: Research in the field of application of membranes for radioactive waste processing and separation of isotopes.

- Membrane distillation plant for concentration of solutions

Technical data: output ~0.05 m^3/h, equipped with spiral-wound PTFE module G-4.0-6-7 (SEP GmbH) with heat recovery in two heat-exchangers.

- Multi-stage MD unit (PROATOM) with 4 chambers equipped with flat sheet membranes for studying isotope separations
- US 150 laboratory stand (Alamo Water) for reverse osmosis tests

Technical data: working pressure – up to 15 bar, flow rate – 200 dm^3/h, equipped with two RO modules.

- Laboratory stand with 5 different RP spiral wound modules and ceramic replaceable tubular modules
- Laboratory set-up for small capillary and frame-and-plate microfiltration and ultrafiltration module examination (capillary EuroSep, pore diameter 0.2 μm and frame-and-plate the INCT modules)
- The system for industrial waste water pretreatment

Technical data: pressure – up to 0.3 MPa; equipped with ceramic filters, bed Alamo Water filters with replaceable cartridge (ceramic carbon, polypropylene, porous or fibrous) and frame-and-plate microfiltration module.

- The set-up for chemically agressive solutions (pH 0-14), high-saline solutions (~50 g/l) in the whole pH range, and of radioactive solutions treatment

Technical data: equipped with TONKAFLO high pressure pump, up to 7 MPa, chemically resistant Kiryat Weizmann module (cut-off 400 MW), and high-pressure RO module.

V. DEPARTMENT OF RADIATION CHEMISTRY AND TECHNOLOGY

1. Laboratory of Radiation Modified Polymers

Activity profile: Modification of polymers by ionising radiation. Radiation-induced radicals in polymers. Optimization of mechanical and chemical properties of biomaterials following electron beam and gamma irradiation, biological application of polymers. Nanocomposites and nanofillers modified by ionising radiation.

- Accelerator ILU-6

INP (Novosibirsk, Russia)

Technical data: beam power – 20 kW, electron energy – 0.7-2 MeV.

Application: Radiation processing.

- Extruder

PLV-151, BRABENDER-DISBURG (Germany)

Technical data: Plasti-Corder consists of: driving motor, temperature adjustment panel, thermostat, crusher, mixer, extruder with set of extrusion heads (for foils, rods, sleevs, tubes), cooling tank, pelleting machine, collecting device.

Application: Preparation of polymer samples.

- Equipment for mechanical testing of polymer samples

INSTRON 5565, Instron Co. (England)

Technical data: High performance load frame with computer control device, equipped with Digital Signal Processing and MERLIN testing software; max. load of frame is 5000 N with accuracy below 0.4% in full range; max. speed of testing 1000 mm/min in full range of load; total crosshead travel – 1135 mm; space between column – 420 mm; the environmental chamber 319-409 (internal dimensions 660x230x240 mm; temperature range from -70 to 250°C).

Application: The unit is designed for testing of polymer materials (extension testing, tension, flexure, peel strength, cyclic test and other with capability to test samples at low and high temperatures).

- Viscosimeter

CAP 2000+H, Brookfield (USA)

Technical data: Range of measurements – 0.8-1500 Pa*s, temperature range – 50-235°C, cone rotation speed – 5-1000 rpm, sample volume – 30 µl. Computer controlled *via* Brookfield CALPCALC® software.

Application: Viscosity measurements of liquids and polymer melts.

- Differential scanning calorimeter

MDSC 2920 CE, TA Instruments

Technical data: equipped with liquid nitrogen cooling adapter (LNCA) for 60 l of liquid nitrogen and sample encapsulating press for open or hermetically sealed pans. Module for Modulated DSC™ is included. Working temperature – from -150°C with the LNCA to 725°C.

Application: Determines the temperature and heat flow associated with material phase transitions as a function of time and temperature. It also provides quantitative and qualitative data on endothermic (heat absorption) and exothermic (heat evolution) processes of materials during physical transitions that are caused by phase changes, melting, oxidation, and other heat-related changes.

- Processor tensiometer K100C

Technical data: supplied with the thermostatable sample vessel. Working temperature is from -10 to +100°C. The height of the sampler carrier is adjusted with the help of a high-precision motor. The balance system is automatically calibrated by a built-in reference weight with a high precision. Resolutions of measurement is 0.01 mN/m.

Application: Surface and interfacial tension measurement of liquids – Du Noüy Ring method and Dynamic Wilhelmy method with range 1-1000 mN/m; dynamic contact angle measurements; surface energy calculations on solids, powders, pigments, fibers, *etc*.; sorption measurements with the Washburn method for determining the surface energy of a powder-form solid. Controlled by LabDesk™ software.

- Spectrophotometer UV-VIS

UNICAM SP 1800 with linear recorder UNICAM AR 25

Technical data: Wavelength – 190-850 nm.

- Equipment for gel electrophoresis

System consists of: horizontal electrophoresis apparatus SUBMINI Electrophoresis Mini-System, transilluminator UV STS-20M JENCONS (United Kingdom), centrifuge EBA 12 Hettich/Zentrifugen, microwave oven KOR 8167 Daewoo.

2. Radiation Sterilization Pilot Plant of Medical Devices and Tissue Grafts

Activity profile: Research and development studies concerning new materials for manufacturing single use medical devices (resistant to radiation up to sterilization doses). Elaboration of monitoring systems and dosimetric systems concerning radiation sterilization processing. Introducing specific procedures based on national and international recommendations of ISO 9000 and PN-EN 552 standards. Sterilization of medical utensils, approx. 70 million pieces per year.

- Electron beam accelerator

UELW-10-10, NPO TORIJ (Moscow, Russia)

Technical data: beam energy – 10 MeV, beam power – 10 kW, supply power – 130 kVA.

Application: Radiation sterilization of medical devices and tissue grafts.

- Spectrophotometer UV-VIS

Model U-1100, Hitachi

Technical data: wavelength range – 200-1100 nm; radiation source – deuterium discharge (D_2) lamp, and tungsten-iodine lamp.

- Spectrophotometer UV-VIS

Model SEMCO S/EC

Technical data: wavelength range – 340-1000 nm, radiation source – halogen lamp.

Application: Only for measurements of dosimetric foils.

- Bacteriological and culture oven with temperature and time control and digital reading

Incudigit 80L

Technical data: maximum temperature – 80°C, homogeneity – ±2%, stability – ±0.25%, thermometer error – ±2%, resolution – 0.1°C.

3. Laboratory of Radiation Microwave Cryotechnique

Activity profile: Radiation processes in solids of catalytic and biological importance: stabilization of cationic metal clusters in zeolites, radical reactions in polycrystalline polypeptides, magnetic properties of transition metals in unusual oxidation states; radical intermediates in heterogeneous catalysis.

- Electron spin resonance X-band spectrometer (ESR)

Bruker ESP-300, equipped with: frequency counter Hewlett-Packard 534 2A, continuous flow helium cryostat Oxford Instruments ESR 900, continuous flow nitrogen cryostat Bruker ER 4111VT, ENDOR-TRIPLE unit Bruker ESP-351.

Application: Studies of free radicals, paramagnetic cations, atoms and metal nanoclusters as well as stable paramagnetic centers.

- Spectrophotometer UV-VIS

LAMBDA-9, Perkin-Elmer

Technical data: wavelength range – 185-3200 nm, equipped with 60 nm integrating sphere.

4. Pulse Radiolysis Laboratory

Activity profile: Studies of charge and radical centres transfer processes in thioether model compounds of biological relevance in liquid phase by means of time-resolved techniques (pulse radiolysis and laser flash photolysis) and steady-state γ-radiolysis.

- Accelerator LAE 10 (nanosecond electron linear accelerator)

INCT (Warszawa, Poland)

Technical data: beam power – 0.2 kW, electron energy – 10 MeV, pulse duration – 7-10 ns and about 100 ns, repetition rate – 1, 12.5, 25 Hz and single pulse, pulse current – 0.5-1 A, year of installation 1999.

Application: Research in the field of pulse radiolysis.

- Gas chromatograph

GC-14B, Shimadzu (Japan)

Specifications: two detectors: thermal conductivity detectors (TCD) and flame ionization detector (FID). Column oven enables installation of stainless steel columns, glass columns and capillary columns. Range of temperature settings for column oven: room temperature to 399°C (in 1°C steps), rate of temperature rise varies from 0 to 40°C/min (in 0.1°C steps). Dual injection port unit with two lines for simultaneous installation of two columns.

Application: Multifunctional instrument for analysis of final products formed during radiolysis of sulphur and porphyrin compounds and for analysis of gaseous products of catalytic reactions in zeolites.

- Dionex DX500 chromatograph system

Dionex Corporation

Specifications: The ED40 electrochemical detector provides three major forms of electrochemical detection: conductivity, DC amperometry and integrated and pulsed amperometry. The AD20 absorbance detector is a dual-beam, variable wavelength photometer, full spectral capability is provided by two light sources: a deuterium lamp for UV detection (from 190 nm) and a tungsten lamp for VIS wavelength operation (up to 800 nm). The GP40 gradient pump with a delivery system designed to blend and pump mixtures of up to four different mobile phases at precisely controlled flow rates. The system can be adapted to a wide range of analytical needs by choice of the chromatography columns: AS11 (anion exchange), CS14 (cation exchange) and AS1 (ion exclusion).

Application: The state-of-the-art analytical system for ion chromatography (IC) and high-performance liquid chromatography (HPLC) applications. Analysis of final ionic and light-absorbed products formed during radiolysis of sulphur compounds. The system and data acquisition are controlled by a Pentium 100 PC computer.

- Digital storage oscilloscope

9354AL, LeCroy

Specifications: Bandwidth DC to 500 MHz; sample rate – 500 Ms/s up to 2 Gs/s (by combining 4 channels); acquisition memory – up to 8 Mpt with 2 Mpt per channel; time/div range – 1 ns/div to 1000 s/div; sensitivity – 2 mV/div to 5 V/div; fully variable, fully programmable *via* GPIB and RS-232C.

Application: Digital storage oscilloscope (DSO) with high speed and long memory controls pulse radiolysis system dedicated to the nanosecond electron linear accelerator (LAE 10). The multiple time scales can be generated by a computer from a single kinetic trace originating from DSO since the oscilloscope produces a sufficient number of time points (up to 8 M points record length).

- Digital storage oscilloscope

9304C, LeCroy

Specifications: Bandwidth DC to 200 MHz; sample rate – 100 Ms/s up to 2 Gs/s (by combining 4 channels); acquisition memory – up to 200 kpt per channel; time/div range – 1 ns/div to 1000 s/div; sensitivity – 2 mV/div to 5 V/div; fully variable.

Application: Digital osciloscope (DO) is used in pulse radiolysis system dedicated to the nanosecond electron linear accelerator (LAE 10).

- Nd:YAG laser

Surelite II-10, Continuum (USA)

Specifications: energy (mJ) at 1064 nm (650), 532 nm (300), 355 nm (160) and 266 nm (80); pulse width – 5-7 ns (at 1064 nm) and 4-6 ns (at 532, 355 and 266 nm); energy stability – 2.5-7%; can be operated either locally or remotely through the RS-232 or TTL interface.

Application: A source of excitation in the nanosecond laser flash photolysis system being currently under construction in the Department.

- Potentiostat/Galvanostat VersaStat II

Princeton Applied Research (USA)

Specifications: Power amplifier compliance voltage single channel – ±20 V, maximum current – ±200 mA, rise time – 100 μs, slew rate – 1 V/μs; system performance: minimum timebase – 100 μs, minimum potential step – 250 μV, noise and ripple <50 μV rms typically, minimum current range – 1 μA (hardware), minimum current range – 100 nA (software), minimum current resolution – 200 pA, drift – *vs*. time <50 μV/°C *vs*. time: <200 μV/week. iR compensation: current interrupt 12-bit potential error correction total int. time <50-2000 μs. Accuracy: applied potential – 0.2% of reading ±2 mV, applied current – 0.2% of full-scale current. Computer interface: GPIB IEEE-488, RS-232. Differential electrometer: input bias current <50 pA at 25°C, typically <20 pA at 25°C. Max. voltage range – ±2 V, max. input voltage differential – ±10 V. Bandwidth – -3 dB at>4 MHz. Offset voltage <100 μV. Offset temperature stability <5 μV/°C. Common mode rejection >70 dB at 100 Hz and >60 dB at 100 kHz. Input impedance >1010 Ω, typically 1011 Ω in parallel with <50 pF.

5. Research Accelerator Laboratory

Activity profile: Laboratory is equipped with accelerators providing electron beams which make capable to perform the irradiation of investigated objects within wide range of electron energy from 100 keV to 13 MeV and average beam power from 0.1 W do 20 kW, as well as with Co-60 gamma sources with activity $1.9x10^{10}$ to $1.3x10^{14}$ Bq and dose rate from 0.03 to 1.8 kGy/h. The described above irradiators are completed in a unique in world scale set of equipment which can be applied in a wide range of electron beam and gamma-ray research and radiation processing.

- Linear electron accelerator

LAE 13/9, Institute of Electro-Physical Equipment (Russia)

Technical data: electron energy – 10-13 MeV; electron beam power – 9 kW.

Application: Radiation processing.

- Cobalt source I

"Spectrophotometric", INCT (Warszawa, Poland)

Technical data: provided for the optical, periscopic access to an irradiation chamber surrounded with Co-60 rods. 6 rods – loaded initially to $3.7x10^{13}$ Bq, after many reloadings actual activity is $1.9x10^{10}$ Bq.

Application: Radiation research.

- Cobalt source II

Issledovatel (Russia)

Technical data: 32 sources with an actual activity of $1.71x10^{14}$ Bq.

Application: Radiation research.

- Cobalt source III

Mineza, INR (Świerk, Poland)

Technical data: 6 rods with an initial activity of $2.66x10^{13}$ Bq; the actual activity is $1.9x10^{10}$ Bq.

Application: Radiation research.

- Transiluminator UV

STS-20M, JENCONS (United Kingdom)

Technical information: six 15 W bulbs, emitted 312 nm wavelength, which corresponds to the fluorescence excitation maximum of ethidium bromide. Product description: For visualisation of ethidium bromide – stained nucleic acids fluorescence detection systems. Fluorescence intensity is enhanced, while photobleaching and photonicking of stained nucleic acids are reduced.

- Electron accelerator

AS-2000 (the Netherlands)

Technical data: energy – 0.1-2 MeV, max. beam current – 100 μA.

Application: Irradiation of materials.

- Spectrometer

DLS-82E, SEMITRAP (Hungary)

Application: Research in radiation physics of semiconductors.

- Argon laser

ILA-120, Carl Zeiss (Jena, Germany)

Application: Measurements of optical properties.

- Spectrometer

DLS-81 (Hungary)

Application: Measurements of semiconductor properties.

- Argon laser

LGN-503 (Russia)

Application: Measurements of optical properties.

VI. DEPARTMENT OF ANALYTICAL CHEMISTRY

1. Laboratory of Spectral Atomic Analysis

Activity profile: atomic absorption and emission spectroscopy, studies on interference mechanisms, interpretation of analytical signals, service analysis.

- Atomic absorption spectrometer

SH-4000, Thermo Jarrell Ash (USA); equipped with a 188 Controlled Furnace Atomizer (CTF 188), Smith-Heftie background correction system and atomic vapor (AVA-440) accessory.

Application: For analyses of samples by flame and furnace AAS.

- Atomic absorption spectrometer

SP9-800, Pye Unicam (England); equipped with SP-9 Furnace Power Supply, PU-9095 data graphics system, PU-9095 video furnace programmer and SP-9 furnace autosampler.

Application: For analyses of samples by flame and furnace AAS.

2. Laboratory of Neutron Activation Analysis

Activity profile: The sole laboratory in Poland engaged for 40 years in theory and practice of neutron activation analysis in which the following methods are being developed: reactor neutron activation analysis (the unique analytical method of special importance in inorganic trace analysis), radiochemical separation methods, ion chromatography. The laboratory is also the main Polish producer of CRMs and the provider for Proficiency Testing exercises.

- Laminar box

HV mini 3, Holten (Denmark)

Technical data: air flow rate 300 m^3/h.

Application: Protection of analytical samples against contamination.

- Ion chromatograph

2000i/SP, Dionex (USA)

Technical data: calculating program AI-450, conductivity detector, UV/VIS detector.

Application: Analyses of water solutions, determination of SO_2, SO_3 and NO_x in flue gases and in air.

- Well HPGe detector

CGW-3223, Canberra, coupled with analog line (ORTEC) and multichannel gamma-ray analyzer TUKAN

Application: Instrumental and radiochemical activation analysis.

- Coaxial HPGe detector

POP-TOP, ORTEC (USA), coupled with analog line (ORTEC) and multichannel gamma-ray analyzer TUKAN

- Well HPGe detector

CGW-5524, Canberra, coupled with multichannel gamma-ray analyzer (hardware and software) Canberra

Application: Instrumental and radiochemical activation analysis.

- Analytical micro-balance

Sartorius MC5

Application: Mostly utilized for the preparation of mono- and multi-elemental standards – a proper solution is dropped onto a filter paper disc – as well as for weighing small mass samples, less than 10 mg, into irradiation PE vials, for the purpose of neutron activation analysis.

- Liquid Scintillator Analyzer

TRI-CARB 2900TR, Packard BioScience Company

Application: β measurements.

- Planetary Ball Mill

PM 100, Retsch

Application: grinding and mixing: soft, medium hard to extremly hard, brittle or fibrous materials.

- Balance-drier

ADS50, AXIS (Poland)

Application: determination of mass and humidity of samples.

- Microwave digestion system

Uniclever II, PLAZMATRONIKA (Poland)

Application: microwave digestion of samples.

- Peristaltic pump

REGLO ANALOG MS-4/6-100, ISMATEC (Switzerland)

Application: regulation of flow of eluents during elution process.

3. Laboratory of Chromatography

Activity profile: Development of HPLC methods for determination of environmental pollutants, application of HPLC and ion-chromatography monitoring of degradation of organic pollutants in waters and wastes using ionizing radiation, development of chromatographic methods, preconcentration of organic environmental pollutants, development of chromatographic methods of identification of natural dyes used for ancient textiles.

- Apparatus for biological oxygen demand determination by respirometric method and dissolved oxygen measurement method

WTW-Wissenschaftlich-Technische Wersttätten (Germany)
Application: analyses of water and waste water samples.

- Apparatus for chemical oxygen demand determination by titrametric method

Behr Labor-Technik (Germany)
Application: analyses of water and waste water samples.

- Set-up for solid phase-extraction (vacuum chamber for 12 columns and vacuum pump)

Application: analyses of water and waste water samples.

- Shimadzu HPLC system consisting of: gradient pump LC-10AT, phase mixer FCV-10AL, diode--array detector SPD-M10A, column thermostat CTO-10AS

Application: analyses of natual dyes, radiopharmaceuticals, water and waste water samples.

- Laboratory ozone generator

301.19, Erwin Sander Elektroapparatebau GmbH (Uetze-Eltze, Germany)
Application: ozone production for degradation pollutants in waste water samples.

VII. DEPARTMENT OF RADIOBIOLOGY AND HEALTH PROTECTION

Laboratory of Cellular Microbiology

Activity profile: The laboratory serves for production of plasmid DNA, subsequently used for studies on DNA recombination repair, determination of topoisomerase I activity and for EPR studies.

- Equipment for electrophoretic analysis of DNA

CHEF III, BIO-RAD (Austria)
Application: Analysis of DNA fragmentation as a result of damage by various physical and chemical agents.

- Microplate reader

ELISA, ORGANON TEKNICA (Belgium)
Application: For measurement of optical density of solutions in microplates.

- Hybridisation oven

OS-91, BIOMETRA (Germany)
Technical data: work temperatures from 0 to 80°C; exchangeable test tubes for hybridisation.
Application: For polymerase chain reaction (PCR).

- Spectrofluorimeter

RF-5000, Shimadzu (Japan)
Application: For fluorimetric determinations.

- Transilluminator for electrophoretic gels

Biodoc, BIOMETRA (Great Britain)
Application: For analysis of electrophoretic gels.

- Laminar flow cabinet

NU-437-400E, Nu Aire (USA)
Application: For work under sterile conditions.

- Liquid scintillation counter

LS 6000LL, BECKMAN (USA)
Application: For determinations of radioactivity in solutions.

- Research microscope universal

NU, Carl Zeiss Jena (Germany)
Application: For examination of cytological preparations.
Comments: Universal microscope for transmission and reflected light/polarised light. Magnification from 25x to 2500x. Possibility to apply phase contrast.

- Incubator

T-303 GF, ASSAB (Sweden)

Technical data: 220 V, temperature range – 25-75°C.
Application: For cell cultures under 5% carbon dioxide.

- Incubator

NU 5500E/Nu Aire (USA)
Technical data: 220 V, temperature range from 18 to 55°C.
Application: for cell cultures under 0-20% carbon dioxide.

- Laminar flow cabinet

V-4, ASSAB (Sweden)
Application: For work under sterile conditions.

- Image analysis system

Komet 3.1, Kinetic Imaging (Great Britain)
Application: For comet (single cell gel electrophoresis) analysis.

- ISIS 3

Metasystem (Germany)
Application: Microscopic image analysis system for chromosomal aberrations (bright field and fluorescence microscopy).

VIII. LABORATORY FOR DETECTION OF IRRADIATED FOODS

Activity profile: Detection of irradiated foods. Specially adapted analytical methods routinely used in the lab are based on electron paramagnetic resonance spectroscopy (EPR) and thermoluminescence measurements (TL). The research work is focused on the development of both methods as well as on validation and implementation of other detection methods as gas chromatographic determination of volatile hydrocarbons in fats, DNA comet assay (decomposition of single cells) and statistical germination study. The quality assurance system is adapted in the Laboratory in agreement with the PN-EN 150/IEC 17025:2001 standard and fully documented. Laboratory possesses Certificate of Testing Laboratory Accreditation NR L 262/I/99 issued by the Polish Centre for Testing and Accreditation and Accreditation Certificate for Testing Laboratory issued by the Polish Centre for Accreditation valid from 25.10.2002 to 25.10.2006.

- Thermoluminescence reader

TL-DA-15 Automated, Risoe National Laboratory (Denmark)
Technical data: turntable for 24 samples, heating range – 50÷500°C, heating speed – 0.5÷10.0°C/s, optical stimulated luminescence (OSL) system.
Application: Detection of irradiated foods, research work on irradiated foods, thermoluminescence dosimetry.

- EPR spectrometer

EPR 10-MINI, St. Petersburg Instruments Ltd. (Russia)
Technical data: sensitivity – $3x10^{10}$, operating frequency (X band) – 9.0-9.6 GHz, max. microwave power – 80 mW, magnetic field range – 30-500 mT, frequency modulation – 100 kHz.
Application: Detection of irradiated foods, bone and alanine dosimetry, research work on irradiated foods and bone tissues.

- Fluorescence microscope

OPTIPHOT Model X-2, NIKON (Japan)
Technical data: halogen lamp 12 V-100 W LL; mercury lamp 100 W/102 DH; lenses (objectives) CF E Plan Achromat 4x, CF E Plan Achromat 40x; CF FLUOR 20x.
Application: Detection of irradiated foods by the DNA comet assay, research work on apoptosis in mammalian cells, biological dosimetry, analysis of DNA damage in mammalian cells.

IX. EXPERIMENTAL PLANT FOR FOOD IRRADIATION

1. Microbiological Laboratory

Activity profile: optimization of food irradiation process by microbiological analysis.

- Sterilizer

ASUE, SMS (Warszawa, Poland)
Application: Autoclaving of laboratory glass, equipment, and microbiological cultures.

- Fluorescence microscope

BX, Olimpus (Germany)
Application: Quantitative and qualitative microbiological analysis.

2. Experimental Plant for Food Irradiation

Activity profile: Development of new radiation technologies for the preservation and hygienization of food products. Development and standarization of the control system for electron beam process-

ing of food. Development of analytical methods for the detection of irradiated food. Organization of consumer tests with radiation treated food products.

- Accelerator ELEKTRONIKA (10 MeV, 10 kW)

UELW-10-10, NPO TORIJ (Moscow, Russia)
Application: Food irradiation.

INDEX OF THE AUTHORS